

Generalized Parton Distributions

M. Diehl

Deutsches Elektronen-Synchrotron DESY, 22603 Hamburg, Germany

Abstract

We give an overview of the theory for generalized parton distributions. Topics covered are their general properties and physical interpretation, the possibility to explore the three-dimensional structure of hadrons at parton level, their potential to unravel the spin structure of the nucleon, their role in small- x physics, and efforts to model their dynamics. We review our understanding of the reactions where generalized parton distributions occur, to leading power accuracy and beyond, and present strategies for phenomenological analysis. We emphasize the close connection between generalized parton distributions and generalized distribution amplitudes, whose properties and physics we also present. We finally discuss the use of these quantities for describing soft contributions to exclusive processes at large energy and momentum transfer.

Contents

1	Introduction	6
2	In a nutshell	8
3	Properties of GPDs and GDAs	11
3.1	Notation and conventions	11
3.2	Definition of GPDs	13
3.3	Basic properties	15
3.3.1	Forward limit	15
3.3.2	Symmetry properties	15
3.3.3	Sum rules and polynomiality	17
3.4	Parton interpretation and the light-cone	19
3.5	Helicity structure	23
3.5.1	Lorentz symmetry on the light-cone	23
3.5.2	Parton helicity flip	24
3.5.3	Helicity amplitudes and GPDs	26
3.5.4	Counting GPDs	27
3.6	The energy-momentum tensor and the spin of the nucleon	28
3.7	Generalized distribution amplitudes	31
3.7.1	General properties	33
3.7.2	Evolution and expansion on polynomials	34
3.8	Evolution of GPDs	36
3.8.1	Evolution of light-cone operators	37
3.8.2	Evolution of GPDs	38
3.8.3	Solving the evolution equations	41
3.8.4	Shuvaev transform	43
3.9	Double distributions	44
3.9.1	General properties and evolution	47
3.9.2	The D -term	49
3.9.3	The crossed channel and the inversion formula	51
3.10	Impact parameter space	53
3.10.1	The case $\xi = 0$	57
3.10.2	GDAs in impact parameter space	58
3.11	The wave function representation	59
3.11.1	Fock space decomposition	59
3.11.2	The overlap formulae	61
3.11.3	Polynomiality and the covariant approach	65
3.11.4	Evolution	67
3.11.5	A remark about the light-cone gauge	68
3.12	Positivity bounds	69
3.12.1	Bounds in momentum representation	70
3.12.2	Bounds in impact parameter representation	71
3.12.3	Derivation and validity	73
3.13	The point $x = \xi$	74
3.14	Transition GPDs	75
3.14.1	Transitions within the baryon octet	76

3.14.2	Transitions to the Δ	77
3.14.3	More transitions	77
3.15	Spin 1 targets	78
4	Dynamics and models	79
4.1	Dynamics of GPDs	80
4.1.1	Chiral symmetry	80
4.1.2	The large- N_c limit	82
4.1.3	The chiral quark-soliton model	83
4.1.4	Quark models	84
4.1.5	Covariant approaches	85
4.1.6	Light-cone wave functions and partons	87
4.1.7	The limit of large t	89
4.1.8	Lessons from impact parameter space	90
4.2	Moments	91
4.3	Ansätze for GPDs	94
4.3.1	Exchange contributions	94
4.3.2	The D -term	95
4.3.3	Double distributions and connection to forward densities	96
4.3.4	Dependence on t	99
4.3.5	GPDs from triangle graphs	101
4.4	GPDs at small x	102
4.5	Nuclei	107
4.6	Dynamics of GDAs	109
4.6.1	Very small s	109
4.6.2	Connection with resonance DAs	109
4.6.3	Very large s	110
4.6.4	Modeling	110
4.6.5	GDAs and the hadronization process	111
5	Exclusive processes to leading power accuracy	112
5.1	Factorization	112
5.1.1	Selection rules	118
5.2	Compton scattering	121
5.3	Meson electroproduction	123
5.3.1	Beyond leading order in α_s	127
5.4	Meson pair production and GDAs	128
5.4.1	Two-photon annihilation	128
5.4.2	Electroproduction	130
6	Beyond leading power	131
6.1	Compton scattering at $1/Q$ accuracy	132
6.1.1	Operator product expansion and twist	132
6.1.2	The DVCS amplitude at $1/Q$ accuracy	136
6.2	Two-photon annihilation	138
6.3	Compton scattering beyond $1/Q$ accuracy	141
6.4	Meson form factors and meson electroproduction	143
6.5	Parton-hadron duality	146

6.5.1	Timelike photons	146
6.5.2	Bloom-Gilman duality	147
7	Beyond the factorization theorems	148
7.1	Transverse vector mesons	148
7.2	Meson pairs with large invariant mass	149
7.3	Access to transversity distributions	149
7.4	Heavy meson production	151
7.4.1	Charmonium	151
7.4.2	Heavy-light mesons	152
7.5	Hadron-hadron collisions	152
8	GPDs and small-x physics	154
8.1	Collinear factorization and beyond	156
8.2	Longitudinal vs. transverse photons	159
8.3	The t dependence	162
8.4	Vector meson production	162
8.4.1	The gluon distribution	163
8.4.2	The meson wave function	164
8.4.3	Dynamics and observables	167
8.5	DVCS	167
8.6	Other diffractive channels	168
9	Phenomenology	169
9.1	DVCS	169
9.1.1	Angular structure	173
9.1.2	Beam and target polarization	175
9.1.3	Cross sections and asymmetries	176
9.1.4	Access to GPDs	179
9.1.5	First data	182
9.1.6	Targets with spin zero or one	183
9.2	Timelike Compton scattering	184
9.3	Two-photon annihilation	185
9.4	Meson production	186
9.4.1	Leading twist and beyond	188
9.4.2	Meson pair production	188
9.5	The deconvolution problem	189
10	Processes at large s, t and u	191
10.1	Hard scattering and soft overlap contributions	191
10.2	The soft overlap for Compton scattering and meson production	193
10.2.1	Calculating the handbag diagrams	193
10.2.2	Phenomenology of Compton scattering	195
10.2.3	Meson production	198
10.3	Two-photon annihilation	198
10.3.1	Baryon pair production	198
10.3.2	Meson pair production	200
11	Conclusions	201

A Acronyms	204
B Light-cone helicity spinors	204

1 Introduction

Among the main open questions in the theory of strong interactions is to understand how the nucleon and other hadrons are built from quarks and gluons, the fundamental degrees of freedom in QCD. An essential tool to investigate hadron structure is the study of deep inelastic scattering processes, where individual quarks and gluons are resolved. The parton densities one can extract from such processes encode the distribution of longitudinal momentum and polarization carried by quarks, antiquarks and gluons within a fast moving hadron. They have provided much to shape our physical picture of hadron structure. Yet important pieces of information are missed out in these quantities, in particular how partons are distributed in the plane transverse to the direction in which the hadron is moving, or how important their orbital angular momentum is in making up the total spin of a nucleon. In recent years it has become clear that appropriate exclusive scattering processes may provide such information, encoded in generalized parton distributions (GPDs).

GPDs have been discovered and rediscovered in different contexts, and the processes where they appear have been considered early on. Let us try to give the main lines of development here, with apologies to those whose contributions we may have overlooked.

- One of the principal reactions involving GPDs is Compton scattering with nonzero momentum transfer to the proton and at least one photon off-shell (see Section 5.1 for specification of the relevant kinematics). The nonforward Compton amplitude has been considered in various contexts, as well as the physical processes where it may be measured such as $ep \rightarrow ep\gamma$, $\gamma p \rightarrow \mu^+\mu^- p$, or $ep \rightarrow ep\mu^+\mu^-$ [1, 2, 3, 4]. A rather detailed treatment of nonforward Compton scattering in the operator product expansion has been given by Watanabe [5, 6], where quantities resembling double distributions (see Section 3.9) appear, but this work has not been pursued.
- A systematic investigation of GPDs and their appearance in virtual Compton scattering has been performed by the Leipzig group in a series of papers [7, 8, 9] culminating in [10]. Using the nonlocal operator product expansion, a unified framework was developed to describe both the DGLAP evolution [11, 12, 13, 14] of parton densities and the ERBL evolution [15, 16] of meson distribution amplitudes. GPDs appeared as functions whose scale evolution “interpolates” between these two limiting cases.
- A different line of research concerns diffractive processes induced by highly virtual photons. Bartels and Loewe [17] considered $\gamma^*p \rightarrow \gamma p$ and $\gamma^*p \rightarrow Zp$ in terms of nonforward gluon ladder diagrams, without recourse to the concept of parton distributions. Ryskin [18] pointed out that $\gamma^*p \rightarrow J/\Psi p$ may provide a sensitive access to the gluon distribution, which appears *squared* in the cross section. Electroproduction of light vector mesons was later investigated by Brodsky et al. [19]. Somewhat ironically, these studies did not emphasize that it is the *generalized* gluon distribution one probes in these reactions: in the leading $\log \frac{1}{x}$ approximation there is indeed no difference between the usual gluon distribution and the generalized one at vanishing invariant momentum transfer t to the proton (see Section 8.1).
- The interest of a wide community in GPDs was raised in 1996, when the nonforward nature of the parton distributions entering virtual Compton scattering [20, 21, 22] and meson production [23] was emphasized by Ji and by Radyushkin, and when Collins et al. [24] provided a proof of factorization of meson electroproduction in diffractive and nondiffractive kinematics. Ji’s work [20] pointed out the potential of such studies to unravel the spin structure of the nucleon: GPDs fulfill a sum rule which may provide access to the *total* angular momentum carried by partons, comprising the spin and the orbital part (see Section 3.6). It also showed how GPDs provide a connection between ordinary parton densities and elastic form factors, and hence

between the principal quantities which so far have provided information on nucleon structure. This connection had previously been pointed out by Jain and Ralston [25].

- The potential of GPDs to study hadron structure in three dimensions (instead of the one-dimensional projection inherent in the ordinary parton densities) has been fully recognized only recently, starting with the work by Burkardt [26] on the impact parameter representation (see Section 3.10).

Experimental measurement of the exclusive processes involving GPDs is a challenge, requiring high luminosity to compensate for small cross sections and detectors capable of ensuring the exclusivity of the final state. Data on electroproduction of vector mesons have been available for some time, whereas virtual Compton scattering in the appropriate kinematics has only been measured recently (see Sections 8.4, 8.5, 9.1.5, 9.4).

A profound property of quantum field theory is crossing symmetry. This symmetry leads to generalized distribution amplitudes (GDAs) as the analogs of GPDs in the crossed channel. GDAs describe the transition from a quark-antiquark or gluon pair to a hadronic system such as $p\bar{p}$ or $\pi^+\pi^-$ and thus involve the physics of hadronization in a very specific situation. Early studies of multi-hadron distribution amplitudes were performed by Baier and Grozin [27, 28]. The close analogy between the short-distance regimes of Compton scattering and of $\gamma^*\gamma^*$ annihilation into two hadrons has been noted by Watanabe [6] and by Müller et al. [10]. The dedicated study of GDAs, with their connections both to GPDs and to the usual distribution amplitudes of single mesons, was initiated by [29]. Although much physics looks quite different in the GPD and GDA channels, there are important similarities and links between them. To profit from these links we will discuss the two types of quantities together rather than treat GDAs in a separate section. Subsections concerning the physics of GDAs are 3.7, 3.9.3, 3.10.2, 4.6, 5.4, 6.2, 9.3, 9.4.2, and 10.3.

In the following section we will set the stage with a non-technical overview. This will introduce several concepts and questions this review is concerned with and anticipate different points to be elaborated on in later sections. In Section 3 we present the general properties of GPDs and GDAs, and discuss different aspects of the physics information contained in these quantities. The status of efforts to understand their dynamics and to model them in practice is reviewed in Section 4.

The theory of leading-twist observables where GPDs or GDAs occur is in a quite advanced state and will be described in Section 5. Much less complete is our grasp of dynamics beyond the leading-twist approximation, which we attempt to sketch in Sections 6 and 7. The appearance of GPDs in small- x physics involves many aspects specific to the high-energy regime, which are discussed in Section 8. The highly developed techniques to extract information about GPDs from experimental observables will be presented in Section 9, as well as the results of phenomenological analyses of available data.

The developments discussed so far concern scattering at small invariant momentum transfer t to the target, or the production of hadronic systems with small invariant mass s . GPDs and GDAs also appear in the description of large-angle scattering processes at high s and t , where they parameterize soft dynamics akin to the Feynman mechanism in form factors at large momentum transfer. For large-angle Compton scattering this was first explored in [30] and [31], whereas the crossed-channel processes have only been considered recently [32, 33, 34]. The driving physics questions in this regime are different from those at small s or t , as is the status of the theory, and both will be described in Section 10. We conclude in Section 11.

A number of dedicated reviews about GPDs have already appeared in the literature. The work of Ji [35] presents the state of the art in an early phase of development of the field. Detailed information about double distributions can be found in a contribution by Radyushkin [36]. The review by Goeke, Polyakov and Vanderhaeghen [37] pays particular attention to the dynamics of GPDs in the context

of chiral symmetry, the large- N_c limit, and their implementation in the chiral quark-soliton model. It also develops detailed models for GPDs and shows their quantitative effects in the cross sections for exclusive processes.

It is a good sign for the liveliness of the field (although a source of occasional despair for the reviewer) that new results have steadily appeared while this article was being written. With some exceptions we have limited ourselves to work that appeared before the end of 2002. More recent work will often be pointed out, but not be discussed in detail.

2 In a nutshell

A convenient starting point to introduce GPDs is the description of inclusive deep inelastic scattering (DIS), $ep \rightarrow eX$. In the Bjorken limit, i.e., when the photon virtuality $Q^2 = -q^2$ and the squared hadronic c.m. energy $(p+q)^2$ both become large with the ratio $x_B = Q^2/(2p \cdot q)$ fixed, the dynamics factorizes into a hard partonic subprocess, calculable in perturbation theory, and a parton distribution, which represents the probability density for finding a parton of specified momentum fraction x in the target. Using the optical theorem to relate the inclusive γ^*p cross section to the imaginary part of the forward Compton amplitude $\gamma^*p \rightarrow \gamma^*p$, the relevant Feynman diagrams at leading order in the strong coupling have the handbag form shown in Fig. 1a. Note that the parton densities appear linearly in the cross section. They can be thought of as the squared amplitudes for the target fluctuating into the parton with momentum fraction x and any remnant system—this gives them their meaning as probabilities in the classical sense, at least to leading logarithmic accuracy in Q^2 .

The simple factorization of dynamics into short- and long-distance parts is not only valid for the forward Compton amplitude, but also for the more general case where there is a finite momentum transfer to the target, provided at least one of the photon virtualities is large. A particular case is where the final photon is on shell, so that it can appear in a physical state. To be more precise, one has to take the limit of large initial photon virtuality Q^2 , with the Bjorken variable (defined as before) and the invariant momentum transfer $t = (p' - p)^2$ remaining fixed. One then speaks of deeply virtual Compton scattering (DVCS) and has again handbag diagrams as shown in Fig. 1b, which can be accessed in the exclusive process $ep \rightarrow e\gamma p$. The long-distance part, represented by the lower blob, is now called a generalized parton distribution (GPD).

An important class of other processes where GPDs occur is the production of a light meson instead of the γ . If the meson quantum numbers permit, the GPDs for gluons enter at the same order in α_s as those for quarks, see Fig. 2. A second nonperturbative quantity in these processes is the meson

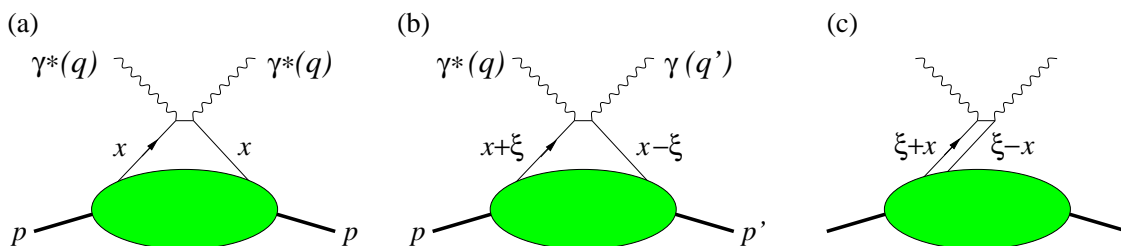


Figure 1: (a) Handbag diagram for the forward Compton amplitude $\gamma^*p \rightarrow \gamma^*p$, whose imaginary part gives the DIS cross section. (b) Handbag diagram for DVCS in the region $\xi < x < 1$. (c) The same in the region $-\xi < x < \xi$. Momentum fractions x and ξ refer to the average hadron momentum $\frac{1}{2}(p+p')$. A second diagram is obtained in each case by interchanging the photon vertices.

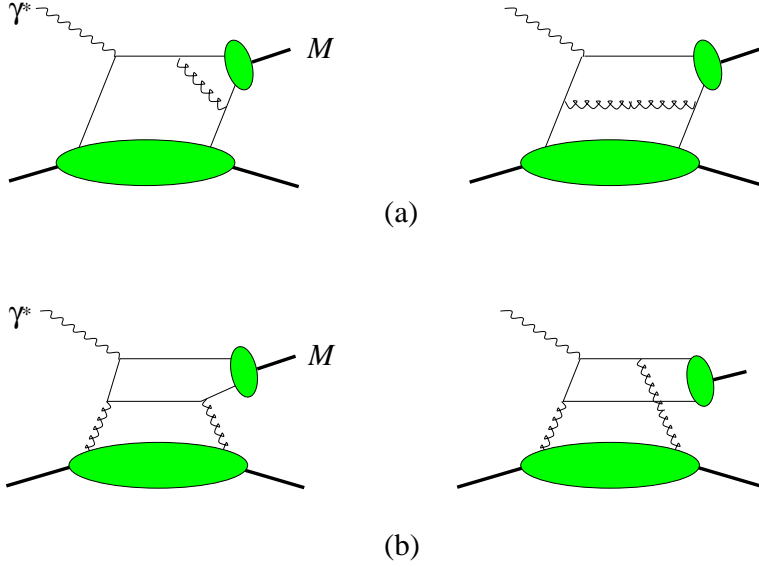


Figure 2: Diagrams for hard meson production $\gamma^*p \rightarrow Mp$ with (a) quark and (b) gluon GPDs.

distribution amplitude, which describes the coupling of the meson to the $q\bar{q}$ (or gluon) pair produced in the hard scattering.

The transformation of a virtual photon into a real photon or a meson requires a finite transfer of longitudinal momentum, where “longitudinal” refers to the direction of the initial proton momentum in a frame where both p and p' move fast (an appropriate frame is for instance the c.m. of the γ^*p collision). One easily sees that the fraction of momentum lost by the proton is determined by x_B . If momentum fractions are parameterized in the symmetric way shown in Fig. 1b, one has

$$\xi \approx \frac{x_B}{2 - x_B} \quad (1)$$

in the Bjorken limit. Proton and parton momenta now are no longer the same on the right- and left-hand sides of the diagrams. Therefore a GPD no longer represents a squared amplitude (and thus a probability), but rather the *interference* between amplitudes describing different quantum fluctuations of a nucleon. This becomes explicit when representing GPDs in terms of light-cone wave functions (Section 3.11).

Apart from the longitudinal momentum, various degrees of freedom can differ between the incoming and outgoing hadron state, each revealing a particular aspect of hadron structure.

- The momentum transfer can have a transverse component (which has to be small to fulfill the condition that t should not be large). This leads to information about the transverse structure of the target, in addition to probing the longitudinal momentum of partons. An intuitive physical picture is obtained in the impact parameter representation (Section 3.10), where GPDs describe the spatial distribution of quarks and gluons in the plane transverse to the momentum of a fast moving hadron. Together with the information on longitudinal parton momentum one thus obtains a fully three-dimensional description of hadron structure.
- Not only the momentum but also the polarization of the target can be changed by the scattering, which leads to a rich spin structure of GPDs. We will see in Section 3.6 how this provides ways to study aspects of the nucleon spin difficult to come by otherwise, in particular the orbital angular momentum carried by partons.

- Because of the finite momentum transfer, the handbag diagrams admit a second kinematical regime, shown in Fig. 1c. Instead of a parton being emitted and reabsorbed by the target, we have emission of a quark-antiquark (or gluon) pair. In this regime, which has no counterpart in the usual parton densities, GPDs probe $q\bar{q}$ and gluon pairs in the hadron wave function and are thus sensitive to physics associated with the dynamics of sea quarks and of meson degrees of freedom (see Section 4).
- Finally, the proton can be scattered inelastically into a different baryon, or a multi-particle state. The factorization just discussed still holds, as long as the invariant mass of that state is small compared with the photon virtuality Q^2 . In this way, information can be obtained about the partonic structure of hadrons not available as targets, like nucleon resonances, the Δ , or hyperons (see Section 3.14).

Factorized amplitudes are written as a convolution of a GPD with a hard scattering kernel depending on the momentum fractions x and ξ , with x being integrated over as a loop variable. The typical integral occurring at lowest order in α_s is

$$\int_{-1}^1 dx f(x, \xi, t) \frac{1}{x - \xi + i\epsilon} = \mathcal{P} \int_{-1}^1 dx f(x, \xi, t) \frac{1}{x - \xi} - i\pi f(\xi, \xi, t), \quad (2)$$

in both DVCS and light meson production, where f stands for a generic GPD and \mathcal{P} for Cauchy's principal value integral. Note that whereas GPDs are real valued quantities due to time reversal invariance, the hard scattering kernel is complex and leads to both a real and an imaginary part of the process amplitude.

If one takes the forward limit of zero ξ and t , the GPDs describing equal polarization of the initial and final state hadron reduce to the usual parton densities. This smooth limit is to be contrasted with the very different ways GPDs and usual parton densities occur in physical observables—the former in exclusive, and the latter in inclusive processes. The forward limit also exists for GPDs with different polarization of the incoming and outgoing hadron, but the corresponding quantities cannot be accessed in inclusive processes where parton densities always occur via the optical theorem.

Taking moments of GPDs in x one obtains form factors of local currents and thus a connection to the quantities which apart from parton densities have historically been one of the main tools to investigate hadron structure. These relations generalize the sum rules for ordinary parton densities, which provide form factors at $t = 0$, i.e., charges. This connection provides constraints on GPDs for those moments where the corresponding form factors are known from direct measurement. On the other hand, knowledge of GPDs can provide access to form factors of currents that do not couple to an elementary probe easily accessible to experiment. Important examples are the energy-momentum tensor (otherwise requiring graviton scattering on hadrons) and currents involving gluon fields.

Crossing symmetry relates Compton scattering $\gamma^*p \rightarrow \gamma^*p$ with two-photon annihilation $\gamma^*\gamma^* \rightarrow p\bar{p}$. In kinematics where at least one of the photon virtualities is large, in particular compared to the invariant mass of the hadron pair, one finds a factorized structure analogous to the one in DVCS, with crossed handbag diagrams as shown in Fig. 3a. In a short-distance process the two photons annihilate into a quark-antiquark (or gluon) pair, and the hadronization of this pair into the final state is described by generalized distribution amplitudes. These quantities are the crossed-channel analogs of GPDs, and although the physics they describe looks quite different, we will see important connections between GDAs and GPDs in Sections 3 and 4. Of course one may consider final states other than $p\bar{p}$, like pion pairs or systems with more than two hadrons. From this point of view GDAs naturally generalize the familiar distribution amplitudes of *single* hadrons, say of a pion. Indeed the factorization in Fig. 3a is completely analogous to the one for $\gamma^*\gamma \rightarrow \pi$ in Fig. 3b, which is among the simplest processes where the pion distribution amplitude can be accessed [38].

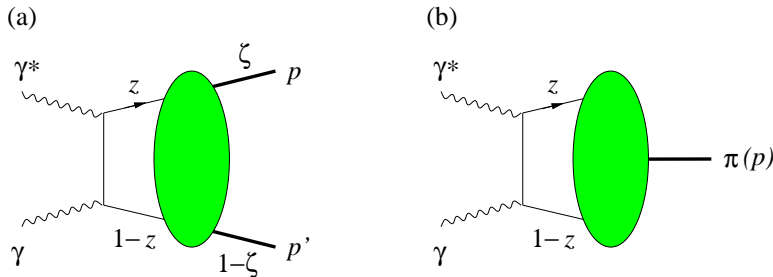


Figure 3: Handbag diagrams for the annihilation of $\gamma^*\gamma$ into a $p\bar{p}$ -pair (a) and into a single pion (b). Momentum fractions z and ζ refer to the sum of momenta in the final state.

3 Properties of GPDs and GDAs

In this section we present the general properties of generalized parton distributions and generalized distribution amplitudes, and provide tools for their physical interpretation. Throughout we will limit ourselves to the distributions of twist two; a discussion of twist three (and of twist in general) will be given in Section 6.1.

3.1 Notation and conventions

The description of parton densities and related quantities is naturally given in light-cone coordinates,

$$v^\pm = \frac{1}{\sqrt{2}}(v^0 \pm v^3), \quad \mathbf{v} = (v^1, v^2) \quad (3)$$

for any four-vector v . To avoid proliferation of subscripts like \perp we will reserve boldface for two-dimensional transverse vectors throughout (but write “ k_T ” to refer to “transverse momentum” in the text). It is often useful to work with two light-like four-vectors $n_+ = (1, 0, 0, 1)/\sqrt{2}$ and $n_- = (1, 0, 0, -1)/\sqrt{2}$, in terms of which the light-cone coordinates are given by

$$v^\mu = v^+ n_+^\mu + v^- n_-^\mu + v_T^\mu \quad (4)$$

with $v^+ = vn_-$, $v^- = vn_+$ and $v_T = (0, \mathbf{v}, 0)$. The invariant product of two four-vectors is given as $vw = v^+w^- + v^-w^+ - \mathbf{v}\mathbf{w}$, and the invariant integration element reads $d^4z = dz^+ dz^- d^2\mathbf{z}$. The derivative operators along the light-cone directions are $\partial^+ = \partial/(\partial z^-)$ and $\partial^- = \partial/(\partial z^+)$.

The physical picture of the parton model holds in frames where hadrons and partons move fast. The light-cone momentum p^+ becomes proportional to the momentum (or energy) of a particle in the infinite momentum frame where $p^3 \rightarrow +\infty$, but can be used to calculate in any convenient reference frame (including the one where a hadron is at rest). For simplicity we often refer to plus-momentum fractions as “momentum fractions”.

For GPDs and the processes where they appear we use the notation

$$P = \frac{p + p'}{2}, \quad \Delta = p' - p, \quad t = \Delta^2, \quad (5)$$

with p for the incoming and p' for the outgoing hadron momentum, and m for the target mass. For γ^*p collisions we use the standard variables

$$Q^2 = -q^2, \quad W^2 = (p + q)^2, \quad x_B = Q^2/(2p \cdot q), \quad (6)$$

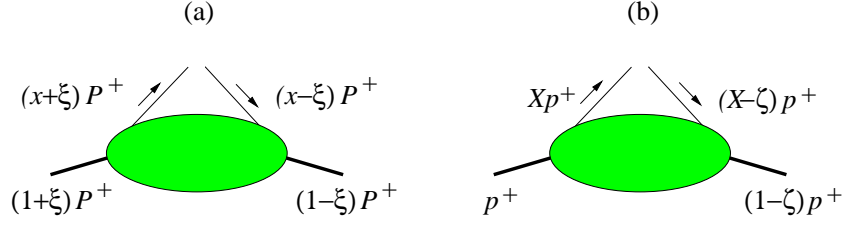


Figure 4: Hadron and parton plus-momenta in the parameterization of (a): Ji [35] and (b): Radyushkin [39].

where q is the momentum of the incident γ^* . At least two parameterizations of momentum fractions for a GPD are common in the literature, shown in Fig. 4. Their relation is

$$X = \frac{x + \xi}{1 + \xi}, \quad \zeta = \frac{2\xi}{1 + \xi}. \quad (7)$$

The variables X and ζ are closer to the ones used in forward kinematics, with the simple relation $\zeta \approx x_B$ for DVCS and light meson production in the Bjorken limit. Ji's variables [35] make symmetry properties between the initial and final hadron more transparent and will be used here. We note that the definition of ξ in Ji's original papers [20, 22] differs from that in [35] and subsequent work, with $\xi_{[35]} = \xi_{[20]}/2$. The variable $\xi_{[20]}$ is occasionally found in the literature, but most work (including this review) uses $\xi_{[35]}$ given by

$$\xi = \frac{p^+ - p'^+}{p^+ + p'^+}. \quad (8)$$

Since plus-momenta of physical states are non-negative, the physical region of ξ is the interval $[-1, 1]$. In all known processes where GPDs may be measured one has $\xi \geq 0$, which we will tacitly assume unless we specifically discuss symmetry properties under $\xi \rightarrow -\xi$ or analytical continuation in ξ .

In the following we specify further conventions used throughout this review. For the momentum fractions of distribution amplitudes (see Fig. 3) we often use the ‘‘bar’’ notation

$$\bar{z} = 1 - z. \quad (9)$$

The electric charges of quarks with flavor q are e_q in units of the positron charge e . For vectors in Hilbert space we work with the usual relativistic normalization. Our convention is

$$\epsilon_{0123} = 1 \quad (10)$$

for the totally antisymmetric tensor, and $\gamma_5 = i\gamma^0\gamma^1\gamma^2\gamma^3$. We also use the transverse tensors

$$g_T^{\alpha\beta} = g^{\alpha\beta} - n_+^\alpha n_-^\beta - n_-^\alpha n_+^\beta, \quad \epsilon_T^{\alpha\beta} = \epsilon^{\alpha\beta\gamma\delta} n_{-\gamma} n_{+\delta}, \quad (11)$$

whose only nonzero components are $g_T^{11} = g_T^{22} = -1$ and $\epsilon_T^{12} = -\epsilon_T^{21} = 1$.

Quark fields will be denoted by $q(x)$, the gluon field by $A^\mu(x)$, the gluon field strength by $G^{\mu\nu}(x)$, and the dual field strength by

$$\tilde{G}^{\alpha\beta}(x) = \frac{1}{2}\epsilon^{\alpha\beta\gamma\delta}G_{\gamma\delta}(x). \quad (12)$$

Finally, we use the abbreviations

$$\overleftrightarrow{\partial}^\mu = \frac{1}{2}(\overrightarrow{\partial}^\mu - \overleftarrow{\partial}^\mu), \quad \overleftrightarrow{D}^\mu = \frac{1}{2}(\overrightarrow{D}^\mu - \overleftarrow{D}^\mu), \quad (13)$$

where $D^\mu = \partial^\mu - igA^\mu$ is the covariant derivative.

3.2 Definition of GPDs

In full analogy to the usual parton densities, GPDs can be defined through matrix elements of quark and gluon operators at a light-like separation. In this section we will restrict ourselves to the case where the partons do not transfer helicity; parton helicity flip will be discussed in Section 3.5.2.

Following the conventions of [35] we define generalized quarks distributions

$$\begin{aligned}
F^q &= \frac{1}{2} \int \frac{dz^-}{2\pi} e^{ixP^+z^-} \langle p' | \bar{q}(-\frac{1}{2}z) \gamma^+ q(\frac{1}{2}z) | p \rangle \Big|_{z^+=0, \mathbf{z}=0} \\
&= \frac{1}{2P^+} \left[H^q(x, \xi, t) \bar{u}(p') \gamma^+ u(p) + E^q(x, \xi, t) \bar{u}(p') \frac{i\sigma^{+\alpha} \Delta_\alpha}{2m} u(p) \right], \\
\tilde{F}^q &= \frac{1}{2} \int \frac{dz^-}{2\pi} e^{ixP^+z^-} \langle p' | \bar{q}(-\frac{1}{2}z) \gamma^+ \gamma_5 q(\frac{1}{2}z) | p \rangle \Big|_{z^+=0, \mathbf{z}=0} \\
&= \frac{1}{2P^+} \left[\tilde{H}^q(x, \xi, t) \bar{u}(p') \gamma^+ \gamma_5 u(p) + \tilde{E}^q(x, \xi, t) \bar{u}(p') \frac{\gamma_5 \Delta^+}{2m} u(p) \right], \tag{14}
\end{aligned}$$

where for legibility we have not displayed the polarization dependence of the hadron states and spinors. Because of Lorentz invariance the GPDs H^q , E^q , \tilde{H}^q , \tilde{E}^q can only depend on the kinematical variables x , ξ , and t . To see this we rewrite the definitions in a frame-independent form,

$$\begin{aligned}
F^q &= \frac{1}{2} \int \frac{d\lambda}{2\pi} e^{ix(Pz)} \langle p' | \bar{q}(-\frac{1}{2}z) \not{n}_- q(\frac{1}{2}z) | p \rangle \Big|_{z=\lambda n_-} \\
&= \frac{1}{2(Pn_-)} \left[H^q(x, \xi, t) \bar{u}(p') \not{n}_- u(p) + E^q(x, \xi, t) \bar{u}(p') \frac{i\sigma^{\alpha\beta} n_{-\alpha} \Delta_\beta}{2m} u(p) \right] \tag{15}
\end{aligned}$$

with an analogous expression for \tilde{H}^q and \tilde{E}^q , where n_- can be any light-like vector. The GPDs are allowed to depend on x and on Lorentz invariant products of the vectors p , p' and n_- , which one may choose as Δn_- , Pn_- and t . Under a boost along the z axis the light-cone vectors n_- and n_+ transform as

$$n_- \rightarrow \alpha n_-, \quad n_+ \rightarrow \alpha^{-1} n_+, \tag{16}$$

and we readily see from (15) that the GPDs are independent under such a boost. Therefore they depend on Δn_- and Pn_- only via the ratio $\xi = -(\Delta n_-)/(2Pn_-)$. In other words they depend only on plus-momentum *fractions*, but not on individual plus-momenta, which are rescaled under boosts.

The above definitions hold in the light-cone gauge $A^+ = 0$ for the gluon field. In other gauges a Wilson line $W[-\frac{1}{2}z^-, \frac{1}{2}z^-]$ along a light-like path appears between the two fields at positions $-\frac{1}{2}z$ and $\frac{1}{2}z$, where

$$W[a, b] = P \exp \left(ig \int_b^a dx^- A^+(x^- n_-) \right) \tag{17}$$

and P denotes ordering along the path from a to b . Most formulae and statements of this review are readily generalized to this case, with exceptions we will indicate.

The distributions we have defined have support in the interval $x \in [-1, 1]$, which falls into the three regions shown in Fig. 5:

1. for $x \in [\xi, 1]$ both momentum fractions $x + \xi$ and $x - \xi$ are positive; the distribution describes emission and reabsorption of a quark.
2. for $x \in [-\xi, \xi]$ one has $x + \xi \geq 0$ but $x - \xi \leq 0$. The second momentum fraction is now interpreted as belonging to a antiquark with momentum fraction $\xi - x$ emitted from the initial proton.

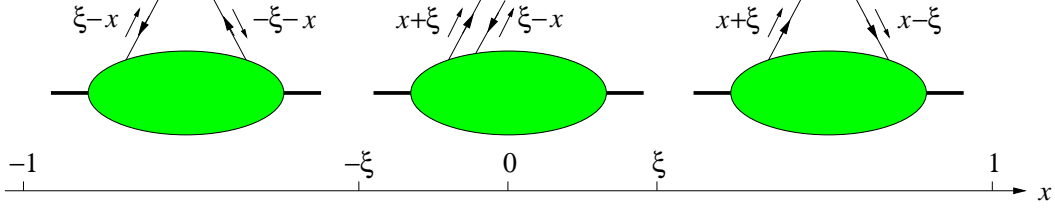


Figure 5: The parton interpretation of GPDs in the three x -intervals $[-1, -\xi]$, $[-\xi, \xi]$, and $[\xi, 1]$.

3. for $x \in [-1, -\xi]$ both $x + \xi$ and $x - \xi$ are negative; one has emission and reabsorption of antiquarks with respective momentum fractions $\xi - x$ and $-\xi - x$.

The first and third case are commonly referred to as DGLAP regions and the second as ERBL region, following the pattern of evolution in the factorization scale (Section 3.8). Why the support of GPDs is restricted to $|x| \leq 1$ will be discussed in Section 3.4.

The above interpretation can be made explicit in the framework of light-cone quantization. As we will see in Section 3.4 one can then decompose the field operators \bar{q} and q in the definitions (14) in terms of annihilation and creation operators b, b^\dagger for quarks and d, d^\dagger for antiquarks [35, 40, 41]. With the constraint that parton states must have positive plus-momentum the above three cases then respectively select the combinations $b^\dagger b$, db , and dd^\dagger .

For gluons we define

$$\begin{aligned}
F^g &= \frac{1}{P^+} \int \frac{dz^-}{2\pi} e^{ixP^+z^-} \langle p' | G^{+\mu}(-\frac{1}{2}z) G_\mu^+(\frac{1}{2}z) | p \rangle \Big|_{z^+=0, \mathbf{z}=0} \\
&= \frac{1}{2P^+} \left[H^g(x, \xi, t) \bar{u}(p') \gamma^+ u(p) + E^g(x, \xi, t) \bar{u}(p') \frac{i\sigma^{\alpha\Delta} u(p)}{2m} \right], \\
\tilde{F}^g &= -\frac{i}{P^+} \int \frac{dz^-}{2\pi} e^{ixP^+z^-} \langle p' | G^{+\mu}(-\frac{1}{2}z) \tilde{G}_\mu^+(\frac{1}{2}z) | p \rangle \Big|_{z^+=0, \mathbf{z}=0} \\
&= \frac{1}{2P^+} \left[\tilde{H}^g(x, \xi, t) \bar{u}(p') \gamma^+ \gamma_5 u(p) + \tilde{E}^g(x, \xi, t) \bar{u}(p') \frac{\gamma_5 \Delta^+}{2m} u(p) \right]. \tag{18}
\end{aligned}$$

These distributions differ by a factor of $2x$ from those of Ji [35] and by a factor of 2 from those of Goeke et al. [37, 42]:

$$2xH_g(x) \Big|_{[35]} = 2H^g(x) \Big|_{[37]} = H^g(x) \Big|_{\text{here}}, \tag{19}$$

with analogous relations for E^g , \tilde{H}^g , and \tilde{E}^g . Taking out a factor of x from our gluon GPDs leads to a more direct relation with the usual gluons densities in the forward limit (see Section 3.3.1). As remarked in [39] this introduces however an additional singularity of the GPDs at $x = 0$ (the point where two gluons with equal plus-momenta are emitted), since at this point the matrix elements in (18) are in general finite but nonzero. In physical processes it is in fact the distributions defined in (18) that appear in the amplitude, without any factor of $1/x$.

The number of GPDs for spin-zero hadrons, say pions or spin-zero nuclei, is smaller. The pion has often been considered in theoretical investigations to avoid the complications of spin (but may also be accessible experimentally, see Section 9.1.6). One defines

$$\begin{aligned}
H_\pi^q(x, \xi, t) &= \frac{1}{2} \int \frac{dz^-}{2\pi} e^{ixP^+z^-} \langle \pi^+(p') | \bar{q}(-\frac{1}{2}z) \gamma^+ q(\frac{1}{2}z) | \pi^+(p) \rangle \Big|_{z^+=0, \mathbf{z}=0}, \\
H_\pi^g(x, \xi, t) &= \frac{1}{P^+} \int \frac{dz^-}{2\pi} e^{ixP^+z^-} \langle \pi^+(p') | G^{+\mu}(-\frac{1}{2}z) G_\mu^+(\frac{1}{2}z) | \pi^+(p) \rangle \Big|_{z^+=0, \mathbf{z}=0}. \tag{20}
\end{aligned}$$

The analogs of \tilde{H}^q and \tilde{H}^g are zero in this case because of parity invariance. The case of targets with spin 1 will be discussed in Section 3.15.

GPDs have also be introduced for scalar partons, in order to facilitate the study of certain theoretical issues. The relevant operator is $\phi^\dagger(-\frac{1}{2}z)\phi(\frac{1}{2}z)$ instead of $\bar{q}(-\frac{1}{2}z)\gamma^+q(\frac{1}{2}z)$, where ϕ is the scalar field representing the partons, for the definitions see [39, 43]. Alternatively the operator $\phi^\dagger(-\frac{1}{2}z)i\overleftrightarrow{\partial}^+\phi(\frac{1}{2}z)$ has been used, which in forward matrix elements gives the number density of the partons [44].

Other parameterizations of GPDs given in the literature are $\tilde{\mathcal{F}}_\zeta^q(X)$ by Radyushkin [39], and $f_{q/p}(x_1, x_2)$, $f_{g/p}(x_1, x_2)$ by Collins et al. [24]. They are related to the distributions given here by normalization factors that can be found in [39, 35], in addition to using different parameterizations of the momentum fractions. Golec-Biernat and Martin [40] have introduced separate distributions $\hat{\mathcal{F}}_q(X, \zeta)$ and $\hat{\mathcal{F}}_{\bar{q}}(X, \zeta)$, which respectively correspond to Ji's distributions in the regions $x \in [-\xi, 1]$ and $x \in [-1, \xi]$. A different separation into ‘‘quark’’ and ‘‘antiquark’’ GPDs $\mathcal{F}_\zeta^q(X)$ and $\mathcal{F}_\zeta^{\bar{q}}(X)$ has been introduced by Radyushkin on the basis of double distributions and will be briefly explained in Section 3.9. The relation between the different parameterizations is discussed in detail in [40]. We finally remark that in the course of history generalized parton distributions have also been termed ‘‘off-diagonal’’, ‘‘off-forward’’, ‘‘nondiagonal’’, ‘‘nonforward’’, or ‘‘skewed’’ parton distributions.

3.3 Basic properties

3.3.1 Forward limit

For $p = p'$ and equal helicities of the initial and final state hadrons, the matrix elements in (14) and (18) reduce to the ones defining the ordinary spin independent or spin dependent densities $q(x)$, $\Delta q(x)$ for quarks and $g(x)$, $\Delta g(x)$ for gluons. One thus obtains reduction formulas

$$\begin{aligned} H^q(x, 0, 0) &= q(x), & \tilde{H}^q(x, 0, 0) &= \Delta q(x) & \text{for } x > 0, \\ H^q(x, 0, 0) &= -\bar{q}(-x), & \tilde{H}^q(x, 0, 0) &= \Delta\bar{q}(-x) & \text{for } x < 0 \end{aligned} \quad (21)$$

in the quark sector. For gluons one has

$$H^g(x, 0, 0) = xg(x), \quad \tilde{H}^g(x, 0, 0) = x\Delta g(x) \quad \text{for } x > 0 \quad (22)$$

and corresponding relations for $x < 0$ (see Section 3.3.2). The forward limits of the pion GPDs H_π^q and H_π^g are as in (21) and (22).

No corresponding relations exist for the quark or gluon distributions E and \tilde{E} in the nucleon: in their defining equations they are multiplied with factors proportional to Δ and therefore decouple in the forward limit. The information residing in these functions at zero ξ and t can thus not be accessed in processes where parton distributions appear in the cross section via the optical theorem; it is only visible in exclusive processes with a finite momentum transfer to the target. We shall see in Section 3.6 that the forward limit of E^q and E^g carries information about the orbital angular momentum of partons.

In analogy to the forward limit, the distributions H and E are sometimes referred to as ‘‘unpolarized’’ and \tilde{H} and \tilde{E} as ‘‘polarized’’. Note that this refers to the spin of the partons and not of the target. More precisely, H and E correspond to the sum over parton helicities, and \tilde{H} and \tilde{E} to the difference.

3.3.2 Symmetry properties

Because gluons are their own antiparticles the distributions $H^g(x, \xi, t)$ and $E^g(x, \xi, t)$ are even functions of x , and $\tilde{H}^g(x, \xi, t)$ and $\tilde{E}^g(x, \xi, t)$ are odd functions of x . Quark distributions are in general

neither even nor odd in x , and it is often useful to consider the combinations

$$\begin{aligned} H^{q(+)}(x, \xi, t) &= H^q(x, \xi, t) - H^q(-x, \xi, t), \\ \tilde{H}^{q(+)}(x, \xi, t) &= \tilde{H}^q(x, \xi, t) + \tilde{H}^q(-x, \xi, t) \end{aligned} \quad (23)$$

and their analogs for E^q and \tilde{E}^q , which correspond to the exchange of charge conjugation $C = +1$ in the t -channel. They are sometimes referred to as ‘‘singlet’’ combinations (even when not summed over quark flavors). In the forward limit one simply has $H^{q(+)}(x, 0, 0) = q(x) + \bar{q}(x)$ and $\tilde{H}^{q(+)}(x, 0, 0) = \Delta q(x) + \Delta \bar{q}(x)$ for $x > 0$. The ‘‘nonsinglet’’ or ‘‘valence’’ combinations

$$\begin{aligned} H^{q(-)}(x, \xi, t) &= H^q(x, \xi, t) + H^q(-x, \xi, t), \\ \tilde{H}^{q(-)}(x, \xi, t) &= \tilde{H}^q(x, \xi, t) - \tilde{H}^q(-x, \xi, t). \end{aligned} \quad (24)$$

and their counterparts for E^q and \tilde{E}^q correspond to $C = -1$ exchange. In the forward limit one has $H^{q(-)}(x, 0, 0) = q(x) - \bar{q}(x)$ and $\tilde{H}^{q(-)}(x, 0, 0) = \Delta q(x) - \Delta \bar{q}(x)$ for $x > 0$. The combinations (23) and (24) are typically accessible in different processes: the transition from a γ^* to a photon or a vector meson selects for instance the C -even combinations, whereas the transition from a γ^* to a pseudoscalar meson selects the C -odd ones. Furthermore, the combinations (23) and (24) do not mix under evolution. For targets with definite charge conjugation parity like the π^0 the C -odd combinations (24) are zero.

Further symmetry properties follow from time reversal invariance. Inserting VV^{-1} in the matrix elements defining the GPDs, where V is the antiunitary operator implementing time reversal in Hilbert space, one obtains

$$H(x, -\xi, t) = H(x, \xi, t) \quad (25)$$

and analogous relations for E , \tilde{H} , \tilde{E} , both for quark and for gluon distributions. That time reversal changes the sign of ξ is not surprising: interchanging initial and final states of the matrix elements in particular interchanges the momenta p and p' and thus reverses the sign of $\xi = (p - p')^+ / (p + p')^+$. Taking the complex conjugate of the defining matrix elements gives on the other hand

$$\left[H(x, -\xi, t) \right]^* = H(x, \xi, t) \quad (26)$$

and corresponding relations for E , \tilde{H} , \tilde{E} . Together with (25) this implies that the GPDs defined here are real valued functions. For the pion GPDs H_π^q and H_π^g one finds the same relations (25) and (26). Note that in deriving the constraints from time reversal we have used that the hadron states in the distribution are stable. For unstable particles such as the Δ resonance the situation is different (see Section 3.14). The relation (25) is a good example for the usefulness of parameterizing the parton momentum fractions by the symmetric variables x and ξ . In terms of Radyushkin’s variables X and ζ (see Fig. 4) the corresponding symmetry is less explicit.

For pions isospin invariance relates the GPDs for π^+ , π^- and π^0 . In particular, one has for the isosinglet combinations

$$H_{\pi^+}^{u+d} = H_{\pi^-}^{u+d} = H_{\pi^0}^{u+d} \quad (27)$$

and for the isotriplet combinations

$$H_{\pi^+}^{u-d} = -H_{\pi^-}^{u-d}, \quad H_{\pi^0}^{u-d} = 0, \quad (28)$$

where we have introduced the notation $H^{u\pm d} = H^u \pm H^d$. The gluon distributions are of course isosinglet and hence equal for the three pion states. For simplicity we will henceforth reserve the notation H_π for the π^+ . From charge conjugation invariance one has in addition

$$H_\pi^{u+d}(x, \xi, t) = -H_\pi^{u+d}(-x, \xi, t), \quad H_\pi^{u-d}(x, \xi, t) = H_\pi^{u-d}(-x, \xi, t), \quad (29)$$

so that the isosinglet sector corresponds to $C = +1$ and the isotriplet sector to $C = -1$.

3.3.3 Sum rules and polynomiality

Moments in the momentum fraction x play an important role in the theory of GPDs, as they do for the ordinary parton distributions. Integrating the matrix elements (14) or (18) over x gives matrix elements of local quark-antiquark or gluon operators, so that x -integrals of GPDs are related with the form factors of these local currents. In particular one has

$$\begin{aligned} \int_{-1}^1 dx H^q(x, \xi, t) &= F_1^q(t), & \int_{-1}^1 dx E^q(x, \xi, t) &= F_2^q(t), \\ \int_{-1}^1 dx \tilde{H}^q(x, \xi, t) &= g_A^q(t), & \int_{-1}^1 dx \tilde{E}^q(x, \xi, t) &= g_P^q(t), \end{aligned} \quad (30)$$

where the Dirac and Pauli form factors

$$\langle p' | \bar{q}(0) \gamma^\mu q(0) | p \rangle = \bar{u}(p') \left[F_1^q(t) \gamma^\mu + F_2^q(t) \frac{i\sigma^{\mu\alpha} \Delta_\alpha}{2m} \right] u(p), \quad (31)$$

and the axial and pseudoscalar ones,

$$\langle p' | \bar{q}(0) \gamma^\mu \gamma_5 q(0) | p \rangle = \bar{u}(p') \left[g_A^q(t) \gamma^\mu \gamma_5 + g_P^q(t) \frac{\gamma_5 \Delta^\mu}{2m} \right] u(p), \quad (32)$$

are defined for each separate quark flavor. Remarkably, the integrals in (30) are independent of ξ . This is a consequence of Lorentz invariance: integrating the matrix elements (14) over x removes all reference to the particular light-cone direction with respect to which ξ is defined, so that the result must be ξ -independent.

Higher Mellin moments in x lead to derivative operators between the two fields according to the relation

$$\begin{aligned} (P^+)^{n+1} \int dx x^n \int \frac{dz^-}{2\pi} e^{ixP^+z^-} \left[\bar{q}(-\tfrac{1}{2}z) \gamma^+ q(\tfrac{1}{2}z) \right]_{z^+=0, \mathbf{z}=0} \\ = \left(i \frac{d}{dz^-} \right)^n \left[\bar{q}(-\tfrac{1}{2}z) \gamma^+ q(\tfrac{1}{2}z) \right] \Big|_{z=0} = \bar{q}(0) \gamma^+ (i\overleftrightarrow{\partial}^+)^n q(0) \end{aligned} \quad (33)$$

and its analogs for the other operators defining GPDs. In a general gauge, where a Wilson line appears between the operators at positions $-\frac{1}{2}z$ and $\frac{1}{2}z$, one obtains the covariant derivative D instead of ∂ on the right-hand side. Higher x -moments of GPDs thus are form factors of the local twist-two operators

$$\begin{aligned} \mathcal{O}_q^{\mu\mu_1 \dots \mu_n} &= \mathbf{S} \bar{q} \gamma^\mu i\overleftrightarrow{D}^{\mu_1} \dots i\overleftrightarrow{D}^{\mu_n} q, \\ \tilde{\mathcal{O}}_q^{\mu\mu_1 \dots \mu_n} &= \mathbf{S} \bar{q} \gamma^\mu \gamma_5 i\overleftrightarrow{D}^{\mu_1} \dots i\overleftrightarrow{D}^{\mu_n} q, \\ \mathcal{O}_g^{\mu\mu_1 \dots \mu_n \nu} &= \mathbf{S} G^{\mu\alpha} i\overleftrightarrow{D}^{\mu_1} \dots i\overleftrightarrow{D}^{\mu_n} G_\alpha^\nu, \\ \tilde{\mathcal{O}}_g^{\mu\mu_1 \dots \mu_n \nu} &= \mathbf{S} (-i) G^{\mu\alpha} i\overleftrightarrow{D}^{\mu_1} \dots i\overleftrightarrow{D}^{\mu_n} \tilde{G}_\alpha^\nu \end{aligned} \quad (34)$$

familiar from deep inelastic scattering. Here \mathbf{S} denotes symmetrization in all uncontracted Lorentz indices and subtraction of trace terms. A form factor decomposition of \mathcal{O}_q can be written as [35]

$$\begin{aligned} \langle p' | \mathcal{O}_q^{\mu\mu_1 \dots \mu_n}(0) | p \rangle &= \mathbf{S} \bar{u}(p') \gamma^\mu u(p) \sum_{\substack{i=0 \\ \text{even}}}^n A_{n+1,i}^q(t) \Delta^{\mu_1} \dots \Delta^{\mu_i} P^{\mu_{i+1}} \dots P^{\mu_n} \\ &+ \mathbf{S} \bar{u}(p') \frac{i\sigma^{\mu\alpha} \Delta_\alpha}{2m} u(p) \sum_{\substack{i=0 \\ \text{even}}}^n B_{n+1,i}^q(t) \Delta^{\mu_1} \dots \Delta^{\mu_i} P^{\mu_{i+1}} \dots P^{\mu_n} \\ &+ \mathbf{S} \frac{\Delta^\mu}{m} \bar{u}(p') u(p) \text{mod}(n, 2) C_{n+1}^q(t) \Delta^{\mu_1} \dots \Delta^{\mu_n}, \end{aligned} \quad (35)$$

where $\text{mod}(n, 2)$ is 1 for odd n and 0 for even n . The Mellin moments of the ordinary quark distribution give forward matrix elements and hence reduce to the $A_{n,0}^q(0)$. Due to the Gordon identities $\bar{u}(p')u(p)$ can be traded for the proton vector and tensor currents when multiplied with P^α , so that it only appears as an independent structure in the form of the last line of (35). The vector Δ^α only appears in even powers because of time reversal invariance. According to (33) the x -moments of GPDs involve the $+$ tensor components of the twist-two operators, and using $\Delta^+ = -2\xi P^+$ one finds

$$\begin{aligned} \int_{-1}^1 dx x^n H^q(x, \xi, t) &= \sum_{\substack{i=0 \\ \text{even}}}^n (2\xi)^i A_{n+1,i}^q(t) + \text{mod}(n, 2) (2\xi)^{n+1} C_{n+1}^q(t), \\ \int_{-1}^1 dx x^n E^q(x, \xi, t) &= \sum_{\substack{i=0 \\ \text{even}}}^n (2\xi)^i B_{n+1,i}^q(t) - \text{mod}(n, 2) (2\xi)^{n+1} C_{n+1}^q(t). \end{aligned} \quad (36)$$

This is the remarkable *polynomiality* property of GPDs: the x -integrals of $x^n H^q$ and of $x^n E^q$ are polynomials in ξ of order $n+1$. Like the ξ -independence of the lowest moments (30) this property is a consequence of the Lorentz invariance encoded in the form factor decomposition (35). A particularity is that the terms with the highest power ξ^{n+1} are equal and opposite for the moments of H^q and E^q , so that the x^n moment of the combination $H^q + E^q$ is only a polynomial in ξ of degree n . The contributions to H^q and E^q going with $\xi^{n+1} C_{n+1}^q(t)$ only occur for odd n and thus in the $C = +1$ sector. They lead to the so-called D term in GPDs and will be discussed further in Section 3.9.2. They have no analog for the spin dependent quark distributions, where the relevant form factor decomposition is

$$\begin{aligned} \langle p' | \tilde{\mathcal{O}}_q^{\mu\mu_1 \dots \mu_n}(0) | p \rangle &= \mathbf{S} \bar{u}(p') \gamma^\mu \gamma_5 u(p) \sum_{\substack{i=0 \\ \text{even}}}^n \tilde{A}_{n+1,i}^q(t) \Delta^{\mu_1} \dots \Delta^{\mu_i} P^{\mu_{i+1}} \dots P^{\mu_n} \\ &+ \mathbf{S} \frac{\Delta^\mu}{2m} \bar{u}(p') \gamma_5 u(p) \sum_{\substack{i=0 \\ \text{even}}}^n \tilde{B}_{n+1,i}^q(t) \Delta^{\mu_1} \dots \Delta^{\mu_i} P^{\mu_{i+1}} \dots P^{\mu_n}. \end{aligned} \quad (37)$$

Here time reversal invariance constrains $\bar{u}(p') \gamma_5 u(p)$ to come with odd powers of Δ^α . One then has sum rules

$$\begin{aligned} \int_{-1}^1 dx x^n \tilde{H}^q(x, \xi, t) &= \sum_{\substack{i=0 \\ \text{even}}}^n (2\xi)^i \tilde{A}_{n+1,i}^q(t), \\ \int_{-1}^1 dx x^n \tilde{E}^q(x, \xi, t) &= \sum_{\substack{i=0 \\ \text{even}}}^n (2\xi)^i \tilde{B}_{n+1,i}^q(t), \end{aligned} \quad (38)$$

where the highest power in ξ is n instead of $n+1$. Notice that the moments considered here correspond to integration over the full x range from -1 to 1 . Integrals $\int dx x^{2n+1} H^q$ and $\int dx x^{2n} \tilde{H}^q$ therefore involve the C -even combinations $H^{q(+)}$ and $\tilde{H}^{q(+)}$, whereas integrals $\int dx x^{2n} H^q$ and $\int dx x^{2n+1} \tilde{H}^q$ involve the C -odd combinations $H^{q(-)}$ and $\tilde{H}^{q(-)}$, in accordance with the C parity of the corresponding local operators (34). The same holds of course for E^q and \tilde{E}^q .

For gluon operators the form factor decompositions are analogous, with

$$\begin{aligned} \langle p' | \mathcal{O}_g^{\mu\mu_1 \dots \mu_{n-1}\nu}(0) | p \rangle \\ = \mathbf{S} \bar{u}(p') \gamma^\mu u(p) \sum_{\substack{i=0 \\ \text{even}}}^n A_{n+1,i}^g(t) \Delta^{\mu_1} \dots \Delta^{\mu_i} P^{\mu_{i+1}} \dots P^{\mu_{n-1}} P^\nu \end{aligned}$$

$$\begin{aligned}
& + \mathbf{S} \bar{u}(p') \frac{i\sigma^{\mu\alpha} \Delta_\alpha}{2m} u(p) \sum_{\substack{i=0 \\ \text{even}}}^n B_{n+1,i}^g(t) \Delta^{\mu_1} \dots \Delta^{\mu_i} P^{\mu_{i+1}} \dots P^{\mu_{n-1}} P^\nu \\
& + \mathbf{S} \frac{\Delta^\mu}{m} \bar{u}(p') u(p) \text{mod}(n, 2) C_{n+1}^g(t) \Delta^{\mu_1} \dots \Delta^{\mu_{n-1}} \Delta^\nu
\end{aligned} \tag{39}$$

and

$$\begin{aligned}
& \langle p' | \tilde{\mathcal{O}}_g^{\mu\mu_1 \dots \mu_{n-1} \nu}(0) | p \rangle \\
& = \mathbf{S} \bar{u}(p') \gamma^\mu \gamma_5 u(p) \sum_{\substack{i=0 \\ \text{even}}}^n \tilde{A}_{n+1,i}^g(t) \Delta^{\mu_1} \dots \Delta^{\mu_i} P^{\mu_{i+1}} \dots P^{\mu_{n-1}} P^\nu \\
& + \mathbf{S} \frac{\Delta^\mu}{2m} \bar{u}(p') \gamma_5 u(p) \sum_{\substack{i=0 \\ \text{even}}}^n \tilde{B}_{n+1,i}^g(t) \Delta^{\mu_1} \dots \Delta^{\mu_i} P^{\mu_{i+1}} \dots P^{\mu_{n-1}} P^\nu.
\end{aligned} \tag{40}$$

The corresponding sum rules read

$$\begin{aligned}
\int_0^1 dx x^{n-1} H^g(x, \xi, t) & = \sum_{\substack{i=0 \\ \text{even}}}^n (2\xi)^i A_{n+1,i}^g(t) + \text{mod}(n, 2) (2\xi)^{n+1} C_{n+1}^g(t), \\
\int_0^1 dx x^{n-1} E^g(x, \xi, t) & = \sum_{\substack{i=0 \\ \text{even}}}^n (2\xi)^i B_{n+1,i}^g(t) - \text{mod}(n, 2) (2\xi)^{n+1} C_{n+1}^g(t)
\end{aligned} \tag{41}$$

for odd n and

$$\begin{aligned}
\int_0^1 dx x^{n-1} \tilde{H}^g(x, \xi, t) & = \sum_{\substack{i=0 \\ \text{even}}}^n (2\xi)^i \tilde{A}_{n+1,i}^g(t), \\
\int_0^1 dx x^{n-1} \tilde{E}^g(x, \xi, t) & = \sum_{\substack{i=0 \\ \text{even}}}^n (2\xi)^i \tilde{B}_{n+1,i}^g(t)
\end{aligned} \tag{42}$$

for even n , where we have used the symmetry properties of the gluon distributions in x to restrict the integration to $x \geq 0$. Note the correspondence between the $(n-1)$ st moment of a gluon GPD and the n th moment of a GPD for quarks. In fact the corresponding quark and gluon operators, and hence their form factors, mix under evolution (see Section 3.8).

3.4 Parton interpretation and the light-cone

Let us discuss in more detail how GPDs can be interpreted as quantities giving us information about partons in hadrons. A useful interpretation of parton distributions (ordinary or generalized) is as amplitudes for the scattering of a parton on a proton; this is the basis of the covariant parton model of Landshoff et al. [45]. To be more precise, parton distributions are Green functions integrated over the k^- and \mathbf{k} of the partons (and thus over their off-shellness). This is seen by writing

$$\begin{aligned}
F^q & = \frac{1}{2} \int \frac{dz^-}{2\pi} e^{ixP^+z^-} \langle p' | \bar{q}(-\frac{1}{2}z) \gamma^+ q(\frac{1}{2}z) | p \rangle \Big|_{z^+=0, \mathbf{z}=0} \\
& = \frac{1}{2} \int \frac{dk^- d^2\mathbf{k}}{(2\pi)^4} \left[\int d^4z e^{i(kz)} \langle p' | \bar{q}(-\frac{1}{2}z) \gamma^+ q(\frac{1}{2}z) | p \rangle \right]_{k^+=xP^+} \\
& = \frac{1}{2} \int \frac{dk^- d^2\mathbf{k}}{(2\pi)^4} \left[\int d^4z e^{i(kz)} \langle p' | T \bar{q}(-\frac{1}{2}z) \gamma^+ q(\frac{1}{2}z) | p \rangle \right]_{k^+=xP^+}
\end{aligned} \tag{43}$$

and the analogous relations for \tilde{F}^q and the gluon distributions. The expression in square brackets in the last line is a Green function $G(p, p', k)$ with on-shell hadrons and off-shell partons. In going from the second to the third line of (43) we have used that the time ordering of operators may be omitted under the integral over k^- . The key ingredient to show this is to locate the singularities of $G(p, p', k)$ in the complex k^- plane according to the general analyticity properties of Green functions. By complex contour deformation one can then replace the k^- integral of $G(p, p', k)$ by the integral of its discontinuity in appropriate external invariants. The resulting cut Green functions are associated with operators that are not time ordered but only normal ordered, as in the second line of (43). For ordinary parton densities this argument was already given in the original work of Landshoff et al. [45]. The situation for nonforward kinematics was discussed in [46, 39] and studied in detail in [47]. A different line of argument was pursued by Jaffe [48] and also applied to higher-twist parton distributions.

The cut Green functions require on-shell intermediate states, and this requirement gives the support of GPDs as $|x| \leq 1$. In physical terms, no parton in a hadron can have a larger plus-momentum than the hadron itself since this would force other partons to have negative plus-momentum, which an on-shell particle cannot have. We remark that the above argument assumes that Green functions with colored external lines have the same analyticity properties as Green functions in perturbation theory, although the “on-shell states” across a cut are colored and hence not part of the physical spectrum.

To obtain this simple interpretation of parton distributions in terms of four-point functions one must take the light-cone gauge $A^+ = 0$, otherwise there is a Wilson line with additional A^+ gluons between the two parton fields. We will therefore adopt this gauge in the rest of this section. There has recently been work pointing out subtle issues of this gauge in connection with parton densities, and we will comment on this in Section 3.11.5.

An alternative to the covariant representation (43) involves partons on their mass shell, which is in particular helpful if we want to assign helicities to them. This can be achieved in a noncovariant framework of light-cone quantization, whose essentials for our context we shall now briefly recall. More detail can be found in the original work by Kogut and Soper [49] or in the reviews [50, 51]. A discussion with focus on spin has been given by Jaffe [52]. In light-cone quantization, the canonical (anti)commutation relations defining the quantum theory are imposed not at a given time, but at a given light-cone time z^+ , which we choose to be $z^+ = 0$. If one introduces projection operators $P_{\pm} = \frac{1}{2}\gamma^{\mp}\gamma^{\pm}$ for Dirac fields and projects the Dirac equation on its P_- component, one obtains

$$i\partial^+ q_-(z) = -\frac{1}{2}\gamma^+(i\not{D}_T - m)q_+(z). \quad (44)$$

with $q_- = P_- q$ and $q_+ = P_+ q$. This equation does not involve derivatives with respect to light-cone time z^+ (remember that $\partial^+ = \partial/(\partial z^-)$). The “bad” field components q_- are therefore dynamically dependent on the “good” components q_+ , and can be eliminated by solving the differential equation (44). Canonical anticommutation relations for free fields are then imposed on the dynamically independent field q_+ at $z^+ = 0$, which can be Fourier decomposed into

$$q_+(z)\Big|_{z^+=0} = \int \frac{d^2\mathbf{k} dk^+}{16\pi^3 k^+} \theta(k^+) \sum_{\mu} \left[b(k^+, \mathbf{k}, \mu) u_+(k^+, \mu) e^{-i(kz)} + d^\dagger(k^+, \mathbf{k}, \mu) v_+(k^+, \mu) e^{i(kz)} \right]_{z^+=0}, \quad (45)$$

where $\mu = \pm\frac{1}{2}$ denotes the light-cone helicity of the parton. (For better legibility we omit color indices throughout.) Light-cone helicity will be discussed in Section 3.5.1; for the moment it is sufficient to know that it is identical to usual helicity for massless particles, and approximately the same if particles

move fast in the positive z -direction. Notice that the good components of the corresponding spinors $u_+ = P_+ u$ and $v_+ = P_+ v$ are independent on \mathbf{k} (this can be easily seen from the matrix representation of the projector P_+ and the explicit spinors in Appendix B). An important consequence is that we can associate a definite light-cone helicity to the partons described by GPDs, which are integrated over \mathbf{k} rather than referring to a particular transverse parton momentum.

For gluons the steps are analogous. One component of the Yang-Mills equations (in $A^+ = 0$ gauge) does not involve derivatives $\partial/(\partial z^+)$ and can be used to eliminate the “bad” component A^- as dynamically dependent. Free-field commutation relations are then imposed on the “good” transverse components of A^μ at $z^+ = 0$, whose Fourier decomposition reads

$$A^i(z)\Big|_{z^+=0} = \int \frac{d^2\mathbf{k} dk^+}{16\pi^3 k^+} \theta(k^+) \sum_{\mu} \left[a(k^+, \mathbf{k}, \mu) \epsilon^i(\mu) e^{-i(kz)} + a^\dagger(k^+, \mathbf{k}, \mu) \epsilon^{i*}(\mu) e^{i(kz)} \right]_{z^+=0}, \quad (46)$$

where $i = 1, 2$ is a transverse index, and the polarization vectors for states with definite light-cone helicity $\mu = \pm 1$ are given by

$$\epsilon(+)= -\frac{1}{\sqrt{2}} \begin{pmatrix} 1 \\ i \end{pmatrix}, \quad \epsilon(-)= \frac{1}{\sqrt{2}} \begin{pmatrix} 1 \\ -i \end{pmatrix}. \quad (47)$$

The operators b , d and a respectively annihilate quarks, antiquarks and gluons, and (anti)commute with the creation operators b^\dagger , d^\dagger and a^\dagger , as do the operators describing free particles. Notice that the good components of quark and gluon fields behave as free *only* at light-cone time $z^+ = 0$, which is just where these operators enter the definition of parton distributions. This reflects the physics of the parton model, where partons are treated as free just during the short time where they are “seen” by a probe like a highly virtual photon in a hard process. Notice also that the parton states obtained by acting with b^\dagger , d^\dagger and a^\dagger on the vacuum are defined with reference to the time of this hard interaction, and not with reference to the far past or far future. In this sense we do not use that partons correspond to observable particles, which of course they are not because of confinement. Let us add that light-cone quantization involves subtle issues well beyond the scope of this review. Among these is the problem of modes with zero plus-momentum (“zero modes”) and their relevance in the physical vacuum; for a discussion we refer to [53].

We now have the ingredients necessary to take a closer look at the operators defining GPDs. As an example we take the operator

$$\begin{aligned} & \int \frac{dz^-}{2\pi} e^{ixP^+z^-} \frac{1}{4} \bar{q}(-\frac{1}{2}z) \gamma^+(1 + \gamma_5) q(\frac{1}{2}z) \Big|_{z^+=0, \mathbf{z}=0} \\ &= \int \frac{d^2\mathbf{k} dk^+}{16\pi^3 k^+} \theta(k^+) \int \frac{d^2\mathbf{k}' dk'^+}{16\pi^3 k'^+} \theta(k'^+) \frac{\sqrt{k^+ k'^+}}{P^+} \\ & \quad \left\{ \delta\left(x - \frac{k^+ + k'^+}{2P^+}\right) b^\dagger(k'^+, \mathbf{k}', +) b(k^+, \mathbf{k}, +) \right. \\ & \quad + \delta\left(x + \frac{k^+ + k'^+}{2P^+}\right) d(k'^+, \mathbf{k}', -) d^\dagger(k^+, \mathbf{k}, -) \\ & \quad - \delta\left(x - \frac{k^+ - k'^+}{2P^+}\right) d(k'^+, \mathbf{k}', -) b(k^+, \mathbf{k}, +) \\ & \quad \left. - \delta\left(x + \frac{k^+ - k'^+}{2P^+}\right) b^\dagger(k'^+, \mathbf{k}', +) d^\dagger(k^+, \mathbf{k}, -) \right\}. \quad (48) \end{aligned}$$

For better legibility we will henceforth give fermion helicities as \pm instead of $\pm\frac{1}{2}$ when they just appear as labels. In matrix elements of the operator (48) between hadron states, momentum conservation fixes $(k - k')^+$ and $\mathbf{k} - \mathbf{k}'$ in the terms with $b^\dagger b$ and $d d^\dagger$, whereas in the terms with db and $b^\dagger d^\dagger$ it fixes $(k + k')^+$ and $\mathbf{k} + \mathbf{k}'$. The parton plus-momenta are hence completely fixed, whereas one still has to integrate over their overall transverse momentum \mathbf{k} . Compared with the representation (43) of the covariant parton model there is however no longer an integration over k^- , because we have expressed the operators defining parton distributions in terms of creation and annihilation operators for *on-shell* partons. Which term of the decomposition (48) contributes in a matrix element is determined by the fraction x , the constraint of positive parton plus-momenta k^+ and k'^+ , and the constraint from momentum conservation. We thus find the different partonic regimes discussed in Section 3.2. For $\xi > 0$ the combination $b^\dagger d^\dagger$ does not appear; it replaces db in the case $\xi < 0$.

Looking at the helicity structure we observe the correspondence of right-helicity quarks and left-helicity antiquarks. In particular, this ensures that the net *transfer* of helicity is always zero, either by emitting a parton and reabsorbing it with the same helicity, or by emitting (or absorbing) a pair of partons with opposite helicities. The formula for the operator $\frac{1}{4}\bar{q}\gamma^+(1 - \gamma_5)q$ is analogous, with all fermion helicities reversed. We also observe that the operator in (48) is invariant under rotations around the z axis and thus carries no angular momentum component J^3 .

The normalization of the operator in (48) is such that taking the forward matrix element with a proton state we obtain the density of positive-helicity quarks $\frac{1}{2}[q(x) + \Delta q(x)]$ for $x > 0$. The operators in (48) should be read as normal ordered, and bringing the combination $d d^\dagger$ in the second term into the form $d^\dagger d$ appropriate for a counting operator one obtains a minus sign. The density of positive-helicity quarks thus goes with the operator $\frac{1}{4}\bar{q}\gamma^+(1 + \gamma_5)q$, and the density for positive-helicity antiquarks with $-\frac{1}{4}\bar{q}\gamma^+(1 - \gamma_5)q$.

For gluon operators we have in analogy to (48)

$$\begin{aligned}
& \frac{1}{P^+} \int \frac{dz^-}{2\pi} e^{ixP^+z^-} \frac{1}{2} \left[G^{+\mu}(-\frac{1}{2}z) G_\mu^+(\frac{1}{2}z) - iG^{+\mu}(-\frac{1}{2}z) \tilde{G}_\mu^+(\frac{1}{2}z) \right]_{z^+=0, \mathbf{z}=0} \\
&= \int \frac{d^2\mathbf{k} dk^+}{16\pi^3 k^+} \theta(k^+) \int \frac{d^2\mathbf{k}' dk'^+}{16\pi^3 k'^+} \theta(k'^+) \frac{k^+ k'^+}{(P^+)^2} \\
& \quad \left\{ \delta\left(x - \frac{k^+ + k'^+}{2P^+}\right) a^\dagger(k'^+, \mathbf{k}', +) a(k^+, \mathbf{k}, +) \right. \\
& \quad + \delta\left(x + \frac{k^+ + k'^+}{2P^+}\right) a(k'^+, \mathbf{k}', -) a^\dagger(k^+, \mathbf{k}, -) \\
& \quad + \delta\left(x - \frac{k^+ - k'^+}{2P^+}\right) a(k'^+, \mathbf{k}', -) a(k^+, \mathbf{k}, +) \\
& \quad \left. + \delta\left(x + \frac{k^+ - k'^+}{2P^+}\right) a^\dagger(k'^+, \mathbf{k}', +) a^\dagger(k^+, \mathbf{k}, -) \right\}. \tag{49}
\end{aligned}$$

Notice that because $G^{\mu\nu}$ and $\tilde{G}^{\mu\nu}$ are antisymmetric tensors, only transverse indices $\mu = 1, 2$ contribute in the operators on the left-hand side. Since in light-cone gauge one has $G^{+\mu} = \partial^+ A^\mu$ we see that only good field components appear in the operators. This is characteristic of both quark and gluon distributions of twist two. Comparing (48) and (49) we notice an extra factor of $\sqrt{k^+ k'^+}/P^+$ for gluons. The forward matrix element of (49) is therefore given by $\frac{1}{2}[xg(x) + x\Delta g(x)]$ for $x > 0$, with an extra factor of x compared to the quark case.

3.5 Helicity structure

Let us now take a closer look at the spin structure of GPDs for a spin $\frac{1}{2}$ target. The structure for spin 0 targets is much simpler and will be briefly discussed at the end of Section 3.5.4. Spin 1 targets and transitions between hadron states with different spin will be discussed in Sections 3.14 and 3.15.

3.5.1 Lorentz symmetry on the light-cone

Parton distributions probe hadron structure with respect to a light-like direction, which is physically singled out by the hard probe in a process where the distributions appear, and technically reflected in the light-like separation of the operators in their definitions (14) and (18). An essential feature of GPDs is that the hadron states are not both “aligned” along this axis, so that there is a nontrivial choice to be made in defining their helicities. As a guide to our choice we will first discuss an important symmetry of light-cone physics.

We have already seen the special role played by plus-momentum in the definition of GPDs. The Lorentz transformations which leave plus-momenta invariant are rotations around the z -axis and the so-called *transverse boosts*, which transform a four-vector k according to

$$k^+ \rightarrow k^+, \quad \mathbf{k} \rightarrow \mathbf{k} - k^+ \mathbf{v}, \quad (50)$$

where \mathbf{v} is a two-dimensional vector parameterizing the transformation. k^- transforms in a more complicated way, ensuring that k^2 remains invariant. Because of Lorentz invariance the GPDs can only depend on the transverse components of p and of p' via the transverse components of the vector

$$D = \frac{p'}{1 - \xi} - \frac{p}{1 + \xi}. \quad (51)$$

Under a transverse boost \mathbf{D} is invariant because by construction $D^+ = 0$. In fact, the invariant t can be written as

$$t = t_0 - (1 - \xi^2) \mathbf{D}^2, \quad (52)$$

where

$$t_0 = -\frac{4\xi^2 m^2}{1 - \xi^2} \quad (53)$$

is the maximum value of t at given ξ . Note that this implies an upper bound $\xi \leq \sqrt{-t} / \sqrt{4m^2 - t}$ on ξ at given t . Only in particular frames is \mathbf{D} proportional to $\mathbf{\Delta}$. Examples are the symmetric case where $\mathbf{p}' = -\mathbf{p} = \frac{1}{2}\mathbf{\Delta}$ so that $\mathbf{D} = (1 - \xi^2)^{-1}\mathbf{\Delta}$, or the case $\mathbf{p} = 0$ where $\mathbf{D} = (1 - \xi)^{-1}\mathbf{\Delta}$.

Given the special role played by transverse boosts it is natural to discuss proton helicity in terms of light-cone helicity states [54, 51]. A light-cone helicity state for a particle with momentum components (k^+, \mathbf{k}) is obtained from the one with momentum components $(k^+, \mathbf{0})$ via the transverse boost specified by $\mathbf{v} = -\mathbf{k}/k^+$. Such states have simple properties under the Lorentz transformations important in light-cone physics. Consider a transformation which changes the momentum k into k' . A state with light-cone helicity λ transforms as $|k, \lambda\rangle \rightarrow |k', \lambda\rangle$ under a longitudinal boost along z and under a transverse boost (50), and as $|k, \lambda\rangle \rightarrow e^{-i\lambda\varphi}|k', \lambda\rangle$ under a rotation by φ around the z -axis. In contrast, the usual helicity state for a particle with (k^+, \mathbf{k}) is obtained from a state with zero transverse momentum by a spatial rotation, and has rather complicated transformation properties under longitudinal and transverse boosts. The distinction between the two types of states is however unimportant for particles having a large positive momentum p^3 , with their difference being of order m/p^+ (and strictly zero if $\mathbf{p} = 0$ and $p^3 > 0$). The situation is hence the same as for light-cone plus-momentum versus usual three-momentum and reflects that the light-cone quantities correspond

to the limit of the infinite-momentum frame. We will henceforth use “helicity” in the sense of “light-cone helicity” unless stated otherwise. The explicit spinors used in our subsequent calculations are given in Appendix B, as well as their relation with usual helicity spinors.

From our discussion it follows that if we consider the matrix elements (14) and (18) for states with definite light-cone helicity, they are invariant under both transverse and longitudinal boosts, and can therefore only depend on the light-cone momentum fractions x and ξ and on \mathbf{D} . For the matrix elements $F_{\lambda'\lambda}$ and $\tilde{F}_{\lambda'\lambda}$ defined in (14) and (18) we explicitly find

$$\begin{aligned}
F_{++} &= F_{--} = \sqrt{1-\xi^2} \left[H - \frac{\xi^2}{1-\xi^2} E \right], \\
\tilde{F}_{++} &= -\tilde{F}_{--} = \sqrt{1-\xi^2} \left[\tilde{H} - \frac{\xi^2}{1-\xi^2} \tilde{E} \right], \\
F_{-+} &= -[F_{+-}]^* = e^{i\varphi} \frac{\sqrt{t_0-t}}{2m} E, \\
\tilde{F}_{-+} &= [\tilde{F}_{+-}]^* = e^{i\varphi} \frac{\sqrt{t_0-t}}{2m} \xi \tilde{E}
\end{aligned} \tag{54}$$

for both quarks and gluons, where the first index λ' refers to the outgoing proton with momentum p' and the second index λ to the incoming proton with momentum p . These relations are of fundamental importance for phenomenology since they specify which GPDs are selected by particular proton helicity transitions. Given the transformation properties of helicity states under rotations about the z axis, the matrix elements (54) depend on \mathbf{D} only via its length $|\mathbf{D}| = \sqrt{t_0-t}/\sqrt{1-\xi^2}$ and a phase factor of the form $e^{in\varphi}$, where the azimuthal angle φ of \mathbf{D} is given by $e^{i\varphi}|\mathbf{D}| = D^1 + iD^2$.

3.5.2 Parton helicity flip

So far we have only discussed quark and gluon operators with total helicity transfer zero, which in the DGLAP regions do not change the helicity of the emitted and reabsorbed parton. There are however twist-two distributions which flip the parton helicity in the DGLAP regions. Both in the DGLAP and ERBL regions they transfer a net helicity of one unit in the case of quarks and of two units in the case of gluons. These distributions are off-diagonal in the parton helicity basis. They become diagonal if one changes basis from eigenstates of helicity to eigenstates of “transversity” [52], which is related to (but not the same as) transverse spin, and are hence also called transversity distributions. They are constructed from the tensor operators

$$\bar{q}\sigma^{+i}q, \quad \frac{1}{2} \left[G^{+i}G^{j+} + G^{+j}G^{i+} \right] - \frac{1}{2} g_T^{ij} G^{+\alpha} G_{\alpha}^+, \quad i, j = 1, 2 \tag{55}$$

with the fields separated by a light-like distance, supplemented by Wilson lines in gauges other than $A^+ = 0$. The Fourier transforms of these non-local operators have representations analogous to (48) and (49). Notice that the operator defining quark transversity is chiral-odd, i.e., it flips quark chirality, in contrast to the chiral-even operators $\bar{q}\gamma^+q$ and $\bar{q}\gamma^+\gamma_5q$.

In a similar manner as for parton helicity conserving GPDs one can define the helicity-flip distributions by a form factor decomposition. Both for quarks and for gluons one has four distributions, given by [55]

$$\begin{aligned}
& \frac{1}{2} \int \frac{dz^-}{2\pi} e^{ixP^+z^-} \langle p' | \bar{q}(-\frac{1}{2}z) i\sigma^{+i} q(\frac{1}{2}z) | p \rangle \Big|_{z^+=0, \mathbf{z}=0} \\
&= \frac{1}{2P^+} \bar{u}(p') \left[H_T^q i\sigma^{+i} + \tilde{H}_T^q \frac{P^+\Delta^i - \Delta^+P^i}{m^2} \right]
\end{aligned}$$

$$\begin{aligned}
& + E_T^g \frac{\gamma^+ \Delta^i - \Delta^+ \gamma^i}{2m} + \tilde{E}_T^g \frac{\gamma^+ P^i - P^+ \gamma^i}{m} \Big] u(p), \\
& \frac{1}{P^+} \int \frac{dz^-}{2\pi} e^{ixP^+z^-} \langle p' | \mathbf{S} G^{+i}(-\frac{1}{2}z) G^{j+}(\frac{1}{2}z) | p \rangle \Big|_{z^+=0, \mathbf{z}=0} \\
& = \mathbf{S} \frac{1}{2P^+} \frac{P^+ \Delta^j - \Delta^+ P^j}{2mP^+} \\
& \quad \times \bar{u}(p') \left[H_T^g i\sigma^{+i} + \tilde{H}_T^g \frac{P^+ \Delta^i - \Delta^+ P^i}{m^2} \right. \\
& \quad \left. + E_T^g \frac{\gamma^+ \Delta^i - \Delta^+ \gamma^i}{2m} + \tilde{E}_T^g \frac{\gamma^+ P^i - P^+ \gamma^i}{m} \right] u(p), \tag{56}
\end{aligned}$$

where \mathbf{S} stands for symmetrization of uncontracted Lorentz indices and removal of the trace (here in the two transverse dimensions). The notation has been chosen to mirror the one in the non-flip sector, but distributions with and without tilde in (56) do *not* correspond to different quantum numbers. The definition for quark distributions can alternatively be expressed in terms of $\sigma^{+\beta}\gamma_5 = -\frac{1}{2}i\epsilon^{+\beta\gamma\delta}\sigma_{\gamma\delta}$ and is given in [55]. Our functions H_T^g and \tilde{H}_T^g respectively coincide with H_G^T and \tilde{E}_G^T defined in [56], and the relation of our convention with the distributions originally introduced by Hoodbhoy and Ji [57] is

$$\begin{aligned}
H_T^g &= H_{Tq}|_{[57]}, & E_T^g &= -E_{Tq}|_{[57]}, \\
\tilde{H}_T^g &= -2xH_{Tg}|_{[57]}, & \tilde{E}_T^g &= -2xE_{Tg}|_{[57]}. \tag{57}
\end{aligned}$$

The existence of the distributions \tilde{H}_T and \tilde{E}_T has been overlooked in the pioneering paper [57] due to a nontrivial error, see the footnote in Section 3.5.4.

For both quarks and gluons, time reversal invariance and hermiticity of the operators give constraints on H_T , \tilde{H}_T and E_T , which read as (25) and (26). For \tilde{E}_T one has

$$\tilde{E}_T(x, \xi, t) = -\tilde{E}_T(x, -\xi, t), \quad \left[\tilde{E}_T(x, \xi, t) \right]^* = -\tilde{E}_T(x, -\xi, t) \tag{58}$$

with extra minus signs, again for both quarks and gluons. The gluon distributions in (56) are even functions of x because gluons are their own antiparticles. Taking Mellin moments in x of the transversity distributions gives form factors of local operators constructed in analogy to (34). Because of polynomiality the lowest moment of \tilde{E}_T^g must be independent of ξ , so that the time reversal constraint in (58) leads to $\int_{-1}^1 dx \tilde{E}_T^g = 0$. In other words, time reversal invariance reduces the number of form factors of the matrix element $\langle p' | \bar{q}(0) \sigma^{\mu\nu} q(0) | p \rangle$ from four to three [55].

An important property of helicity-flip distributions is that they evolve independently in the renormalization scale μ , i.e., quarks do not mix with gluons and vice versa. In particular, gluon transversity probes glue in the target which is “intrinsic” in the sense that it cannot be generated from quarks by the perturbative DGLAP parton splitting processes.

From (58) and the factors of Δ in (56) we immediately see that only the quark GPDs H_T^q can be measured in the forward limit. There they become equal to the quark transversity distributions, usually denoted by $\delta q(x)$ or $h_1(x)$. These distributions have been introduced long ago [58], but so far not much is known experimentally about them. This will hopefully change with the progress of the spin programs at HERMES, COMPASS, and RHIC [59, 60]. Concerning gluons it is clear that the helicity-flip distributions must all decouple in the forward limit for a spin $\frac{1}{2}$ target, since the change of gluon helicity by two units cannot be compensated by the target. For targets with spin

1 or higher, such as a deuteron or a photon, gluon transversity is however visible in forward matrix elements [61, 62].

As we will see in Section 5.1.1, gluon transversity GPDs appear to leading-twist accuracy in DVCS. Prospects of their measurement will be discussed in Sections 6.3 and 7.3. Experimental access to quark transversity GPDs seems much less trivial and will also be discussed in Section 7.3.

3.5.3 Helicity amplitudes and GPDs

We can now give a systematic account of the helicity structure of GPDs in terms of the matrix elements

$$\begin{aligned} A_{\lambda'\mu',\lambda\mu}^q &= \int \frac{dz^-}{2\pi} e^{ixP^+z^-} \langle p', \lambda' | \mathcal{O}_{\mu'\mu}^q(z) | p, \lambda \rangle \Big|_{z^+=0, \mathbf{z}=0}, \\ A_{\lambda'\mu',\lambda\mu}^g &= \frac{1}{P^+} \int \frac{dz^-}{2\pi} e^{ixP^+z^-} \langle p', \lambda' | \mathcal{O}_{\mu'\mu}^g(z) | p, \lambda \rangle \Big|_{z^+=0, \mathbf{z}=0}. \end{aligned} \quad (59)$$

In Table 1 we list the relevant operators $\mathcal{O}_{\mu'\mu}$ for parton transitions in the region $x \in [\xi, 1]$, where the combinations $b^\dagger(\mu')b(\mu)$ or $a^\dagger(\mu')a(\mu)$ are active. The helicity transitions in the other regions of x are easily deduced from the correspondence between outgoing left-helicity partons and incoming right-helicity partons, as we saw in (48) and (49). Note that the ordering of helicity labels in (59) corresponds to Fig. 6a and differs from the conventions for the familiar s -channel helicity amplitudes in elastic scattering (where helicities are defined in the collision c.m.). The matrix elements (59) share important features with helicity amplitudes, in particular they obey constraints

$$A_{-\lambda'-\mu', -\lambda-\mu} = (-1)^{\lambda'-\mu'-\lambda+\mu} [A_{\lambda'\mu',\lambda\mu}]^* \quad (60)$$

from parity invariance. The sign factor on the right-hand side corresponds to our choice of spinors given in Appendix B.

Explicitly we obtain parton helicity conserving matrix elements

$$\begin{aligned} A_{+,+,++} &= \sqrt{1-\xi^2} \left(\frac{H+\tilde{H}}{2} - \frac{\xi^2}{1-\xi^2} \frac{E+\tilde{E}}{2} \right), \\ A_{-+,-,+} &= \sqrt{1-\xi^2} \left(\frac{H-\tilde{H}}{2} - \frac{\xi^2}{1-\xi^2} \frac{E-\tilde{E}}{2} \right), \end{aligned}$$

Table 1: Operators $\mathcal{O}_{\mu'\mu}^q$ and $\mathcal{O}_{\mu'\mu}^g$ for leading-twist GPDs, and the parton helicity transitions they describe in the region $x \in [\xi, 1]$. It is implied that the first field is taken at $-\frac{1}{2}z$ and the second at $\frac{1}{2}z$. The label μ refers to the emitted parton and μ' to the reabsorbed one.

$\mathcal{O}_{\mu'\mu}^q$	operator		helicities	
	$\mathcal{O}_{\mu'\mu}^g$		μ'	μ
$\frac{1}{4}\bar{q}\gamma^+(1+\gamma_5)q$	$\frac{1}{2}[G^{+\alpha}G_\alpha^+ - iG^{+\alpha}\tilde{G}_\alpha^+]$		+	+
$\frac{1}{4}\bar{q}\gamma^+(1-\gamma_5)q$	$\frac{1}{2}[G^{+\alpha}G_\alpha^+ + iG^{+\alpha}\tilde{G}_\alpha^+]$		-	-
$-\frac{1}{4}i\bar{q}(\sigma^{+1}-i\sigma^{+2})q$	$\frac{1}{2}[G^{+1}G^{1+} - G^{+2}G^{2+} - iG^{+1}G^{2+} - iG^{+2}G^{1+}]$		-	+
$\frac{1}{4}i\bar{q}(\sigma^{+1}+i\sigma^{+2})q$	$\frac{1}{2}[G^{+1}G^{1+} - G^{+2}G^{2+} + iG^{+1}G^{2+} + iG^{+2}G^{1+}]$		+	-

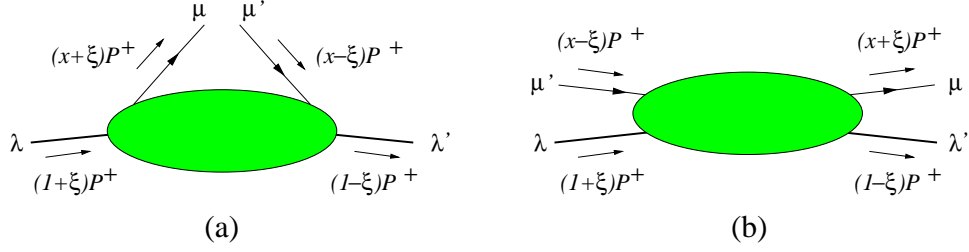


Figure 6: Representation of a generalized parton distribution in the region $x \in [\xi, 1]$. The flow of plus-momentum is indicated by arrows, and the labels $\lambda, \lambda', \mu, \mu'$ denote helicities. (a) shows the ordering of lines as “proton in, quark out, quark back in, proton out” that is common for parton distributions. (b) displays the order “proton in, quark in, quark out, proton out” appropriate for a scattering amplitude.

$$\begin{aligned}
A_{++,--} &= -e^{-i\varphi} \frac{\sqrt{t_0-t}}{2m} \frac{E-\xi\tilde{E}}{2}, \\
A_{-+,++} &= e^{i\varphi} \frac{\sqrt{t_0-t}}{2m} \frac{E+\xi\tilde{E}}{2},
\end{aligned} \tag{61}$$

for both quarks and gluons, where φ is the azimuthal angle of the vector D as before. In the parton helicity flip sector we have [55]

$$\begin{aligned}
A_{++,-+}^q &= e^{i\varphi} \frac{\sqrt{t_0-t}}{2m} \left(\tilde{H}_T^q + (1-\xi) \frac{E_T^q + \tilde{E}_T^q}{2} \right), \\
A_{-+,-}^q &= e^{i\varphi} \frac{\sqrt{t_0-t}}{2m} \left(\tilde{H}_T^q + (1+\xi) \frac{E_T^q - \tilde{E}_T^q}{2} \right), \\
A_{++,-}^q &= \sqrt{1-\xi^2} \left(H_T^q + \frac{t_0-t}{4m^2} \tilde{H}_T^q - \frac{\xi^2}{1-\xi^2} E_T^q + \frac{\xi}{1-\xi^2} \tilde{E}_T^q \right), \\
A_{-+,-}^q &= -e^{2i\varphi} \sqrt{1-\xi^2} \frac{t_0-t}{4m^2} \tilde{H}_T^q
\end{aligned} \tag{62}$$

for quarks, and analogous expressions with an additional global factor $e^{i\varphi} \sqrt{1-\xi^2} \sqrt{t_0-t}/(2m)$ on the right-hand side for gluons.

An essential feature of GPDs is that they can mediate transitions where overall helicity is not conserved. This is because angular momentum along the z axis is not given by the helicities alone, but also receives an orbital contribution as soon as there is a transfer of transverse momentum between the hadrons. That the helicity mismatch is compensated by orbital angular momentum is in fact signaled by the prefactors $\sqrt{t_0-t}^{|\lambda'-\mu'-\lambda+\mu|}$ in the above matrix elements, where each factor of $\sqrt{t_0-t} \propto |\mathbf{D}|$ corresponds to one unit of angular momentum along z . This observation makes it clear why GPDs are sensitive to orbital angular momentum, which we will see again in Sections 3.6 and 3.11.2.

3.5.4 Counting GPDs

The connection between GPDs and helicity amplitudes offers a convenient method to determine the number of independent GPDs for targets with arbitrary spin. The method is well-known for the usual parton distributions [52], but must be modified in the nonforward case [55]. Taking the proton GPDs as an example, we start with $2^4 = 16$ helicity amplitudes for quark-proton scattering, and an equal

number for gluon-proton scattering. The parity constraints (60) relate amplitudes pairwise, which for each parton species brings us to 8 independent amplitudes parameterized by eight GPDs. One easily sees that 4 of them flip parton helicity and 4 do not. It is important to realize that, whereas time reversal invariance provides two further constraints for ordinary s -channel helicity amplitudes, it does *not* further reduce the number of GPDs.¹ The reason for this difference is that s -channel helicity amplitudes kinematically depend on Lorentz invariants s and t , which do not change under time reversal. In contrast, the helicity matrix elements (59) refer to a particular light-cone direction, given by the vector n_- in the definition (15), and depend on light-cone fractions x and ξ . Time reversal changes the sign of ξ as seen in (25) and hence constrains GPDs to be even or odd in ξ . Together with the hermiticity constraints (26) this fixes the phase of GPDs, but does not set any of them to zero. This happens only in the case $\xi = 0$ (which still allows for nonzero t). From (61) and (62) together with (58) and (60) we see that for vanishing ξ one has indeed the time reversal constraints $A_{+,+,-}^q = -[A_{-+,++}^q]^*$ and $A_{+,+,-}^g = -[A_{+,-,++}^g]^*$ familiar for s -channel helicity amplitudes.

The general “counting rules” for GPDs are then (i) to determine the total number of helicity transitions for a given parton species and given hadron states, and then (ii) to eliminate those transitions which are dependent due to the parity constraints (60). This counting can be done separately for parton helicity conserving or changing transitions. Time reversal invariance results in certain properties of the GPDs but does not further reduce their number. The same holds for charge conjugation invariance for hadrons of definite charge parity like neutral pions: the x dependence of the GPDs then corresponds to $C = +1$ exchange in the t -channel as discussed in Section 3.3.2.

Applying these rules to spin-zero targets we find that for each parton species there is one parton helicity conserving GPD, given in (20), and one parton helicity flip GPD, defined from the tensor operators (55). For a spin-zero target both quark and gluon helicity flip GPDs decouple of course in the forward limit.

The counting for the *form factors* of the local twist-two matrix elements associated with GPDs is yet different. A general method has been constructed by Ji and Lebed and applied to the nucleon [63]. Instead of parity and time reversal invariance for matrix elements $\langle p' | \mathcal{O} | p \rangle$ the authors used parity and charge conjugation invariance for the matrix elements $\langle \bar{p} p | \mathcal{O} | 0 \rangle$ in the crossed channel. Because of overall CPT invariance, the two types of constraints are equivalent and lead to the same structure for the allowed form factor decompositions. We note that the explicit results for the number of form factors given in [63] hold for the parity-even operators $\mathcal{O}_q^{\mu\mu_1\dots\mu_n}$ and $\mathcal{O}_g^{\mu\mu_1\dots\mu_n\nu}$ in (34) and have to be appropriately modified for the other twist-two operators.

3.6 The energy-momentum tensor and the spin of the nucleon

A fundamental question about nucleon structure is how its total spin is made up from quarks and gluons. The polarized quark densities measurable in DIS specify the distribution of quark spins aligned or antialigned with the spin of the nucleon. Evaluating their lowest moments $\int dx [\Delta q(x) + \Delta \bar{q}(x)]$ and summing over flavors one finds that the fraction of the total proton spin carried by quarks and antiquarks is moderate, not more than 30% to 50% depending on the renormalization scheme defining the quark distributions, see e.g. [64, 65]. The corresponding contribution $\int dx \Delta g(x)$ from the gluon helicity is presently not well constrained by measurements. An important contribution of the proton spin may however be due to the orbital angular momentum of partons, as proposed long ago by Sehgal [66]. That the parton splitting processes $q \rightarrow qg$ and $g \rightarrow q\bar{q}$ responsible for the DGLAP evolution of parton densities generate orbital angular momentum was observed by Ratcliffe [67].

The possibility to access orbital angular momentum through GPDs has been realized by Ji [20].

¹This was incorrectly assumed in [57], whose authors looked for 6 independent GPDs and thus missed \tilde{H}_T and \tilde{E}_T .

Starting point of the argument is the Belinfante improved energy-momentum tensor

$$T^{\mu\nu} = \sum_{i=q,g} T_i^{\mu\nu} \quad (63)$$

with individual quark and gluon contributions

$$T_q^{\mu\nu} = \bar{q}\gamma^{(\mu}i\overleftrightarrow{D}^{\nu)}q, \quad T_g^{\mu\nu} = G^{\mu\alpha}G_{\alpha}{}^{\nu} + \frac{1}{4}g^{\mu\nu}G^{\alpha\beta}G_{\alpha\beta}, \quad (64)$$

where $t^{(\mu\nu)} = \frac{1}{2}(t^{\mu\nu} + t^{\nu\mu})$ denotes symmetrization for any tensor. The angular momentum density is given by

$$M^{\alpha\mu\nu} = T^{\alpha\nu}x^{\mu} - T^{\alpha\mu}x^{\nu}, \quad (65)$$

and the operator for angular momentum along the z direction by

$$\int d^3x M^{012}(x), \quad (66)$$

with analogous expressions for the individual quark and gluon contributions. Let us consider the expectation values $\langle J_q^3 \rangle$ and $\langle J_g^3 \rangle$ of the operator (66) for a proton state at rest with spin along the positive z axis. Ji has shown [68] that one obtains identical expectation values if the proton moves along the positive or negative z direction, and also if instead of (66) one takes the light-cone helicity operator

$$J^3 = \int dx^- d^2\mathbf{x} M^{+12}(x), \quad (67)$$

which naturally arises in the context of light-cone quantization [49] and hence of the parton interpretation presented in Section 3.4. The quark and gluon parts of the energy-momentum tensor can be decomposed on form factors as

$$\begin{aligned} \langle p' | T_{q,g}^{\mu\nu} | p \rangle &= A_{q,g}(t) \bar{u} P^{(\mu} \gamma^{\nu)} u + B_{q,g}(t) \bar{u} \frac{P^{(\mu} i\sigma^{\nu)\alpha} \Delta_{\alpha}}{2m} u \\ &+ C_{q,g}(t) \frac{\Delta^{\mu} \Delta^{\nu} - g^{\mu\nu} \Delta^2}{m} \bar{u} u + \bar{C}_{q,g}(t) m g^{\mu\nu} \bar{u} u, \end{aligned} \quad (68)$$

where for legibility we have omitted the momentum labels in the spinors \bar{u} and u for the outgoing and incoming proton. A , B and C coincide with the form factors $A_{2,0}$, $B_{2,0}$ and C_2 introduced in (35) for quarks and in (39) for gluons. The angular momentum carried by each parton species is found to be

$$\langle J_q^3 \rangle = \frac{1}{2}[A_q(0) + B_q(0)], \quad \langle J_g^3 \rangle = \frac{1}{2}[A_g(0) + B_g(0)], \quad (69)$$

and can be represented in terms of the moments of GPDs according to our discussion in Section 3.3.3 since

$$\begin{aligned} A_q(t) + B_q(t) &= \int_{-1}^1 dx x [H_q(x, \xi, t) + E_q(x, \xi, t)], \\ A_g(t) + B_g(t) &= \int_0^1 dx [H_g(x, \xi, t) + E_g(x, \xi, t)]. \end{aligned} \quad (70)$$

The combination of (69) and (70) is often referred to as Ji's sum rules [20]. Notice their similarity to the momentum sum rules

$$\begin{aligned} \langle P_q^+ \rangle &= A_q(0) = \int_0^1 dx x [q(x) + \bar{q}(x)], \\ \langle P_g^+ \rangle &= A_g(0) = \int_0^1 dx x g(x) \end{aligned} \quad (71)$$

where $P_{q,g}^+ = \int dx^- d^2 \mathbf{x} T_{q,g}^{++}$ is the plus-momentum operator. Evaluating Ji's sum rules from data is highly demanding: it requires knowledge of GPDs as functions of x at fixed ξ and t , including the separation of the spin combinations H and E , and of individual parton species. These sum rules are however the only known way to experimentally access the total angular momentum carried by quarks or by gluons in the nucleon.

Several further remarks on Ji's sum rules can be made.

- The individual contributions $\langle J_q^3 \rangle$, $\langle J_g^3 \rangle$ depend on the scale μ at which the operators are renormalized, i.e., on the scale at which quarks and gluons are resolved. Their evolution is exactly as the one for the momentum fractions $\langle P_q^+ \rangle$, $\langle P_g^+ \rangle$, since the A and B form factors belong to the same operator. In particular one asymptotically has

$$\langle J_q^3 \rangle : \langle J_g^3 \rangle = \langle P_q^+ \rangle : \langle P_g^+ \rangle = 3 : 16 \quad \text{as } \mu \rightarrow \infty \quad (72)$$

for any single quark flavor q . At asymptotic scale the partition of angular momentum between quarks and gluons hence becomes the same as the partition of plus-momentum.

- The sum rules for the total spin and momentum of the proton,

$$\sum_q \langle P_q^+ \rangle + \langle P_g^+ \rangle = 1, \quad \sum_q \langle J_q^3 \rangle + \langle J_g^3 \rangle = \frac{1}{2}, \quad (73)$$

imply together with (69) and (71) that

$$\sum_q B_q(0) + B_g(0) = \sum_q \int_{-1}^1 dx x E^q(x, 0, 0) + \int_0^1 dx E^g(x, 0, 0) = 0 \quad (74)$$

at any renormalization scale. Brodsky et al. [69] have derived the same result using the wave function representation of form factors discussed in Section 3.11. Explicitly calculating the B form factors for an electron to one-loop accuracy in QED (with electrons and photons taking the roles of quarks and gluons) they confirmed the sum rule (74). Furthermore, they found that $\sum_q B_q(t) + B_g(t)$ at finite t was nonzero, as well as the individual contributions from quarks and gluons at $t = 0$. Nonzero values of $\sum_q B_q(0)$ and $B_g(0)$ are hence not in conflict with general symmetries, contrary to a claim made in [70]. Only at asymptotically large μ must $B_q(0)$ and $B_g(0)$ evolve to zero according to (72).

We note on the other hand that recent calculations in lattice QCD [71, 72] obtain small values for the flavor summed combination $B_u(t) + B_d(t)$, due to large cancellations between $B_u(t)$ and $B_d(t)$. Such a behavior is also predicted in the large- N_c limit of QCD (see Section 4.1.2).

- An explicit decomposition $\langle J_q \rangle = \langle S_q \rangle + \langle L_q \rangle$ into spin and orbital angular momentum has been given by Ji [20, 35], with

$$S_q^3 = \frac{1}{2} \int d^3 x q^\dagger \sigma^{12} q, \quad L_q^3 = - \int d^3 x q^\dagger (x^1 i D^2 - x^2 i D^1) q. \quad (75)$$

For the spin part one finds $\langle S_q^3 \rangle = \frac{1}{2} \int dx [\Delta q(x) + \Delta \bar{q}(x)]$ as expected. For gluons there is no gauge invariant separation into spin and orbital angular momentum operators, and Ji and collaborators [20, 73] have proposed to *define* the orbital angular momentum part as $\langle L_g^3 \rangle = \langle J_g^3 \rangle - \int dx \Delta g(x)$, assuming the usual interpretation of $\int dx \Delta g(x)$ as the total helicity carried by gluons in the proton.

We note that there is a controversy in the literature concerning the question whether a decomposition of angular momentum operators needs to be gauge invariant in the context of a parton

interpretation, and that there is a decomposition of J^3 into separate spin and orbital contributions for both quarks and gluons, going back to Jaffe and Manohar [74]. For the arguments of the different sides we refer to [75, 73] and [76].

- Using QCD sum rules, Balitsky and Ji estimated $\langle J_g^3 \rangle \approx 0.25$ at $\mu = 1$ GeV for the gluon angular momentum in the proton [77]. Barone et al. obtained $\langle J_g^3 \rangle \approx 0.24$ at $\mu = 0.5$ GeV in a quark model [78]. The quark angular momentum $\langle J_q^3 \rangle$ in the proton has been studied in lattice QCD by several groups [79, 80, 71, 72]. Comparing with lattice results for the contribution $\langle S_q^3 \rangle$ from quark helicity, one gets information about the orbital part $\langle L_q^3 \rangle$. Whereas an early study by Mathur et al. [79] suggests a substantial contribution from quark orbital angular momentum, recent results by Gökeler et al. [71] and Hägler et al. [72] find its contribution to be very small when summing over flavors. To settle this issue will require better control over systematic errors in the lattice calculations.
- The axial anomaly of QCD leads to notorious problems in separating quark and gluon helicity beyond leading order in α_s . Bass [81] has pointed out that these problems are yet more subtle in nonforward matrix elements, and that nonforward analogs of the AB and JET schemes for spin dependent parton densities cannot be defined in a gauge invariant way. On the other hand, the operators and matrix elements for the total angular momentum components J_q^3 and J_g^3 are *not* affected by the problems related with the axial anomaly, since they involve the parity-even operators $T_q^{\alpha\beta}$ and $T_g^{\alpha\beta}$. This implies that anomaly related ambiguities in renormalizing $\langle S_q^3 \rangle$ must be compensated by corresponding ambiguities in renormalizing $\langle L_q^3 \rangle$, so that they cancel in the sum $\langle J_q^3 \rangle$.
- As mentioned above the matrix elements $\langle J_{q,g}^3 \rangle$ can be understood as the expectation values of the light-cone helicity (67) carried by quarks and gluons in a fast moving proton. Polyakov and Shuvaev [82, 83] have elaborated on interpreting the same quantities as the usual orbital angular momentum (66) in a proton at rest, using the same framework that leads to the interpretation of the Sachs form factors G_E and G_M at $t = 0$ as the electric charge and magnetic moment of the nucleon [84]. In this framework one can in addition relate the form factors $C_{q,g}$ at $t = 0$ with the traceless part of the three-dimensional stress tensor $T_{q,g}^{ij}$ and thus to shear forces experienced by quarks and gluons in a hadron [82, 83]. Representations of the form factors $A_{q,g}$, $B_{q,g}$, $C_{q,g}$ at nonzero t have also been given in [83]. It is not obvious whether a light-cone equivalent can be found to illuminate the physical meaning of the form factors $C_{q,g}(t)$.

3.7 Generalized distribution amplitudes

Let us now investigate generalized distribution amplitudes, which are the crossed-channel analogs of GPDs [10, 29]. GDAs parameterize the matrix elements of the same light-cone operators as GPDs, but not between two different hadron states, but between the vacuum and a system of hadrons. Much of the literature has focused on pion pairs, which have a simpler spin structure than for instance the $p\bar{p}$ system. The quark and gluon GDAs for the $\pi^+\pi^-$ system are defined as [85]

$$\begin{aligned}
\Phi^q(z, \zeta, s) &= \int \frac{dx^-}{2\pi} e^{i(2z-1)(p+p')^+x^-/2} \\
&\quad \times \text{out} \langle \pi^+(p)\pi^-(p') | \bar{q}(-\frac{1}{2}x) \gamma^+ q(\frac{1}{2}x) | 0 \rangle \Big|_{x^+=0, \mathbf{x}=0}, \\
\Phi^g(z, \zeta, s) &= \frac{1}{(p+p')^+} \int \frac{dx^-}{2\pi} e^{i(2z-1)(p+p')^+x^-/2} \\
&\quad \times \text{out} \langle \pi^+(p)\pi^-(p') | G^{+\mu}(-\frac{1}{2}x) G_\mu^+(\frac{1}{2}x) | 0 \rangle \Big|_{x^+=0, \mathbf{x}=0}, \tag{76}
\end{aligned}$$

they are also called “two-pion distribution amplitudes” in the literature. Due to Lorentz invariance these functions depend on the plus-momentum fraction z of the quark with respect to $p + p'$, on the fraction $\zeta = p^+/(p + p')^+$ describing how the pions share their plus-momentum (see Fig. 3a), and on the invariant mass $s = (p + p')^2$. Our convention for Φ^g coincides with Φ^G defined in [86]; the relation of our Φ^q with the GDAs $\Phi^{J=0,1}$ with definite isospin of Polyakov [87] is given in Section III.A of [85].

The close connection between GDAs and GPDs is obvious from their respective definitions (76) and (20). Crossing the final-state $\pi^-(p')$ to an initial-state $\pi^+(p)$ we must respectively identify p and p' in the GDA with p' and $-p$ in the GPD, and thus identify the corresponding pairs of light-cone variables in GDAs and GPDs as

$$1 - 2\zeta \leftrightarrow \frac{1}{\xi}, \quad 1 - 2z \leftrightarrow \frac{x}{\xi}. \quad (77)$$

Note that in order to have the simple forward limit (21) one needs a prefactor $\frac{1}{2}$ in the definition of H^q , which conventionally does not appear in Φ^q . Notice also different factors of $\frac{1}{2}$ between the definitions in the gluon sector.

Due to parity invariance there are no corresponding matrix elements of the operators $\bar{q}\gamma^+\gamma_5q$ and $G^{+\mu}\tilde{G}_\mu^+$. There are however GDAs Φ_T^q and Φ_T^g defined from the tensor operators $\bar{q}\sigma^{+i}q$ and $\mathbf{S}G^{+i}G^{j+}$ in (55), whose GPD analogs flip parton helicity. The GDAs Φ^q and Φ^g describe a hadronic system with total light-cone helicity $J^3 = 0$ (the light-cone operators defining them carry zero J^3 as discussed in Section 3.4). In contrast, Φ_T^q describes hadrons in a $J^3 = \pm 1$ state, and Φ_T^g describes a $J^3 = \pm 2$ state. No process has so far been identified where one could access the chiral-odd quantity Φ_T^q . The tensor gluon GDA Φ_T^g does however appear in several processes, see Sections 5.4 and 7.3. For the two-pion system it was introduced by Kivel et al. [86], to which we refer for its definition and general properties.

The definitions (76) are reminiscent of those for the leading-twist distribution amplitudes (DAs) of a single meson M with natural parity $P = (-1)^J$,

$$\begin{aligned} \Phi^q(z) &= \int \frac{dx^-}{2\pi} e^{i(2z-1)p^+x^-/2} \langle M(p) | \bar{q}(-\frac{1}{2}x) \gamma^+ q(\frac{1}{2}x) | 0 \rangle \Big|_{x^+=0, \mathbf{x}=0}, \\ \Phi^g(z) &= \frac{1}{p^+} \int \frac{dx^-}{2\pi} e^{i(2z-1)p^+x^-/2} \langle M(p) | G^{+\mu}(-\frac{1}{2}x) G_\mu^+(\frac{1}{2}x) | 0 \rangle \Big|_{x^+=0, \mathbf{x}=0}, \end{aligned} \quad (78)$$

where M is in the polarization state with light-cone helicity zero. Of course, the gluon DA only exists for $C = +1$ mesons, e.g. for an f_0 or f_2 but not for a ρ . All that changes between a DA and a GDA is the replacement of a single meson by the state of several hadrons, and the introduction of variables describing the internal degrees of freedom of this state. We already pointed out in Section 2 the close analogy between $\gamma^*\gamma^* \rightarrow \pi\pi$ and the simpler annihilation process $\gamma^*\gamma^* \rightarrow \pi$. In this case the relevant distribution amplitude is defined by

$$\Phi^q(z) = \int \frac{dx^-}{2\pi} e^{i(2z-1)p^+x^-/2} \langle M(p) | \bar{q}(-\frac{1}{2}x) \gamma^+ \gamma_5 q(\frac{1}{2}x) | 0 \rangle \Big|_{x^+=0, \mathbf{x}=0} \quad (79)$$

as appropriate for states with unnatural parity $P = (-1)^{J+1}$. Note that meson DAs are often defined with an additional factor i in (79), in order to match the standard definition of pseudoscalar decay constants while having a real-valued function Φ^q . The same convention is also sometimes taken for mesons with other quantum numbers. This factor i corresponds to redefining the phase of the meson state and is hence unobservable.

GDAs can also be defined for more complicated systems. The case of three pions has been studied in [88] and the case of two ρ mesons in [89]. The spin structure of GDAs for baryon-antibaryon pairs

can be parameterized as [33]

$$\begin{aligned}
& \int \frac{dx^-}{2\pi} e^{i(2z-1)(p+p')^+x^-/2} \text{out} \langle p(p)\bar{p}(p') | \bar{q}(-\frac{1}{2}x) \gamma^+ q(\frac{1}{2}x) | 0 \rangle \Big|_{x^+=0, \mathbf{x}=0} \\
&= \frac{1}{(p+p')^+} \left[\Phi_V^q \bar{u}(p) \gamma^+ v(p') + \Phi_S^q \frac{(p+p')^+}{2m} \bar{u}(p) v(p') \right], \\
& \int \frac{dx^-}{2\pi} e^{i(2z-1)(p+p')^+x^-/2} \text{out} \langle p(p)\bar{p}(p') | \bar{q}(-\frac{1}{2}x) \gamma^+ \gamma_5 q(\frac{1}{2}x) | 0 \rangle \Big|_{x^+=0, \mathbf{x}=0} \\
&= \frac{1}{(p+p')^+} \left[\Phi_A^q \bar{u}(p) \gamma^+ \gamma_5 v(p') + \Phi_P^q \frac{(p+p')^+}{2m} \bar{u}(p) \gamma_5 v(p') \right], \tag{80}
\end{aligned}$$

for quarks, where for simplicity we have omitted helicity labels for the baryons and the arguments z, ζ, s of the GDAs. In analogy one defines gluon GDAs, with $\bar{q}\gamma^+q$ replaced by $G^{+\mu} G_\mu^+ / (p+p')^+$ and $\bar{q}\gamma^+\gamma_5 q$ by $-iG^{+\mu} \tilde{G}_\mu^+ / (p+p')^+$. We should remark on a subtle point in the relation between proton GPDs and the $p\bar{p}$ distribution amplitudes just introduced. Comparing the Lorentz structures in (80) and (14), and taking into account the change of momentum variables under crossing, we recognize Φ_A and Φ_P as the respective counterparts of \tilde{H} and \tilde{E} . In the vector channel one may use the Gordon decomposition to trade the scalar current for the tensor one. By crossing the defining relation for H and E one would obtain the scalar current $\bar{u}(p)v(p')$ multiplied with $(p'-p)^+ = (1-2\zeta)(p+p')^+$ instead of $(p+p')^+$. A distribution amplitude $\hat{\Phi}_S$ defined with such a prefactor would however have an artificial singularity at $\zeta = \frac{1}{2}$, since there is no symmetry by which $(p'-p)^+ \hat{\Phi}_S(z, \zeta, s) = (p+p')^+ \Phi_S(z, \zeta, s)$ has to vanish at $p^+ = p'^+$. This is in contrast to the definition of \tilde{E} , where due to time reversal invariance the product $(p'-p)^+ \tilde{E}$ is zero for $p^+ = p'^+$.

3.7.1 General properties

Parity invariance has the same consequences for GPDs and for GDAs, restricting the number of independent functions that parameterize a matrix element and, as in the case of pions, constraining the matrix elements of certain operators to vanish altogether. If they describe a particle-antiparticle system, GDAs are subject to further constraints from charge conjugation invariance. In the case of the two-pion system they read

$$\begin{aligned}
\Phi^g(1-z, 1-\zeta, s) &= -\Phi^g(z, \zeta, s), \\
\Phi^g(1-z, 1-\zeta, s) &= \Phi^g(z, \zeta, s). \tag{81}
\end{aligned}$$

In a similar fashion as for quark GPDs, it is useful to separate out the quark GDA combinations

$$\Phi^{g(\pm)}(z, \zeta, s) = \frac{1}{2} \left[\Phi^g(z, \zeta, s) \pm \Phi^g(z, 1-\zeta, s) \right], \tag{82}$$

which respectively describe a $\pi\pi$ system in its $C = \pm 1$ state. These combinations do not mix under evolution, and they are selected in certain hard processes (although in some cases both combinations contribute, see Section 5.3). Since gluons are their own antiparticles we further have $\Phi^g(z, 1-\zeta, s) = \Phi^g(z, \zeta, s)$, so that the two gluons only couple to the $C = +1$ state of the $\pi\pi$ system. In the case of pions further constraints are provided by isospin invariance [87, 85], which relate the GDAs for $\pi^+\pi^-$ and $\pi^0\pi^0$, as well as those for u and d quarks. These relations are the exact analogs of the relations between the GPDs of charged and neutral pions in Section 3.3.2. The charge conjugation properties of $p\bar{p}$ distribution amplitudes are given in [33].

In contrast to the case of GPDs, time reversal invariance does not provide constraints on GDAs.² In the matrix elements (76) the two-pion state appears as ${}_{\text{out}}\langle\pi^+\pi^+|$, in accordance to the physical process where these matrix elements appear. Time reversal transforms this into $|\pi^+\pi^-\rangle_{\text{in}}$, whereas complex conjugation of the matrix element gives $|\pi^+\pi^-\rangle_{\text{out}}$. “In” and “out” states are only identical for states with a single stable particle, whereas a two-pion state interacts and changes between the far past and the far future. GDAs are hence not constrained to be real-valued functions, rather they have dynamical phases reflecting the interactions within the multiparticle system. What time reversal tells us is that the GDA for the transition $q\bar{q} \rightarrow \pi\pi$ is the same as for the transition $\pi\pi \rightarrow q\bar{q}$. Analogous statements hold for proton-antiproton GDAs (with some fine print concerning minus signs, see [33]). It is not obvious to find processes where GDAs with “in” states appear, but they do have applications as we will see in Section 10.3.

According to the relation (33), polynomial moments in $(2z-1)^n$ of the GDAs in (76) give matrix elements of the local twist-two operators (34) between the vacuum and the two-pion state. These moments are polynomials in $(2\zeta-1)$ whose coefficients are form factors corresponding to the ones describing the x^n moments of the GPDs (20). The form factors of local operators have known analyticity properties in their Mandelstam variables, given by s for GDAs and by t for GPDs. This makes explicit how GDAs and GPDs are related by crossing: they are connected by analytic continuation in s or t of their polynomial moments in $2z-1$ or x [87, 90]. In particular, the lowest moments $\int_0^1 dz \Phi^q(z, \zeta, s)$ and $\int_{-1}^1 dx H^q(x, \xi, t)$ are respectively proportional to the pion form factor F_π in the timelike and in the spacelike region.

3.7.2 Evolution and expansion on polynomials

As any matrix element of light-cone separated operators, GDAs depend on a factorization scale μ^2 . Their evolution in this scale is the same as the one for single-particle DAs with the corresponding quantum numbers, and therefore given by the ERBL equations [15, 16]. We will discuss these in Section 3.8 and give here only some results of specific interest for GDAs. We restrict ourselves to evolution at leading logarithmic accuracy, i.e., to the leading-order approximation in α_s of evolution kernels and anomalous dimensions. The variables s and ζ concern the hadronic system but not the partons and are passive in the evolution equations, which involve only μ^2 and z . The evolution can be explicitly solved by an expansion in Gegenbauer polynomials $C_n^k(2z-1)$. For GDAs a double expansion is useful [87, 86]:

$$\begin{aligned}
\Phi^{q(-)}(z, \zeta, s; \mu^2) &= 6z(1-z) \sum_{\substack{n=0 \\ \text{even}}}^{\infty} \sum_{\substack{l=1 \\ \text{odd}}}^{n+1} B_{nl}^q(s, \mu^2) C_n^{3/2}(2z-1) P_l(2\zeta-1) \\
\Phi^{q(+)}(z, \zeta, s; \mu^2) &= 6z(1-z) \sum_{\substack{n=1 \\ \text{odd}}}^{\infty} \sum_{\substack{l=0 \\ \text{even}}}^{n+1} B_{nl}^q(s, \mu^2) C_n^{3/2}(2z-1) P_l(2\zeta-1) \\
\Phi^g(z, \zeta, s; \mu^2) &= 9z^2(1-z)^2 \sum_{\substack{n=1 \\ \text{odd}}}^{\infty} \sum_{\substack{l=0 \\ \text{even}}}^{n+1} B_{nl}^g(s, \mu^2) C_{n-1}^{5/2}(2z-1) P_l(2\zeta-1). \tag{83}
\end{aligned}$$

Our normalization of the gluon coefficients B_{nl}^g has been chosen to obtain a simple form of the energy-momentum relation in (90) and differs from the one in [86] by a factor of $\frac{3}{10}$. The coefficients $B_{nl}^{q,g}$ used here should not be confused with the form factors $B_{n,i}^{q,g}$ introduced in (35) and (39).

²Notice however the similarity between the time reversal constraints (25) for GPDs and the charge conjugation constraints (81) for GDAs, taking into account the relation (77) between momentum fractions. See also our comment at the end of Section 3.5.4.

Before discussing the evolution properties of the expansion coefficients B_{nl}^q and B_{nl}^g let us elaborate on the expansion itself. The restrictions on n and l to be odd or even implement the charge conjugation constraints discussed above, and the restriction $l \leq n+1$ reflects the polynomiality property of GDAs, which is derived in analogy to the one for GPDs. The expansion in Legendre polynomials $P_l(2\zeta - 1)$ is motivated by the following: in the rest frame of the two-pion system one has $2\zeta - 1 = \beta \cos \theta$, where $\beta = (1 - 4m_\pi^2/s)^{1/2}$ is the relativistic velocity of each pion and θ the polar angle of the π^+ with respect to the z -axis defining the light-cone direction in the GDAs. In the limit $\beta \rightarrow 1$ the coefficients B_{nl}^q and B_{nl}^g are therefore associated with the l th partial wave of the two-pion system. An exact partial wave decomposition is obtained by rearranging the finite sum $\sum_l B_{nl} P_l(2\zeta - 1)$ for given n into $\sum_l \tilde{B}_{nl} P_l(\cos \theta)$, see [87, 85]. One then finds in particular the usual phase space suppression $\tilde{B}_{nl} \propto \beta^l$ for each partial wave.

The expansion (83) also allows one to obtain information about the phases of GDAs [87, 85]. In the s region where $\pi\pi$ scattering is strictly elastic, “in” and “out” two-pion states in a definite partial wave l are simply related by the phase shifts as $|\pi\pi(l)\rangle_{\text{in}} = e^{2i\delta_l} |\pi\pi(l)\rangle_{\text{out}}$. The relations from time reversal discussed above then fix the phase of the expansion coefficients to be $\tilde{B}_{nl} = \eta_{nl} e^{i\delta_l} |\tilde{B}_{nl}|$, up to a sign factor $\eta_{nl} = \pm 1$. In analogy to a different context this is called Watson’s theorem [91]. Since low-energy $\pi\pi$ scattering is rather well studied experimentally and known to be approximately elastic up to $s \sim 1 \text{ GeV}^2$, information about the phases of the two-pion DAs is available in this region. The dynamical phases of GDAs can have characteristic signatures in experimental observables (see Sections 9.3 and 9.4.2).

To leading logarithmic accuracy, the coefficients B_{nl}^q of $\Phi^{q(-)}$ renormalize multiplicatively, so that one has

$$B_{nl}^q(s, \mu^2) = B_{nl}^q(s, \mu_0^2) \left(\frac{\alpha_s(\mu^2)}{\alpha_s(\mu_0^2)} \right)^{2\gamma_n/\beta_0} \quad \text{for even } n \quad (84)$$

where $\beta_0 = 11 - \frac{2}{3}n_f$ for n_f quark flavors, and where the γ_n are the same anomalous dimensions which govern the evolution of the DA for a single ρ or π [15, 16],

$$\gamma_n = \frac{4}{3} \left(\frac{1}{2} - \frac{1}{(n+1)(n+2)} + 2 \sum_{k=2}^{n+1} \frac{1}{k} \right). \quad (85)$$

Numerically one has $\gamma_n \approx \frac{8}{3} \log(n+1)$ within at most 6% for all n . For the difference of $\Phi^{q(+)}$ between any two quark flavors q_1 and q_2 one has accordingly

$$\left[B_{nl}^{q_1}(s, \mu^2) - B_{nl}^{q_2}(s, \mu^2) \right] = \left[B_{nl}^{q_1}(s, \mu_0^2) - B_{nl}^{q_2}(s, \mu_0^2) \right] \left(\frac{\alpha_s(\mu^2)}{\alpha_s(\mu_0^2)} \right)^{2\gamma_n/\beta_0} \quad (86)$$

for odd n . The flavor singlet combination $\sum_q \Phi^{q(+)}$ and Φ^g mix under evolution, and for odd n

$$\begin{aligned} \frac{1}{n_f} \sum_q B_{nl}^q(s, \mu^2) &= B_{nl}^+ \left(\frac{\alpha_s(\mu^2)}{\alpha_s(\mu_0^2)} \right)^{2\gamma_n^+/\beta_0} + B_{nl}^- \left(\frac{\alpha_s(\mu^2)}{\alpha_s(\mu_0^2)} \right)^{2\gamma_n^-/\beta_0}, \\ B_{nl}^g(s, \mu^2) &= a_n^+ B_{nl}^+ \left(\frac{\alpha_s(\mu^2)}{\alpha_s(\mu_0^2)} \right)^{2\gamma_n^+/\beta_0} + a_n^- B_{nl}^- \left(\frac{\alpha_s(\mu^2)}{\alpha_s(\mu_0^2)} \right)^{2\gamma_n^-/\beta_0}. \end{aligned} \quad (87)$$

The anomalous dimensions γ_n^\pm and mixing coefficients a_n^\pm were first calculated in [92, 93], results corresponding to the the definitions of GDAs used here are given in [85]. For $n = 1$ one explicitly has

$$\begin{aligned} \gamma_1^- &= 0, & \gamma_1^+ &= \frac{16}{9} + \frac{1}{3}n_f \\ a_1^- &= \frac{16}{3}, & a_1^+ &= -n_f. \end{aligned} \quad (88)$$

Note that the superscripts \pm in this notation do not refer to the C parity, but label the two eigenvalues of the anomalous dimension matrix for the mixing between the quark flavor singlet and gluons.

All of the above anomalous dimensions above are positive except for $\gamma_0 = \gamma_1^- = 0$, so the asymptotic forms for the GDAs are

$$\begin{aligned}\Phi^{q(-)}(z, \zeta, s; \mu^2) &\xrightarrow{\mu \rightarrow \infty} 6z(1-z)(2\zeta-1)B_{01}^q(s), \\ \Phi^{q(+)}(z, \zeta, s; \mu^2) &\xrightarrow{\mu \rightarrow \infty} 18z(1-z)(2z-1)\left[B_{10}^-(s) + B_{12}^-(s)P_2(2\zeta-1)\right], \\ \Phi^g(z, \zeta, s; \mu^2) &\xrightarrow{\mu \rightarrow \infty} 48z^2(1-z)^2\left[B_{10}^-(s) + B_{12}^-(s)P_2(2\zeta-1)\right],\end{aligned}\tag{89}$$

where $P_2(2\zeta-1) = 1 - 6\zeta(1-\zeta)$. The coefficients B_{01}^q and B_{1l}^- are form factors of conserved currents and hence μ -independent. B_{01}^q belongs to the vector current $\bar{q}\gamma^\mu q$ and is just given by the timelike electromagnetic pion form factor as $B_{01}^u = -B_{01}^d = F_\pi(s)$. The coefficients B_{1l}^- belong to the total energy-momentum tensor $T^{\mu\nu}$ (summed over all quark flavors and gluons). In contrast, B_{1l}^q and B_{1l}^g are associated with the individual contributions of quarks and gluons to $T^{\mu\nu}$ and do evolve with μ . Further information can be obtained by analytic continuation to the point $s = 0$, which corresponds to the forward matrix element $\langle \pi^+ | T^{\mu\nu} | \pi^+ \rangle$. The normalization of the energy-momentum tensor provides the identification

$$B_{12}^q(0, \mu^2) = \frac{9}{10} A_q(0, \mu^2), \quad B_{12}^g(0, \mu^2) = \frac{9}{10} A_g(0, \mu^2),\tag{90}$$

where $A_q(0) = \int_0^1 dx x[q(x) + \bar{q}(x)]$ is the fraction of plus-momentum carried by quarks and antiquarks of flavor q in the pion and $A_g(0) = \int_0^1 dx xg(x)$ its analog for gluons. Asymptotically one has the well-known limit $A^q(0, \mu^2) \xrightarrow{\mu \rightarrow \infty} 3/(3n_f + 16)$.

The proton GDAs Φ_V^q and Φ_S^q and their analogs for gluons are defined with the same operators as the corresponding two-pion GDAs and hence follow the same evolution equations. Their expansion in $p\bar{p}$ partial waves is similar to (83) but differs in detail because of spin (see Section 4.2). The evolution of the parity-odd GDAs Φ_A^q and Φ_P^q in the nonsinglet sector (i.e. for the C -odd combinations or for the difference of two quark flavors) is the same as the nonsinglet evolution of Φ_V^q and Φ_S^q , since the anomalous dimensions for vector and axial vector quark operators are identical at leading order in α_s . For gluons and their mixing with quarks the anomalous dimensions differ in the parity-even and odd sectors. In particular, the only vanishing anomalous dimension in the parity-odd case is γ_0 , belonging now to the axial current $\bar{q}\gamma^+\gamma_5 q$. This leads to an asymptotic form going like $z(1-z)$ for the $C = +1$ combinations of quark GDAs. The $C = -1$ combinations of quark GDAs and the GDAs for gluons tend to zero when evolved to $\mu \rightarrow \infty$ (the same holds for the tensor GDAs for quarks or gluons briefly discussed above). The anomalous dimensions and mixing coefficients in the parity-odd sector can e.g. be found in [94], which includes a comparison with earlier results in the literature.

3.8 Evolution of GPDs

GPDs depend on a factorization scale μ^2 , which technically arises as the renormalization scale of the bilocal operators in their definitions and physically represents the scale at which the partons are resolved. Early results on evolution kernels for nonforward kernels were given by Gribov, Levin and Ryskin (Section 6.2.2.1 of [95]), but their formulae contain mistakes [96]. Detailed investigations of the leading-order (LO) evolution equations and kernels for GPDs have been carried out by the Leipzig group [7, 8, 9] and led to the classical paper [10] on GPDs and nonforward Compton scattering. Later work was done by Ji [22], by Radyushkin and Balitsky [39, 97, 98], and by Blümlein et al. [99, 100]. Anomalous dimensions and kernels at next-to-leading order (NLO) accuracy have been obtained in a

series of papers by Belitsky et al. [101, 102, 103, 104, 105]. The evolution of gluon transversity GPDs was studied in [57, 56], and the kernels for gluon and quark transversity at NLO accuracy have been given in [106]. We note that the leading-order nonforward kernels relevant for GPDs were also studied by Bukhostov et al. [107] as building blocks for the evolution of higher-twist parton distributions.

3.8.1 Evolution of light-cone operators

To understand the intimate relationship between the evolution for GPDs, the one of usual parton distributions, and the one for meson DAs or GDAs, it is useful to consider the renormalization group evolution of the defining operators themselves. This can be done for local operators (see Section 3.8.3) but also directly for the nonlocal operators

$$\begin{aligned}
\mathcal{O}^q(\kappa_1, \kappa_2) &= z_\alpha \bar{q}(\kappa_1 z) \gamma^\alpha q(\kappa_2 z) \Big|_{z^2=0}, \\
\mathcal{O}^g(\kappa_1, \kappa_2) &= z_\alpha z_\beta G^{\alpha\mu}(\kappa_1 z) G_\mu^\beta(\kappa_2 z) \Big|_{z^2=0}, \\
\tilde{\mathcal{O}}^q(\kappa_1, \kappa_2) &= z_\alpha \bar{q}(\kappa_1 z) \gamma^\alpha \gamma_5 q(\kappa_2 z) \Big|_{z^2=0}, \\
\tilde{\mathcal{O}}^g(\kappa_1, \kappa_2) &= z_\alpha z_\beta (-i) G^{\alpha\mu}(\kappa_1 z) \tilde{G}_\mu^\beta(\kappa_2 z) \Big|_{z^2=0}.
\end{aligned} \tag{91}$$

The C -odd quark sector evolves without mixing with gluons and one has the nonsinglet evolution equation [108]

$$\mu^2 \frac{d}{d\mu^2} [\mathcal{O}^q(\kappa_1, \kappa_2) + \mathcal{O}^q(\kappa_2, \kappa_1)] = \int_0^1 d\alpha_1 \int_0^1 d\alpha_2 K_{NS}(\alpha_1, \alpha_2) [\mathcal{O}^q(\kappa'_1, \kappa'_2) + \mathcal{O}^q(\kappa'_2, \kappa'_1)] \tag{92}$$

with

$$\kappa'_1 = \kappa_1(1 - \alpha_1) + \kappa_2 \alpha_1, \quad \kappa'_2 = \kappa_1 \alpha_2 + \kappa_2(1 - \alpha_2), \tag{93}$$

where for simplicity we omit μ as an explicit argument of the light-cone operators or of their matrix elements. An analogous equation holds for the C -odd operators $\tilde{\mathcal{O}}^q(\kappa_1, \kappa_2) - \tilde{\mathcal{O}}^q(\kappa_2, \kappa_1)$, and also for flavor differences $\mathcal{O}^{q_1} - \mathcal{O}^{q_2}$ and $\tilde{\mathcal{O}}^{q_1} - \tilde{\mathcal{O}}^{q_2}$ of quark operators in the C -even sector. To leading order in α_s the evolution kernel is the same for all cases and reads [108, 99]

$$\begin{aligned}
K_{NS}(\alpha_1, \alpha_2) &= \frac{\alpha_s}{2\pi} C_F \theta(\alpha_1 + \alpha_2 \leq 1) \left\{ 1 + \frac{3}{2} \delta(\alpha_1) \delta(\alpha_2) - \delta(\alpha_1) - \delta(\alpha_2) \right. \\
&\quad \left. + \delta(\alpha_1) \left[\frac{1}{\alpha_2} \right]_+ + \delta(\alpha_2) \left[\frac{1}{\alpha_1} \right]_+ \right\},
\end{aligned} \tag{94}$$

where $C_F = \frac{4}{3}$ and the plus distribution is defined as

$$\int_0^1 d\alpha f(\alpha) \left[\frac{1}{\alpha} \right]_+ = \int_0^1 d\alpha \frac{f(\alpha) - f(0)}{\alpha}. \tag{95}$$

In the singlet sector quarks mix with gluons, and one has a matrix equation

$$\mu^2 \frac{d}{d\mu^2} \mathcal{O}(\kappa_1, \kappa_2) = \int_0^1 d\alpha_1 \int_0^1 d\alpha_2 K(\alpha_1, \alpha_2, \kappa_2 - \kappa_1) \mathcal{O}(\kappa'_1, \kappa'_2) \tag{96}$$

with

$$\mathcal{O}(\kappa_1, \kappa_2) = \begin{pmatrix} (2n_f)^{-1} \sum_q^{n_f} [\mathcal{O}^q(\kappa_1, \kappa_2) + \mathcal{O}^q(\kappa_2, \kappa_1)] \\ \mathcal{O}^g(\kappa_1, \kappa_2) \end{pmatrix}, \tag{97}$$

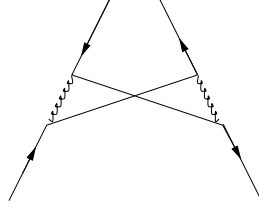


Figure 7: A diagram contributing to the region $\alpha_1 + \alpha_2 > 1$ of the evolution kernel K_{NS} at $O(\alpha_s^2)$.

and

$$K = \begin{pmatrix} K^{qq}(\alpha_1, \alpha_2) & -i(\kappa_2 - \kappa_1)K^{qg}(\alpha_1, \alpha_2) \\ i(\kappa_2 - \kappa_1)^{-1}K^{gq}(\alpha_1, \alpha_2) & K^{gg}(\alpha_1, \alpha_2) \end{pmatrix}. \quad (98)$$

The dependence of the off-diagonal elements on the light-cone distance $\kappa_2 - \kappa_1$ can be traced back to the different powers of z appearing in the quark and gluon operators (91). An analogous equation describes the singlet evolution for the parity-odd operators $\tilde{\mathcal{O}}^q$ and $\tilde{\mathcal{O}}^g$. At LO (but not beyond) one has $\tilde{K}^{qq} = K^{qq} = K_{\text{NS}}$, whereas the kernels K^{gg} , K^{gq} , K^{qg} differ from those in the parity-odd sector already at LO. Explicit forms of the LO kernels for the parity-even operators can be found in [108, 39], and for the parity-odd ones in [97, 100]. Evolution equations analogous to (92) but with different kernels hold for the operators describing quark or gluon transversity (see Section 3.5.2), which again evolve by themselves without mixing.

The support properties of the evolution kernels can be determined using the α -parameter representation of Feynman diagrams and are $0 \leq \alpha_1 \leq 1$ and $0 \leq \alpha_2 \leq 1$ [10]. The region $\alpha_1 + \alpha_2 > 1$ (which corresponds to opposite orientation along the light-cone of the operators on the two sides of the evolution equation) only appears in K_{NS} at two-loop order and comes from diagrams “mixing” quarks and antiquarks as in Fig. 7 [109].

3.8.2 Evolution of GPDs

The evolution equations of the light-cone operators readily generate the various evolution equations for their matrix elements and thus for GPDs. From the definitions (14) one obtains in the C -odd sector

$$\mu^2 \frac{d}{d\mu^2} H^{q(-)}(x, \xi, t) = \int_{-1}^1 dx' \frac{1}{|\xi|} V_{\text{NS}}\left(\frac{x}{\xi}, \frac{x'}{\xi}\right) H^{q(-)}(x', \xi, t). \quad (99)$$

Analogous equations hold for $E^{q(-)}$, $\tilde{H}^{q(-)}$, $\tilde{E}^{q(-)}$ and for the difference of quark distributions for two flavors in the C -even sector, with identical kernels at $O(\alpha_s)$. Notice that both x and ξ are active variables in the evolution equation since they specify the parton momenta, whereas the momentum fraction ζ for GDAs is passive in the evolution. The evolution kernel is obtained as

$$\begin{aligned} & \frac{1}{|\xi|} V_{\text{NS}}\left(\frac{x}{\xi}, \frac{x'}{\xi}\right) \\ &= \int_0^1 d\alpha_1 \int_0^1 d\alpha_2 \delta(x - x'(1 - \alpha_1 - \alpha_2) - \xi(\alpha_1 - \alpha_2)) K_{\text{NS}}(\alpha_1, \alpha_2) \end{aligned} \quad (100)$$

and to LO accuracy reads

$$\begin{aligned} & V_{\text{NS}}(x, x') \\ &= \frac{\alpha_s}{4\pi} C_F \left[\rho(x, x') \left\{ \frac{1+x}{1+x'} \left(1 + \frac{2}{x'-x} \right) \right\} + \{x \rightarrow -x, x' \rightarrow -x'\} \right]_+ \end{aligned} \quad (101)$$

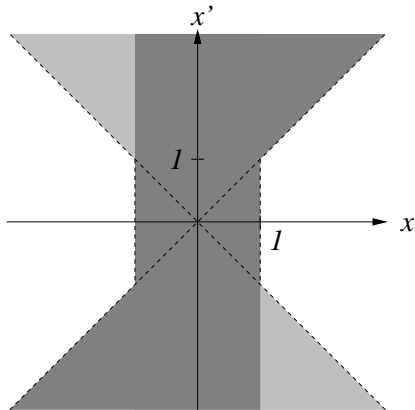


Figure 8: Support region of the quark evolution kernel $V_{\text{NS}}(x, x')$. The dark shaded region corresponds to the LO kernel, and the light shaded region starts contributing at NLO.

with its support controlled by

$$\rho(x, x') = \theta(x' \geq x \geq -1) - \theta(x' \leq x \leq -1), \quad (102)$$

where we use a shorthand notation $\theta(x \leq y \leq z) = \theta(y - x)\theta(z - y)$. The plus-distribution is here defined with respect to the first argument, i.e.,

$$\left[f(x, x') \right]_+ = f(x, x') - \delta(x - x') \int dx'' f(x'', x'), \quad (103)$$

where the integral on the right-hand side is over the full support region in x'' , which is finite thanks to the function ρ in the kernels. One finds that this prescription also makes the integral over the second argument finite, which is needed in the evolution equation (99). From (99), (101) and (103) one directly sees that $\int dx H^q(x)$ is independent of μ^2 , as befits the form factors of conserved currents.

The support region of the kernels for GPDs follows from the support of the kernels for light-cone operators and is as shown in Fig. 8 [10]. The leading-order result (101) corresponds to the dark-shaded region. The light-shaded region starts contributing at NLO and corresponds to $\alpha_1 + \alpha_2 > 1$ in the position-space kernels, i.e., to diagrams like in Fig. 7 which in momentum space describe radiation of an antiquark from a quark [109].

The evolution equation in the singlet sector is obtained from (99) by replacing

$$H^{q(-)} \rightarrow \left(\begin{array}{c} (2n_f)^{-1} \sum_q^{n_f} H^{q(+)} \\ H^g \end{array} \right) \quad (104)$$

and [105]

$$V_{\text{NS}}\left(\frac{x}{\xi}, \frac{x'}{\xi}\right) \rightarrow \left(\begin{array}{cc} V^{qq}\left(\frac{x}{\xi}, \frac{x'}{\xi}\right) & \frac{1}{\xi} V^{qg}\left(\frac{x}{\xi}, \frac{x'}{\xi}\right) \\ \xi V^{gq}\left(\frac{x}{\xi}, \frac{x'}{\xi}\right) & V^{gg}\left(\frac{x}{\xi}, \frac{x'}{\xi}\right) \end{array} \right). \quad (105)$$

The kernels V^{qq} and V^{gg} are obtained as in (100), whereas due to the factors $(\kappa_2 - \kappa_1)$ and $(\kappa_2 - \kappa_1)^{-1}$ in the matrix kernel (98) the corresponding relations for V^{qg} and V^{gq} respectively involve the derivative and the integral of the δ function in (100). Compilations of these kernels at LO, as well as the

ones for the singlet evolution of $\tilde{H}^{q(+)}$ and \tilde{H}^g can be found in [100]. The corresponding results for Radyushkin's distributions $\mathcal{F}_\zeta(X)$ are given in [98] and those for the distributions $\hat{\mathcal{F}}_q(X, \zeta)$ of Golec-Biernat and Martin in [40]. The NLO kernels are listed in [105] (with some misprints in the skewed DGLAP kernels pointed out in [110]). Different forms of the off-diagonal kernels are given in the literature, but note that only the even part in x' of V^{qg} and the odd part in x' of V^{gq} survive the convolution with the corresponding GPDs in the evolution equations. An analogous statement (with opposite symmetry properties in x') holds in the parity-odd sector.

The evolution kernels $V(x, x')$ for GPDs include the ERBL and DGLAP kernels as limiting cases. The limit $\xi \rightarrow \pm 1$ of a GPD corresponds to an initial or final state with zero plus-momentum, which for the evolution equations is as good as the vacuum state appearing in DAs or GDAs. The ERBL equations have hence the same form as (99) and its singlet counterparts, with ξ set to ± 1 . The momentum fraction x we use for GPDs is proportional to the difference of quark and antiquark momenta in the ERBL region and corresponds to $2z - 1$ in terms of the quark momentum fraction z we use for distribution amplitudes. Taking this correspondence into account, the ERBL evolution kernels are just given by $V(x, x')$ restricted to the interval $[-1, 1]$ in both arguments. Indeed one recognizes in (101) the familiar ERBL kernel with $\rho(x, x')$ instead of $\theta(x' - x)$. Müller et al. [10] have shown that one can obtain the evolution kernels for GPDs as a unique extension of the usual ERBL kernels to the full (x, x') -plane. The argument consists in showing that the Fourier transform $\int dx \exp(i\lambda x) V(x, x')$ is analytic in both λ and x' and can hence be obtained by analytic continuation from the region $|x'| \leq 1$, where $V(x, x')$ reduces to the usual ERBL kernels according to Fig. 8. The kernel $V(x, x')$ in the full (x, x') -plane is then obtained by inverting the Fourier transform. At $O(\alpha_s)$ this procedure reduces to replacing $\theta(x' - x)$ in the ERBL kernels by $\rho(x, x')$.

The DGLAP evolution kernels are obtained by taking the forward limit $\xi \rightarrow 0$ of (99) and its singlet counterparts. Comparing with the conventional form of the DGLAP equations in the nonsinglet sector,

$$\mu^2 \frac{d}{d\mu^2} q(z) = \int_z^1 \frac{dz'}{z'} P_{\text{NS}}\left(\frac{z}{z'}\right) q(z'), \quad (106)$$

where $z > 0$, one finds

$$P_{\text{NS}}(z) = \lim_{\xi \rightarrow 0} \frac{1}{|\xi|} V_{\text{NS}}\left(\frac{z}{\xi}, \frac{1}{\xi}\right) = \frac{\alpha_s}{2\pi} C_F \left[\theta(0 \leq z \leq 1) \frac{1+z^2}{1-z} \right]_+ + O(\alpha_s^2). \quad (107)$$

Analogous relations hold for the other kernels. Notice that the DGLAP evolution equations are relevant not only for the usual parton distributions but also for GPDs at $\xi = 0$ but nonzero t .

For nonzero skewness ξ the evolution in the DGLAP region $\xi \leq |x|$ is very similar to the usual DGLAP evolution. In particular we see from Fig. 8 that the change of a GPD $f^i(x, \xi, t)$ with μ is influenced only by GPDs $f^j(x', \xi, t)$ at values $|x'| \geq |x|$, i.e. by partons with the same or larger plus-momentum. Qualitatively, evolution to higher scales μ “shifts” partons from larger to smaller momentum fractions $|x|$, as suggested by the physical picture of partons losing momentum by radiating other partons before they are probed in the hard process.

In the ERBL region, the change of $f^i(x, \xi, t)$ with μ depends on GPDs $f^j(x', \xi, t)$ in the full range of x' . Rewriting (99) as

$$\begin{aligned} \mu^2 \frac{d}{d\mu^2} H^{q(-)}(y\xi, \xi, t) &= \int_{-1}^1 dy' V_{\text{NS}}(y, y') H^{q(-)}(y'\xi, \xi, t) \\ &+ \int dy' \left[\theta(y' < -1) + \theta(y' > 1) \right] V_{\text{NS}}(y, y') H^{q(-)}(y'\xi, \xi, t) \end{aligned} \quad (108)$$

we see that the evolution equation in the ERBL region can be regarded as an inhomogeneous equation, with the homogeneous part identical to the usual ERBL equations for distribution amplitudes and

an inhomogeneous term due to the GPDs in the DGLAP region (Belitsky et al. have proposed to use this decomposition in the actual solution of the evolution equations [106]). In the ERBL region, evolution tends to “equalize” the plus-momenta of the two emitted partons towards a symmetric or antisymmetric shape in x (depending on the channel) and eventually to their asymptotic shapes discussed below. Dedicated numerical studies of leading-order evolution have been performed by various groups in [46, 111], [96, 112, 113], [114], [115]. Belitsky et al. [116, 109] numerically studied the two-loop corrections to evolution at moderate ξ and found small to moderate effects, depending on how small the starting scale μ_0 was taken. Similar results were reported by Freund and McDermott [117]. As is to be expected, two-loop effects become more important when starting evolution at low scales, where the running coupling is large.

3.8.3 Solving the evolution equations

As in the case of forward parton densities, the evolution of GPDs may also be treated in terms of the ultraviolet renormalization of the *local* operators that correspond to their moments in x (Section 3.3.3). What complicates the nonforward case is that the set of leading-twist operators in (34) mixes under renormalization with operators having additional overall derivatives. Projecting all Lorentz indices on the plus-direction for simplicity, one has

$$\mu^2 \frac{d}{d\mu^2} [\bar{q}\gamma^+(\overleftrightarrow{D}^+)^n q] = \sum_{\substack{m=0 \\ \text{even}}}^n \Gamma_{nm} [(\partial^+)^{n-m} \bar{q}\gamma^+(\overleftrightarrow{D}^+)^m q] \quad (109)$$

for even n . In matrix elements between states with momenta p' and p the overall derivatives ∂^+ translate into factors of $i\Delta^+$. It is therefore only for $\Delta^+ = 0$ that one has the simple multiplicative renormalization of Mellin moments familiar from the usual parton densities. To leading logarithmic accuracy the system (109) is diagonalized by the so-called conformal operators [118, 119, 120]

$$\mathcal{O}_n^q = (\partial^+)^n \bar{q}\gamma^+ C_n^{3/2} \left(\frac{\overleftrightarrow{D}^+ - \overleftarrow{D}^+}{\overrightarrow{\partial}^+ + \overleftarrow{\partial}^+} \right) q \quad (110)$$

with even n (where the inverse derivatives in the polynomial cancel against derivatives ∂^+ in front of the operator). To leading logarithmic accuracy the conformal moments

$$C_n^q(\xi, t; \mu^2) = \xi^n \int_{-1}^1 dx C_n^{3/2} \left(\frac{x}{\xi} \right) H^q(x, \xi, t; \mu^2) \quad (111)$$

of GPDs thus renormalize multiplicatively for even n , as written in (84) for the Gegenbauer coefficients of GDAs. For gluon distributions the corresponding moments are

$$C_n^g(\xi, t; \mu^2) = \xi^{n-1} \int_{-1}^1 dx C_{n-1}^{5/2} \left(\frac{x}{\xi} \right) H^g(x, \xi, t; \mu^2), \quad (112)$$

and the mixing between C_n^g and the flavor singlet combination $\sum_q C_n^q$ for odd n is solved as in (87) for GDAs (with different mixing coefficients due to the different relative normalization of B_{nl}^q , B_{nl}^g and C_n^q , C_n^g). The conformal moments of the parton helicity dependent GPDs \tilde{H}^q , \tilde{H}^g and of quark or gluon transversity distributions evolve in a similar manner: the relevant Gegenbauer polynomials are always $C_n^{3/2}$ for quarks and $C_{n-1}^{5/2}$ for gluons, and the differences in the evolution arise from the differences in the anomalous dimensions. The moments of E and \tilde{E} evolve of course as their counterparts for

H and \tilde{H} . An explicit form of conformal moments sometimes used in the literature is based on the relation between Gegenbauer and Jacobi polynomials:

$$\begin{aligned}\xi^n C_n^{3/2}\left(\frac{x}{\xi}\right) &= \frac{n+1}{2^{n+1}} \sum_{k=0}^n \binom{n}{k} \binom{n+2}{k+1} (x+\xi)^k (x-\xi)^{n-k}, \\ \xi^n C_n^{5/2}\left(\frac{x}{\xi}\right) &= \frac{(n+1)(n+2)}{3 \cdot 2^{n+2}} \sum_{k=0}^n \binom{n}{k} \binom{n+4}{k+2} (x+\xi)^k (x-\xi)^{n-k}.\end{aligned}\quad (113)$$

Notice that for $\xi = 0$ the conformal moments reduce to the usual Mellin moments up to a normalization factor.

At NLO the conformal operators (110) mix under renormalization, and one has

$$\mu^2 \frac{d}{d\mu^2} \mathcal{O}_n^q = \sum_{\substack{m=0 \\ \text{even}}}^n \hat{\Gamma}_{nm} [(\partial^+)^{n-m} \mathcal{O}_m^q] \quad (114)$$

for even n . At NLO the change with μ of the n th conformal moment C_n^q thus depends also on the lower moments. Corresponding results hold for the quark and gluon operators in the C -even sector. The off-diagonal entries of the anomalous dimension matrix $\hat{\Gamma}_{nm}$ start at order α_s^2 and are specific to nonforward kinematics, whereas the diagonal entries coincide with the anomalous dimensions known from DGLAP evolution. The solution of the coupled system of equations (114) and its analogs in the favor singlet sector is discussed in [102, 116, 109].

When evolving to asymptotically large μ^2 the running coupling decreases, and the asymptotic forms of the GPDs are controlled by the leading-order anomalous dimensions as already discussed in Sect. 3.7.2. Only the Gegenbauer moments (or their quark-gluon combinations) corresponding to zero anomalous dimensions survive and one finds [37]

$$\begin{aligned}H^{q(+)}(x, \xi, t) &\xrightarrow{\mu \rightarrow \infty} \theta(|x| < \xi) \frac{3}{3n_f + 16} \frac{15x}{4\xi} \left(1 - \frac{x^2}{\xi^2}\right) \left(\frac{A(t)}{\xi^2} + 4C(t)\right), \\ E^{q(+)}(x, \xi, t) &\xrightarrow{\mu \rightarrow \infty} \theta(|x| < \xi) \frac{3}{3n_f + 16} \frac{15x}{4\xi} \left(1 - \frac{x^2}{\xi^2}\right) \left(\frac{B(t)}{\xi^2} - 4C(t)\right), \\ H^g(x, \xi, t) &\xrightarrow{\mu \rightarrow \infty} \theta(|x| < \xi) \frac{16}{3n_f + 16} \frac{15\xi}{8} \left(1 - \frac{x^2}{\xi^2}\right)^2 \left(\frac{A(t)}{\xi^2} + 4C(t)\right), \\ E^g(x, \xi, t) &\xrightarrow{\mu \rightarrow \infty} \theta(|x| < \xi) \frac{16}{3n_f + 16} \frac{15\xi}{8} \left(1 - \frac{x^2}{\xi^2}\right)^2 \left(\frac{B(t)}{\xi^2} - 4C(t)\right)\end{aligned}\quad (115)$$

in the C -even sector, where $A = \sum_q A_q + A_g$ and its analogs B and C are the form factors of the total energy-momentum tensor discussed in Section 3.6. Note that at $t = 0$ one has $A = 1$ and $B = 0$ due to the momentum and angular momentum sum rules. One further has

$$\begin{aligned}H^{q(-)}(x, \xi, t) &\xrightarrow{\mu \rightarrow \infty} \theta(|x| < \xi) \frac{3}{4\xi} \left(1 - \frac{x^2}{\xi^2}\right) F_1^q(t), \\ E^{q(-)}(x, \xi, t) &\xrightarrow{\mu \rightarrow \infty} \theta(|x| < \xi) \frac{3}{4\xi} \left(1 - \frac{x^2}{\xi^2}\right) F_2^q(t), \\ \tilde{H}^{q(+)}(x, \xi, t) &\xrightarrow{\mu \rightarrow \infty} \theta(|x| < \xi) \frac{3}{4\xi} \left(1 - \frac{x^2}{\xi^2}\right) g_A^q(t), \\ \tilde{E}^{q(+)}(x, \xi, t) &\xrightarrow{\mu \rightarrow \infty} \theta(|x| < \xi) \frac{3}{4\xi} \left(1 - \frac{x^2}{\xi^2}\right) g_P^q(t),\end{aligned}\quad (116)$$

whereas the remaining combinations $\tilde{H}^{q(-)}$, $\tilde{E}^{q(-)}$ and \tilde{H}^g , \tilde{E}^g asymptotically evolve to zero, as well as the quark and gluon transversity distributions. In the limit $\xi \rightarrow 0$ the functions in (115) and (116) become proportional to either $\delta(x)$ or $\delta'(x)$ and one recovers the singular asymptotic forms of the forward densities.

For distribution amplitudes, whose kinematics corresponds to $\xi = \pm 1$, the conformal moments (111) and (112) are readily inverted and thus provide a solution of the evolution equations in momentum space. This is however not the case for $|\xi| < 1$, where the Gegenbauer polynomials $C_n^k(x/\xi)$ do not form an orthogonal set of functions on the interval $x \in [-1, 1]$. The reconstruction of GPDs from the moments (111) and (112) is then nontrivial, as is the inversion of Mellin moments in the forward limit. A strategy proposed in [121] leads to the Shuvaev transform discussed in the next section. Another method is to expand the GPDs in a set of orthogonal polynomials on the interval $x \in [-1, 1]$. Choosing Gegenbauer polynomials $C_n^{3/2}(x)$ one finds a structure

$$H^q(x, \xi, t) = (1 - x^2) \sum_{n=0}^{\infty} C_n^{3/2}(x) \sum_{\substack{m=0 \\ \text{even}}}^n a_{nm}(\xi) C_{n-m}^q(\xi) \quad (117)$$

where the $a_{nm}(\xi)$ are known even polynomials in ξ of order m [114, 122]. The method is not restricted to expanding on $C_n^{3/2}(x)$, and the relevant coefficients for Jacobi polynomials have been given in [116, 109]. Solutions based on polynomial expansion have also been presented in [108, 122] for the position space operators (91) or their hadronic matrix elements (termed ‘‘coordinate space distributions’’).

Expansion on different polynomials has been used for the numerical solution of the evolution equations at leading order by several groups [114, 123, 112, 122]. Belitsky et al. [116, 109, 124] have treated NLO evolution in this way. Expanding on Legendre polynomials, the authors report that a rather large number of terms (several tens to hundreds) was necessary to achieve a reliable accuracy because of the oscillatory behavior of the polynomials, and found the method intractable or unreliable for x close to ξ or for small ξ , when the GPDs can have rapid variations in x . It is not known whether there is an adequate choice of polynomials for which a smaller number of terms would be sufficient. Direct numerical integration of the evolution equations has been used as an alternative method; some technical information is given in [46, 110]. For the case where evolution is performed over a limited range in μ , Musatov and Radyushkin [115] have proposed an iterative solution of the evolution equations.

3.8.4 Shuvaev transform

Shuvaev [121] has proposed a method to reduce the leading logarithmic evolution of GPDs to the usual DGLAP evolution, making use of the fact that the Gegenbauer moments of GPDs evolve in the same way as the Mellin moments of forward distributions. The method introduces ‘‘effective forward distributions’’ $f_\xi^q(x)$, $f_\xi^g(x)$, whose Mellin moments are equal to the Gegenbauer moments of a given GPD $H^{q,g}(x, \xi)$, up to a normalization factor which ensures that in the forward limit one has $f_0^q(x) = H^q(x, 0, 0)$ and $x f_0^g(x) = H^g(x, 0, 0)$:

$$\int_{-1}^1 dx x^n f_\xi^{q,g}(x) = c_n^{q,g} C_n^{q,g}(\xi) \quad (118)$$

with

$$c_n^q = \frac{2^n [n!]^2}{(2n+1)!}, \quad c_n^g = \frac{3 \cdot 2^n [n!]^2}{n(2n+1)!}. \quad (119)$$

For simplicity we suppress the dependence of both H and f on t and on μ^2 here. The leading order evolution of a nonforward distribution can then be performed by transforming H to f , solving the usual DGLAP evolution for f , and transforming back to H at the new factorization scale.

A detailed investigation of the Shuvaev transform has been given by Noritzsch [125]. The Shuvaev transform is an integral transform

$$H^q(x, \xi) = \int_{-y_\xi}^{y_\xi} dy \mathcal{K}_q(x, \xi, y) f_\xi^q(y), \quad (120)$$

with $y_\xi = \frac{1}{2}(1 + \sqrt{1 - \xi^2})$. In the DGLAP regions $|x| \geq \xi$ the kernel further restricts the integration to the two intervals $y \geq \frac{1}{2}(x + \sqrt{x^2 - \xi^2})$ and $y \leq \frac{1}{2}(x - \sqrt{x^2 - \xi^2})$, whereas no such restriction occurs for x in the ERBL region [125]. The inverse transform is given by

$$\begin{aligned} f_\xi^q(y) &= \int_{|x| \geq \xi} dx \mathcal{K}_q^{-1}(y, \xi, x) H^q(x, \xi) \\ &+ \sum_{n=0}^{\infty} \frac{(-1)^n}{n!} \delta^{(n)}(y) c_n^q \int_{|x| \leq \xi} dx \xi^n C_n^{3/2}\left(\frac{x}{\xi}\right) H^q(x, \xi). \end{aligned} \quad (121)$$

Analogous expressions hold for gluons. Different equivalent expressions for the integral kernels $\mathcal{K}_{q,g}$ and $\mathcal{K}_{q,g}^{-1}$ can be found in [121, 125, 126]. For $|x| \gg \xi$ one finds $\mathcal{K}_q(x, \xi, y) = \delta(x - y) + x^{-1}O(\xi^2/x^2)$ and $\mathcal{K}_g(x, \xi, y) = x\delta(x - y) + O(\xi^2/x^2)$ so that in this limit GPDs and effective forward distributions almost coincide [125].

In practice the Shuvaev transform has not been used to solve the evolution of GPDs, possibly because of the infinite sum over δ functions and their derivatives in the inverse transform (121), overlooked in [121] and pointed out in [125]. The transform has however been useful for approximating GPDs at small ξ , by replacing $f_\xi(x)$ with the forward densities times a t dependent factor in (120). This will be discussed in Section 4.4.

3.9 Double distributions

Double distributions are an alternative way to parameterize the hadronic matrix elements which define GPDs and which appear in several hard processes. Their study provides insight into the properties of these matrix elements, and it provides a strategy to make ansätze for GPDs, which we will discuss in Section 4.3. Double distributions have been introduced by Müller et al. [10], who called them “spectral functions”. They were rediscovered and studied by Radyushkin, who has given a detailed review on the subject [36].

Starting point for introducing double distributions are the matrix elements of the light-cone operators we already encountered when discussing evolution in Section 3.8, namely

$$\langle p' | \bar{q}(-\frac{1}{2}z) \not{z} q(\frac{1}{2}z) | p \rangle \Big|_{z^2=0} \quad (122)$$

and its analogs in the parity-odd sector and for gluons. Because of Lorentz invariance these matrix elements only depend on scalar products pz , $p'z$, pp' or alternatively on Pz , Δz , t once appropriate spinor structures have been taken off. Double distributions are defined through a Fourier transform in the two independent variables Pz and Δz ,

$$\begin{aligned} \langle p' | \bar{q}(-\frac{1}{2}z) \not{z} q(\frac{1}{2}z) | p \rangle \Big|_{z^2=0} &= \bar{u}(p') \not{z} u(p) \int d\beta d\alpha e^{-i\beta(Pz) + i\alpha(\Delta z)/2} f^q(\beta, \alpha, t) \\ &+ \bar{u}(p') \frac{i\sigma^{\mu\alpha} z_\mu \Delta_\alpha}{2m} u(p) \int d\beta d\alpha e^{-i\beta(Pz) + i\alpha(\Delta z)/2} k^q(\beta, \alpha, t) \\ &- \bar{u}(p') \frac{\Delta z}{2m} u(p) \int d\alpha e^{i\alpha(\Delta z)/2} D^q(\alpha, t). \end{aligned} \quad (123)$$

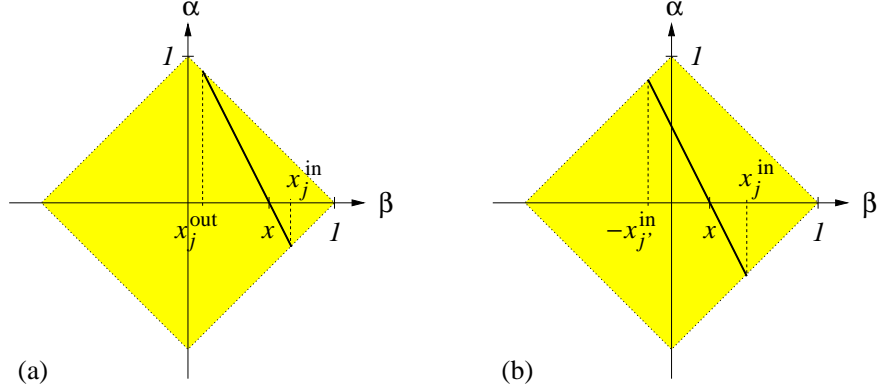


Figure 9: Support region for double distributions, and lines of integration to obtain GPDs in the regions (a) $x \in [\xi, 1]$ and (b) $x \in [-\xi, \xi]$ according to (124). The momentum fractions x_j^{in} , x_j^{out} , x_j^{in} are given in (167) and (170) with $x_j = x$.

The alphabetic order of the variables β and α follows the convention of [37].³ The so-called D -term in the last line had for a long time been overlooked and was only introduced by Polyakov and Weiss [90]. For the moment we will leave it aside and discuss it in Section 3.9.2.

The support region of the double distributions f and k is given by the rhombus $|\beta| + |\alpha| \leq 1$ shown in Fig 9, and D has support for $|\alpha| \leq 1$ (for simplicity we do not write out the corresponding limits in the integrals over β and α). These spectral properties can be shown using the α -representation of Feynman diagrams [39, 128]. Note that double distributions need not be smooth functions; one explicitly encounters δ distributions and their derivatives in meson exchange contributions (see Section 4.3.3).

To obtain the relation between double distributions and GPDs one can take a given lightlike z and choose a frame where $z^+ = 0$ and $\mathbf{z} = 0$. Dividing the matrix element (122) by z^- and taking the Fourier transform with respect to z^- one finds the relations

$$\begin{aligned} H^q(x, \xi, t) &= \int d\beta d\alpha \delta(x - \beta - \xi\alpha) f^q(\beta, \alpha, t) + \text{sgn}(\xi) D^q\left(\frac{x}{\xi}, t\right), \\ E^q(x, \xi, t) &= \int d\beta d\alpha \delta(x - \beta - \xi\alpha) k^q(\beta, \alpha, t) - \text{sgn}(\xi) D^q\left(\frac{x}{\xi}, t\right). \end{aligned} \quad (124)$$

Notice that because of its support property, the D -term only contributes in the region $|x| < |\xi|$. The lines of integration over the double distributions in the β - α plane are shown in Fig. 9. They have slope $-1/\xi$ and cut the β axis at x . Furthermore, they intersect the edges of the support rhombus at points where $|\beta|$ is the momentum fraction of one or the other parton with respect to its parent hadron in the GPD (given in (167) and (170)). The forward quark density is simply obtained by integration over the vertical line $\beta = x$,

$$q(x) = \int_{x-1}^{1-x} d\alpha f^q(x, \alpha, 0) \quad (125)$$

for $x > 0$, with an analogous relation for $x < 0$.

From the arguments of the Fourier transform in (123) one can associate the two variables β and α with a flow of momentum as shown in Fig. 10. For $\Delta = 0$ one clearly obtains the kinematics of a

³Radyushkin [127] had earlier introduced the variables (x, α) instead of (β, α) , but we reserve x for the first argument of GPDs.

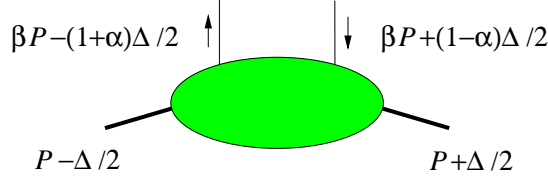


Figure 10: Momenta associated with the partons and hadrons in a double distribution, as explained in the text.

forward parton density, whereas the opposite case $P = 0$ is reminiscent of a distribution amplitude (this will become yet more explicit in Sect. 3.9.3). This suggests that the dependence of the double distribution on β will resemble the pattern of a parton density, and the dependence on α that of a DA. It is however important to realize that the picture in Fig. 10 is only a guide. pz and $p'z$ are treated as *independent* variables when defining the double distribution through a two-dimensional Fourier transform. As a consequence, a double distribution refers to fixed $t = (p - p')^2$ but *not* to fixed individual hadron momenta p and p' (and hence does not depend on the plus-momentum fraction ξ). This is in contrast to GPDs, whose definition (14) is readily turned into a one-dimensional Fourier transform

$$\begin{aligned} \langle p' | \bar{q}(-\frac{1}{2}z) \not{z} q(\frac{1}{2}z) | p \rangle \Big|_{z^2=0} &= \bar{u}(p') \not{z} u(p) \int dx e^{-ix(Pz)} H^q(x, \xi, t) \\ &+ \bar{u}(p') \frac{i\sigma^{\mu\alpha} z_\mu \Delta_\alpha}{2m} u(p) \int dx e^{-ix(Pz)} E^q(x, \xi, t). \end{aligned} \quad (126)$$

Here pz and $p'z$ are understood as dependent variables subject to the constraint $\xi = -(\Delta z)/(2Pz)$, so that p and p' can both be taken fixed. The above feature of double distributions leads to their simple properties regarding Lorentz invariance (see Section 3.9.1), but at the same time makes their physical interpretation less immediate than the one of GPDs. In particular, no interpretation comparable to the ones we will develop in Sections 3.10 and 3.11 has been found so far.

For gluons double distributions can be defined by

$$\begin{aligned} \langle p' | z_\alpha z_\beta G^{\alpha\mu}(-\frac{1}{2}z) G_\mu^\beta(\frac{1}{2}z) | p \rangle \Big|_{z^2=0} &= \bar{u}(p') \not{z} u(p) \frac{Pz}{2} \int d\beta d\alpha e^{-i\beta(Pz)+i\alpha(\Delta z)/2} \beta f^g(\beta, \alpha, t) \\ &+ \bar{u}(p') \frac{i\sigma^{\mu\alpha} z_\mu \Delta_\alpha}{2m} u(p) \frac{Pz}{2} \int d\beta d\alpha e^{-i\beta(Pz)+i\alpha(\Delta z)/2} \beta k^g(\beta, \alpha, t) \\ &+ \bar{u}(p') \frac{\Delta z}{2m} u(p) \frac{\Delta z}{4} \int d\alpha e^{i\alpha(\Delta z)/2} D^g(\alpha, t). \end{aligned} \quad (127)$$

This definition of f^g follows the convention of [115, 36]; definitions with other prefactors have also been used in the literature. With the above choice one obtains the forward gluon density as $g(x) = \int d\alpha f^g(x, \alpha, 0)$. The reduction formulae to the gluon GPDs H^g and E^g read

$$\begin{aligned} H^g(x, \xi, t) &= \int d\beta d\alpha \delta(x - \beta - \xi\alpha) \beta f^g(\beta, \alpha, t) + |\xi| D^g\left(\frac{x}{\xi}, t\right), \\ E^g(x, \xi, t) &= \int d\beta d\alpha \delta(x - \beta - \xi\alpha) \beta k^g(\beta, \alpha, t) - |\xi| D^g\left(\frac{x}{\xi}, t\right). \end{aligned} \quad (128)$$

Double distributions corresponding to the quark or gluon helicity dependent GPDs \tilde{H} and \tilde{E} are defined as

$$\langle p' | \bar{q}(-\frac{1}{2}z) \not{z} \gamma_5 q(\frac{1}{2}z) | p \rangle \Big|_{z^2=0}$$

$$\begin{aligned}
&= \bar{u}(p') \not{z} \gamma_5 u(p) \int d\beta d\alpha e^{-i\beta(Pz)+i\alpha(\Delta z)/2} \tilde{f}^q(\beta, \alpha, t) \\
&+ \bar{u}(p') \frac{\gamma_5(\Delta z)}{2m} u(p) \int d\beta d\alpha e^{-i\beta(Pz)+i\alpha(\Delta z)/2} \tilde{k}^q(\beta, \alpha, t), \\
&\langle p' | z_\alpha z_\beta (-i) G^{\alpha\mu}(-\frac{1}{2}z) \tilde{G}_\mu^\beta(\frac{1}{2}z) | p \rangle \Big|_{z^2=0} \\
&= \bar{u}(p') \not{z} \gamma_5 u(p) \frac{Pz}{2} \int d\beta d\alpha e^{-i\beta(Pz)+i\alpha(\Delta z)/2} \beta \tilde{f}^g(\beta, \alpha, t) \\
&+ \bar{u}(p') \frac{\gamma_5(\Delta z)}{2m} u(p) \frac{Pz}{2} \int d\beta d\alpha e^{-i\beta(Pz)+i\alpha(\Delta z)/2} \beta \tilde{k}^g(\beta, \alpha, t). \tag{129}
\end{aligned}$$

Except for the absence of D -terms in this sector (see Section 3.9.2) the corresponding reduction relations read as in (124) and (128).

There are different variants of the double distributions defined above. Radyushkin has discussed double distributions $\tilde{F}^q(x, y) = 2f^q(\beta, \alpha)$ using different variables

$$x = \beta, \quad y = \frac{1}{2}(1 - \beta + \alpha), \tag{130}$$

which match more naturally the variables X and ζ for GPDs mentioned in Section 3.1. He has also introduced separate ‘‘quark’’ and ‘‘antiquark’’ double distributions $F^q(x, y)$ and $F^{\bar{q}}(x, y)$, which respectively describe the regions $x > 0$ and $x < 0$ of $\tilde{F}^q(x, y)$. Separate ‘‘quark’’ and ‘‘antiquark’’ GPDs $\mathcal{F}_\zeta^q(X)$ and $\mathcal{F}_\zeta^{\bar{q}}(X)$ are then defined by integrals in the x - y plane. In the DGLAP regions they respectively correspond to Ji’s $H^q(x, \xi)$ in the quark and antiquark regions $x > \xi$ and $x < -\xi$, whereas in the ERBL region $H^q(x, \xi)$ is a linear combination of $\mathcal{F}_\zeta^q(X)$ and $\mathcal{F}_\zeta^{\bar{q}}(X)$. This type of distributions has been discussed in detail in earlier work but not much been used in the recent literature. Details on their relation with Ji’s GPDs can be found in [127, 40].

3.9.1 General properties and evolution

In a similar way as for GPDs one finds that time reversal invariance and hermiticity constrains double distributions to be real valued and even functions of α . This is sometimes referred to as ‘‘Munich symmetry’’ with reference to [123], where it was discovered as a much less obvious symmetry in terms of the variables x and y mentioned above. As we did for GPDs in Section 3.3.2, one can form combinations with definite C -parity,

$$\begin{aligned}
f^{q(\pm)}(\beta, \alpha, t) &= f^q(\beta, \alpha, t) \mp f^q(-\beta, \alpha, t), \\
\tilde{f}^{q(\pm)}(\beta, \alpha, t) &= \tilde{f}^q(\beta, \alpha, t) \pm \tilde{f}^q(-\beta, \alpha, t)
\end{aligned} \tag{131}$$

and their analogs for k^q and \tilde{k}^q . The gluon double distributions f^g and k^g are odd in β , and \tilde{f}^g and \tilde{k}^g are even in β .

Probably the most important aspect of double distributions for practical purposes is that they generate GPDs which automatically satisfy the polynomiality conditions discussed in Section 3.3.3. This is readily checked by taking Mellin moments in x of the reduction formulae (124) and their analogs for the other distributions. In other words, Lorentz invariance restricts the functional form of the x and ξ dependence for GPDs, but not the dependence on double distributions on β and α . To see how this difference comes about one can choose $z^+ = 0$, $\mathbf{z} = 0$ in the definitions (123) and (126), divide by z^- , take the n -th derivative $(d/dz^-)^n$, and then set z^- to zero. On the left-hand sides one then obtains the local twist-two operators (34). The right-hand side of the double distribution definition (123) automatically has the required polynomial dependence on Δ^+ , but not the right-hand

side of the GPD definition (126), where the dependence on Δ^+ is implicit in the ξ dependence of H and E .

Double distributions satisfy evolution equations of the form

$$\mu^2 \frac{d}{d\mu^2} f(\beta, \alpha, t; \mu^2) = \int d\beta' d\alpha' R_{\text{NS}}(\beta, \alpha; \beta' \alpha') f(\beta', \alpha', t; \mu^2) \quad (132)$$

for the quark non-singlet combination, and corresponding matrix equations for the mixed evolution of the quark singlet and gluon distributions. The kernels R readily follow from the kernels K for the evolution of the light-cone operators discussed in Section 3.8.1. Up to global factors R_{NS} , R^{qq} and R^{gg} are obtained by a simple change of arguments, whereas the quark-gluon mixing kernels require differentiation or integration with respect to β because of the factors $(\kappa_2 - \kappa_1)$ and $(\kappa_2 - \kappa_1)^{-1}$ in the matrix kernels (98). Explicit results for the LO kernels can be found in [99, 100], and for the double distribution variables x, y of Radyushkin in [98]. After suitable integration along a line in the β - α plane the kernels R reduce to the evolution kernels for GPDs, including the limiting cases of the DGLAP or ERBL kernels, as shown in detail in [39, 98].

A strategy for solving the evolution equations is to connect the conformal moments (111) of GPDs with the moments of double distributions (see [36] for details)

$$\begin{aligned} C_n^{q,g}(\xi, t; \mu) &= \sum_{\substack{m=0 \\ n-m \text{ even}}}^n a_{nm}^{q,g} \xi^{n-m} \int d\beta d\alpha \beta^m C_{n-m}^{3/2+m}(\alpha) f^{q,g}(\beta, \alpha, t; \mu) \\ &+ (D\text{-term contribution}) \end{aligned} \quad (133)$$

with known numerical coefficients $a_{nm}^{q,g}$. The D -term contribution goes with ξ^{n+1} and only occurs for odd n . We see that the quantities that renormalize multiplicatively (after orthogonalization in the case of quark-gluon mixing) are combined Mellin moments in β and Gegenbauer moments in α of double distributions. Notice that quarks and gluons come with the same Gegenbauer polynomials here. Using their orthogonality one finds from (133) that the Mellin moments have the form

$$\int_{|\alpha|=1}^{1-|\alpha|} d\beta \beta^m f^{q,g}(\beta, \alpha, t; \mu) = (1 - \alpha^2)^{m+1} \sum_{\substack{k=0 \\ \text{even}}}^{\infty} A_{mk}^{q,g}(t; \mu) C_k^{3/2+m}(\alpha), \quad (134)$$

where A_{mk} is related to the conformal moments by

$$C_n^{q,g}(\xi, t; \mu) = \sum_{\substack{m=0 \\ n-m \text{ even}}}^n b_{nm}^{q,g} \xi^{n-m} A_{m,n-m}^{q,g}(t; \mu) + (D\text{-term contribution}) \quad (135)$$

with known numerical coefficients $b_{nm}^{q,g}$. In the above sums n and m are even for the quark nonsinglet and odd for the quark singlet and the gluon distributions. The quark nonsinglet coefficients A_{mk}^q are renormalized multiplicatively with anomalous dimension γ_{m+k} , in analogy to the moments of GDAs in (84). Appropriate linear combinations of quark singlet and gluon coefficients evolve with γ_{m+k}^+ or γ_{m+k}^- instead of γ_{m+k} . One can now easily deduce the behavior of the Mellin moments (134) under evolution to $\mu \rightarrow \infty$. In all cases the term with smallest anomalous dimension is the $k = 0$ term in the sum, so that the moments (134) asymptotically go like $(1 - \alpha^2)^{m+1}$. Furthermore, all Mellin moments vanish asymptotically except those associated with the anomalous dimensions $\gamma_0 = \gamma_1^- = 0$. This leads to asymptotic forms of double distributions going like

$$\begin{aligned} f^{q(-)}(\beta, \alpha) &\stackrel{\mu \rightarrow \infty}{\sim} (1 - \alpha^2) \delta(\beta), \\ f^g(\beta, \alpha), f^{q(+)}(\beta, \alpha) &\stackrel{\mu \rightarrow \infty}{\sim} (1 - \alpha^2)^2 \delta'(\beta). \end{aligned} \quad (136)$$

The resulting GPDs are those given in Section 3.8.3. The evolution of the polarized double distributions $\tilde{f}^{q,g}$ can be solved in analogy to (133) to (135). Apart from the absence of D -terms the difference to the unpolarized case is due to the anomalous dimensions. The asymptotic form for the C -even combinations is thus given by

$$\tilde{f}^{q(+)}(\beta, \alpha) \stackrel{\mu \rightarrow \infty}{\sim} (1 - \alpha^2) \delta(\beta), \quad (137)$$

whereas \tilde{f}^g and $\tilde{f}^{q(-)}$ asymptotically evolve to zero. Analogous forms are of course obtained for $k^{q,g}$ and $\tilde{k}^{q,g}$.

3.9.2 The D -term

We now discuss in more detail the functions D^q and D^g in (123) and (127). As we have seen in Section 3.3.3 the Mellin moments $\int dx x^n H^q$ and $\int dx x^{n-1} H^g$ with odd n are polynomials in ξ of degree $n+1$. As one readily sees from the reduction formulae (124) and (128), the double distributions $f^{q,g}$ and $k^{q,g}$ give maximal powers of ξ^n for these moments, so that the general decompositions of the light-cone matrix elements in (123) and (127) require extra terms. It has been shown in [90] that these extra terms can be chosen to depend only on α but not on β , and that the resulting decomposition in spectral functions f , k , and D is unique.

Important properties of the D -terms are

- The D -term contributions to GPDs have support only in the ERBL region $x \in [-\xi, \xi]$. This makes them an example of information inaccessible in the forward parton distributions.
- There is a D -term for each separate quark flavor and for the gluon. It contributes to either H^g and E^g or to $H^{q(+)}$ and $E^{q(+)}$, but not to the C -odd combinations of quark GPDs. There is no analog of the D term for the helicity dependent distributions $\tilde{H}^{q,g}$ or $\tilde{E}^{q,g}$: as we discussed in Section 3.3.3 their appropriate Mellin moments do not have maximal power ξ^{n+1} but only ξ^n , which is generated by double distributions alone.
- The same function $D^{q,g}$ contributes with opposite sign to $H^{q,g}$ and to $E^{q,g}$ as seen in the reduction formulas (124) and (128). In a sense this is a particularity of decomposing the GPD matrix elements (14) and (18) on the proton vector and tensor currents. If instead one were to take the vector and scalar current of the proton, the corresponding set of GPDs would be $(H + E)$ and E , and the D -term would only contribute to E .
- D -terms also appear for targets with spin zero. For a pion one has

$$\begin{aligned} & \langle \pi^+(p') | \bar{q}(-\frac{1}{2}z) \not{z} q(\frac{1}{2}z) | \pi^+(p) \rangle \Big|_{z^2=0} \\ &= 2(Pz) \int d\beta d\alpha e^{-i\beta(Pz) + i\alpha(\Delta z)/2} f^q(\beta, \alpha, t) \\ &- (\Delta z) \int d\alpha e^{i\alpha(\Delta z)/2} D^q(\alpha, t) \end{aligned} \quad (138)$$

and its analog for gluons. The reduction formulae to the GPDs H_π^q and H_π^g read as in (124) and (128). Due to isospin invariance the $C = +1$ quark combinations have isospin $I = 0$ and the $C = -1$ combinations have isospin $I = 1$. Hence there is a D -term contribution to the isosinglet combination H_π^{u+d} but none to the isotriplet combination H_π^{u-d} . A corresponding statement does *not* hold for the nucleon GPDs, *except* if one considers the large N_c limit (see Section 4.1.2).

- From time reversal one obtains that $D^q(\alpha, t)$ is odd and $D^g(\alpha, t)$ even in α , in accordance with the properties of the corresponding GPDs under the replacement $x \rightarrow -x$.
- D^q and D^g evolve according to the ERBL equations, just like distribution amplitudes with the same quantum numbers. Their Gegenbauer coefficients d_n^q and d_n^g , defined by⁴

$$\begin{aligned} D^q(x, t; \mu) &= (1-x^2) \sum_{\substack{n=1 \\ \text{odd}}}^{\infty} d_n^q(t; \mu) C_n^{3/2}(x), \\ D^g(x, t; \mu) &= \frac{3}{2} (1-x^2)^2 \sum_{\substack{n=1 \\ \text{odd}}}^{\infty} d_n^g(t; \mu) C_{n-1}^{5/2}(x), \end{aligned} \quad (139)$$

thus evolve multiplicatively with anomalous dimension γ_n for the difference of any two quark flavors, and with γ_n^+ and γ_n^- after appropriate diagonalization for the quark flavor singlet and the gluon. Asymptotically one has [37]

$$d_1^q(t; \mu) \stackrel{\mu \rightarrow \infty}{=} \frac{3}{3n_f + 16} d(t), \quad d_1^g(t; \mu) \stackrel{\mu \rightarrow \infty}{=} \frac{16}{3n_f + 16} d(t), \quad (140)$$

with all higher moments going to zero. Note that $d(t) = 5C(t)$ is given by one of the form factors of the total energy-momentum tensor (see Section 3.6), with individual contributions $d_1^q = 5C_q$ and $d_1^g = 5C_g$ from quarks and gluons.

- As we will see in Section 5.1, the contribution of a D -term to hard process amplitudes is energy independent at fixed photon virtuality.

As already mentioned, the D term is uniquely defined for a given hadronic matrix element (122), and one may ask about its direct relation to a given GPD. The D -term contribution is fixed by the coefficients of the appropriate highest power in ξ of the Mellin moments. This can be used to obtain the Mellin moments of D as

$$\begin{aligned} \int_{-1}^1 dx x^{n-1} D^q(x) &= \frac{1}{n!} \left(\frac{\partial}{\partial \xi} \right)^n \int_{-1}^1 dx x^{n-1} H^q(x, \xi, t), \\ \int_{-1}^1 dx x^{n-2} D^g(x) &= \frac{1}{n!} \left(\frac{\partial}{\partial \xi} \right)^n \int_{-1}^1 dx x^{n-2} H^g(x, \xi, t), \end{aligned} \quad (141)$$

where the right-hand sides can be evaluated at any ξ due to the polynomiality condition. In analogy, the Gegenbauer moments of the D term are given by

$$\begin{aligned} \int_{-1}^1 dx C_{n-1}^{3/2}(x) D^q(x) &= \frac{1}{n!} \left(\frac{\partial}{\partial \xi} \right)^n C_{n-1}^q(\xi), \\ \int_{-1}^1 dx C_{n-2}^{5/2}(x) D^g(x) &= \frac{1}{n!} \left(\frac{\partial}{\partial \xi} \right)^n C_{n-1}^g(\xi) \end{aligned} \quad (142)$$

in terms of the conformal moments (111) of the GPDs. Another consequence of polynomiality, reported in [37],

$$\int_{-1}^1 dx \frac{H^q(x, \xi + xz) - H^q(x, \xi)}{x} = \sum_{n=1}^{\infty} z^n \int_{-1}^1 dx x^{n-1} D^q(x) \quad (143)$$

⁴The moments d_n^g defined here coincide with the d_n^G of [37]. The different factors in their eq. (24) and our eq. (139) reflect the different definitions of H^g .

and its analog for gluons is readily checked against (141) by taking the derivative $\partial^n / (\partial z)^n$ and setting z to zero. Resumming the geometric series on the right-hand side we get

$$\int_{-1}^1 dx \frac{D^q(x)}{1-xz} = \int_{-1}^1 dx \frac{H^q(x, \xi + xz) - H^q(x, \xi)}{xz}, \quad (144)$$

where one may take any ξ and $|z| < 1 - |\xi|$, thus staying within the physical region for the second argument of the GPD.

We note that there are alternative ways to generate GPDs with the correct polynomiality properties. For definiteness let us consider the quark distributions in a pion. As observed in the pioneering paper of Polyakov and Weiss [90] a more general parameterization than (138) is

$$\begin{aligned} \langle \pi^+(p') | \bar{q}(-\frac{1}{2}z) \not{z} q(\frac{1}{2}z) | \pi^+(p) \rangle \Big|_{z^2=0} &= 2(Pz) \int d\beta d\alpha e^{-i\beta(Pz)+i\alpha(\Delta z)/2} f^q(\beta, \alpha, t) \\ &- (\Delta z) \int d\beta d\alpha e^{-i\beta(Pz)+i\alpha(\Delta z)/2} g^q(\beta, \alpha, t), \end{aligned} \quad (145)$$

where $2Pz$ and $-\Delta z$ are treated in a symmetric way. This leads to a reduction formula

$$H_\pi^q(x, \xi, t) = \int d\beta d\alpha \delta(x - \beta - \xi\alpha) \left[f^q(\beta, \alpha, t) + \xi g^q(\beta, \alpha, t) \right]. \quad (146)$$

In analogy one may generalize the D -term in the decompositions (123) for a spin $\frac{1}{2}$ target to a double distribution depending on both β and α [90]. The decomposition (145) into functions f^q and g^q is not unique. Teryaev [129] has pointed out its invariance under the combined transformations

$$\begin{aligned} f^q(\beta, \alpha, t) &\rightarrow f^q(\beta, \alpha, t) + \frac{\partial}{\partial \alpha} \varphi(\beta, \alpha, t), \\ g^q(\beta, \alpha, t) &\rightarrow g^q(\beta, \alpha, t) - \frac{\partial}{\partial \beta} \varphi(\beta, \alpha, t), \end{aligned} \quad (147)$$

for a sufficiently regular function φ vanishing at the boundary $|\beta| + |\alpha| = 1$ of the support region. He has also noted the analogy with a gauge transformation in two-dimensional magnetostatics, with (f, g) being the analog of the potential (A^x, A^y) and $(\alpha, -\beta)$ playing the role of the spatial coordinates (x, y) . The freedom (147), which readily follows from (145) via integration by parts, may be used to transform g^q to a function independent of β . This function is then just the D -term of (138) in the C -even sector, and zero in the C -odd sector. The invariance property (147) of the general decomposition (145) has important consequences for constructing models (see Section 4.3.4).

Suggestions have also been made to parameterize the matrix element in (145) by a single function. In [130] it was proposed to define double distributions that reduce to $x^{-1} H_\pi^q(x, \xi, t)$ instead of H_π^q as in (124). This clearly raises the highest power in ξ of the Mellin moments by 1. A different possibility [129] is to take double distributions to generate $\partial / (\partial x) H_\pi^q(x, \xi, t)$. Neither suggestion has much been pursued in the literature, because the $\xi = 0$ limits of $x^{-1} H_\pi^q$ and $\partial / (\partial x) H_\pi^q$ have stronger singularities than H_π^q at $x = 0$, which turns out to be unpleasant for modeling purposes, see Section 4.3. More recently Pobylytsa [43] has considered double distributions which reduce to $(1-x)^{-1} H_\pi^q(x, \xi, t)$ instead of H_π^q .

3.9.3 The crossed channel and the inversion formula

It is straightforward to obtain a GPD from the corresponding double distribution (and the associated D -term if appropriate), and it is natural to ask how to compute a double distribution from a given GPD. This inversion problem has been solved in [130, 129], with an earlier partial result in [127].

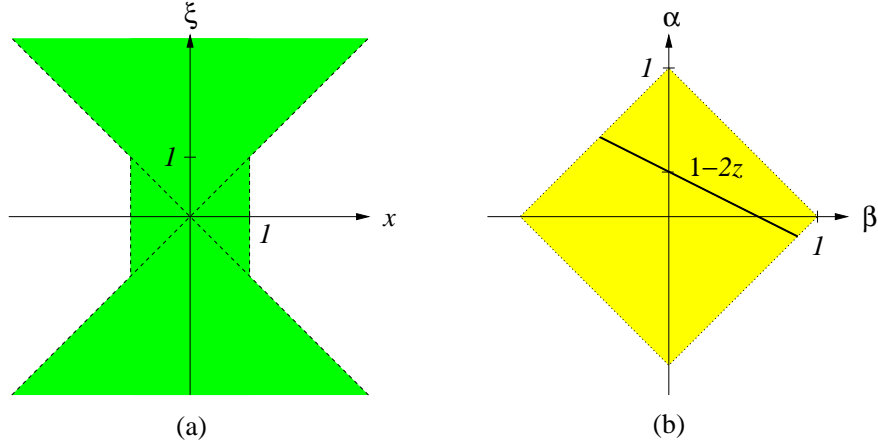


Figure 11: (a) Support region of GPDs following from the reduction formula (124). (b) Line of integration to obtain a GDA from a double distribution according to the reduction formula (149).

Unfortunately this solution is difficult to use in practice; it is however instructive to see why that is the case.

Let us first try to invert the double Fourier transform (123) defining our double distributions, after appropriately projecting out a chosen proton spinor structure. Given the finite support of the double distributions (assumed to be sufficiently well-behaved), the Fourier integrals in (123) are defined for all Pz and Δz . The matrix element on the left-hand side is however restricted to the region $|\Delta z| < 2|Pz|$. To see this, choose a frame with $z^+ = 0$ with $\mathbf{z} = 0$, where this condition reads $|p'^+ - p^+| < p'^+ + p^+$, i.e. $|\xi| < 1$ and follows from the positivity of the plus-momentum for physical states. To invert the double Fourier transform in (123) one thus needs an appropriate continuation of the light-cone matrix elements to the unphysical region $|\Delta z| \geq 2|Pz|$.

Similarly, the right-hand side of the reduction formula (124) gives a nonzero result outside the physical region $|x| < 1$ and $|\xi| < 1$. Given the support properties of double distributions and the D -term this additional region is given by $|x| < |\xi|$ for $|\xi| > 1$. The full region of support of the functions H, E defined by the representation (124) is the hour-glass shaped region shown in Fig. 11a, and for $|\xi| > 1$ the corresponding lines in the β - α plane have a slope $-1/\xi$ between -1 and 1 as shown in Fig. 11b.

Clearly $|\xi| > 1$ requires one of the plus-momentum fractions p^+ or p'^+ to be negative. This should remind us of the crossing relation between GPDs and GDAs discussed in Section 3.7. In fact, one can represent the crossed matrix element relevant for GDAs by double distributions and a D -term in full analogy to (123). For the simpler case of pions one has [129, 131]

$$\begin{aligned}
& \langle \pi^+(p) \pi^-(p') | \bar{q}(-\frac{1}{2}x) \not{x} q(\frac{1}{2}x) | 0 \rangle \Big|_{x^2=0} \\
&= (p - p')x \int d\beta d\alpha e^{-i\beta(p-p')x/2 + i\alpha(p+p')x/2} f^q(\beta, \alpha, s) \\
&- (p + p')x \int d\alpha e^{i\alpha(p+p')x/2} D^q(\alpha, s)
\end{aligned} \tag{148}$$

as crossed version of (138), and a reduction formula

$$\begin{aligned}
-\frac{1}{2}\Phi^q(z, \zeta, s) &= (1 - 2\zeta) \int d\beta d\alpha \delta\left((1 - 2z) - \beta(1 - 2\zeta) - \alpha\right) f^q(\beta, \alpha, s) \\
&+ D^q(1 - 2z, s).
\end{aligned} \tag{149}$$

Analogous expressions hold for gluons. The spectral functions $f^q(\beta, \alpha, s)$ and $D^q(\alpha, s)$ are the analytic continuation of the double distributions to positive values of the invariant t (which in the GDA channel we call s). For positive t , integrals of double distributions over the lines with slope between -1 and 1 in Fig. 11b thus generate GDAs in their physical region, with the slope equal to $2\zeta - 1$ and the intercept with the α -axis at $1 - 2z$. The case of zero slope, i.e. integration over β at fixed α corresponds to a GDA at the particular point $\zeta = \frac{1}{2}$. This confirms the interpretation of α as a DA-like variable, which underlies most intuition about what the functional dependence of double distribution may be.

Let us assume that one has obtained H or E in the unphysical region $|\xi| \geq 1$, for instance by analytically continuing the corresponding $p\bar{p}$ distribution amplitudes from their physical region to $s < 0$. It is then indeed possible to invert the reduction formula (124): the particular integral over the double distribution there is known as a Radon transform (for references see [130, 129]), whose inversion can be obtained via its relation to Fourier transformation. One finds [129]

$$f^q(\beta, \alpha) = -\frac{1}{2\pi^2} \int_{-\infty}^{\infty} d\xi \int_{-\infty}^{\infty} dz \frac{H_{DD}^q(z + \beta + \alpha\xi, \xi) - H_{DD}^q(\beta + \alpha\xi, \xi)}{z^2} \quad (150)$$

where $H_{DD}^q(x, \xi) = H^q(x, \xi) - \text{sgn}(\xi)D^q(x/\xi)$ has the D -term subtracted. Analogous relations exist for the gluon distributions. For the case where $H^q(x, \xi)$ has a non-integrable singularity at $x = 0$ we refer to [130].

A similar task is to calculate the D -term for a given GPD. Also here there is no known closed expression which would not either involve a moment inversion or knowledge of H or E outside their physical regions. As remarked in [130] one has $D^q(z) = \frac{1}{2} \lim_{\xi \rightarrow \infty} H^{q(+)}(z\xi, \xi)$, which can be seen from the reduction formula (124). For gluons one has correspondingly $D^g(z) = \lim_{\xi \rightarrow \infty} \xi^{-1} H^g(z\xi, \xi)$. We remark that the relation (144) for D has the form of a Hilbert transform and admits an explicit inversion, which requires one to know the right-hand side of (144) for all values of z . This needs again a continuation of the GPDs to skewness $|\xi| > 1$. It is amusing to note that in the crossed channel, the D term is easily reconstructed from the GDA at $\zeta = \frac{1}{2}$, as seen in (149).

3.10 Impact parameter space

Our discussion and interpretation of GPDs so far was in momentum space. An intuitive physical picture can also be obtained in position space, which we will now present. More precisely, we will use a “mixed representation”, keeping momentum in the light-cone plus-direction, but Fourier transforming from transverse momentum to transverse position, called “impact parameter” in this context. This representation is useful in a variety of contexts, such as high-energy scattering (see Section 8) or the resummation of Sudakov logarithms in hard processes [132]. Its use in the context of GPDs has been pioneered by Burkardt with emphasis on the case $\xi = 0$, where a density interpretation is possible, see the original work [26] and the detailed review [133]. This framework has been extended to nonzero ξ in [134]. From a more general perspective, Ralston and Pire [135] have highlighted the analogy with imaging techniques: the Fourier transform occurs in geometrical optics, with light rays corresponding to momentum space and an image plane to transverse position, or in X -ray diffraction of crystals, where the diffraction pattern has to be Fourier transformed to recover spatial information.

The first step in constructing impact parameter GPDs is to form hadron states with definite plus-momentum and definite position \mathbf{b} in the transverse plane (and hence undetermined transverse momentum):

$$|p^+, \mathbf{b}, \lambda\rangle = \int \frac{d^2\mathbf{p}}{16\pi^3} e^{-i\mathbf{p}\mathbf{b}} |p^+, \mathbf{p}, \lambda\rangle. \quad (151)$$

Choosing states of definite light-cone helicity on the right-hand side we find that under a rotation by φ about the z axis this state transforms as $|p^+, \mathbf{b}, \lambda\rangle \rightarrow e^{-i\lambda\varphi} |p^+, \mathbf{b}', \lambda\rangle$, where \mathbf{b}' is related to \mathbf{b} by the

same rotation. Under a spatial translation by \mathbf{a} the state transforms like $|p^+, \mathbf{b}, \lambda\rangle \rightarrow |p^+, \mathbf{b} + \mathbf{a}, \lambda\rangle$, as one would expect.

Of course, the proton is an extended object, and we should make it more explicit what “localized in the transverse plane” means. The key to this is the analogy of transverse boosts (50) with Galilean transformations in two-dimensional nonrelativistic mechanics. In this analogy, \mathbf{v} in (50) corresponds to the velocity characterizing the transformation, and k^+ to the mass of the particle. The conserved quantity following from Galilean invariance is the center-of-mass coordinate, $\mathbf{r} = \sum m_i \mathbf{r}_i / \sum m_i$ of a many-body system, and by analogy the conserved quantity following from invariance under transverse boosts is the “center of plus-momentum” [136] or “transverse center of momentum” [137] $\mathbf{b} = \sum p_i^+ \mathbf{b}_i / \sum p_i^+$ of the partons in the proton state (151). We will explicitly obtain this result in the wave function representation, see Section 3.11. The field-theoretical operator for the center of plus-momentum is constructed from the generators B^i of transverse boosts as [54]

$$R^i = -(P^+)^{-1} B^i, \quad i = 1, 2. \quad (152)$$

It has commutation relations $[R^i, P^j] = i\delta^{ij}$ and $[J^3, R^i] = i\epsilon^{3ij} R^j$ as befits a position operator in the transverse plane. From the explicit form $B^i = \int dx^- d^2\mathbf{x} M^{++i}(x)$, where $M^{\alpha\mu\nu}$ is the angular-momentum density (65), we get

$$R^i = (P^+)^{-1} \int dx^- d^2\mathbf{x} x^i T^{++}(x) \Big|_{x^+=0} \quad (153)$$

in terms of the energy-momentum tensor T^{++} . Having taken T^{++} at $x^+ = 0$ we can rewrite it in terms of the parton creation and annihilation operators in light-cone quantization, and confirm our interpretation of \mathbf{R} : it is determined by the transverse positions of the partons, weighted by their plus-momentum fractions with respect to the total plus-momentum P^+ of the hadron [133].

Taking matrix elements of the precisely localized states $|p^+, \mathbf{b}, \lambda\rangle$ can lead to infinities due to their normalization. This can be avoided by forming wave packets, integrating over \mathbf{p} in (151) with a weight that falls off sufficiently fast at large $|\mathbf{p}|$. There is a further condition if we wish to identify the state $|p^+, \mathbf{b}, \lambda\rangle$ of definite p^+ as a hadron moving along the z axis with a definite three-momentum, since $p^3 = (p^+ - p^-)/\sqrt{2}$ and $p^- = (\mathbf{p}^2 + m^2)/(2p^+)$. To prevent p^3 from varying too much at given p^+ (and from becoming negative for too large $|\mathbf{p}|$) we must restrict the relevant range of integration in (151) to $|\mathbf{p}| \ll p^+$. By the uncertainty principle we can then achieve a transverse localization $\Delta b_T \sim 1/\Delta p_T \gg 1/p^+$. This is however not a strong restriction in a frame where the proton moves sufficiently fast in the z -direction, and it is anyway in such a frame that the parton picture is most adequate. With this in mind we will use the sharply localized states $|p^+, \mathbf{b}, \lambda\rangle$ in the following; explicit calculations with wave packets can be found in [26, 134].

The impact parameter representation of GPDs is obtained by Fourier transforming the light-cone matrix elements $F_{\lambda'\lambda}$ and $\tilde{F}_{\lambda'\lambda}$ with respect to the vector \mathbf{D} defined in (51). The result reads [134]

$$\begin{aligned} & \int \frac{d^2\mathbf{D}}{(2\pi)^2} e^{-i\mathbf{D}\mathbf{b}} \left[H - \frac{\xi^2}{1-\xi^2} E \right] \\ &= \mathcal{N}^{-1} \frac{1+\xi^2}{(1-\xi^2)^{5/2}} \left\langle p'^+, -\frac{\xi\mathbf{b}}{1-\xi}, +\frac{1}{2} \left| \mathcal{O}(\mathbf{b}) \right| p^+, \frac{\xi\mathbf{b}}{1+\xi}, +\frac{1}{2} \right\rangle, \\ & \frac{i}{2m} \left(\frac{\partial}{\partial b^1} + i \frac{\partial}{\partial b^2} \right) \int \frac{d^2\mathbf{D}}{(2\pi)^2} e^{-i\mathbf{D}\mathbf{b}} E \\ &= \mathcal{N}^{-1} \frac{1+\xi^2}{(1-\xi^2)^{5/2}} \left\langle p'^+, -\frac{\xi\mathbf{b}}{1-\xi}, -\frac{1}{2} \left| \mathcal{O}(\mathbf{b}) \right| p^+, \frac{\xi\mathbf{b}}{1+\xi}, +\frac{1}{2} \right\rangle \end{aligned} \quad (154)$$

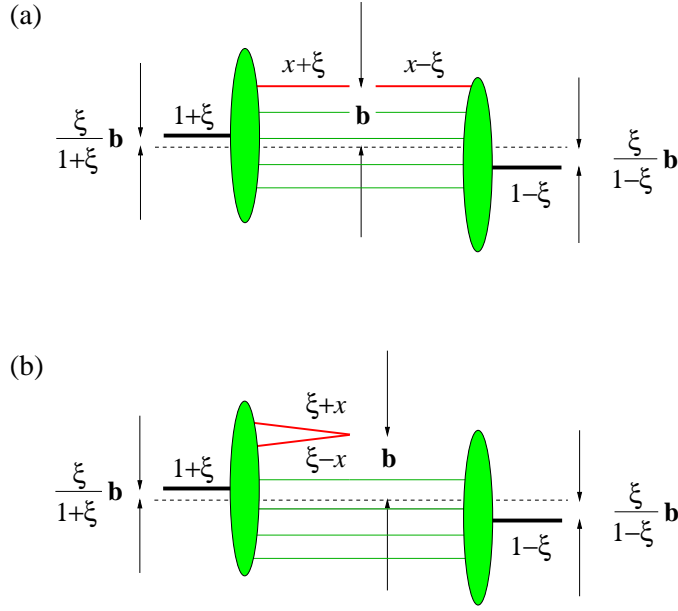


Figure 12: Representation of a GPD in impact parameter space. Plus-momentum fractions refer to the average proton momentum $\frac{1}{2}(p+p')$ and are indicated above or below lines. The region $x \in [\xi, 1]$ is shown in (a), and the region $x \in [-\xi, \xi]$ in (b).

with the quark-antiquark operator

$$\mathcal{O}(\mathbf{b}) = \int \frac{dz^-}{4\pi} e^{ixP^+z^-} \bar{q}(0, -\frac{1}{2}z^-, \mathbf{b}) \gamma^+ q(0, \frac{1}{2}z^-, \mathbf{b}), \quad (155)$$

where position arguments of fields are given in the form $q(z) = q(z^+, z^-, \mathbf{z})$. Analogous expressions exist for the Fourier transforms of helicity dependent and gluon GPDs. Note that the Fourier transform is to be taken at fixed x and ξ , so that the t dependence of the GPDs has to be rewritten using (52). Under this transform the prefactor $e^{i\varphi}|\mathbf{D}| = D^1 + iD^2$ in the helicity flip matrix element F_{-+} has turned into derivatives with respect to the components of \mathbf{b} . The factor $\mathcal{N} = (64\pi^4)^{-1} \int d^2\mathbf{p}$ in (154) comes from the normalization of the states $|p^+, \mathbf{b}, \lambda\rangle$ and is singular like $\delta^{(2)}(\mathbf{0})$ as hinted at above. It becomes finite for proton states whose transverse position is smeared out.

Let us now discuss several aspects of the representation (154), visualized in Fig. 12.

- The impact parameter representation offers an intuitive picture of the information encoded in GPDs. According to the range of x the quark-antiquark operator either describes the emission and reabsorption of a quark (or antiquark) at transverse position \mathbf{b} , or the emission of a quark-antiquark pair at position \mathbf{b} . The transverse locations of the initial and final state proton are shifted relative to each other by an amount of order $\xi\mathbf{b}$. In the DGLAP region the struck quark suffers a loss of plus-momentum proportional to ξ , so that the weighting of transverse parton positions in the proton is different in the initial and the final state. Similarly, in the ERBL region the proton “loses” a quark-antiquark pair, which leads to a shift of its center of plus-momentum.
- Since this shift is proportional to ξ , it makes sense to say that for small ξ the impact parameter GPDs are “almost” diagonal in transverse space. This is in contrast to the longitudinal degrees

of freedom, because the plus-momenta are still very asymmetric between the initial and final state if x is of order ξ , even if ξ is small.

We also notice that the transverse shift depends on ξ but not on x . In this sense, the transverse information is not “washed out” if one integrates the GPDs over x with a weight depending on x and ξ . This is of practical importance, because it is in such a convolution that GPDs appear in the amplitudes of hard processes, and to reconstruct functions of x from the convolution is a delicate problem. The information that *is* affected by integration over x is the separation of the DGLAP and ERBL regimes, which correspond to different physical configurations in terms of quarks and antiquarks. Note however that for processes like DVCS and meson electroproduction the imaginary part of the amplitude comes only from the point $x = \xi$ to lowest order in α_s , and only from the DGLAP region beyond tree approximation. Similarly, the separation of the two partonic regimes of Fig. 12 is lost when one goes from the mixed representation with its definite plus-momenta to the position representation in full three-dimensional space. This was proposed in [135] but has not been very much explored yet. The position space operators appearing in the matrix elements defining GPDs contain both quark and antiquark modes, and the distinction of the two is naturally made in the space of frequencies or (on the light-cone) of plus-momenta.

- In practice one will only ever have experimental information on GPDs in a limited range of t and thus of \mathbf{D} , so that the integrals in (154) can only be evaluated if one either cuts off the integration range or extrapolates the integrand. One may also weight the integrand in (154) with a smooth function that suppresses values $|\mathbf{D}|$ above some ΔD_T . As shown in [134] this corresponds to smoothly smearing out the relative transverse positions of hadrons and partons in Fig. 12 by an amount of order $\Delta b_T \sim 1/\Delta D_T$. Whatever the procedure, with information on GPDs up to a momentum transfer $|t|_{\max}$ one can only localize partons up to order $(|t|_{\max} - |t_0|)^{-1/2}$.

It is important to distinguish this resolution limit from the resolution described by the renormalization scale μ of the GPDs, set by the hardness of the probe in the reaction where GPDs are measured. Since the evolution equations involve GPDs at fixed ξ and t , their Fourier transform with respect to \mathbf{D} is straightforward, and impact parameter GPDs evolve exactly like their t -dependent counterparts. As for ordinary parton distributions one may think of μ as a cutoff on transverse momenta in the theory (with a sufficient amount of caution concerning the effects of a cutoff regularization on Lorentz and gauge symmetries). The partons described by the bilocal operators then have an effective size or extension of order $1/\mu$, and may reveal themselves as consisting of several partons at finer spatial resolution [138]. The scale μ thus specifies *what* the partons are that are probed in the two regimes of Fig. 12, whereas the maximum $|t|$ of the measurement limits the ability to determine *where* these partons are located in the proton.

In the preceding discussion we have again assumed the $A^+ = 0$ gauge, which is natural for the parton interpretation. We remark that (154) holds in any other gauge, with a Wilson line along a light-like path inserted between the two quark fields. Although this will modify the partonic interpretation in a way that has not much been explored so far, it should not alter the basic picture we have obtained on the transverse structure, since the additional A^+ gluons in the Wilson line are all at the same impact parameter \mathbf{b} as the struck partons in Fig. 12.

A brief comment is in order concerning the choice of the momentum variable \mathbf{D} and the Fourier conjugate impact parameter \mathbf{b} . In [139, 140] the impact parameter was defined with respect to $\tilde{\mathbf{D}} = (1 - \xi^2)\mathbf{D}$, which equals $\mathbf{\Delta}$ in frames where $\mathbf{p}' = -\mathbf{p} = \frac{1}{2}\mathbf{\Delta}$. With this choice of variables one has e.g.

$$\int \frac{d^2\tilde{\mathbf{D}}}{(2\pi)^2} e^{-i\tilde{\mathbf{D}}\tilde{\mathbf{b}}} \left[H - \frac{\xi^2}{1 - \xi^2} E \right] = \mathcal{N}^{-1} \frac{1 + \xi^2}{(1 - \xi^2)^{1/2}} \left\langle p'^+, -\xi\tilde{\mathbf{b}}, +\frac{1}{2} \left| \mathcal{O}(\tilde{\mathbf{b}}) \right| p^+, \xi\tilde{\mathbf{b}}, +\frac{1}{2} \right\rangle, \quad (156)$$

which looks even simpler than (154). We will however find that the variable \mathbf{b} leads to more natural expressions in the context of the wave function representation, see Section 3.11. In fact, the different transverse variables in (154) reflect the difference of longitudinal momenta. The variables \mathbf{b} and $\tilde{\mathbf{b}}$ describe of course the same physics, just as the different sets of plus-momentum fractions common in the literature.

3.10.1 The case $\xi = 0$

We have seen that for nonzero skewness ξ GPDs are nondiagonal both in longitudinal momenta and in impact parameter. For $\xi = 0$ one recovers a symmetric configuration in both variables, and if one chooses the same polarization for the initial and final state proton, one obtains the interpretation as a density of quarks or gluons with momentum fraction x and transverse distance \mathbf{b} from the proton center [26]. More precisely, for $x > 0$ the Fourier transform of H^q gives the density of quarks with any helicity, whereas the transform of \tilde{H}^q is the difference of densities for positive-helicity and negative-helicity quarks, with $x < 0$ corresponding to antiquarks as usual. This joint information about longitudinal momentum and transverse location can be reduced in two ways. Taking the integral over \mathbf{b} one recovers the case $t = 0$ in momentum space and thus the usual parton distributions with their familiar density interpretation.

Integrating over x one obtains the Fourier transforms of elastic form factors, F_1^q from H^q and g_A^q from \tilde{H}^q , as *two-dimensional* densities (or density differences) [136]. As emphasized in [26] this is different from the more familiar interpretation of Fourier transformed form factors as *three-dimensional* densities in the non-relativistic limit, which goes back to Sachs [84] and underlies the work of Polyakov and Shuvaev [82, 83] briefly discussed at the end of Section 3.6. The three-dimensional density interpretation refers to a hadron at rest and receives relativistic corrections, see the discussion in [26]. These corrections reflect that one cannot localize the hadron in all three dimensions more accurately than within its Compton wavelength. An extension of this framework using the concept of phase space distributions has recently been proposed by Belitsky [141] and Ji [142]. In contrast, the interpretation obtained here refers to a hadron moving fast. It gives a density in the plane transverse to the direction of motion and is fully relativistic. Even the Fourier transforms from momentum to position space are different in the two cases, being two-dimensional in one and three-dimensional in the other.

One may wonder how form factors like $F_1(t)$ at small to moderate t can carry any information about partons, which can only be resolved by probes with large virtuality. The solution of this apparent paradox is that F_1 is the form factor of the conserved current $\bar{q}(x)\gamma^\mu q(x)$ and thus does not depend on a renormalization scale μ : it is the same whether directly measured in elastic scattering at moderate t or obtained via a sum rule from GPDs measured in hard processes. In more physical terms, F_1 measures the transverse distribution of charge, which is insensitive to whether one resolves individual partons or not.

Whereas the integrals of quark GPDs over x have lost any reference to the longitudinal parton momentum, some information about it is retained when taking higher moments in x . Fourier transforming the integral $\int dx x H^q$ to impact parameter space gives the transverse distribution of partons weighted with their momentum fraction. Such higher moments do depend on a resolution scale μ , which is physically plausible since for instance the DGLAP-type splitting of a quark into a quark and a gluon transfers momentum from quarks to gluons. Only the sum $\sum_q \int_{-1}^1 dx x H^q + \int_0^1 dx H^g$ over all partons, corresponding to the conserved total energy-momentum tensor, gives a transverse density of plus-momentum which does not evolve with the resolution scale μ .

A density interpretation of the distributions E^q and E^g at $\xi = 0$ is more subtle, since the corresponding matrix elements are still non-diagonal in the proton helicity, see (154). One can however

diagonalize by the usual trick of changing basis from helicity states $|+\rangle_z$ and $|-\rangle_z$ to transversity states $|\pm\rangle_x = \frac{1}{\sqrt{2}}(|+\rangle_z \pm |-\rangle_z)$. For a particle at rest the new basis states are polarized along the positive or negative x -axis, but for our fast-moving and transversely localized protons (151) they are not eigenstates of the angular momentum operator J^1 along the x -axis, and their physical meaning is not quite clear. This reflects the notorious difficulty of defining transverse spin for relativistic particles and the complicated nature of transverse spin operators in the light-cone framework, see e.g. [51]. Proceeding nevertheless along this line, Burkardt has obtained several physically rather intuitive results [133]. The Fourier transforms of E^q and E^g describe a relative shift in the transverse density of partons along the y direction between the polarization states $|+\rangle_x$ and $|-\rangle_x$, or between the states $|+\rangle_x$ and $|+\rangle_z$. The moments $F_2^q = \int dx E^q$ and $\int dx x E^q$ at $\xi = 0$ and $t = 0$ are related with the corresponding averages $\langle b^y \rangle$ and $\langle x b^y \rangle$ for quarks. Conservation of the transverse center of momentum implies that the sum of $\langle x b^y \rangle$ over all parton species is zero in a hadron with zero center of momentum, which provides another derivation of the sum rule (74) for the distributions E^q and E^g in the forward limit. Burkardt also notes that the shift in the transverse distribution of partons in a polarized state $|+\rangle_x$ is consistent with the classical picture of a polarized proton as a rotating sphere.

The distributions \tilde{E}^q and \tilde{E}^g have no representation analogous to the ones we have just discussed, since at $\xi = 0$ they decouple from the matrix elements $\tilde{F}_{\lambda'\lambda}$ in (54). As discussed in Section 3.5.4 this is a constraint from time reversal invariance. In the present context it implies that the densities in x and \mathbf{b} one can form with the light-cone operators $\bar{q}\gamma^+\gamma_5 q$ and $G^{+\mu}\tilde{G}_\mu^+$ are described by the Fourier transforms of \tilde{H}^q and \tilde{H}^g alone, for any superposition of the helicity states $|+\rangle_z$ and $|-\rangle_z$.

To conclude this subsection let us point out that there is another class of hadronic matrix elements that carries information on both the transverse and longitudinal structure of partons, namely k_T dependent or k_T unintegrated parton distributions (see e.g. [143, 144] and also Section 8.1). In momentum space they specify the transverse momentum of the struck parton. This corresponds to different transverse positions of the emitted and the reabsorbed parton in the DGLAP regime, and to different transverse positions of the two emitted partons in the ERBL region. The centers of plus-momentum of the incoming and outgoing hadron are shifted accordingly. The Fourier transforms of unintegrated parton distributions with respect to the parton k_T thus describe correlations of the transverse location of partons within a hadron, and thus never represent densities in impact parameter space. A more detailed discussion is given in [134]. The connection between parton distributions in impact parameter space and those depending on parton k_T has recently been explored by Burkardt [145, 146] with focus on the spin and angular momentum structure of the nucleon.

3.10.2 GDAs in impact parameter space

In close analogy to the case of GPDs one can derive an impact parameter representation for GDAs, as shown by Pire and Szymanowski [147]. One starts by introducing two-pion states in the impact parameter representation,

$$|\pi^+(p^+, \mathbf{b}) \pi^-(p'^+, \mathbf{b}')\rangle_{\text{out}} = \int \frac{d^2\mathbf{p}}{16\pi^3} \frac{d^2\mathbf{p}'}{16\pi^3} e^{-i\mathbf{p}\mathbf{b} - i\mathbf{p}'\mathbf{b}'} |\pi^+(p^+, \mathbf{p}) \pi^-(p'^+, \mathbf{p}')\rangle_{\text{out}}. \quad (157)$$

Strictly speaking, one has to form appropriate wave packets to ensure that in the far future one has two pions with a large separation along the z axis (even though their separation in the transverse plane may be small, even compared with the pion radius). Only then may one neglect their interactions, treat them as individual free particles, and interpret (157) as two separate pions with fixed plus-momenta and transverse positions. One proceeds by decomposing the invariant mass of the pair into

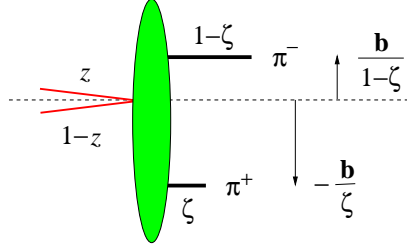


Figure 13: Impact parameter representation of the two-pion distribution amplitude. Plus-momentum fractions z and ζ refer to the sum of the pion plus-momenta

terms coming from longitudinal and transverse momentum components,

$$s = \frac{m^2}{\zeta(1-\zeta)} + \zeta(1-\zeta)\mathbf{D}^2, \quad (158)$$

where the vector D is defined in the GDA channel by

$$D = \frac{p}{\zeta} - \frac{p'}{1-\zeta}. \quad (159)$$

One then finds for the GDA in impact parameter space

$$\begin{aligned} & \int \frac{d^2\mathbf{D}}{(2\pi)^2} e^{-i\mathbf{D}\mathbf{b}} \Phi^q(z, \zeta, s) \\ &= \mathcal{N}^{-1} \frac{\zeta^2 + (1-\zeta)^2}{\zeta^2(1-\zeta)^2} \left\langle \pi^+ \left(p^+, -\frac{\mathbf{b}}{\zeta} \right) \pi^- \left(p'^+, \frac{\mathbf{b}}{1-\zeta} \right) \left| \mathcal{O}(\mathbf{0}) \right| 0 \right\rangle \end{aligned} \quad (160)$$

with the same quark-antiquark operator \mathcal{O} and normalization factor \mathcal{N} as above. The physical interpretation is shown in Fig. 13: a quark-antiquark pair at transverse position zero hadronizes into two pions with transverse separation $\zeta^{-1}(1-\zeta)^{-1}\mathbf{b}$. The overall center of plus-momentum is conserved in this process. As discussed in [147] one can for instance see how hadronization into a pion pair with s close to a squared resonance mass m_R^2 translates into typical transverse distances of order $1/m_R$. Hadronization into pairs of very large invariant mass s corresponds to small transverse distances between the initial $q\bar{q}$ pair and the center of momentum of each final-state pion, which provides a physical picture for the perturbative mechanism discussed in Section 4.6.3.

3.11 The wave function representation

GPDs can be represented in terms of the wave functions for the target. This offers a further way to make explicit which kind of information on hadron structure is contained in these quantities. Certain properties of GPDs, in particular the positivity constraints discussed in Section 3.12 are naturally derived from this representation, which furthermore has been used as a strategy to model GPDs, see Section 4.1.6. It can equally be given in momentum space and in the impact parameter representation.

3.11.1 Fock space decomposition

The wave function representation is most naturally obtained in the framework of light-cone quantization and of $A^+ = 0$ gauge, and has been derived and discussed in [41, 134] (whose notation we

will follow here) and in [148]. Starting point is the Fock state expansion in QCD quantized on the light-cone [50], where a hadron state is represented in terms of the partonic Fock states created from the vacuum by the operators b^\dagger , d^\dagger , a^\dagger , which appear in the decompositions (45), (46) of the good components of quark and gluon fields. This expansion reads

$$\begin{aligned}
|p^+, \mathbf{p}, \lambda\rangle &= \sum_{N, \beta} \frac{1}{\sqrt{f_{N\beta}}} \int [dx]_N [d^2\mathbf{k}]_N \Psi_{N\beta}^\lambda(x_i, \mathbf{k}_i) \\
&\times \prod_{i=1}^{N_q} \frac{1}{\sqrt{x_i}} b^\dagger(x_i p^+, \mathbf{k}_i + x_i \mathbf{p}) \prod_{i=N_q+1}^{N_q+N_{\bar{q}}} \frac{1}{\sqrt{x_i}} d^\dagger(x_i p^+, \mathbf{k}_i + x_i \mathbf{p}) \\
&\times \prod_{i=N_q+N_{\bar{q}}+1}^N \frac{1}{\sqrt{x_i}} a^\dagger(x_i p^+, \mathbf{k}_i + x_i \mathbf{p}) |0\rangle, \tag{161}
\end{aligned}$$

where N specifies the number of partons in a Fock state, and β collectively labels its parton composition and the discrete quantum numbers (flavor, color, helicity) for each parton. $f_{N\beta}$ is a normalization constant providing a factor $n!$ for each subset of n partons with identical discrete quantum numbers (not explicitly labeled in the operators for brevity). For the N -parton integration elements we have used the shorthand notation

$$\begin{aligned}
[d^2\mathbf{k}]_N &= (16\pi^3)^{-N+1} \prod_{i=1}^N d^2\mathbf{k}_i \delta^{(2)}\left(\sum_{i=1}^N \mathbf{k}_i\right), \\
[dx]_N &= \prod_{i=1}^N dx_i \delta\left(1 - \sum_{i=1}^N x_i\right). \tag{162}
\end{aligned}$$

The wave functions Ψ depend on the momentum variables of each parton only via its light-cone momentum fraction $x_i = k_i^+/p^+$ and via its transverse momentum \mathbf{k}_i relative to the transverse momentum of the hadron. This is an important consequence of Lorentz invariance on the light-cone: the state $|p^+, \mathbf{p}, \lambda\rangle$ can be obtained from a proton state at rest by a combination of a longitudinal boost (to the state $|p^+, \mathbf{0}, \lambda\rangle$) and a transverse boost. In the literature different conventions for light-cone wave functions are used as far as kinematical and overall factors are concerned. Our wave functions here are normalized such that

$$P_{N\beta}^\lambda = \int [dx]_N [d^2\mathbf{k}]_N \left| \Psi_{N\beta}^\lambda(x_i, \mathbf{k}_i) \right|^2 \tag{163}$$

is the probability to find the corresponding Fock state in the proton, so that in total $\sum_{N, \beta} P_{N\beta}^\lambda = 1$.

Light-cone wave functions can be represented as matrix elements between the hadron state and the vacuum, with operators formed from the relevant quark or gluon field components at vanishing light-cone time z^+ . As a simple example consider the $q\bar{q}$ Fock state in a pion, with opposite parton helicities. Its wave function can be projected out as

$$\begin{aligned}
\Psi_{+-}(x, \mathbf{k} - x\mathbf{p}) & \tag{164} \\
&= -\frac{1}{2\sqrt{3}} \int dz^- d^2\mathbf{z} e^{i(2x-1)p^+z^-/2} e^{-i(2\mathbf{k}-\mathbf{p})\mathbf{z}/2} \langle \pi(p) | \bar{q}(-\frac{1}{2}z) \gamma^+ \gamma_5 q(\frac{1}{2}z) | 0 \rangle \Big|_{z^+=0},
\end{aligned}$$

where for simplicity we have only given the momentum arguments of the quark.⁵ The subscripts $+$ and $-$ respectively refer to the quark and antiquark helicities, and we have used the parity constraint

⁵Following common usage we have summed over quark colors on the right-hand side of (164), corresponding to the wave function for a $q\bar{q}$ state coupled to zero color.

$\Psi_{+-} = -\Psi_{-+}$ for a pion. Configurations with equal parton helicities are obtained from the tensor operator $\bar{q}\sigma^{+i}q$ we have encountered in the discussion of helicity flip GPDs, see [149]. The operators projecting out three-quark wave functions in a proton have been given in [150].

Integrating a light-cone wave function over the transverse momenta of all partons (after weighting with appropriate factors of \mathbf{k}_i if the partons carry nonzero orbital angular momentum) one obtains matrix elements of operators with light-like separation between the fields, and thus distribution amplitudes. For our simple example we have

$$\int \frac{d^2\mathbf{k}}{16\pi^3} \Psi_{+-}(z, \mathbf{k}) = -\frac{1}{4\sqrt{3}} \Phi_\pi^q(z) \quad (165)$$

as easily seen from the definition (79). Leading-twist DAs correspond to the lowest Fock states $q\bar{q}$ of mesons and qqq for baryons, involve only the good components of the quark fields, and describe vanishing orbital angular momenta of the partons. In particular, the twist-two meson DAs are generated from the same operators as the twist-two GPDs. Beyond leading twist the situation is more involved; results on meson and baryon DAs can respectively be found in [151, 152] and [153] and the references therein.

3.11.2 The overlap formulae

The wave function representation of GPDs is obtained by (i) inserting the Fock state expansions (161) into the matrix elements defining GPDs, (ii) representing the quark-antiquark or two-gluon operators in the matrix elements by parton creation and annihilation operators as in (48), (49), and (iii) using the (anti)commutation relations of these operators. The resulting formulae may appear somewhat involved because of the parton kinematics, but their physics content and interpretation is rather simple.

In the region $x \in [\xi, 1]$ the result for the combinations of H^q and E^q in (54) is

$$F_{\lambda'\lambda}^q(x, \xi, t) = \sum_{N,\beta} \sqrt{1-\xi}^{2-N} \sqrt{1+\xi}^{2-N} \sum_{j=q} [dx]_N [d^2\mathbf{k}]_N \quad (166)$$

$$\times \delta(x - x_j) \Psi_{N\beta}^{*\lambda'}(x_i^{\text{out}}, \mathbf{k}_i^{\text{out}}) \Psi_{N\beta}^\lambda(x_i^{\text{in}}, \mathbf{k}_i^{\text{in}}),$$

where the label j denotes the struck parton and is summed over all quarks with appropriate flavor in a given Fock state, and the labels (N, β) are summed over Fock states. The wave function arguments are given by momentum fractions, referring to the plus-momenta of either the initial or the final state hadron,

$$\begin{aligned} x_i^{\text{in}} &= \frac{x_i}{1+\xi}, & x_i^{\text{out}} &= \frac{x_i}{1-\xi} & \text{for } i \neq j, \\ x_j^{\text{in}} &= \frac{x_j + \xi}{1+\xi}, & x_j^{\text{out}} &= \frac{x_j - \xi}{1-\xi}, \end{aligned} \quad (167)$$

and by transverse parton momenta relative to the transverse momentum of their parent hadron,

$$\begin{aligned} \mathbf{k}_i^{\text{in}} &= \mathbf{k}_i - \frac{x_i}{1+\xi} \mathbf{p}, & \mathbf{k}_i^{\text{out}} &= \mathbf{k}_i - \frac{x_i}{1-\xi} \mathbf{p}' & \text{for } i \neq j, \\ \mathbf{k}_j^{\text{in}} &= \mathbf{k}_j + \frac{1-x_j}{1+\xi} \mathbf{p}, & \mathbf{k}_j^{\text{out}} &= \mathbf{k}_j + \frac{1-x_j}{1-\xi} \mathbf{p}'. \end{aligned} \quad (168)$$

These transverse momentum arguments can readily be determined by performing a transverse boost to a frame where the corresponding hadron moves along the z axis. The representation in the region

$x \in [-1, -\xi]$ is obtained from (177) by reversing the overall sign according to (48), by changing $\delta(x - x_j)$ into $\delta(x + x_j)$, and by summing j over antiquarks. We thus find that in the DGLAP regions a GPD is essentially given by the product $\Psi_{\text{in}} \Psi_{\text{out}}^*$ of wave functions for the initial and final state hadron, summed over all partonic configurations where the emitted and the reabsorbed parton have specified flavor and plus-momenta. The parton configurations in the initial and final state differ in their kinematics unless one has the forward case $p' = p$.

In the ERBL region we have instead the overlap of wave functions where the initial-state hadron has two partons more than the final-state one,⁶

$$\begin{aligned}
F_{\lambda\lambda}^q(x, \xi, t) &= - \sum_{N, \beta, \beta'} \sqrt{1 - \xi}^{3-N} \sqrt{1 + \xi}^{1-N} \\
&\times \sum_{j, j'} \frac{1}{\sqrt{n_j n_{j'}}} \int dx_j \prod_{i \neq j, j'} dx_i \delta\left(1 - \xi - \sum_{i \neq j, j'} x_i\right) \\
&\times (16\pi^3)^{-N+1} \int d^2\mathbf{k}_j \prod_{i \neq j, j'} d^2\mathbf{k}_i \delta^{(2)}\left(\mathbf{p}' - \sum_{i \neq j, j'} \mathbf{k}_i\right) \\
&\times \delta(x - x_j) \Psi_{N-1, \beta'}^{*\lambda'}(x_i^{\text{out}}, \mathbf{k}_i^{\text{out}}) \Psi_{N+1, \beta}^\lambda(x_i^{\text{in}}, \mathbf{k}_i^{\text{in}}). \tag{169}
\end{aligned}$$

The partons j, j' are the ones emitted from the initial proton. One has to sum over all quarks j and antiquarks j' with opposite helicities, opposite color, and appropriate flavor in the initial state proton, over all Fock states $(N + 1, \beta)$ containing such a $q\bar{q}$ pair, and over all Fock states $(N - 1, \beta')$ of the outgoing proton whose quantum numbers match those of the spectator partons $i \neq j, j'$. The statistical factors n_j ($n_{j'}$) give the number of (anti)quarks in the Fock state $(N + 1, \beta)$ that have the same discrete quantum numbers as the (anti)quark pulled out of the target. The wave function arguments of the spectator partons $i \neq j, j'$ are given as before in (167) and (168), whereas for the partons removed from the target they now read

$$\begin{aligned}
x_j^{\text{in}} &= \frac{\xi + x_j}{1 + \xi}, & x_{j'}^{\text{in}} &= \frac{\xi - x_j}{1 + \xi}. \\
\mathbf{k}_j^{\text{in}} &= \mathbf{k}_j - \frac{\xi + x_j}{1 + \xi} \mathbf{p} - \frac{1}{2} \mathbf{\Delta}, & \mathbf{k}_{j'}^{\text{in}} &= -\mathbf{k}_j - \frac{\xi - x_j}{1 + \xi} \mathbf{p} - \frac{1}{2} \mathbf{\Delta}. \tag{170}
\end{aligned}$$

In this region GPDs thus probe a color-singlet $q\bar{q}$ pair in the initial-state hadron wave function, specifying the plus-momentum for the q and the \bar{q} , and the overall transverse momentum and helicity of the pair.

Going now to the impact parameter representation we introduce operators describing quarks or antiquarks of definite transverse position,

$$\begin{aligned}
\tilde{b}(k^+, \mathbf{b}, \mu) &= \int \frac{d^2\mathbf{k}}{16\pi^3} b(k^+, \mathbf{k}, \mu) e^{i\mathbf{k}\mathbf{b}}, \\
\tilde{d}(k^+, \mathbf{b}, \mu) &= \int \frac{d^2\mathbf{k}}{16\pi^3} d(k^+, \mathbf{k}, \mu) e^{i\mathbf{k}\mathbf{b}}, \tag{171}
\end{aligned}$$

with an analogous definition for gluons at definite transverse position. The corresponding Fock state expansion is

$$|p^+, \mathbf{b}, \lambda\rangle = \sum_{N, \beta} \frac{1}{\sqrt{f_{N\beta}}} \int [dx]_N [d^2\mathbf{b}]_N \tilde{\Psi}_{N\beta}^\lambda(x_i, \mathbf{b}_i)$$

⁶The overlap formulae (169) and (178) in the ERBL region differ by a global sign from those in [41, 134], due to the phase convention (404) for antiquark spinors used here.

$$\begin{aligned}
& \times \prod_{i=1}^{N_q} \frac{1}{\sqrt{x_i}} \tilde{b}^\dagger(x_i p^+, \mathbf{b}_i + \mathbf{b}) \prod_{i=N_q+1}^{N_q+N_{\bar{q}}} \frac{1}{\sqrt{x_i}} \tilde{d}^\dagger(x_i p^+, \mathbf{b}_i + \mathbf{b}) \\
& \times \prod_{i=N_q+N_{\bar{q}}+1}^N \frac{1}{\sqrt{x_i}} \tilde{a}^\dagger(x_i p^+, \mathbf{b}_i + \mathbf{b}) |0\rangle
\end{aligned} \tag{172}$$

with an integration element

$$[d^2\mathbf{b}]_N = (4\pi)^{N-1} \prod_{i=1}^N d^2\mathbf{b}_i \delta^{(2)}\left(\sum_{i=1}^N x_i \mathbf{b}_i\right), \tag{173}$$

and wave functions normalized as

$$P_{N\beta}^\lambda = \int [dx]_N [d^2\mathbf{b}]_N \left| \tilde{\Psi}_{N\beta}^\lambda(x_i, \mathbf{b}_i) \right|^2. \tag{174}$$

The wave functions for definite transverse momentum or impact parameter are related by Fourier transforms

$$\Psi_{N\beta}^\lambda(x_i, \mathbf{k}_i - x_i \mathbf{p}) = \int [d^2\mathbf{b}]_N \exp\left[-i \sum_{i=1}^N \mathbf{k}_i \mathbf{b}_i\right] \tilde{\Psi}_{N\beta}^\lambda(x_i, \mathbf{b}_i) \tag{175}$$

with $\mathbf{p} = \sum_{i=1}^N \mathbf{k}_i$ and

$$\tilde{\Psi}_{N\beta}^\lambda(x_i, \mathbf{b}_i - \mathbf{b}) = \int [d^2\mathbf{k}]_N \exp\left[i \sum_{i=1}^N \mathbf{k}_i \mathbf{b}_i\right] \Psi_{N\beta}^\lambda(x_i, \mathbf{k}_i) \tag{176}$$

with $\mathbf{b} = \sum_{i=1}^N x_i \mathbf{b}_i$. The latter condition confirms that the transverse position \mathbf{b} of the proton is the center of plus-momentum of the partons (in each Fock state) as we anticipated in Section 3.10.

The overlap formulae are very similar to the one in transverse momentum space. For $x \in [\xi, 1]$ we have

$$\begin{aligned}
& \int \frac{d^2\mathbf{D}}{(2\pi)^2} e^{-i\mathbf{D}\mathbf{b}} F_{\lambda'\lambda}^q(x, \xi, t) = \sum_{N,\beta} \sqrt{1-\xi}^{2-N} \sqrt{1+\xi}^{2-N} \sum_{j=q} [dx]_N [d^2\mathbf{b}]_N \\
& \times \delta(x - x_j) \delta^{(2)}(\mathbf{b} - \mathbf{b}_j) \tilde{\Psi}_{N\beta}^{\lambda'}(x_i^{\text{out}}, \mathbf{b}_i - \mathbf{b}_0^{\text{out}}) \tilde{\Psi}_{N\beta}^\lambda(x_i^{\text{in}}, \mathbf{b}_i - \mathbf{b}_0^{\text{in}})
\end{aligned} \tag{177}$$

and for $x \in [-\xi, \xi]$

$$\begin{aligned}
& \int \frac{d^2\mathbf{D}}{(2\pi)^2} e^{-i\mathbf{D}\mathbf{b}} F_{\lambda'\lambda}^q(x, \xi, t) = - \sum_{N,\beta,\beta'} \sqrt{1-\xi}^{3-N} \sqrt{1+\xi}^{1-N} \\
& \times \sum_{j,j'} \frac{1}{\sqrt{n_j n_{j'}}} \int dx_j \prod_{i \neq j, j'} dx_i \delta\left(1 - \xi - \sum_{i \neq j, j'} x_i\right) \\
& \times (4\pi)^{N-1} \int d^2\mathbf{b}_j \prod_{i \neq j, j'} d^2\mathbf{b}_i \delta^{(2)}\left(\xi \mathbf{b}_j + \sum_{i \neq j, j'} x_i \mathbf{b}_i\right) \\
& \times \delta(x - x_j) \delta^{(2)}(\mathbf{b} - \mathbf{b}_j) \tilde{\Psi}_{N-1,\beta'}^{\lambda'}(x_i^{\text{out}}, \mathbf{b}_i - \mathbf{b}_0^{\text{out}}) \tilde{\Psi}_{N+1,\beta}^\lambda(x_i^{\text{in}}, \mathbf{b}_i - \mathbf{b}_0^{\text{in}})
\end{aligned} \tag{178}$$

with $\mathbf{b}_{j'} = \mathbf{b}_j$. The transverse positions of the hadrons are given by

$$\mathbf{b}_0^{\text{in}} = \frac{\xi}{1+\xi} \mathbf{b}_j, \quad \mathbf{b}_0^{\text{out}} = -\frac{\xi}{1-\xi} \mathbf{b}_j \quad (179)$$

in both cases. The interpretation of these expressions is exactly the one we have previously given in Fig. 12, where the blobs represent the hadronic wave functions in the mixed representation of plus-momentum and impact parameter. In addition to the results obtained in Section 3.10 we see that the transverse locations of the spectator partons are conserved, as well as the relative distance between the struck parton and the spectators in the DGLAP region. What *does* change if $\xi \neq 0$ are the relative positions of partons with respect to the center of plus-momentum of their parent hadron.

Analogous representations can be obtained for all other twist-two GPDs we have discussed so far. The appropriate restrictions on the helicities of the struck partons are readily determined from the operators in Table 1 and the correspondence between left-handed incoming and right-handed outgoing partons. The relevant global signs and factors are given in [41].⁷ An important difference between quark and gluon distributions is that for gluons an extra factor of $(x+\xi)^{1/2} |x-\xi|^{1/2}$ appears on the right-hand sides of the overlap formulae, both in the DGLAP and the ERBL regions. To understand this we note that the derivatives in the gluon field strength operators $G^{+\mu}$ provide a factor of the plus-momentum for both partons being probed, whereas the spinors from the quark fields provide only a square root for each momentum. Gluon GPDs need however not vanish at $x = \xi$ due to the extra factor $|x-\xi|^{1/2}$ since the relevant wave functions can diverge at these points (see Section 3.13). We also note that the overlap formula for GPDs of scalar partons has a factor of $(x+\xi)^{-1/2} |x-\xi|^{-1/2}$ on the right-hand side [154].

Corresponding representations exist for targets with different spin. Comparing (14) and (20) one finds that the analogs of the overlap formulae (166), (169), (177), (178) for a spin-zero target are simply obtained by replacing $F_{\lambda'\lambda}^q(x, \xi, t)$ on the left-hand sides with $H^q(x, \xi, t)$ and by omitting the helicity labels λ, λ' in the wave functions. We finally remark that a representation of twist-three GPDs (see Section 6.1.1) in terms of wave functions should also be possible, along the lines of the studies of the forward twist-three structure functions in [155, 156]. A perturbative study of the twist-three quark and gluon GPDs in a quark target was performed in [157].

The overlap formulae in momentum or position space provide a concrete interpretation of GPDs and related quantities:

- Taking the forward limit $p = p'$ and equal hadron helicities, our matrix elements represent the usual parton densities. The momentum space wave functions in the DGLAP region then have the same arguments, i.e., parton densities are given by *squared* wave functions $|\Psi(x_i, \mathbf{k}_i)|^2$ summed over all parton configurations with a given flavor and momentum fraction x of the struck parton. This justifies the interpretation as classical probability densities in the parton model, as has long been known [50].
- For $\xi = 0$ and nonzero t the momentum space wave functions have a relative shift in their transverse momentum arguments. After Fourier transforming to impact parameter space, the wave function arguments of the initial and final state wave functions are however identical. This makes the density interpretation discussed in Section 3.10.1 explicit in terms of squared impact parameter wave functions $|\tilde{\Psi}(x_i, \mathbf{b}_i)|^2$, provided one has the same polarization for both hadron states.

⁷In [41] the overall sign in the formula (68) for unpolarized gluon GPDs in the ERBL region is incorrect and should be reversed. The same correction must be made in the corresponding formula for polarized gluon GPDs.

- Integrating over the momentum fraction x and choosing a frame with $\xi = 0$ one obtains the wave function representations of elastic form factors, going back to Drell and Yan [158], which become again densities in impact parameter space [136].
- For nonzero ξ GPDs are *not* expressed through squared wave functions, neither in momentum space nor in the mixed representation using impact parameter. Instead, they express the *interference* or *correlation* between wave functions for different parton configurations in a hadron. In the ERBL region, even the parton content of the two wave functions is different.

The distributions E and \tilde{E} for quarks or gluons appear in matrix elements between hadrons with opposite helicities. On the other hand, the overlap representations (166) or (177) in the DGLAP region imply that the Fock states in the initial and final hadron have the same quantum numbers, and in particular the same helicity for each parton. This means that in at least one of the wave functions Ψ_{in} or Ψ_{out} the helicity of the hadron is *not* the sum of helicities of its partons. Conservation of angular momentum along the z axis (in a frame where the relevant parent hadron has zero transverse momentum) implies that E and \tilde{E} are overlaps of wave functions whose orbital angular momentum L^3 of the partons differs by one unit. This reflects from a different point of view the finding of Ji's sum rule (Section 3.6), where E^q and E^g intervene. $L^3 \neq 0$ wave functions cannot all be small in the nucleon, because the Pauli form factors $F_2 = \int dx E$ at small t are large for both proton and neutron. The role of $F_2(t)$ as an indicator for light-cone wave functions with nonvanishing orbital angular momentum has long been known [159], for recent discussions see for instance [25, 160]. A dedicated study of the overlap representation for $F_2(t)$ and $\int dx x E$ and its connection with orbital angular momentum was done by Brodsky et al. [69]. Explicit overlap formulae for the three-quark state of a proton target have recently been derived by Ji et al. [150], and further work on light-cone wave functions with orbital angular momentum can be found in [161, 162].

It is natural to ask about a wave function representation for GDAs. They cannot be written as the simple overlap of the wave functions of the individual hadrons. Physically this is because the properties of a multi-hadron state are not simply described by the individual structure of each hadron because of the strong interaction between the hadrons. One can however write down a Fock state decomposition of the interacting *multi-hadron states* like $|\pi\pi\rangle$ or $|p\bar{p}\rangle$ and understand the twist-two GDAs we have discussed as the quark-antiquark wave functions of these states integrated over the transverse parton momenta.

3.11.3 Polynomiality and the covariant approach

Since the wave function representation we have derived are exact, the resulting GPDs must satisfy the general properties we have discussed in Section 3.3. For some of them this is easily verified: in the forward limit one obtains the known wave function representations of usual parton densities. It is also straightforward to show [41] that the GPDs obtained by the overlap formulae are even functions of ξ . What is *not* obvious to see from the wave function representation is however the continuity of GPDs at $x = \pm\xi$ (discussed in Section 3.13) and the polynomiality condition. In these cases both the DGLAP and the ERBL regions must cooperate to lead to the required properties, and this implies nontrivial relations between the wave functions for the different Fock states relevant in the two regions. An *ad hoc* ansatz for the wave functions would almost certainly lead to GPDs that violate the above requirements.

It is instructive to see how the light-cone overlap representation we have discussed so far comes about in a covariant framework, and how polynomiality is achieved there. Consider for simplicity a pion and start with the Bethe-Salpeter wave function for the $q\bar{q}$ state. This is the covariant vertex

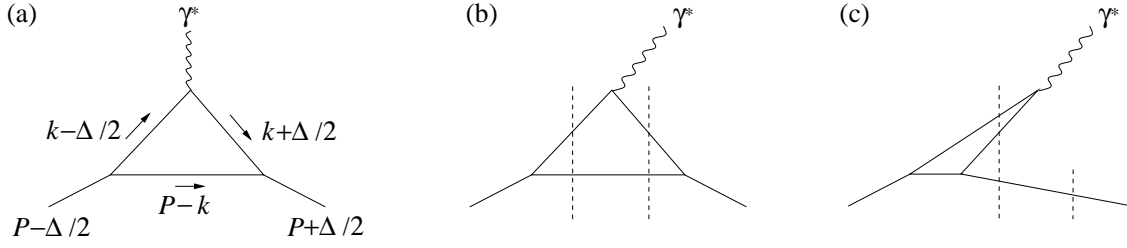


Figure 14: Triangle diagram in covariant perturbation theory (a), and its light-cone representation in the regions $\xi < x < 1$ (b) and $0 < x < \xi$ (c). Vertical lines show the intermediate states in the wave function representation.

function between the pion and the two quarks, including the full quark propagators,

$$\Psi_{\alpha\beta}^{\text{BS}}(k) = \int d^4x e^{i(kx)} \langle \pi(p) | T \bar{q}_\alpha(-\frac{1}{2}x) q_\beta(\frac{1}{2}x) | 0 \rangle \quad (180)$$

where k is half the difference between the quark and antiquark four-momenta. Choosing a particular frame and integrating over k^- puts the relative light-cone time x^+ of the fields to zero, and contracting with the Dirac matrix $\gamma^+ \gamma_5$ selects the “good” field components which correspond to opposite helicities of quark and antiquark. Writing the quark operators at $x^+ = 0$ in terms of annihilation and creation operators for quarks and using the Fock state decomposition of the meson one readily identifies the result with the light-cone wave function Ψ_{+-} given in (164),

$$\begin{aligned} & \int dk^- \sum_{\alpha\beta} (\gamma^+ \gamma_5)_{\alpha\beta} \Psi_{\alpha\beta}^{\text{BS}}(k) \\ &= 2\pi \int dx^- d^2\mathbf{x} e^{i(kx)} \langle \pi(p) | \bar{q}(-\frac{1}{2}x) \gamma^+ \gamma_5 q(\frac{1}{2}x) | 0 \rangle \Big|_{x^+=0} \\ &= -4\pi\sqrt{3} \Psi_{+-}. \end{aligned} \quad (181)$$

We have omitted the time ordering of the quark operators in the second line of (181) following our discussion in Section 3.4. Further integration of Ψ_{+-} over the transverse parton momentum also puts \mathbf{x} to zero and gives the meson distribution amplitude defined in (79).

Let us now restrict ourselves to the overlap representation of the elastic meson form factor, where polynomiality just means independence of ξ . Sawicki [163] has shown how this independence comes about in a toy model, where scalar particles couple to themselves by a ϕ^3 interaction, and to a photon by the usual derivative coupling of scalar QED. The scalars play the role both of quarks and of the meson. In usual covariant perturbation theory at leading order, the form factor is then given by the triangle diagram of Fig. 14a. Restricting oneself to the plus-component of the current, which is enough to extract the form factor, the diagram is proportional to

$$\int d^4k k^+ D(P-k) D(k - \frac{1}{2}\Delta) D(k + \frac{1}{2}\Delta) \quad (182)$$

with scalar quark propagators $D(l) = (l^2 - m^2 + i\epsilon)^{-1}$.

After choosing a particular frame, one can perform the integral over k^- by complex contour integration using Cauchy’s theorem, with poles originating from the quark propagators. Defining $x = k^+/P^+$ and $\xi = -\Delta^+/(2P^+)$ as usual and taking a frame where $\xi > 0$, one has to distinguish the following cases:

1. If $x < 0$ or $x > 1$ then the poles of all three propagators are on the same side of the real k^- axis. Closing the integration contour in the other half-plane one obtains a zero integral.
2. For $\xi < x < 1$, corresponding to the kinematics of Fig. 14b, one can close the contour so as to pick up only the pole of $D(P - k)$. The result is proportional to

$$\int dk^+ d^2\mathbf{k} k^+ (P^+ - k^+)^{-1} D(k - \frac{1}{2}\Delta)D(k + \frac{1}{2}\Delta)\Big|_{k^- = k_{\text{os}}^-}, \quad (183)$$

where k_{os}^- is the value where $D(P - k) = 0$. The Bethe-Salpeter wave function of the incoming meson in this theory is to lowest order in the coupling just given by a factor times the product $D(k - \frac{1}{2}\Delta) D(P - k)$ of quark propagators. To obtain the corresponding light-cone wave function one integrates over k^- . Using again complex contour integration one finds a nonzero wave function only for $x \in [0, 1]$, which can be written as a factor times $D(k - \frac{1}{2}\Delta)$ evaluated at k_{os}^- . In analogy one can express the propagator $D(k + \frac{1}{2}\Delta)$ at k_{os}^- through the light-cone wave function of the final state meson. All together (183) thus takes the form of an overlap integral of the wave functions for the two mesons, as in the overlap representation (166) for the DGLAP region.

3. For $0 < x < \xi$ one can either pick up the pole of $D(k - \frac{1}{2}\Delta)$ or the poles of the two other propagators. The result cannot be written in terms of the wave functions for the mesons. This is physically clear since the right-hand vertex in Fig. 14c corresponds to a quark splitting into a meson and a quark, which is not the kinematics of a wave function. Brodsky and Hwang [164] have realized that the result can however be written as the light-cone wave function for three particles in the meson (see the dotted line in the diagram) and the one-particle wave function to find a meson in a meson, which is just proportional to a δ function in momentum. This is precisely the overlap of wave functions with different particle content we have seen in the ERBL region.

Only when summing the contributions from the DGLAP and the ERBL regions does one obtain a result for the meson form factor that is independent of ξ , i.e. of the frame in which one has performed the reduction from Bethe-Salpeter to light-cone wave functions. The wave functions for two and three partons in the meson are related in a way so as to preserve Lorentz invariance: in fact they have been identified from the same covariant Feynman diagrams in different kinematical regimes.

It is not known which form corresponding relations between light-cone wave functions take in general and in more realistic theories. Such relations can be provided by the equations of motion, since the Dirac operator $i\not{D} - m$ contains terms which either conserve parton number, or add or remove one gluon.

3.11.4 Evolution

Because of the ultraviolet divergences of QCD, the quantities we have manipulated in our derivation need to be renormalized. This concerns the fields q_+ and hence the parton operators and light-cone wave functions, as well as the bilocal operators defining GPDs. The renormalization must ensure that the integrals one has to perform in the overlap representations are finite, and the corresponding renormalization scale μ provides the scale at which the wave functions and parton distributions are defined. It is intuitive to think of μ as a cutoff in transverse momenta, so that the available \mathbf{k} in the wave functions and their overlap are at most of order μ . There are similar cutoff schemes, for instance in the light-cone energy of the Fock states [50], which also cuts off small plus-momenta k^+ . For certain purposes, cutoff regularization will of course be insufficient since it breaks Lorentz and gauge invariance of the theory.

A study of the renormalization scale dependence for usual parton densities in the context of the Fock state representation has been performed in [149], where evolution equations were given for the contributions of individual Fock states to the parton densities. The evolution of an N parton Fock state was seen to depend also on the $(N-1)$ parton Fock states (which can radiate a parton to become an N parton state). Summing over all Fock state contributions the usual DGLAP equations were obtained. In [165] the nonforward case was studied, and it was shown how the splitting functions of the evolution are related with the k_T divergences of the perturbatively calculated wave functions of a quark and gluon within a quark.

3.11.5 A remark about the light-cone gauge

Brodsky et al. [166] have claimed that the representation of forward parton distributions as probabilities, which follows from the wave function representation in Section 3.11.2 is not correct. At the center of the arguments in [166] are the effects of gluons polarized in the plus-direction, which are described by a Wilson line in the definition of parton distributions for a general gauge (Section 3.2) but are absent in the light-cone gauge $A^+ = 0$, where the parton picture and the overlap representation of this section is derived. Subsequent investigations of the theoretical issues raised in [166] have been made by Collins [167, 168] and by Ji and collaborators [169, 170]. We will not attempt a full discussion of these problems, which are not finally settled in our view, but nevertheless make some points relevant in the context of this review.

- The arguments in [166] do not affect the leading-twist factorization theorems presented in Section 5.1, which connect GPDs to physical processes. (In fact these theorems were proven in covariant gauges, where the Wilson lines summing up the effects of A^+ gluons explicitly appear.)
- The general properties of GPDs discussed in Sections 3.2, 3.3 and 3.6 to 3.10 are not affected either, since they can be derived in covariant gauges, taking explicitly into account the Wilson lines. The discussion of helicity structure in Section 3.5 should not be affected either since A^+ gluons carry zero light-cone helicity.
- Both the hard-scattering kernels and the matrix elements defining GPDs are gauge invariant quantities, and it should in particular be possible to evaluate them in $A^+ = 0$ gauge. This was indeed found in an explicit calculation of the quark density in scalar QED [170] from the same diagrams that were considered in [166]. The regularization and renormalization prescriptions needed to define parton distributions must of course be gauge invariant to obtain this result, and simple cutoff schemes are in general not suitable for this purpose.
- The condition $A^+ = 0$ is not sufficient to fully fix the gauge since it is preserved by gauge transformations which do not depend on the coordinate x^- . To specify the gauge completely one may impose boundary conditions on the gauge field at $x^- \rightarrow \pm\infty$, see [170] and references therein. In momentum space this is related with providing a prescription for the $1/k^+$ singularity of the gluon propagator

$$\frac{1}{k^2 + i\epsilon} \left(g^{\alpha\beta} - \frac{k^\alpha n_-^\beta + n_-^\alpha k^\beta}{k^+} \right). \quad (184)$$

Light-cone wave functions as defined in Section 3.11.1 are not gauge invariant quantities and depend in particular on how the residual gauge freedom is fixed. In some of these prescriptions the wave functions of stable particles have dynamical phases: regulators like $1/(k^+ + i\epsilon)$ for instance introduce imaginary parts in addition to those from the Feynman prescription in the propagator $1/(k^2 + i\epsilon)$.

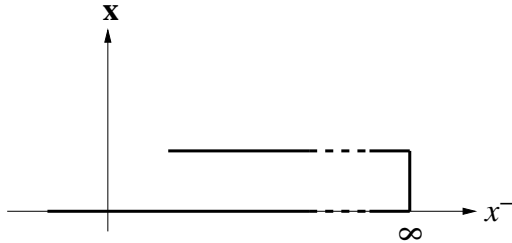


Figure 15: One of the possible paths for the Wilson line in k_T dependent parton distributions (see text). The part of the path going in the transverse direction is at $x^- \rightarrow \infty$.

- Gauge issues are more prominent in distributions depending on the parton k_T . As remarked at the end of Section 3.10.1 the field operators in their definition appear at finite transverse separation \mathbf{x} and hence cannot be connected by a Wilson line along a purely light-like path. A path often considered in the literature is shown in Figure 15, and one may naively expect that in light-cone gauge the Wilson line along this path reduces to unity. This is however not true in general since in $A^+ = 0$ gauge the gauge fields at $x^- \rightarrow \infty$ do not vanish, except for particular choices of the residual gauge fixing. The Wilson line along the transverse direction at $x^- \rightarrow \infty$ then does appear in k_T dependent parton distributions, but reduces to unity in the k_T integrated distributions, where $\mathbf{x} = \mathbf{0}$ [170]. In k_T dependent distributions the gluons described by the Wilson line have important physical consequences for various spin and azimuthal asymmetries in inclusive or semi-inclusive processes [171, 172, 167, 169].
- The $1/k^+$ singularity of the light-cone gauge gluon propagator (184) also shows up as a singular term in the wave function renormalization of the quark field, which directly affects the definition of light-cone wave functions [50]. A cutoff in k^+ is sufficient to regulate the singularity in simple situations as for instance in [149] but may not be in general.⁸

Little is known about how to appropriately define light-cone wave functions in $A^+ = 0$ gauge taking into account the issues of renormalization, of gauge fixing and of a proper regularization of gauge artifacts. It is not known how such a scheme should look like in order to have physically appealing features such as the overlap representation we have presented. In this sense the overlap formulae and their consequences presently do not have the status of all-order results, and it remains to be seen which of these results will require modification. Ultimately these issues lead to the question of how to properly implement the physical picture of the parton model in QCD.

3.12 Positivity bounds

In the DGLAP regions GPDs are very similar to the usual parton distributions, and one may expect quantitative relations between these quantities. Such relations indeed exist and provide upper bounds on GPDs in terms of conventional parton densities. That the wave function representation of GPDs leads to such bounds was observed by Martin and Ryskin [96], who derived an upper bound on GPDs in terms of the arithmetic mean of the usual parton densities at two different momentum fractions. Pire, Soffer and Teryaev [173] later showed that stronger bounds exist which involve the geometric mean instead. A missing kinematical factor in these bounds was corrected by Radyushkin [98], and [41] corrected the incorrect treatment of the proton spin structure in previous work, which

⁸I thank J. Collins for discussions about this point.

had missed out the contribution from the distributions E . Bounds on GPDs in impact parameter space were derived in [174, 134]. An extensive investigation of several aspects of positivity bounds was given by Poblitsa [175, 176, 139, 43, 177, 178]. All bounds discussed in the literature are restricted to the DGLAP regions $x \in [\xi, 1]$ and $x \in [-1, -\xi]$, and it is not known whether anything similar holds in the ERBL region.

The positivity constraints we will discuss in the next subsection provide upper bounds on GPDs in terms of the forward parton densities, which are rather well known. In contrast, the upper bounds on impact parameter GPDs in Section 3.12.2 are given in terms of parton densities in impact parameter space. These are not known phenomenologically, but the corresponding bounds provide constraints on models or ansätze for the impact parameter dependence of GPDs (and thus on their t -dependence after Fourier transform). In fact, not all current modeling strategies automatically respect the positivity constraints, see Section 4.3.4.

3.12.1 Bounds in momentum representation

A convenient method to derive the positivity constraints is to use the wave function representation of GPDs given in Section 3.11.2. One readily sees that the overlap formula (166) has the form of a scalar product in the space of wave functions. Taking a spin-zero target for simplicity, one can then write $H_\pi^q(x, \xi, t)$ for $x \in [\xi, 1]$ as a scalar product $(\phi_{-\xi, \mathbf{p}'} | \phi_{\xi, \mathbf{p}})$ with

$$\begin{aligned}\phi_{-\xi, \mathbf{p}'}(x_i, \mathbf{k}_i, N, \beta) &= \sqrt{1 - \xi}^{2-N} \Psi_{N\beta}(x_i^{\text{out}}, \mathbf{k}_i^{\text{out}}), \\ \phi_{\xi, \mathbf{p}}(x_i, \mathbf{k}_i, N, \beta) &= \sqrt{1 + \xi}^{2-N} \Psi_{N\beta}(x_i^{\text{in}}, \mathbf{k}_i^{\text{in}}).\end{aligned}\quad (185)$$

The Schwartz inequality $|(\phi_{-\xi, \mathbf{p}'} | \phi_{\xi, \mathbf{p}})|^2 \leq (\phi_{-\xi, \mathbf{p}'} | \phi_{-\xi, \mathbf{p}'}) (\phi_{\xi, \mathbf{p}} | \phi_{\xi, \mathbf{p}})$ translates into

$$\left| H_\pi^q(x, \xi, t) \right| \leq \sqrt{q_\pi(x_{\text{in}}) q_\pi(x_{\text{out}})} \quad \text{for } x \in [\xi, 1], \quad (186)$$

where

$$x_{\text{in}} = \frac{x + \xi}{1 + \xi}, \quad x_{\text{out}} = \frac{x - \xi}{1 - \xi} \quad (187)$$

are the momentum fractions of the struck parton before and after the scattering, referring respectively to the initial and final hadron momentum. An analogous result holds for $x \in [-1, -\xi]$ and involves antiquark instead of quark distributions. For gluons one has

$$\left| H_\pi^g(x, \xi, t) \right| \leq \sqrt{1 - \xi^2} \sqrt{x_{\text{in}} g_\pi(x_{\text{in}})} \sqrt{x_{\text{out}} g_\pi(x_{\text{out}})} \quad \text{for } x \in [\xi, 1] \quad (188)$$

instead.

To extend these results to cases with nontrivial spin structure it is useful to rewrite (186) as a positivity condition for a matrix [176],

$$\begin{pmatrix} q_\pi(x_{\text{in}}) & H_\pi^q(x, \xi, t) \\ H_\pi^q(x, \xi, t) & q_\pi(x_{\text{out}}) \end{pmatrix} \geq 0, \quad (189)$$

again for $x \in [\xi, 1]$, which we will always imply in the following. Analogs hold of course for the antiquark region and for gluons. For a spin $\frac{1}{2}$ target the overlap representation of $F_{\lambda'\lambda}^q$ in (166) is a scalar product $(\phi_{-\xi, \mathbf{p}'}^{\lambda'} | \phi_{\xi, \mathbf{p}}^\lambda)$, whose vectors are labeled by the proton helicity in addition to the kinematical variables. Positivity of the scalar product implies a positive semidefinite 4×4 matrix

$$\begin{pmatrix} F^q(x_{\text{in}}, 0, 0) & F^q(x, \xi, t) \\ [F^q(x, \xi, t)]^\dagger & F^q(x_{\text{out}}, 0, 0) \end{pmatrix} \geq 0 \quad (190)$$

where $F^q(x, \xi, t)$ is the matrix

$$F^q = \begin{pmatrix} \sqrt{1 - \xi^2} \left(H^q - \frac{\xi^2}{1 - \xi^2} E^q \right) & -e^{-i\varphi} \frac{\sqrt{t_0 - t}}{2m} E^q \\ e^{i\varphi} \frac{\sqrt{t_0 - t}}{2m} E^q & \sqrt{1 - \xi^2} \left(H^q - \frac{\xi^2}{1 - \xi^2} E^q \right) \end{pmatrix} \quad (191)$$

obtained from (54). The positivity condition (190) can be written as [175]

$$(1 - \xi^2) \left(H^q - \frac{\xi^2}{1 - \xi^2} E^q \right)^2 + \frac{t_0 - t}{4m^2} (E^q)^2 \leq q(x_{\text{in}}) q(x_{\text{out}}). \quad (192)$$

For better legibility we have omitted the arguments x, ξ, t of the GPDs in (191) and (192).

More involved bounds are obtained when also taking into account the spin structure on the quark side. The matrix F^q in (190) is then replaced with a 4×4 matrix formed by the helicity combinations $A_{\lambda'\mu',\lambda\mu}^q$ given in Section 3.5.3, where the rows of the matrix are associated with the four helicity combinations (λ', μ') and the columns with the four helicity combinations (λ, μ) . The analog of (190) then states the positivity of an 8×8 matrix. Using the parity constraints (60) on $A_{\lambda'\mu',\lambda\mu}^q$ this can be rewritten as the positivity of two 4×4 matrices, which differ by the relative signs between quark helicity conserving and quark helicity changing GPDs [176]. These positivity conditions, which contain in particular the well-known bound $|\Delta q(x)| \leq q(x)$ and the Soffer bound [179] on the forward transversity distribution, can be translated into inequalities involving GPDs by a general method given in [176]. In the same reference it is shown how to obtain an upper bound on any given linear combination of GPDs in terms of forward densities. Examples are

$$\left| \sqrt{1 - \xi^2} \left(H^q - \frac{\xi^2}{1 - \xi^2} E^q \right) \right| \leq \frac{1}{2} \left(\sqrt{(q + \Delta q)_{\text{in}} (q + \Delta q)_{\text{out}}} + \sqrt{(q - \Delta q)_{\text{in}} (q - \Delta q)_{\text{out}}} \right), \quad (193)$$

$$\left| \frac{\sqrt{t_0 - t}}{2m} E^q \right| \leq \frac{1}{2} \left(\sqrt{(q + \Delta q)_{\text{in}} (q - \Delta q)_{\text{out}}} + \sqrt{(q - \Delta q)_{\text{in}} (q + \Delta q)_{\text{out}}} \right), \quad (194)$$

where we have used a shorthand notation $(q + \Delta q)_{\text{in}} = q(x_{\text{in}}) + \Delta q(x_{\text{in}})$ etc. Stricter bounds involve in addition the forward transversity distributions on the right-hand sides. Looser bounds are obtained by setting the polarized parton densities to zero, compare also with (192). We remark that the bound involving only the distribution H^q comes with a factor on the left-hand side that vanishes like $\sqrt{t_0 - t}$ in the zero-angle limit, as happens in (194). Bounds for the polarized quark GPDs are obtained by replacing $H \rightarrow \tilde{H}$ and $E \rightarrow \tilde{E}$ in (193) and $E \rightarrow \xi \tilde{E}$ in (194), with the same expressions on the right-hand sides.

3.12.2 Bounds in impact parameter representation

Bounds on GPDs in the impact parameter representation are readily derived from their overlap representation in (177). Taking again a pion target for simplicity, the impact parameter GPD has

the form of a scalar product $(\tilde{\phi}_{-\xi}|\tilde{\phi}_\xi)$ with

$$\begin{aligned}\tilde{\phi}_{-\xi}(x_i, \mathbf{b}_i, N, \beta) &= \sqrt{1-\xi}^{2-N} \tilde{\Psi}_{N\beta}(x_i^{\text{out}}, \mathbf{b}_i - \mathbf{b}_0^{\text{out}}), \\ \tilde{\phi}_\xi(x_i, \mathbf{b}_i, N, \beta) &= \sqrt{1+\xi}^{2-N} \tilde{\Psi}_{N\beta}(x_i^{\text{in}}, \mathbf{b}_i - \mathbf{b}_0^{\text{in}}).\end{aligned}\quad (195)$$

This leads to

$$(1-\xi^2) \left| \mathcal{F}H_\pi^q(x, \xi, \mathbf{b}) \right| \leq \sqrt{\mathcal{F}H_\pi^q(x_{\text{in}}, 0, \frac{\mathbf{b}}{1+\xi}) \mathcal{F}H_\pi^q(x_{\text{out}}, 0, \frac{\mathbf{b}}{1-\xi})}, \quad (196)$$

where \mathcal{F} denotes the Fourier transform

$$\mathcal{F}f(x, \xi, \mathbf{b}) = \int \frac{d^2\mathbf{D}}{(2\pi)^2} e^{-i\mathbf{D}\mathbf{b}} f(x, \xi, t) \quad (197)$$

passing from momentum to impact parameter space, where it is understood that t depends on \mathbf{D}^2 as given in (52). Analogous expressions are obtained for proton GPDs by replacing H_π^q under the Fourier transform with the matrix (191) or its generalization including the quark spin dependent GPDs. The impact parameter arguments on the right-hand side of (196) are readily identified as the distance between the probed quark and the center of the incoming or outgoing proton in Figure 12a.

A more general class of positivity conditions has been derived by Pobylitsa [139, 43]. For a spinless target (and after translating Pobylitsa's convention for the impact parameter into ours) they can be written as the requirement that

$$(1-\xi^2)^{3/2-s} \mathcal{F}H_\pi(x, \xi, \mathbf{b}) = \sum_n Q_n^*\left(x_{\text{out}}, \frac{\mathbf{b}}{1-x}\right) Q_n\left(x_{\text{in}}, \frac{\mathbf{b}}{1-x}\right) \quad (198)$$

with arbitrary functions Q_n , where the sum over n may be discrete or involve integration over continuous variables. Here s denotes the spin of the partons, $s = \frac{1}{2}$ for quarks, $s = 1$ for gluons, and $s = 0$ for spinless partons in toy models. The overlap representation (177) can indeed be cast into the form (198). To see this one changes variables to $x'_i = x_i/(1-x)$ and $\mathbf{b}'_i = \mathbf{b}_i + \mathbf{b}x/(1-x)$ for the spectators $i \neq j$. The delta function constraints in the overlap formula then become $\delta(1 - \sum_{i \neq j} x'_i) \delta^{(2)}(\sum_{i \neq j} x'_i \mathbf{b}'_i)$ and hence independent of x_{in} , x_{out} and \mathbf{b} . The functions Q_n are just the wave functions $\tilde{\Psi}$ times a scale factor $(1-x_{\text{out}})^{N-4}$ or $(1-x_{\text{in}})^{N-4}$, and the label n includes the dependence on the spectator variables x'_i and \mathbf{b}'_i .

Note that the distance $\mathbf{b}/(1-x)$ between the probed quark and the center of momentum of the *spectator* system is the same before and after the scattering, as was observed in [133]. If one rescales \mathbf{b} by $(1-x)$ then the right-hand side of (198) depends on x and ξ only through x_{out} and x_{in} . As a consequence one has

$$\int_0^1 dx_{\text{in}} \int_0^1 dx_{\text{out}} p^*(x_{\text{out}}, \mathbf{b}) p(x_{\text{in}}, \mathbf{b}) (1-\xi^2)^{3/2-s} \mathcal{F}H_\pi(x, \xi, (1-x)\mathbf{b}) \geq 0 \quad (199)$$

for any function $p(z, \mathbf{b})$ and for any fixed \mathbf{b} . By a change of variables and a rescaling of the function p this is equivalent to the condition

$$\int_{-1}^1 d\xi \int_{|\xi|}^1 dx (1-x)^{-2s} p^*(x_{\text{out}}, \mathbf{b}) p(x_{\text{in}}, \mathbf{b}) \mathcal{F}H_\pi(x, \xi, (1-x)\mathbf{b}) \geq 0. \quad (200)$$

Equivalent forms hold of course in the antiquark region $x < -|\xi|$. The constraint (200) is the most general one known so far. As shown in [139], the positivity conditions (186) and (196) are obtained from (200) by special choices of $p(z, \mathbf{b})$, followed by integration over \mathbf{b} in the case of (186).

For targets with spin the derivation goes in analogy, including the matrix structure in the helicities of the target and the partons as explained in the previous subsection. The final result (200) then involves multiplication of the matrix $\mathcal{F}A_{\lambda'\mu', \lambda\mu}$ with vector valued functions $p_{\lambda'\mu'}^*$ and $p_{\lambda\mu}$.

3.12.3 Derivation and validity

The constraints (200) and their generalization to targets with spin are stable under leading-logarithmic evolution to higher evolution scales μ as shown in [139]. The essence of the argument is the interpretation of the LO evolution kernels in the DGLAP region as the generalized parton distributions of a parton target. As is the case for the positivity constraints on forward parton densities [180], the same is however not generally true for NLO evolution nor for backward evolution to smaller scales, depending on the scheme used to renormalize the distributions. A model calculation [177] of perturbative triangle diagrams as in Fig. 14, with a Yukawa coupling between a scalar target and spin $\frac{1}{2}$ partons, gave for instance an additive term proportional to $\theta(x) \log \mu^2$ in the quark distribution $q(x)$, which will violate its positivity at small renormalization scales.

The derivation of the positivity bounds we have sketched here relies on the overlap representation and is hence subject to the caveats concerning the proper definition and renormalization of light-cone wave functions mentioned in Section 3.11.5. This derivation is in essence equivalent to inserting a complete set of intermediate states between the operators $\bar{q}(-\frac{1}{2}z)$ and $q(\frac{1}{2}z)$ in the definition of quark densities [173], or to using positivity of the norm in the Hilbert space of mixed quark-hadron states $q(\frac{1}{2}z|p)$, as done in Poylyitsa's work. All these derivation require the $A^+ = 0$ gauge in order to have no Wilson line between the quark fields, and they all involve the manipulation of "states" with net color (see our brief remark in Section 3.4 in the context of light-cone quantization).

An alternative derivation of the positivity bounds given in [178] sheds further light onto the question of their validity, and we will sketch the essence of the argument. Starting point are the positivity properties of the matrix element

$$\begin{aligned} 4\pi\epsilon_\alpha W^{\alpha\beta} \epsilon_\beta^* &= \epsilon_\alpha \left[\int d^4x e^{i(q+q')x/2} \langle p' | J^\beta(\frac{1}{2}x) J^\alpha(-\frac{1}{2}x) | p \rangle \right] \epsilon_\beta^* \\ &= \sum_X (2\pi)^4 \delta^{(4)}(p+q-p_X) \langle p' | \epsilon^* J(0) | X \rangle \langle X | \epsilon J(0) | p \rangle \end{aligned} \quad (201)$$

with the local current $J^\alpha = \bar{q}\gamma^\alpha q$, where the sum is over all *physical* states with momentum p_X . At this point we anticipate the results of Sections 5.1 and 5.2. In the region where q^2 and q'^2 are both spacelike $2\pi W^{\alpha\beta}$ is simply the absorptive part of the hadronic tensor $T^{\alpha\beta}$ for doubly virtual Compton scattering (up to the quark charges and the sum over flavors). Notice that in order to obtain this simple relation one must avoid the region where one or both photons are timelike, since then the Compton amplitude has additional cuts in the photon virtualities. In the generalized Bjorken limit (large q^2 and q'^2 and small t) the absorptive part of the Compton amplitude at leading order in α_s is simply proportional to $H^{q^{(+)}}(\rho, \xi, t)$. Having both photons spacelike selects the DGLAP region $|\rho| \geq |\xi|$, as seen in the definitions (260). To proceed one transforms (201) to impact parameter space and obtains $\mathcal{F}H^{q^{(+)}}(\rho, \xi, \mathbf{b})$ represented as in (198). The functions Q_n are now matrix elements of $J \cdot \epsilon$ between states of the target and the system X at definite plus-momentum and definite impact parameter, and n labels the different intermediate states X . To separate quarks from antiquarks, as well as the different parton helicity combinations, one can use appropriate currents J and polarization vectors ϵ . The current $J^\alpha = \bar{q}\gamma^\alpha(1 - \gamma_5)q$ for instance only couples to quarks with negative and antiquarks with positive helicity. To get the absorptive part of the amplitude one has to cut the handbag diagrams in Fig. 27, so that the parton is on shell before and after scattering on the current. In the Breit frame of this subprocess one sees that one can select the positive or negative helicity parton by taking a polarization vector ϵ corresponding to positive or negative helicity.

What this derivation requires is that q^2 and q'^2 be in a region where the Compton amplitude is well approximated by the leading-twist expression at leading order in α_s . This requires in particular μ^2 to be of the order of the hard scale of the process. The upshot of the argument is that the positivity

bounds should be valid at sufficiently large factorization scales μ^2 . We note in passing that positivity constraints on the absorptive part of the nonforward Compton amplitude have long ago been studied by De Rújula and De Rafael [3].

3.13 The point $x = \xi$

The point $x = \xi$ (or $x = -\xi$) where the DGLAP and ERBL regimes meet is of particular interest and importance. On one hand it is rather directly accessible to experiment: at leading order in α_s the imaginary parts of the amplitudes for DVCS and for meson electroproduction just involve GPDs at $x = \pm\xi$, as we see from the form (2) of the hard scattering kernels. Physically the point $x = \xi$ corresponds to very peculiar parton configurations, involving one parton with vanishing plus-momentum in the initial or final state hadron (according to whether one approaches the point from the ERBL or DGLAP region). Intuitively one might fear that such configurations are dangerous for the factorization of the hard-scattering process, but one can show that this is not the case for the processes we will consider (see Section 5.1).

GPDs around $x = \xi$ are sensitive to the physics of partons with small plus-momentum, but in a different way than the usual parton distributions at small x . In the wave function representation we see that, as x approaches ξ from above, the kinematical mismatch between the initial and final state wave functions becomes extreme, with a parton momentum fraction going to zero in the final state but staying finite (equal to $2\xi/(1 + \xi)$ with respect to the parent hadron) in the initial state. As x approaches ξ from below, one probes a parton pair with one momentum fraction finite and the other going to zero, a configuration similar to the one of a meson distribution amplitude at its endpoints $z = 0$ or $z = 1$. We note that the inequalities from positivity discussed in Section 3.12.1 do not provide constraints in the limit $x \rightarrow \xi$ since the parton distributions on their right-hand sides diverge for $x_{\text{out}} \rightarrow 0$ (unless the factorization scale is very low).

The real parts of the amplitudes for DVCS and for meson electroproduction involve principal value integrals as in (2). Consistency of factorization thus requires leading-twist GPDs to be *continuous* at $x = \pm\xi$, otherwise the scattering amplitude would be logarithmically divergent. An analog to this is that leading-twist distribution amplitudes must vanish at the endpoints $z = 0$ and $z = 1$ in order to give finite convolutions with hard scattering kernels (see e.g. Section 5.3).

Using the connection between GPDs and parton-proton scattering amplitudes discussed in Section 3.4, Collins and Freund [181] have related the analyticity properties in x of GPDs with the analytic properties of Feynman graphs. They find that GPDs can be written as the sum of a term analytic at $x = \xi$ and a contribution which is nonanalytic but zero at this point. This ensures of course continuity at $x = \xi$. A nonanalytic behavior at this point is also suggested by the reduction formula (124) from double distributions to GPDs. For fixed ξ the length of the integration line in the β - α plane is constant in the ERBL region and proportional to $1 - |x|$ in the DGLAP regions, i.e., the change in this length has a jump at $x = \xi$. Even with a smooth double distribution one will then in general have a jump in some derivative of the GPD at this point.

A discontinuity of the first derivative of GPDs has been found in several model studies, for instance by Radyushkin [39] in scalar ϕ^3 theory, where the GPD of the scalar particle was evaluated perturbatively to first order in the coupling. Tiburzi and Miller [154] and Theußl et al. [182] studied the GPDs of a bound state in different toy field theories, using perturbation theory in a Bethe-Salpeter approach (see Section 4.1.5). Both groups obtain GPDs at $x = \xi$ that are continuous but have a jump in the first derivative. The same was found by Burkardt [183] for the GPD of a meson state in the 't Hooft model (QCD in $1 + 1$ dimensions and the large- N_c limit [184]), which is exactly solvable without recourse to perturbation theory. A discontinuous derivative is thus at least not in contradiction with general principles of field theory. The precise behavior of the GPD at the transition

point may depend on further details such as the spin of the partons. We note that the behavior of gluon GPDs at $x = \xi$ has not much been investigated in the literature.

In the overlap representation the continuity of GPDs at the boundary between the DGLAP and the ERBL regimes is nontrivial and requires relations between the wave functions for different Fock states when the plus-momentum of one parton goes to zero. Similarly to those needed to guarantee polynomiality (see Section 3.11.3) such relations can be provided by the equations of motion. From the constraint equation (44) of light-cone quantization Antonuccio et al. [185] have in fact obtained relations between wave functions for Fock states with N , $N - 1$ and $N + 1$ partons when a quark or antiquark plus-momentum goes to zero. Explicit calculations in toy models do provide continuous GPDs, which has been checked in the field theory examples mentioned above [39, 154, 182, 183], and also for the perturbatively calculable GPDs of an electron target in QED [148]. Not every approximation scheme in model calculations will however correctly lead to continuous GPDs, as has been seen in the Bethe-Salpeter framework, see Section 4.1.5.

It is sometimes assumed that light-cone wave functions vanish when a parton plus-momentum goes to zero. For those wave functions that reduce to leading-twist distribution amplitudes when integrated over the parton k_T this may be true, but in general it is most probably not. The work by Antonuccio et al. [185] suggests that there are wave functions for higher Fock states that do not vanish when a quark or antiquark momentum fraction x tends to zero. The usual argument [50] that such wave functions would describe configurations with infinite light-cone energy is invalidated by cancellations between the free (kinetic) and interacting parts of the light-cone Hamiltonian. The perturbative wave function for an electron and a photon within an electron (given e.g. in [148]) also remains finite for a vanishing momentum fraction of the electron if the helicities of all particles are aligned. If the photon becomes slow, the same wave function diverges like the inverse square root of the photon momentum fraction, thus compensating the factor $|x - \xi|^{1/2}$ in the overlap representation for spin-one partons (see Section 3.11.2). For scalar partons on the other hand, a finite GPD at $x = \xi$ is already generated by wave functions not vanishing faster than the square root of a parton momentum fraction, given the factor $|x - \xi|^{-1/2}$ in the overlap formula.

The GPDs calculated from the lowest Fock states of the target were indeed found to be nonzero at $x = \xi$ in ϕ^3 theory and in QED [39, 148], as well as in the bound state calculations of [154, 182] with scalar or spin $\frac{1}{2}$ partons. We remark however that the meson GPDs in the 't Hooft model do tend to zero at $x = \xi$ [183], with the $q\bar{q}$ wave functions of the meson vanishing at the endpoints.

In QCD it is not plausible that GPDs should vanish at $x = \xi$. Such a situation is only stable under evolution if the GPD vanishes in the entire DGLAP region (as it does in the limit $\mu \rightarrow \infty$), otherwise evolution to a higher scale μ will immediately “fill up” a zero at $x = \xi$. We also recall the link between evolution and the perturbative wave functions of two partons within a free parton state (see Section 3.11.4), which do not vanish at the end points. A better understanding of these issues would further our knowledge of how hadronic wave functions behave at their end points.

3.14 Transition GPDs

In hard exclusive processes where GPDs can be accessed one is not limited to an elastic transition on the target side, say from a proton to a proton. One also has quasielastic transitions, say $p \rightarrow n$ or $p \rightarrow \Delta$ to other baryons, and even to continuum states like $p \rightarrow N\pi$ (where N stands for a nucleon, p or n). As long as the invariant mass of this hadronic system is small compared with the hard scale Q^2 of the process, factorization works in the same way, with the soft input being GPDs for the relevant hadron transition.

Transitions to final states like Δ , N^* or $N\pi$ compete with the elastic transition and can thus present a background in experiments. To estimate its size, some phenomenological knowledge of the

relevant transition GPDs will be useful. If on the other hand the final state hadronic system can be sufficiently well detected, one can think of studying transition GPDs to a given final state as a signal. In fact they are quantities that allow one to study properties of baryons not available as targets. Moreover they are among the rare quantities (apart from fragmentation functions) that specifically contain information on their structure at *parton* level. In the wave function representation they are interpreted as the overlap of the final state hadron wave functions with the “reference” wave functions of the target.

The definition of transition GPDs is a straightforward extension of the usual one, e.g.

$$\begin{aligned} & \frac{1}{2} \int \frac{dz^-}{2\pi} e^{ixP^+z^-} \langle n(p') | \bar{d}(-\frac{1}{2}z) \gamma^+ u(\frac{1}{2}z) | p(p) \rangle \Big|_{z^+=0, \mathbf{z}=0} \\ &= \frac{1}{2P^+} \left[H_{p \rightarrow n}^{du}(x, \xi, t) \bar{u}(p') \gamma^+ u(p) + E_{p \rightarrow n}^{du}(x, \xi, t) \bar{u}(p') \frac{i\sigma^{+\alpha} \Delta_\alpha}{2m} u(p) \right]. \end{aligned} \quad (202)$$

The symmetry relations (25) and (26) discussed in Section 3.3.2 change for transition GPDs, because the actions of time reversal and of complex conjugation now relate e.g. $H_{A \rightarrow B}$ with $H_{B \rightarrow A}$. One thus no longer has functions even in ξ , except if there is another symmetry relating $H_{A \rightarrow B}$ with $H_{B \rightarrow A}$ such as isospin or SU(3) flavor symmetry.

The combined action of time reversal and complex conjugation does however constrain the transition GPDs to be real valued, provided that they involve stable single hadrons. Otherwise, a state like $|N\pi\rangle_{\text{out}}$ becomes $|N\pi\rangle_{\text{in}}$ under time reversal. The transition GPDs to unstable states thus contain dynamical phases, just as we saw in the case of GDAs in Section 3.7.

For the same reasons, transition form factors (related to transition GPDs by sum rules) are real-valued only for transitions between stable hadrons, and the number of independent form factors for the transition $A \rightarrow B$ is different from the number of form factors for elastic transitions, unless flavor symmetry provides further relations between $A \rightarrow B$ and $B \rightarrow A$. On the other hand the counting of independent GPDs still proceeds according to the rules given in Section 3.5.4, because they do not make use of time reversal or hermiticity.

3.14.1 Transitions within the baryon octet

Transition GPDs between members of the ground state baryon octet have the same spin structure as the proton GPDs, namely there are four quark helicity conserving GPDs H , E , \tilde{H} , \tilde{E} for each possible quark flavor transition. There are no gluon GPDs for transitions between different octet baryons because two gluons carry zero isospin and hypercharge. We remark that for determining quantum number constraints one may either consider GPD matrix elements of the type $\langle n | \bar{d} \gamma^+ u | p \rangle$ or the appropriate one in the crossed channel $\langle n \bar{p} | \bar{d} \gamma^+ u | 0 \rangle$.

GPDs for the proton-neutron transitions occur for instance in the electroproduction processes $\gamma^* p \rightarrow \pi^+ n$ or $\gamma^* p \rightarrow \rho^+ n$. Scattering off neutrons in nuclei involves the reverse transitions $\gamma^* n \rightarrow \pi^- p$ or $\gamma^* n \rightarrow \rho^- p$. The transition GPDs are related to the flavor diagonal ones by [186]

$$H_{p \rightarrow n}^{du} = H_{n \rightarrow p}^{ud} = H_p^u - H_p^d, \quad (203)$$

at equal arguments x, ξ, t . In the flavor diagonal sector one has isospin relations $H_p^u = H_n^d$, $H_p^d = H_n^u$, $H_p^s = H_n^s$ as for the usual parton densities. Analogous relations hold for the other GPDs E, \tilde{H}, \tilde{E} .

Among the other transitions within the ground state baryon octet, those from a nucleon to a Σ or Λ are of practical relevance, since they appear in kaon electroproduction processes, such as $\gamma^* p \rightarrow K^+ \Lambda$, $\gamma^* p \rightarrow K^+ \Sigma^0$, $\gamma^* p \rightarrow K^0 \Sigma^+$. For a detailed account on the GPDs for nucleon to

hyperon transitions we refer to [37]. Flavor SU(3) symmetry relates again these distributions to the flavor diagonal ones in the nucleon, namely [187, 37]

$$\begin{aligned}
H_{p \rightarrow \Lambda}^{su} &= \frac{1}{\sqrt{6}} [H_p^d + H_p^s - 2H_p^u], \\
H_{p \rightarrow \Sigma^0}^{su} &= \frac{1}{\sqrt{2}} [H_p^s - H_p^d], \\
H_{p \rightarrow \Sigma^+}^{sd} &= H_p^s - H_p^d,
\end{aligned} \tag{204}$$

with similar relations for the transitions $n \rightarrow \Lambda, \Sigma^0, \Sigma^-$. Analogous relations hold for E and \tilde{H} . For \tilde{E} one expects substantial flavor SU(3) breaking effects, see Section 5.3.

As discussed in [37], some quantities may be rather sensitive to the SU(3) breaking. The lowest x -moments of the four GPDs H , E , \tilde{H} , \tilde{E} for a given transition are now related to six transition form factors, instead of the four elastic form factors in (31) and (32). The additional form factors are zero in the SU(3) limit, where they are related to elastic form factors that vanish due to time reversal. One of these additional form factors (which is unaccessible in weak hyperon decays and thus experimentally unknown) contributes to sum rule for \tilde{E} with a prefactor $1/\xi$. This does not imply a steep rise of cross sections, where \tilde{E} appears multiplied with ξ , but it does provide an enhancement of this SU(3) suppressed form factor compared with the SU(3) allowed one in the same sum rule. Information on the size of the \tilde{E} transition GPDs may be obtained from a transverse spin asymmetry in kaon electroproduction, see Section 9.4.

3.14.2 Transitions to the Δ

The nucleon- Δ transition is of particular practical importance because it can contaminate the elastic $p \rightarrow p$ transition in experiments. $N \rightarrow \Delta$ GPDs have briefly been discussed in [188, 189]; more detail can be found in the review [37] and in the recent study [190].

Isospin relates transition GPDs $f_{p \rightarrow \Delta^0}^{du}$ and $f_{p \rightarrow \Delta^{++}}^{ud}$ to $f_{p \rightarrow \Delta^+}^u = -f_{p \rightarrow \Delta^+}^d$ so that there is only one independent flavor structure. For this a set of seven independent quark helicity conserving GPDs has been introduced in [37], corresponding to the number of independent $N \rightarrow \Delta$ transition form factors. This set must be incomplete, since the spin counting rules of Section 3.5.4 give eight independent helicity transitions. On the other hand, phenomenological studies have made use of the large- N_c limit, where only three of the previous $N \rightarrow \Delta$ GPDs are leading in $1/N_c$. In this limit, the nucleon and the Δ appear as different excitations of the same object, namely of a soliton. The three leading $N \rightarrow \Delta$ GPDs are then respectively proportional to the isovector combinations \tilde{H}_p^{u-d} , E_p^{u-d} , \tilde{E}_p^{u-d} .

When writing down hadronic matrix elements involving the Δ one implicitly approximates it as a stable particle, in the same sense as one assumes the ρ to be stable when defining its distribution amplitude. In this formalism the $N \rightarrow \Delta$ GPDs are real valued, and the dynamical phases associated with the decay of the resonance must explicitly be taken into account when describing the transition from Δ to $N\pi$, see e.g. [190]. An alternative treatment of the same process considers the transition GPDs to an $N\pi$ state from the start, projecting the $N\pi$ system on the partial wave and isospin combination corresponding to the Δ resonance. This formalism directly deals with the physically observed $N\pi$ states with the appropriate quantum numbers, in the same sense that one can trade a ρ distribution amplitude for a two-pion DA in a P -wave and the $C = -1$, $I = 1$ projection.

3.14.3 More transitions

GPDs for the $N \rightarrow N\pi$ transitions have been discussed in [37]. The classification of their structure is more involved than for single-particle states. In addition to the usual variables x , ξ , t the transition

GPDs depend on three kinematical variables describing the internal degrees of freedom of the $N\pi$ state (similar to the variables ζ and s we have encountered in GDAs). There are now three independent momentum fraction variables, both in the GPDs and in the analog of double distributions, which have been studied by Blümlein et al. [191]. Apart from the Δ resonance region just mentioned, the study of $N \rightarrow N\pi$ GPDs is particularly interesting close to threshold, where again they are of practical importance to experiment and where they are related to chiral dynamics (see Section 4.1.1).

GPDs for other quantum number changing transitions have been discussed in the literature. Feldmann and Kroll have considered the $B \rightarrow \pi$ transition in [192]. The lowest x moment of the corresponding GPDs are the $B \rightarrow \pi$ transition form factors, which are an essential ingredient to the study of various exclusive B meson decays. The GPD formalism has been used in order to classify contributions to these form factors of different dynamical nature, which can then be added without double counting. The main tool in this classification was the representation of GPDs in terms of light-cone wave functions. This representation had earlier been considered for the $B \rightarrow \pi$ transition in [164], whose main observation was that for this transition reference frames with vanishing skewness ξ are kinematically not possible if $\Delta^2 > 0$. The ERBL regime with its emission of a $u\bar{b}$ or $d\bar{b}$ -pair from the initial B meson then always appears in the overlap representation of the form factors.

Frankfurt et al. [188] have pointed out that one can even define GPDs for fermion number changing transitions such as $p \rightarrow \pi$. They involve operators with three quark fields (similarly to the three-quark DA in the proton) and involve several partonic regimes corresponding to the DGLAP and ERBL regions of ordinary GPDs. They are for instance sensitive to components of the nucleon wave functions with three quarks at a small transverse distance, plus a number of spectator partons that form the outgoing pion. Such GPDs appear in electroproduction processes like $\gamma^*p \rightarrow \pi p$ at large Q^2 and small Mandelstam variable u , i.e. in kinematics where in the collision c.m. the π moves in the direction of the initial proton, and the final p in the direction of the γ^* . Note however that the hard scattering process in this case is related to the one for the elastic transition $\gamma^*p \rightarrow p$ at large Q^2 ; experience with that reaction suggests that the leading-twist regime may only be reached at extremely large values of Q^2 (see Section 10.3).

3.15 Spin 1 targets

GPDs for hadrons with spin $J = 1$ are of practical importance for experiments on nuclear targets, in particular on the deuteron (see Section 4.5). Their spin classification and basic properties (in the parton helicity conserving sector) have been given by Berger et al. [193]. The helicity counting rules of Section 3.5.4 tell us that for each quark flavor and the gluons there are 9 parton helicity conserving GPDs, 5 of them averaged over parton helicities and 4 sensitive to parton polarization. For quarks one has⁹

$$\begin{aligned} \frac{1}{2} \int \frac{d\lambda}{2\pi} e^{ix(Pz)} \langle p' | \bar{q}(-\frac{1}{2}z) \not{n}_- q(\frac{1}{2}z) | p \rangle \Big|_{z=\lambda n_-} &= -(\epsilon'^* \epsilon) H_1 \\ &+ \frac{(\epsilon n_-)(\epsilon'^* P) + (\epsilon'^* n_-)(\epsilon P)}{P n_-} H_2 - \frac{2(\epsilon P)(\epsilon'^* P)}{m^2} H_3 \\ &+ \frac{(\epsilon n_-)(\epsilon'^* P) - (\epsilon'^* n_-)(\epsilon P)}{P n_-} H_4 \\ &+ \left[m^2 \frac{(\epsilon n_-)(\epsilon'^* n_-)}{(P n_-)^2} + \frac{1}{3}(\epsilon'^* \epsilon) \right] H_5, \end{aligned}$$

⁹Note that the vector P in [193] is defined with an extra factor of 2 compared with our convention (5) here.

$$\begin{aligned}
\frac{1}{2} \int \frac{d\lambda}{2\pi} e^{ix(Pz)} \langle p' | \bar{q}(-\frac{1}{2}z) \not{n}_- \gamma_5 q(\frac{1}{2}z) | p \rangle \Big|_{z=\lambda n_-} &= -i \frac{\epsilon_{\mu\alpha\beta\gamma} n_-^\mu \epsilon'^{\ast\alpha} \epsilon^\beta P^\gamma}{P n_-} \tilde{H}_1 \\
+ 2i \frac{\epsilon_{\mu\alpha\beta\gamma} n_-^\mu \Delta^\alpha P^\beta}{P n_-} \frac{\epsilon^\gamma(\epsilon'^{\ast} P) + \epsilon'^{\ast\gamma}(\epsilon P)}{m^2} \tilde{H}_2 & \\
+ 2i \frac{\epsilon_{\mu\alpha\beta\gamma} n_-^\mu \Delta^\alpha P^\beta}{P n_-} \frac{\epsilon^\gamma(\epsilon'^{\ast} P) - \epsilon'^{\ast\gamma}(\epsilon P)}{m^2} \tilde{H}_3 & \\
+ \frac{i}{2} \frac{\epsilon_{\mu\alpha\beta\gamma} n_-^\mu \Delta^\alpha P^\beta}{P n_-} \frac{\epsilon^\gamma(\epsilon'^{\ast} n_-) + \epsilon'^{\ast\gamma}(\epsilon n_-)}{P n_-} \tilde{H}_4, & \tag{205}
\end{aligned}$$

where ϵ and ϵ' are the respective polarization vectors of the incoming and outgoing deuteron. Time reversal invariance gives that H_4 and \tilde{H}_3 are odd in ξ and all other GPDs even in ξ . Taking the lowest moments in x we recover the vector and axial vector form factors for elastic deuteron transitions,

$$\begin{aligned}
\int_{-1}^1 dx H_i(x, \xi, t) &= G_i(t) \quad (i = 1, 2, 3), \\
\int_{-1}^1 dx \tilde{H}_i(x, \xi, t) &= \tilde{G}_i(t) \quad (i = 1, 2),
\end{aligned} \tag{206}$$

with

$$\begin{aligned}
\langle p' | \bar{q}(0) \gamma^\mu q(0) | p \rangle &= -2(\epsilon'^{\ast} \epsilon) P^\mu G_1(t) \\
+ 2 \left[\epsilon^\mu(\epsilon'^{\ast} P) + \epsilon'^{\ast\mu}(\epsilon P) \right] G_2(t) &- 4(\epsilon P)(\epsilon'^{\ast} P) \frac{P^\mu}{m^2} G_3(t), \\
\langle p' | \bar{q}(0) \gamma^\mu \gamma_5 q(0) | p \rangle &= -2i \epsilon^\mu_{\alpha\beta\gamma} \epsilon'^{\ast\alpha} \epsilon^\beta P^\gamma \tilde{G}_1(t) \\
+ 4i \epsilon^\mu_{\alpha\beta\gamma} \Delta^\alpha P^\beta \frac{\epsilon^\gamma(\epsilon'^{\ast} P) + \epsilon'^{\ast\gamma}(\epsilon P)}{m^2} &\tilde{G}_2(t).
\end{aligned} \tag{207}$$

One furthermore has

$$\int_{-1}^1 dx H_4(x, \xi, t) = \int_{-1}^1 dx \tilde{H}_3(x, \xi, t) = 0 \tag{208}$$

because of time reversal invariance, and

$$\int_{-1}^1 dx H_5(x, \xi, t) = \int_{-1}^1 dx \tilde{H}_4(x, \xi, t) = 0 \tag{209}$$

because the definitions of these GPDs involve the tensor $n^\mu n^\nu$, whose analog is forbidden by Lorenz invariance in the decomposition of the local vector and axial vector currents.

In the forward limit H_1 , H_5 , and \tilde{H}_1 tend to the well-known quark densities in the deuteron, which at leading twist and leading order in α_s are respectively proportional to the structure functions $F_1(x)$, $b_1(x)$, and $g_1(x)$ [194]. The vanishing of the integral of H_5 over x is directly related to the sum rule for $b_1(x)$ found by Close and Kumano [195].

4 Dynamics and models

At present GPDs are still mostly unknown functions, apart from the constraints from the forward limit and from sum rules relating them to elastic form factors. In this section we will review the current strategies to make ansätze for these functions, which are needed for two practical reasons. One is that the projection of experiments requires at least roughly correct predictions for cross sections and

event distributions. On the other hand, the only known strategy at present to “extract” GPDs from measurements is to assume a functional form of GPDs with a number of adjustable parameters, and to fit these by comparing the resulting cross sections and distributions with experimental data, just as one does in the standard analyses of usual parton densities. For this to be reliable one needs some confidence that the assumed functional dependence is adequate to capture the actual shape of GPDs as functions of three kinematical variables. A better understanding of these issues finally means a better understanding of hadron structure itself, which is the ultimate goal of studying GPDs.

Among the features of GPDs one needs to understand is first the interplay between the two momentum fractions, i.e. between the x and ξ dependence.

- In the DGLAP region, a way to put this question is how strongly GPDs at a given x and ξ differ from the forward distributions at the same x or some combination of x and ξ like $x_{\text{in}} = (x + \xi)/(1 + \xi)$.
- The structure of GPDs in the ERBL region is yet more difficult to guess from the usual parton densities. Lorentz invariance (and its realization by double distributions) indicates that there is cross talk between the two regions, but also that there are contributions to the ERBL region which are invisible in the DGLAP regions and hence in the forward limit (see Section 3.9.2).
- As discussed in Section 3.13 a particularly important point is the behavior of GPDs for x in the vicinity of ξ , both for the physics it reflects and for its prominent role in physical scattering amplitudes.

A second feature is the correlation between the dependence on t and the longitudinal variables x and ξ . This concerns the interplay between transverse and longitudinal momenta of partons, or in the impact parameter representation the relation between the transverse location of quarks or gluons and their longitudinal momenta. In yet a different form the question is how different the t dependence is for the various form factors one obtains by taking x -moments of GPDs for the various parton species.

Some of these issues have been addressed in toy models. These do not claim to reflect the dynamics of QCD but allow one to explore which structures can be generated in relativistic quantum field theories where calculations can be pushed further than in QCD, since one may use perturbation theory or can exactly solve the theory. We have already mentioned examples of such studies [39, 148, 154, 182, 183] when discussing the behavior of GPDs at the point $x = \xi$ in Section 3.13. Perturbative studies also provide a glimpse into the relation between physics in the DGLAP and ERBL regimes, which look very different in a partonic picture but in these examples are generated by the same covariant Feynman diagrams in different kinematical regions.

4.1 Dynamics of GPDs

There is also a growing number of studies using either dynamical symmetries of QCD or models that aim to capture at least part of QCD dynamics. Whereas no dynamical model can presently give predictions detailed enough to obtain, say, the full scattering amplitude of deeply virtual Compton scattering, models can make predictions concerning general features like those just mentioned. Turning these into predictions on observable quantities, one can hope to test aspects of such models against experiment. Ideally, this will allow one to put to test the physical picture of the dynamics responsible for the many nontrivial features of hadron structure encoded in GPDs.

4.1.1 Chiral symmetry

Since GPDs are low-energy quantities in QCD it is natural to ask what chiral symmetry has to say about them. A number of properties can indeed be inferred from chiral symmetry and its implementa-

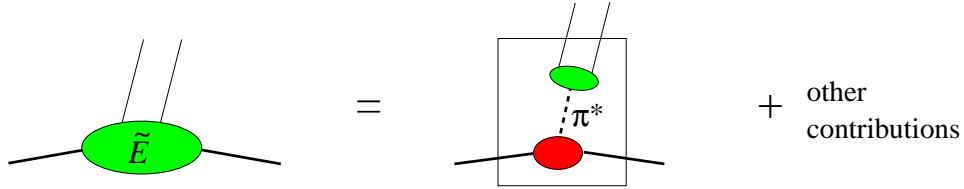


Figure 16: Pion exchange contribution to \tilde{E}^{u-d} at t close to m_π^2 .

tion in chiral perturbation theory. Notice however that, contrary to most of the “usual” applications of these concepts, GPDs involve quark and gluon fields. Applying concepts of chiral physics therefore requires a matching procedure to link low-energy degrees of freedom such as pions to the parton degrees of freedom which manifest themselves in processes at sufficiently high virtualities.

Probably the most prominent manifestation of chiral symmetry is the pion exchange contribution to the nucleon GPDs \tilde{E}^q , briefly mentioned in [188] and analyzed in [196, 197]. Physically it corresponds to the emission of a virtual pion by the initial nucleon, which for small $|t|$ is only weakly off-shell. The pion then annihilates into the $q\bar{q}$ pair probed in the hard process, see Fig. 16. This contribution is only present in the ERBL region. Due to its quantum numbers it only contributes to the C -even part of the isovector combination \tilde{E}^{u-d} and to the corresponding proton-neutron transition GPDs following the isospin relation (203). More precisely, one has a contribution from an on-shell pion if one analytically continues to $t = m_\pi^2$, where [196, 197]

$$\tilde{E}^{u-d}(x, \xi, t) \xrightarrow{t \rightarrow m_\pi^2} \theta(|x| < |\xi|) \frac{1}{2|\xi|} \phi_\pi \left(\frac{x + \xi}{2\xi} \right) \frac{4m^2 g_A(0)}{m_\pi^2 - t}. \quad (210)$$

Here we have used the pion distribution amplitude ϕ_π normalized as

$$\int_0^1 dz \phi_\pi(z) = 1, \quad (211)$$

which is related to our definition in (79) by $\phi_\pi(z) = \sqrt{2} f_\pi^{-1} \Phi_{\pi_0}^{u_0}(z)$ with $f_\pi \approx 131$ MeV. Note that both \tilde{E} and ϕ_π depend on the factorization scale μ . In (210) use has been made of the Goldberger-Treiman relation, which in the chiral limit relates the axial charge $g_A(0) \approx 1.26$ of the nucleon to the pion-nucleon coupling constant $g_{\pi NN}$ and is phenomenologically valid with about 6% accuracy [198]. The pion pole contribution to \tilde{E} may be seen as one particular instance of a resonance exchange contribution to GPDs, but it is special in that for the pion it is least questionable that one single resonance contribution may dominate at small t in the physical region, due to the smallness of m_π^2 . Even for the pion there are corrections to the pole contribution (210) that are not negligible at $-t$ of a few 0.1 GeV², according to estimates in the chiral soliton model (see Section 4.1.3).

Another application of chiral dynamics is to study nonanalytic terms in the dependence of GPDs on t and on the pion mass. Whereas the t dependence is of obvious physical concern, the dependence on m_π is important for instance in lattice QCD studies, which require extrapolation of results from unphysically large values of m_π to its physical value. In particular, a logarithmic behavior of GPDs in t and m_π^2 is generated by loop corrections in chiral perturbation theory. Belitsky and Ji [199] have studied these terms for the Mellin moments of the nucleon GPDs H^q and E^q , matching the relevant local quark-antiquark operators to operators constructed from pion and nucleon fields, and then calculating the corresponding one loop corrections in heavy-baryon chiral perturbation theory. Non-analytic terms in t only occur for the isoscalar combination of second moments $\int dx x H^{u+d}$ and $\int dx x E^{u+d}$ and the isovector combination of first moments $\int dx H^{u-d}$ and $\int dx E^{u-d}$. For the other

isospin combinations and for all higher moments, the t dependence is hence at most linear at small t to first order in chiral perturbation theory.

For GPDs involving pions, constraints can be obtained for configurations where a pion momentum becomes soft, more precisely when its four-momentum goes to zero in the chiral limit. Such soft-pion theorems relate for instance the transition GPDs for $N \rightarrow N\pi$ in the limit of a soft pion momentum to nucleon and pion GPDs. Already mentioned in [37], this has recently been investigated in [190].

Not surprisingly, soft pion theorems also exist for GPDs of the pion. Here the zero-momentum limit for the outgoing pion means $\xi \rightarrow 1$ and $t \rightarrow 0$, and one finds [87]

$$\lim_{\xi \rightarrow 1} H_{\pi}^{u-d}(x, \xi, 0) = \phi_{\pi} \left(\frac{1+x}{2} \right), \quad \lim_{\xi \rightarrow 1} H_{\pi}^{u+d}(x, \xi, 0) = 0 \quad (212)$$

in the chiral limit of QCD. Note that $\xi = 1$ is not in the physical region in a world with massive pions, so that the above relations are to be understood in the sense of an analytic continuation. The constraints (212) have consequences for the GPDs at ξ away from 1. They imply for instance that at $t = 0$ the second moment of H_{π}^{u+d} is given by one instead of two parameters [90]:

$$\int_{-1}^1 dx x H_{\pi}^{u+d}(x, \xi, 0) = (1 - \xi^2) A_{\pi}^{u+d}(0), \quad (213)$$

where $A_{\pi}^{u+d}(0)$ is the momentum fraction carried by u and d quarks and antiquarks in the pion. Taking the $\xi = 1$ limit of (124) also fixes the quark D -term at $t = 0$ in terms of the corresponding double distribution. In particular its first Gegenbauer moment defined in (139) is fixed to be $d_1^{u+d}(0, \mu^2) = -\frac{5}{4} A_{\pi}^{u+d}(0, \mu^2)$, which is sizeable and of definite sign [200].

A systematic treatment of pion GPDs in the context of chiral perturbation theory has been given in [131]. In lowest order of the chiral expansion, the double distributions $f(\beta, \alpha)$ of the pion coincide with generating functions for the low-energy constants that match the local twist-two quark-antiquark operators onto pion operators in the effective theory. The soft pion theorems (212) are readily obtained in the chiral limit. At one-loop level one obtains corrections to these theorems, which involve logarithms of t or m_{π}^2 and are parametrically suppressed by $m_{\pi}^2/(4\pi f_{\pi})^2$ as usual in chiral perturbation theory. An interesting finding is that to this order a nonanalytic t -dependence is generated only in the ERBL region; this predicts in particular a different t -behavior of the real and imaginary parts of hard scattering amplitudes. Taking $\xi = 0$ and converting to impact parameter space, one obtains the transverse distributions of quarks at large impact parameter. It is found to come from low-momentum quarks, and by inspection of the relevant diagrams it is naturally attributed to the long range pion “cloud” of the target.

4.1.2 The large- N_c limit

The limit of $SU(N_c)$ gauge theory with the number N_c of colors going to infinity has proven to be a valuable guide to the physics of QCD with $N_c = 3$, both for mesons [201] and for baryons [202]. We have already mentioned in Section 3.14.2 that the large- N_c limit relates the GPDs for the $N \rightarrow \Delta$ transitions with the GPDs of the nucleon. The large- N_c properties of nucleon GPDs for u - and d -quarks have been investigated in [203, 197] and are summarized in the review [37]. In the large- N_c limit baryon masses scale as $m \sim N_c$, and to fix a power-counting scheme the kinematical region with $t \sim N_c^0$ and $\xi \sim 1/N_c$, $x \sim 1/N_c$ has been specified. Note that the scaling of the quark momentum fractions $x \pm \xi \sim 1/N_c$ matches the large- N_c picture of a baryon as a bound state of N_c quarks.

The large- N_c limit then predicts the relative size of different combinations of GPDs. For leading isospin combinations one has [37]

$$\begin{aligned} H^{u+d} &\sim N_c^2, & E^{u-d} &\sim N_c^3, \\ \tilde{H}^{u-d} &\sim N_c^2, & \tilde{E}^{u-d} &\sim N_c^4. \end{aligned} \quad (214)$$

In each case, the other isospin combination is suppressed by one power of N_c . For the D -term one finds $D^{u+d} \sim N_c^2$ and $D^{u-d} \sim N_c$, so that it contributes at leading order to H^u , H^d and the isosinglet combination E^{u+d} , but appears with a relative suppression by $1/N_c^2$ in E^{u-d} . Taking into account the power counting for the kinematical variables one obtains the scaling behavior of the matrix elements $F_{\lambda'\lambda}^q$ and $\tilde{F}_{\lambda'\lambda}^q$ in (54), which correspond to definite nucleon helicities and occur in physical amplitudes. For the quark helicity averaged case one has

$$\begin{aligned} F_{++}^{u+d} &\sim N_c^2, & F_{-+}^{u-d} &\sim N_c^2 \\ F_{++}^{u-d} &\sim N_c, & F_{-+}^{u+d} &\sim N_c, \end{aligned} \tag{215}$$

whereas the isovector combinations \tilde{F}_{++}^{u-d} and \tilde{F}_{-+}^{u-d} scale like N_c^2 , and the isoscalar combinations \tilde{F}_{++}^{u+d} and \tilde{F}_{-+}^{u+d} scale like N_c . We note in passing that in physical applications one may have a mix of isosinglet and isotriplet combinations, for instance $\frac{4}{9}u + \frac{1}{9}d = \frac{5}{18}(u+d) + \frac{3}{18}(u-d)$ in Compton scattering processes.

It may be useful to “check” the above relations in limits where the GPDs are known. Taking the forward limit, one finds the relations $(u+d) : (u-d) \sim N_c$ and $(\Delta u - \Delta d) : (\Delta u + \Delta d) \sim N_c$ for the parton distributions. At momentum fractions $x \sim 1/N_c$ in the valence region and for moderately large factorization scale μ this is quite well satisfied in the real world with $N_c = 3$. Another test case are the anomalous magnetic moments $\kappa^q = F_2^q(0)$ for each separate quark flavor in the proton, related to the anomalous magnetic moments of proton and nucleon by $\kappa_p = \frac{2}{3}\kappa^u - \frac{1}{3}\kappa^d$ and $\kappa_n = \frac{2}{3}\kappa^d - \frac{1}{3}\kappa^u$ if one neglects the contribution from strange quarks. Numerically one has $(\kappa^u - \kappa^d) : (\kappa^u + \kappa^d) \approx 3.7 : (-0.36)$, whose size should be of order N_c according to (214). These exercises indicate that (i) terms suppressed by $1/N_c$ can indeed be as large as 30% of the leading terms, as they are entitled to be, and that (ii) as with any power counting argument one should allow for extra factors in phenomenological applications, which may be of order 3 in one direction or the other. With these caveats in mind, one may still use $1/N_c$ counting as a guide for the relative orders of magnitude between the different flavor and spin combinations of GPDs.

4.1.3 The chiral quark-soliton model

Quite detailed studies of GPDs have been performed in the chiral quark-soliton model [203, 197]; a review and references can be found in [37]. Essential ingredients of this model are the spontaneously broken chiral symmetry of QCD and the large- N_c limit, which we have just discussed. It is based on an effective field theory of QCD, obtained from the instanton model of the QCD vacuum. Degrees of freedom are pions and quarks. The quarks have a momentum dependent dynamical mass of order $M = 350$ MeV at low scale, which drops sharply at a momentum scale $1/\rho \approx 600$ MeV given by the typical instanton size ρ in the vacuum of the model. This scale provides an ultraviolet cutoff to the effective theory when calculating parton distributions. The quarks and antiquarks in these distributions should then be seen as “constituent quarks” that have an unresolved substructure at length scales smaller than ρ [204]. A simpler (but not obviously equivalent) interpretation is to associate the distributions obtained in the effective theory as the QCD quark and antiquark distributions at a factorization scale $\mu \sim 1/\rho$. Gluon GPDs are parametrically suppressed by $\rho^2 M^2$ in this framework, and have not been studied yet.

In this model the nucleon appears as a bound state of quarks in a semi-classical pion field (the “chiral soliton”). The single-particle spectrum of quarks in this field contains a bound state and continuum states of positive or negative energy. The nucleon is obtained by occupying the bound state with N_c quarks and by filling the negative-continuum Dirac sea. This leads to a “two-component” structure of nucleon GPDs with distinct contributions from the “valence” bound state level and from

the Dirac sea. Notice that the terms “valence” and “sea” have a dynamical meaning in the context of this model, which is *not* equivalent to the usual meaning of “valence” distributions as the difference $q - \bar{q}$ and of “sea” as \bar{q} . In particular, both the contributions from the “valence” and “sea” levels have support in then entire regions $-1 < x < 1$ (although the valence contribution is largest for moderate positive x).

So far, u and d quark GPDs in the nucleon have been studied in this model to leading order in the large- N_c expansion. We note that the model provides a fair description of the unpolarized and polarized forward u and d quark distributions (including the $1/N_c$ suppressed combination $u - d$ [205]) and of the elastic nucleon form factors for $|t|$ up to about 1 GeV^2 (except for the electric form factor of the neutron) [206]. The analytic results in this model fulfill various consistency requirements, namely the forward limit and the reduction of the first Mellin moment to the elastic form factors [203, 197]. Schweitzer et al. [207, 208] have shown that the higher Mellin moments satisfy polynomiality in ξ when analytically continued to $t = 0$. Several features of GPDs were found in this model [203, 197, 37]:

- The distribution H^{u+d} exhibits rapid variations in x around $x = \pm\xi$, due to a rather smooth valence contribution and an oscillating contribution from the Dirac sea. Both H^{u+d} and \tilde{H}^{u-d} have considerable structure in the ERBL region. The Dirac sea only contributes to the C -even combinations of H^{u+d} and of \tilde{H}^{u-d} .
- The pion pole contribution (210) to \tilde{E}^{u-d} can be obtained analytically. Perhaps even more important, corrections to the pole term were also obtained and parameterized for intermediate values of t . These corrections were found to have a non-negligible impact on observables in a phenomenological study [209].
- Study of both $H(x, \xi, t)$ and $\tilde{H}(x, \xi, t)$ shows that the model does *not* support a factorized t dependence of the form $F(t)f(x, \xi)$, which is often taken as an ansatz (see Section 4.3.4).
- The isosinglet D -term for the nucleon is found to be rather large. The lowest Gegenbauer moments (139) for $t = 0$ were fitted numerically in [200] and obtained analytically in [207].

Since the pion appears as an explicit degree of freedom in the effective theory, its quark GPDs can also readily be studied, which has been done in [90, 210]. Since the model is constructed to respect the chiral symmetry breaking pattern of QCD, it respects in particular the soft-pion relations (212) in the chiral limit.

4.1.4 Quark models

The very first dynamical study of quark GPDs was carried out in the MIT bag model [211] by Ji et al. [212]. At a very low factorization scale of order 450 MeV , quark GPDs were obtained with support in the entire region $-1 < x < 1$, although strongly concentrated at $x > 0$. The curves of all four distributions H , E , \tilde{H} , \tilde{E} as a function of x were found to have an extremely weak dependence on ξ . The physics reason for this is not understood, nor is the reliability of the results in the region $x < \xi$, where antiquarks play an essential role. Also using the MIT bag model, Anikin et al. [213] have calculated the GPDs in a pion, including the twist-three distributions to be discussed in Section 6.1.1. The reliability of the model remains unclear in the ERBL region, which requires nonvalence configurations in the initial pion.

GPDs calculated in constituent quark models have support only in the region $x > \xi$. They are obtained as an overlap of Schrödinger wave functions for three constituent quarks (corresponding to equal time z^0 of the quark and antiquark operators, not to equal light-cone time z^+). Scopetta and Vento have given expressions for nonrelativistic kinematics (requiring $|t| \ll m^2$ and hence small ξ)

and studied the quark distributions H^u , H^d for different quark potentials [214]. The distributions H and E in fully relativistic kinematics have been treated by Boffi et al. [215], including the effect of the Melosh transformation for the quarks (which relates the usual states with spin quantized along the z axis with states of definite light-cone helicity). General features of the results of both groups are:

- GPDs that vanish at $x = \xi$ since the constituent wave functions vanish for zero quark momentum.
- As functions of x , the GPDs have a peak whose position shifts to the right with increasing ξ and also with increasing $|t|$.
- To the right of this peak the shape in x varies very little with ξ .

Whereas the nonrelativistic approximation in [214] leads to the artifact that GPDs are small but nonvanishing at $x = 1$, the relativistic treatment does not have this drawback.

An interesting feature of the results in [215] is that the distributions E fall off faster at $x \rightarrow 1$ than the distributions H . We have seen in Section 3.11.2 that E can be represented at the overlap of light-cone wave functions where at least one wave function involves nonzero orbital angular momentum L^3 . The Schrödinger wave functions of the constituent quarks are in an S -wave, but the Melosh transform to light-cone helicity states generates light-cone wave functions with nonzero L^3 . The effect of this transform diminishes when the quark momentum increases. This may be the reason for the stronger decrease of E at large x , where the struck parton becomes fast (a more careful analysis would have to take into account the orbital angular momentum of the spectators). The importance of the Melosh transform for generating the proton helicity flip form factor $F_2(t)$ has also been stressed by Miller and Frank [216].

As x approaches the boundary to the ERBL region, the results of constituent quark models become more problematic. A way to capture the physics of higher Fock states and in particular of antiquarks in the nucleon may be to assign a substructure to constituent quarks [214]. Simply applying the evolution equations to constituent quark GPDs does of course also generate antiquarks and gluons, fill up the zero at $x = \xi$, and populate the region $x < \xi$ when going to higher scales μ . It will be interesting to test such scenarios against data for hard processes, where GPDs at $x \sim \xi$ are of prime importance.

Restricted to the three-quark configurations in the proton, constituent quark models will in general not respect the polynomiality constraints. In particular, elastic form factors can be obtained in this framework by integrating over x , but only in frames with $\xi = 0$.

4.1.5 Covariant approaches

Attempts for a consistent description of the physics in the ERBL region have been made in the covariant approach of reducing Bethe-Salpeter to light-cone wave functions, whose essentials we explained in Section 3.11.3. The different Fock states required in the ERBL and the DGLAP regions are here generated by the same covariant diagrams. Remember that in the perturbative example of Section 3.11.3 the triangle diagram in the ERBL region could be written in terms of the light-cone wave functions for three particles or for one particle in a single-particle state. The situation is however more complicated if the external state is not an elementary particle as in that example, but a bound state. Interpreting the external lines in Fig. 14c as “hadrons” and the internal lines as “partons”, one would obtain the “wave function” for one hadron plus two partons in a single hadron, which as it stands is not part of the Fock state expansion.

A strategy that has been pursued in the literature is to replace the pointlike vertices in the triangle diagram Fig. 14 with the bound-state Bethe Salpeter wave functions Ψ_{BS} and to make use

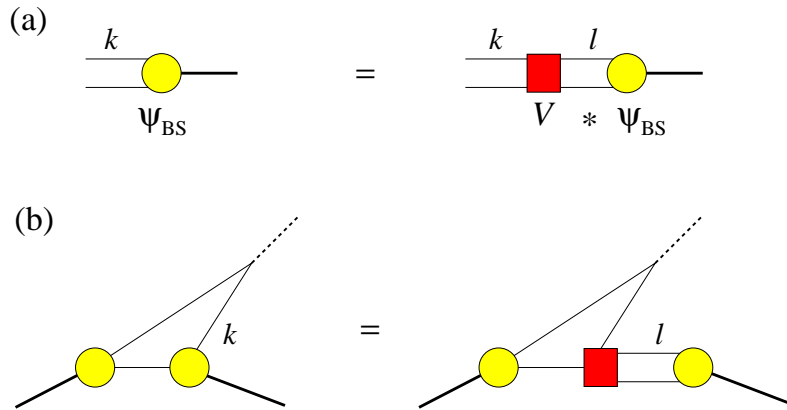


Figure 17: (a) Schematic representation of the Bethe-Salpeter equation. (b) The Bethe-Salpeter equation may be used to trade a crossed wave function for the crossed interaction kernel. The dashed line denotes the external (local or nonlocal) current.

of the Bethe-Salpeter equation, depicted schematically in Fig. 17a. The crossed vertex function for the final state hadron in Fig. 17b is not in the correct kinematics to reduce to a light-cone wave function after integration over k^- . Using the Bethe-Salpeter equation as in Fig. 17b one obtains a form where crossing has to be performed for the two-parton interaction kernel V instead. Integrating over the momentum l^- and using Cauchy's theorem to pick up appropriate singularities one may then hope to reduce Ψ_{BS} to a light-cone wave function. In general this still is nontrivial since in addition to $\Psi_{\text{BS}}(l)$ the interaction kernel $V(k, l)$ can have a nontrivial dependence on l^- . One also needs to take into account interactions at the vertex with the external current operator, which involve configurations as in Fig. 18b. We remark that in the 't Hooft model the interaction between quarks is exactly instantaneous in light-cone time (i.e., V is independent on k^- and l^-), and the physical picture of Fig. 18 indeed appears in the evaluation of GPDs in the ERBL region [183]. For other interactions the implementation of this program still requires approximation schemes, which must be chosen with care in order to obtain consistent results, in particular continuity of GPDs at $x = \xi$. This was clearly seen in the work of Choi et al. [217] compared with their earlier attempt [218]. Different approximations were studied by Tiburzi and Miller [219]. In subsequent work [220, 154] these authors used a particular expansion scheme in the reduction to the light cone and found that configurations as in Fig. 18 can be systematically replaced by higher Fock states, thus recovering the overlap representation. So far such work has had to resort to the weak-coupling limit, and it may be that the results obtained are more immediately applicable not to bound states of quarks but rather to bound states of nucleons (see Section 4.5). No scheme is known where polynomiality of GPDs is exactly satisfied, but in practice it may be sufficient to have approximate polynomiality in kinematics where the scheme is valid, especially if there is a systematic way of taking into account corrections as proposed in [220, 154]. The problems discussed here are not only relevant for describing GPDs, but equally occur in form factors for the transition from heavy to light hadrons at timelike momentum transfer, see Section 3.14.3.

Theußl et al. [182] have taken a different route and calculated GPDs directly from the covariant diagrams with four-dimensional Bethe-Salpeter vertices, without projecting on the light-cone. In this case full covariance is retained, and polynomiality is exact. To obtain the required wave functions one must now solve the full Bethe-Salpeter equation, instead of its light-cone projection. The field theories considered in [182] are scalar electrodynamics and the Nambu Jona-Lasinio model.

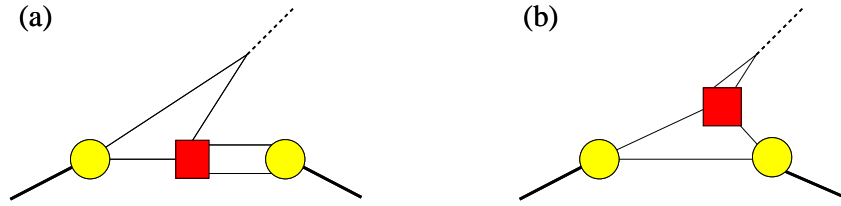


Figure 18: Relevant configurations of the triangle diagram in the ERBL region.

4.1.6 Light-cone wave functions and partons

The approaches discussed so far deal with *effective* quark degrees of freedom, which are not connected in a simple way to the quark fields in the QCD Lagrangian. A different line of work, initiated in [31], deals directly with the overlap representation of GPDs in terms of light-cone wave functions for parton Fock states (Section 3.11), which directly correspond to the QCD quark fields defining GPDs. The rationale of such efforts is to model the wave functions for the lowest Fock state and to link a variety of processes where one can reasonably expect the leading Fock state to provide the dominant contribution. These are in particular parton distributions at large x , and GPDs or form factors at large values of t . We make here the additional assumption that in an important kinematical region parton configurations with low internal virtualities provide the bulk contribution to GPDs, and that contributions involving partons far off-shell become dominant only very close to the limits $x \rightarrow 1$ or $|t| \rightarrow \infty$. Such off-shell configurations involve hard gluon exchange and lead to the well-known dimensional counting rules of Brodsky and collaborators, see e.g. [50]. In which kinematics such perturbative configurations take over remains controversial (see our discussion in Section 10.1).

Bolz and Kroll [221] have developed a model wave function for the three-quark Fock state in the nucleon, adjusting parameters to describe the unpolarized u and d quark distributions at large x , the Dirac form factor $F_1(t)$ at large t , and the decay $J/\Psi \rightarrow p\bar{p}$. The wave function is restricted to the configurations with orbital angular momentum $L^3 = 0$, principally because theoretical and phenomenological information on the $L^3 \neq 0$ wave functions is even more scarce. The wave function is understood to be *soft* (associated with a normalization scale $\mu_0 = 1$ GeV), excluding configurations with large virtualities and in particular the perturbative tail at large transverse momenta that is generated by hard gluon exchange. Its dependence on the \mathbf{k}_i is taken as

$$\Psi(x_i, \mathbf{k}_i) = N_3 \phi(x_1, x_2, x_3) \frac{(4\pi a_3)^4}{x_1 x_2 x_3} \exp \left[-a_3^2 \sum_{i=1}^3 \frac{\mathbf{k}_i^2}{x_i} \right], \quad (216)$$

where N_3 is a normalization constant. The probability for the corresponding Fock state comes out as $P_3 \approx 0.17$. This alone makes it clear that one is not dealing with a constituent wave function, which would be normalized to one. The impact parameter form of (216) is

$$\tilde{\Psi}(x_i, \mathbf{b}_i) = N_3 \phi(x_1, x_2, x_3) \exp \left[-\frac{1}{4a_3^2} \sum_{i=1}^3 x_i \mathbf{b}_i^2 \right], \quad (217)$$

and shows that the constant a_3 describes the average transverse size of this particular Fock state. A Gaussian ansatz for the \mathbf{k}_i dependence has the virtue of allowing one to perform integrals analytically. A dependence on the combination \mathbf{k}_i^2/x_i naturally arises in light-cone perturbation theory [38, 50], or equivalently when integrating covariant Feynman diagrams over k^- as discussed in Section 3.11.3.

The Gaussian ansatz for the \mathbf{k}_i dependence in (216) goes back to Brodsky et al. [222]. Its analog for two partons instead of three has some theoretical support from studies of the $q\bar{q}$ wave functions

with $L_3 = 0$ in a π or a ρ . Szczepaniak et al. [223] found this form for the pion using QCD sum rules, although a different dependence can be obtained in the same framework (namely by using local parton hadron duality instead of the Borel transform). Halperin and Zhitnitsky [224, 225] strongly argue in favor of a Gaussian dependence as in (216) near the endpoints $x_i \rightarrow 0$, based on a study of high moments $\int dx d^2\mathbf{k} (2x-1)^n \mathbf{k}^{2m} \Psi(x, \mathbf{k}^2)$ with QCD sum rule techniques.¹⁰ We caution that a discussion of the behavior of wave functions at large \mathbf{k}_i^2/x_i , corresponding to large off-shellness, requires careful consideration of the renormalization and factorization scheme in which they are defined. In the context where we use them, wave functions at small scale μ^2 are to describe the region of small off-shellness, the hard region being explicitly included in hard-scattering kernels. From a pragmatic point of view this is just what the above Gaussian ansatz ensures: in practical applications there is little difference whether one includes the region of high \mathbf{k}_i^2/x_i in integrals or not.

The function $\phi(x_1, x_2, x_3)$ in (216) is the leading-twist distribution amplitude in the proton at normalization scale μ_0 . In [221] a simple polynomial form was taken for $\phi(x_1, x_2, x_3)$, with a weak deviation from its asymptotic form under evolution. It has been argued that in the exponent of (216) the combination $\mathbf{k}_i^2 + m_{\text{eff}}^2$ should appear, where m_{eff} is a quark mass of some 100 MeV generated by nonperturbative physics [38, 226]. This would generate a factor

$$\exp \left[-a_3^2 \sum_{i=1}^3 \frac{m_{\text{eff}}^2}{x_i} \right] \quad (218)$$

in $\phi(x_1, x_2, x_3)$. A polynomial form was taken in [221, 31] to retain simplicity of expressions. We emphasize that the corresponding wave function has been used to describe the physics for configurations with parton momentum fractions going down to order 0.1. In such a limited region a polynomial or a polynomial times the exponential (218) should be practically equivalent, given an adequate adjustment of the wave function parameters. The ansatz is *not* intended for extremely small values of x_i or for the limit $x_i \rightarrow 0$, where there is a qualitative difference between a polynomial and a polynomial times (218).

An attempt has been made in [31] to also model the wave functions for the next highest Fock states with an extra gluon or with an extra $q\bar{q}$ pair. The principal aim was to obtain an indication of how important higher Fock state contributions are for various quantities. The ansatz was tailored along the form (216) with simplicity as the main guide and free parameters fitted to describe the unpolarized antiquark and gluon distributions at large x . A good description was obtained for valence distributions $q - \bar{q}$ and $\Delta q - \Delta \bar{q}$ of u and d quarks at $x \gtrsim 0.5$, with the three-quark Fock component dominating for $x \gtrsim 0.6$. Notice that the polarized quark densities were not used to constrain the model wave functions, so that agreement in this sector is a nontrivial test of the model. A fair description of the Dirac form factors F_1 of proton and neutron was also obtained for large t .

An important outcome of the study in [31] is that the nominal leading power behavior in $(1-x)$ of the soft contributions to parton densities (which is easily identified in the analytical expressions) gave a poor representation of the full result in a large range of x . The same holds for the nominal leading power behavior in t of elastic form factors. This recommends care in using power counting arguments for soft physics contributions of this particular type.

Using the above ansatz to evaluate GPDs at large x or large t , one finds again that higher Fock states become gradually important as x decreases, with the leading three-quark contribution dominating roughly for $x \gtrsim 2\xi$. An important feature is that the t dependence is intimately related

¹⁰Note that the wave functions in [224, 225] are defined such that these moments correspond to local operators containing covariant derivatives D^μ in the transverse direction. The nonlocal operator associated with $\Psi(x, \mathbf{k}^2)$ thus involves gluon fields with transverse polarization and hence differs from our definition using the Fock state expansion in Section 3.11.

with x and ξ , as suggested by the generic structure of the overlap representation (166). For $\xi = 0$ the Gaussian ansatz for the wave functions leads to the simple structure

$$H(x, 0, t) = q(x) \exp \left[\frac{a^2}{2} \frac{1-x}{x} t \right] \quad (219)$$

for the separate contributions from each Fock state, which are summed over in the end. An analogous expression relates \tilde{H} and Δq . Taking x -moments one obtains elastic form factors, which at large t are dominated by large x . With the model parameters in [31] the dominant values of x in the integral giving the proton Dirac form factor range between 0.45 and 0.75 for $|t|$ between 5 GeV² and 20 GeV², indicating that in this region one is indeed far away from the $x \rightarrow 1$ limit. The expression (219) makes it clear why for this mechanism the typical momentum scale of the t -dependence is not given by the inverse of a typical transverse size a^{-1} , which is below 1 GeV, but by this scale times a typical value of $(1-x)^{-1/2}$. This results in a momentum scale of several GeV.

The form (219) has also been used as a guide for an ansatz with a larger range of validity and less dependence on model parameters, assuming that the transverse size parameter a is similar for the lowest few Fock states. In kinematics where these dominate, one can then just sum over them and read (219) as a relation between the full parton distributions, where a is now an ‘‘average’’ transverse size of the relevant contributing Fock states. From its origin it is however clear that (219) is not sensible for all x and t . If both variables are small, an increasing number of Fock states becomes relevant for which the assumption of a common dependence of the type (216) with one average size parameter a is less and less plausible. In particular, (219) leads to an infinite value of $dF_1/(dt)$ at $t = 0$ since the relevant integrand $x^{-1}(q - \bar{q})$ is too singular at $x = 0$. Restricting oneself to the contributions from the lowest Fock states in the model, one obtains a quark distribution $q(x)$ vanishing at $x = 0$ and hence a finite value of $dF_1/(dt)$ at $t = 0$. These contributions have however no claim to dominate the actual charge radius of the proton.

The ansatz (216) refers to a low factorization scale of $\mu_0 = 1$ GeV, and hence also the approximate relation (219). When going to higher scales both $H(x, 0, t; \mu^2)$ and $q(x; \mu^2)$ evolve according to the usual DGLAP equations. In a study of the pion GPDs, Vogt [227] has found that for large x and t the relation (219) is approximately valid over a finite range of μ if the parameter a is taken to decrease logarithmically with μ (without allowing it to depend on x). This shows a certain robustness of the ansatz (219), although its motivation from the overlap of soft wave function comes from low scales μ .

An ansatz analogous to (219) has also been proposed by Radyushkin on the basis of the overlap of ‘‘effective’’ two-body wave functions [30]. It has further been explored in [228, 229, 230] for the nucleon, and in [231] for the pion.

Clearly the Gaussian \mathbf{k} dependence in (216) has the status of an ansatz and may not capture all important features of light-cone wave functions. Tiburzi and Miller have explored the overlap of wave functions for weakly bound two-body systems [232]. They point out that, contrary to wave functions with a power-law falloff such as $1/\mathbf{k}^4$, a Gaussian dependence has special features (the product of two Gaussians with shifted \mathbf{k} arguments, which appears in the overlap formula (166), is again a Gaussian). We also remark that in wave functions with nonzero L^3 additional factors \mathbf{k}_i must appear in order to have the correct properties under rotations about the 3-axis.

4.1.7 The limit of large t

The dynamics discussed in the previous section involves low internal virtualities. At very large t , the perturbative contributions given by the hard scattering mechanism will be dominant according to general power counting arguments [38, 50]. This limit may not be achievable in any realistic experiment, but its features are of theoretical interest similar to those of the toy field theory studies

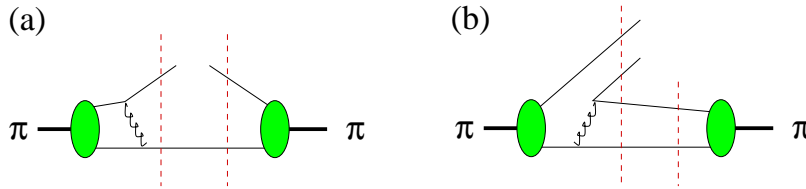


Figure 19: (a) One of the two diagrams for H_π^q in the limit of large t in the DGLAP region $x \in [\xi, 1]$. In the second diagram the gluon is exchanged after the struck quark returns. (b) The diagram contributing in the ERBL region. Dashed lines indicate the representation as an overlap of light-cone wave functions.

discussed earlier. For the quark GPDs of the pion this was investigated by Vogt [233]. In the large- t limit H_π^q can be expressed in terms of the leading-twist DAs of each pion, convoluted with a hard-scattering kernel. To leading order in α_s the relevant diagrams are those given in Fig. 19, provided one uses light-cone gauge $A^+ = 0$. The scale of virtualities in these diagrams is set by t , which thus provides the factorization scale of the obtained GPDs, and the scale of α_s . Salient features of the results in [233] are:

- The t dependence is given as $H_\pi^q(x, \xi, t) = \alpha_s(t) t^{-1} h^q(x, \xi)$. This is compatible with dimensional counting behavior, as for the pion form factor, which is obtained from the lowest Mellin moment of H_π^q . Corrections to the result are power suppressed in $1/t$.
- At $x = \xi$ the GPDs are finite and continuous, but their derivative has a singular behavior like $\log|x - \xi|$. This confirms once more the suspected behavior discussed in Section 3.13.
- For $x \rightarrow 1$ the GPDs develop an unphysical logarithmic singularity like $\log(1 - x)$. In this region the spectator quark in one of the pions becomes slow and the internal virtualities of the diagrams of Fig. 19 small, so that the collinear hard scattering approximation is no longer justified.
- From the diagrams in Fig. 19 one readily sees that to this level of accuracy H_π^s is zero. Similarly, H_π^u is zero for $x < -\xi$ since the diagrams cannot generate \bar{u} antiquarks in a π^+ .
- The obtained GPDs exactly satisfy the polynomiality property.

The results of the calculation can also be cast into the form of a wave function overlap. The analysis is similar as for the pion form factor, see Section 4 of [50] and also the discussion in [232]. The perturbative tail at large \mathbf{k} generated by one-gluon exchange for a $q\bar{q}$ wave function is now essential and easily identified in the diagram of Fig. 19a. The integration over \mathbf{k} turns one of the light-cone wave functions into a distribution amplitude. In the ERBL region the hard-scattering diagrams generate the overlap of a 4-parton wave function with the 2-parton one as shown in Fig. 19b.

4.1.8 Lessons from impact parameter space

The impact parameter representation of GPDs can be used to motivate general features of the t -dependence in certain limits [133]. Consider first the case where $x \rightarrow 1$. For any parton configuration in a hadron localized at \mathbf{b} one has the constraint $\mathbf{b} = x_j \mathbf{b}_j + \sum_{i \neq j} x_i \mathbf{b}_i$. If j denotes the struck parton, the momentum fraction x_j both in the initial and in the final state hadron goes to 1, and the spectator momentum fractions x_i in both hadrons go to zero. Barring the possibility that the

transverse distribution of the spectators becomes so wide that $\sum_{i \neq j} x_i \mathbf{b}_i$ can give a finite contribution even as all $x_i \rightarrow 0$, one finds that the centers of plus-momentum of both initial and final hadron should approximately coincide with the position \mathbf{b}_j of the fast struck parton. The \mathbf{b} profile of impact parameter GPDs should hence become a narrow peak around $\mathbf{0}$ for $x \rightarrow 1$ and any ξ . In momentum representation this translates into a flat t dependence of the GPDs in this limit. Note that the wave function ansatz (217) and its consequence (219) do satisfy this requirement.

As already discussed, the relation (219) is not acceptable in the opposite limit $x \rightarrow 0$, where it would give a transverse extension of partons growing as fast as $\langle \mathbf{b}^2(x) \rangle \sim 1/x$. Gribov diffusion, i.e., the physical picture of repeated parton branching at small x as a diffusion process in impact parameter space, leads to a growth as $\langle \mathbf{b}^2(x) \rangle \sim \log(x_0/x)$ with a Gaussian profile both in impact parameter and momentum space [234]. This gives a t -dependence of the form

$$H(x, 0, t) \stackrel{x \rightarrow 0}{\sim} \exp \left[\alpha' \left(\log \frac{x_0}{x} \right) t \right] \quad (220)$$

with constants α' and x_0 . One recognizes the interplay of t and x -dependence of Regge theory; we will come back to this point in Sections 4.3.4 and 8.

Dedicated studies of impact parameter dependent GPDs at $\xi = 0$ have recently been performed for the pion within transverse lattice gauge theory by Dalley [235] and within quark models by Broniowski and Ruiz Arriola [236].

4.2 Moments

Moments of GPDs are important in different respects. They provide a particular reduction of the rich information contained in functions of three kinematical variables, which can be very useful for certain aspects. In Section 3.10.1 we have seen that a different t dependence of different Mellin moments reflects how partons are distributed in the transverse plane depending on their momentum fraction. The second moments of H^q and E^q (and the first moments of H^g and E^g) are of particular importance since the associated operator of energy-momentum is of fundamental importance in field theory and in particular provides access to the angular momentum sum rule (Section 3.6). We have also seen that conformal moments of GPDs have particularly simple properties under evolution in leading logarithmic accuracy.

Among the dynamical investigations discussed above, dedicated results on moments have been given in the MIT bag study [212], in the study of chiral loop contributions [199] and in the chiral soliton model [197]. In the future one can expect important contributions from lattice QCD, where moments are the adequate quantities to be calculated, and which presents a perspective to obtain results from first principles in QCD. Lattice calculations for moments of forward parton distributions have been pursued for some time, see e.g. [237, 238] for recent reviews. Evaluating matrix elements of local operators between hadron states of different momentum is also possible using lattice methods, as has been shown in first studies of the elastic nucleon form factors $F_1(t)$, $F_2(t)$, $g_A(t)$ for values of $|t|$ up to about 2.5 GeV^2 [239, 240]. First lattice studies of the energy-momentum form factors $A_q(t)$, $B_q(t)$, $C_q(t)$ for u and d quarks in the proton have appeared recently [71, 72].

The moments of GPDs are given as polynomials in ξ whose coefficients are form factors. These are the quantities which have simple analytic behavior in t and are suitable for analytical continuation to the crossed channel corresponding to GDAs. Let us see which quantum number combinations are allowed in the $p\bar{p}$ channel for the various moments of GPDs. This is relevant for determining which t -channel exchanges of resonances can contribute to a given GPD, or for writing down dispersion relations for the moments. To identify the relevant quantum numbers one has to analytically continue

the form factor decompositions (35) and (37) to positive t (which we write again as s),

$$\begin{aligned}
& \langle p(p)\bar{p}(p') | \mathcal{O}_q^{\mu\mu_1\dots\mu_n} | 0 \rangle \\
&= \mathbf{S} \bar{u}(p)\gamma^\mu v(p') \sum_{\substack{i=0 \\ \text{even}}}^n [A_{n+1,i}^q(s) + B_{n+1,i}^q(s)] P^{\mu_1} \dots P^{\mu_i} \frac{1}{2}\Delta^{\mu_{i+1}} \dots \frac{1}{2}\Delta^{\mu_n} \\
&- \mathbf{S} \frac{\Delta^\mu}{2m} \bar{u}(p)v(p') \sum_{\substack{i=0 \\ \text{even}}}^n B_{n+1,i}^q(s) P^{\mu_1} \dots P^{\mu_i} \frac{1}{2}\Delta^{\mu_{i+1}} \dots \frac{1}{2}\Delta^{\mu_n} \\
&+ \mathbf{S} \frac{P^\mu}{m} \bar{u}(p)v(p') \text{mod}(n, 2) C_{n+1}^q(s) P^{\mu_1} \dots P^{\mu_n}, \\
& \langle p(p)\bar{p}(p') | \tilde{\mathcal{O}}_q^{\mu\mu_1\dots\mu_n} | 0 \rangle \\
&= \mathbf{S} \bar{u}(p)\gamma^\mu \gamma_5 v(p') \sum_{\substack{i=0 \\ \text{even}}}^n \tilde{A}_{n+1,i}^q(s) P^{\mu_1} \dots P^{\mu_i} \frac{1}{2}\Delta^{\mu_{i+1}} \dots \frac{1}{2}\Delta^{\mu_n} \\
&+ \mathbf{S} \frac{P^\mu}{2m} \bar{u}(p)\gamma_5 v(p') \sum_{\substack{i=0 \\ \text{even}}}^n \tilde{B}_{n+1,i}^q(s) P^{\mu_1} \dots P^{\mu_i} \frac{1}{2}\Delta^{\mu_{i+1}} \dots \frac{1}{2}\Delta^{\mu_n}, \tag{221}
\end{aligned}$$

where in the first equation we have used the Gordon identities to trade the tensor current for the vector and scalar currents. We write $P = p + p'$ and $\Delta = p - p'$ in the crossed channel, in contrast to our notation for GPDs. To find which partial waves can contribute to these matrix elements, one evaluates the spinor products on the right-hand side for spinors of definite (usual) helicity in the $p\bar{p}$ c.m. Taking the plus-components of (221) one then finds

$$\begin{aligned}
& \langle p(p)\bar{p}(p') | \mathcal{O}_q^{++++} | 0 \rangle = \eta_{\lambda'\lambda} (P^+)^{n+1} 2\beta^{-1} (1 - \beta^2)^{1/2} \\
& \times \left\{ \sum_{\substack{i=0 \\ \text{even}}}^n \left[A_{n+1,i}^q(s) + \frac{s}{4m^2} B_{n+1,i}^q(s) \right] \left(\frac{1}{2}\beta \cos \theta \right)^{n-i+1} \right. \\
& \left. + \text{mod}(n, 2) \left[1 - \frac{s}{4m^2} \right] C_{n+1}^q(s) \right\}, \\
& \langle p(p)\bar{p}(p') | \tilde{\mathcal{O}}_q^{++++} | 0 \rangle = \tilde{\eta}_{\lambda'\lambda} (P^+)^{n+1} (1 - \beta^2)^{1/2} \\
& \times \sum_{\substack{i=0 \\ \text{even}}}^n \left[\tilde{A}_{n+1,i}^q(s) + \frac{s}{4m^2} \tilde{B}_{n+1,i}^q(s) \right] \left(\frac{1}{2}\beta \cos \theta \right)^{n-i} \tag{222}
\end{aligned}$$

for the case where the helicities of proton and antiproton couple to $\lambda - \lambda' = 0$, and

$$\begin{aligned}
& \langle p(p)\bar{p}(p') | \mathcal{O}_q^{++++} | 0 \rangle = \eta_{\lambda'\lambda} (P^+)^{n+1} \\
& \times \sum_{\substack{i=0 \\ \text{even}}}^n \left[A_{n+1,i}^q(s) + B_{n+1,i}^q(s) \right] \sin \theta \left(\frac{1}{2}\beta \cos \theta \right)^{n-i}, \\
& \langle p(p)\bar{p}(p') | \tilde{\mathcal{O}}_q^{++++} | 0 \rangle = \tilde{\eta}_{\lambda'\lambda} (P^+)^{n+1} \beta \\
& \times \sum_{\substack{i=0 \\ \text{even}}}^n \tilde{A}_{n+1,i}^q(s) \sin \theta \left(\frac{1}{2}\beta \cos \theta \right)^{n-i} \tag{223}
\end{aligned}$$

when they couple to $|\lambda - \lambda'| = 1$. Here $\beta = (1 - 4m^2/s)^{1/2}$ is the velocity and θ the polar angle of the proton in the $p\bar{p}$ c.m., and $\eta, \tilde{\eta}$ are phase factors which may depend on the azimuthal angle φ of the

proton. One can decompose (222) and (223) on partial wave states with total angular momentum J . They have $J^3 = 0$ because all Lorentz indices of the operators were chosen as $+$. The θ dependence of the partial waves is given by the rotation functions $d_{J^3, |\lambda-\lambda'|}^J$ (see e.g. [241]) and hence by

$$\begin{aligned} d_{00}^J &= P_J(\cos \theta) && \text{for } \lambda - \lambda' = 0, \\ d_{01}^J &= [J(J+1)]^{-1/2} \sin \theta P_J'(\cos \theta) && \text{for } |\lambda - \lambda'| = 1. \end{aligned} \quad (224)$$

Comparing with the relations (36) and (38) for the moments of the GPDs, one finds that when continued to positive t they receive contributions from states with the quantum numbers

$$\begin{aligned} \int dx x^n \left(H^q + \frac{t}{4m^2} E^q \right) & J^{PC} = 1^{--}, 3^{--}, \dots, (n+1)^{--} \\ \int dx x^n (H^q + E^q) & J^{PC} = 1^{--}, 3^{--}, \dots, (n+1)^{--} \\ \int dx x^n \left(\tilde{H}^q + \frac{t}{4m^2} \tilde{E}^q \right) & J^{PC} = 0^{-+}, 2^{-+}, \dots, n^{-+} \\ \int dx x^n \tilde{H}^q & J^{PC} = 1^{++}, 3^{++}, \dots, (n+1)^{++} \end{aligned} \quad (225)$$

for n even and

$$\begin{aligned} \int dx x^n \left(H^q + \frac{t}{4m^2} E^q \right) & J^{PC} = 0^{++}, 2^{++}, \dots, (n+1)^{++} \\ \int dx x^n (H^q + E^q) & J^{PC} = 2^{++}, 4^{++}, \dots, (n+1)^{++} \\ \int dx x^n \left(\tilde{H}^q + \frac{t}{4m^2} \tilde{E}^q \right) & J^{PC} = 1^{+-}, 3^{+-}, \dots, n^{+-} \\ \int dx x^n \tilde{H}^q & J^{PC} = 2^{--}, 4^{--}, \dots, (n+1)^{--} \end{aligned} \quad (226)$$

for n odd, where as usual the integrals are over $x \in [-1, 1]$. Corresponding relations hold for the conformal moments \mathcal{C}_n^q , which are just linear combinations of the Mellin moments with powers x^n , x^{n-2} , etc. For gluon GPDs the results are analogous with x^n replaced by x^{n-1} . These quantum number assignments agree with the results of the general method of [63], which does however not identify the relevant combinations of distributions H , E and of \tilde{H} , \tilde{E} . Notice that for $H + E$ and for \tilde{H} no contributions with $J = 0$ appear since the proton helicities in (223) are coupled to ± 1 . In particular we see that for the moment $\int dx x (H^q + E^q)$ of Ji's sum rule only states with the quantum numbers $J^{PC} = 2^{++}$ of f_2 mesons contribute.

In (222) and (223) the factors $(\beta \cos \theta)^{n-i}$ come from $n-i$ powers of Δ^+ in the form factor decompositions (221). The partial wave decomposition we have discussed is closely related to a decomposition on polynomials in $2\zeta - 1 = \beta \cos \theta$, which we have encountered for the pion GDAs in Section 3.7.2. In the proton case the appropriate decomposition is on Legendre polynomials P_l or their first derivatives P_l' , depending on the proton helicity combinations. Under crossing of matrix elements $\langle p(p) \bar{p}(p') | \mathcal{O} | 0 \rangle$ to $\langle p(p') | \mathcal{O} | p(p) \rangle$ one has to change

$$(p^+ + p'^+)^n Q_l \left(\frac{p^+ - p'^+}{p^+ + p'^+} \right) \rightarrow (p'^+ - p^+)^n Q_l \left(\frac{p'^+ + p^+}{p'^+ - p^+} \right) \quad (227)$$

where $l \leq n$ and Q_l is either P_l or P_l' . An expansion in $Q_l(2\zeta - 1)$ for $t > 0$ hence becomes an expansion in $(-\xi)^n Q_l(-1/\xi)$ for $t < 0$. For GDAs and GPDs of the pion more detail can be found in [90].

4.3 Ansätze for GPDs

For full-fledged phenomenological studies the dynamical considerations discussed in the previous section are not sufficient to calculate the scattering amplitudes of hard processes, which require knowledge of GPDs for several quark flavors and over the full range of x (or at least at $x = \pm\xi$). For this purpose one has to develop general ansätze for GPDs, whose basics we shall now present. Before starting we should say that the need to obtain a full description presently forces one to make simplifications that are likely too simple to capture important physics features. Guidance and correction from comparing with data, and further theoretical insight into the dynamics of GPDs should lead to improvement. The following can thus only be a snapshot, focusing on basics and current problems, and some of it will hopefully be outdated in the future.

The principal input for making an ansatz for GPDs is our knowledge of the “boundary conditions” on GPDs provided by the forward parton densities and also by the elastic form factors. It is however clear that important pieces of information about GPDs cannot be obtained from knowing their forward limits. In particular there are contributions in the ERBL region that become “invisible” when ξ is taken to zero.

4.3.1 Exchange contributions

Among these contributions is for instance the pion pole contribution to \tilde{E}^{u-d} we have discussed in Section 4.1.1. More generally one can think of the exchange of any resonance in the t -channel, which then annihilates into a parton pair, see Fig. 20a. The corresponding contribution to a generic GPD f has the form

$$f(x, \xi, t) = p_n \left(\frac{1}{\xi} \right) \phi \left(\frac{x}{\xi}, t \right), \quad (228)$$

where we have assumed $\xi > 0$ for simplicity. $\phi(u, t)$ has support in $u \in [-1, 1]$ and p_n is a polynomial of order n . Polynomiality requires that the moments $\int dx x^m f(x, \xi, t) = \xi^{m+1} p_n(1/\xi) \int du u^m \phi(u, t)$ vanish for $m < n - 1$. The identification of (228) as the contribution from a resonance with mass m_R and width Γ_R becomes clear when one analytically continues t to the vicinity of m_R^2 , see Fig. 20b. According to our discussion in Section 4.6.2, $\phi(u, t)$ should then be given by the DA of the resonance times a Breit-Wigner propagator $(t - m_R^2 + i\Gamma_R m_R)^{-1}$ times a factor describing the coupling of the resonance to the nucleon. The pion pole contribution (210) to \tilde{E} has exactly this form (with zero width of course). The spin of the resonance determines the form of the polynomial p_n according to the partial wave decomposition presented in Section 4.2.

For describing GPDs in their physical region $t < 0$ one has to keep in mind that, except for the pion with its small mass, there is a large interval between t and squared resonance masses, so that one would not expect any single resonance to dominate. As we remarked in Section 4.1.3, even the

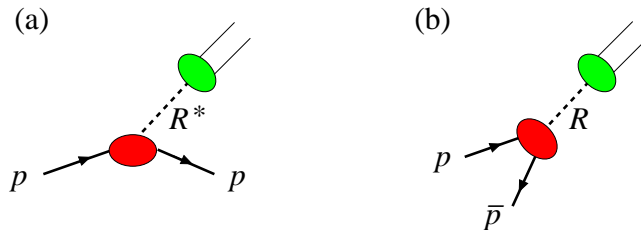


Figure 20: (a) Resonance exchange contribution to a GPD and (b) its analytic continuation to $t \sim m_R^2$ in the GDA channel.

pion pole contribution (210) may receive non-negligible corrections at moderate t . The issues here are similar to those in modeling the Dirac and Pauli form factors by vector meson dominance.

One readily sees from the hard-scattering kernel in (2) that a single resonance term of the form (228) gives a contribution to the real part of a scattering amplitude which grows like ξ^{-n} at small ξ . Unless n is small enough, this is an unacceptably steep behavior. This problem is reminiscent of Regge theory, where it is the *coherent sum* over an infinite number of t -channel exchange terms that ensures a proper behavior of amplitudes in the high-energy limit (corresponding to small ξ in our context), see e.g. [242]. Polyakov and Shuvaev [82] have recently proposed a parameterization of GPDs based on their representation as an infinite sum of t -channel exchanges of the form (228). Taking for example a pion target, one starts with the double expansion (83) of Φ^q in a series of $C_n^{3/2}(2z-1)$ and $P_l(2\zeta-1)$ and obtains a series representation of H_π^q by analytic continuation, as was already done in [90]. The strategy in [82] is to resum subsets of terms in this series in order to obtain a simple approximation of GPDs for small ξ . The methods employed for this are similar to those in the Shuvaev transform (Section 3.8.4). It will be interesting to see the further development of this proposal.

Extending the ideas just discussed, one may also consider t -channel exchange of continuum states instead of resonances. An important example is two-pion exchange, see the next subsection.

4.3.2 The D -term

Another contribution which is invisible in the forward limit is the D -term, whose theory we have presented in Section 3.9.2. An input used in many recent phenomenological analyses is the isoscalar combination D^{u+d} obtained in the chiral soliton model for the nucleon (Section 4.1.3) or an extension to the flavor SU(3) singlet combination D^{u+d+s} by Goeke et al. [37]. In accordance with the expansion scheme of the model, isovector and gluon D -terms are neglected. Kivel et al. [200] have extrapolated the numerical result obtained in [203] to $t=0$ and fitted to Gegenbauer polynomials as in (139). They provide the lowest coefficients $d_1^{u+d} \approx -4.0$, $d_3^{u+d} \approx -1.2$, $d_5^{u+d} \approx -0.4$, with higher coefficients being small. We remark that these values refer to the low factorization scale $\mu_0 \approx 600$ GeV of the chiral soliton model and become significantly smaller at larger scales, given the large size of α_s at small μ . Assuming a zero D -term of the gluon at the input scale and evolving up to $\mu^2 = 5$ GeV² reduces for instance d_1^{u+d} to the value -2.9 in leading logarithmic approximation [243] (see also [244]).

Notice that according to the crossed-channel relations (222) and (223) the only θ independent terms for the parity even operators are the C_n . They are resummed in the D term contribution to the distributions H and E . Exchanges with quantum numbers $J^{PC} = 0^{++}$ are thus exclusively contained in the D -term, but not in the double distributions, which are related to the form factors $A_{n,i}$ and $B_{n,i}$. Exchanges with higher even spin contribute both to the D -term and to double distributions, and odd-spin exchange contributes only to the double distributions. An explicit discussion for the case of pion GPDs is given in [90].

From a dynamical point of view, D^{u+d} in the chiral soliton model receives important contributions

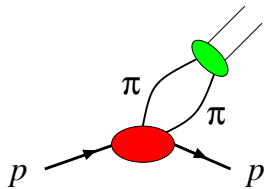


Figure 21: A two-pion exchange graph contributing to the D term in the chiral quark-soliton model.

from diagrams as shown in Fig. 21. In this framework the D -term is mainly generated from the “pion cloud” of nucleon. In different terms one may view the corresponding contributions as due to the t -channel exchange of two pions in partial waves $0^{++}, 2^{++}, \dots$.

4.3.3 Double distributions and connection to forward densities

Ansätze for GPDs used in the literature so far are typically taken as an “extrapolation” of the forward densities to nonzero skewness ξ and nonzero t , possibly supplemented with the quark D -term contribution just discussed. This strategy is of course only possible for the distributions H and \tilde{H} , whose forward limits are the known parton densities. The modeling of E and \tilde{E} does not have this guide and most often these distributions are neglected in phenomenological studies, with the exceptions of the D -term contribution to E^{u+d} and the pion pole contribution (210) to \tilde{E}^{u-d} (sometimes including the corrections to the pion pole obtained in the chiral soliton model, see Section 4.1.3). It is clear that this is not always appropriate: the C -odd part of E^{u-d} for instance cannot be small since at $t = 0$ its integral over x gives the large isotriplet anomalous magnetic moment $\kappa^u - \kappa^d \approx 3.7$. For many observables, however, the contributions from E or \tilde{E} are suppressed compared with those from H or \tilde{H} by small kinematic prefactors ξ^2 or $t/(4m^2)$, see e.g. (365) and (366). A first attempt of more sophisticated modeling for E^q has been made by Goeke et al. [37], with general features obtained in the chiral soliton model as a guide.

A direct ansatz for GPDs has in general little chance to satisfy the polynomiality constraints, so that the favored strategy in the literature is to make instead an ansatz for double distributions, which automatically leads to GPDs satisfying polynomiality. Notice that double distributions are indeed “distributions” in the mathematical sense and need not be smooth functions. An example of a singular term in double distributions is $\delta^{(n)}(\beta) h(\alpha, t)$ with $n \geq 0$. It leads to GPDs of the form (228) with $p_n(1/\xi) = 1/\xi^{n+1}$ and $\phi(\alpha, t) = \partial^n/(\partial\alpha)^n h(\alpha, t)$, which only has support in the ERBL region and is invisible in the forward limit. In models, such contributions concentrated at $\beta = 0$ may just be added to a double distribution with support in the full region $|\beta| + |\alpha| \leq 1$, which generates both the forward parton densities and a contribution to GPDs in the DGLAP and ERBL regions.

The connection with forward densities can of course only be made at $t = 0$, and in this section we will focus on the modeling of the interplay between the x and ξ dependence, leaving the discussion of the t -dependence for the next section. We will thus suppress the t dependence of all functions, which may be understood as taken at $t = 0$. Notice that for $\xi \neq 0$ this point is outside the physical region due to the constraint $t \leq -4\xi^2 m^2/(1 - \xi^2)$, so that the corresponding functions are to be understood in the sense of analytic continuation.

To have a simple notation for the forward limit it is useful to extend the definition of quark and gluon distributions to the full interval $x \in [-1, 1]$ by

$$\begin{aligned} q(-x) &\stackrel{\text{def}}{=} -\bar{q}(x), & \Delta q(-x) &\stackrel{\text{def}}{=} \Delta\bar{q}(x), \\ g(-x) &\stackrel{\text{def}}{=} -g(x), & \Delta g(-x) &\stackrel{\text{def}}{=} \Delta g(x) \end{aligned} \quad (229)$$

for $x > 0$. Without assumption one can write the double distributions as

$$f^q(\beta, \alpha) = q(\beta) h^q(\beta, \alpha), \quad f^g(\beta, \alpha) = g(\beta) h^g(\beta, \alpha), \quad (230)$$

with analogous forms for $\tilde{f}^{q,g}$, where the “profile functions” $h^{q,g}$ are normalized to

$$\int_{|\beta|-1}^{1-|\beta|} d\alpha h(\beta, \alpha) = 1 \quad (231)$$

in order to produce the correct forward limit of the GPDs. An ansatz due to Radyushkin is to take the same α shape of the profile function for all β , up to a rescaling by the length of the integration interval in (231),

$$h(\beta, \alpha) = \frac{1}{1 - |\beta|} \rho\left(\frac{\alpha}{1 - |\beta|}\right) \quad (232)$$

with ρ normalized to $\int_{-1}^1 d\alpha \rho(\alpha) = 1$. A particular form for this function is [115]

$$\rho^{(b)}(\alpha) = \frac{\Gamma(2b + 2)}{2^{2b+1} \Gamma^2(b + 1)} (1 - \alpha^2)^b, \quad (233)$$

where b is a parameter that remains to be chosen.

One may refine this type of ansatz by separating the quark double distributions into different components and choosing different profile functions for each of them.

1. A natural decomposition, used for instance in [127], is into the C -even and C -odd combinations $f^{q(+)}$, $\tilde{f}^{q(+)}$ and $f^{q(-)}$, $\tilde{f}^{q(-)}$ defined in (131).
2. One can also separate the double distributions into contributions from positive and negative β , i.e. $f^q = f^> + f^<$ with $f^>(\beta, \alpha) = \theta(\beta)f^q(\beta, \alpha)$ and $f^<(\beta, \alpha) = \theta(-\beta)f^q(\beta, \alpha)$. Integration of $f^>$ and $f^<$ over α respectively gives the quark and antiquark densities. The respective contributions to GPDs have support in the regions $x \in [-\xi, 1]$ and $x \in [-1, \xi]$, both including the ERBL region. This corresponds to Radyushkin's separation into "quark" and "antiquark" distributions discussed briefly in Section 3.9, but has not been used for modeling in the literature.
3. A hybrid of the previous schemes has been used in [37, 244], decomposing $f^q = f_{\text{val}}^q + f_{\text{sea}}^q$ with

$$\begin{aligned} f_{\text{val}}(\beta, \alpha) &= \begin{cases} f(\beta, \alpha) + f(-\beta, \alpha) & \text{for } \beta > 0 \\ 0 & \text{for } \beta < 0 \end{cases} \\ f_{\text{sea}}(\beta, \alpha) &= \begin{cases} -f(-\beta, \alpha) & \text{for } \beta > 0 \\ f(\beta, \alpha) & \text{for } \beta < 0 \end{cases} \end{aligned} \quad (234)$$

Integration of f_{val} and f_{sea} over α for $\beta > 0$ respectively gives the familiar valence and sea quark distributions $q_{\text{val}} = q - \bar{q}$ and $q_{\text{sea}} = \bar{q}$, which explains the naming scheme. Notice however that f_{val} generates GPDs with support $x \in [-\xi, 1]$ including the ERBL region. This clearly describes physics beyond the simple idea of a distribution due to "the three valence quarks" in the nucleon. An analogous decomposition can be made for the polarized double distributions \tilde{f}^q , replacing $f(\beta, \alpha) \rightarrow \tilde{f}(\beta, \alpha)$ and $f(-\beta, \alpha) \rightarrow -\tilde{f}(-\beta, \alpha)$ in (234).

Let us return to the choice of b in the profile function (233). In the limit $b \rightarrow \infty$ one obtains a simple profile $h^{(\infty)}(\beta, \alpha) = \delta(\alpha)$ and corresponding GPDs

$$\begin{aligned} H^q(x, \xi) &= q(x), & \tilde{H}^q(x, \xi) &= \Delta q(x), \\ H^g(x, \xi) &= xg(x), & \tilde{H}^g(x, \xi) &= x\Delta g(x) \end{aligned} \quad (235)$$

with no effect of skewness at all. This may be the only consistent ansatz for GPDs one can make without resort to double distributions. It is however questionable from a physics point of view. In the global parton analyses the quark distributions $q(x)$ and $\Delta q(x)$ come out singular at $x = 0$. For the gluon many parameterizations have a singular behavior of $xg(x)$ at $x = 0$, unless one takes a rather low factorization scale. A singular behavior of a GPD at $x = 0$ and nonzero ξ is difficult to understand physically, since this is the point in the ERBL region where the two partons have equal

and *finite* plus-momenta. This is in contrast to the forward case $\xi = 0$, where $x = 0$ entails *zero* plus-momentum of both partons, which is indeed a singular situation. Note also that DGLAP evolution does not drive GPDs at nonzero ξ to become singular at $x = 0$.

A choice made in many studies is to take $b = 1$ for quark and $b = 2$ for gluon distributions [127]. This is motivated by the interpretation of α as a DA-like variable and the fact that the asymptotic form of distribution amplitudes under evolution is like $(1 - \alpha^2)$ for quarks and $(1 - \alpha^2)^2$ for gluons (corresponding to $z(1 - z)$ and $z^2(1 - z)^2$ in terms of the momentum variable we use for distribution amplitudes, see Section 3.9.3). Taking a simple analytic ansatz for the forward quark distribution $q(x) = cx^a(1 - x)^3$ allows analytic evaluation of the integral necessary to obtain the GPD [127, 115]. Among the characteristic features of the result is a continuous but nonanalytic behavior at the points $x = \pm\xi$, both for $H^{q(+)}$ and $H^{q(-)}$. In the model defined by (230) to (233) the behavior of the GPDs at these points is strongly influenced by the behavior of the double distributions at the upper “tip” of the rhombus $|\beta| + |\alpha| \leq 1$ and thus by the behavior of the forward parton densities at $x \rightarrow 0$. We recall that in parameterizations of parton densities the small- x behavior is usually parameterized by a power law,

$$xf(x) \sim x^{-\lambda}. \quad (236)$$

Typical values of λ at factorization scale $\mu = 1$ GeV are slightly above zero for $f = \bar{q}$, and below zero for $f = q - \bar{q}$ and the polarized quark valence and sea distributions, see e.g. [245, 246, 247]. The behavior for gluons at this scale is rather uncertain, with λ of either sign for $f = g$ and clearly below zero for $f = \Delta g$. At the low scales $\mu \sim 500$ MeV of the GRV and GRSV parameterizations λ is negative for all distributions, and smaller than -1 for unpolarized and polarized gluons [248, 249].

With a behavior (236) the first derivative of GPDs in the model (230) to (233) can become infinite. Starting from (124) and trading $\partial/(\partial x)$ for $\partial/(\partial\alpha)$ under the integral one finds

$$\frac{\partial}{\partial x} H^q(x, \xi) \stackrel{x \rightarrow \xi}{\sim} - \int_{|x-\xi|} d\beta \beta^{b-2-\lambda}, \quad (237)$$

which is divergent for $\lambda \geq b - 1$ (see also [243]). This is in particular relevant for the C -even combination $H^{q(+)}$ and a profile function with $b = 1$. Note that the principal-value integral (2) appearing in the real part of scattering amplitudes is very sensitive to such a steep behavior. For gluons, one has instead

$$\frac{\partial}{\partial x} H^g(x, \xi) \stackrel{x \rightarrow \xi}{\sim} - \int_{|x-\xi|} d\beta \beta^{b-1-\lambda}, \quad (238)$$

which for practically relevant cases leads to a finite and continuous first derivative of H^g at $x = \xi$.

The sensitivity of the above model to forward parton densities at small momentum fraction is not restricted to the points $x = \pm\xi$. The integral in the β - α plane shown in Fig. 9 involves values of $|\beta|$ down to $x_{\text{out}} = |x - \xi|/(1 - \xi)$ in the DGLAP regions. In the ERBL region the integration is over a region around $\beta = 0$ and thus even involves parton densities down to $x = 0$. With $b = 1$ for quark distributions, the integral giving the GPD in the ERBL region has an integrand behaving like $\beta^{-(1+\lambda)}$ for quark densities going like (236). For the C -even unpolarized combinations, where $\lambda > 0$ at moderate scales μ , this is a non-integrable singularity, but since $f^{q(+)}(\beta, \alpha)$ is odd in β the corresponding integral can be taken using the principal value prescription. Equivalently one can use the antisymmetry of $f^{q(+)}(\beta, \alpha)$ to rewrite the integrand so as to have a small- β behavior as $\beta^{-\lambda}$, which is integrable [250, 243]. The fact remains that in this model GPDs at finite ξ depend on forward densities at $x \ll \xi$. This was quantitatively investigated for $H^{q(+)}$ and a profile parameter $b = 1$ in [243, 251]. Although differing in detail, both studies found a sensitivity of the model GPDs to the sea quark density at x values one or more orders of magnitude below ξ , especially for the region $x \sim \xi$ of the GPDs, which has strong impact on the corresponding hard-scattering amplitudes. For modeling

GPDs at very small ξ this drives one into a region where the forward densities are unknown. We note that for the unpolarized gluon GPD, where the small- x power λ is also positive, the corresponding sensitivity is much less since $f^g(\beta, \alpha)$, and hence $g(\beta)$ in the model, enters the reduction formula (128) with an extra factor β .

One may expect some sensitivity of GPDs to the physics of parton momentum fractions x below ξ . Unlike forward parton distributions at small x , GPDs around $x \approx \xi$ involve however small momentum fractions in the initial but *not* in the final state wave function, so that a strong link between GPDs at finite ξ and parton densities at $x \ll \xi$ is not obvious to understand physically. From a different point of view, double distributions in some narrow band of β around zero on one hand generate the small- x behavior of forward densities. They hence must be large somewhere in this band, since the forward densities have a strong rise towards $x = 0$. On the other hand the reduction of double distributions to GPDs also involves this narrow band, even for ξ much larger than the width of the band. How important the influence of this band is depends on the detailed shape of the profile function $h(\beta, \alpha)$ in (230), and it is not clear whether an α dependence only via the rescaled variable $\alpha/(1 - |\beta|)$ as in (232) is a viable representation of the relevant physics.

The particular ansatz (230) to (233) must be made at a specific factorization scale μ . A study of H^g and $H^{q(\pm)}$ for $\xi \approx 0.05$ in [115] compared the results obtained when either (i) making the profile ansatz at $\mu^2 = 1.5 \text{ GeV}^2$ and evolving the obtained GPDs up to $\mu^2 = 20 \text{ GeV}^2$ or (ii) directly making the profile ansatz with the same forward densities evolved to $\mu^2 = 20 \text{ GeV}^2$. For b between 1 and 2 little deviation between the two versions was found. We note that the problem of sensitivity to the small- x limit of the forward densities is alleviated when making this ansatz at very small scale μ , where parton densities are less singular at small x [252]. It would be interesting to know how evolution to larger scale then changes the double distribution and its profile function.

4.3.4 Dependence on t

An adequate description of the t dependence of GPDs is essential in all physical applications, because physical processes are measured for $t \leq t_0$ and the small- t falloff of GPDs is in general expected to be similarly steep as for elastic form factors. The most widely used ansatz of the t dependence has so far been a factorized form $F(t)f(x, \xi)$ for the GPD, with the form factors $F(t)$ chosen to guarantee the correct sum rules (30). In particular cases one can make contact with experimentally known form factors and has [253]

$$\begin{aligned} H^u(x, \xi, t) &= \frac{1}{2} F_1^u(t) H^u(x, \xi, 0), & H^d(x, \xi, t) &= F_1^d(t) H^d(x, \xi, 0), \\ \tilde{H}^q(x, \xi, t) &= \frac{g_A(t)}{g_A(0)} \tilde{H}^q(x, \xi, 0), & \text{for } q &= u, d. \end{aligned} \quad (239)$$

The GPDs continued to $t = 0$ can then be modeled along the lines described in the previous subsection. Neglecting the small s quark contribution to the elastic nucleon form factors one can use isospin invariance to obtain

$$F_1^u(t) = 2F_1^p(t) + F_1^n(t), \quad F_1^d(t) = 2F_1^n(t) + F_1^p(t), \quad (240)$$

and use the electromagnetic form factors F_1^p, F_1^n of proton and neutron, which are quite well measured at small to intermediate t (see e.g. [254, 255]). For the axial form factor the above ansatz neglects again the s quark contribution in the nucleon and assumes that the isoscalar combination $g_A^{u+d}(t)$ has the same dependence on t as the isovector one,

$$g_A(t) = g_A^{u-d}(t). \quad (241)$$

The latter is accessible in neutral current scattering, and also in charged current nucleon transitions via the isospin relation (203). It is experimentally known up to $|t|$ of about 1 GeV^2 [256].

An ansatz analogous to (239) can be made for E^q , with F_1^q replaced by the Pauli form factor F_2^q . In this case one can of course not proceed modeling by using the forward limit. A form sometimes used is to set

$$E^u(x, \xi, t) = \frac{1}{2} F_2^u(t) H^u(x, \xi, 0), \quad E^d(x, \xi, t) = F_2^d(t) H^d(x, \xi, 0), \quad (242)$$

which has not much motivation beyond simplicity. In (239) and (242) it is understood that the factorized form does not include the D -term, which does not appear in the Mellin moment giving the elastic form factors and has of course the same t -dependence in H and in E . Here one typically assumes a factorized form $D^{u+d}(x, \xi, t) = F(t) D^{u+d}(x, \xi, 0)$, with some choice for $F(t)$ and the term for $t = 0$ taken as described in Section 4.3.2. A factorized ansatz as in (239) can of course also be directly written down at the level of double distributions.

Ansätze analogous to (239) have also been made for the gluon distributions H^g and \tilde{H}^g , where one must model the unmeasured form factors of the local currents $G^{\mu\alpha} G_\mu^\beta$ and $G^{\mu\alpha} \tilde{G}_\mu^\beta$, see e.g. [250, 244]. We remark that in processes at small ξ the t dependence is often described in a different way, using an exponential form $\exp(bt)$ for the relevant gluon or quark GPDs which will be briefly discussed in Section 8.3.

The ansatz (239) has the virtue of being simple and not introducing additional free parameters. It can probably describe the overall drop in t of scattering amplitudes at moderate ξ , but is likely to fail in situations when different contributions to an observable have different signs and can partially cancel, and in observables sensitive to the interplay between t and ξ . From a theoretical point of view it is for instance clear that the electromagnetic and weak form factors in (239) can only constrain the t -dependence of $H^{q(-)}$ and $\tilde{H}^{q(+)}$, but not of $H^{q(+)}$ and $\tilde{H}^{q(-)}$. Along similar lines of reasoning, Belitsky et al. [244] have taken separate factorized expressions for the “valence” and “sea” components of GPDs defined by (234), with different form factors in the valence and sea sectors. Notice that for strange quarks an ansatz like (239) is clearly inadequate: since the proton has no net strangeness the vector form factor $F_1^s(t)$ vanishes at $t = 0$, whereas the C -even combination $H^{s(+)}(x, 0, 0) = s(x) + \bar{s}(x)$ in the forward limit is nonzero. Not even for $H^{s(-)}$ would a factorized form be adequate beyond a certain accuracy, since $s(x) - \bar{s}(x)$ has a vanishing lowest Mellin moment and is overall small but does not vanish.

More generally one expects that the t dependence of GPDs, or equivalently the transverse spatial distributions of partons, will depend on whether the partons are slow or fast. This expectation is borne out by explicit dynamical considerations, as we have discussed for contributions from chiral logarithms (Section 4.1.1), from the chiral soliton model (Section 4.1.3), from the overlap of wave functions at large x (Section 4.1.6), or from the impact parameter representation in the limits of small or large x (Section 4.1.8). Factorization of the t dependence from x and ξ does occur for particular contributions or special limits: the pion pole contribution (210) for $t \rightarrow m_\pi^2$ has a global factor $(t - m_\pi^2)^{-1}$ and the deviations from the pole form found in the chiral soliton model induce little correlation between t and x/ξ [197]. Another example is the global power behavior in t in the large- t limit we saw in Section 4.1.7, valid for x not too close to 1.

First attempts to incorporate a correlation between t and the longitudinal variables in a practicable way have been made, with focus on the simpler case $\xi = 0$ so far. As seen in (219) and (220), global factors

$$F_L(x, t) = \exp \left[\frac{a^2}{2} \frac{1-x}{x} t \right], \quad F_R(x, t) = \exp \left[\alpha' \left(\log \frac{x_0}{x} \right) t \right] \quad (243)$$

for the t dependence of the GPDs are motivated by dynamical considerations in the respective limits of large and small x (note that neither form is stable under DGLAP evolution and must be taken

at a definite scale μ). Combined with a power-law dependence (236) of the forward quark or gluon densities at small x , the form $F_R(x, t)$ can be seen as the extension to finite t of a behavior like $(x_0/x)^{\alpha(t)}$, with the form $\alpha(t) = \alpha(0) + \alpha' t$ familiar from Regge theory (see Sections 4.4 and 8). In the chiral soliton model such a behavior was reported to give a qualitative description of H^{u+d} and \tilde{H}^{u-d} [37, 197], with values $\alpha' \approx 0.8 \text{ GeV}^{-2}$ and $x_0 = 1$ quoted for H^{u+d} in [37]. This value of α' is remarkably close to the slope parameter for meson Regge trajectories in hadronic collisions. Notice that accidentally the large- x behavior of $F_R(x, t)$ with $x_0 = 1$ is $\exp[\alpha'(1-x)t]$ and hence the same as for $F_L(x, t)$ [133]. The constants α' and $\frac{1}{2}a^2$ in the respective forms have however very different physical origins (the first being related to Fock states with large parton number and the second to the lowest Fock states with three quarks and possibly a few extra gluons or $q\bar{q}$ pairs). The study [31] found a value of $\frac{1}{2}a^2 \approx 0.5 \text{ GeV}^{-2}$ or smaller for the large- x form $F_L(x, t)$ at scale $\mu \approx 1 \text{ GeV}$, which according to the considerations of Vogt [227] is expected to increase when evolving to the lower scale $\mu \approx 600 \text{ MeV}$ of the chiral quark-soliton model, so that the values of α' and $\frac{1}{2}a^2$ may be accidentally rather close to each other. Further investigation would be required to see whether the simple form $F_R(x, t)$ with $x_0 = 1$ can be used as a quantitatively adequate ansatz for both small and large x . Goeke et al. [37] “promoted” this form to an ansatz $f^q(\beta, \alpha, t) = h^q(\beta, \alpha) q(\beta) |\beta|^{-\alpha' t}$ for a double distribution with a nontrivial interplay between t and the other variables.

A nontrivial t dependence was obtained in a study for the pion by Mukherjee et al. [257]. Starting point was the $q\bar{q}$ wave function obtained in a dynamical model. This wave function, having a power-law falloff as $|\mathbf{k}|^{-2\kappa}$ at large $|\mathbf{k}|$ with $\kappa \approx 2$, was used to calculate the quark GPD at $\xi = 0$ from the overlap representation (166). The result was then rewritten in the form $H_\pi^q(x, 0, t) = \int d\alpha f^q(x, \alpha, t)$, where the integrand had support for $|\alpha| \leq 1 - |x|$ and thus could be interpreted as a double distribution. At $t = 0$ the form of f^q is found to coincide with the profile function ansatz (230) to (233) with $b = \kappa - 1$. The t dependence does however *not* factorize from the dependence on β and α , and at nonzero t the shape in α depends on β beyond the simple rescaling in (232). We note that the procedure just described gives a result for $H_\pi^q(x, \xi, t)$ that differs from the one obtained in the overlap representation at nonzero ξ with the same light-cone wave function. As pointed out in [44] the result of [257] actually violates the positivity bound (186), which a GPD obtained from the overlap formula respects by construction. Tiburzi and Miller [258] have clarified the origin of this mismatch: from $H_\pi^q(x, 0, t)$ one can construct a double distribution $f^q(\beta, \alpha, t)$ but not the second function $g^q(\beta, \alpha, t)$ in the decomposition (145), which according to the reduction formula (146) is invisible in the GPD at $\xi = 0$. Without knowing both functions one can however not calculate $H_\pi^q(x, \xi, t)$ unambiguously. The procedure in [257] tacitly assumed $g^q = 0$ when calculating $H_\pi^q(x, \xi, t)$ from f^q alone, which no longer guarantees consistent results even when starting from a consistent dynamical model. Lorentz invariance is not sufficient to reconstruct a GPD from its knowledge at $\xi = 0$.

4.3.5 GPDs from triangle graphs

Ansätze for GPDs based on the double distribution representation respect polynomiality by construction, but they do not necessarily fulfill the positivity constraints unless the double distributions possess certain properties, as already observed in [98]. An integral representation of double distributions satisfying the most general positivity constraint (200) has been given in [43] but not used in practice so far. A different ansatz for double distributions that respects positivity has very recently been suggested in [257].

Pobylitsa [177] has proposed a different way to construct parameterizations of GPDs which fulfill the necessary consistency requirements. It is based on the calculation of GPDs in perturbative toy models, which in lowest order of the coupling leads to evaluating triangle graphs as we discussed in Section 3.11.3. Pobylitsa considered GPDs for a spin-zero target, both in scalar ϕ^3 theory and with

spin $\frac{1}{2}$ partons coupling to the target by a Yukawa interaction. By construction the GPDs calculated in covariant perturbation theory respect polynomiality. On the other hand the triangle graphs can be rewritten in terms of light-cone wave functions and hence satisfy the general positivity requirement (200). An exception are ultraviolet divergences (occurring in the Yukawa case as mentioned in Section 3.12.3), whose regularization can violate positivity at low renormalization scale μ^2 . The consistency properties of the GPDs obtained in this way are retained if different masses are taken for the different lines in the graphs.

Clearly one cannot expect GPDs obtained in perturbative models to be close to those of hadrons in QCD. The strategy pursued in [177] is to take a superposition of GPDs obtained with different parton masses m_1, m_2, m_3 in the graphs (and also a superposition of the forms obtained in the ϕ^3 and Yukawa models). The structure of the hadron GPDs is then encoded in the weight functions $s(m_1, m_2, m_3)$ of this superposition. Modeling along these lines had previously been suggested by Brodsky et al. [69] for the nucleon, where the lines in the triangle loop were associated with effective quark-diquark degrees of freedom in the target. Under suitable conditions on the weight functions (which need not be positive definite) the positivity properties of GPDs are preserved, as shown in [177]. The ultraviolet divergence of the triangle graphs can be removed in the superposition by an additional condition on the weights. It will be interesting to see whether the form of GPDs obtained by this strategy is suitable in practice for parameterizing the structure of QCD bound states.

4.4 GPDs at small x

As we mentioned in the Introduction, an important context where GPDs appear are exclusive processes at very high energy and hence very small x . The small- x regime has a number of specialties compared with moderate or large x . Here we focus on GPDs in the small- x limit; broader aspects of the dynamics in this region will be discussed in Section 8. In the context of GPDs it is more correct to speak of “small ξ ”, but we follow common usage, where “small x ” refers to the typical relevant scale of momentum fractions in a process, which is indeed set by the external kinematic variable ξ .

Most small- x studies have focused on the gluon GPD H^g and to a lesser extent on the quark distributions H^q . These are assumed to dominate the experimentally most accessible observables as we will explain in Section 8. There we will also see why one may concentrate on the imaginary part of the scattering amplitude, which for DVCS and light meson production involves GPDs only in the DGLAP region (see Section 5.2) and at Born level just at $x = \pm\xi$. Indicators for the effect of skewness in the small- x regime which have become rather common in the literature are

$$R^g = \frac{H^g(\xi, \xi)}{2\xi g(2\xi)}, \quad R^q = \frac{H^q(\xi, \xi)}{q(2\xi)}, \quad (244)$$

where t is set to zero in the spirit discussed in Section 4.3.3. Corresponding ratios defined for other parameterizations of GPDs differ from those here by global factors $(1+\xi)$, which can be approximated by 1 to the precision of interest here.

Early studies by Frankfurt et al. [46] and by Martin and Ryskin [96] have approximated the skewed gluon distribution $H^g(x, \xi)$ with the forward gluon distribution at $x_{\text{in}} = (x + \xi)/(1 + \xi)$, i.e., with $1 + \xi \approx 1$ they set

$$H^g(x, \xi) = (x + \xi) g(x + \xi), \quad (245)$$

which in particular implies $R^g = 1$ (this explains the choice of momentum fraction 2ξ instead of ξ in the denominators of (244)). In terms of Radyushkin’s conventions (Sections 3.1 and 3.2) the ansatz (245) reads more naturally $\mathcal{F}_\xi^g(X) = Xg(X)$. Making this ansatz at input scales μ_0^2 of order 1 GeV² and evolving to higher scales it was found that the ratio R^g increases with μ^2 , with typical values up to 1.6 for μ^2 around 100 GeV² and a weak ξ dependence for small $\xi < 10^{-2}$. The ansatz (245)

appears at odds with the symmetry of GPDs under $\xi \leftrightarrow -\xi$ (although strictly speaking it does not violate general principles when only used for positive ξ) and has in later work mostly been supplanted by the ansatz

$$H^g(x, \xi) = xg(x), \quad (246)$$

we already introduced in (235). For $x \geq \xi$ and small ξ Freund and Guzey [111] found this relation to be stable within 10% to 20% under evolution from μ^2 around 0.6 GeV² to above 100 GeV². Note that with the ansatz (246) one has

$$R^g = \frac{\xi g(\xi)}{2\xi g(2\xi)}, \quad (247)$$

which increases with μ since at higher scales the gluon density at small x becomes steeper. With a power-law behavior $xg(x) \sim x^{-\lambda}$ or $xq(x) \sim x^{-\lambda}$ as in (236) one obtains

$$R^g = 2^\lambda, \quad R^q = 2^{\lambda+1}. \quad (248)$$

from (246) and from its analog $H^q(x, \xi) = q(x)$ for quarks. Numerical values of R^g up to 1.6 were found in [111] for μ^2 as quoted above (247). We remark that both (245) and (246), as well as simply setting $R^g = 1$ from the start, are equivalent in the leading $\log \frac{1}{x}$ approximation, where small- x arguments different by factors of order 2 cannot be distinguished, see Section 8.1. The spread in values of R^g just quoted indicates the precision of such an approximation in the application at hand.

A more general connection between GPDs and their forward limit was advocated in [46] and [96]. It starts from the observation that for $x \gg \xi$ one should have $H(x, \xi) \approx H(x, 0)$ to a good precision. In this region the kinematical asymmetry between the two gluons is negligible, and one may for instance expand $H(x, \xi) = \sum_n (\xi/x)^{2n} h_n(x)$ and only keep the leading term. The second point of the argument is to calculate GPDs at high scale μ (where measurements are performed) from input GPDs at low input scale μ_0 . In the region $x \gg \xi$ the input distributions may be approximated with their diagonal counterparts. This is the region which controls the behavior of GPDs at large μ and small momentum fraction $x \gtrsim \xi$ (which is most relevant in the convolution with hard scattering kernels) since under evolution to higher scales partons in the DGLAP region migrate towards smaller momentum fractions. Put differently, effects of nonzero ξ in the GPDs at the input scale μ_0 are concentrated in a region where $x \sim \xi$, and evolution to high μ shifts these effects into the ERBL region. At $x \gtrsim \xi$ and large μ the difference between H and its forward counterpart is then of perturbative origin, due to the effect of nonzero ξ in the nonforward evolution kernels. Whereas all studies discussed so far confined themselves to the DGLAP region, Shuvaev et al. [126] argue that the “washing out” of skewness effects in the input distributions is also effective in the ERBL region. In fact we have seen in Section 3.8.3 that in this region evolution to large μ generates a universal shape in the variable x/ξ .

A crucial question for using these observations in practice is how long the evolution interval in μ must be to make this “washing out” of the initial conditions effective. Unless $\alpha_s(\mu)$ is very large, evolution can indeed be rather slow, and its “speed” depends on the shape of the initial conditions. We also note that in many applications the relevant hard scale μ of the process is not *very* high, see Section 8.4.1. A numerical study by Golec-Biernat et al. [113] evolved different input distributions at $\mu_0^2 = 0.26$ GeV² up to higher scales, both for small and for moderate ξ , and found indeed that the shapes come closer to each other for $\mu^2 = 4$ GeV² (and somewhat more for $\mu^2 = 100$ GeV²). It is difficult to assess the general speed of this convergence: in the DGLAP regions the GPDs at μ_0^2 were already quite close to each other, whereas in the ERBL region they differed widely at μ_0^2 and still did considerably after evolution (except for H^g).

A quantitative implementation of the above idea was developed in [126, 113], which makes use of the Shuvaev transform (Section 3.8.4). It is based on neglecting the ξ dependence of the conformal

moments $\mathcal{C}_n(\xi)$ defined in (111) and (112). This is equivalent to approximating Shuvaev's effective forward distribution $f_\xi^q(x)$ or $f_\xi^g(x)$ by the forward density $q(x)$ or $g(x)$. One then has

$$H^{q,g}(x, \xi; \mu) \approx \int_{-1}^1 dy \mathcal{K}_{q,g}(x, \xi, y) f^{q,g}(y; \mu) \quad (249)$$

with $f^q(x) = q(x)$ and $f^g(x) = g(x)$, where the ξ dependence of the GPD is generated only by the integral kernel $\mathcal{K}_q(x, \xi, y)$. Such an ansatz is by construction stable under evolution and thus relates GPDs with forward densities at any scale μ . To justify this ansatz Golec-Biernat et al. [113] argue that the ξ dependence of $H^{q,g}$ which comes from higher conformal moments can be neglected at sufficiently large μ , since all moments with $n > 1$ asymptotically evolve to zero. In consequence, they claim that (249) becomes more reliable as μ increases, but is valid even if ξ is not very small. We find this argument problematic since the ξ independent parts of higher moments $\mathcal{C}_n(\xi)$ evolve to zero with the same speed as their ξ dependent parts. Neglecting higher moments altogether would give the asymptotic forms of GPDs (with $H(\xi, \xi) = 0$ in particular) and clearly be insufficient at scales μ of practical relevance.

A different line of argument [126] is to point out that $\mathcal{C}_n(\xi) = \mathcal{C}_n(0) + \xi^2 \mathcal{R}_n(\xi)$, so that neglecting the ξ dependence of the moments induces an error of $O(\xi^2)$. This argument seems in fact independent on whether μ is small or large. The crucial question is then how small the induced corrections are in the GPDs at a given value of x , since the inversion of conformal moments is a nontrivial procedure (see Section 3.8.3).

Given the form of the parton densities and of the kernels $\mathcal{K}_{q,g}(x, \xi, y)$, the transformation (249) for $\xi \ll 1$ is dominated by $q(x)$ or $g(x)$ at small values of x . Approximating the forward densities by a power-law (236) as before, one can perform the integration explicitly and obtains skewness ratios [126, 125]

$$R^g = \frac{2^{2\lambda+3}}{\sqrt{\pi}} \frac{\Gamma(\lambda + \frac{5}{2})}{\Gamma(\lambda + 4)}, \quad R^q = \frac{2^{2\lambda+3}}{\sqrt{\pi}} \frac{\Gamma(\lambda + \frac{5}{2})}{\Gamma(\lambda + 3)}. \quad (250)$$

For modeling GPDs by double distributions, Musatov and Radyushkin have given an approximate representation for small ξ [115],

$$\begin{aligned} H^g(x, \xi) &= \int_{-1}^1 d\alpha \rho(\alpha) (x - \xi\alpha) g(x - \xi\alpha), \\ H^q(x, \xi) &= \int_{-1}^1 d\alpha \rho(\alpha) q(x - \xi\alpha), \end{aligned} \quad (251)$$

where one has neglected the β dependence in the profile function $h(\beta, \alpha)$ of (230) and thus obtains a function of just one variable as in (232). At small $x \sim \xi$ this approximation has corrections of relative order ξ for sufficiently regular profile functions such as (232) with (233). This follows from expanding $h(\beta, \alpha)$ around $\beta = 0$, which is justified since for $x \sim \xi$ the reduction formula (124) implies $\beta \sim \xi$. For $x \gg \xi$ one can expand $x - \xi\alpha$ around x in (251) and thus has $H(x, \xi)$ approximated by the forward density up to order $(\xi/x)^2$.

With this model a power law for the small- x behavior of the forward densities translates into a power behavior

$$H^g(x, \xi) = \xi^{-\lambda} \hat{H}^g(x/\xi), \quad H^q(x, \xi) = \xi^{-(1+\lambda)} \hat{H}^q(x/\xi). \quad (252)$$

With $\rho \propto (1 - \alpha^2)^b$ as given in (233), the integral in (251) can explicitly be performed and yields [115]

$$R^g = \frac{\Gamma(2 + 2b)}{\Gamma(2 + 2b - \lambda)} \frac{\Gamma(1 + b - \lambda)}{\Gamma(1 + b)}, \quad R^q = \frac{\Gamma(2 + 2b)}{\Gamma(1 + 2b - \lambda)} \frac{\Gamma(b - \lambda)}{\Gamma(1 + b)}, \quad (253)$$

where the different forms for gluons and quarks originate in the different forward limits $H^g(x, 0) = xg(x)$ and $H^q(x) = q(x)$ and the corresponding extra factor β in the relation (128) between H^g and its double distribution. As long as $0 < \lambda < 1 + b$ for gluons and $-1 < \lambda < b$ for quarks, these ratios decrease as b increases, and tend to (248) in the limit $b \rightarrow \infty$, which corresponds to the “forward model” (235). Other special cases often used in the literature are

$$R_{(b=2)}^g = \frac{1}{(1 - \frac{1}{3}\lambda)(1 - \frac{1}{4}\lambda)(1 - \frac{1}{5}\lambda)}, \quad R_{(b=1)}^q = \frac{3}{(1 - \lambda)(1 - \frac{1}{2}\lambda)}. \quad (254)$$

We recall that the ansatz $b^g = 1$ and $b^g = 2$ is based on the analogy with meson DAs and their asymptotic behavior. For the asymptotic behavior of double distributions under evolution we saw in (136) that all double distributions become concentrated at $\beta = 0$, with the shape in α being like $(1 - \alpha^2)$ for $f^{q(-)}$ and like $(1 - \alpha^2)^2$ for f^g , in accordance with the above powers. In contrast, the α shape for $f^{q(+)}$ tends to $(1 - \alpha^2)^2$, which does not correspond to $b^g = 1$. Taking $b^g = 2$ one obtains

$$R_{(b=2)}^q = \frac{2.5}{(1 - \frac{1}{2}\lambda)(1 - \frac{1}{3}\lambda)(1 - \frac{1}{4}\lambda)}, \quad (255)$$

which for $|\lambda| < 1$ provides less enhancement than $R_{(b=1)}^q$ but still more than $R_{(b=2)}^g$.

Musatov and Radyushkin [115] have considered a model based on a “less asymptotic” limit of the double distributions, retaining for each separate Mellin moment $\int d\beta \beta^m f(\beta, \alpha)$ in (134) the asymptotically dominant term, which is proportional to $(1 - \alpha^2)^{m+1}$ times the corresponding Mellin moment of the forward quark or gluon density. According to (135) this is tantamount to retaining only the ξ -independent term in the conformal moments \mathcal{C}_n of H and thus to the model based on the Shuvaev transform discussed above. With a further approximation (which still allows one to calculate H at small x and ξ from the double distribution) one can explicitly invert the Mellin moments of $f(\beta, \alpha)$. For a power-law behavior (236) of parton densities the result has the form (251) with $\rho(\alpha) \propto (1 - \alpha^2)^b$ and $b = \lambda + 1$ for both gluons and quarks. The corresponding enhancement ratios are of course given by (250). In Fig. 22 we plot the ratios R^g and R^q for the various models we have discussed in this section. We emphasize that λ describes the forward densities in the relevant range $x \sim \xi$, and as an effective power depends weakly on the range of x and rather strongly on the scale μ (see Section 8).

In the phenomenologically relevant region of λ the enhancement factors for gluons are almost identical for the choice $b = 2$ and for the Shuvaev model. For $\lambda \lesssim 0.4$ there is in fact little difference for all profile parameters between $b = 1$ and $b = \infty$. The ratio R^g is relevant for vector meson production at small x , where the gluon distribution dominates. Compton scattering receives important contributions from the C -even combination of quark distributions even at small x (see Section 5.2). For this combination one has $\lambda > 0$ at scales relevant for the process and obtains enhancement factors of appreciable size.

Freund et al. [251] have made the strong claim that, except when taking $b = \infty$, the underlying ansatz (230) to (233) fails to describe the available data on DVCS at LO or NLO in α_s , overshooting both the H1 cross section data at small x_B [259] and the beam spin asymmetries from HERMES and CLAS [260, 261] at moderate x_B . They propose an alternative ansatz using the forward model (235) in the DGLAP region (corresponding to $b = \infty$). In the ERBL region they take a simple polynomial in x with ξ -dependent coefficients chosen such that the resulting GPD satisfies polynomiality for the lowest Mellin moments, arguing that higher moments are practically irrelevant in the small ξ region. We caution that higher Mellin moments are essential for reconstructing parton distributions (and the associated scattering amplitudes) at achievable resolution scales μ , and it remains to study how small violations of polynomiality in higher Mellin moments propagate to these quantities.

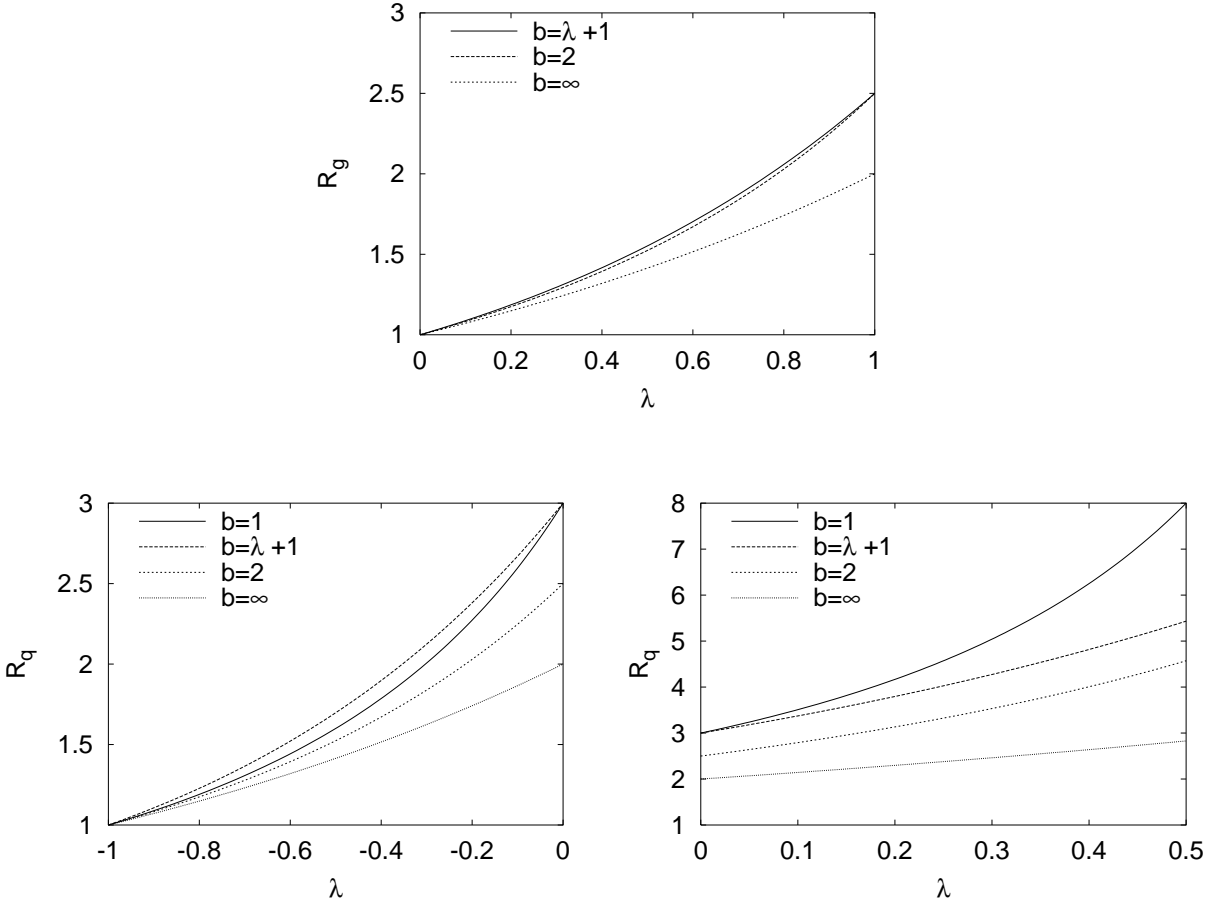


Figure 22: The skewness ratios (253) for gluons and quarks for forward densities with a power behavior (236). The choice $b = \infty$ corresponds to the simple forward model in (235), and $b = \lambda + 1$ to the ansatz (249) based on the Shuvaev transform.

We finally remark that the general results presented in this section, in particular the various expressions for the skewness ratios, can readily be extended to the polarized GPDs, with the replacements $H^g \rightarrow \tilde{H}^g$, $H^q \rightarrow \tilde{H}^q$ and their analogs for the forward densities.

4.5 Nuclei

Some of the experimental facilities that can study hard exclusive processes also run with nuclear targets, and it is natural to ask what can be learned from the corresponding generalized parton distributions.

Let us begin by discussing the deuteron, which in some respects is the simplest case to be studied. According to whether the deuteron stays intact or breaks up one will deal with GPDs for the deuteron, or for the breakup $d \rightarrow p + n$, or for the breakup to a more complicated state (containing for instance additional soft pions). Each case offers characteristic physics information, whose extraction requires of course that the final state can be experimentally identified.

The $d \rightarrow p + n$ transition may provide access to the GPDs of the neutron (and thus to a flavor decomposition of the nucleon GPDs) in kinematics where the neutron takes nearly all of the momentum transfer Δ . In the impulse approximation the scattering then takes place on a quasifree neutron in the deuteron, with the proton being a spectator. The $d \rightarrow p + n$ transition GPDs are thus given by the neutron GPDs convoluted with the nuclear wave functions ψ_{p+n} of the target. Other nuclei might be used to the same end. No detailed studies of these issues have yet been performed in the literature.

The spin structure of the GPDs for the elastic $d \rightarrow d$ process has been presented in Section 3.15. Consider again the approximation of the deuteron as a weakly bound state of a proton and a neutron, described by two-body wave functions ψ_{p+n} with the appropriate momentum and spin dependence. In analogy to the convolution model for the usual parton densities of the deuteron, the deuteron GPDs are then a convolution of these nuclear light-cone wave functions and the relevant nucleon GPDs, as shown in Fig. 23a and b. As detailed in [193] the GPDs H_3 , H_5 , \tilde{H}_2 , \tilde{H}_3 require D -wave configurations of the proton and neutron in the deuteron. If extracted experimentally, they may provide information on the corresponding part of the nuclear wave function, in addition to what can be inferred from the elastic deuteron form factors.

The GPDs of a nuclear system are interesting beyond their spin structure. For the mechanism of Fig. 23a and b, we observe that at nonzero ξ the longitudinal momentum fraction of the active nucleon in the bound state before and after the scattering is different. The ξ dependence of the generalized parton distribution reflects rather directly the width of the deuteron wave function in longitudinal momentum: if the plus-momentum fraction of the nucleon in the deuteron has width w , the deuteron GPDs will drop at $\xi \sim w$ [193]. Note that the dependence on the longitudinal variable ξ comes in correlation with the dependence on transverse momentum, controlled by the variable t . In kinematics

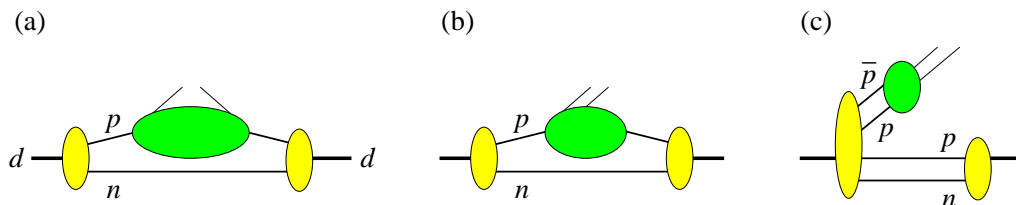


Figure 23: Different contributions to the generalized parton distributions of the deuteron in a convolution model.

where the motion of the nucleons in the deuteron is dominantly nonrelativistic the deuteron wave functions are rather well known, and one may again use such processes to investigate the GPDs of the neutron. A similar statement holds for other nuclei. A first quantitative study of the deuteron GPDs in a convolution model has been performed by Cano and Pire [262].

The extension of the convolution model to GPDs of heavier nuclei has been considered by Guzey and Strikman [263], who have also estimated the relative importance of the case when the nucleus breaks up. In a phenomenological study by Kirchner and Müller [264], a simplification of the convolution picture was used to obtain the x and ξ dependence, neglecting the relative momenta of nucleons in the initial-state nucleus. Note that this implies nonzero relative nucleon momenta in the final-state nucleus and hence violates the symmetry in ξ of the nuclear GPDs. By construction GPDs at $\xi \neq 0$ do not allow both the initial and final nucleus to be treated as static systems of nucleons. To neglect the momentum mismatch between the initial and final state wave functions is only consistent as an approximation for values of ξ small compared with the typical momentum fractions over which the nuclear wave functions vary significantly.

It follows from our discussion in Section 3.11.3 that the convolution model described so far is not sufficient to guarantee the polynomiality properties of GPDs. In the ERBL region there is also the possibility that a nucleon-antinucleon pair in the initial nucleus annihilates into a $q\bar{q}$ system which is then emitted (Fig. 23c). Experimental and theoretical studies of nuclear GPDs at different ξ may provide a glimpse on how important such highly relativistic configurations are in a nuclear system. For deuteron GPDs at not too large ξ , only small to moderate deviations from the sum rules (206), (208), (209) were found for the convolution model used in [262].

Clearly the description of a nucleus in terms only of nucleon degrees of freedom is an approximation. The possible role of meson degrees of freedom has briefly been discussed in [264]. If ξ is so large that in the convolution picture one is forced into the tail of the nuclear wave function, one will be sensitive to quantum fluctuations of the deuteron that are more complicated than a system of two almost free nucleons. To study such configurations in deeply inelastic scattering at $x_B > 1$ has proven to be difficult since one scatters on quarks with a very large momentum fraction in the target. For GPDs however one can have any plus-momentum fraction of the struck quark, even for large ξ .

An additional observable for nuclear targets is the dependence on the atomic number A , which can distinguish different dynamical mechanisms. An example is a study of Polyakov [83], which obtained a characteristic A dependence of the D -term, appealing to its connection with the spatial components of the energy-momentum tensor described at the end of Section 3.6, and using a simple model for a large nucleus. Nuclear medium effects in GPDs and their consequences in the scattering amplitude for DVCS have recently been investigated by Freund and Strikman [265].

The occurrence of GPDs in a quite different context was studied by Osborne and Wang [266]. Applying the convolution model to twist-four parton correlations in nuclei, contributions as shown in Fig. 24 were identified as involving nucleon GPDs, which are not close to the forward limit in

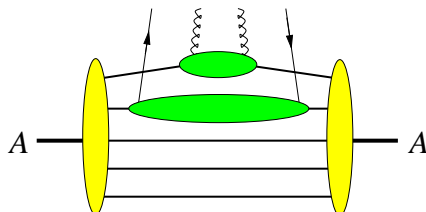


Figure 24: Contribution to a twist-four parton distribution in a nucleus which involves two nucleon GPDs.

all kinematics. These contributions scale as $A^{4/3}$ and can hence become important for large nuclei since their twist-two parton densities only grow like A in the region where the convolution model is applicable.

4.6 Dynamics of GDAs

We have seen the intimate connection between GPDs and generalized distribution amplitudes through analytic continuation in the invariants t or s . Dynamical studies of the respective quantities show similar connections but also important differences between the physics in the t and in the s channel. One important difference already mentioned in Section 3.11.2 is that GDAs cannot be represented in terms of the wave functions of individual hadrons they involve: they describe the formation of a hadronic system including the interactions between hadrons. A representation in terms of the bound state wave function *and* the corresponding interaction kernel has been given by Tiburzi and Miller [219, 154] in the covariant framework we discussed in Section 4.1.5.

Dynamical studies of GDAs have so far concentrated on the two-pion system, both because of its relative theoretical simplicity and phenomenological importance. Moreover, most work has focused on the quark GDAs.

4.6.1 Very small s

At low invariant two-pion mass \sqrt{s} the two-pion DAs have important connections with the chiral symmetry of QCD and its spontaneous breaking, and studies similar to those described in Sections 4.1.1 and 4.1.3 for the pion GPDs have been performed. In the chiral limit there are soft-pion theorems for GDAs analogous to those for GPDs in (212). At $s \rightarrow 0$ and $\zeta \rightarrow 0$ or 1, where one pion momentum becomes soft, one has [87]

$$\begin{aligned} \lim_{\zeta \rightarrow 1} \Phi^{u-d}(z, \zeta, 0) &= -\lim_{\zeta \rightarrow 0} \Phi^{u-d}(z, \zeta, 0) = 2\phi_\pi(z), \\ \lim_{\zeta \rightarrow 1} \Phi^{u+d}(z, \zeta, 0) &= \lim_{\zeta \rightarrow 0} \Phi^{u+d}(z, \zeta, 0) = 0. \end{aligned} \tag{256}$$

Similarly, one has $\lim_{\zeta \rightarrow 0,1} \Phi^g(z, \zeta, 0) = 0$ for the gluon GDA [86]. This type of relation can be generalized to the three-pion DAs for the case where one or two pion momenta become soft [88]. One-loop contributions in chiral perturbation theory generate nonanalytic terms in s or in m_π^2 for the two-pion DAs and have been calculated by Kivel and Polyakov [131]. In particular, these terms provide corrections to the soft-pion theorem (256). They also lead to an imaginary part of the two-pion DAs for $s > 4m_\pi^2$, due to rescattering of the two pions.

The two-pion DAs have been evaluated in the chiral quark-soliton model by Polyakov and Weiss [267]. Valid for $s \lesssim 4M^2 \approx (700 \text{ MeV})^2$ and referring to a low factorization scale $\mu \approx 600 \text{ MeV}$, the GDAs obtained have a rather rich structure in z , with sharp crossovers at the points $z = \zeta$ and $z = 1 - \zeta$ where one pion carries the same plus-momentum as the quark. Their shape also exhibits a clear dependence on s . A detailed study of both pion GDAs and pion GPDs in this model has recently been performed by Praszalowicz and Rostworowski [210].

4.6.2 Connection with resonance DAs

When \sqrt{s} is in the vicinity of the mass of a resonance, a close connection can be established between the GDA and the corresponding DA of the resonance [87]. This involves first a projection on the appropriate partial wave of the two-pion state through Legendre polynomials $P_l(\cos \theta)$ with $\beta \cos \theta = 2\zeta - 1$. One can also directly work with the partial wave Gegenbauer coefficients \tilde{B}_{nl} discussed in

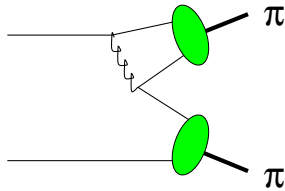


Figure 25: One of the diagrams for the pion two-pion DA Φ^q in the limit of large s .

Section 3.7.2. Assuming that in some region s the resonance contribution dominates the appropriate partial wave in the GDA, one can then match its behavior around the resonance peak onto the DA of the resonance times a factor describing its decay to the two-pion channel. The latter is described by a Breit-Wigner propagator $(s - m_R^2 + i\Gamma_R m_R)^{-1}$ and a constant related to the relevant branching ratio.

From a conceptual point of view it is important that the GDA describes both the “resonance” and “continuum” contribution in the two-pion system, without the need to even separate the two unless one explicitly wants to connect the GDA with resonance properties. In hard processes where a resonance DA appears, one can thus alternatively work with the GDA of the resonance decay products. This can be especially useful when a separation of resonance “signal” and continuum “background” is nontrivial, for instance for the very broad ρ resonance, or if one wants to extend study to invariant masses \sqrt{s} away from the resonance peak. We will mention practical applications of this in Sections 5.4.2 and 9.4.2.

4.6.3 Very large s

The behavior of the two-pion DAs in the limit $s \rightarrow \infty$ is fully analogous to the large- t limit of the pion GPDs discussed in Section 4.1.7 and has been discussed in [268]. The GDAs in this limit can be described by the hard scattering mechanism, with diagrams as shown in Fig. 25.

The features of the result are analogous to those discussed in Section 4.1.7. In particular one obtains a power-law behavior $\Phi^q(z, \zeta, s) = \alpha_s(s) s^{-1} \phi^q(z, \zeta)$ for the GDAs, whose factorization scale is understood to be of order s . As in the case of GPDs, one obtains GDAs that exactly satisfy the polynomiality conditions. In their z -dependence a change of sign is observed at $z = \zeta$. As z approaches ζ one finds a logarithmic singularity like $\log|z - \zeta|$, which signals the breakdown of the hard scattering approximation in the vicinity of this point, where the momentum of the quark or antiquark in one of the pions (the lower one in Fig. 25) becomes soft. In an improved evaluation one expects to find finite GDAs with a rapid change between positive and negative values at this point. Note that according to the crossing rules (77) its location $z = \zeta$ corresponds to the point $x = 1$ of GPDs, where the hard scattering formalism breaks down as well (see Section 4.1.7).

4.6.4 Modeling

A modeling strategy for the two pion DAs Φ^u and Φ^d in the mass region up to about $s \approx 1 \text{ GeV}^2$ has been developed by Polyakov [87], with an extension to Φ^g in [86, 269]. It makes use of the various connections of GDAs with other hadronic quantities we have discussed so far.

Its first ingredient is the restriction to the asymptotic form in z given in (89). We note that the only distribution amplitudes which are strongly constrained from data are for a single pion or a single η or η' , where in particular the processes $\gamma^* \gamma \rightarrow \pi^0$, η , η' suggest a form rather close to the asymptotic one, $\phi(z) = 6z(1 - z)$, already at low factorization scale $\mu \sim 1 \text{ GeV}$ (see Section 5.4.1).

The same assumption for GDAs should be taken with due care, given that the results of the chiral quark-soliton model (Section 4.6.1) give shapes very different from the asymptotic one at the very low scale $\mu \approx 600$ MeV, while giving a single-pion DA quite close to $\phi(z) = 6z(1-z)$ at the same scale [270]. Evolving the GDA up to $\mu \sim 1$ GeV will bring its shape closer to the asymptotic form since α_s in that region is quite large, but no quantitative study of this has been performed. Evolution from this scale upward is rather slow because the anomalous dimensions are not very large, so that strong differences from the asymptotic shape in z will persist over a long interval of μ .

When taking the asymptotic shape in z , the isovector GDA Φ^{u-d} is expressed through the timelike pion form factor, which is phenomenologically well known for small and moderate s . This leaves one to model the Gegenbauer coefficients for the isoscalar and gluon GDAs. More generally one may keep the z dependence as in (89) but retain the scale dependent Gegenbauer coefficients $B_{1l}^{u+d}(s, \mu^2)$ and $B_{1l}^g(s, \mu^2)$ instead of their respective asymptotic limits, which depend only on $B_{1l}^-(s)$ [85].

The second ingredient in the method of [87] is to use a dispersion relation in s for these Gegenbauer coefficients. As an input one needs the subtraction constants in this dispersion relation, given by the B_{1l} or their derivatives at the point $s = 0$. At this point one has various pieces of information from chiral symmetry and from the moments of quark densities in the pion, which are phenomenologically known to some extent. In particular, the soft-pion theorem (256) gives $B_{10}^{u+d}(0) = -B_{12}^{u+d}(0)$ and the analog for gluons, with corrections of parametric suppression $m_\pi^2/(4\pi f_\pi)^2$. Furthermore, $B_{12}^{u+d}(0)$ and $B_{12}^g(0)$ are respectively related to the momentum fraction carried by u and d quarks or gluons in the pion, see (90). As remarked in [85] these fractions at moderate scales μ are still rather different from their asymptotic values under evolution, and the corresponding difference can have notable effects on physical amplitudes calculated in this model [271]. The momentum fraction of s quarks in the pion at moderate scale is presumably small, which provides some justification for neglecting Φ^s in the pion at not too large values of s and μ^2 . At s of order m_π^2 the coefficients $B_{1l}(s)$ of the two-pion DAs can also be related with parameters in the Lagrangian of chiral perturbation theory, namely with the couplings constants for the interaction of soft pions with a gravitational field [272]. Polyakov [87] has also studied these parameters within the chiral soliton model.

A further ingredient in the dispersion relation are the phases of the Gegenbauer coefficients \tilde{B}_{1l} for definite partial waves. As discussed in Section 3.7.2 they equal the measured phase shifts $\delta_l(s)$ of elastic $\pi\pi$ scattering for s up to the region where inelastic scattering becomes important. This limits the region of validity in s of the simple dispersive method described here. Up to about $\sqrt{s} = 1.2$ GeV the D wave is approximately elastic and well described by a Breit-Wigner phase from the $f_2(1270)$ resonance. In the S wave, a rather complicated structure appears around $\sqrt{s} = 1$ GeV, where the narrow $f_0(980)$ resonance and the opening of the two-kaon channel almost coincide. A first attempt to describe the behavior of the S wave beyond this energy has been made in [273] by including an inelasticity parameter. A full treatment will likely require a two-channel analysis, which has not been performed as yet.

As we saw in Section 3.9.3 not only GPDs but also GDAs can be represented in terms of double distributions. Only recently has this been exploited for modeling purposes [257].

4.6.5 GDAs and the hadronization process

GDAs describe the hadronization from quarks or gluons to a specified system of hadrons. This can be regarded as the “exclusive” counterpart of hadronization in the regime of large multiplicities, where observables typically are taken to be more inclusive. Among the models used to describe this regime is the Lund string model [274]. In this framework Maul [275] has studied $\gamma^*\gamma$ annihilation into two pions and other exclusive channels at $Q^2 \gg s$, thus taking the Lund model to its “exclusive limit”, where the Lund string breaks only once before the desired final state is obtained. As the Lund model

is semiclassical, this study was performed at the cross section level, in contrast to the description of the same process by GPDs, which enter at amplitude level. At $s = 1 \text{ GeV}^2$ the cross section obtained in [275] differs by a factor of about 3.5 from the cross section calculated with GPDs modeled along the lines of the previous subsection [85]. This is remarkably close given considerable uncertainties in both model studies and above all the very different dynamical pictures they represent, the chosen value of s being at the lower limit of applicability for one model and at the upper limit for the other.

5 Exclusive processes to leading power accuracy

5.1 Factorization

The possibility to study GPDs in suitable exclusive scattering processes rests on factorization theorems, as does the program to extract usual parton densities from inclusive and semi-inclusive measurements. Collins, Frankfurt and Strikman [24] have given a detailed proof for factorization in light meson production, and Collins and Freund [181] for Compton scattering, see [276] for a brief account of both works. These proofs are based on the properties of Feynman diagrams and very similar to the factorization proofs for inclusive DIS or Drell-Yan pair production [277]. Radyushkin has analyzed Compton scattering and meson production using the α -representation of Feynman graphs [39]. Another analysis of Compton scattering has been given by Ji and Osborne [278]. Recently, Bauer et al. [279] have investigated Compton scattering in an effective field theory framework. An effective field theory formulation had earlier been used by Derkachov and Kirschner in a study focusing on evolution [280].

Consider first the amplitude for virtual Compton scattering

$$\gamma^*(q) + p(p) \rightarrow \gamma^*(q') + p(p'). \quad (257)$$

So far we have discussed DVCS, where q^2 is large and spacelike, whereas the final photon is on shell. Another relevant case is when the outgoing photon is timelike and decays into a lepton pair $\ell^+\ell^-$. The factorization proof [181] requires that at least one of the photons be far off-shell. This includes the case where the initial photon is real and q'^2 is large and timelike [281], which was called “timelike Compton scattering” (TCS) in [243]. The case where both photons are off shell has been dubbed “double deeply virtual Compton scattering” (DDVCS) by Guidal and Vanderhaeghen [282] and appears in the process $ep \rightarrow ep \ell^+\ell^-$. The factorization theorem for Compton scattering is valid in the generalized Bjorken limit

$$|q^2| + |q'^2| \rightarrow \infty \quad \text{at fixed } q^2/W^2, q'^2/W^2, t. \quad (258)$$

With the case of a timelike final-state photon in mind we define $Q^2 = -q^2$ and $Q'^2 = q'^2$. The amplitude can be written as

$$\mathcal{A}(\gamma^*p \rightarrow \gamma^*p) = \sum_i \int_{-1}^1 dx T^i(x, \rho, \xi, Q^2 - Q'^2) F^i(x, \xi, t), \quad (259)$$

up to terms suppressed by inverse powers of the large momentum scale Q or Q' . Here F^i stands for the matrix elements F^q , F^g and \tilde{F}^q , \tilde{F}^g . The corresponding hard scattering amplitudes T^i further depend on the photon helicities, as will be discussed in Section 5.1.1. There are now two scaling variables,¹¹

$$\rho = -\frac{(q+q')^2}{2(p+p') \cdot (q+q')}, \quad \xi = -\frac{(q-q') \cdot (q+q')}{(p+p') \cdot (q+q')}, \quad (260)$$

¹¹A variety of notations is used for these variables in the literature. In particular, “ ξ ” sometimes has the meaning of ρ in (260).

which up to terms of order t/W^2 and m^2/W^2 equal

$$\begin{aligned}\rho &\approx \frac{Q^2 - Q'^2}{2W^2 + Q^2 - Q'^2} \approx -\frac{(q + q')^+}{(p + p')^+}, \\ \xi &\approx \frac{Q^2 + Q'^2}{2W^2 + Q^2 - Q'^2} \approx \frac{(p - p')^+}{(p + p')^+}.\end{aligned}\tag{261}$$

Special cases are DVCS with $Q'^2 = 0$ and $\rho = \xi$, and TCS with $Q'^2 = 0$ and $\rho = -\xi$. For simplicity we will in the following refer to the large scale as Q , keeping in mind the exception of TCS. In (259) we have not written out the dependence on the factorization scale μ_F of the GPDs and on the renormalization scale μ_R of the running coupling. Explicit logarithms $\log(Q^2 - Q'^2)/\mu_F^2$ appear in the hard scattering kernel starting at $O(\alpha_s)$, and logarithms $\log(Q^2 - Q'^2)/\mu_R^2$ appear starting at $O(\alpha_s^2)$. The dependence of the amplitude on μ_F and μ_R cancels of course order by order in the strong coupling. In choosing $Q^2 - Q'^2$ as argument of the logarithms we have assumed that one does not have $Q'^2 = Q^2$, in which case one would take the argument $Q^2 + Q'^2$ instead. We note that in part of the literature the generalized Bjorken limit is defined not by $|q^2| + |q'^2| \rightarrow \infty$ but by $|q^2 + q'^2| \rightarrow \infty$, which excludes the point $Q'^2 = Q^2$. It is not clear why factorization should not hold in this case, but there is no dedicated investigation of this issue in the literature.

The plus-momenta in (261) refer to a frame where the external momenta of the Compton amplitude have small transverse components of order $\sqrt{-t}$. Various particular choices have been made in the literature, for instance $\mathbf{p} = 0$ or $\mathbf{p} = -\mathbf{p}' = -\frac{1}{2}\mathbf{\Delta}$ on the proton side, and $\mathbf{q} = 0$ or $\mathbf{q}' = 0$ or $\mathbf{q} = -\mathbf{q}' = \frac{1}{2}\mathbf{\Delta}$ on the photon side. At leading order in the large scale all these frames are equivalent.

The relevant limit for the production of a meson M

$$\gamma^*(q) + p(p) \rightarrow M(q') + p(p')\tag{262}$$

is

$$Q^2 \rightarrow \infty \quad \text{at fixed } Q^2/W^2, t.\tag{263}$$

In this limit, the amplitude for longitudinal polarization of photon and meson reads

$$\mathcal{A}(\gamma_L^* p \rightarrow M_L p) = \frac{1}{Q} \sum_{ij} \int_{-1}^1 dx \int_0^1 dz T^{ij}(x, \xi, z, Q^2) F^i(x, \xi, t) \Phi^j(z)\tag{264}$$

up to power corrections in $1/Q$. All other helicity transitions are of order $1/Q^2$ or higher. Again we have not displayed the dependence on the factorization scale μ_F of the GPDs and the meson DAs and on the renormalization scale μ_R of α_s . The dependence of T^{ij} on Q^2 is through logarithms $\log Q^2/\mu_F^2$ and $\log Q^2/\mu_R^2$, both starting at $O(\alpha_s^2)$. In a suitable reference frame the external momenta in (262) have small transverse components, the incoming and outgoing protons have large plus-momentum, and the outgoing meson has large minus-momentum. x and ξ then represent plus-momentum fractions as before. z is now the minus-momentum fraction of a quark or gluon in the meson and thus corresponds to reversing plus- and minus-components in the definitions (78) and (79) of distribution amplitudes Φ^j for the relevant quark flavors or gluons.

The factorization theorems apply to a larger class of processes than (257) and (262). One may replace the outgoing proton $p(p')$ by any single- or multiparticle state Y with appropriate quantum numbers; transition GPDs then appear in the factorization formula. Similarly one may replace the outgoing meson M by a system X of particles and the meson DA by the appropriate GDA, see [283] for a more detailed discussion. What counts for factorization is that the invariant masses M_Y and M_X of these systems remain fixed in the limits (258) or (263). In practice this means $M_Y^2, M_X^2 \ll W^2$ so that Y is well separated in rapidity from the outgoing γ^* or X .

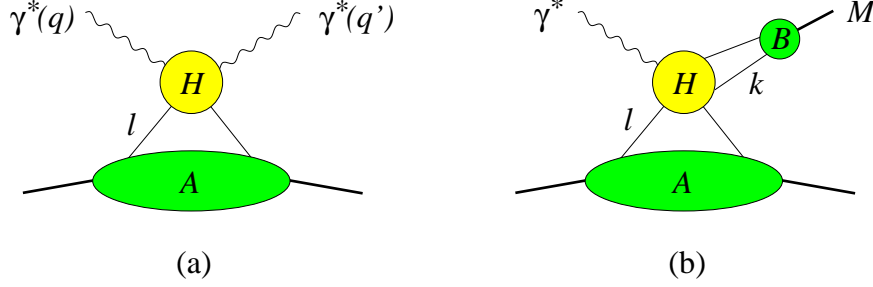


Figure 26: Graphs for the factorization formulae of Compton scattering (a) and meson production (b). An arbitrary number of additional gluons with suitable polarizations can connect H with A and with B . Diagrams with soft subgraphs as in Fig. 28 are discussed in the text.

Let us discuss some important points in the construction of the factorization theorem, following the approach of [181, 276]. Although it technically uses Feynman diagrams, the key elements are general principles (gauge invariance, dimensional analysis, boost properties and analyticity of scattering amplitudes) and should hold beyond perturbation theory.

- The factorization formulae are associated with the graphs shown in Fig. 26, which provide the leading power behavior of the limit (258) or (263). These “reduced graphs” specify both the topology of the relevant Feynman graphs and regions of loop momentum space. Lines in subgraph A are collinear to the incoming and outgoing proton, lines in subgraph B are collinear to the outgoing meson, while lines in H have large components in both the plus- and minus directions and are thus far off-shell.
- To leading power accuracy one can Taylor expand the hard subgraph H in those components of its external momenta that are small on the scale of Q . For Fig. 26a we have

$$\int d^4l H(l)A(l) \approx \int dl^+ H(l)|_{l^-=0, \mathbf{l}=0} \int dl^- d^2\mathbf{l} A(l). \quad (265)$$

Writing $A(l)$ as the Fourier transform of a position space operator sandwiched between proton states, we then obtain a light-cone operator, as shown in (43). On the other hand, the hard scattering H is now evaluated with external partons on shell and strictly collinear. For meson production one also expands H around $k^+ = 0$ and $\mathbf{k} = 0$. The collinear expansion has important consequences, in particular the helicity selection rules we will shortly discuss.

- The operators for the external partons in the subgraphs A and B are time ordered, whereas those in the definition of parton distributions and distribution amplitudes are not. It is therefore crucial that the time ordering of the operators can be dropped in the integral $\int dl^- A(l)$ and analogously in $\int dk^+ B(k)$, as we discussed in Section 3.4.
- In addition to the lines shown in Fig. 26 there can be an arbitrary number of collinear gluons with polarization along the plus-direction between H and A , and an arbitrary number of collinear gluons with polarization along the minus-direction between H and B . Using Ward identities, these graphs can be summed so that Wilson lines appear in the definitions of GPDs and DAs, whereas the hard scattering H is evaluated with the minimum number of external lines shown in Fig. 26. At this stage one also obtains that the operators associated with the subgraphs A and B are gauge invariant.

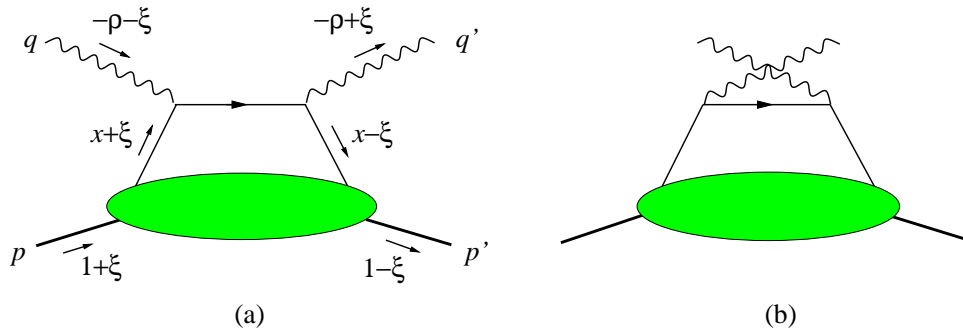


Figure 27: Born graphs for the Compton amplitude with independent photon virtualities, with plus-momentum fractions referring to the average proton momentum $\frac{1}{2}(p + p')$.

- The integrals over momentum fractions in the factorization formulae (259) and (264) involve configurations where lines in H are not far off-shell. A simple example is the point $x = \rho$ in the Born level diagram of the Compton amplitude in Fig. 27a (which corresponds to $x = x_B$ in the forward case describing inclusive DIS). The quark struck by the initial photon has zero plus-momentum and (in the collinear approximation) is on shell for these configurations. The corresponding pole provides the imaginary part of the scattering amplitude via Feynman's $i\epsilon$ in the propagator. The important point is that one can avoid these poles by deforming the x integration in the complex plane into a region where the plus-momenta in H are of order Q . In contrast this is not possible for the lines joining H to the other subgraphs: the integration path in complex loop momenta becomes pinched between different singularities in the limit $Q \rightarrow \infty$ and hence cannot be deformed. In this sense the lines going into the collinear subgraphs represent partons with “truly” small virtualities, whereas on-shell configurations inside the hard scattering graph H (obtained in particular when calculating its imaginary part by cutting lines) do not. A physically intuitive representation of reduced diagrams as in Fig. 26 is obtained from the Coleman-Norton theorem [284], which states that lines pinched in this manner correspond to the space-time trajectories of a particle in a classically allowed scattering process.
- In addition to the graphs in Fig. 26 there are reduced graphs with a further soft subgraph (whose momenta have all components small compared with Q) connected to any other subgraph. Important examples are shown in Fig. 28. Other examples have the form of Fig. 26b with an additional soft subgraph connected to A and B by soft gluons. For a detailed classification see [24, 181]. Such configurations correspond to nonperturbative cross talk between the target and the produced photon and meson, and an important piece of the factorization proofs is to show that they do not occur in the final result.

Note that configurations of this type occur in the momentum integrals of the factorization formulae at the transition $x \approx \pm\xi$ between ERBL and DGLAP regions and in the endpoint regions $z \approx 0$ or 1 of the meson DA. Examples are shown in Fig. 29. Consider for instance the region in the DVCS graph of Fig. 29a where the momentum l becomes soft. The horizontal quark line in the diagram is then of low virtuality and no longer belongs to a hard subgraph (and neglecting its transverse momentum as is done in the hard scattering subprocess is no longer justified). The reduced graph of this configuration is then of the form of Fig. 28 rather than of Fig. 26. As shown in the factorization proof [181], the contribution from the region where $l^+l^- \sim \mathbf{l}^2 \sim \Lambda^2$ is power suppressed and may hence be included in the integral over x in the factorization formula to leading power accuracy. Here Λ stands for a typical hadronic scale,

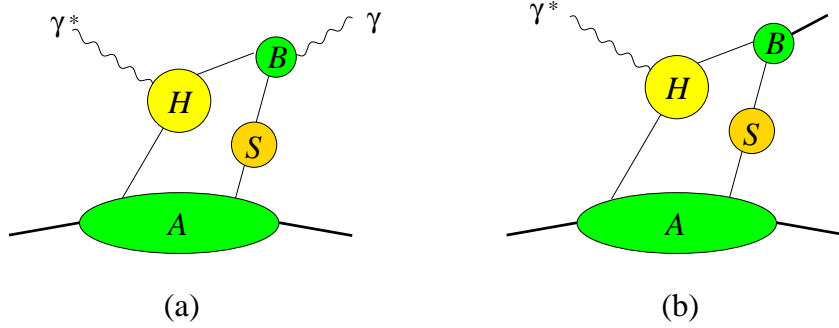


Figure 28: Examples of graphs with extra soft subgraphs for DVCS (a) and meson production (b).

say 1 GeV. The region where $l^2 \sim \Lambda^2$ while l^+ and l^- are of order Λ^2/Q does contribute to leading power, but in this case one can deform the integration over l^+ in the complex plane to a region where $l^+ \sim Q$, as mentioned in the previous point.

For meson production one finds [24] that with longitudinal γ^* the soft region contributes to the amplitude only as $1/Q^2$ and is hence power suppressed compared with the dominant behavior $1/Q$. Gauge invariance is important to establish this: the soft region can provide leading $1/Q$ contributions for individual Feynman diagrams, but these cancel in the sum over all diagrams. A similar finding in the small- x approximation was made by Hebecker and Landshoff [285]. Another important ingredient of the argument is the possibility to deform the integration contour in the region $k^+k^- \ll \mathbf{k}^2 \sim \Lambda^2$ and relies heavily on the fact that in the initial state there is no hadron moving in the direction of the final meson. This would fail in processes where there are oppositely moving hadrons in both the initial and the final state (see Section 7.5). If the γ^* in meson production is transverse, the amplitude is power suppressed. Contributions at level $1/Q^2$ come from *both* the collinear and the soft region, i.e. from both $k^- \sim Q$ and $k^- \sim \Lambda$.

- For DVCS and TCS only one of the two photons is far off-shell in the limit (258) and one may wonder whether using the pointlike photon-quark coupling is adequate. We have already remarked that configurations where one of the quarks coupling to the photon is soft (so that the other has small virtuality) are power suppressed or can be avoided by complex contour deformation. Configurations where both quarks coupling to the photon are approximately collinear to it (and will thus be subject to strong interactions among themselves) are described by reduced graphs as in meson production (Fig. 26b). These are power suppressed compared with the leading diagrams for Compton scattering (Fig. 26a).

The hard scattering kernels in (259) and (264) have important general properties which we now discuss. The hard scattering diagrams depend on the photon and parton momenta, but not on the average proton momentum P , to which the momentum fractions x , ξ , ρ refer. Thus one can write the Compton amplitude as

$$\begin{aligned}
\mathcal{A}(\gamma^*p \rightarrow \gamma^*p) &= \sum_q \int_{-1}^1 \frac{dx}{\xi} t^q \left(\frac{x}{\xi}, \frac{\rho}{\xi}, \log(Q^2 - Q'^2) \right) F^q(x, \xi, t) + \left(t^q \rightarrow \tilde{t}^q, F^q \rightarrow \tilde{F}^q \right) \\
&+ \int_{-1}^1 \frac{dx}{\xi} t^g \left(\frac{x}{\xi}, \frac{\rho}{\xi}, \log(Q^2 - Q'^2) \right) \frac{1}{\xi} F^g(x, \xi, t) + \left(t^g \rightarrow \tilde{t}^g, F^g \rightarrow \tilde{F}^g \right).
\end{aligned} \tag{266}$$

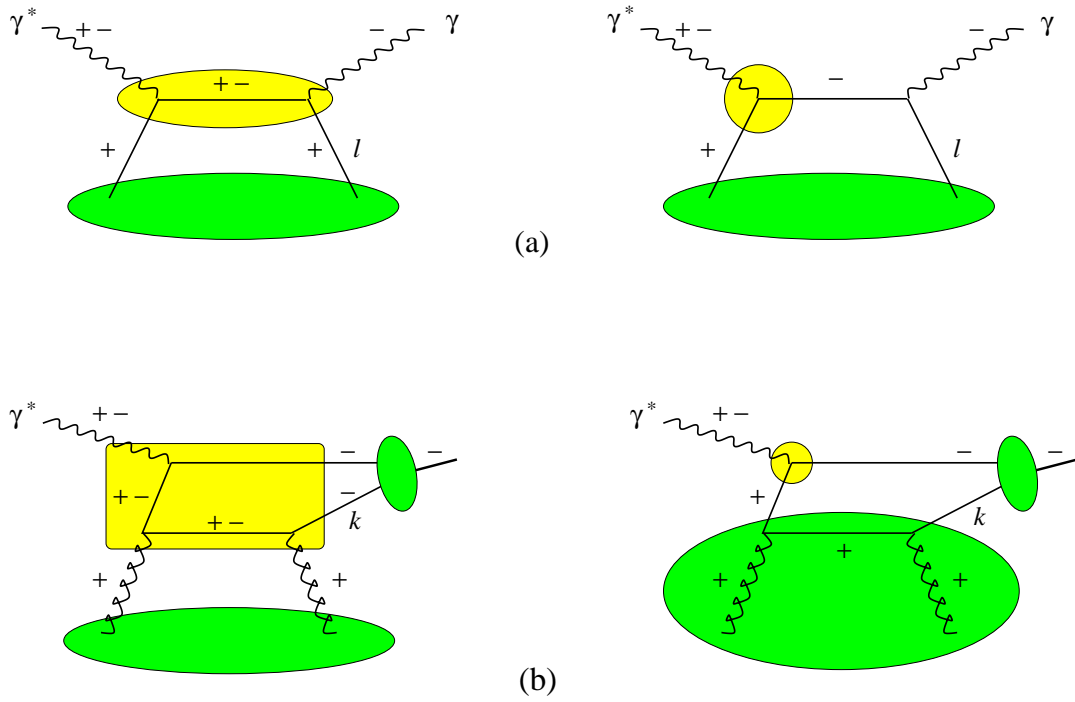


Figure 29: Feynman diagrams whose reduced graphs are either as in Fig. 26 or as in Fig. 28. A + or - next to a line indicates large plus- or minus-momenta. Lines with both + and - are hard, and lines without labels are soft and constitute the soft subgraphs here. The external proton lines are omitted for simplicity.

It is understood that the scale restoring the proper dimension in the logarithms is μ_F^2 or μ_R^2 . The overall factor of $1/\xi$ can be traced back to rewriting $dl^+ = P^+ dx$, and for gluons there is a further factor of $1/\xi$ originating from the explicit $1/P^+$ in the definition (18) of gluon GPDs. For meson production one similarly has

$$\begin{aligned} \mathcal{A}(\gamma_L^* p \rightarrow M_L p) = & \frac{1}{Q} \int_{-1}^1 \frac{dx}{\xi} \int_0^1 dz \left[\sum_{qj} t^{qj} \left(\frac{x}{\xi}, z, \log Q^2 \right) F^q(x, \xi, t) \Phi^j(z) \right. \\ & \left. + \sum_j t^{gj} \left(\frac{x}{\xi}, z, \log Q^2 \right) \frac{1}{\xi} F^g(x, \xi, t) \Phi^j(z) \right] \end{aligned} \quad (267)$$

for mesons with natural parity, and an analogous relation with \tilde{F}^q and \tilde{F}^g for mesons with unnatural parity. The factorization formulae predict the scaling of the Compton amplitude for large $Q^{(\prime)}$ at fixed ξ , ρ and t , up to logarithmic corrections. This is the exact analog of Bjorken scaling in DIS. For meson production, the dominant amplitude is predicted to decrease as $1/Q$ for large Q at fixed ξ and t , again up to logarithms.

The forms (266) and (267) have immediate consequences on the ξ or (ξ, ρ) dependence of the amplitude. If the quark or gluon GPDs at small ξ scale as in (252), $H^q(x, \xi) = \xi^{-\lambda} \hat{H}^q(x/\xi)$ or $H^g(x, \xi) = \xi^{-(1+\lambda)} \hat{H}^g(x/\xi)$, their contribution to the Compton amplitude gives a power law

$$\mathcal{A}_{q,g} = \xi^{-(1+\lambda)} C_{q,g}(\rho/\xi) \quad (268)$$

for $\xi \ll 1$. At fixed Q^2 and Q'^2 this translates into a high-energy behavior as $W^{2(1+\lambda)}$. For meson production amplitudes the result is analogous, with $C_{q,g}(\rho/\xi)$ replaced by constants. Such a power behavior was explicitly found in numerical studies, see [123, 286, 244].

Resonance exchange contributions (228) to GPDs also lead to a power behavior in ξ times a function of ρ/ξ . Replacing in particular \tilde{F}^q in (266) with the pion pole contribution (210) to \tilde{E}^q gives a term $\xi^{-1} C_\pi(\rho/\xi)$. According to (54) the distribution \tilde{E}^q appears in amplitudes with at least one factor of ξ , which leads to at most a constant high-energy behavior of the amplitude at fixed Q^2 and Q'^2 , as it must be for spin-zero exchange. Finally, replacing F^q or F^g in (266) with the D -term contributions (124) or (128) to H^q , E^q or H^g , E^g gives a result depending only on ρ/ξ for both quarks and gluons. Further ξ dependence comes from the appropriate prefactors in the proton matrix elements (54).

5.1.1 Selection rules

Because the hard scattering kernels express collinear scattering, the helicities of incoming and outgoing particles must balance to ensure conservation of angular momentum J^3 . Together with chirality conservation in the hard scattering (where light quark masses are set to zero) this leads to selection rules for the photon (or meson) helicities. It can be shown that the axial anomaly of QCD does not invalidate chirality conservation in hard scattering coefficients [287]. For Compton scattering this allows at leading power the transitions summarized in Table 2. The transition $\gamma_L^* \rightarrow \gamma_L^*$ is of course absent if one of the photons is real. In DDVCS this transition only starts at one-loop level, as does its forward analog, the longitudinal structure function F_L of inclusive DIS. For the hadronic tensor (270) at leading order in $1/Q$ and in α_s this implies a nonforward analog of the Callan-Gross relation $F_2 = 2xF_1$ between deep inelastic structure functions [100, 288]. Note that in the $\gamma_L^* \rightarrow \gamma_L^*$ transition $\tilde{H}^{q,g}$ and $\tilde{E}^{q,g}$ do not appear because of parity invariance. Photon helicity flip by two units can be balanced by gluon helicity flip GPDs, and thus also occurs at one-loop level. Amplitudes with one

Table 2: Allowed photon helicity transitions in Compton scattering at leading power in $1/Q$ or $1/Q'$, together with the relevant GPDs and the order of the hard scattering where they occur. LO corresponds to Born level and NLO to $O(\alpha_s)$. Further allowed transitions are obtained by reversing both helicities. For each parton species H stands for H , E and \tilde{H} for \tilde{H} , \tilde{E} , whereas H_T represents all four transversity distributions.

$\gamma^* \rightarrow$	γ^*	LO	NLO
+	+	$H^{q(+)}, \tilde{H}^{q(+)}$	$H^{q(+)}, \tilde{H}^{q(+)}, H^g, \tilde{H}^g$
0	0		$H^{q(+)}, H^g$
+	-		H_T^g

longitudinal and one transverse photon are suppressed by a power $1/Q^{(\prime)}$ and explicitly appear at twist-three level (see Section 6.1.2).

The selection rules for meson production are more intricate. To make the symmetry between the proton and meson side in the factorization formula explicit, it is useful to consider the GPDs in the ERBL region, where they have the parton kinematics of a distribution amplitude. The hard scattering is then the same as for an elastic meson form factor or a meson transition form factor, with the incoming partons moving to the right and the outgoing ones to the left in the Breit frame.

The leading-twist operators for DAs and GPDs describe coupling of the parton pair to helicity 0, helicity ± 1 (with quark transversity), or helicity ± 2 (with gluon transversity). Because of chirality conservation in the hard scattering, chiral-odd DAs and GPDs must occur in pairs. This was originally thought to offer a way for measuring quark transversity GPDs in the production of a transversely polarized meson [181]. The hard scattering kernel is however zero, as was explicitly checked at leading [123] and next-to-leading [289] order in α_s . It holds in effect to all orders [290, 287]: quark helicity conservation would force the initial and final quark pair to have opposite total helicity in the Breit frame, and a photon cannot mediate a change of J^3 by two units.

The matrix elements of the tensor operator $\mathbf{S}G^{+i}G^{j+}$ cannot appear either. Helicity conservation in the hard scattering would only allow them in pairs, but one cannot have a gluon GPD and a gluon GDA in the same diagram: two gluons couple only to $C = +$ and a photon does not couple to the transition between two C -even states. One is thus left with transitions $q\bar{q} \rightarrow q\bar{q}$, $gg \rightarrow q\bar{q}$, or $q\bar{q} \rightarrow gg$ from helicity 0 to helicity 0. This also establishes that only γ_L^* amplitudes are leading in $1/Q$. The corresponding statement for meson form factors is the well-known hadron helicity conservation in hard exclusive scattering processes [291].

The parity constraints for the hard scattering with a γ_L^* require the operators of the DAs and the GPDs to have the same parity, so that natural parity mesons only go with H , E and unnatural parity ones only with \tilde{H} , \tilde{E} . In Table 3 we list the relevant combinations for several mesons. This compilation is not complete.¹² The selection of GPDs and DAs for a_1 mesons is the same as for pions, and for f_1 the same as for the η , η' system. The combinations for a_0 and a_2 coincide with those for f_0 and f_2 except that there is no Φ^g . For neutral b_1 and h_1 mesons one has access to $\tilde{H}^{q(+)}$, and for charged b_1 to $\tilde{H}^{q(+)} \pm 3\tilde{H}^{q(-)}$. One can however expect experimental study of these mesons to be difficult because they have many-body decay modes or poorly known branching ratios.

¹²Detailed tables including quark flavor combinations are given by Goeke et al. [37]. In their Table 3 the entries in the first column correctly read $(2u + \bar{u}) - (2d + \bar{d})$, $(2u - \bar{u}) - (2d - \bar{d})$, $(2\Delta u + \Delta \bar{u}) - (2\Delta d + \Delta \bar{d})$, $(2\Delta u - \Delta \bar{u}) - (2\Delta d - \Delta \bar{d})$ [292].

Table 3: Combinations of GPDs and DAs entering in selected meson electroproduction channels at leading order in $1/Q$ and in α_s . The same results hold with appropriate GDAs if the meson is replaced by a many-body system with appropriate quantum numbers. For each parton species H stands for H , E and \tilde{H} for \tilde{H} , \tilde{E} . In the charged meson channels the isospin relations (203) have been used to relate the $p \rightarrow n$ and $\bar{p} \rightarrow \bar{n}$ GPDs to the flavor diagonal ones in the proton.

J^{PC} or J^P	meson	GPD	DA
1^{--}	ρ^0, ω, ϕ	$H^{q(+)}, H^g$	Φ^q
$0^{++}, 2^{++}$	f_0, f_2	$H^{q(-)}$	Φ^q, Φ^g
0^{-+}	π^0, η, η'	$\tilde{H}^{q(-)}$	Φ^q
1^-	ρ^\pm	$H^{q(+)} \pm 3H^{q(-)}$	Φ^q
0^-	π^\pm	$\tilde{H}^{q(-)} \pm 3\tilde{H}^{q(+)}$	Φ^q

One may expect that for isoscalar mesons with unnatural parity the gluon DA, going with the operator $G^{+\mu} \tilde{G}_\mu^+$ also enters. At leading order in α_s the corresponding collinear scattering kernel is however zero, as was found in a study of η and η' production [94]. At one-loop level the gluon DA should appear explicitly in the hard scattering, since it mixes with the quark DA under evolution. The symmetry between the meson and proton side in the hard scattering implies that likewise the gluon GPD \tilde{H}^g appears in h_1 production only at $O(\alpha_s^2)$.

From Tables 2 and 3 we see that access to H^g and E^g is provided in Compton scattering at NLO and in the production of neutral vector mesons. \tilde{H}^g and \tilde{E}^g can only be accessed Compton scattering at NLO (assuming that a NLO analysis of h_1 production is not practical). Possibilities to access the polarized gluon GPDs in processes beyond leading twist have been proposed and will be discussed in Section 7. Access to the C -even combinations of quark GPDs is given in Compton scattering, with each quark flavor weighted by its squared charge e_q^2 . From

$$\sum_q e_q^2 H^q = \frac{5}{18} H^{u+d} + \frac{3}{18} H^{u-d} + \frac{1}{9} H^s \quad (269)$$

and the analog for the other GPDs one sees in particular that the isoscalar combination is slightly enhanced over the isotriplet one by the charge weighting.

Information for flavor separation of $H^{q(+)}$ and $E^{q(+)}$ may be obtained from vector meson production, and for $\tilde{H}^{q(+)}$, $\tilde{E}^{q(+)}$ from charged pseudoscalar production at small ξ , where one may expect that $|\tilde{H}^{q(+)}| \gg |\tilde{H}^{q(-)}|$ in analogy with the forward densities. The C -odd combinations of quark GPDs may be studied in the relevant neutral meson channels. A different possibility to access combinations of GPDs not occurring in Compton scattering is in principle given by replacing photons in the Compton process by weak gauge bosons, but this has not been studied so far. Finally, flavor separation of u and d quark GPDs could be obtained with nuclear targets by scattering on a neutron instead of a proton (see Section 4.5). In analogy to the situation for flavor separation of inclusive parton densities this requires sufficient knowledge of the nuclear wave functions.

5.2 Compton scattering

Compton scattering is the most thoroughly studied process involving GPDs, with most work focused on DVCS so far. The process is conveniently analyzed in terms of the hadronic tensor

$$T^{\alpha\beta} = i \int d^4x e^{i(q+q')x/2} \langle p' | T J_{\text{em}}^\alpha(-\frac{1}{2}x) J_{\text{em}}^\beta(\frac{1}{2}x) | p \rangle, \quad (270)$$

where $eJ_{\text{em}}^\alpha(x)$ is the electromagnetic current. The helicity amplitudes for $\gamma^*p \rightarrow \gamma^*p$ are then given by

$$e^2 M_{\lambda'\mu',\lambda\mu} = e^2 \epsilon_\alpha T^{\alpha\beta} \epsilon_\beta'^* \quad (271)$$

where ϵ (ϵ') and μ (μ') denote the polarization and helicity of the initial (final) photon, and λ (λ') the helicity of the initial (final) proton. From parity invariance one has

$$M_{-\lambda'-\mu',-\lambda-\mu} = (-1)^{\lambda'-\mu'-\lambda+\mu} M_{\lambda'\mu',\lambda\mu}, \quad (272)$$

provided one takes a frame where the initial and final proton momenta are in the x - z plane, which we will assume from now on. We further choose a frame where both protons move fast into the positive z direction.

To leading order in $1/Q$ one can write

$$T^{\alpha\beta} = -g_T^{\alpha\beta} \mathcal{F} - i\epsilon_T^{\alpha\beta} \tilde{\mathcal{F}} + \dots, \quad (273)$$

where the \dots indicate terms which appear at $O(\alpha_s)$ and go with the photon helicity combinations $(\mu'\mu) = (00)$, $(+-)$ or $(-+)$. The handbag diagrams in Fig. 27 give

$$\begin{aligned} \mathcal{F}(\rho, \xi, t) &= \sum_q e_q^2 \int_{-1}^1 dx F^q(x, \xi, t) \left(\frac{1}{\rho - x - i\epsilon} - \frac{1}{\rho + x - i\epsilon} \right) + O(\alpha_s), \\ \tilde{\mathcal{F}}(\rho, \xi, t) &= \sum_q e_q^2 \int_{-1}^1 dx \tilde{F}^q(x, \xi, t) \left(\frac{1}{\rho - x - i\epsilon} + \frac{1}{\rho + x - i\epsilon} \right) + O(\alpha_s), \end{aligned} \quad (274)$$

where at $O(\alpha_s)$ one has also contributions from F^g in \mathcal{F} and from \tilde{F}^g in $\tilde{\mathcal{F}}$. Following the convention of Belitsky et al. [293, 244] we further define \mathcal{H} , \mathcal{E} by replacing $F^{q,g}$ with $H^{q,g}$ or $E^{q,g}$, and $\tilde{\mathcal{H}}$, $\tilde{\mathcal{E}}$ by replacing $\tilde{F}^{q,g}$ with $\tilde{H}^{q,g}$ or $\tilde{E}^{q,g}$ in (274).

To obtain explicit amplitudes we choose polarization vectors

$$\epsilon(\pm) = \frac{1}{\sqrt{2}}(0, \mp 1, i, 0) \quad (275)$$

for both photons when their momentum points in the negative z direction in the photon-proton c.m., and correspondingly if they have a small momentum in the x direction. Since deviations from strict collinearity are suppressed by $1/Q$ in the hard scattering, one then has

$$-\epsilon_\alpha g_T^{\alpha\beta} \epsilon_\beta'^* = 1, \quad -i\epsilon_\alpha \epsilon_T^{\alpha\beta} \epsilon_\beta'^* = \mu \quad (276)$$

for $\mu = \mu' = \pm 1$, up to corrections in $1/Q$. Explicitly one obtains from (54) and (273)

$$\begin{aligned} M_{++;++} &= \sqrt{1-\xi^2} \left(\mathcal{H} + \tilde{\mathcal{H}} - \frac{\xi^2}{1-\xi^2} (\mathcal{E} + \tilde{\mathcal{E}}) \right), \\ M_{-+;-+} &= \sqrt{1-\xi^2} \left(\mathcal{H} - \tilde{\mathcal{H}} - \frac{\xi^2}{1-\xi^2} (\mathcal{E} - \tilde{\mathcal{E}}) \right), \\ M_{++;-+} &= \frac{\sqrt{t_0-t}}{2m} (\mathcal{E} - \xi\tilde{\mathcal{E}}), \\ M_{-+;++} &= -\frac{\sqrt{t_0-t}}{2m} (\mathcal{E} + \xi\tilde{\mathcal{E}}). \end{aligned} \quad (277)$$

These amplitudes correspond to the phase conventions of the light-cone helicity spinors (404) in a frame where the incoming proton momentum p points along the positive z axis, whereas the components of the outgoing proton momentum satisfy $p^1 \leq 0$, $p^2 = 0$, $p^3 > 0$. Up to $1/Q$ suppressed terms, the amplitudes are the same for the usual helicity spinors in the γ^*p c.m., where both protons move fast (see Appendix B).

In the case where the final or initial state photon is real, the imaginary part of the amplitudes is given by GPDs at the boundaries $x = \pm\xi$ of the ERBL and DGLAP regions. The same is true for vector meson production. In contrast, with two nonzero photon virtualities one has access to the quark GPDs evaluated at fixed $x = \pm\rho$ in the ERBL region, since kinematics enforces $|\rho| \leq \xi$. This unique possibility of DDVCS has been emphasized already in [39].

The hard scattering kernels in (274) provide a simple relation between DVCS and TCS at leading order in α_s . From

$$\mathcal{H}(-\xi, \xi, t) = [\mathcal{H}(\xi, \xi, t)]^*, \quad \tilde{\mathcal{H}}(-\xi, \xi, t) = -[\tilde{\mathcal{H}}(\xi, \xi, t)]^*, \quad (278)$$

and the analogs for \mathcal{E} and $\tilde{\mathcal{E}}$ one finds that at leading-twist accuracy

$$M_{\lambda'\mu, \lambda\mu} \Big|_{\text{TCS}} = [M_{\lambda'-\mu, \lambda-\mu}]_{\text{DVCS}}^* + O(\alpha_s) \quad (279)$$

with $\mu = \pm 1$, where it is understood that the amplitudes are evaluated at the same ξ and t and at equal values of Q^2 and Q'^2 , which set the factorization scale in the GPDs. In this approximation the amplitudes for DVCS and for TCS thus carry the same information. Relations similar to (278) and (279) hold for $|\rho| < \xi$ and connect the amplitudes for DDVCS at equal $(Q^2 + Q'^2)$ and opposite $(Q^2 - Q'^2)$. Verification of the relations (279) would constitute a model independent test of leading-twist dominance and the Born level approximation for the Compton amplitude. At $O(\alpha_s)$ accuracy these relations no longer hold, neither for the NLO corrections to the quark handbag diagrams nor for the diagrams involving gluon GPDs.

The hard scattering kernels at NLO have been calculated by several groups. They can be found in [294, 295, 296, 278]¹³ for the photon helicity transition $(\mu'\mu) = (++)$, and in [295] for $(\mu'\mu) = (00)$. These results are given for independent ρ and ξ , explicit kernels for DVCS can be found in [124].¹⁴ The helicity flip case $(\mu'\mu) = (+-)$ has been calculated in [57, 56]. For DVCS one finds a rather simple result [55]

$$M_{\lambda'\mu', \lambda\mu} = -\frac{\alpha_s}{4\pi} \sum_q e_q^2 \int_{-1}^1 \frac{dx}{x} A_{\lambda'\mu', \lambda\mu}^g(x, \xi, t) \left(\frac{1}{\xi - x - i\epsilon} - \frac{1}{\xi + x - i\epsilon} \right) \quad (280)$$

for $(\mu'\mu) = (+-)$ and $(-+)$, with the phase conventions (275). Here A^g stands for the combinations of gluon transversity GPDs given in Section 3.5.3. The term in brackets is proportional to x , so that the integrand has no $1/x$ singularity.

Beyond leading order in α_s , both real and imaginary parts of the Compton amplitude involve GPDs in integrals over x . For DVCS the imaginary part of the amplitude involves only the DGLAP regions, with $x \geq \xi$ corresponding to the s -channel cut and $x \leq -\xi$ to the u -channel cut of the parton-photon subprocess. The same holds for light meson production amplitudes. If the final state photon in the Compton process is timelike the situation is more complicated since there are additional cuts in

¹³The journal version of [295] contains a typo in the coefficient of \tilde{F}^g , which is corrected in version 3 in the hep-ph archive.

¹⁴The global factor $1/|\eta|$ in eq. (6) of [124] should be omitted, and for gluon kernels it must read $\mp(t \rightarrow -t)$ instead of $\pm(t \rightarrow -t)$ in eq. (9) [297].

q^2 , and the imaginary part of the amplitude is no longer related in a simple way to the discontinuities in the external invariants.

Numerical studies of DVCS amplitudes at NLO accuracy have been performed by Belitsky et al. in [124] and later in [244], and by Freund and McDermott [298, 286, 110]. Both groups find a significant dependence of the size and pattern of NLO corrections on the input GPDs, so that general conclusions are to be taken with some caution. The input dependence in [298, 286, 110] is generally larger in the small- x_B region and larger for the real than for the imaginary part of the amplitude. With identical input GPDs at a given scale, NLO corrections tend to decrease the unpolarized DVCS cross section. For a factorization scale $\mu = Q$, both groups find that even at moderate $x_B \sim 0.1$ the contributions from the gluon GPDs are not always negligible. On the other hand even at small $x_B \sim 10^{-3}$ the contribution from quark GPDs cannot be ignored. This is in contrast to vector meson production, where quarks and gluons enter at the same order in α_s , so that at small x_B the gluon contribution should strongly dominate over quarks. Note that for DVCS at NLO the distinction between quark and gluon contributions depends on the factorization scale and scheme (the $\overline{\text{MS}}$ scheme has been used in all studies). Belitsky et al. [244] have pointed out that the contribution of gluon GPDs at NLO can be made very small by choosing a scale which for their model GPDs was about $\mu \approx 3.8Q$. A physics reason for taking such a high μ is however not obvious. Comparing on the other hand the NLO results obtained with $\mu^2 = Q^2$, $\mu^2 = 2Q^2$ and $\mu^2 = Q^2/2$ the studies [124] and [286] found rather moderate effects.

We remark that the one-loop kernels going with gluon GPDs are so far only available for massless quarks. This leads to an uncertainty in the range of x_B and Q^2 where the collision energy is large enough for charm to be important but Q^2 is not so large that the charm quark mass can be neglected in the loop. This is presumably the case for the kinematical region of the DVCS measurements of H1 and ZEUS [259, 299]. Notice for comparison that the charm contribution to the inclusive proton structure function F_2 is in the 10% to 20% range for the same values of x_B and Q^2 [300, 301].

5.3 Meson electroproduction

Meson production processes offer the possibility to study various aspects of GPDs that are inaccessible in Compton scattering, in addition to being sensitive to the structure of the produced meson itself. Dedicated phenomenological studies of meson production at leading $1/Q$ accuracy have been performed by Mankiewicz et al. for neutral [123] and charged [186] mesons, by Frankfurt et al. for pseudoscalar mesons [187] and for processes with a Δ or a strange baryon in the final state [189], by Eides et al. [302] and by Mankiewicz et al. [196] for neutral pseudoscalars, and by Vanderhaeghen et al. [303, 304].

To leading order in α_s the diagrams involving quark GPDs and quark DAs give a contribution [123, 186, 303, 187]

$$\mathcal{A}_1 = e \frac{16\pi\alpha_s}{9} \frac{1}{Q} \int_0^1 dz \sum_{qq'} \Phi^{qq'}(z) \int_{-1}^1 dx F^{q'q}(x, \xi, t) \left[\frac{1}{\bar{z}} \frac{e_q}{\xi - x - i\epsilon} - \frac{1}{z} \frac{e_{q'}}{\xi + x - i\epsilon} \right] \quad (281)$$

to the amplitude for a longitudinal γ^* and a longitudinal meson with natural parity. Here $\Phi^{qq'}(z)$ is defined as in (78) with the operator $\bar{q}\gamma^+q'$, so that z is the momentum fraction of the quark q and $\bar{z} = 1 - z$ the momentum fraction of the antiquark \bar{q}' . For $F^{q'q}$ the relevant operator is $\bar{q}'\gamma^+q$, so that the momentum fraction $x + \xi$ belongs to flavor q and $x - \xi$ to flavor q' . The expression for mesons with unnatural parity is analogous with the appropriate DA and $\tilde{F}^{q'q}$ instead of $F^{q'q}$. If the meson quantum numbers admit there is in addition a contribution with either gluon GPDs [123, 269, 272],

$$\mathcal{A}_2 = e \frac{\pi\alpha_s}{3} \frac{1}{Q} \int_0^1 dz \sum_q e_q \frac{\Phi^q(z)}{z\bar{z}} \int_{-1}^1 dx \frac{F^g(x, \xi, t)}{x} \left[\frac{1}{\xi - x - i\epsilon} - \frac{1}{\xi + x - i\epsilon} \right] \quad (282)$$

or with the gluon DA of the meson [269, 272],

$$\mathcal{A}_3 = e \frac{4\pi\alpha_s}{3} \frac{1}{Q} \int_0^1 dz \frac{\Phi^g(z)}{z\bar{z}} \int_{-1}^1 dx \sum_q e_q F^q(x, \xi, t) \left[\frac{1}{\xi - x - i\epsilon} + \frac{1}{\xi + x - i\epsilon} \right]. \quad (283)$$

Note that to leading order in $1/Q$ and in α_s the meson structure only enters through a few constants. For each quark flavor combination one needs $\int dz (z\bar{z})^{-1} \Phi$ and $\int dz (z\bar{z})^{-1} (z - \bar{z}) \Phi$, one of which is zero if the meson is a C eigenstate. If applicable there is a further constant $\int dz (z\bar{z})^{-1} \Phi^g$ from the gluon DA. Relations between DAs for different quark flavors follow from flavor symmetry. Isospin invariance gives for instance $\Phi_{\pi^+}^{ud} = \Phi_{\pi^-}^{du} = \sqrt{2} \Phi_{\pi^0}^u = -\sqrt{2} \Phi_{\pi^0}^d$ and corresponding relations for the ρ mesons.¹⁵ In analogy to GPDs we use the shorthand notation $\Phi^{u-d} = \Phi^u - \Phi^d$ etc.

Let us discuss some aspects of the phenomenology following from these expressions, and of the possibilities to extract information on GPDs and meson structure from various channels. We caution that in experimental observables one has no direct access to the amplitudes discussed here, but rather to their squares or interference terms, summed over appropriate proton spin combinations (see Section 9.4).

For the neutral vector mesons ρ^0 , ω , ϕ both quark and gluon GPDs contribute. The ratio of their production amplitudes is

$$\begin{aligned} \mathcal{A}_{\rho^0} : \mathcal{A}_{\omega} : \mathcal{A}_{\phi} &= \int_{-1}^1 \frac{dx}{\xi - x - i\epsilon} \left(\frac{2F^{u(+)} + F^{d(+)}}{\sqrt{2}} + \frac{9}{8\sqrt{2}} \frac{F^g}{x} \right) \\ &: \int_{-1}^1 \frac{dx}{\xi - x - i\epsilon} \left(\frac{2F^{u(+)} - F^{d(+)}}{\sqrt{2}} + \frac{3}{8\sqrt{2}} \frac{F^g}{x} \right) \\ &: \int_{-1}^1 \frac{dx}{\xi - x - i\epsilon} \left(-F^{s(+)} - \frac{3}{8} \frac{F^g}{x} \right), \end{aligned} \quad (284)$$

if one assumes that their respective $q\bar{q}$ content is $\frac{1}{\sqrt{2}}(|u\bar{u}\rangle - |d\bar{d}\rangle)$, $\frac{1}{\sqrt{2}}(|u\bar{u}\rangle + |d\bar{d}\rangle)$ and $|s\bar{s}\rangle$, and that their distribution amplitudes are related as $\Phi_{\rho^0}^{u-d}(z) = \Phi_{\omega}^{u+d}(z) = \sqrt{2} \Phi_{\phi}^s(z)$.¹⁶ This hypothesis reproduces rather well the combinations $(M_V \Gamma_{V \rightarrow e^+e^-})^{1/2}$ of mass and partial leptonic width for these mesons, which are proportional to $\sum_q \int dz e_q \Phi^q(z)$. Measurement gives $(M_{\rho} \Gamma_{\rho \rightarrow e^+e^-}) : (M_{\omega} \Gamma_{\omega \rightarrow e^+e^-}) : (M_{\phi} \Gamma_{\phi \rightarrow e^+e^-}) \approx 9 : 0.8 : 2.2$, compared with the ratios $9 : 1 : 2$ obtained under the above assumptions. With (284) the same ratios are obtained for the electroproduction cross sections σ_{ρ^0} , σ_{ω} , σ_{ϕ} in the region where the gluon GPDs dominate over those for quarks. This is expected and found in the data at small x_B , see Section 8.4. At larger values of x_B one expects the quark contributions to become important, at least for the ρ^0 and the ω . How important the respective contributions are at intermediate x_B and from which point quarks dominate is not clear at present. Existing studies by Vanderhaeghen et al. [303, 304] (see also [37]) have added the cross sections modeled for quark and gluon GPDs but not taken into account their interference. For the gluon contributions they furthermore used a model by Frankfurt et al. [305], which specifically used approximations for the region of very small x_B (see Section 8.4).

In a region of x_B and Q^2 where one can argue for the dominance of quark GPDs for ρ and ω production (possibly by comparison with the ϕ channel) the cross section ratio $d\sigma_{\omega}/d\sigma_{\rho^0}$ in the approximation of (284) gives rather direct information about the relative size of unpolarized u and d quark GPDs. Note that quark dominance and the simple assumption $F^u : F^d = 2 : 1$ yield a ratio

¹⁵Note that the relative sign between DAs for different isospin states is convention dependent, see Appendix A of [85].

¹⁶These relations do not simply follow from SU(3) flavor symmetry. They neglect in addition the mixing of $q\bar{q}$ with gluons, which induces e.g. differences between $\Phi_{\rho^0}^{u-d}$ and Φ_{ω}^{u+d} .

$d\sigma_{\rho^0} : d\sigma_{\omega} = 25 : 9$, which is significantly smaller than in the gluon dominated region, as already observed in [24].

The production of charged mesons involves a combination of C -even and C -odd GPDs as seen in Table 3. In analogy to forward parton distributions one expects that at small x_B the C -even combinations will become dominant, so that for instance the cross sections for $\gamma^*p \rightarrow \rho^+n$ and $\gamma^*n \rightarrow \rho^-p$ or their analogs for π^+ and π^- production will become equal. In a model study [186] for ρ^\pm production this was found to hold for $x_B \lesssim 0.1$. Using the isospin relations $\Phi_{\rho^+}^{ud} = \Phi_{\rho^-}^{du} = \sqrt{2}\Phi_{\rho^0}^u$ and those in (203) relating the nucleon transition GPDs to the flavor diagonal ones, one finds the three ρ channels connected by

$$\begin{aligned} \mathcal{A}_{\rho^0} : \mathcal{A}_{\rho^+} : \mathcal{A}_{\rho^-} &= \int_{-1}^1 \frac{dx}{\xi - x - i\epsilon} \left(\frac{2F^{u(+)} + F^{d(+)}}{\sqrt{2}} + \frac{9}{8\sqrt{2}} \frac{F^g}{x} \right) \\ &: \int_{-1}^1 \frac{dx}{\xi - x - i\epsilon} \left(\frac{F^{u(+)} - F^{d(+)}}{2} + \frac{3F^{u(-)} - 3F^{d(-)}}{2} \right) \\ &: \int_{-1}^1 \frac{dx}{\xi - x - i\epsilon} \left(\frac{F^{u(+)} - F^{d(+)}}{2} - \frac{3F^{u(-)} - 3F^{d(-)}}{2} \right). \end{aligned} \quad (285)$$

Together with the relation (284) between ρ^0 and ω production we see that these four channels offer in principle enough observables to separate F^g , $F^{u(+)}$, $F^{d(+)}$, and $F^{u(-)} - F^{d(-)}$. The simple estimate $F^u : F^d = 2 : 1$ also suggests that the cross section for charged ρ production is significantly smaller than for ρ^0 production, even in a region where the latter is not enhanced by gluon exchange.

Note that the vector meson channels offer the possibility to obtain flavor information beyond the combination (269) from Compton scattering for the distributions $H^{q(+)}$ and $E^{q(+)}$, which enter in Ji's sum rule (70). ϕ production is one of the very few known processes where one could separately access $F^{s(+)}$, although in direct competition with F^g , apart possibly from K^* production (see below) and neutrino induced processes (Section 7.4.2).

The production of π^0 involves the C -odd combination $2\tilde{F}^{u(-)} + \tilde{F}^{d(-)}$ of polarized quark GPDs. Note that the pion pole contribution to \tilde{E} is C -even and does not appear in this process. In the η , η' system there is a nontrivial pattern of mixing and flavor SU(3) breaking, related to the U(1) axial anomaly of QCD, for reviews we refer to [306, 307]. Studies of electroproduction focusing on this issue have been performed in [302] and [94]. Neglecting isospin violation, one has a set Φ_η^{u+d} , Φ_η^s and $\Phi_{\eta'}^{u+d}$, $\Phi_{\eta'}^s$ of independent quark DAs. In the naive SU(3) limit one has $\Phi_\eta^{u+d} = -\Phi_\eta^s$ and $\Phi_{\eta'}^{u+d} = 2\Phi_{\eta'}^s$. As we mentioned in Section 5.1.1 the gluon DAs of η and η' enter in electroproduction only through mixing in the LO evolution and at order α_s^2 in the hard scattering. The relative weight of the quark DAs is given by

$$\mathcal{A}_\eta \propto \int_{-1}^1 \frac{dx}{\xi - x - i\epsilon} \int_0^1 \frac{dz}{z\bar{z}} \left[(2\tilde{F}^{u(-)} - \tilde{F}^{d(-)})\Phi_\eta^{u+d} - 2\tilde{F}^{s(-)}\Phi_\eta^s \right] \quad (286)$$

for the η . This involves the same z integral as the process $\gamma^*\gamma \rightarrow \eta$ at leading order in $1/Q$ and α_s (see Section 5.4.1):

$$\mathcal{A}(\gamma^*\gamma \rightarrow \eta) \propto \int_0^1 \frac{dz}{z\bar{z}} \left[5\Phi_\eta^{u+d} + 2\Phi_\eta^s \right], \quad (287)$$

Relations analogous to (286) and (287) hold for the η' . We see that electroproduction and two-photon annihilation probe different quark flavor combinations of the DAs. The forward limit of $\tilde{F}^{s(-)}$ is $\Delta s - \Delta \bar{s}$, so that one may plausibly neglect $\tilde{F}^{s(-)}$ in (286), especially at larger values of ξ [302]. The electroproduction ratio $d\sigma_\eta/d\sigma_{\eta'}$ then gives rather direct information about the relative size

of Φ_η^{u+d} and $\Phi_{\eta'}^{u+d}$, which is independent from what is measured in $\gamma^*\gamma$ annihilation. Conversely, particular scenarios for η , η' mixing and for the shape of their DAs can be tested in $d\sigma_\eta/d\sigma_{\eta'}$ without uncertainties from the nucleon GPDs if the above approximations are valid. With knowledge about the relative size of η , η' and π^0 quark DAs as input one could finally obtain information about the relative size of $2\tilde{F}^{u(-)} - \tilde{F}^{d(-)}$ and $2\tilde{F}^{u(-)} + \tilde{F}^{d(-)}$.

Charged pion production receives a contribution from the pion pole part (210) of \tilde{E}^{u-d} , which according to phenomenological estimates [196, 304] strongly dominates the cross section for sufficiently large x_B and small t . This pole contribution to the amplitude can be written as

$$\mathcal{A}_{\pi^+}^{\text{pole}} = -\mathcal{A}_{\pi^-}^{\text{pole}} = -e \frac{Q F_\pi(Q^2)}{f_\pi} \frac{2m g_A(0)}{m_\pi^2 - t} \bar{u}(p') \gamma_5 u(p) \quad (288)$$

with $f_\pi \approx 131$ MeV, where

$$F_\pi(Q^2) = \frac{2\pi\alpha_s}{9} \frac{f_\pi^2}{Q^2} \left[\int_0^1 dz \frac{\phi_\pi(z)}{z\bar{z}} \right]^2 \quad (289)$$

is the electromagnetic pion form factor to leading order in $1/Q$ and α_s in the hard scattering picture [50], which is the exact analog for form factors of the factorization scheme discussed in Section 5.1. The relation (288) readily generalizes to higher orders in α_s . As in (211) we have used the pion distribution amplitude $\phi_\pi(z)$ normalized to unit integral. The physical picture behind (288) is that the nucleon emits a pion (whose off-shellness is neglected as one approaches the pion pole) on which the photon scatters, see Fig. 30. This is the basis of the attempt to measure the electromagnetic pion form factor in $\gamma^*p \rightarrow \pi^+ n$. In the large Q^2 limit the GPD formalism offers ways to study the extent to which the pion pole dominates the amplitude in given kinematics. As we have emphasized in Section 4.1.3 the chiral soliton model estimates important non-pole contributions to \tilde{E}^{u-d} if t is not small enough. The minimal kinematically allowed value of $|t|$ is $m^2 x_B^2 / (1 - x_B)$ at large Q^2 , which favors measurement at smaller x_B . On the other hand, as x_B decreases the contributions from \tilde{H}^{u-d} are expected to become increasingly important, in analogy with the increase of the forward polarized quark densities with x_B . In contrast the pion pole contribution (288) does not grow with decreasing x_B . A model estimate of the relative size of the two contributions has been given by Mankiewicz et al. [196], who in particular point out the importance of an adequate description of the t -dependence of \tilde{H} . We note that the physical process corresponding to the contribution from \tilde{H} and \tilde{E} in the DGLAP region, including the boundary $x = \xi$ which provides the imaginary part of the amplitude at leading $O(\alpha_s)$, has been discussed long ago by Carlson and Milana [308]. To obtain information on the size of non-pole contributions in π^\pm production from the π^0 channel is unfortunately difficult, given the different combinations of quark flavor and C -parity for the GPDs. On the other hand, information on the relative size of the contributions from \tilde{H} and \tilde{E} in the π^\pm channels can be obtained with

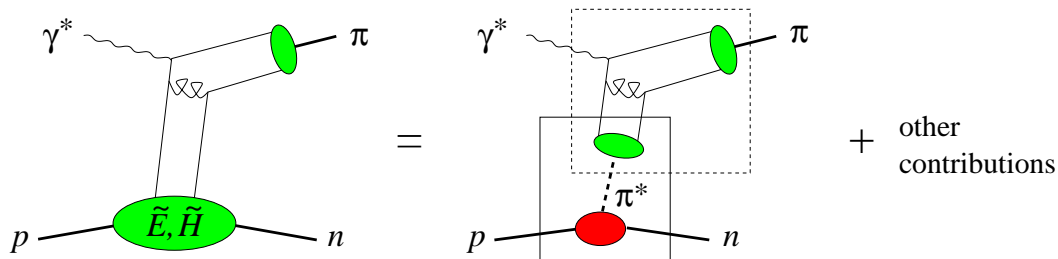


Figure 30: Pion exchange contribution to $\gamma^*p \rightarrow \pi^+ n$. The dashed box gives the pion form factor at leading twist when t is analytically continued to m_π^2 .

transverse target polarization [187], as we will discuss in Section 9.4. We remark in passing that the pion pole term in \tilde{E}^{u-d} also contributes to DVCS. In this case it has however to compete not only with contributions from \tilde{H} but above all from H , which is expected to be larger than \tilde{H} in analogy with the situation for the forward densities (where this follows from positivity). In addition, the squared quark charges favor the isosinglet over the isotriplet GPDs in DVCS, see (269).

In addition to the production of pions from spacelike photons, one may consider the production of a timelike photon with large virtuality Q'^2 from charged pion beams, with the γ^* decaying into an e^+e^- or $\mu^+\mu^-$ pair [209]. This process factorizes in analogy to its spacelike counterpart if the photon is longitudinally polarized, which can be studied using the angular distribution of the lepton pair. To leading order in $1/Q^{(l)}$ and in α_s the amplitudes of space- and timelike processes are closely related [209],

$$\begin{aligned}\mathcal{A}(\pi^- p \rightarrow \gamma^* n) &= \left[\mathcal{A}(\gamma^* p \rightarrow \pi^+ n) \right]^*, \\ \mathcal{A}(\pi^+ n \rightarrow \gamma^* p) &= \left[\mathcal{A}(\gamma^* n \rightarrow \pi^- p) \right]^*,\end{aligned}\tag{290}$$

where both sides are evaluated for equal proton and neutron helicities, for equal values of ξ and t , and with Q'^2 in the timelike processes equal to Q^2 in the spacelike ones. These relations will be modified by corrections in α_s , in a similar way as in Compton scattering, and also by higher twist effects. Comparison of the channels may thus provide indications for the size of such corrections, and more generally on the relation between analogous space- and timelike processes. The timelike channels receive a pion pole contribution, which reads like (288) with the pion form factor in the timelike region. This can directly be measured in $e^+e^- \rightarrow \pi^+\pi^-$ (although the available data [309] at high Q'^2 has large experimental errors). Good data for both processes would provide a rather unique chance to directly test pion pole dominance, which does not seem experimentally feasible in the spacelike case for large Q^2 .

Let us finally point out some specialties of strangeness production, studied in [189] and reviewed in detail in [37]. Due to flavor SU(3) breaking, the distribution amplitudes for neutral and charged kaons cannot be expected to be symmetric in $z \leftrightarrow \bar{z}$, in contrast to pions and ρ mesons. The relative contribution of C -even and C -odd GPDs then depends on the relative size of the integrals $\int dz (z\bar{z})^{-1} \Phi$ and $\int dz (z\bar{z})^{-1} (z - \bar{z}) \Phi$. As a consequence one finds kaon pole contributions not only for $\gamma^* p \rightarrow K^+ \Sigma^0$ and $\gamma^* p \rightarrow K^+ \Lambda$ but also for $\gamma^* p \rightarrow K^0 \Sigma^+$. This pole contribution in the relevant flavor transition GPDs \tilde{E} has a form similar to the pion pole contribution (210) in the nucleon sector. Due to the large mass splitting between π and K one expects a substantial violation of the flavor SU(3) relations for \tilde{E} , which as in (204) relate the strangeness transition GPDs with the flavor diagonal ones for the proton. We finally note that when using these relations for the H and E distributions, independent flavor information about s quarks in the nucleon may in principle be obtained in the production of $K^*(892)$ mesons, without the presence of gluon distributions.

5.3.1 Beyond leading order in α_s

An important question is how well the Born level expressions we have discussed so far approximate the physical scattering amplitudes. The only NLO study to date has been performed by Belitsky and Müller [310] for $\gamma^* p \rightarrow \pi^+ n$. The hard-scattering kernel can be taken over from the known results for the electromagnetic pion form factor by appropriate analytic continuation. In fact, for the pion pole contribution to \tilde{E} , which is believed to dominate the cross section at larger x_B , the NLO corrections are the same in both cases, as expressed in (288). Since the meson production amplitude is proportional to α_s already at leading order, the choice of renormalization scale μ_R is of particular importance for the result. One particular way of setting this scale is the BLM procedure [311], which

in the case at hand can be implemented by choosing μ_R such that the term multiplying $\beta_0 = 11 - \frac{2}{3}n_f$ in the NLO expressions vanishes. With the model they used for \tilde{H} , Belitsky and Müller found a small scale μ_{BLM}^2 below $0.1 Q^2$ in a wide range of x_B . The BLM scale is particularly small for the pion form factor and hence for the pion pole part of \tilde{E} . For the asymptotic pion DA one finds $\mu_{\text{BLM}}^2 \approx 0.01 Q^2$. At such low scales one can of course not evaluate the perturbative running coupling for practically relevant values of Q^2 , and the study [310] froze α_s/π to a value of 0.1 for $\mu_R \leq 1$ GeV. The result was a considerable size of the NLO corrections, and a huge spread of the NLO result when comparing the results for the BLM scale and the choice $\mu_R^2 = Q^2$. We do however not think that, as it stands, this implies the process to be beyond perturbative control at any Q^2 available in experiment. The intimate connection between the $\log(Q/\mu_R)$ dependence of the one-loop kernels and the running of $\alpha_s(\mu_R)$ in the tree level term is destroyed when modifying α_s for non-perturbative effects. Another point is that, as discussed in [310, 312], the NLO kernel contains large terms which do not go with β_0 , so that BLM scale setting cannot render the size of one-loop corrections small. We remark that in a study of the pion form factor, Melić et al. [313] have found that for $\mu_R^2 \approx 0.05 Q^2$ and the asymptotic pion DA, the NLO corrections are small and show little variation when μ_R^2 is changed.¹⁷ For moderate Q^2 this choice, which has also been discussed in [312], still leads to scales where α_s is large and one may doubt the applicability of perturbation theory. For $Q^2 \gtrsim 10$ GeV the total NLO result for $F_\pi(Q^2)$ in [313] was found to have important but not extremely large variation when μ_R^2 was chosen between Q^2 and $0.05 Q^2$. NLO corrections not only affect the overall size of the cross section but also its dependence on kinematical variables and spin. The study by Belitsky and Müller reports that the transverse target spin asymmetry in $\gamma^* p \rightarrow \pi^+ n$ (see Section 9.4) is rather stable under NLO corrections.

Notice that the Born level expressions (281) to (283) can be written as an integral over x involving the GPDs times an integral over z involving the DAs, or as a sum of two such terms if the DA is neither symmetric nor antisymmetric under $z \leftrightarrow \bar{z}$. This simple property is lost at the level of α_s^2 corrections, where there is a nontrivial interplay between x and z in the hard scattering kernels. In other words, the meson structure determines how the nucleon GPDs are probed, and the process amplitude can have different ξ and t dependence for one and the same set of GPDs but different choices of the meson DA. How important this cross talk is has however not been studied so far. Whether and how a trustworthy perturbative description of $F_\pi(Q^2)$ and meson electroproduction can be obtained for achievable Q^2 , and how well different observables can be theoretically controlled, remains to be further investigated.

5.4 Meson pair production and GDAs

GDAs appear in a variety of hard scattering processes. We will discuss in some detail their occurrence in two-photon annihilation and in hard electroproduction. They also appear in decay processes where a large scale is set by a heavy quark mass. Studies have been performed for the decays of J/Ψ or Υ into $\gamma \pi^+ \pi^-$ [314] and $\ell^+ \ell^- \pi^+ \pi^-$ [315], which at leading order in α_S are sensitive only to the gluon GDA Φ^g , and for exclusive semileptonic [316, 315] and hadronic [317] decays of B mesons.

5.4.1 Two-photon annihilation

The analog of Compton scattering in the crossed channel is two-photon annihilation

$$\gamma^*(q) + \gamma^*(q') \rightarrow h(p) + \bar{h}(p'), \quad (291)$$

¹⁷The choice $\mu_R^2 = e^{-5/3} Q^2/4 \approx 0.05 Q^2$ is referred to as BLM scale in [313], but the scale that renders the β_0 dependent term in the NLO amplitude zero for the asymptotic DA is $\mu_R^2 = e^{-14/3} Q^2 \approx 0.01 Q^2$.

where h can be either a baryon or a meson. In analogy to the Compton case one can show factorization of this process [283] in the limit

$$|q^2| + |q'^2| \rightarrow \infty \quad \text{at fixed } q'^2/q^2, W^2, \cos \theta, \quad (292)$$

where $W^2 = (p + p')^2$ is the squared invariant mass of the hadronic system and θ the polar angle of the hadron h in the c.m. If both photons are spacelike this process can be observed in e^+e^- collisions (Section 9.3), and we define $Q^2 = -q^2$ and $Q'^2 = -q'^2$. As in the Compton channel one may have both photons off shell or only one of them. The scaling behavior and helicity selection rules are analogous to those of Compton scattering. Amplitudes with both photons transverse or longitudinal are leading, and those with one transverse and one longitudinal photon are power suppressed by $1/Q^{(\prime)}$.

Studies in the literature have so far focused on the channels $\gamma^*\gamma \rightarrow \pi^+\pi^-$ and $\gamma^*\gamma \rightarrow \pi^0\pi^0$. To lowest order in $1/Q$ and α_s the hadronic tensor is given by

$$\begin{aligned} T^{\alpha\beta} &= i \int d^4x e^{i(q-q')x/2} \langle \pi(p)\pi(p') | T J_{\text{em}}^\alpha(-\frac{1}{2}x) J_{\text{em}}^\beta(\frac{1}{2}x) | 0 \rangle \\ &= -\frac{1}{2} g_T^{\alpha\beta} \sum_q e_q^2 \int_0^1 dz \frac{2z-1}{z(1-z)} \Phi^q(z, \zeta, W^2) \end{aligned} \quad (293)$$

in terms of the quark GDAs for the pion pair. For pairs of hadrons with spin like $p\bar{p}$ or $\rho\rho$ there are also terms with the tensor $\epsilon_T^{\alpha\beta}$. Both $g_T^{\alpha\beta}$ and $\epsilon_T^{\alpha\beta}$ filter out the photon helicity combinations $(\mu'\mu) = (++)$ and $(\mu'\mu) = (--)$ in the collision c.m., so that the hadrons are produced in a state with total $J^3 = 0$ along the photon axis. The hard scattering kernels at $O(\alpha_s)$ can be obtained from those of Compton scattering by crossing and are explicitly given in [86] for the $\pi\pi$ channel. Modeling the two-pion DAs along the lines described in Section 4.6.4 Kivel et al. [86, 271] found that the contribution from the gluon GDA at NLO depends rather strongly on the Gegenbauer coefficient B_{12}^g in the model, which is related to the momentum fraction taken by gluons in the pion. The process is thus rather sensitive to the relative strength of $q\bar{q}$ and gg coupling to a pion pair.

A different probe of the gluon coupling is given by the helicity amplitudes with $(\mu'\mu) = (+-)$ or $(-+)$, corresponding to pion pairs with $J^3 = \pm 2$, which to leading order in $1/Q$ receive only contributions going with the tensor gluon GDA Φ_7^g . The corresponding amplitudes at $O(\alpha_s)$ have been discussed in [86]. As pointed out by Braun and Kivel [318] this may also be used to investigate the gluon content of meson resonances, for instance in $\gamma^*\gamma \rightarrow f_2$. Notice that in hard processes one is sensitive to $q\bar{q}$ or gg configurations at small transverse separation, which is quite different from and complementary to the quark-antiquark or two-gluon picture in constituent models and meson spectroscopy.

The annihilation of $\gamma^*\gamma$ into a single light pseudoscalar meson factorizes in an analogous way for large Q^2 , with the hadronic tensor being proportional to

$$\sum_q e_q^2 \int_0^1 dz \frac{1}{z(1-z)} \Phi^q(z). \quad (294)$$

Measurements by CLEO [319] for π^0 , η , η' and by L3 [320] for η' indicate that the scaling behavior of the leading twist-mechanism sets in already at moderate Q^2 . The data for this process gives probably the cleanest available constraints on the $q\bar{q}$ distribution amplitudes of these mesons and is consistent with a shape close to the asymptotic one, $\Phi^q \propto z(1-z)$, at low factorization scale $\mu \sim 1$ GeV. For a recent analysis and references for π^0 we refer to [321], and for η and η' to [306, 94]. We will discuss limitations of the leading-twist description in Section 6.2.

Using the model two-pion DAs we discussed in Section 4.6.4 it was estimated in [85] that the cross section for $\gamma^*\gamma \rightarrow \pi^0\pi^0$ integrated over W from threshold to 1 GeV is only about 10% of the one for

$\gamma^*\gamma \rightarrow \pi^0$. In the leading-twist mechanism the pion pair is produced by an intermediate $q\bar{q}$ or gg state, so that it can only have total isospin $I = 0$ but not $I = 2$. As a consequence the production amplitudes for $\pi^0\pi^0$ and for $\pi^+\pi^-$ are equal (up to a convention dependent phase).

It is instructive to compare the exclusive annihilation of $\gamma^*\gamma$ with the inclusive annihilation into hadrons, both in the limit of large Q^2 at fixed W^2 . The inclusive channel is then described by the transverse and longitudinal photon structure functions F_T^γ and F_L^γ in the limit $x_B = Q^2/(W^2 + Q^2) \rightarrow 1$. It can be calculated at partonic level as $\gamma^*\gamma \rightarrow q\bar{q}$ to leading order in α_s , provided that one explicitly regulates the region where either the quark or antiquark carry the entire momentum of the hadronic system in the Breit frame. In the leading-twist description of the exclusive channels this corresponds to the endpoint regions $z \rightarrow 0, 1$ and is regulated by the behavior of the distribution amplitudes, i.e. by the hadronization process. Taking the limit of large Q^2 at fixed W^2 one finds a scaling behavior [85]

$$F_T^\gamma \sim c(W^2), \quad F_L^\gamma \sim W^2/Q^2 \quad (295)$$

with some function c . This coincides indeed with the Q^2 dependence predicted for the exclusive channels discussed above. The study [85] also compared the total cross section for $\gamma^*\gamma$ calculated (i) as open $q\bar{q}$ production with a quark mass around 300 MeV as regulator (or equivalently a transverse momentum cutoff of the same size) and (ii) as the sum of leading-twist cross sections for the exclusive channels. Amusingly, the inclusive $q\bar{q}$ cross section integrated up to $W = 1$ GeV is comparable in size with the sum of the exclusive channels π^0, η, η' and the (small) estimated $\pi\pi$ continuum.

5.4.2 Electroproduction

The concept of GDAs allows one to extend meson production studies to a wider class of processes. Of particular practical importance is the case of pion pairs. When the invariant mass $m_{\pi\pi}$ of the pair is in the vicinity of the $\rho(770)$ or $f_2(1270)$ resonances, an analysis in terms of GDAs can be complementary to a more conventional one in terms of single-meson states and provide additional physics insights.

Clerbaux and Polyakov have used $\pi^+\pi^-$ electroproduction data from H1 and ZEUS to analyze the spectrum in the two-pion invariant mass $m_{\pi\pi}$. As we saw in Section 3.7.2, the $m_{\pi\pi}$ dependence of $\Phi^{q(-)}$ is given by the timelike pion form factor $F_\pi(m_{\pi\pi}^2)$ if the z dependence has its asymptotic shape $z(1-z)$. This predicts the invariant mass distribution in electroproduction at asymptotically large Q^2 to be

$$\frac{1}{N} \frac{dN}{dm_{\pi\pi}^2} \xrightarrow{\log Q^2 \rightarrow \infty} \beta^3 |F_\pi(m_{\pi\pi}^2)|^2, \quad (296)$$

where $\beta = (1 - 4m_\pi^2/m_{\pi\pi}^2)^{1/2}$. Note that $|F_\pi(m_{\pi\pi}^2)|$ around the ρ mass is well measured from e^+e^- annihilation data. The form (296) shows very clearly that leading-twist dominance does *not* predict the nonresonant “background” under the ρ peak to vanish at large photon virtuality, since F_π contains a contribution from the continuum in addition to the resonance. Clerbaux and Polyakov find that a fit to (296) of the measured $m_{\pi\pi}$ spectrum between about 550 and 1100 MeV becomes increasingly good with larger Q^2 (with the highest bin being around 20 GeV²). This is consistent with $\Phi^{q(-)}$ in this mass range being close to its asymptotic $z(1-z)$ shape, although it might also be that the coefficients of higher terms in the Gegenbauer expansion (83) have an $m_{\pi\pi}$ dependence similar to that of $F_\pi(m_{\pi\pi}^2)$. In [322] an attempt was made to extract some of the parameters describing the deviation from the asymptotic form of the GDA, but the statistical errors in the data were too large to permit strong conclusions.

This study was performed for the mass spectrum integrated over the angular distribution of the pion pair. It is known that at moderate values of Q^2 the contribution from $J^3 = \pm 1$ states (such as a transverse ρ) is not negligible, whereas the leading-twist description only holds for the amplitudes

with $J^3 = 0$. The authors of [322] point out that the $J^3 = \pm 1$ contributions can be suppressed by taking appropriate moments in the polar angle θ of the π^+ in the two-pion c.m.

The production of pion pairs in the C -even projection has been studied by Lehmann-Dronke et al. [269, 272], for an earlier discussion see [323]. The invariant mass regions with the clearest signal for this channel, compared with the overwhelming dominance of the ρ resonance, were estimated to be close to the $\pi\pi$ threshold and around the f_2 resonance. In addition it is advantageous to go to larger values of x_B , since the C -even two-pion state involves the GPD combinations $F^{q(-)}$, which at small x_B are well below $F^{q(+)}$ and F^g occurring in the C -odd $\pi\pi$ channel. One can however make use of the strong C -odd contribution by measuring its interference with the C -even channel, which can be filtered out from the θ distribution, see Section 9.4.2.

The electroproduction of C -even states involves both their quark and gluon GDAs. It was reported in [272] that for the model of the GDAs described in Section 4.6.4 the total amplitude is only weakly sensitive to the relative size of Φ^{u+d} and Φ^g . It would require further study to assess whether this process alone or together with two-photon annihilation could be used to estimate the relative quark and gluon coupling to pion pairs or in particular to the f resonances.

6 Beyond leading power

In order to extract twist-two GPDs and GDAs from data one must have sufficient control over power corrections to the leading-twist description reviewed in Section 5.1. Moreover, in certain situations it may be possible to treat power suppressed effects as a signal which by itself carries information about hadron structure and dynamics at the quark-gluon level.

In the leading-twist approximation the amplitude is factorized into a hard and one or several collinear subgraphs. The subgraphs are connected by the minimal necessary number of partons, which is two in the cases we deal with. The hard scattering is evaluated in the collinear approximation, and the masses of hadrons and quarks are neglected. The study of power corrections thus involves hadronic matrix elements with more than two external partons, corrections to evaluating the hard scattering for collinear on-shell partons, and target mass corrections. Further contributions can arise from soft subgraphs as in Fig. 28. As discussed in Section 5.1 they are intimately related with configurations where partons entering the hard scattering become soft.

A systematic approach to power corrections in Compton scattering and two-photon annihilation is the operator product expansion (OPE) of the product of two electromagnetic currents. Here information about hadron structure is encoded in matrix elements of higher-twist operators. These operators are not all independent since they satisfy the QCD equations of motion when physical matrix elements are taken. In order not to over-parameterize nonperturbative physics one needs to choose an appropriate operator basis. Different choices are possible, as discussed in the analysis of deep inelastic scattering by Ellis, Furmanski and Petronzio [324]. Since the equations of motion involve operators with different parton content, effects due to parton transverse momentum or off-shellness and effects due to extra partons are related. One hence needs to specify a particular framework in order to state which is the “dynamical origin” of a particular contribution. Note also that gauge invariance relates different terms. The operators $\bar{q}\gamma^+(i\overleftrightarrow{\partial}_T)q$ and $\bar{q}\gamma^+(gA_T)q$ for instance, respectively describing quark transverse momentum and an additional gluon, mix under gauge transformations, and only their sum is gauge invariant.

Complications arise for real photons. A real photon can split into a quark and antiquark that are both of low virtuality and almost collinear to each other. Such configurations are prone to long-range interactions, so that the pointlike quark-photon vertex is insufficient to represent them. In analogy to quark-antiquark configurations in a meson they can be described by distribution amplitudes for

the photon, which have been discussed in detail by Ball et al. [325]. Furthermore, a real photon can split into one fast near-shell quark and a soft one. Such end-point configurations are associated with soft subgraphs and hence with dynamics that cannot obviously be described by the hadronic matrix elements of the OPE. At the level of some subleading power one may thus expect the OPE description to break down when one photon is on shell. A signal of this would be the occurrence of divergences in the convolution of the appropriate hard scattering kernels with the appropriate parton distributions or distribution amplitudes.

In this case, as well as for processes like exclusive meson production, one cannot use the OPE and there is to date no systematic way of describing the dynamics beyond leading-power accuracy. A suitable framework to achieve this may be an effective field theory formulation. First steps in this direction (with main focus on B meson decays) have been made but this field is still in an early stage of development, see e.g. [326], [327, 328] and [329, 330, 331]. Existing methods attempt to estimate or model power suppressed effects, typically focusing on particular sources of power corrections and making assumptions going beyond first principles of QCD. A detailed account of these methods is well beyond the scope of this review. We rather aim to give an overview of what has been done for the processes where GPDs or GDAs occur, and point out related work on processes that are very similar.

We note that there are processes that cannot be described within the OPE but where nevertheless power corrections up to a certain accuracy can be expressed in terms of hard scattering coefficients and hadronic matrix elements of higher-twist operators. An example are the $1/Q^2$ power corrections in the unpolarized Drell-Yan pair cross section [332, 333]. What has to be shown is that the reduced diagrams contributing to that accuracy still have the form of a hard subgraph connected to several collinear ones, without soft interactions between the collinear graphs that would imply non-perturbative cross talk between the two incoming hadrons.

6.1 Compton scattering at $1/Q$ accuracy

The $1/Q$ suppressed power corrections to virtual Compton scattering have been studied at leading order in α_s by a number of groups. To this level of accuracy the structure of the process is well understood and can be written again as the convolution of hard scattering kernels with hadronic matrix elements. The theoretical analysis closely resembles that of the $1/Q$ suppressed terms in deep inelastic scattering on a polarized target, but there are important particularities due to the nonforward kinematics in our case. Just recently, part of the α_s corrections to the $1/Q$ suppressed DVCS amplitudes was obtained by Kivel and Mankiewicz [334].

6.1.1 Operator product expansion and twist

A framework to treat factorization in Compton scattering is given by the OPE. If at least one of the photons is far off-shell, the time ordered product of currents in the hadronic tensor (270) is dominated by distances z^2 close to the light-cone and one can expand

$$\begin{aligned}
& iT J_{\text{em}}^\alpha(-\tfrac{1}{2}z) J_{\text{em}}^\beta(\tfrac{1}{2}z) \\
&= \bar{q}(-\tfrac{1}{2}z) \frac{\gamma^\alpha \not{z} \gamma^\beta}{2\pi^2 z^4} W[-\tfrac{1}{2}z, \tfrac{1}{2}z] q(\tfrac{1}{2}z) + \{z \rightarrow -z, \alpha \leftrightarrow \beta\} + O(z^{-2}) \\
&= \frac{z_\rho}{2\pi^2 z^4} \left(s^{\alpha\rho\beta\sigma} \left\{ \bar{q}(-\tfrac{1}{2}z) \gamma_\sigma W[-\tfrac{1}{2}z, \tfrac{1}{2}z] q(\tfrac{1}{2}z) - \{z \rightarrow -z\} \right\} \right. \\
&\quad \left. - i\epsilon^{\alpha\rho\beta\sigma} \left\{ \bar{q}(-\tfrac{1}{2}z) \gamma_\sigma \gamma_5 W[-\tfrac{1}{2}z, \tfrac{1}{2}z] q(\tfrac{1}{2}z) + \{z \rightarrow -z\} \right\} \right) + O(z^{-2})
\end{aligned} \tag{297}$$

up to higher-order corrections in α_s . Here $s^{\alpha\rho\beta\sigma} = g^{\alpha\rho}g^{\beta\sigma} + g^{\alpha\sigma}g^{\beta\rho} - g^{\alpha\beta}g^{\rho\sigma}$, and $W[a, b]$ denotes a Wilson line along the straight-line path from a^μ to b^μ , generalizing our notation of Section 3.2. The expression (297) directly corresponds to the handbag diagrams for Compton scattering in Fig. 27, supplemented by the gluons summed in the Wilson lines.

In the *local* OPE one expands the product of currents in terms of local operators. This can be obtained from (297) using

$$\bar{q}(-\tfrac{1}{2}z)\gamma^\sigma W[-\tfrac{1}{2}z, \tfrac{1}{2}z]q(\tfrac{1}{2}z) = \sum_{n=0}^{\infty} \frac{1}{n!} z_{\alpha_1} \dots z_{\alpha_n} \left[\bar{q}\gamma^\sigma \overleftrightarrow{D}^{\alpha_1} \dots \overleftrightarrow{D}^{\alpha_n} q \right] \quad (298)$$

and its analog for the axial vector operator, where all fields on the right-hand side are evaluated at $z = 0$. An early treatment of the nonforward virtual Compton amplitude in this framework has been given by Watanabe [5, 6], and more recent ones by Chen [335] and by Ji and Osborne [278]. These works are confined to leading power accuracy, whereas a study by White [336] includes $1/Q$ power corrections. In close analogy to the classical analysis of inclusive DIS, the local OPE provides an expansion of the Compton tensor $T^{\alpha\beta}$ in powers of $1/\rho$, i.e. for $|\rho| \rightarrow \infty$ in the unphysical region. The coefficients of this expansion can be identified with the Mellin moments of the discontinuity of $T^{\alpha\beta}$ in ρ , and the full amplitude is recovered by a dispersion relation in this variable [336]. At leading $1/Q$ accuracy the $1/\rho$ expansion involves the Mellin moments of the twist-two GPDs we discussed in Section 3.3.3; the corresponding Wilson coefficients at $O(\alpha_s)$ can be found in [278]. We must remark that the considerations of [336] cannot be taken as a proof for factorization as claimed in that work, since the arguments crucially depend on properties of the Wilson coefficients which are not proven (but do hold in the explicit Born level and one-loop calculations).

An alternative approach, developed independently by Anikin and Zavyalov [337] and by Balitsky and Braun [108], is to expand directly in terms of “string” operators as in (297), where fields occur at positions along a straight line from $-\kappa z$ to κz . For $z^2 = 0$ these operators are also called “light-ray operators”. The local OPE expansion is organized in terms of operators with definite “twist”, which is defined as the spin of an operator minus its canonical mass dimension. The twist-two projections of the operators on the right-hand side of (298) are obtained by symmetrization in $\sigma, \alpha_1, \dots, \alpha_n$ and by subtractions making the operators traceless in any two indices; higher-twist operators are antisymmetric in some of their indices. A string operator of definite twist is defined by resumming the corresponding twist projections of the local operators in (298). The construction of the string operators with definite twist relevant for the Compton amplitude has been performed in a series of works by Geyer et al. [338, 339, 340]. One finds in particular that for light-like distance z the decomposition of these operators involves only a finite number of twists.

The notion of twist defined in this way is also called “geometrical twist”. It differs from the “dynamical twist”, which refers to matrix elements of light-ray operators and specifies at which power in $1/Q$ they first appear in hard processes. Dynamical twist is closely related to the decomposition of operators in terms of “good” and “bad” field components in light-cone quantization (see Section 3.4); for a discussion see [52]. For twist two the geometrical and dynamical twist definitions coincide, but not for higher twist. We will continue to call the GPDs and GDAs introduced in Section 3 “twist-two” or “leading-twist” quantities, even when they appear in power suppressed amplitudes. When referring to the “twist” of a scattering amplitude, we will imply the notion of dynamical twist.

An important finding is that the projection of operators on geometrical twist two gives a Compton amplitude which in nonforward kinematics respects electromagnetic gauge invariance at leading power in $1/Q$ but not beyond, as can be seen by explicit calculation [288]. Radyushkin and Weiss [341] have emphasized that the twist-two projection of the operator expanded product $TJ_{\text{em}}^\alpha(z_1)J_{\text{em}}^\beta(z_2)$ does not satisfy electromagnetic current conservation. The terms which break current conservation are

“total derivatives” of operators, i.e. derivatives with respect to an overall translation such as

$$\frac{\partial}{\partial X_\mu} \left[\bar{q}(X - \frac{1}{2}z) \gamma^\sigma W[X - \frac{1}{2}z, X + \frac{1}{2}z] q(X + \frac{1}{2}z) \right]_{X=0}. \quad (299)$$

In matrix elements these derivatives turn into factors of $i\Delta^\mu$, so that their forward matrix elements are zero but not their nonforward ones. A consistent evaluation of nonforward Compton scattering at $1/Q$ accuracy requires the inclusion of operators with geometrical twist three. As already mentioned, the QCD equations of motion are needed at this level in order to obtain a basis of independent operators. Belitsky and Müller [342] have given an explicit representation for the geometrical twist-three parts of the string operators in (297) at $z^2 = 0$. It involves total derivatives of their geometrical twist-two projections, and quark-antiquark-gluon operators $\bar{q}\gamma^+G^{+\rho}q$ and $\bar{q}\gamma^+\gamma_5\tilde{G}^{+\rho}q$ with all fields along the light-cone (for simplicity we have omitted Wilson line factors). A representation away from the light-cone has recently been given by Kiptily and Polyakov [343].

The contribution to the nonforward Compton amplitude from the geometrical twist-two operators and their total derivatives is separately gauge invariant. This provides a minimal set of operators to restore current conservation of the handbag amplitude to order $1/Q$ [344, 345, 341]. The resulting $1/Q$ terms are often called “kinematical” twist-three corrections. Radyushkin and Weiss have pointed out that to $1/Q$ accuracy in the Compton amplitude the effect of the operators with total derivatives can be represented as a “spin rotation” of the twist-two string operators, which acts on the Dirac indices of the quark and antiquark fields [346]. The contributions from the quark-antiquark-gluon operators are commonly referred to as “dynamical” or “genuine” twist-three terms.

As a result of the operator decomposition just mentioned the hadronic matrix elements

$$\begin{aligned} F^\mu &= P^+ \int \frac{dz^-}{2\pi} e^{ixP^+z^-} \langle p' | \bar{q}(-\frac{1}{2}z) \gamma^\mu q(\frac{1}{2}z) | p \rangle \Big|_{z^+=0, \mathbf{z}=0}, \\ \tilde{F}^\mu &= P^+ \int \frac{dz^-}{2\pi} e^{ixP^+z^-} \langle p' | \bar{q}(-\frac{1}{2}z) \gamma^\mu \gamma_5 q(\frac{1}{2}z) | p \rangle \Big|_{z^+=0, \mathbf{z}=0}, \end{aligned} \quad (300)$$

can be represented in terms of functions parameterizing the quark-antiquark-gluon contributions, and of a “Wandzura-Wilczek part” involving the twist-two GPDs or double distributions discussed so far in this review. This representation is limited to $1/Q$ accuracy in the Compton amplitude, which will be implied in the remainder of this section. Only the plus and transverse components of (300) are relevant then, since the minus components only appear at order $1/Q^2$. Most studies in the literature have used the “Wandzura-Wilczek approximation”, where the quark-antiquark-gluon matrix elements are neglected. For the forward Compton amplitude this leads to the well-known relation between the polarized structure functions g_1 and g_2 of DIS [347], which agrees rather well with recent measurements and a number of theoretical calculations [348]. Little has been done so far to explore whether one may expect this approximation to be valid in nonforward kinematics. A recent study in the chiral quark-soliton model [343] has estimated that the first nonvanishing moments of the quark-antiquark-gluon distributions, which are matrix elements of the local operators $\bar{q}\gamma^+G^{+\rho}q$ and $\bar{q}\gamma^+\gamma_5\tilde{G}^{+\rho}q$, are parametrically suppressed at low normalization scale and small t (as are the twist-two gluon distributions in the same model, see Section 4.1.3).

The Wandzura-Wilczek part of the above matrix elements on the proton reads [349]

$$\begin{aligned} F_W^\mu &= \left(P^\mu - \frac{\Delta_T^\mu}{2\xi} \right) \frac{1}{P^+} \left[H(x, \xi) \bar{u}\gamma^+u + E(x, \xi) \bar{u} \frac{i\sigma^{+\alpha}\Delta_\alpha}{2m} u \right] \\ &\quad + \frac{1}{2} \int_{-1}^1 dy \left[W(x, y, \xi) + W(-x, -y, \xi) \right] G^\mu(y, \xi) \end{aligned}$$

$$\begin{aligned}
& + \frac{1}{2} \int_{-1}^1 dy \left[W(x, y, \xi) - W(-x, -y, \xi) \right] i\epsilon_T^{\mu\nu} \tilde{G}_\nu(y, \xi), \\
\tilde{F}_W^\mu & = \left(P^\mu - \frac{\Delta_T^\mu}{2\xi} \right) \frac{1}{P^+} \left[\tilde{H}(x, \xi) \bar{u}\gamma^+\gamma_5 u + \tilde{E}(x, \xi) \bar{u} \frac{\gamma_5 \Delta^+}{2m} u \right] \\
& + \frac{1}{2} \int_{-1}^1 dy \left[W(x, y, \xi) + W(-x, -y, \xi) \right] \tilde{G}^\mu(y, \xi) \\
& + \frac{1}{2} \int_{-1}^1 dy \left[W(x, y, \xi) - W(-x, -y, \xi) \right] i\epsilon_T^{\mu\nu} G_\nu(y, \xi), \tag{301}
\end{aligned}$$

where

$$W(x, y, \xi) = \frac{1}{\xi - y} \left[\theta(\xi > x > y) - \theta(\xi < x < y) \right] \tag{302}$$

is the Wandzura-Wilczek kernel, and

$$\begin{aligned}
G^\mu(x, \xi) & = \bar{u}\gamma_T^\mu u \left[H(x, \xi) + E(x, \xi) \right] - \frac{\Delta_T^\mu}{2\xi} \left[\frac{\bar{u}\gamma^+ u}{P^+} \left(x \frac{\partial}{\partial x} + \xi \frac{\partial}{\partial \xi} \right) \left[H(x, \xi) + E(x, \xi) \right] \right. \\
& \quad \left. - \frac{\bar{u}u}{m} \left(x \frac{\partial}{\partial x} + \xi \frac{\partial}{\partial \xi} \right) E(x, \xi) \right], \\
\tilde{G}^\mu(x, \xi) & = \bar{u}\gamma_T^\mu \gamma_5 u \tilde{H}(x, \xi) - \frac{\Delta_T^\mu}{2\xi} \left[\frac{\bar{u}\gamma^+ \gamma_5 u}{P^+} \left(x \frac{\partial}{\partial x} + \xi \frac{\partial}{\partial \xi} \right) \tilde{H}(x, \xi) \right. \\
& \quad \left. - \frac{\bar{u}\gamma_5 u}{m} \left(x \frac{\partial}{\partial x} + \xi \frac{\partial}{\partial \xi} \right) \xi \tilde{E}(x, \xi) \right]. \tag{303}
\end{aligned}$$

For legibility we have not displayed the t dependence of GPDs, and omitted spinor arguments and quark flavor labels. The plus-components of (301) reduce to $2P^+$ times the matrix elements F^q and \tilde{F}^q defining twist-two GPDs, as it must be. As noted in [349] the D -term contribution to H and E , as well as the pion pole part of \tilde{E} cancel in G^μ and \tilde{G}^μ . These terms hence appear in F^μ and \tilde{F}^μ in the same form as in twist-two matrix elements, in particular without being convoluted with the Wandzura-Wilczek kernels. For a spin-zero target there are expressions similar to the above [344, 341, 350]. They are simpler since there are no twist-two distributions for the axial vector operator due to parity invariance. Expressions of the matrix elements F^μ and \tilde{F}^μ for targets with spin zero or $\frac{1}{2}$ including the quark-antiquark-gluon contributions are given in [342], and a general form factor decomposition of F^μ and \tilde{F}^μ for spin $\frac{1}{2}$ targets can be found in [343]. Notice that the evolution of the Wandzura-Wilczek parts of F^μ and \tilde{F}^μ directly follows from the known evolution at twist two-level. The evolution of the genuine twist-three operators is discussed in [342].

The structure of (301) to (303) is similar to the Wandzura-Wilczek relations for meson distribution amplitudes [151, 152] or GDAs [350], which originate from the same decompositions of string operators. We recall that these relations involve the inclusion of operators with geometrical twist three, the use of the QCD equations of motion, and the neglect of quark-antiquark-gluon matrix elements. They are hence different in form and content from the Wandzura-Wilczek relations between matrix elements of geometrical twist-two operators in [100, 288, 191]. A discussion of these differences in the case of distribution amplitudes is given in [351].

Let us finally mention sum rules for the matrix elements F^μ and \tilde{F}^μ , which were discussed in [352, 349, 37, 343] and in particular give the Burkhardt-Cottingham [353] and Efremov-Leader-Teryaev [354] sum rules in the forward limit. The first and second moments $\int_{-1}^1 dx F^\mu$ and $\int_{-1}^1 dx x F^\mu$ as well as their analogs for \tilde{F}^μ receive no contributions from the quark-antiquark-gluon operators and are

hence readily obtained from the Wandzura-Wilczek relations (301). The first moments simply lead to the form factors F_1 , F_2 and g_A , g_P for each quark flavor, whereas the second moments involve these form factors and the second moments of the GPDs H , E and \tilde{H} , \tilde{E} .

6.1.2 The DVCS amplitude at $1/Q$ accuracy

The DVCS amplitude at $1/Q$ accuracy has been studied to leading order in α_s by several groups with different methods. The investigation of Anikin et al. [355] is for spinless targets and closely follows the techniques of Ellis, Furmanski and Petronzio, using in particular the “transverse” basis of operators introduced in [324]. Belitsky and Müller give a complete treatment for targets of spin 0 or $\frac{1}{2}$ in [342]. Other studies have used the Wandzura-Wilczek approximation. Penttinen et al. [352] consider a nucleon target and proceed in a manner motivated by parton model ideas. The work of Kivel et al. for targets of spin 0 [344] and spin $\frac{1}{2}$ [349], and the work of Radyushkin and Weiss [345, 341, 346] for spin-zero targets closely follows the string operator formalism of Balitsky and Braun [108]. Studies concerning the phenomenology of DVCS at twist-three level are reviewed in Section 9.1.

At $1/Q$ accuracy the calculation of DVCS involves the handbag diagrams of Fig. 27, to be evaluated beyond the collinear approximation by performing the Taylor expansion in (265) one order further, and in addition diagrams with an extra (transversely polarized) gluon connecting the quark line of the hard scattering with the collinear subgraph of the proton. Applying the equations of motion for the quark field operator one finds [355, 342] that the complete amplitude can be expressed in terms of the matrix elements F^μ and \tilde{F}^μ defined in (300). It can hence be parameterized by twist-two quark-antiquark GPDs and quark-antiquark-gluon GPDs of twist three. These steps ensure that the result respects electromagnetic current conservation and involves only QCD operators that are gauge invariant. The hadronic tensor for DVCS then reads [349]

$$\begin{aligned}
T^{\alpha\beta} = & \sum_q e_q^2 \int_{-1}^1 dx \left(-g_T^{\alpha\gamma} \frac{F^{q+}}{2P^+} C - i\epsilon_T^{\alpha\gamma} \frac{\tilde{F}^{q+}}{2P^+} \tilde{C} \right. \\
& \left. + \frac{(q+4\xi P)^\alpha}{2qP} \left\{ g_T^{\gamma\delta} F_\delta^q C - i\epsilon_T^{\gamma\delta} \tilde{F}_\delta^q \tilde{C} \right\} \right) \left(g_\gamma^\beta + \frac{\Delta_T \gamma P^\beta}{qP} \right)
\end{aligned} \tag{304}$$

up to $1/Q^2$ suppressed corrections, with the familiar hard-scattering kernels

$$\begin{aligned}
C(x, \xi) &= \frac{1}{\xi - x - i\epsilon} - \frac{1}{\xi + x - i\epsilon}, \\
\tilde{C}(x, \xi) &= \frac{1}{\xi - x - i\epsilon} + \frac{1}{\xi + x - i\epsilon}.
\end{aligned} \tag{305}$$

The tensor is given for a coordinate system where the transverse directions are defined with respect to the initial photon momentum q and to the average hadron momentum P , and where p and p' have large components along the positive z axis. For a spinless target one has in particular $\tilde{F}^{q+} = 0$ from parity invariance, and the parameterization of the amplitude requires one GPD for the transverse components of each matrix element $F^{q\mu}$ and $\tilde{F}^{q\mu}$ in addition to the GPDs H^q parameterizing F^{q+} [355]. The Compton amplitude for two off-shell photons is given in [342]. It involves the same hadronic matrix elements, with hard-scattering kernels $C(x, \rho)$ and $\tilde{C}(x, \rho)$ and appropriately modified tensor structures.

Let us discuss the electromagnetic gauge invariance of the Compton amplitude, which requires $q_\alpha T^{\alpha\beta} = T^{\alpha\beta} q'_\beta = 0$. The Compton tensor (273) in leading-twist approximation is gauge invariant except for terms of order Δ_T/Q and is hence consistent to the accuracy at which it is calculated.

Vanderhaeghen et al. [303, 253] have proposed to use an exactly gauge invariant amplitude by the replacement

$$T^{\alpha\beta} \rightarrow T^{\alpha\gamma} \left(g_{\gamma}^{\beta} - \frac{q'_{\gamma} v^{\beta}}{q'v} \right), \quad (306)$$

where v is an appropriately chosen auxiliary vector with $q'v$ of order Q^2 . If the Compton tensor calculated up to corrections of order $1/Q^{n+1}$ satisfies $T^{\alpha\beta} q'_{\beta} = O(1/Q^n)$ then this replacement is allowed within the accuracy of the calculation. An analogous prescription can of course be used for the initial photon, but with the coordinate system chosen here the tensor already satisfies $q_{\alpha} T^{\alpha\beta} = 0$. We remark that the prescription (306) is equivalent to using the axial gauge $vA_{\text{em}} = 0$ for the electromagnetic field, where the polarization vectors of the final state photon in Feynman gauge are to be replaced according to

$$\epsilon_{\beta} \rightarrow \epsilon_{\beta} - \frac{\epsilon v}{q'v} q'_{\beta}. \quad (307)$$

Taking $v = P$ and using that $q'P = qP$ and $q'_T = -\Delta_T$ one finds that the terms going with F^{q+} and \tilde{F}^{q+} in the Compton tensor (304) are precisely those anticipated by the prescription (306). Note that the terms in (304) where F_{δ}^q or \tilde{F}_{δ}^q is multiplied with $\Delta_{T\gamma}$ contribute to the amplitude only at order $1/Q^2$. They have been added by hand following the above rationale in order to obtain an exactly gauge invariant tensor.

No general analysis comparable to the leading-twist factorization theorem guarantees that at $1/Q$ accuracy the Compton amplitude *can* actually be represented in terms of hadronic matrix elements and hard-scattering kernels. According to our discussion at the beginning of this section this is particularly problematic when one photon is on shell. A consistency check of the factorized result (304) is the absence of collinear or soft singularities which would signal a breakdown of the factorization scheme at this order. As has been discussed in [344] and [345, 341] for the pion and in [349] for the nucleon, the convolution of the Wandzura Wilczek kernels with smooth GPDs leads to functions with a discontinuity. Namely, the convolution

$$\begin{aligned} f_W(x, \xi) &= \int_{-1}^1 dy W(x, y, \xi) f(y, \xi) \\ &= \theta(x > \xi) \int_x^1 dy \frac{f(y, \xi)}{y - \xi} - \theta(x < \xi) \int_{-1}^x dy \frac{f(y, \xi)}{y - \xi}, \end{aligned} \quad (308)$$

where $f(y, \xi)$ stands for a generic GPD, has a discontinuity

$$f_W(\xi + \delta, \xi) - f_W(\xi - \delta, \xi) \xrightarrow{\delta \rightarrow 0} \int_{-1}^1 dy \frac{f(y, \xi)}{y - \xi} \quad (309)$$

at $x = \xi$, which involves the same integral as the real part of the twist-two amplitude and has little chance to be zero. The convolution with $W(-x, -y, \xi)$ is discontinuous at $x = -\xi$ in turn. The Compton tensor (304) involves however only the combinations $(\xi + x - i\epsilon)^{-1} W(x, y, \xi)$ and $(\xi - x - i\epsilon)^{-1} W(-x, -y, \xi)$ where these discontinuities are harmless. In the calculation of $T^{\alpha\beta}$ one also finds a contribution

$$\sum_q e_q^2 \int_{-1}^1 dx \left\{ g_T^{\alpha\delta} F_{\delta}^q C + i\epsilon_T^{\alpha\delta} \tilde{F}_{\delta}^q \tilde{C} \right\} \frac{(q + 2\xi P)^{\beta}}{2qP} \quad (310)$$

which involves $(\xi - x - i\epsilon)^{-1} W(x, y, \xi)$ and $(\xi + x - i\epsilon)^{-1} W(-x, -y, \xi)$ and thus has logarithmic singularities. As emphasized in [344, 345, 341, 349] this tensor gives however a $1/Q^2$ suppressed term when contracted with any *physical* polarization vector of the final photon. This is beyond the accuracy

of the calculation and therefore has been omitted in (304). Indeed, one has $(q + 2\xi P)^\beta \approx (q' + \Delta_T)^\beta$ up to yet higher terms in $1/Q$, and physical polarization vectors are of course orthogonal to q'^β . Anikin and Teryaev [350] have pointed out the analog of this situation in the crossed channel, where the twist-three GDAs for pion pairs have finite values at the end points $z = 0$ or $z = 1$. This leads to logarithmic singularities in the unphysical sector when convoluted with z^{-1} or $(1 - z)^{-1}$ from the hard-scattering kernels, but no singularities appear in the physical part of the hadronic tensor. Note that the discontinuities of the matrix elements F^μ and \tilde{F}^μ at $x = \pm\xi$ do not lead to problems in the doubly virtual Compton amplitude, where the hard-scattering kernels have their poles at $x = \pm\rho$, as remarked in [344].

Radyushkin and Weiss have explicitly shown that to order $1/Q^2$ accuracy the total derivative operators discussed in the previous subsection provide terms which result in replacing $(q + 2\xi P)^\beta$ by q'^β in the contribution (310), so that its factorization breaking singularities do not appear in the physical sector of the Compton tensor [341]. A result free of singularities was also obtained in a recent evaluation of α_s corrections to DVCS at order $1/Q$, which was restricted to the Wandzura Wilczek approximation and to the contribution involving quark GPDs [334]. In general it remains however unknown whether factorization still holds for DVCS at $1/Q^2$ or at α_s/Q accuracy.

Calculating amplitudes for definite photon helicity in the γ^*p c.m. from the Compton tensor (304), one finds that the $1/Q$ corrections do not affect the transverse photon amplitudes (277) calculated at leading-twist accuracy. Instead they give nonzero transitions for a longitudinal photon, which are absent at leading power. The new amplitudes can be expressed in terms of (i) the Compton form factors \mathcal{H} , \mathcal{E} , $\tilde{\mathcal{H}}$, $\tilde{\mathcal{E}}$ already appearing at leading twist, (ii) form factors given by

$$\begin{aligned} \mathcal{H}_W &= \sum_q e_q^2 \int_{-1}^1 dx \frac{1}{\xi - x - i\epsilon} \int_{-1}^1 dy W(-x, -y, \xi) H^{q(+)}(y, \xi, t) \\ &= \sum_q e_q^2 \int_{-1}^1 dx \frac{1}{\xi + x} \ln \frac{2\xi}{\xi - x - i\epsilon} H^{q(+)}(x, \xi, t) \end{aligned} \quad (311)$$

and its analogs with $E^{q(+)}$, $\tilde{H}^{q(+)}$, $\tilde{E}^{q(+)}$, and (iii) four independent form factors involving quark-antiquark-gluon distributions [244]. The derivatives in (303) can be written according to

$$\sum_q e_q^2 \int_{-1}^1 dx \frac{1}{\xi + x} \ln \frac{2\xi}{\xi - x - i\epsilon} \left(x \frac{\partial}{\partial x} + \xi \frac{\partial}{\partial \xi} \right) H^{q(+)}(x, \xi, t) = \xi \frac{\partial}{\partial \xi} \mathcal{H}_W. \quad (312)$$

The form factors \mathcal{H} , \mathcal{E} , $\tilde{\mathcal{H}}$, $\tilde{\mathcal{E}}$ can in principle be extracted from the four independent leading-twist amplitudes $M_{\lambda'+, \lambda+}$. The four independent twist-three amplitudes $M_{\lambda'+, \lambda 0}$ then depend on another eight unknowns, namely on \mathcal{H}_W , \mathcal{E}_W , $\tilde{\mathcal{H}}_W$, $\tilde{\mathcal{E}}_W$ and on the genuine twist-three form factors. To decide from measured Compton amplitudes whether the Wandzura-Wilczek approximation is adequate would hence require sufficient knowledge of the x -dependence of GPDs at given ξ , so that both the \mathcal{H} and the \mathcal{H}_W type convolutions can be evaluated. If in turn this approximation can be sufficiently motivated from other sources, measurement of the twist-three amplitudes will provide information about H^q , E^q , \tilde{H}^q , \tilde{E}^q beyond what can be deduced from the leading amplitudes $M_{\lambda'+, \lambda+}$.

6.2 Two-photon annihilation

Among all hard exclusive processes $\gamma^* \gamma \rightarrow \pi^0$ plays a special role. On one hand rather good experimental data exist for Q^2 up to about 8 GeV². On the other hand this is one of the simplest processes from a theoretical point of view, and several investigations of power corrections have been carried out. The methods they employ are of direct relevance for processes where GDAs or GPDs can be measured.

For two-photon annihilation into a meson one can write down the operator product expansion. The first power corrections to the amplitude appear at order $1/Q^2$ and can be found in [356]. Taking the asymptotic forms of the relevant twist-two and twist-four distribution amplitudes one finds a ratio $\mathcal{A}_4/\mathcal{A}_2 = -\frac{8}{9}\delta^2/Q^2$ of the twist-four and twist-two contributions to the amplitude. Here δ parameterizes the local matrix element $\langle\pi(p)|\bar{d}g\tilde{G}^{\mu\nu}\gamma_\nu u|0\rangle$. Light-cone sum rule estimates give $\delta^2 \approx 0.2 \text{ GeV}^2$ at a scale $\mu = 1 \text{ GeV}$, with an error of about 30% being quoted in [357].

Twist-four corrections of similar size have been estimated in [358] using the renormalon technique (see [359]). This method starts with a resummation to all orders in perturbation theory of fermion loop insertions in the gluon lines of the relevant hard scattering subgraphs (which are those at NLO in the present case). Due to the infrared behavior of the running coupling this resummation contains an ambiguity which is power suppressed by $1/Q^2$, and which must be compensated in the process amplitude by a corresponding ambiguity in the twist-four contributions. One obtains an estimate for the power corrections under the assumption that the size of this ambiguity approximates the size of the twist-four corrections themselves.

As explained in the beginning of this section, the process $\gamma^*\gamma \rightarrow \pi$ differs from $\gamma^*\gamma^* \rightarrow \pi$ in that the real photon can lead to additional power corrections, associated with soft regions of phase space and signaled by endpoint divergences in the amplitude calculated from hard scattering graphs. Such corrections do indeed show up in the renormalon calculation of [358]. A different method to estimate them is based on light-cone sum rules, whose principal ingredients are parton-hadron duality and the use of dispersion relations. In the analysis by Khodjamirian [356] the amplitude for $\gamma^*\gamma \rightarrow \pi$ is expressed in terms of the one for $\gamma^*\gamma^* \rightarrow \pi$ in the region where both photons are far off-shell, so that soft end-point contributions for the photon are not kinematically possible. In [356] the twist-two and twist-four terms of the $\gamma^*\gamma \rightarrow \pi$ amplitude were evaluated to lowest order in α_s , whereas the one-loop corrections to the leading-twist term were included in [360, 361]. A different way of using light-cone sum rules for $\gamma^*\gamma \rightarrow \pi$ has been taken by Radyushkin and collaborators [362, 363, 364]. Here the $\gamma^*\gamma\pi$ vertex was related to the Green function between two photons and the axial current, in kinematics where the momentum transfer by the axial current is sufficiently far off-shell to use perturbation theory. No input of pion distribution amplitudes is required in this case.

Building on the work of Sterman and collaborators [365, 366], Jakob et al. have developed a different approach to estimating power corrections [367, 368]. Instead of expanding hard scattering graphs in the parton momenta around the point where they are on-shell and collinear to each other, one explicitly keeps the dependence of the hard scattering on transverse parton momenta. This is then convoluted not with the distribution amplitudes of the external hadrons, but with their light-cone wave functions, thus keeping the full nonperturbative k_T dependence. This formalism incorporates the Sudakov factors of the “modified hard scattering approach” of Sterman et al. [365, 366]. Going beyond the “standard hard scattering approach” [50], these Sudakov form factors resum effects of soft gluons in the hard scattering to all orders in perturbation theory. Calculations in this framework are conveniently performed in impact parameter space rather than transverse momentum. Both the behavior of the impact parameter wave function and the Sudakov factors tend to suppress the region of large impact parameters, where the use of perturbation theory is problematic. In particular this suppresses the contribution from the soft endpoint regions of the wave functions.¹⁸ In the momentum space formulation, it is precisely in the endpoint regions when the neglect of parton k_T in the hard scattering is not justified, since parton virtualities become small there. Note that this way of including transverse momentum in the hard scattering (as well as the light-cone sum rule approaches discussed above) does not include power suppressed effects order by order in $1/Q$, but rather sums certain types of power corrections to all orders in a $1/Q^n$ expansion. The relation between the inclusion of k_T in

¹⁸There are cases where the suppression from the Sudakov factor is not efficient enough to suppress large impact parameters, as pointed out by Descotes-Genon and Sachrajda for the $B \rightarrow \pi$ transition form factor [369].

the hard scattering kernel and the operator product expansion is not clear, as has been pointed out by Musatov and Radyushkin [364]. We also remark that the question of gauge invariance in this approach has not much been discussed in the literature.

In a phenomenological study, Jakob et al. [368] used a Gaussian form as in (216) for the \mathbf{k} dependence of the $q\bar{q}$ wave function of the pion,

$$\Psi_{+-}(z, \mathbf{k}) = N \frac{(4\pi a)^2}{z(1-z)} \exp \left[-a^2 \frac{\mathbf{k}^2}{z(1-z)} \right] \Phi_\pi(z) \quad (313)$$

with a normalization factor N fixed by (165). Taking the asymptotic form for the distribution amplitude $\Phi_\pi(z)$ the authors obtain a $\gamma^*\gamma \rightarrow \pi$ scattering amplitude smaller than the leading-twist one by about 33% at $Q^2 = 2 \text{ GeV}^2$ and by about 15% at $Q^2 = 8 \text{ GeV}^2$. In this kinematics, the effect of the Sudakov form factors turns out to be negligible compared to the intrinsic k_T dependence of the pion wave function and of the quark propagator in the hard scattering [321].

Given the precision of experimental data, an analysis of the leading-twist contribution calls for the inclusion of the $O(\alpha_s)$ corrections to the hard scattering. Contrary to the elastic pion form factor discussed in Section 5.3.1, these are relatively moderate in $\gamma^*\gamma \rightarrow \pi$ for Q^2 larger than about 2 GeV^2 . A recent evaluation of the full $O(\alpha_s^2)$ corrections [370] also suggests that the perturbation series is well behaved in this range (whereas the $O(\alpha_s^2)$ terms become of the same size as the $O(\alpha_s)$ ones when going down to $Q^2 = 1 \text{ GeV}^2$, given the increase of the strong coupling constant). The evaluation of the $O(\alpha_s^2)$ terms with fermion loops also allows one to determine the BLM scale for the running coupling in this process, which for the asymptotic pion DA and in the $\overline{\text{MS}}$ scheme is $\mu_R^2 \approx 0.11 Q^2$ when taken to be independent of parton momentum fractions [371]. This leads to rather small scales for most relevant Q^2 . To use the BLM scale one must hence modify the running of α_s in the infrared region, and thus go beyond the usual leading-twist formalism. Such an approach has in particular been pursued in [372] and [226].¹⁹

The CLEO data [319] for the $\gamma^*\gamma \rightarrow \pi$ amplitude show an approximate leading-twist scaling behavior already at moderate Q^2 above 2 GeV^2 . The normalization of the amplitude is rather close to its asymptotic value at $\log Q^2 \rightarrow \infty$ (given by the leading-twist expression with the asymptotic pion DA and without α_s corrections). It is difficult to assess whether the remaining difference for Q^2 between 2 and 8 GeV^2 is due to the shape of $\Phi_\pi(z)$ or to power suppressed contributions. A pure leading-twist analysis at $O(\alpha_s)$ can describe the data with Φ_π mildly deviating from its asymptotic form [321], and so can several descriptions including the power corrections discussed above. Analyses agree that very asymmetric shapes of Φ_π are strongly disfavored by the $\gamma^*\gamma \rightarrow \pi$ data [373, 360, 361], but by just how much Φ_π deviates from its asymptotic form strongly depends on the theory assumptions concerning power suppressed terms. In other words, values and errors on the leading-twist pion DA obtained in existing analyses crucially depend on the values and errors assumed for the power corrections. Attempts to determine the latter from present data as well will likely give results with poor statistical significance.

We also note that the amplitude for $\gamma^*\gamma \rightarrow \pi$ depends on Φ_π through the integral (294) over z and does not allow one to reconstruct the function $\Phi_\pi(z)$ without further theoretical assumptions. The leading-twist logarithmic scaling violations provide only little further constraints in the Q^2 range available [321]. In scenarios where power suppressed terms also depend on Φ_π , this situation is somewhat better [360, 361]. An often made assumption is that one can truncate the Gegenbauer expansion of Φ_π after a few terms. As a theoretical ansatz this is corroborated by several attempts to calculate or model Φ_π within QCD, where the coefficients of higher Gegenbauer polynomials tend to decrease with the degree of the polynomial.

¹⁹Notice that in [372] the BLM scale for $\gamma^*\gamma \rightarrow \pi$ is assumed to be the one for the pion form factor (Section 5.3.1) and is hence too small.

Summarizing this discussion, the annihilation process $\gamma^*\gamma \rightarrow \pi$ is a case where a leading-twist description with a plausible shape for the nonperturbative input describes the data rather well, even at moderate Q^2 . Compared with data from other processes it provides the cleanest constraints on Φ_π we have. Attempts to determine the integral (294) of $\Phi_\pi(z)$ with high precision are limited by theoretical control over power corrections. Precise data at higher Q^2 may help to overcome these limitations. Further and similarly clean information on the shape of $\Phi_\pi(z)$ could be obtained from $\gamma^*\gamma^* \rightarrow \pi$ in the region where one photon virtuality is much smaller than the other, as has been discussed in [321, 370].

The production of pion pairs, $\gamma^*\gamma \rightarrow \pi\pi$, which gives access to generalized distribution amplitudes, is very similar to $\gamma^*\gamma \rightarrow \pi$, and one can expect a similar situation concerning power corrections. The analysis in [85] observed that the production of pion pairs may be more sensitive to the soft physics at the endpoints $z = 0$ and $z = 1$. This is because compared with single pion production the z region around $\frac{1}{2}$ is suppressed by an extra factor $(2z - 1)^2$, with one factor $(2z - 1)$ coming from the hard-scattering kernel (293) and one from the Gegenbauer expansion (83) of the two-pion DA. A light-cone sum rule analysis by Kivel and Mankiewicz [271], following closely the treatment of $\gamma^*\gamma \rightarrow \pi$ by Khodjamirian [356], obtains rather moderate power corrections. At $Q^2 = 2 \text{ GeV}^2$ they reduce the leading-twist result by about 30% and are completely negligible at $Q^2 = 8 \text{ GeV}^2$.

The study just mentioned focused on the helicity amplitude where the $\pi\pi$ pair is produced in the $L^3 = 0$ partial wave. The situation for the case $L^3 = \pm 1$ and $L^3 = \pm 2$ can be inferred from work by Braun and Kivel [318] on $\gamma^*\gamma$ annihilation into $f_2(1270)$ (which in fact predominantly decays into $\pi\pi$). The transition amplitudes to the various meson helicity states were calculated using the operator product expansion on the light-cone, i.e., the same formalism described in Section 6.1 for DVCS. The transition to $L^3 = \pm 1$ is suppressed by $1/Q$ and in the Wandzura-Wilczek approximation depends on the twist-two quark DA. The production of the $L^3 = \pm 2$ state has a leading-twist part involving the tensor gluon DA briefly discussed in Section 3.7. This competes with a $1/Q^2$ suppressed contribution, which in the Wandzura-Wilczek approximation again involves the twist-two quark DA. Taking the asymptotic forms for the z dependence of the respective distribution amplitudes and assuming that the decay constants describing their normalization are of similar size, one finds that the relative size of leading and subleading power contributions is α_s/π versus m^2/Q^2 , where m is the meson mass. Unless the two-gluon DA has a significantly larger normalization than the quark DA one will hence need rather large Q^2 to have clean access to the two-gluon component in this process, given its suppression by α_s/π .

6.3 Compton scattering beyond $1/Q$ accuracy

Whereas the structure of the virtual Compton amplitudes is well understood including $1/Q$ contributions, no systematic treatment yet exists for higher power suppressed terms. This concerns in particular the corrections to the leading helicity amplitudes conserving the photon polarization.

First attempts have been made to resum target mass corrections to all orders in m^2/Q^2 in DDVCS. Belitsky and Müller [374] have performed this resummation for the vector and axial vector quark operators of geometrical twist two. The resulting hadronic tensor is conveniently expressed in terms of double distributions, convoluted with a modified hard scattering kernel, where the target mass and invariant momentum transfer appear via the variable

$$\mathcal{M}^2 = -4\rho^2 \frac{(4m^2 - t)\beta^2 + t\alpha^2}{(q + q')^2 (\beta + \xi\alpha)^2}, \quad (314)$$

where ρ is defined in (260). In the forward limit $t = 0$, $\xi = 0$, this reduces to the well-known combination $4x_B^2 m^2/Q^2$ in the target mass corrections of deep inelastic scattering. An important

feature of this result is that the target mass corrections are proportional to ρ^2 and should thus be rather small in much of the experimentally relevant kinematics. As it stands, the result can however not be used for phenomenology: as in the case of $1/Q$ corrections, the hadronic tensor obtained from geometrical twist-two operators does not respect electromagnetic gauge invariance. A full treatment will therefore require the inclusion of operators with higher geometrical twist. Building on results of [340], Eilers and Geyer [375] have done this for scalar quark operators (but not for the vector and axial vector ones) and found again that the target mass appears through the variable (314).

In a similar fashion as for $\gamma^*\gamma \rightarrow \pi$ one may estimate twist-four corrections to DVCS using the renormalon technique discussed in the previous subsection. Belitsky and Schäfer [376] have given a detailed presentation of the necessary resummation of fermion loops in the NLO hard-scattering diagrams. A numerical estimate has been reported by Vanttinen et al. [377]. At $Q^2 = 4 \text{ GeV}^2$ the authors found an enhancement of the squared DVCS amplitude growing from about 20% at $x_B = 0.1$ to about 60% at $x_B = 0.8$, with some dependence on the particular ansatz taken for the twist-two GPDs.

Vanderhaeghen et al. [304] have estimated power corrections due to parton k_T by extending to DVCS the framework of Jakob et al. presented in the previous subsection. In analogy to the ansatz (313), which extends a distribution amplitude to a wave function, the authors introduced a k_T dependence in the proton GPDs by multiplying the usual double distributions with

$$\frac{a^2}{(1 - |\beta|)^2 - \alpha^2} \exp \left[-a^2 \frac{4\mathbf{k}^2}{(1 - |\beta|)^2 - \alpha^2} \right] \quad (315)$$

times an appropriate normalization factor, taking a transverse size parameter $a \approx 0.86 \text{ GeV}^{-1}$ as in the pion wave function. The k_T dependent forward quark densities obtained with the ansatz in [304] give an average parton transverse momentum of $\langle k_T^2 \rangle^{1/2} \approx (1 - x) \times 520 \text{ MeV}$ at fixed parton plus-momentum fraction x . With $x_B = 0.3$ the authors find a reduction of the squared leading-twist amplitude by about 40% for $Q^2 = 2 \text{ GeV}^2$, going down to about 20% reduction for $Q^2 = 6 \text{ GeV}^2$.

To estimate the effect of the hadron-like component of the real photon in DVCS it is suggestive to compare this process with the electroproduction of a ρ meson. Donnachie and Gravelis [378] have used a model that gives a fair description of the H1 and ZEUS data on ρ production, and converted $\gamma_T^* p \rightarrow \rho_T p$ into a contribution to the $\gamma_T^* p \rightarrow \gamma p$ amplitude using the standard $\rho - \gamma$ conversion factor of the vector dominance model. Comparing with the measured DVCS cross section from H1 [259], they found that for $Q^2 = 2$ to 4 GeV^2 the so defined ρ contribution to the DVCS amplitude is about 18%. For the range $Q^2 = 11$ to 20 GeV^2 this ratio decreased to about 12%. In a similar study, Cano and Laget [379] used a model which describes well the HERMES data for transverse ρ electroproduction [380]. The corresponding ρ contribution to the DVCS amplitude accounts for about 50% of the electron beam spin asymmetries measured at CLAS (for $Q^2 = 1.25 \text{ GeV}^2$) [261] and at HERMES (for $Q^2 = 2.6 \text{ GeV}^2$) [260]. In both studies the dependence on the particular model used for ρ -production should be rather weak since ρ -production and DVCS are compared in similar kinematics (one needs however assumptions about the proton spin dependence in both processes and about the yet unmeasured t dependence of DVCS). We remark that the above conversion between amplitudes with a real photon and amplitudes with a $\rho(770)$ corresponds to the simplest form of vector dominance, which is by itself a model. It may be used as an estimate of how important the hadronic part of the photon is in DVCS, but should be taken as an indicator of power-suppressed contributions only with great care. Nevertheless, the studies cited above suggest some caution concerning a pure leading-twist interpretation of DVCS at rather low Q^2 . The situation for timelike photons with virtuality around the ρ mass will be discussed in Section 6.5.1.

We conclude this subsection by reporting a study by Kivel and Mankiewicz [381] on $1/Q^2$ corrections to the Compton amplitude with double photon helicity flip. These were calculated in the

Wandzura-Wilczek approximation, with the result expressed in terms of the twist-two GPDs H^q , E^q , \tilde{H}^q , \tilde{E}^q . Their convolution with hard-scattering kernels was found to have only integrable logarithmic singularities at $x = \pm\xi$, so that factorization does not manifestly break down in this amplitude at $O(\alpha_s^0/Q^2)$. In close analogy to the study [318] of $\gamma^*\gamma \rightarrow f_2$ mentioned in Section 6.2, the ratio of the leading-twist amplitude to the $1/Q^2$ corrections was found to go like α_s/π to m^2/Q^2 , where m is the proton mass. There is however a rather complicated dependence of the hard-scattering kernels on ξ and x , and the tensor gluon GPDs in the leading-twist term are completely unknown. Without further study it is hence difficult to say whether in a suitable range of ξ and Q^2 the leading-twist contribution may be favored.

6.4 Meson form factors and meson electroproduction

The elastic pion form factor has been the object of rather detailed studies of power corrections. This observable may be a case where the leading-twist contribution is not a good approximation of the total amplitude, even for Q^2 values of 10 GeV² and higher. Jakob et al. [367] have included the transverse parton momentum in the hard scattering in the way discussed in Section 6.2, and found a substantial suppression of the leading-twist result in this Q^2 range. Most of the suppression is not due to the Sudakov form factors but rather to the k_T dependence of the pion wave function and of the gluon propagator in the hard scattering. Note that transverse momentum enters a typical gluon virtuality as $z_1\bar{z}_2 Q^2 + (\mathbf{k}_1 - \mathbf{k}_2)^2$, where the indices refer to one or the other pion, whereas in a quark virtuality it appears in the form $z_1 Q^2 + \mathbf{k}_1^2$ (see Fig. 36c). The dominant effect of k_T is hence in the gluon propagator. The k_T in the quark propagator is neglected in most investigations, including the one just cited. The integration over one of the impact parameters conjugate to \mathbf{k}_1 and \mathbf{k}_2 then conveniently simplifies to a delta function. A study by Li found only a moderate further suppression when taking into account k_T in the quark propagator as well [382].

The strong suppression found in [367] indicates that even for Q^2 of several GeV² a substantial part of the leading-twist expression (289) is due to the regions where a quark or antiquark in one or both pions becomes soft. A power suppressed contribution to F_π not included in the hard-scattering diagram of Fig. 31a is the soft overlap of the $q\bar{q}$ Fock states for both pions, shown in Fig. 31b. Evaluating both contributions with the same wave functions Jakob et al. [368] found the soft overlap to be dominant over the graphs with one-gluon exchange. Notice that one has here a partial cancellation of negative power corrections from parton k_T in the $O(\alpha_s)$ graphs and of the positive soft overlap contribution at $O(\alpha_s^0)$. How large each contribution is depends not only on the pion wave function but also on the details of the perturbative treatment, compare e.g. the results of [368] and of [226].

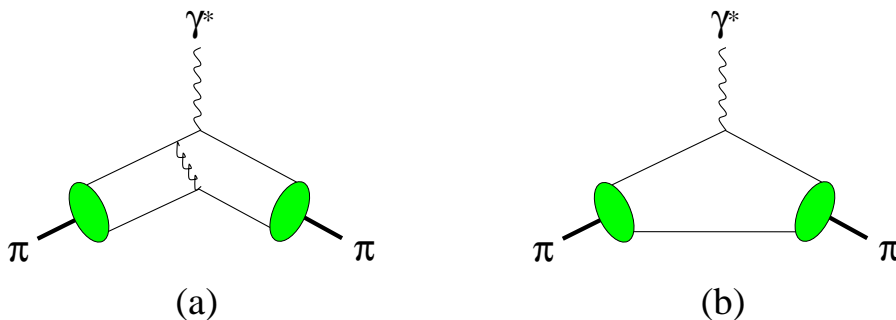


Figure 31: (a) Hard-scattering diagram for the pion form factor. (b) Soft overlap contribution to the pion form factor.

The sum of all contributions in [367] is close to the data if Φ_π is close to its asymptotic form, whereas strongly asymmetric pion DAs strongly overshoot the data. We caution however that the data for $F_\pi(Q^2)$ at large Q^2 (see [383] and references therein) are obtained from $\gamma^*p \rightarrow \pi^+n$ by an extrapolation to the pion pole, which is subject to criticism (see Section 5.3).

A model-dependent way to treat both hard-scattering and soft contributions in the same framework is provided by the light-cone sum rule technique. A detailed investigation has been given by Braun et al. [384], where one of the pions was replaced with the local axial current and the other was kept and described by its distribution amplitudes up to twist four. Calculating the graphs of $O(\alpha_s^0)$ and $O(\alpha_s)$, the authors find a large positive contribution to $F_\pi(Q^2)$ from regions where a quark or antiquark in the pion is soft. These power suppressed contributions are in part canceled by negative power suppressed terms from the hard-scattering region, due in this case to higher-twist pion DAs.

Given the model dependence of any existing treatment it is difficult to assess how large power corrections are to F_π in the experimentally relevant Q^2 range. The cancellations found in the above studies also show the dangers of discussing only selected sources of power corrections. Moreover, the separation of different contributions, in particular of “hard” versus “soft” ones, requires definition within a given framework, with care taken not to double count.

Comparing this situation for F_π with the one for $\gamma^*\gamma \rightarrow \pi$ one can identify why F_π is much more sensitive to power corrections at the same value of Q^2 . A typical virtuality inside the leading-twist graphs for $\gamma^*\gamma \rightarrow \pi$ is z_1Q^2 . The leading-twist graphs for F_π start with an additional gluon line, and the hard momentum of the external photon is diluted more strongly inside a graph: in particular the typical virtuality of the gluon is $z_1\bar{z}_2Q^2$ and hence tends to be significantly smaller than in $\gamma^*\gamma \rightarrow \pi$. This leads to greater sensitivity to corrections due for instance to the parton k_T , and ultimately to the soft end-point regions. Furthermore the soft overlap contribution to F_π in Fig. 31b comes with a factor of α_s less than the leading power contribution, which starts at $O(\alpha_s)$. In contrast, the soft overlap contribution between the real photon and the pion in $\gamma^*\gamma \rightarrow \pi$ (corresponding to the endpoint region of z_1) comes with the same power of α_s as the leading-twist hard scattering piece.

Vanderhaeghen et al. [304] have estimated the effect of parton k_T in meson electroproduction, using meson light-cone wave function with a Gaussian k_T dependence and a similar k_T dependence for GPDs, as described in Section 6.3. They considered the quark GPD contributions to both vector and pseudoscalar production. The inclusion of k_T dependence in the relevant diagrams shifts the point giving the imaginary part of the scattering amplitude from $x = \xi$ to $x > \xi$, which reduces the result for current models of GPDs. Note that the imaginary part of the amplitude is typically larger than the real part, except for charged pion production, which is dominated by the pion pole contribution. In the case of $\gamma_L^*p \rightarrow \rho_L p$, the study [304] found indeed a rather strong reduction of the leading-twist cross section, by a factor of about 3.5 at $x_B = 0.3$ and $Q^2 = 4 \text{ GeV}^2$ and a factor of about 2.5 at $x_B = 0.3$ and $Q^2 = 8 \text{ GeV}^2$, with yet bigger effects at larger x_B . A strong suppression for the same process in the small- x regime of the H1 and ZEUS data has been reported by Postler [385] in a study including the k_T dependence for the ρ wave function, but staying collinear for the gluon GPDs in the proton.

Like the elastic pion form factor, meson electroproduction admits a soft overlap regime at $O(\alpha_s^0)$, shown in Fig. 32. Vanderhaeghen et al. [304] have modeled this in the ERBL region of Fig. 32a, where the pion can be described by its light-cone wave function. How to estimate the contribution from the DGLAP configurations of Fig. 32b is not known. Note that the soft overlap (at least as calculated in this model) contributes only to the real part of the amplitude, so that its effect was found negligible for ρ production in [304]. For the production of charged pions, however, the pion pole contribution described by (288) was strongly enhanced and led to a strong enhancement of the cross section for $\gamma_L^*p \rightarrow \pi^+n$, clearly outweighing the suppression from parton k_T in the hard scattering contributions.

The renormalon approach described in Section 6.2 has been applied to meson production by

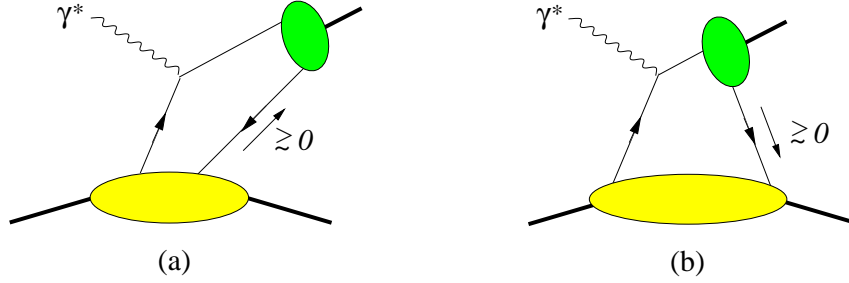


Figure 32: Soft overlap contributions to meson electroproduction in (a) the ERBL and (b) the DGLAP regime. Plus-momentum fractions $\gtrsim 0$ refer to the average nucleon momentum.

Vänttinen et al. [377]. For $\gamma^*p \rightarrow \pi^0p$ at $Q^2 = 4 \text{ GeV}^2$ a substantial enhancement of the cross section was found, with a strong dependence on the GPD model used. Substantial power corrections estimated from renormalons have also been reported for $\gamma^*p \rightarrow \pi^+n$ by Belitsky [141], who finds in addition that they tend to cancel in the transverse target spin asymmetry (see Section 9.4) for the kinematics considered in his study.

The pion form factor at large *timelike* photon virtuality is measured to be significantly larger than at the corresponding *spacelike* virtualities. The leading-twist formula gives $F_\pi(q^2) = F_\pi(-q^2)$ at $O(\alpha_s)$; whether the NLO corrections would significantly enhance the timelike region has not been studied. Gousset and Pire [386] have studied the effect of finite parton k_T in the same formalism as Jakob et al., and found an *enhancement* over the leading-twist $O(\alpha_s)$ result (although not quite large enough to describe the data). This trend is readily understood from the gluon virtuality in the hard scattering, which is $(z_1\bar{z}_2q^2 - \mathbf{k}^2)$ when transverse parton momentum is included. For $q^2 > 0$ this inclusion can provide an enhancement of the propagator, whereas for $q^2 < 0$ it always gives suppression. The soft overlap contribution to the timelike form factor cannot be described in terms of pion light-cone wave functions, as is seen in Fig. 33. A study using light-cone sum rule techniques has been performed by Bakulev et al. [312], with both pions replaced by local axial currents. The authors also calculated Sudakov-type radiative corrections to the quark-photon vertex in this mechanism. These are found to decrease F_π in the spacelike region, whereas for timelike photons they increase F_π and also provide an imaginary part. Power corrections to the timelike process $\pi N \rightarrow \gamma^*N$ discussed in Section 5.3 have not been studied in the literature. Here one may expect a similar pattern compared to pion electroproduction $\gamma^*N \rightarrow \pi N$ as between the time- and spacelike pion form factors.

A number of studies of power corrections to the leading meson production amplitude have been performed in the specific context of small x_B . These will be reviewed in Section 8.4.

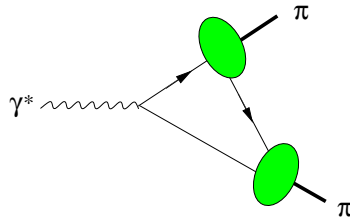


Figure 33: Soft overlap for the timelike pion form factor.

6.5 Parton-hadron duality

Parton-hadron duality appears in several contexts in the reactions of interest for us. We have already mentioned the technique of light-cone sum rules, where duality is used to relate amplitudes involving hadrons and Green functions involving local currents, which are more readily accessible for perturbative evaluation in suitable kinematics. In Section 8.4.2 we will report on the use of parton-hadron duality to relate the diffractive amplitude $\gamma^*p \rightarrow q\bar{q} + p$ with vector meson production.

6.5.1 Timelike photons

The application of the leading-twist formalism to processes with timelike photons, in particular to $\gamma^*p \rightarrow \gamma^*p$, $\gamma p \rightarrow \gamma^*p$ and to $\pi N \rightarrow \gamma^*N$, requires care in kinematics where the produced photon has an invariant mass Q' in the vicinity of meson resonances. Note that the limit for which factorization is derived implies $Q'^2 \rightarrow \infty$ and hence does not address this issue. This also holds for DDVCS, where the Q^2 of the incident photon provides a second hard scale: here the limit (258) sends both Q^2 and Q'^2 to infinity.

It is suggestive to compare the above cases to other processes involving the coupling of a quark line to a timelike photon with large virtuality, such as Drell-Yan pair production and e^+e^- annihilation into hadrons (Fig. 34). As discussed in [243] one must however be careful when using such analogies, since the relevant kinematic configurations are qualitatively different. In the γ^* production processes where we want to study GPDs, one of the quark lines attached to the timelike photon is part of a hard scattering kernel and thus to be regarded as far off shell, whereas the other quark line is connected to the proton GPD and corresponds to propagation over long distances. In contrast, both q and \bar{q} have small virtualities in the Drell-Yan process, and both are hard in $e^+e^- \rightarrow \text{hadrons}$. (In the tree-level graph $e^+e^- \rightarrow q\bar{q}$ the final quarks are on shell, but such singularities can be avoided by analytic continuation as explained in Section 5.1.) Moreover, the space-time structure is not the same in these cases: in Compton scattering at tree level the final γ^* is formed by $q\bar{q}$ in the ERBL region, but in the DGLAP region the corresponding vertex is $q \rightarrow \gamma^*q$ or $\bar{q} \rightarrow \gamma^*\bar{q}$, which does not suggest resonant behavior.

With these caveats in mind one may nevertheless use the analogy with Drell-Yan and e^+e^- annihilation to estimate the importance of resonance effects in exclusive γ^* production processes. Drell-Yan production data [387, 388] permit a leading-twist description for heavy-photon masses Q' above 4 or 5 GeV, excluding the region of the Υ resonances. Below this mass range, problems arise due to decay leptons from charm production, a background of course absent in the exclusive processes

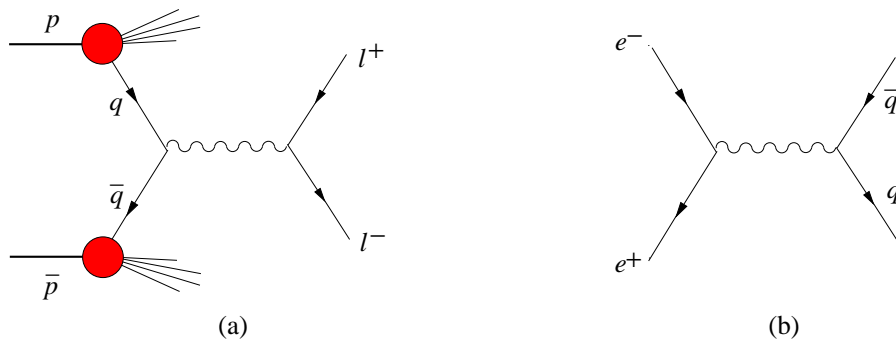


Figure 34: Born-level diagrams for (a) Drell-Yan lepton pair production and (b) e^+e^- annihilation into hadrons.

we are interested in. As to $e^+e^- \rightarrow \text{hadrons}$, the data [389, 390] show little resonance structure and good agreement with the leading-twist perturbative result in the Q' range from 2 to 3 GeV and above 5 GeV, excluding again the Υ resonances. One may thus regard these ranges as hopeful candidates for a leading-twist analysis of $\gamma p \rightarrow \gamma^* p$ and $\pi N \rightarrow \gamma^* N$.

For $\gamma^* p \rightarrow \gamma^* p$ one may extend this range if the initial photon virtuality Q^2 provides a hard scale to the process, and in particular also include the low Q' region down to the limit $Q' = 0$ of DVCS. Care is nevertheless advised, especially in a Q' band of several 100 MeV around 770 MeV, given the strong ρ peak in many similar situations. The importance of the resonance effects in this region can directly be assessed by converting data on $\gamma^* p \rightarrow \rho p \rightarrow (\pi^+\pi^-)p$ to $\gamma^* p \rightarrow \rho p \rightarrow (\ell^+\ell^-)p$ using the known ρ branching ratios. The latter contributes directly to the amplitude $\gamma^* p \rightarrow \gamma^* p \rightarrow (\ell^+\ell^-)p$, where DDVCS can be observed. This contribution is of the same order in the electromagnetic coupling since the $\rho \rightarrow \ell^+\ell^-$ decay proceeds via a γ^* . At moderately large Q^2 the amplitudes for $\gamma_L^* p \rightarrow \rho_L p$ and $\gamma_T^* p \rightarrow \rho_T p$ are experimentally known to be of comparable size, whereas for very large Q^2 the longitudinal contribution dominates. Guidal and Vanderhaeghen [282] have estimated the “ ρ contribution” to DDVCS by calculating $\gamma_L^* p \rightarrow \rho_L p$ in the leading-twist approximation, and report rather little effect on DDVCS observables in the kinematics they considered.

Given the above theoretical caveats it may be best from a phenomenological point of view to assess the importance of resonance effects directly from the data of the processes under study, since such effects will likely show up in the Q' distribution. Such a study and its comparison to other processes may itself provide information on the mechanism of parton-hadron duality in different environments. In Q' regions where resonance structures do appear, a leading-twist analysis of the data will need to invoke parton-hadron duality after averaging over a suitable Q' range, as can be done for $e^+e^- \rightarrow \text{hadrons}$.

6.5.2 Bloom-Gilman duality

This particular type of parton-hadron duality has recently been studied with increasing interest in inclusive DIS, both experimentally and theoretically, see e.g. [391] for a recent overview. An extension of such studies to DVCS and DDVCS for W^2 in the resonance region seems natural. It is amusing to note that virtual Compton scattering with a timelike final γ^* can simultaneously involve parton-hadron duality in two channels, corresponding to the variables Q' and W .

Close and Zhao [392] have investigated a toy model for the proton, consisting of two scalar constituents with electromagnetic charges e_1 and e_2 bound by a potential. They have shown how the superposition of resonances reproduces features of the leading-twist mechanism, namely Bjorken scaling and the absence of terms with $e_1 e_2$, where the photons couple to different constituents. These features are found both for the imaginary part of the forward Compton amplitude and for $\text{Im } \mathcal{A}(\gamma^* p \rightarrow \gamma^* p)$ in nonforward kinematics at large Q^2 and small t . The authors proceed by discussing the imaginary part of the DVCS amplitude in terms of two independent scaling variables, $Q^2/(2pq)$ and $-t/(2pq)$, and draw conclusions on generalized parton distributions as functions of the independent variables x , ξ , and t . Since the leading-twist expression of $\text{Im } \mathcal{A}(\gamma^* p \rightarrow \gamma p)$ at Born level only gives access to GPDs at $x = \pm\xi$, these conclusions are unfortunately incorrect. It may be possible to apply the considerations of [392] to $\text{Im } \mathcal{A}(\gamma^* p \rightarrow \gamma^* p)$ for small t and different spacelike q^2 and q'^2 , which involves the GPDs in the DGLAP region at leading-twist accuracy (although no practicable way is known to measure it).

7 Beyond the factorization theorems

A number of investigations have been concerned with processes or observables to which the leading-twist factorization theorems discussed in Section 5.1 cannot be applied, with the prime motivation to see whether information about GPDs or GDAs can be obtained nevertheless. The most advanced example is Compton scattering at the $1/Q$ level (Section 6.1). The hope of such studies is often to probe GPDs or GDAs to which leading-twist observables give only little or no access, for instance the polarized gluon GPD \tilde{H}^g or transversity GPDs.

7.1 Transverse vector mesons

The electroproduction of transverse vector mesons from transverse photons is power suppressed by $1/Q$ compared with the dominant longitudinal amplitude, and there is no factorization theorem which allows one to calculate it in terms of meson distribution amplitudes and nucleon GPDs. It is nevertheless instructive to see what an attempt at such a calculation gives. This has been done by Mankiewicz and Piller [393], and later by Anikin and Teryaev [394] with a different method. The results of both studies agree. Only the chiral-even meson wave functions were considered in both cases. To make a transverse meson from a $q\bar{q}$ pair with helicities coupled to zero, one needs one unit of orbital angular momentum or one extra gluon, and the relevant meson distribution amplitudes start at dynamical twist three. To obtain the dominant part of $\gamma_T^* p \rightarrow \rho_T p$ one is then restricted to dynamical twist two on the GPD side. The calculation of Mankiewicz and Piller uses the distribution amplitudes defined in the QCD string operator approach of Braun and collaborators [151] and stays within the Wandzura-Wilczek approximation. Anikin and Teryaev use the “transverse” operator basis of Ellis et al. [324] and give results both with and without the Wandzura-Wilczek approximation, restricting themselves to a spinless target.

Calculation of the graphs in Fig. 2 (plus those with an additional gluon line attached to the meson in the case of [394]) gives logarithmic singularities, which affect both the meson DAs and the target GPDs. For the meson they take the form

$$\int_0^1 \frac{dz}{z} \int_z^1 \frac{du}{u} \Phi^q(u), \quad (316)$$

where Φ^q is the usual twist-two DA. This integral is only finite if $\int_0^1 du u^{-1} \Phi^q(u)$ is accidentally zero, which can at most occur at a particular factorization scale. On the GPD side the result involves the familiar convolutions with $(\xi \mp x - i\epsilon)^{-1}$, but in addition the integrals

$$\int_{-1}^1 dx \frac{1}{(\xi \mp x - i\epsilon)^2} H^{q,g}(x, \xi, t) = \mp \int_{-1}^1 dx \frac{1}{\xi \mp x - i\epsilon} \frac{\partial}{\partial x} H^{q,g}(x, \xi, t) \quad (317)$$

and analogous ones with E, \tilde{H}, \tilde{E} for quarks and gluons. To be well defined and finite, they require the x -derivative of the GPDs to be finite at $x = \pm\xi$. As we discussed in Section 3.13, this is not the case for the quark GPDs in a large number of field theoretical models, where this derivative has a discontinuity at these points. We have also seen that the double distribution formalism suggests that such discontinuities can occur. The situation for the gluon GPDs is less clear. One may observe that the asymptotic form of a gluon D -term goes like $\theta(|x| < |\xi|) [1 - (x/\xi)^2]^2$ and has a vanishing first derivative at $x = \pm\xi$, whereas the asymptotic form $\theta(|x| < |\xi|) [1 - (x/\xi)^2]$ of a quark D -term has a first derivative jumping from a finite value to zero at that point. No further investigation of this point has been made.

These findings show that for the amplitude at hand an expansion of the partonic scattering amplitude around zero k_T of the partons (or equivalently an expansion of nonlocal operators around

$z_T = 0$ in position space) is not adequate. The occurrence of divergences in the calculation may be cured by keeping finite parton k_T in the partonic scattering. This will regulate end point divergences by replacing for instance an inverse propagator zQ^2 by $zQ^2 + \mathbf{k}^2$. An even simpler phenomenological prescription is to cut off z -integrals like (316) at a value $\langle \mathbf{k}^2 \rangle / Q^2$, with $\langle \mathbf{k}^2 \rangle$ being of typical hadronic size. The integral will then have a logarithmic enhancement by $\log \langle \mathbf{k}^2 \rangle / Q^2$. As remarked in [394], this may explain why the observed ratio $R = \sigma_L / \sigma_T$ of longitudinal to transverse ρ production seems to grow more slowly with Q^2 than expected from simple power counting arguments (see Section 9.4.1). On the GPD side, the inclusion of transverse momentum would change the location of the singularity in (317) from $x = \xi$ to $x > \xi$, where the GPDs are expected to be regular.

As a matter of principle, the above divergences signal however the presence of soft contributions to the amplitude, in full accordance with the general analysis of the factorization theorems we presented in Section 5.1. Such soft exchanges between the meson and target side break the factorization into soft matrix elements depending only on either the meson or the target. It is not known how serious such violations of universality are, and it remains controversial in the literature if phenomenological prescriptions as discussed above are adequate to describe the essential dynamics. We will again come across this issue in Sections 8.2 and 8.4.

7.2 Meson pairs with large invariant mass

Lehmann-Dronke et al. [250] have studied the electroproduction production of $\pi^+\pi^-$ and K^+K^- pairs with an invariant pair mass M of a few GeV. In contrast to the case $M^2 \ll Q^2$, where the formation of the meson pair can be described by the appropriate GDA, the process was modeled by calculating the production of a $q\bar{q}$ pair at the cross section level and describing the subsequent hadronization to a meson pair using the Lund string fragmentation model [274]. This is reminiscent of the study of exclusive $\gamma^*\gamma$ annihilation into hadrons we reported on in Section 4.6.5. The authors of [250] estimated cross sections for kinematics achievable at HERMES and found them to be too small for the luminosity one may expect there.

The description of open $q\bar{q}$ production in the GPD framework (which we will again discuss in Section 8.6) is of theoretical interest by itself. Lehmann-Dronke et al. use the collinear factorization formalism to calculate the amplitudes for both transverse and longitudinal photons. The result for gluon exchange diagrams involves the convolution (317) for the GPDs $H^g, E^g, \tilde{H}^g, \tilde{E}^g$. In contrast, the scattering kernels for the quark distributions $H^q, E^q, \tilde{H}^q, \tilde{E}^q$ are found to have only simple poles at $x = \pm\xi$ and $x = \pm\rho$, with ρ defined in (260) if we set $Q' = M$. Dangerous double poles would thus only occur for $M \rightarrow 0$, where ξ and ρ coincide. The momentum fractions z and $1 - z$ of the final q and \bar{q} are external kinematical variables in this case. One may hence avoid the dangerous soft regions $z \rightarrow 0, 1$ by imposing a minimum transverse momentum \mathbf{k} for the $q\bar{q}$ pair, given that $\mathbf{k}^2 = z(1 - z)M^2$. In physical applications one must of course assume that the quark momentum is sufficiently correlated with a measured momentum in the final state.

7.3 Access to transversity distributions

We have seen in Sections 5.2 and 5.4.1 that one may access the gluon transversity GPDs at leading-twist level in Compton scattering with photon helicity flip, and the corresponding tensor gluon DA or GDA in two-photon annihilation with $L^3 = \pm 2$. Kivel [395] has investigated the occurrence of these quantities in power suppressed meson electroproduction amplitudes with helicity transfer between the photon and the meson. He calculated the diagrams of Fig. 2 in the light-cone string operator formalism of Braun et al., giving results for a spinless target. Two cases were found where tensor gluon GPDs or DAs provide the only contribution to the considered amplitude at level $1/Q^2$. Both involve one unit of orbital angular momentum in the hard scattering kernel, which gives the $1/Q$

A large subenergy s_2 was taken in order to select gluon exchange in the upper part of the diagram, whereas the charge of the ρ_T^+ ensures quark exchange in the lower part. The leading-twist collinear approximation, which should be relevant for large \mathbf{p}^2 , selects the chiral-odd distribution amplitudes Φ_T^g for the transverse meson. This in turn selects the chiral-odd nucleon GPDs, which appear in the amplitude through a convolution in x restricted to the ERBL region, at skewness $\xi \approx \zeta/(2 - \zeta)$ with $\zeta \approx (Q^2 + s_1)/s \approx \mathbf{p}^2/(s_2 + \mathbf{p}^2)$. Further investigation will have to show whether this proposal can be used in practice to provide access to chiral-odd GPDs, about which nothing is presently known.

7.4 Heavy meson production

7.4.1 Charmonium

Exclusive production of heavy quarkonium states, in particular of the J/Ψ , has repeatedly been investigated as a process to access gluon GPDs. Some of these studies are dedicated to the small x regime and will be reviewed in Section 8.4.2.

The relevant graphs for heavy meson production are as for light mesons in Fig. 2b. In the limit where $Q^2 \gg M_{J/\Psi}^2$, the charm quarks in the loop may be treated as massless, so that one recovers the predictions of the leading-twist factorization theorem: the dominant $\gamma^* p \rightarrow J/\Psi p$ transition has both photon and meson longitudinally polarized, and this transition is described in terms of nucleon GPDs and the leading-twist distribution amplitude $\Phi_{J/\Psi}(z)$ of the J/Ψ .

The opposite of this situation is photoproduction, $Q^2 = 0$. In this situation it is the charm quark mass that provides a hard scale to the process and protects the off-shell propagators in the graphs of Fig. 2b from going close to their mass shell. Of course, the charm quark mass is not negligible if Q^2 is comparable in size to $M_{J/\Psi}^2$. The finite quark mass also cuts off the endpoint regions $z = 0, 1$ of the meson wave function, where factorization breaks down, so that both amplitudes with γ_T^* and γ_L^* can be investigated in a GPD framework. A further characteristic of the process is that charmonium bound states are approximately nonrelativistic. The simplest approximation of their $c\bar{c}$ wave function corresponds to the static case, where c and \bar{c} equally share the meson four-momentum, with zero relative momentum and m_c approximated by half the bound state mass. This static approximation is widely used in the literature. As a refinement, one may expand the wave function in powers of the relative velocity v of the quarks in the meson rest frame, as is done in the non-relativistic QCD approach [398]. So far, no systematic analysis has been given for issues of factorization and power counting in $\gamma^{(*)} p \rightarrow J/\Psi p$ when the quark mass cannot be neglected.

Hoodbhoy [399] has studied the deviation from the static wave function approximation to order v^2 in the non-relativistic expansion *and* to leading accuracy in the $1/Q$ expansion of J/Ψ electroproduction. A very small reduction of the amplitude was found compared with the static wave function. We note that the static approximation implies a distribution amplitude $\Phi(z) \propto \delta(z - \frac{1}{2})$, and that the integral $\int dz z^{-1} \Phi(z)$ *increases* when this delta-peak becomes wider, unless there are cancellations between regions with positive and negative $\Phi(z)$. It is hence not clear how the departure from the static approximation could lead to *suppression* of the electroproduction amplitude in the large Q limit. We also observe that for $Q^2 \gg m_c^2$ it is appropriate to use the meson DA at a renormalization scale of order Q^2 to prevent large logarithms $\log Q/m_c$ appearing in loop corrections to the hard-scattering process. The physics of modes with virtualities between m_c and Q is however not included in a wave function obtained in a non-relativistic approximation.

A study by Ryskin [400] of J/Ψ electro- and photoproduction suggested that one may access the polarized gluon distributions (\tilde{H}^g and \tilde{E}^g in our notation) in suitable polarization observables. Unfortunately, this hope was the consequence of a mistake in the calculation, as pointed out by Vanttinen and Mankiewicz [401]. Calculating the graphs of Fig. 2b with the collinear approximation for the gluons, keeping the charm quark mass in the loop, one finds that \tilde{H}^g and \tilde{E}^g do not contribute

to $\gamma^{(*)}p \rightarrow J/\Psi p$ in the static approximation for the meson wave function. Taking into account the corrections of $O(v^2)$ in a non-relativistic expansion, Vanttinen and Mankiewicz [402] found only very small effects. The double polarization asymmetry of J/Ψ photoproduction with the helicities of photon and target proton aligned or antialigned in the c.m. is proportional to the ratio of polarized to unpolarized gluon GPDs, but a value of at most 1% was estimated for this observable.

One should finally remark that the charm quark mass is not very large, and that the treatment of the charmonium as a non-relativistic system is not undisputed, see Section 8.4.2. This is less problematic for the Υ resonances.

7.4.2 Heavy-light mesons

With the prospect of future high-intensity neutrino beam facilities, charged and neutral current production process may be studied at the same footing as the photon induced reactions we have discussed so far. Due to the quantum numbers of W and Z bosons, these currents give access to different combinations of GPDs than those one can probe in electromagnetic reactions.

Lehmann-Dronke and Schäfer [403] have studied the process $\bar{\nu}_\mu p \rightarrow \mu^+ p D_s^-$ for large virtuality Q^2 and longitudinal polarization of the exchanged W^- boson. The graphs of Fig. 2a and Fig. 2b were calculated in the collinear hard scattering approximation. Both the mass of the charm quark and of the meson were kept finite, neglecting terms of order $M_{D_s}^4/(Q^2 + M_{D_s}^2)^2$. The result involves the $s\bar{c}$ distribution amplitude of the meson and the proton GPDs H^g , $H^s - \tilde{H}^s$, \tilde{H}^g together with their E -counterparts. The polarized gluon GPDs \tilde{H}^g , \tilde{E}^g appeared with a factor $M_{D_s}^2/(Q^2 + M_{D_s}^2)$ and were completely negligible in a numerical study of the amplitude for $Q^2 > 12 \text{ GeV}^2$. In this region, effects from the finite masses m_c and M_{D_s} were found to be quite small, so that the results of the massless leading-twist approach gave a good approximation of the result.

7.5 Hadron-hadron collisions

The reactions we have discussed so far are all in photon or lepton induced scattering on a hadronic target.²⁰ It is natural to ask if one cannot also use hadron-hadron collisions to study GPDs, as one does for the extraction of the usual parton densities. This turns out to be difficult, since the factorization theorems which provide a sound basis to extract GPDs do not hold for hadron-hadron scattering processes.

A simple example of the problems which occur is the exclusive analog of Drell-Yan pair production, i.e., $pp \rightarrow \gamma^* pp$ or $p\bar{p} \rightarrow \gamma^* n\bar{n}$ with the timelike photon decaying into a lepton pair.²¹ Naively employing leading-twist factorization one obtains the diagram of Fig. 36a and further diagrams with different attachments of the photon to a quark line. The hard-scattering subprocess is the same as for $\pi^- p \rightarrow \gamma^* n$ in Fig. 36b and for the timelike pion form factor $\pi^- \pi^+ \rightarrow \gamma^*$ in Fig. 36c, where leading-twist factorization does hold. The corresponding parton scattering amplitudes are related by the correspondence between z in a meson DA and $(\xi + x)/(2\xi)$ for a GPD, both giving the momentum fraction of the quark with respect to the total momentum carried by the two partons. This gives hard scattering kernels

$$K_a \propto \frac{e_{q'}}{(\xi_1 + x_1)(\xi_2 - x_2) + i\epsilon} - \frac{e_q}{(\xi_1 - x_1)(\xi_2 + x_2) + i\epsilon},$$

$$K_b \propto \frac{e_{q'}}{(\xi_1 + x_1)(1 - z_2) + i\epsilon} - \frac{e_q}{(\xi_1 - x_1)z_2 + i\epsilon},$$

²⁰An exception are cases like $\pi^- p \rightarrow \gamma^* n$ where an off-shell photon is in the final instead of the initial state. When referring to hadron-hadron scattering here, we imply more than one hadron in both the initial and the final state.

²¹I thank B. Pire and O. Teryaev for discussions about this issue.

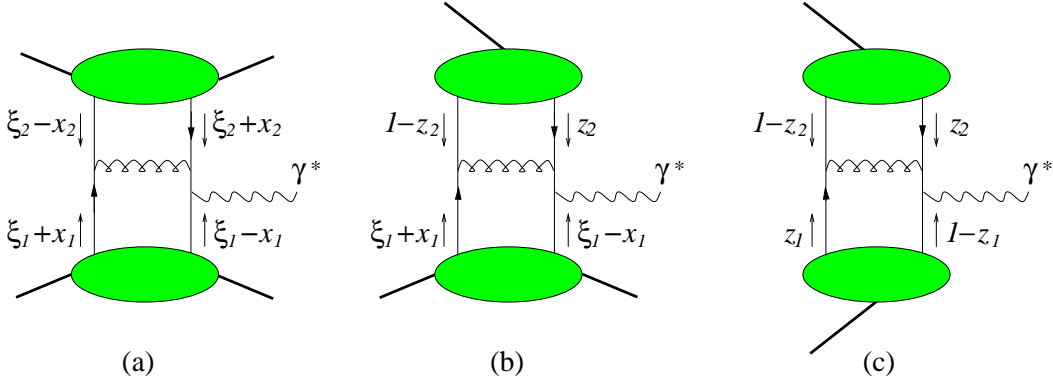


Figure 36: Example graphs of the hard scattering mechanism for $pp \rightarrow \gamma^* pp$ (a), for $\pi^- p \rightarrow \gamma^* n$ (b), and for the timelike meson form factor (c). Momentum fractions refer to the meson for DAs and to the average hadron momentum for GPDs.

$$K_c \propto \frac{e_{q'}}{z_1(1-z_2) + i\epsilon} - \frac{e_q}{(1-z_1)z_2 + i\epsilon}, \quad (320)$$

for the three cases of Fig. 36, where the $i\epsilon$ prescription follows directly from the Feynman prescription for the gluon propagator in the diagrams (the denominators of the quark propagators cancel against the numerators in the sum of the relevant diagrams). e_q and $e_{q'}$ respectively are the charges of the quark on the left- and right-hand sides of the graphs. The crucial difference between the case of a meson DA and a GPD is that the poles of the gluon propagators in $z_{1,2}$ are at the endpoints of the $z_{1,2}$ integration and will be canceled by the zeroes of the meson DA. In contrast, the poles in $x_{1,2}$ are at $\pm\xi_{1,2}$, where the corresponding GPDs do in general not vanish. For K_b this poses no problem, since the $i\epsilon$ prescription makes the integral well defined. For K_a however, this prescription is not sufficient to regulate the simultaneous poles in x_1 and x_2 in the convolution with the corresponding GPDs. Explicitly one finds that the imaginary part of this convolution diverges as $\log(1/\epsilon)$. The divergence cannot be canceled between the terms with e_q and $e_{q'}$ in the hard scattering, since the GPDs are in general different at $x = \xi$ and $x = -\xi$. This shows that the “hard scattering kernel” naively calculated in the collinear expansion for $pp \rightarrow \gamma^* pp$ is not actually hard: the configuration in Fig. 36a where the gluon and both quark lines on the left have soft momenta is not suppressed.

As we mentioned in Section 5.1, the factorization proof for meson electroproduction had to resort to complex contour deformation of loop momenta in order to show that nonfactorizable soft interactions do not contribute to the scattering amplitude, and that this was only possible because there were not two hadrons both in the initial and in the final state. Nonfactorizable soft interactions in hadron-hadron scattering can be shown to interfere destructively only in *inclusive* processes like Drell-Yan production, where one sums over all remnant states of the initial hadrons. For a brief discussion and references see [404].

An example where factorization breaking expected for the above reasons seems to be observed in data are diffractive processes. For diffraction in ep collisions one can establish factorization in terms of hard scattering coefficients and diffractive parton densities [405]. Taking densities fitted to diffractive ep scattering at HERA and calculating processes like diffractive W production, $p\bar{p} \rightarrow W + p + X$ with a large gap in rapidity between the scattered p and all other final-state particles, one finds cross sections significantly larger than measured at the Tevatron [406, 407]. Suggestive of the picture that factorization is broken by *soft* interactions is the observation that the momentum distribution of the particles produced in the hard subprocess does seem to agree with predictions obtained by assuming

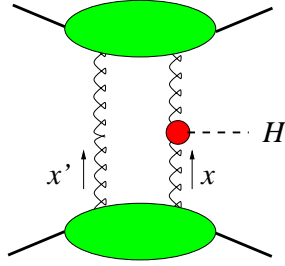


Figure 37: Diagram for exclusive Higgs production in hadron-hadron collisions. The coupling between gluons and Higgs is via a top quark loop.

factorization [407]. There are attempts in the literature to model the effect of such soft interactions, which is often called “rapidity gap survival” with the idea in mind that a potential rapidity gap left behind from a hard subprocess can subsequently be filled by particles from soft interactions.

This was for instance done by Khoze et al. [408, 409, 410] in an investigation of exclusive Higgs production, $pp \rightarrow p + H + p$, which has long been proposed as a very clean process to detect and study the Higgs at the LHC. In this work the survival probability multiplies the result obtained from calculating the diagram in Fig. 37. Note that, unlike in Fig. 36a, one parton exchanged between the two protons is now disconnected from the hard scattering subgraph $gg \rightarrow H$. Khoze et al. calculate this graph using k_T dependent GPDs (see Section 8.1), including a Sudakov form factor which suppresses the region of small parton k_T . The authors find the typical transverse gluon momentum to satisfy $\Lambda_{\text{QCD}}^2 \ll k_T^2 \ll M_H^2$, and typical longitudinal momentum fractions

$$\frac{\Lambda_{\text{QCD}}}{\sqrt{s}} \ll |x'| \sim \frac{k_T}{\sqrt{s}} \ll x \sim \frac{M_H}{\sqrt{s}}, \quad (321)$$

so that the gluon which “bypasses” the hard scattering is not actually soft. We remark that the theoretical description of $pp \rightarrow p + H + p$ is not uncontroversial, with a wide spread in size of cross section estimates in the literature, see e.g. [411, 412].

8 GPDs and small- x physics

Hard exclusive processes at high energy and hence at small x have been investigated in theory and experiment for some time, in particular since the operation of the HERA ep collider at DESY. In this section we will discuss some of the dynamical issues which render the small- x regime special compared with moderate and large x , and put into context the role played by GPDs. As in Section 4.4 we will use the term “small x ” having in mind that the small external variable is ξ or x_B in the electroproduction processes we focus on.

To start with let us recall some general results for high-energy reactions and parton distributions at small x .

- The dominant parton densities at small x are the unpolarized gluon and next the flavor singlet combination of unpolarized quarks and antiquarks, for scales $\mu^2 = Q^2$ large enough to make contact with physical observables. Evolution to higher scales enhances this trend. It is natural to expect the same situation for GPDs. The small- x behavior of parton helicity dependent distributions is interesting in itself, but these distributions will presumably be hard to access experimentally.

- Helicity flip amplitudes in hadron-hadron scattering at high energy are measured to be relatively small, although nonzero, so that at small ξ one may expect H^g and $\sum_q H^q$ to dominate over E^g and $\sum_q E^q$. This is in line with the comparison between the isoscalar combinations of the Dirac and Pauli form factors $(F_1^p + F_1^n)$ and $(F_2^p + F_2^n)$, with the caveats spelled out in Section 4.3.4.
- The real and imaginary parts of scattering amplitudes are related by dispersion relations, which involve the imaginary part in the entire physical region of squared c.m. energy s .²² As an example consider a once subtracted dispersion relation at fixed t for an amplitude even under crossing $s \leftrightarrow u$, see e.g. [241, 242],

$$\operatorname{Re} \frac{\mathcal{A}_+(s, t)}{s} \approx \frac{2s}{\pi} \int_{s_{\min}}^{\infty} \frac{ds'}{s'^2 - s^2} \operatorname{Im} \frac{\mathcal{A}_+(s', t)}{s'}, \quad (322)$$

where we have taken the limit of large s and small t and neglected subtraction and pole terms (which would decrease as s^{-1} on the right-hand side). This relation can be simplified by Taylor expanding $\operatorname{Im} \mathcal{A}_+(s', t)/s'$ in $\log(s'/s)$ and approximating $s_{\min} \approx 0$. The Taylor series can be summed explicitly, and one obtains a so-called derivative analyticity relation [413]

$$\operatorname{Re} \frac{\mathcal{A}_+(s, t)}{s} \approx \tan\left(\frac{\pi}{2} \frac{d}{d \log s}\right) \frac{\operatorname{Im} \mathcal{A}_+(s, t)}{s} \approx \frac{\pi}{2} \frac{d}{d \log s} \operatorname{Im} \frac{\mathcal{A}_+(s, t)}{s}. \quad (323)$$

For amplitudes odd under crossing one starts with

$$\operatorname{Re} \mathcal{A}_-(s, t) \approx \frac{2s}{\pi} \int_{s_{\min}}^{\infty} \frac{ds'}{s'^2 - s^2} \operatorname{Im} \mathcal{A}_-(s', t), \quad (324)$$

and finds

$$\operatorname{Re} \mathcal{A}_-(s, t) \approx \tan\left(\frac{\pi}{2} \frac{d}{d \log s}\right) \operatorname{Im} \mathcal{A}_-(s, t) \approx \frac{\pi}{2} \frac{d}{d \log s} \operatorname{Im} \mathcal{A}_-(s, t). \quad (325)$$

A more sophisticated version of these relations is also given in [413]. Most small- x studies calculate the imaginary part of a scattering amplitude and recover the real part by a relation of the type (323).

- The parameterization (236) of small- x parton densities as a power of x is motivated by Regge theory, which describes strong interactions at high s and small t starting from general principles like analyticity of scattering amplitudes [241, 242]. In accordance with these principles, Regge behavior is also found for scattering amplitudes in QCD [414, 415]. The simplest energy dependence obtained in Regge theory is a sum of “Regge poles”

$$\mathcal{A}(s, t) \sim \sum_j c_j(t) \left(\frac{s}{s_0}\right)^{\alpha_j(t)} (1 + S_j e^{-i\pi\alpha_j(t)}), \quad (326)$$

where the real-valued coefficients $c_j(t)$ depend on the scattering particles, but the “Regge trajectories” $\alpha_j(t)$ do not. Phenomenologically, trajectories are well described by a linear form $\alpha_j(t) = \alpha_j(0) + \alpha'_j t$ for $-t$ not too large. Each term j is associated with a t -channel exchange of definite quantum numbers, including the “signature” $S_j = \pm 1$ which distinguishes even and odd terms under $s \leftrightarrow u$ crossing (equivalent to $s \leftrightarrow -s$ at high energies). Notice that the relations

$$\operatorname{Re} \mathcal{A}_+ = \tan\left[\frac{\pi}{2}(\alpha - 1)\right] \operatorname{Im} \mathcal{A}_+, \quad \operatorname{Re} \mathcal{A}_- = \tan\left[\frac{\pi}{2}\alpha\right] \operatorname{Im} \mathcal{A}_- \quad (327)$$

²²To be precise, one should replace $\operatorname{Im} \mathcal{A}$ in this discussion by the energy discontinuity $\operatorname{disc}_s \mathcal{A}(s, t) = [\mathcal{A}(s + i\epsilon, t) - \mathcal{A}(s - i\epsilon, t)]/(2i)$. This makes for instance a difference when \mathcal{A} involves phases due to spinors.

for a single term with positive or negative signature are in agreement with (323) and (325) as it must be. More complicated dependence on s involves logarithms from “Regge cuts” in addition to the powers in (326).

The form (326) translates into a representation of quark and gluon densities as a sum over powers $x^{-\alpha_j(0)}$ [45]. This can be seen by representing the parton distributions as parton-hadron scattering amplitudes (see Section 3.4), or by using (326) for the forward Compton amplitude $\gamma^*p \rightarrow \gamma^*p$ and comparing with its expression through parton densities. An extension of these arguments underlies the ansatz (243) for the t -dependence of GPDs at small x and $\xi = 0$, where the trajectory $\alpha_j(t)$ appears.

- A special role is played by exchanges with vacuum quantum numbers ($P = C = 1$ and isospin $I = 0$ and positive signature), which dominate elastic amplitudes in the high-energy limit. In QCD these quantum numbers correspond to two-gluon exchange in the t -channel. Data for hadron-hadron scattering and for DIS down to $x_B \approx 10^{-2}$ can be well described by Regge poles corresponding to meson exchange in addition to a “Pomeron” pole with vacuum quantum numbers and a trajectory with $\alpha_P(0) \approx 1.08$ and $\alpha'_P \approx 0.25 \text{ GeV}^{-2}$ [416, 417]. The HERA data for deep inelastic processes at x_B down to about 10^{-4} have however shown that the situation is not as simple, with the rise in energy becoming considerably steeper as Q^2 increases. The nature of this phenomenon and its description in QCD remains a major unsettled and controversial issue. Cudell et al. [418] have emphasized that in Regge theory the powers of energy in (326) depend on t but not on the virtuality Q^2 of a scattering particle. When parameterizing the high-energy behavior of cross sections by a single power-law with a Q^2 dependent exponent, one should hence keep in mind that this is an “effective power”, which approximates a sum of powers or a more complicated form involving logarithms in a certain region of energy. Correspondingly, a single power-law term $xf(x) \sim x^{-\lambda}$ in a parton distribution can provide an approximate description over a finite x -range and for a given factorization scale μ .

We already observed in Section 5.1 that a power-law behavior of GPDs as in (252) leads to a power-law behavior in ξ of the scattering amplitude, due to the general structure of hard-scattering kernels. The relations (327) between real and imaginary part of the amplitude have also been reproduced, both in numerical [286] and analytical [125, 244] studies with appropriate input GPDs. It is believed that the leading-twist factorization formulae satisfy in fact the dispersion relations underlying (327). We remark however that the proof given for this in [24] is incorrect as it stands, since the argument does not properly take into account the ξ dependence of the GPDs .

We finally note that for electroproduction processes the Regge limit means $x_B \rightarrow 0$ at fixed Q^2 , whereas the limit underlying the collinear factorization theorems is $Q^2 \rightarrow \infty$ at fixed x_B . Whether for finite values of Q^2 and x_B one approximation scheme of the other is appropriate (or both) can at present not be decided from theory and is at times controversial in practice.

8.1 Collinear factorization and beyond

The description of hard scattering processes we have used so far is based on collinear factorization, hard scattering kernels evaluated at fixed order in α_s , and the resummation of logarithms $\alpha_s^m (\alpha_s \log Q^2)^n$ to all orders in n by DGLAP evolution or its nonforward generalization. In the small- x limit one has however a two-scale problem, $s \gg Q^2 \gg \Lambda_{\text{QCD}}^2$, and large logarithms $\log \frac{1}{x}$ appear in loops. Their resummation to all orders of perturbation theory can be performed using different schemes with different accuracy of the resulting scattering amplitudes, such as leading power in $1/Q$, resummed leading logarithms $(\alpha_s \log \frac{1}{x})^n$, resummed leading double logarithms $(\alpha_s \log Q^2 \log \frac{1}{x})^n$, etc. An important ingredient in this context are k_T dependent, or unintegrated parton distributions and

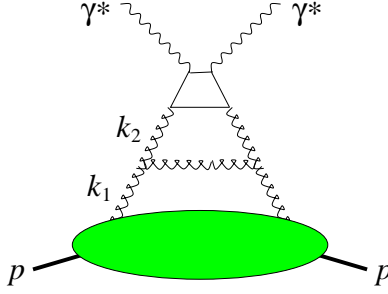


Figure 38: Two-loop diagram for the forward Compton amplitude.

corresponding hard scattering kernels, where k_T denotes the transverse momentum of the partons entering the hard scattering [419, 420]. The simplest definition of the k_T dependent gluon density is through

$$xg(x, \mu^2) = \int^{\mu^2} \frac{d\mathbf{k}^2}{\mathbf{k}^2} f(x, \mathbf{k}^2), \quad (328)$$

but there are more sophisticated versions taking into account k_T effects to different accuracy, which may include an additional dependence of the unintegrated density on a renormalization scale μ^2 . For a recent overview we refer to [421]. k_T dependent GPDs have been discussed in a particular scheme by Martin and Ryskin [422]. Notice that the usual collinear factorization framework also partly takes into account finite k_T of partons within hadrons: this is the case for the gluon with momentum k_2 in the two-loop diagram of Fig. 38, where the transverse momentum resulting from the splitting of the gluon with momentum k_1 explicitly appears in the hard scattering kernel. Conversely, using only the one-loop hard scattering coefficient together with the unintegrated gluon density takes into account part of the two-loop corrections of the collinear framework.

A particular factorization scheme for amplitudes like $\gamma^* p \rightarrow \gamma^* p$ at high energy originates in the BFKL framework [423, 424, 425, 414] at leading $\log \frac{1}{x}$ accuracy. It can be formulated in terms of color dipoles [426, 427, 428], as shown in Fig. 39a for $\gamma^* p \rightarrow \gamma^* p$ with longitudinal γ^* polarization. The imaginary part of the forward scattering amplitude then takes the form

$$\text{Im } \mathcal{A}(\gamma_L^* p \rightarrow \gamma_L^* p) \propto \int d^2 \mathbf{r} \int dz \tilde{\Psi}^*(\mathbf{r}, z) \sigma_{q\bar{q}}(\mathbf{r}, x_B) \tilde{\Psi}(\mathbf{r}, z), \quad (329)$$

where $\tilde{\Psi}$ denotes the impact parameter wave function for a $q\bar{q}$ pair in a photon of virtuality Q^2 , see Section 3.11.2. Because of translation invariance $\tilde{\Psi}$ only depends on the difference $\mathbf{r} = \mathbf{b}_q - \mathbf{b}_{\bar{q}}$ of quark and antiquark positions. $\sigma_{q\bar{q}}$ is the total cross section for scattering a $q\bar{q}$ dipole with transverse size \mathbf{r} on the target (related to the corresponding forward elastic amplitude by the optical theorem). This scattering conserves the quark helicities, which are to be summed over in (329) and have not been displayed. The factorization formula has a natural interpretation in the target rest frame, where it corresponds to a sequence of processes: the γ^* splitting into $q\bar{q}$ far ahead of the target by a distance of order $1/(x_B m)$, the interaction of this $q\bar{q}$ pair with the target, and its recombination into a γ^* .

This dipole factorization scheme can be derived in the leading $\log \frac{1}{x}$ approximation, requiring Q^2 only to be sufficiently large to use perturbation theory. Its result coincides with the one of collinear factorization if one takes the limit of leading power in $1/Q$ and of the leading double logarithm $\log Q^2 \log \frac{1}{x}$ in each scheme. Identifying the two results one obtains the relation

$$\sigma_{q\bar{q}}(\mathbf{r}, x) \sim \mathbf{r}^2 \alpha_s xg(x) \quad (330)$$

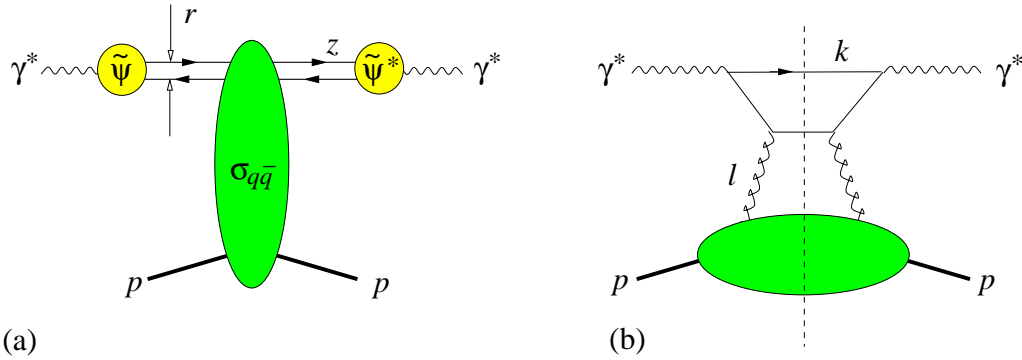


Figure 39: Imaginary part of the forward Compton amplitude in the dipole picture (a) and in collinear factorization (b).

at small dipole separation \mathbf{r} , which is selected in the process by taking large Q^2 . The factorization scale of the gluon density here is of order $\mu^2 \sim 1/r^2$, corresponding to $\mu^2 \sim Q^2$ after convoluting with the γ^* wave functions in (329), and the same holds for the scale of α_s . A more precise statement cannot be made at leading $\log Q^2$ accuracy. Similarly, since one has taken the leading $\log \frac{1}{x}$ limit one obtains the gluon distribution evaluated at x_B and not as an integral over gluon momentum fractions x as in the full calculation in the collinear factorization diagram shown in Fig. 39b.

The BFKL dipole formalism can be extended to scattering at finite t , or equivalently at definite impact parameter between the dipole and the target state, with a dipole-target scattering amplitude depending in addition on t or on the impact parameter [429]. In the analog of (330) the GPD H^g or its impact parameter equivalent will then appear instead of $xg(x)$. We also note that BFKL dynamics is not restricted to the unpolarized sector, and there are studies of the polarized proton structure function g_1 [430] and of the double helicity-flip structure function of a photon target [431].

The simple physical picture expressed in the dipole formalism makes it appealing to use it beyond the limits where its validity has so far been firmly established. Strictly speaking, we already did this in applying (329) to a proton target, since the derivation of the dipole representation requires a target whose structure is amenable to perturbation theory, such as a heavy quarkonium state [427, 428]. A further step is to use dipole factorization also for processes like $\gamma^*p \rightarrow \rho p$ or $\gamma p \rightarrow \gamma p$, where one or both wave functions in (329) cease to be perturbatively calculable. As \mathbf{r} becomes comparable to a hadronic scale, the relation between the dipole cross section and the gluon distribution no longer holds, and one can currently only model the behavior of $\sigma_{q\bar{q}}$ in this region.

There are other limits of extending the dipole formalism in its simple form, namely when going beyond the leading $\log \frac{1}{x}$. Bialas et al. [432] have shown that exactly taking into account the kinematical correlation between the plus-momentum fractions and the k_T of the gluons in the diagram of Fig. 39b is incompatible with the conservation of the dipole size in Fig. 39a. BFKL calculations at the next-to-leading $\log \frac{1}{x}$ level further indicate that not only $q\bar{q}$ dipoles but also higher Fock states in the photon like $q\bar{q}g$ will need to be explicitly taken into account [433].

Finally, the effect of nonzero skewness ξ in nonforward processes is beyond the leading $\log \frac{1}{x}$ approximation, which cannot distinguish between different small momentum fractions of the same order. This was already observed in the early study of Bartels and Loewe [17], who considered BFKL dynamics in processes like $\gamma^*p \rightarrow Zp$ and found that the relevant variable for the energy logarithm is the larger of ξ and ρ defined in (260). By the same token, $H^g(x, \xi, 0)$ for $x \gtrsim \xi$ and the usual gluon density $xg(x)$ taken at momentum fraction ξ cannot be distinguished to this precision, as emphasized by Brodsky et al. [19]. It remains to be seen whether and how the effect of different parton momentum

fractions can be taken into account beyond leading $\log \frac{1}{x}$ in the dipole picture or in an extension of it.

There is on the other hand physics at small x which goes beyond the description in terms of parton distributions and collinear factorization. An example of topical interest is the phenomenon of parton saturation (see [434] for a recent overview). Under DGLAP evolution to high scales μ , the density of partons at small x continues to increase, but one can expect that the density of partons in a given phase space cannot become arbitrarily large and at some point will “saturate”. This phenomenon can be implemented phenomenologically into the dipole formalism through a corresponding behavior of the dipole cross section $\sigma_{q\bar{q}}(\mathbf{r}, x_B)$, and even a simple model ansatz as the one of Golec-Biernat and Wüsthoff [435] is remarkably successful in describing data for a large class of small- x processes in ep scattering. For presently available energies and observables the situation remains however ambiguous as to whether the leading-twist description breaks down and saturation sets in.

Another example of physics that cannot be described by leading-twist GPDs (but can within the BFKL approach) is given by processes where due to quantum numbers the minimal number of gluons exchanged in the t -channel is three instead of two. In the framework of Regge theory this corresponds to the odderon, which is the $P = C = -1$ counterpart of the pomeron. Compared with quark-antiquark exchange in the t -channel this does not correspond to the minimal number of external partons in the hard scattering subprocess and is hence power suppressed in the hard scale at given x . On the other hand, three-gluon exchange increases faster than $q\bar{q}$ exchange as x decreases at given Q^2 and should hence dominate at high energies. No firm evidence for odderon exchange in hard or soft processes so far exists. Suggestions to search for three-gluon exchange in hard processes have been made for $\gamma^*p \rightarrow \eta_c p$ in [436, 437], for electroproduction of various mesons with positive charge parity in [438], and for $\gamma^*p \rightarrow \pi^+\pi^- p$ in [439, 273]. In the latter case the interference between pion pairs in the C -odd and C -even state (respectively produced by the exchange of two and three gluons) can be accessed in C -odd angular asymmetries (see Section 9.4.2).

Whether GPDs and collinear factorization, or an appropriate generalization to k_T dependent GPDs as suggested in [422], provide an appropriate framework to describe physics in a given range of Q^2 and small x remains to be seen (as it does for the description of DIS by collinear factorization). On the other hand, GPDs so far present the only framework where effects of skewness, which are beyond a description at leading $\log \frac{1}{x}$ precision, are explicitly taken into account.

8.2 Longitudinal vs. transverse photons

In processes involving light quarks longitudinal and transverse virtual photons play distinct roles in the context of factorization. We have already seen this in Section 7.1 and shall now investigate this issue in the specific context of small x . To this end, consider the forward Compton amplitude as shown in Fig. 39b. Calculating the relevant four cut diagrams in the small- x limit and expressing the lower blob by the unintegrated gluon distribution (328) one obtains

$$\text{Im } \mathcal{A} \propto \int d^2\mathbf{l} d^2\mathbf{k} dz K(\mathbf{l}, \mathbf{k}, z) \frac{f(x_B, \mathbf{l}^2)}{\mathbf{l}^4}. \quad (331)$$

The plus-momentum fraction of the gluon in the cut diagrams is $x = x_B$ up to terms of order \mathbf{k}^2/Q^2 or \mathbf{l}^2/Q^2 . To simplify the discussion we have taken the leading $\log \frac{1}{x}$ approximation and set $x = x_B$. The quark loop kernel can be written as the overlap of photon wave functions,

$$K(\mathbf{l}, \mathbf{k}, z) = \Psi^*(\mathbf{k}, z) \left[\Psi(\mathbf{k} + \mathbf{l}, z) + \Psi(\mathbf{k} - \mathbf{l}, z) - 2\Psi(\mathbf{k}, z) \right]. \quad (332)$$

The crucial difference between transverse and longitudinal photons can be traced back to their wave functions. For massless quarks they read²³

$$\begin{aligned}
\Psi_{\lambda\lambda'}^0(\mathbf{k}, z) &= 2ee_q \frac{z\bar{z}Q}{z\bar{z}Q^2 + \mathbf{k}^2} \delta_{\lambda, -\lambda'}, \\
\Psi_{+-}^+(\mathbf{k}, z) &= -\sqrt{2}ee_q \frac{z(k^1 + ik^2)}{z\bar{z}Q^2 + \mathbf{k}^2}, \\
\Psi_{-+}^+(\mathbf{k}, z) &= \sqrt{2}ee_q \frac{\bar{z}(k^1 + ik^2)}{z\bar{z}Q^2 + \mathbf{k}^2}, \\
\Psi_{++}^+ &= \Psi_{--}^+ = 0,
\end{aligned} \tag{333}$$

where the upper index refers to the photon helicity and the lower indices to the quark and antiquark, respectively. The wave functions $\Psi_{\lambda\lambda'}^-$ are obtained from $\Psi_{-\lambda-\lambda'}^+$ via parity invariance. The denominators in (333) correspond to the off-shell quark propagators in the cut diagrams of Fig. 39b. The quark or antiquark is guaranteed to be off-shell by an order Q^2 , except for asymmetric configurations where z or \bar{z} is close to 0. Such configurations are suppressed by the numerator factors of the wave functions for longitudinal photons, but not for transverse ones.

The typical scale for the dependence of the quark loop kernel (332) on \mathbf{l}^2 is $\mu^2 \sim z\bar{z}Q^2 + \mathbf{k}^2$. For z away from the endpoints this is much larger than the hadronic scale governing the \mathbf{l}^2 dependence of $f(x_B, \mathbf{l}^2)$. The leading logarithmic behavior in Q^2 is then obtained by Taylor expanding $K(\mathbf{l}, \mathbf{k}, z)$ around $\mathbf{l} = 0$, corresponding to the region $\mathbf{l}^2 \ll \mu^2$, and taking μ^2 as the upper integration limit. The lowest nonvanishing term in this expansion is proportional to \mathbf{l}^2 after integration over the azimuth of \mathbf{l} , and one obtains

$$\text{Im } \mathcal{A} \propto \int d^2\mathbf{k} dz \Psi^*(\mathbf{k}, z) \left[\frac{\partial}{\partial k^i} \frac{\partial}{\partial \bar{k}^i} \Psi(\mathbf{k}, z) \right] \int^{\mu^2} \frac{d\mathbf{l}^2}{\mathbf{l}^2} f(x_B, \mathbf{l}^2). \tag{334}$$

With the help of (328) one readily identifies the last integral as the usual gluon density at a factorization scale μ^2 . For longitudinal photon polarization the integral over z in (334) is dominated by values of $z \sim \frac{1}{2}$ due to the factor $z\bar{z}$ in the photon wave functions, and one has recovered the collinear factorization at the leading $\log Q^2$ level.

For transverse photons, however, the end-point regions in z are not suppressed. Taking the scale μ^2 of the gluon density fixed one can explicitly perform the integration over \mathbf{k} and obtains a logarithmically divergent integral $\int_0^1 dz (z\bar{z})^{-1}$. One may formally render this finite by taking literally the dependence $\mu^2 \sim z\bar{z}Q^2$ in the gluon density (328), which for $z\bar{z} \rightarrow 0$ will then also vanish and make the z integration finite [440, 396]. In the region of small $z\bar{z}$ the initial approximation $\mathbf{l}^2 \ll z\bar{z}Q^2 + \mathbf{k}^2$ leading to (334) was however not justified from the start, and such a procedure can only be sensible if the endpoint regions do not give a substantial contribution to the result. Even without approximating (331) by (334) one has an amplitude with contributions from the region where \mathbf{l}^2 , \mathbf{k}^2 , and $z\bar{z}Q^2$ are of hadronic size. In this region the starting expression (331) does not reflect a separation of soft and hard physics, since the quark virtualities in the kernel K are not perturbatively large. For these ‘‘aligned jet’’ configurations it is then appropriate to factorize the diagrams into the quark or antiquark distributions and a hard scattering $\gamma^*q \rightarrow \gamma^*q$ or $\gamma^*\bar{q} \rightarrow \gamma^*\bar{q}$, where the parton entering the hard scattering is the one with small z or \bar{z} .²⁴ The same discussion holds not only for

²³The normalization of the photon wave function used in the context of small- x physics differs in general from the one we have introduced in Section 3.11.

²⁴Note that the calculation discussed here uses Feynman gauge for the gluons. A gluon attached to the parton with large z or \bar{z} in Fig. 39b then contributes to the Wilson line in the definition of the quark distribution.

the forward Compton amplitude $\gamma_T^* p \rightarrow \gamma_T^* p$ but also for DVCS, $\gamma_T^* p \rightarrow \gamma p$, where the aligned jet region leads to the quark handbag diagram in Fig. 1b.

For light meson production such as $\gamma^* p \rightarrow \rho p$ the discussion goes along similar lines, with $\Psi^*(\mathbf{k}, z)$ in (332) replaced by the relevant meson light-cone wave function, and $f(x_B, \mathbf{l}^2)$ with the corresponding unintegrated generalized gluon distribution, which at $t = 0$ is equal to the forward distribution in the leading $\log \frac{1}{x}$ limit. With longitudinal photons one obtains the collinear approximation for the gluons in the leading $\log Q^2$ approximation as above. A definite statement about the situation for transverse photon or meson polarization can only be made when specifying the behavior of the meson wave function. Unless one takes this to be strongly suppressed for $z\bar{z} \rightarrow 0$ one finds again the above problem of infrared sensitivity, see e.g. [396]. How important this region is and whether a perturbative factorization as in (331) can be justified for the production of light mesons from transverse photons remains controversial in the literature, compare e.g. [440] and [441]. Contrary to Compton scattering one cannot factorize the diagram in terms of a quark distribution and a hard scattering subprocess, since the coupling of the meson to the quark lines is itself nonperturbative.

In the case where both the γ^* and the meson have longitudinal polarization, one can proceed and take the collinear approximation on the meson side by neglecting \mathbf{k}^2 compared with $z\bar{z}Q^2$ in the photon wave function. The integration over \mathbf{k} then concerns only the meson wave function (when taking a \mathbf{k} independent scale μ^2 in the gluon distribution) and gives the meson distribution amplitude at a factorization scale of order Q^2 . Together with the approximation leading to the k_T integrated gluon distribution, one then has obtained the collinear factorization formula of Section 5.1 at leading double $\log \frac{1}{x} \log Q^2$.

For massive quarks the starting expression (331) remains valid, with the appropriate photon wave functions given e.g. in [442]. The quark helicities in the $\gamma^* p$ c.m. are not changed by the interaction with the gluons; this is a feature of the coupling of a vector particle to a fast-moving fermion. For heavy quarks the end-point region in z is not associated with low virtualities in the quark loop, since the denominator of the photon wave functions then reads $(z\bar{z}Q^2 + \mathbf{k}^2 + m_q^2)$. Assuming that m_c is large enough to warrant a perturbative treatment one can hence use the factorized expressions (331) or (334) for the charm quark loop in the Compton amplitude with either longitudinal or transverse photons, and for any polarization in charmonium production from a real or virtual photon. For the production of heavy mesons, the appropriate argument of the gluon density in the leading $\log \frac{1}{x}$ approximation is

$$x = \frac{Q^2 + M_V^2}{W^2} \quad (335)$$

instead of $x_B \approx Q^2/W^2$. This corresponds to $\xi \approx x/2$ as given in (261) for DDVCS kinematics, with Q' replaced by M_V .

It is easy to translate the preceding discussion into the impact parameter representation, which is used in the dipole picture. Starting from (332) one rewrites

$$\int d^2\mathbf{k} K(\mathbf{l}, \mathbf{k}, z) = -64\pi^4 \int d^2\mathbf{r} \tilde{\Psi}^*(\mathbf{r}, z) (1 - e^{i\mathbf{l}\mathbf{r}}) (1 - e^{-i\mathbf{l}\mathbf{r}}) \tilde{\Psi}(\mathbf{r}, z). \quad (336)$$

Inserting this into the starting expression (331) and comparing with (329) one finds that

$$\sigma_{q\bar{q}}(\mathbf{r}, x_B) \propto \int \frac{d^2\mathbf{l}}{\mathbf{l}^4} f(x_B, \mathbf{l}^2) (1 - e^{i\mathbf{l}\mathbf{r}}) (1 - e^{-i\mathbf{l}\mathbf{r}}). \quad (337)$$

Under the same requirements as discussed above one now obtains the leading $\log Q^2$ approximation by Taylor expanding $(1 - e^{i\mathbf{l}\mathbf{r}}) (1 - e^{-i\mathbf{l}\mathbf{r}})$ around $\mathbf{l} = 0$ for the region $\mathbf{l}^2 \mathbf{r}^2 \ll 1$ and integrating over \mathbf{l}^2 up to $\mu^2 \sim 1/\mathbf{r}^2$. The leading term is proportional to $\mathbf{l}^2 \mathbf{r}^2$ after integration over the azimuth of \mathbf{l} and

gives the double leading logarithmic relation (330) between the dipole cross section and the gluon density.

For $\gamma_L^* p \rightarrow \rho_L p$ one obtains (336) with $\tilde{\Psi}^*$ replaced by the impact parameter wave function of the meson. The photon wave function has a logarithmic divergence at $\mathbf{r} = 0$ and varies with \mathbf{r} over typical distances of order $1/Q$, whereas the \mathbf{r} dependence of the meson wave function is controlled by the much larger meson radius. Approximating \mathbf{r}^2 with a value of order $1/Q^2$ in the meson wave function one obtains the impact parameter analog of the collinear approximation on the meson side.

8.3 The t dependence

Our discussion so far has focused on the scattering amplitude at $t = 0$ (or more precisely at $t = t_0 \approx -4\xi^2 m^2$, which is negligible in the kinematics of interest). Important physics resides however in the dependence on t or on the impact parameter, and on its interplay with the other variables. Within the dipole formalism one can identify the impact parameter \mathbf{b} as the distance between the transverse centers of momentum of the dipole and of the target [442]. The dipole cross section then depends on two transverse vectors \mathbf{r} and \mathbf{b} with a nontrivial interplay. In the limit where one can connect the dipole cross section with the nonforward gluon distribution, \mathbf{b} becomes the distance between the gluon on which one scatters and the transverse center of the target, as we already have seen in Section 3.10.

The t dependence is correlated with the longitudinal variable x . In a Regge theory description, a single pole with a linear trajectory gives for instance a factor $x^{-\alpha' t} = \exp[\alpha' t \log \frac{1}{x}]$. Translated to impact parameter this states that the transverse extension of the target increases logarithmically with energy. Bartels and Kowalski [443] have argued that in processes with a hard scale this phenomenon is intimately related with the dynamics of confinement.

On a practical level, most small- x studies of meson production or DVCS describe the t -dependence by an exponential ansatz

$$\frac{d\sigma(\gamma^* p)}{dt} \propto e^{Bt}, \quad (338)$$

where B may depend on x_B and on Q^2 in the sense of an “effective power”. We remark that the validity of such an exponential form may be restricted to rather small t and should not be taken for granted over a wide t range.

8.4 Vector meson production

The production of vector mesons ρ^0 , ω , ϕ and J/Ψ , $\Psi(2S)$, Υ at small x_B and small t has been studied quite extensively in theory. Measurements in the x_B range from 10^{-4} to 10^{-2} have been made by H1 and ZEUS at HERA. We do not attempt here a complete review of the subject but concentrate on issues regarding the description in terms of GPDs and the wider question of how adequate a leading-twist description is in experimentally accessible kinematics. An extensive review of the experimental situation up to 1997 has been given by Crittenden [444], for a recent overview see [445]. Original references are [446, 447, 448, 449, 450] and [451, 452, 453, 454, 455] for electroproduction of light mesons, and [446, 456, 457, 458, 459, 460] and [453, 461, 462, 463] for photo- and electroproduction of heavy mesons. Salient features of the data are [445]:

- The dependence on W for photoproduction of light mesons is comparable to the energy dependence of elastic hadron-hadron scattering, whereas it becomes significantly steeper if either Q^2 or the meson mass are large. This is in line with the change in energy dependence of $\sigma_{\text{tot}}(\gamma^* p)$ as one goes from the photoproduction limit to the deeply inelastic region.
- In ρ production the slope parameter B defined by (338) decreases as Q^2 increases from zero to several GeV^2 , down to values comparable to those measured in J/Ψ photoproduction [459, 463].

- The production cross sections of ρ , ω , ϕ plotted as a function of $Q^2 + M_V^2$ closely follow a common curve when rescaled by the factors $\rho : \omega : \phi = 9 : 1 : 2$ explained in Section 5.3. To a lesser degree of accuracy the same holds for J/Ψ production when rescaling according to $\rho : J/\Psi = 9 : 8$ (see our comment in Section 8.4.2).
- Preliminary data are consistent with the ratio of $d\sigma/dt$ for elastic and proton dissociative ρ electroproduction being independent of Q^2 .

These features support the qualitative picture of $\gamma^*p \rightarrow Vp$ at large Q^2 or large M_V^2 which follows from Fig. 2b, with

- a quark loop at the top, which has little t -dependence and satisfies flavor SU(3) symmetry, up to SU(3) breaking effects due to the meson wave functions (see [305] for a discussion) and due to quark masses in kinematics where they are important,
- a quantity describing gluon exchange with the proton, whose behavior at fixed small t is similar to the x behavior of the usual gluon density at scale $\mu^2 \sim Q^2 + M_V^2$.

The γ^*p cross section just discussed corresponds to a mixture of transverse and longitudinal photons, and is to a good approximation $\sigma(\gamma^*p) \approx \sigma_T + \sigma_L$ in the kinematics of the experiments. Detailed studies of the helicity structure in vector meson production have been carried out using angular distributions, with the most precise data available for ρ production [448, 450, 454]:

- The ratio $R = \sigma_L/\sigma_T$ increases as a function of Q^2 , but is significantly smaller than $R = Q^2/M_\rho^2$ in electroproduction, taking a value of $R = 1$ for $Q^2 \approx 2 \text{ GeV}^2$. The behavior of R above $Q^2 = 10 \text{ GeV}^2$ is not easy to assess because statistical errors are still rather large. Preliminary data suggest that for fixed Q^2 there is little dependence of R on W in the high-energy region $W > 40 \text{ GeV}$ [445].
- s -channel helicity conservation (SCHC) is approximately observed in the data but broken at the 10% level, with the dominant helicity changing transition at large Q^2 being $\gamma_T^* \rightarrow \rho_L$.

8.4.1 The gluon distribution

The description of ρ electroproduction by two-gluon exchange and a quark loop has a long history, starting with work by Donnachie and Landshoff [464]. Brodsky et al. [19] have analyzed the process in the framework of factorization: the scattering amplitude for $\gamma_L^* p \rightarrow \rho_L p$ at $t = 0$ was obtained in terms of the meson distribution amplitude, and of the forward gluon density evaluated at $x = x_B$ and $\mu^2 = Q^2$ since the analysis was done to leading double $\log \frac{1}{x} \log Q^2$ accuracy.

The choice of factorization scale in the gluon distribution entails a considerable uncertainty at small x_B , where the scaling violation in $g(x_B, \mu^2)$ is particularly strong. This affects both the overall normalization of the cross section and its dependence on x_B and Q^2 . Although the choice of scale remains principally undetermined at leading $\log Q^2$ accuracy, an “educated guess” of appropriate scale is phenomenologically of great importance in the absence of a full NLO calculation of the process. We remark that commonly the renormalization scale in α_s is taken equal to the scale of the gluon distribution, or equal to $\mathbf{1}^2$ if the unintegrated gluon density (328) is used. Frankfurt et al. [305, 465, 466, 467] estimate the scale in $g(x_B, \mu^2)$ by a procedure based on the dipole representation (329) and (330) for $\gamma_L^* p \rightarrow \gamma_L^* p$ and for $\gamma_L^* p \rightarrow \rho_L p$. The estimated scale for ρ production is found to be lower than Q^2 , corresponding to larger average dipole sizes \mathbf{r}^2 in ρ production than in the forward longitudinal Compton amplitude. The same procedure was applied by the authors to heavy quarkonium production. Martin et al. [468, 440, 469, 470] advocate the scale $\mu^2 = \frac{1}{4}(Q^2 + M_V^2)$ as

argument of $g(x, \mu^2)$. In numerical studies they use the unintegrated density. For \mathbf{I}^2 above a value \mathbf{I}_0^2 where $g(x, \mathbf{I}^2)$ is available from global parton analyses $f(x, \mathbf{I}^2)$ is calculated from (328), supplemented by a Sudakov form factor in [470], whereas for \mathbf{I}^2 below \mathbf{I}_0^2 different procedures are used, see [471]. Compared with using the collinear gluon density, an increase of the cross section was found when including the gluon k_T .

Efforts have also been undertaken to improve on the leading $\log \frac{1}{x}$ approximation and take into account the finite skewness in meson production. Kinematics tells us that x in (335) is the difference $x_1 - x_2$ of plus-momentum fractions for the emitted and the reabsorbed gluon, where both fractions refer to the incoming proton. In the DGLAP region, which gives the imaginary part of the amplitude, one has $x_1 \geq x$. In studies of Υ and J/Ψ production, Frankfurt et al. [466, 467] have estimated typical values for x_1 , identified the generalized and forward gluon at a starting scale and then evolved up to the hard scale of the process. In [467] the relation (330) between the dipole cross section and the gluon density was only used at small \mathbf{r} , whereas an ansatz was made for the behavior of $\sigma_{q\bar{q}}$ at larger \mathbf{r} , thereby going beyond a leading-twist description. Martin et al. [469, 470] estimated skewness effects with the relation (250) obtained in the Shuvaev model for the ratio R^g of $H^g(\xi, \xi)$ and $2\xi g(2\xi)$, with $2\xi \approx x$ given by (335). The authors report significant enhancement factors from skewness for the cross sections of ρ and J/Ψ electroproduction at large Q^2 . These factors also influence the Q^2 dependence, since the effective power λ in the gluon density depends on Q^2 . Put in more general terms, the scale dependence of the nonforward and the forward gluon distribution is not the same.

For photoproduction of Υ , both groups [466, 469] find significant enhancement from their estimates of skewness, since at the corresponding large scales μ^2 the gluon density is very steep. They emphasize that the enhancement factor for the cross section is essential for describing data [462, 459], being about 2 with $\mu^2 = \frac{1}{4}M_\Upsilon^2$ in [469] and about 2.3 with μ^2 between 40 and 75 GeV² in [466]. Ma and Xu [472] obtain a description of the data using the forward model (235) for the gluon GPD, with an enhancement factor $R^g = 2^\lambda$ and a scale $\mu^2 = m_b^2$. In all three studies the contribution from the real part of the scattering amplitude, obtained from the imaginary part using (323), is significant given the steepness of the gluon density.

We remark that vector meson production has been studied in the dipole formalism by several groups, using the analog of (329) together with a model for the dipole cross section, see e.g. [473, 474, 475, 476]. Munier et al. [477] have taken the “reverse” approach and attempted to extract the dipole cross section at given impact parameter using the measured cross section for $\gamma_L^* p \rightarrow \rho_L p$ and different models for the ρ wave function. No definite conclusion concerning the onset of parton saturation (which implies the breakdown of the leading-twist description) in current data could be drawn in this study. The same holds for J/Ψ production: Gotsman et al. [478] find better agreement with the data when including saturation effects, whereas Frankfurt et al. [467] do not require saturation while making a particular choice of factorization scale. Dosch and Ferreira [476] have modeled saturation effects in J/Ψ photoproduction in the dipole approach and found them too small to be identified in present data, given other theoretical uncertainties and experimental errors.

8.4.2 The meson wave function

A substantial source of theoretical uncertainty in the normalization and the Q^2 dependence of light meson electroproduction is due to the \mathbf{k} dependence of the meson light-cone wave functions. Frankfurt et al. [305, 465] have compared the convolution (334) of wave functions for $\gamma_L^* p \rightarrow \rho_L p$ with its collinear approximation, where \mathbf{k} in the photon wave function is set to zero, and found large suppression factors in the cross section due to the meson \mathbf{k} . Values at $Q^2 = 10$ GeV² are between about 0.64 and 0.06, with variations due to the parameters taken in the wave functions but above all to its assumed large- \mathbf{k} behavior, which ranged from a Gaussian falloff at large \mathbf{k}^2 to a power-law decrease

like $1/\mathbf{k}^2$. The $1/\mathbf{k}^2$ behavior is generated by hard gluon exchange between the quark and antiquark, which gives rise to the ERBL evolution of the distribution amplitude. Rather than an estimate of higher-twist effects, its explicit inclusion in the hard scattering thus is an estimate of higher-loop corrections, similar to the use of unintegrated parton distributions we discussed after (328). Comparison with experiment [453] indicates that the very strong suppression from a $1/\mathbf{k}^2$ falloff, together with the choice made in [305] for the scale of the gluon distribution underestimates the data. The suppression factor of 0.64 quoted above corresponds to a wave function proposed by Halperin and Zhitnitsky [225], who report large cancellations between the $1/Q^2$ and the $1/Q^4$ corrections to the collinear approximation when expanding (334) in moments $\int d^2\mathbf{k} \mathbf{k}^{2n} \Psi_\rho(\mathbf{k}^2, z)/Q^{2n}$. In such a situation, successive improvement of the leading-twist expression by higher-power terms in $1/Q^2$ would be an unfortunate strategy.

Martin et al. [440, 470] have proposed to describe the transition from $q\bar{q}$ to the meson not by a wave function but by using parton-hadron duality, based on the picture that a $q\bar{q}$ pair with invariant mass M in the vicinity of m_ρ has few other channels to hadronize into (an isospin factor of 9/10 allowing for ω production is taken into account). They project the amplitude for open $q\bar{q}$ production onto the relevant partial wave and integrate over a certain range of $M^2 = \mathbf{k}^2/(z\bar{z})$ at the level of the cross section. This approach is taken for both $\gamma_L^* p \rightarrow \rho_L p$ and $\gamma_T^* p \rightarrow \rho_T p$. In the latter case there are non-negligible contributions from soft regions of phase space, but the integrals are finite and the authors report little variation of the results when changing the parameter \mathbf{l}_0^2 mentioned above, which separates the hard and the soft regime in the unintegrated gluon density. The overall normalization is difficult to predict in this framework (due to the choice of mass window in M^2), and a substantial K -factor estimating higher-order corrections in α_S was used in [440]. In particular the measured Q^2 dependence of the ratio $R = \sigma_L/\sigma_T$ is however well described. That its growth is slower than a linear behavior like Q^2/M_ρ^2 can be traced back to the fact that σ_T is sensitive to the gluon density at lower scale μ^2 than σ_L (as emphasized earlier by Nemchik et al. [479]), and that the increase of $g(x, \mu^2)$ with μ^2 is faster at low values of μ^2 . This result is not special to using parton-hadron duality. In fact, Ivanov and Kirschner [396] have obtained the same expression for R as in [440], using a particular ansatz for the structure of the meson wave function. The helicity dependence of the ρ wave function in this ansatz is taken as for a photon, given by $\bar{u}\not{\epsilon}_\rho v$, where u and v are massless on-shell spinors for the quark and antiquark and ϵ_ρ is the meson polarization vector. This is proportional to the corresponding rotation functions $e^{i\mu\varphi} d_{1\mu}^1(\theta)$, where μ denotes the meson helicity and φ, θ the azimuthal and polar angles of the quark in the meson rest frame. The meson production cross section in [396] has the structure

$$\frac{d\sigma}{dt} \propto \left| \int dM^2 \int d(\cos\theta) d\varphi \mathcal{A}_{q\bar{q}}(M, \theta, \varphi) w(M) e^{-i\mu\varphi} d_{1\mu}^1(\theta) \right|^2, \quad (339)$$

where $\mathcal{A}_{q\bar{q}}$ describes the production of a $q\bar{q}$ -pair with squared invariant mass $M^2 = \mathbf{k}^2/(z\bar{z})$, and $w(M)$ comes from the meson wave function. This is similar to the structure of the result using parton-hadron duality,

$$\frac{d\sigma}{dt} \propto \int_{M_1^2}^{M_2^2} dM^2 \left| \int d(\cos\theta) d\varphi \mathcal{A}_{q\bar{q}}(M, \theta, \varphi) e^{-i\mu\varphi} d_{1\mu}^1(\theta) \right|^2, \quad (340)$$

in particular in the dependence on $\cos\theta = 2z - 1$, which is sensitive to the polarizations of meson and photon and which determines the typical scale of hardness in the quark propagators $z\bar{z}Q^2 + \mathbf{k}^2 = z\bar{z}(Q^2 + M^2)$. Ivanov and Kirschner have used the ansatz (339) to calculate not only the helicity conserving transitions with longitudinal and transverse photons, but also the helicity violating ones.

Their leading power behavior was found to be

$$\begin{aligned} \mathcal{A}_{0,0} &\sim 1/Q, & \mathcal{A}_{1,1} &\sim 1/Q^2, \\ \mathcal{A}_{0,1} &\sim 1/Q^2, & \mathcal{A}_{1,0} &\sim 1/Q^3, & \mathcal{A}_{1,-1} &\sim 1/Q^2, \end{aligned} \quad (341)$$

where the first subscript refers to the meson and the second to the photon helicity. A sensitivity like $(z\bar{z})^{-1}$ to aligned-jet configurations was found in $\mathcal{A}_{1,1}$, $\mathcal{A}_{0,1}$, $\mathcal{A}_{1,0}$, as well as in a $1/Q^4$ contribution to $\mathcal{A}_{1,-1}$. A rather good description of the HERA data on the helicity structure of ρ [448, 450, 454] and ϕ [449] production can be obtained in the model. Similar results were obtained by Kuraev et al. [480], who used constituent wave functions for the ρ .

For heavy-quark systems like the J/Ψ or the Υ the simplest approximation to the light-cone wave function is the static ansatz $\Psi(\mathbf{k}, z) \propto \delta^{(2)}(\mathbf{k}) \delta(z - \frac{1}{2})$ together with a quark mass $m_q = \frac{1}{2}M_V$. Ryskin et al. [468] have investigated corrections to this, including a Gaussian \mathbf{k} dependence of the wave function in the hard scattering while keeping $z = \frac{1}{2}$. They find that the ensuing suppression tends to be canceled by taking a current quark mass m_c instead of $\frac{1}{2}M_{J/\Psi}$ in the hard scattering (especially for photoproduction the cross section depends on a high power of m_c^{-1}). Frankfurt et al. [465] have reached different conclusions, in particular including in $\Psi(\mathbf{k}, z)$ a nontrivial z dependence of and taking a perturbative falloff like $1/\mathbf{k}^2$ at large \mathbf{k} . They obtain suppression factors for the photoproduction cross section as small as 0.25 relative to taking the static wave function and $m_q = \frac{1}{2}M_{J/\Psi}$. This suppression becomes weaker for large Q^2 and eventually turns into an enhancement, in accordance with our arguments in Section 7.4.

A commonly used way to obtain the meson light-cone wave function is by a kinematical transformation of the Schrödinger wave function calculated e.g. in a potential model. This corresponds to the calculation of GPDs in constituent quark models discussed in Section 4.1.4. Hüfner et al. [474] have pointed out the importance in charmonium production of including the Melosh transform between the different spin bases used in rest-frame Schrödinger wave functions and in light-cone wave functions. They further caution that the purely kinematic transform between the two wave functions has the status of a model since in quantum field theory the connection between matrix elements at equal time x^0 and equal light-cone time x^+ includes dynamical effects.

Frankfurt et al. [465] have pointed out that a non-relativistic description of charmonium is problematic since it typically yields wave functions with a significant part of high-momentum modes not satisfying $v \ll c$. For bottomonium the situation is less critical, and the suppression compared with the static approximation found in [465] for Υ is rather mild.

An expectation often encountered in the literature is that at small x the electroproduction cross sections for ρ , ω , ϕ , J/Ψ should behave as 9 : 1 : 2 : 8 in the limit where $Q^2 \gg M_{J/\Psi}$. This holds if these ratios are followed by the squared integrals $[\sum_q e_q \int dz z^{-1} \Phi^q(z)]^2$ of the respective distribution amplitudes. The squared integrals $[\sum_q e_q \int dz \Phi^q(z)]^2$ are proportional to $M_V \Gamma_{V \rightarrow e^+e^-}$, whose measured values for the *light* mesons (see Section 5.3) fit rather well with the above ratios, which follow from flavor SU(3) and the neglect of mixing between $q\bar{q}$ and gluon configurations. As pointed out in [305] the extension to flavor SU(4) fails however quite badly, with experimental values $(M_\rho \Gamma_{\rho \rightarrow e^+e^-}) : (M_{J/\Psi} \Gamma_{J/\Psi \rightarrow e^+e^-}) \approx 9 : (3.5 \times 8)$. This is not surprising for quantities determined by physics at scales not larger than the respective meson masses. Furthermore, the respective z dependence of the distribution amplitudes may well differ between light and heavy mesons, unless $\log Q^2$ is so large that even $\Phi_{J/\Psi}(z)$ has evolved to the asymptotic shape. If the quantities $[\sum_q e_q \int dz z^{-1} \Phi^q(z)]^2$ relevant for electroproduction were to follow the naive SU(4) expectation 9 : 8 for ρ versus J/Ψ at some factorization scale, this would be a rather accidental conspiracy of two SU(4) breaking effects.

8.4.3 Dynamics and observables

The description of $\gamma_L^* p \rightarrow V_L p$ at small x to leading-twist and leading $O(\alpha_s)$ accuracy (implying the leading $\log Q^2$ approximation) allows very direct access to the gluon structure of the proton. In particular, the meson structure only appears through a global factor $\sum_q e_q \int dz z^{-1} \Phi^q(z)$ in the amplitude. Let us try and assess how particular observables are affected by the various corrections we have discussed.

- *The overall normalization* of the cross section may be severely affected by finite meson \mathbf{k} in the hard scattering subprocess according to estimates. It is hence most sensitive to the details of the meson wave function.
- *The Q^2 dependence* is influenced by several sources. It may be strongly affected by the finite \mathbf{k} effects just mentioned. Its theoretical description is subject to the uncertainty in relating the factorization scale of the gluon distribution with Q^2 .

We note that in many experimental studies the Q^2 dependence of the $\gamma^* p$ cross section is given and parameterized at fixed W^2 , whereas the predictions of the factorization theorems are for fixed x_B .

- *The dependence on x_B* is again strongly influenced by the choice of scale in the gluon distribution. Physics beyond leading twist such as saturation will affect the x_B behavior, but the data does at present not allow one to decide whether such effects are at work in HERA kinematics.

One may expect less impact on the x_B dependence from the details of the meson structure. Such a cross-talk does exist at some level: in the approach of Frankfurt et al. the choice of scale in the gluon distribution is for instance connected with the relevant dipole sizes in the convolution $\int dz \tilde{\Psi}^*(\mathbf{r}, z) \tilde{\Psi}(\mathbf{r}, z)$ of photon and meson wave functions. How important such cross-talk may be has however not been studied quantitatively.

- *The t dependence* may also be expected to be rather independent of the detailed meson structure. Again there is a caveat of cross-talk via the resolution scale of the process: in the leading-twist approximation the behavior of $H^g(x, \xi, t)$ with t depends on the scale μ^2 where the gluons are probed. Indeed evolution in μ^2 changes the t dependence unless it is completely uncorrelated with the dependence on x .

In light of this discussion a better control of the relevant resolution scale in meson production would be of great importance. To put the theoretical discussion on a firmer footing, a full next-to-leading order calculation is called for, which would also include effects of the meson structure at small distance (i.e. at large \mathbf{k}).

8.5 DVCS

Let us now turn to DVCS in the small- x regime of the H1 and ZEUS measurements [259, 299]. In Section 5.2 we have already discussed the NLO analyses in the GPD framework by McDermott and Freund [298, 286, 110] and by Belitsky et al. [244]. Contrary to vector meson production, the forward and nonforward Compton amplitudes for transverse photons receive important contributions from the quark distributions (at least for “standard” choices of the factorization scale). In the dipole representation this is related to the importance of aligned-jet configurations for transverse photons. Apart from the leading-twist analyses, a number of other approaches have been applied to DVCS at small x , which we shall briefly present.

An early study by Frankfurt et al. [481] starts by modeling the ratio

$$R(Q^2, x_B) = \frac{\text{Im}[\mathcal{A}(\gamma_T^* p \rightarrow \gamma_T^* p)]}{\text{Im}[\mathcal{A}(\gamma_T^* p \rightarrow \gamma p)]_{t=0}} \quad (342)$$

at $Q_0^2 = 2.6 \text{ GeV}^2$, using an ansatz based on the aligned-jet model. The change of the amplitudes with Q^2 is then investigated using nonforward evolution, which at small x is dominated by the gluon distribution. H^g at the starting scale was fixed by the ansatz (245). The authors find little variation of the ratio R for Q^2 between Q_0^2 and 45 GeV^2 , with R between 0.5 and 0.58 for x_B of order 10^{-2} to 10^{-4} . The real part of the DVCS amplitude is recovered by a derivative analyticity relation and the t -dependence as described in Section 8.3. The numerator of (342) is proportional to the transverse inclusive structure function $F_T = F_2 - F_L$. For estimating the DVCS cross section in [481], F_L was assumed to be negligible in the relevant kinematics, and F_T was approximated with the measured F_2 [482].

DVCS has been analyzed in the dipole formalism by Donnachie and Dosch [483], by McDermott et al. [484], and by Favart and Machado [485] with different models for the dipole cross section. We remark that, even though $\sigma_{q\bar{q}}(\mathbf{r}, x_B)$ does not take skewness into account, the amplitudes for $\gamma_T^* p \rightarrow \gamma_T^* p$ and for DVCS differ in the dipole formulation because the analog of the master formula (329) involves the overlap of different wave functions for DIS and for DVCS. The studies [484, 485] compared the \mathbf{r} dependence of $\sigma_{q\bar{q}}(\mathbf{r}, x_B) \int dz \tilde{\Psi}^*(\mathbf{r}, z) \tilde{\Psi}(\mathbf{r}, z)$ in both cases. As expected, the typical dipole size is larger in DVCS than in F_T at equal Q^2 (except in the limit $Q^2 \rightarrow 0$ where both agree by definition); by exactly how much is somewhat model dependent. The results of all the studies mentioned here [481, 483, 484, 485] are in agreement with the H1 data within errors.

A special feature of DVCS is that through interference with the Bethe-Heitler process in $ep \rightarrow ep\gamma$ it allows measurement of both imaginary and real part of the scattering amplitude (see Section 9.1). The derivative analyticity relation (323) suggests that $\text{Re}\mathcal{A}$ does not carry any new information compared to $\text{Im}\mathcal{A}$ in the high-energy region. This does not seem to hold in practice. Frankfurt et al. [486] report that different parameterizations of the small- x data for $F_2(x_B, Q^2)$ lead to quite distinct predictions for $\text{Re}\mathcal{A}_{\text{DVCS}}$, in particular when comparing power-law and logarithmic parameterizations of the x_B -dependence. A similar finding has been made in the study by McDermott et al. [484], where the predictions of two different models for the dipole cross section are much more similar for $\text{Im}\mathcal{A}_{\text{DVCS}}$ than for $\text{Re}\mathcal{A}_{\text{DVCS}}$. This indicates that in a finite range of x_B different curves may describe the cross section data within errors, but have rather different slopes in $\log x_B$. Note that assessing the importance of higher derivatives with respect to $\log x_B$ in (323) requires even higher quality of data for $\text{Im}\mathcal{A}$, so that direct measurement of $\text{Re}\mathcal{A}$ may indeed contribute important extra information.

We finally note that DVCS gives direct access to the Compton amplitude with a transverse γ^* (the transition $\gamma_L^* p \rightarrow \gamma p$ being suppressed at large Q^2 and small t), in contrast to inclusive DIS, where the separation of F_T and F_L requires measurement at different beam energies. The inclusive structure function F_2 and the DVCS amplitude may thus show important differences beyond the effects of skewness. We remark in particular that an estimate by Bartels et al. [487] found in certain regions of small x_B and moderate Q^2 important twist-four effects in F_T and in F_L , which largely canceled in their sum F_2 .

8.6 Other diffractive channels

A different type of small- x processes which can be studied at HERA and where gluon GPDs are relevant are diffractive reactions $\gamma^{(*)} p \rightarrow Xp$ with suitable non-exclusive final states X . For a general review we refer to [488]. Golec-Biernat et al. [112] have investigated the effect of skewness in the “exclusive” production of dijets, described by $\gamma^{(*)} p \rightarrow q\bar{q} + p$ at parton level, and pointed out interesting

effects due to the kinematical correlation between the longitudinal momenta of the gluons and the large transverse momentum \mathbf{k} of the jets. This reaction is not easy to access: states corresponding to $q\bar{q}g$ or more complicated configurations at parton level dominate in a large part of phase space, and a dedicated experimental study is not yet available for events in a region where a sole $q\bar{q}$ pair should adequately describe the diffractive final state.

Another case of interest is the diffractive production of charm, where the channel $\gamma^{(*)}p \rightarrow c\bar{c} + p$ allows description in terms of gluons GPDs. Here the charm quark mass protects against the infrared sensitive region of aligned-jet configurations, as in the case of J/Ψ production. Again, this channel has to be separated from states with additional gluons at parton level. Dominance of $c\bar{c}$ over $c\bar{c}g$ and higher states can be expected at large values of $\beta = Q^2/(Q^2 + M^2)$, i.e., at small invariant mass M of the diffractive system [471].

For inclusive diffraction $\gamma^*p \rightarrow X + p$ the situation is similar. In order to have X adequately represented by a $q\bar{q}$ pair one needs to go to large β [488]. For light quarks, however, the aligned-jet region is part of the phase space. With the collinear approximation for the gluons in the hard scattering one finds integrals behaving as $\sigma_L \sim \int dz (z\bar{z})^{-1}$ and $\sigma_T \sim \int dz (z\bar{z})^{-2}$, depending on the photon polarization, so that one has to go back to the unintegrated gluon distribution or introduce some infrared regularization. A detailed study of this process in the context of GPDs has been performed by Hebecker and Teubner [489]. The authors estimate in particular that a region where a GPD based description is viable and where the cross section is dominated by σ_L (which is less infrared sensitive than σ_T) is given by $\Lambda^2/Q^2 \ll 1 - \beta \ll (\Lambda^2/Q^2)^{1/2}$, where Λ is a hadronic scale.

9 Phenomenology

In this section we present the basic phenomenology of the reactions where GPDs and GDAs can be accessed. The phenomenological analysis can be separated into two distinct steps, as was discussed in detail for DVCS in [490]. The first step is to go from differential cross sections of processes like $ep \rightarrow ep\gamma$ or $ep \rightarrow epp$ to amplitudes for $\gamma^*p \rightarrow \gamma p$ or $\gamma^*p \rightarrow \rho p$. These can then be analyzed making use of the factorization theorems. This first means to test whether the general scaling and helicity structure is as predicted for the regime of leading-twist dominance (see Section 5.1). If this is the case, the task remains to extract GPDs from the appropriate process amplitudes, where they appear in convolutions with the hard scattering kernels. How to tackle this “deconvolution” problem remains an outstanding task for theory, and its status will be discussed in Section 9.5.

The principles of analyzing meson electroproduction have long been established, see for instance the detailed work on vector meson production by Schilling and Wolf [491]. The phenomenology of two-photon reactions like DVCS is special because of competing Bethe-Heitler processes. On one hand this makes their analysis more involved, but on the other hand it provides much more detailed access to the amplitudes at two-photon level which one aims to study. We will report on the detailed work that has been done for DVCS. The situation for the cross-channel counterparts $\gamma p \rightarrow \gamma^*p$ and the annihilation of $\gamma^*\gamma$ into hadron pairs is very similar, and we shall point out important special aspects of these reactions. For processes involving two off-shell photons the corresponding theory is in the process of development. First brief results have been given for DDVCS in [282, 492], whose phenomenology combines the cases of DVCS and of TCS.

9.1 DVCS

DVCS is measured in electro- or muoproduction of real photons, $ep \rightarrow ep\gamma$ or $\mu p \rightarrow \mu p\gamma$. In the kinematics of relevance for the factorization theorems the lepton mass is negligible and will be set to zero in the following. The two cases can then be considered on equal footing. For definiteness we

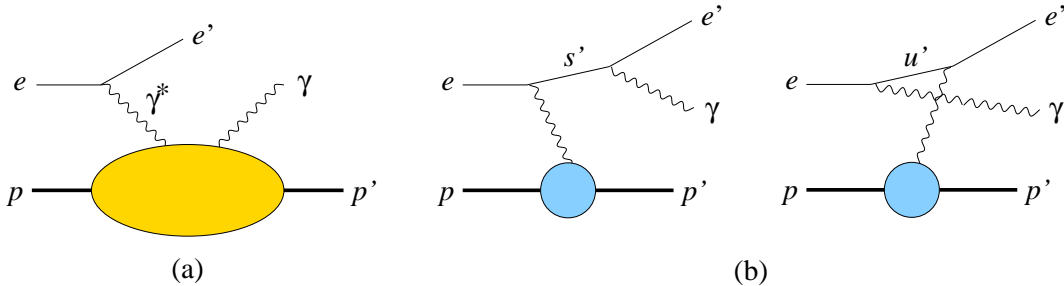


Figure 40: (a) Compton scattering and (b) Bethe-Heitler contributions to $ep \rightarrow ep\gamma$.

will refer to electroproduction in the following and also specialize to targets with spin $\frac{1}{2}$. Aspects of targets with spin zero or one will be discussed in Section 9.1.6. Apart from Compton scattering, the Bethe-Heitler process contributes to the same final state (see Fig. 40), and both mechanisms have to be added in the amplitude. In particular situations, the interference term between both mechanisms can be used to study $\gamma^*p \rightarrow \gamma p$ at amplitude level, including its phase. Belitsky and Müller [140] have compared this situation with holography, in the sense that the phase of the Compton amplitude is measured against the known “reference phase” of the Bethe-Heitler process. With lepton beams of both charges one can filter out the interference term, as remarked long ago by Brodsky et al. [493]. In a similar way one can use the beam polarization asymmetry, as was observed by Kroll et al. [494] in the context of virtual Compton scattering at large t . The general structure of $ep \rightarrow ep\gamma$ at twist-two level was first discussed by Ji [22]. A strategy to analyze DVCS in the context of the $1/Q$ expansion was proposed in [490] and forms the basis of our presentation here. Belitsky et al. have investigated in detail how the cross section of $ep \rightarrow ep\gamma$ is related to integrals involving GPDs at twist-two [293] and twist-three [495, 244] accuracy. Detailed numerical predictions for DVCS observables using models for twist-two GPDs were made by Vanderhaeghen et al. [303, 253, 304], by Belitsky et al. [293], and by Freund and McDermott [298, 110]. Studies for particular fixed-target experiments can be found in [496] for JLAB, in [497, 498] for HERMES, and in [499] for COMPASS. Predictions at twist-three level were made in [200, 37], [244], and [500]. DVCS with the $p \rightarrow \Delta$ transition, $ep \rightarrow e\Delta^+\gamma$, is briefly discussed in [188, 37], and the more general case of the $p \rightarrow p\pi^0$ and $p \rightarrow n\pi^+$ transitions has recently been investigated in [190].

The dynamics of the $\gamma^*p \rightarrow \gamma p$ subprocess can be parameterized in different ways. A form factor decomposition of the hadronic tensor $T^{\alpha\beta}$ defined in (270) has for instance been used in [244]. Alternatively one may use the helicity amplitudes $e^2 M_{\lambda\mu',\lambda\mu}$ defined in (271), which we find particularly suitable given their immediate physical interpretation. With the constraints from parity invariance there are 12 such amplitudes for DVCS, of which four conserve the photon helicities, four describe single helicity flip and four describe double helicity flip of the photon. Both the Compton form factors and the helicity amplitudes depend only on the kinematical variables Q^2 , t , and x_B (which may be traded for ξ). Additional variables needed to describe the electroproduction process are the usual inelasticity parameter y or the ratio ϵ of longitudinal and transverse polarization of the virtual photon in DVCS,

$$y = \frac{k \cdot p}{q \cdot p}, \quad \epsilon = \frac{1 - y - \delta}{1 - y + y^2/2 + \delta} \quad (343)$$

with $\delta = y^2 x_B^2 m^2 / Q^2$, and the azimuthal angle ϕ between hadron and lepton planes defined in Fig. 41.²⁵

²⁵This definition follows the convention used by HERMES [501] and by CLAS [502]. It is related to the angle used in [490] by $\phi_{\text{here}} = -\varphi_{[490]}$ and to the one in [244] by $\phi_{\text{here}} = \pi - \phi_{[244]}$.

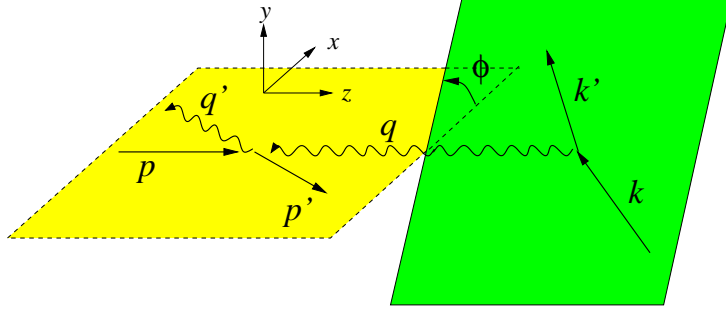


Figure 41: Kinematics of $ep \rightarrow ep\gamma$ in the c.m. of the final-state proton and photon.

The Bethe-Heitler process can be calculated given the knowledge of the electromagnetic proton form factors, which are well measured at small t (see e.g. [254]). One can hence give exact expressions for the differential $ep \rightarrow ep\gamma$ cross section in terms of the Compton amplitudes. Since however the theoretical description of the Compton process is based on an expansion in $1/Q$ at fixed x_B and t , it is meaningful to apply the same expansion to the Bethe-Heitler process. This expansion reveals a simple structure of the electroproduction cross section in the kinematics of DVCS [490, 293, 244]. Treating the Bethe-Heitler process exactly (while approximating the Compton process to twist-two or three accuracy) is of course possible at the level of a numerical analysis, as has for instance been done in [303, 200].

The differential electroproduction cross section on an unpolarized target is given by

$$\frac{d\sigma(ep \rightarrow ep\gamma)}{d\phi dt dQ^2 dx_B} = \frac{\alpha_{\text{em}}^3}{8\pi} \frac{x_B y^2}{Q^4} \frac{1}{\sqrt{1 + 4x_B^2 m^2/Q^2}} \frac{1}{e^6} \sum'_{\text{spins}} |\mathcal{T}_{\text{VCS}} + \mathcal{T}_{\text{BH}}|^2, \quad (344)$$

where \sum'_{spins} denotes the sum over the spins of the final-state proton and photon and the average over the initial proton polarization. The contribution from Compton scattering is

$$\begin{aligned} \frac{1}{e^6} \sum'_{\text{spins}} |\mathcal{T}_{\text{VCS}}|^2 &= \frac{1}{Q^2} \frac{2}{1-\epsilon} \sum_{\lambda'\lambda} \left[\frac{|M_{\lambda'+,\lambda+}|^2 + |M_{\lambda'+,\lambda-}|^2}{2} + \epsilon |M_{\lambda'+,\lambda 0}|^2 \right. \\ &\quad - \cos\phi \sqrt{\epsilon(1+\epsilon)} \operatorname{Re} \left\{ M_{\lambda'+,\lambda+}^* M_{\lambda'+,\lambda 0} - M_{\lambda'+,\lambda-}^* M_{\lambda'+,\lambda 0} \right\} - \cos 2\phi \epsilon \operatorname{Re} \left\{ M_{\lambda'+,\lambda+}^* M_{\lambda'+,\lambda-} \right\} \\ &\quad \left. - P_\ell \sin\phi \sqrt{\epsilon(1-\epsilon)} \operatorname{Im} \left\{ M_{\lambda'+,\lambda+}^* M_{\lambda'+,\lambda 0} - M_{\lambda'+,\lambda-}^* M_{\lambda'+,\lambda 0} \right\} \right] \end{aligned} \quad (345)$$

where P_ℓ is the lepton beam polarization, $-1 \leq P_\ell \leq 1$. The full expression of the Bethe-Heitler contribution can be found in [244]. To make its behavior in DVCS kinematics apparent we take the limit of large Q at fixed t , x_B , y and ϕ , and require in particular that $1 - x_B$ and $1 - y$ be large compared with m^2/Q^2 . Expanding in $1/Q$ we get

$$\frac{1}{e^6} \sum'_{\text{spins}} |\mathcal{T}_{\text{BH}}|^2 = -\frac{1}{t} \frac{4}{\epsilon} \frac{1}{P} \left[\frac{1-\xi^2}{\xi^2} \frac{t-t_0}{t} \left(F_1^2 - \frac{t}{4m^2} F_2^2 \right) + 2(F_1 + F_2)^2 + O\left(\frac{1}{Q}\right) \right] \quad (346)$$

with the Dirac and Pauli form factors F_1 , F_2 evaluated at momentum transfer t . The factor $P = 1 + \cos\phi O(1/Q)$ will be discussed shortly. In the same expansion the interference term reads

$$\frac{1}{e^6} \sum'_{\text{spins}} (\mathcal{T}_{\text{BH}}^* \mathcal{T}_{\text{VCS}} + \mathcal{T}_{\text{VCS}}^* \mathcal{T}_{\text{BH}}) = e_\ell \frac{1}{t} \frac{m}{Q} \frac{8\sqrt{2}}{\xi} \frac{1}{P}$$

$$\begin{aligned}
& \times \left[\cos \phi \frac{1}{\sqrt{\epsilon(1-\epsilon)}} \operatorname{Re} \widehat{M}_{++} - \cos 2\phi \sqrt{\frac{1+\epsilon}{1-\epsilon}} \operatorname{Re} \widehat{M}_{+0} - \cos 3\phi \sqrt{\frac{\epsilon}{1-\epsilon}} \operatorname{Re} \widehat{M}_{+-} \right. \\
& \left. + P_\ell \sin \phi \sqrt{\frac{1+\epsilon}{\epsilon}} \operatorname{Im} \widehat{M}_{++} - P_\ell \sin 2\phi \operatorname{Im} \widehat{M}_{+0} + O\left(\frac{1}{Q}\right) \right], \tag{347}
\end{aligned}$$

where $e_\ell = \pm 1$ is the lepton beam charge. We have not yet used the Q^2 behavior of the Compton amplitudes $M_{\lambda'\mu',\lambda\mu}$ at this point, i.e., the terms denoted by $O(1/Q)$ in (347) involve Compton amplitudes multiplied with kinematical factors going at least like $1/Q$. We have introduced linear combinations

$$\widehat{M}_{\mu'\mu} = \frac{1}{2} \sum_{\lambda'\lambda} g_{\lambda'\lambda} M_{\lambda'\mu',\lambda\mu} \tag{348}$$

with coefficients

$$\begin{aligned}
g_{++} &= \frac{\sqrt{t_0-t}}{2m} [F_1 + \xi(F_1 + F_2)], \\
g_{--} &= \frac{\sqrt{t_0-t}}{2m} [F_1 - \xi(F_1 + F_2)], \\
g_{+-} &= \sqrt{1-\xi^2} \frac{t_0-t}{4m^2} F_2, \\
g_{-+} &= -\sqrt{1-\xi^2} \frac{t_0-t}{4m^2} F_2 - \frac{2\xi^2}{\sqrt{1-\xi^2}} (F_1 + F_2). \tag{349}
\end{aligned}$$

Notice that $\widehat{M}_{+\mu} \propto \sqrt{t_0-t}$ since g_{-+} is multiplied with $M_{-+,\mu}$, which due to angular momentum conservation vanishes at $t = t_0$ at least like $\sqrt{t_0-t}$. Our phase convention for the Compton amplitudes is to take the (usual) helicity spinors of Appendix B for the proton and the photon polarizations specified in Section 5.2, using the coordinate system shown in Fig. 41.²⁶

The relative weight of the Compton and Bethe-Heitler cross sections is parametrically given by

$$|\mathcal{T}_{\text{VCS}}|^2 : |\mathcal{T}_{\text{BH}}|^2 \sim \left(\frac{1}{Q^2} \frac{1}{1-\epsilon} \right) : \left(-\frac{1}{t} \frac{1}{\epsilon} \right), \tag{350}$$

with the interference term being of order of their geometric mean. The condition $Q^2 \gg -t$ of DVCS favors the Bethe-Heitler contribution to start with. This can be counteracted by having ϵ close to 1, i.e., small y . This means a large ep c.m. energy \sqrt{s} at given Q^2 and x_B , or large x_B at given Q^2 and \sqrt{s} , given the relation $yx_B = Q^2/(s-m^2)$. We notice in (346) that the Bethe-Heitler cross section grows like ξ^{-2} at small ξ , except in the very forward region where $|t_0-t| \ll |t_0|$. According to our discussion in Section 4.4 one expects a small- x behavior like $\xi^{-(1+\lambda)}$ with some $\lambda > 0$ for the leading-twist Compton amplitudes, so that the Compton cross section should increase somewhat faster than the Bethe-Heitler one at small ξ .

The lepton virtualities in the Bethe-Heitler graphs of Fig. 40 are $s' = (q' + k')^2$ and $u' = (q' - k')^2$. They are given by

$$\begin{aligned}
s' &= \frac{Q^2}{y} \left[1 - \frac{2\sqrt{1-y}\sqrt{t_0-t}}{Q} \sqrt{\frac{1-\xi}{1+\xi}} \cos \phi \right] + O(t, m^2), \\
-u' &= \frac{Q^2}{y} \left[1 - y + \frac{2\sqrt{1-y}\sqrt{t_0-t}}{Q} \sqrt{\frac{1-\xi}{1+\xi}} \cos \phi \right] + O(t, m^2) \tag{351}
\end{aligned}$$

²⁶Different phase conventions were used in [490], and the proton helicity conserving DVCS amplitudes there differ from the ones used here by a global sign.

and hence ϕ independent to leading order in $1/Q$. It turns however out that for experimentally relevant kinematics, this dependence is numerically not always negligible, as has been emphasized in [293, 244]. Because the leading term in u' is proportional to $1 - y$, this holds in particular for the kinematics of the HERMES and CLAS measurements [260, 261], where y is not small. Neglecting the $\cos \phi$ terms is an even worse approximation in $1/(s'u')$, which appears in the cross section, because the geometric series $(1 - x)^{-1} = 1 + x + \dots$ converges rather slowly. This is why we have kept the ratio of exact and approximated propagators

$$P = \frac{-s'u'}{(1-y)y^{-2}Q^4} \quad (352)$$

in the expressions of the Bethe-Heitler and interference terms above (the exact expressions for the propagators can be found in eqs. (28) to (32) of [244]). Taking this ratio into account is particularly important in an angular analysis of the Compton process, which we now discuss.

9.1.1 Angular structure

Let us take a closer look on how the simple angular structure in (346) and (347) comes about and how general it is. To this end we write both \mathcal{T}_{VCS} and \mathcal{T}_{BH} as a product of a leptonic and a hadronic tensor, the latter being the Compton tensor for VCS and the proton-photon vertex for Bethe-Heitler. For Compton scattering we have introduced polarization vectors (275) of the intermediate photon with momentum q , and in analogy we introduce polarizations for the photon of momentum Δ in the Bethe-Heitler process. We choose these vectors, as well as the polarizations of the external particles, with reference only to the hadronic plane (i.e., define them in terms of the momenta p, p', q) and contract them with the hadronic and leptonic tensors. The hadronic parts of the amplitudes are then ϕ independent and all ϕ dependence is explicit in the leptonic parts. Further ϕ dependence arises if the target has a definite polarization longitudinal or transverse to the lepton beam (see Section 9.1.2). We obtain the expression (345) for the unpolarized Compton cross section and a similar one with target polarization. For the Bethe-Heitler part we get

$$\sum_{\text{spins}} \rho_{\tilde{\lambda}\lambda} |\mathcal{T}_{\text{BH}}|^2 = \sum_{\substack{\lambda', \tilde{\lambda}, \lambda \\ \tilde{\nu}, \nu}} L_{\text{BH}}(P_\ell, \tilde{\nu}, \nu) \Gamma_{\tilde{\nu}\lambda'\tilde{\lambda}}^* \Gamma_{\nu\lambda\lambda} \rho_{\tilde{\lambda}\lambda}, \quad (353)$$

where \sum_{spins} denotes summation over the spins of incoming and outgoing particles. $\rho_{\tilde{\lambda}\lambda}$ is the spin density matrix of the target, with helicities λ and $\tilde{\lambda}$ in the amplitude and its complex conjugate. The leptonic part L_{BH} of the squared amplitude depends on the lepton beam polarization (taken as longitudinal since transverse polarization effects are suppressed by the lepton mass) and on the helicities ν and $\tilde{\nu}$ of the photon with momentum Δ in the amplitude and its complex conjugate. Γ is the proton-photon vertex for fixed helicities. One finds that the denominators of the lepton propagators appear as $(s' - m_\ell^2)^{-1}(u' - m_\ell^2)^{-1}$ and $m_\ell^2(s' - m_\ell^2)^{-2}(u' - m_\ell^2)^{-2}$. If we neglect the lepton mass, L_{BH} can thus be written as $1/P$ times a trigonometric polynomial in ϕ . The P_ℓ independent part of this polynomial is of order 2, and the P_ℓ dependent part of order 1. Both parts are of order 0 to leading order in $1/Q$ as we see in (346).

Similarly, the interference term is

$$\begin{aligned} & \sum_{\text{spins}} \rho_{\tilde{\lambda}\lambda} \left(\mathcal{T}_{\text{BH}}^* \mathcal{T}_{\text{VCS}} + \mathcal{T}_{\text{VCS}}^* \mathcal{T}_{\text{BH}} \right) \\ &= \sum_{\substack{\lambda', \tilde{\lambda}, \lambda \\ \tilde{\nu}, \mu', \mu}} L_{\text{INT}}(P_\ell, \mu', \mu, \tilde{\nu}) \Gamma_{\tilde{\nu}\lambda'\tilde{\lambda}}^* M_{\lambda'\mu', \lambda\mu} \rho_{\tilde{\lambda}\lambda} + \text{c.c.} \end{aligned} \quad (354)$$

The leptonic part now has the form $1/P$ times a trigonometric polynomial in ϕ , with a P_ℓ independent part of order 3, and the P_ℓ dependent part of order 2. Its dependence on ϕ and the photon polarizations is

$$L_{\text{INT}} \propto \frac{1}{P(\cos \phi)} e^{i(\mu-2\mu')\phi} \delta_{\tilde{\nu}\mu'} + O\left(\frac{1}{Q}\right), \quad (355)$$

where the coefficient of $e^{\pm 3i\phi}$ does not depend on P_ℓ . This simple structure readily translates into the angular dependence in (347), where for fixed μ' each helicity μ comes with a different angular dependence, and where a $\sin 3\phi$ term is missing in the P_ℓ dependent part. The constraint $\tilde{\nu} = \mu'$ in the leading order part of L_{INT} has important consequences: in the interference term the Compton amplitudes $M_{\lambda'\mu',\lambda\mu}$ are summed over the proton helicities with weights $\Gamma_{\mu'\lambda'\tilde{\lambda}}^* \rho_{\tilde{\lambda}\lambda}$ that are

- dependent on ξ and t but not on ϵ ,
- the same for the P_ℓ independent and dependent part,
- the same for all μ at fixed μ' .

These properties are of course realized in (347) to (349), with the coefficients $g_{\lambda'\lambda}$ being just the proton-photon vertices $\Gamma_{+\lambda'\lambda}^*$ up to a global kinematical factor. They are also found in the explicit calculation for a polarized target [244]. One finds in particular that with different target polarizations one can obtain enough different weighting factors $\Gamma_{\mu'\lambda'\tilde{\lambda}}^* \rho_{\tilde{\lambda}\lambda}$ to separate the Compton amplitudes for different λ' , λ (see Section 9.1.4).

Going beyond the leading order in $1/Q$ one finds that for given μ and μ' other frequencies $e^{in\phi}$ appear in L_{INT} , suppressed by powers of $1/Q$. The interference term for an unpolarized target has the general ϕ dependence

$$P(\cos \phi) \frac{d\sigma_{\text{INT}}(ep \rightarrow ep\gamma)}{d\phi dt dQ^2 dx_B} = c_0 + c_1 \cos \phi + c_2 \cos 2\phi + c_3 \cos 3\phi + P_\ell (s_1 \sin \phi + s_2 \sin 2\phi), \quad (356)$$

where the c_i , s_i are linear combinations of the Compton amplitudes with prefactors depending on Q^2 , t , ξ and ϵ . Closer inspection reveals in particular that the amplitudes appear in the hierarchy

- $Q^{-1}M_{\lambda'+,\lambda+}$, $Q^{-2}M_{\lambda'+,\lambda 0}$, $Q^{-3}M_{\lambda'+,\lambda-}$ in c_0 ,
- $M_{\lambda'+,\lambda+}$, $Q^{-1}M_{\lambda'+,\lambda 0}$, $Q^{-2}M_{\lambda'+,\lambda-}$ in c_1 and s_1 ,
- $M_{\lambda'+,\lambda 0}$, $Q^{-1}M_{\lambda'+,\lambda-}$, $Q^{-3}M_{\lambda'+,\lambda+}$ in c_2 and s_2 .

The linear combination of the different twist-two amplitudes $M_{\lambda'+,\lambda+}$ in the subleading coefficient c_0 differs from the one in c_1 . We will come back to this in Section 9.1.4.

If one takes into account the power behavior predicted by the dynamical analysis of the factorization theorem (where $M_{\lambda'+,\lambda 0}$ is $1/Q$ suppressed compared with $M_{\lambda'+,\lambda+}$) one altogether finds that each Fourier coefficient in (356) is given by the leading-order formula (347) up to corrections of order $1/Q^2$ and not only $1/Q$. An analysis based on (347) should therefore be feasible even at moderately large Q^2 . In the analogous case of timelike Compton scattering (see Section 9.3) this was corroborated by numerical comparison of the interference term obtained with and without expanding the Bethe-Heitler amplitude in the inverse large scale [243].

An important corollary to the preceding discussion is that the ϕ dependence is a consequence of the *leptonic* part of the Bethe-Heitler and interference terms. The results of this subsection therefore

hold not only for the process $ep \rightarrow ep\gamma$, but for targets of *any* spin, and for the case where the target is scattered into a different hadron or hadronic system, whose details (including polarization) are unobserved in the measured cross section. This implies in particular that the principles of the angular analysis of $ep \rightarrow ep\gamma$ using the above results are not invalidated if there is a background of proton dissociation.

9.1.2 Beam and target polarization

Let us again specialize to a spin $\frac{1}{2}$ target, but allow for the possibility that the proton dissociates into a system of any spin. The angular analysis described in the previous subsection becomes modified in the presence of target polarization, since this polarization is experimentally fixed in the laboratory and not with respect to the scattering plane of the Compton process. Let us recall the essentials of the transformation from definite polarization in the laboratory (defined to be the target rest frame or a frame where electron and proton collide head on) to polarization with respect to the “hadronic” coordinate system of Fig. 41, where we have also defined the helicity states for the initial proton.

- Longitudinal polarization in the lab induces in the hadronic system a longitudinal polarization, plus a transverse polarization which is suppressed by a factor of order $2x_B m/Q$ and whose direction in the x - y plane depends on ϕ . The spin density matrix of the target is hence ϕ dependent to $1/Q$ accuracy, and an analysis of $1/Q$ suppressed terms in the interference term or the Compton part of the ep cross section will have the ϕ dependence modified compared with the unpolarized case.
- Transverse polarization in the lab induces in the hadronic system a transverse polarization whose direction depends on ϕ and on the azimuthal angle Ψ between the target polarization and the lepton scattering plane in the laboratory. It further induces a longitudinal polarization whose size depends on Ψ and is again suppressed by a factor of order $2x_B m/Q$. In this case the spin-density matrix of the target hence depends on ϕ already to leading order and accordingly modifies the angular structure compared with the unpolarized case.

Important constraints on the structure of the ep cross section follow from parity and time reversal invariance:

- Since the helicity and the covariant spin vector of a spin $\frac{1}{2}$ particle are parity odd, a single (beam or target) spin asymmetry must be proportional to the antisymmetric tensor $\epsilon_{\alpha\beta\gamma\delta}$, which is the only other parity odd structure available. This leads to an azimuthal dependence via $\sin(n\phi)$ (and $\sin(n\phi \pm \Psi)$ for transverse target polarization) with integer n . Conversely, the unpolarized cross section or a double (beam and target) spin asymmetry cannot be proportional to $\epsilon_{\alpha\beta\gamma\delta}$ and thus has an azimuthal dependence via $\cos(n\phi)$ and $\cos(n\phi \pm \Psi)$.
- The tensor $\epsilon_{\alpha\beta\gamma\delta}$ is odd under time reversal. Time reversal invariance implies that terms proportional to this tensor must involve absorptive parts of the scattering amplitude, i.e., correspond to possible on-shell intermediate states in the process. As we are working to leading order in α_{em} , the leptonic parts of the Compton and Bethe-Heitler amplitudes do not have absorptive parts. Together with the above consequence of parity invariance one thus finds that single spin asymmetries must go with $\text{Im}(M^*M)$, $\text{Im}(\Gamma^*M)$ or $\text{Im}(\Gamma^*\Gamma)$, whereas the unpolarized cross section and double spin asymmetries are proportional to the real parts of these products, where for simplicity we have omitted the helicity labels.²⁷ The elastic proton-photon vertex Γ does not have an imaginary part, so that $\text{Im}(\Gamma^*M) = \Gamma \text{Im} M$ and $\text{Im}(\Gamma^*\Gamma) = 0$.

²⁷The identification of the “imaginary” with the “absorptive” parts for M and Γ only holds if no further phases come from the proton or photon polarizations. This is the case for our phase convention.

An important consequence is that the Bethe-Heitler contribution is zero for *any* single-spin asymmetry on a spin $\frac{1}{2}$ target. This is an exact result to leading order in α_{em} ,²⁸ confirmed by the explicit calculation in [244] and generalizing the observation for the beam spin asymmetry of [494]. Notice that it no longer holds for proton dissociation, where the Bethe-Heitler contribution to single spin asymmetries must be estimated from the phases of the electromagnetic transition Γ from the proton to the final state. If however the cross section for $ep \rightarrow eX\gamma$ is summed over all hadronic final states X of given invariant mass (as is done when the proton remnant is not experimentally detected) one has again a zero Bethe-Heitler contribution to single spin asymmetries. This is readily seen by writing the Bethe-Heitler cross section as the contraction of a leptonic tensor with the imaginary part of the hadronic tensor for the forward Compton amplitude $\gamma^*(\Delta) + p \rightarrow \gamma^*(\Delta) + p$. Due to parity and time reversal invariance the respective lepton and proton polarization dependent parts of these tensors are antisymmetric, whereas the polarization independent parts are symmetric.

9.1.3 Cross sections and asymmetries

There are different observables from which information on the Compton amplitudes can be extracted. The pure Bethe-Heitler part of the differential ep cross section is calculable and can be subtracted, provided it does not dominate so strongly that the remainder would have unacceptably large errors. Such a subtraction has been performed in the cross section measurements at small x by H1 and ZEUS [259, 299]. As discussed in the previous subsection, a different possibility to eliminate the Bethe-Heitler contribution is to take the difference of cross sections for opposite beam or target polarization (the latter either longitudinal or transverse). In both cases, the cross section difference receives contributions from both Compton scattering and the Compton-Bethe-Heitler interference. The cleanest separation of these pieces can be achieved in experiments with beams of either charge. Since the Compton contribution to the ep amplitude is linear and the Bethe-Heitler contribution quadratic in the lepton charge, the interference term is projected out in the difference $d\sigma(e^+p) - d\sigma(e^-p)$ of cross sections, whereas it is absent in their sum.

To understand the relative importance of Compton and interference contributions in different observables, we schematically write

$$\begin{aligned} \frac{d\sigma_{\text{VCS}}}{d\phi dt dQ^2 dx_B} &= \frac{1}{Q^2} \sum_{\lambda'\lambda} \left[\dots |M_{\lambda'+,\lambda+}|^2 + \dots \cos \phi \operatorname{Re} (M_{\lambda'+,\lambda+}^* M_{\lambda'+,\lambda 0}) \right. \\ &\quad \left. + \dots P_\ell \sin \phi \operatorname{Im} (M_{\lambda'+,\lambda+}^* M_{\lambda'+,\lambda 0}) + O(Q^{-2}) + O(\alpha_s) \right] \end{aligned} \quad (357)$$

$$\begin{aligned} \frac{d\sigma_{\text{INT}}}{d\phi dt dQ^2 dx_B} &= \frac{1}{Q} \frac{e_\ell}{P(\cos \phi)} \sum_{\lambda'\lambda} \left[\dots Q^{-1} \operatorname{Re} M_{\lambda'+,\lambda+} \right. \\ &\quad \left. + \dots \cos \phi \operatorname{Re} M_{\lambda'+,\lambda+} + \dots \cos 2\phi \operatorname{Re} M_{\lambda'+,\lambda 0} \right. \\ &\quad \left. + \dots P_\ell \sin \phi \operatorname{Im} M_{\lambda'+,\lambda+} + \dots P_\ell \sin 2\phi \operatorname{Im} M_{\lambda'+,\lambda 0} + O(Q^{-2}) + O(\alpha_s) \right], \end{aligned} \quad (358)$$

with

$$P(\cos \phi) = 1 + \dots Q^{-1} \cos \phi + O(Q^{-2}), \quad (359)$$

where we have made explicit the dependence on ϕ and on the lepton charge and polarization. For the

²⁸The result even holds for the QED radiative corrections which are enhanced by logarithms of the lepton mass. These correspond to the additional emission of soft or collinear photons from the lepton and to the associated virtual corrections, and do not generate absorptive parts.

power counting we have now also used $M_{\lambda'+, \lambda_0} \sim 1/Q$ and $M_{\lambda'+, \lambda_-} \sim \alpha_s$. We see that when integrated over ϕ , the subtracted cross section $d\sigma/(dt dQ^2 dx_B) - d\sigma_{\text{BH}}/(dt dQ^2 dx_B)$ receives a contribution

- from Compton scattering, proportional to the squared leading twist amplitudes $|M_{\lambda'+, \lambda_+}|^2$,
- and from the interference term, at the level of $1/Q$ suppressed terms. Part of this contribution comes from the ϕ independent contribution in brackets and part from the $\cos \phi$ term, with both pieces involving the leading-twist amplitudes $\text{Re } M_{\lambda'+, \lambda_+}$. We remark that with the model GPDs used in [244], the total interference contribution to the ϕ integrated cross section was estimated to be at the percent level in the kinematics of the H1 measurement.

Another important observable is the cross section difference for different lepton helicities

$$P(\cos \phi) \left[\frac{d\sigma(e^\uparrow p)}{d\phi dt dQ^2 dx_B} - \frac{d\sigma(e^\downarrow p)}{d\phi dt dQ^2 dx_B} \right], \quad (360)$$

where the prefactor removes the ϕ dependence due to the lepton propagators. This observable has a $\sin \phi$ term, which receives a contribution from $d\sigma_{\text{INT}}$ going with $\text{Im } M_{\lambda'+, \lambda_+}$, and a contribution from $d\sigma_{\text{VCS}}$ involving the product of twist-two and twist-three amplitudes. Similarly, the subtracted unpolarized cross section

$$P(\cos \phi) \left[\frac{d\sigma(ep)}{d\phi dt dQ^2 dx_B} - \frac{d\sigma_{\text{BH}}(ep)}{d\phi dt dQ^2 dx_B} \right] \quad (361)$$

has a $\cos \phi$ term with an interference contribution involving $\text{Re } M_{\lambda'+, \lambda_+}$ and a contribution from $1/Q$ suppressed terms in $P(\cos \phi) d\sigma_{\text{VCS}}/(d\phi dt dQ^2 dx_B)$. It was estimated in [244] that despite being power suppressed, this Compton contribution can be comparable to the interference one, especially in the small x regime. To understand this, notice that $\text{Re}(M_{\lambda'+, \lambda_+}^* M_{\lambda'+, \lambda_0})$ contains the product of the imaginary parts of two Compton amplitudes, which at small x tend to be larger than the real parts. This recommends care when trying to extract $\text{Re } M_{\lambda'+, \lambda_+}$ from an angular analysis of the cross section alone, without the benefit of the beam charge asymmetry.

In cases where information on the Compton process is sought from the interference term, the analysis of the ϕ dependence becomes considerably cleaner if the measured cross section is re-weighted by the propagator factor $P(\cos \phi)$ as in (360) and (361), provided one has sufficient experimental resolution for the kinematic quantities $(q' + k')^2$ and $(q' - k')^2$. The weighted cross section is then a trigonometric polynomial, whose coefficients have a simple relation to the fundamental quantities describing the Compton process, at least for sufficiently large Q^2 (see Section 9.1.1). These coefficients are readily extracted by fitting the ϕ dependence or by additional weighting with $\cos(n\phi)$ and $\sin(n\phi)$, i.e., by measuring quantities like

$$\int d\phi \sin(\phi) P(\cos \phi) \frac{d\sigma(ep)}{d\phi dt dQ^2 dx_B} \quad (362)$$

and its analog for appropriate cross section differences. The weighted cross sections including the factor $P(\cos \phi)$ may be smaller than the ones without. This does *not* determine which of the two is more sensitive to the quantities to be extracted, since not only the size of the observable but also its error depends on the weight chosen. The same holds for the comparison of other weighting factors, for instance of $\text{sgn}(\sin \phi)$ instead of $\sin \phi$, which leads to an “up-down” asymmetry $\int_0^\pi d\phi (d\sigma/d\phi) - \int_\pi^{2\pi} d\phi (d\sigma/d\phi)$.

As discussed in Section 9.1.1 the coefficients of $\cos \phi$ or $\sin \phi$ in the re-weighted interference term are proportional to \widehat{M}_{++} and those of $\cos 2\phi$ or $\sin 2\phi$ are proportional to \widehat{M}_{+0} , up to corrections

in $1/Q^2$ if one is in a region where the Compton amplitudes have the power behavior predicted by the large Q^2 analysis. In contrast, angular distributions without re-weighting by $P(\cos \phi)$ have the dynamical information about Compton scattering entangled with $1/Q$ effects from the Bethe-Heitler propagators, which can be numerically important. These propagators depend strongly on t , see (351), and their effect cannot readily be separated in ϕ spectra integrated over a certain t range. For a particular parameterization of the relevant GPDs one can of course calculate the corresponding twist-two and twist-three Compton amplitudes and directly evaluate observables from them, as was for instance done in the study by Kivel et al. [200]. Given however the considerable freedom in modeling the dependence of the different GPDs on their three variables, the connection between the shape of GPDs and the differential ep cross section is highly nontrivial. The studies [200] and [244] found that twist-three amplitudes can have quite visible effects on observables in the kinematics of current experiments, for instance on the beam charge and to a lesser extent on the beam spin asymmetry. Only if one assumes twist-three quark-gluon correlation to be negligible are these twist-three amplitudes expressed in terms of the leading-twist input GPDs. A separation of Compton amplitudes with different dynamical twist, or similarly of Compton form factors as proposed in [244], should help towards keeping the analysis transparent and assessing possible ambiguities in attempting to extract GPDs from the data.

As discussed in [244], differences of absolute cross sections (for different polarizations or beam charges) are simpler to analyze theoretically than the corresponding asymmetries (normalized to the sum of relevant cross sections). This is because the denominator of these asymmetries also depends on unknown Compton amplitudes, which are in general different from those in the numerator. Notice that there are different versions of normalized observables. The complications in the analysis introduced by the normalization factor are for instance different for

$$A(\phi) = \frac{d\sigma(e^\uparrow p) - d\sigma(e^\perp p)}{d\sigma(e^\uparrow p) + d\sigma(e^\perp p)}, \quad (363)$$

and for

$$A^{\sin \phi} = \frac{2 \int d\phi \sin \phi \left[\frac{d\sigma(e^\uparrow p)}{d\phi} - \frac{d\sigma(e^\perp p)}{d\phi} \right]}{\int d\phi \left[\frac{d\sigma(e^\uparrow p)}{d\phi} + \frac{d\sigma(e^\perp p)}{d\phi} \right]} \quad (364)$$

or the analog with additional weighting factors $P(\cos \phi)$ under the integrals.²⁹ Note that the factor $1/P$ in the Bethe-Heitler and the interference term cancels only approximately in (363) when numerator and denominator are separately integrated over a range in t . Which observable presents the best compromise between theoretical and experimental uncertainties can only be decided case by case.

We finally remark on the specific situation for experiments with muon beams, which can e.g. be performed by the COMPASS experiment at the CERN SPS [499]. The natural polarization of muon beams produced from pion decays changes with the beam charge, and one may wonder what the separation power is for the combined reversal of beam charge and polarization. From (357) and (358) one readily finds that the corresponding difference of cross sections (where the Bethe-Heitler contribution drops out) contains the $\sin \phi$ term of $d\sigma_{\text{VCS}}$ and the $\cos(n\phi)$ terms of $d\sigma_{\text{INT}}$. The sum of cross sections involves the $\cos(n\phi)$ terms in $d\sigma_{\text{VCS}}$ and the $\sin(n\phi)$ terms in $d\sigma_{\text{INT}}$. This is a consequence of parity invariance as discussed in Section 9.1.2. Unless one of them strongly dominates, the Compton and interference contributions can hence be separated in such an experiment by the angular distribution, requiring in fact only a separation between terms even and odd under $\phi \rightarrow -\phi$.

²⁹The factor 2 in the numerator of $A^{\sin \phi}$ follows the HERMES convention [260] and has the effect that $A^{\sin \phi} = s/c$ for $d\sigma/d\phi = c + s P_\ell \sin \phi$.

9.1.4 Access to GPDs

The ultimate goal of studying Compton scattering in our context is the extraction of amplitudes which carry information about GPDs. Using the polarization and ϕ dependence of the ep cross section discussed in the previous sections one can first test in a model independent way whether the behavior in Q^2 is as predicted by the power counting arguments underlying the factorization theorem, and whether at given Q^2 power suppressed amplitudes like $M_{\lambda'+, \lambda_0}$ are indeed smaller than the leading-twist ones $M_{\lambda'+, \lambda+}$. To be sure, the detailed dynamics contributing to the $1/Q$ amplitudes $M_{\lambda'+, \lambda_0}$ and to the $1/Q^2$ corrections in $M_{\lambda'+, \lambda+}$ is different, and either of them may be untypically small or large. With this caveat in mind one can take the smallness of twist-three amplitudes as a generic consistency check for the relevance of the $1/Q$ expansion. If this check is passed one may proceed and analyze the relevant Compton amplitudes in terms of GPDs.

The detailed analysis of Belitsky et al. [244] shows that one can in principle separate all Compton form factors corresponding to the amplitudes $M_{\lambda'+, \lambda+}$ and $M_{\lambda'+, \lambda_0}$ from the ϕ dependent terms in the weighted interference term (356) and its analogs for a longitudinally and for a transversely polarized target. One further finds that the same reconstruction is in principle possible without transverse target polarization if one has the full information from the Compton cross section and from the interference term, including the ϕ independent term c_0 in (356) and its analog for longitudinal target polarization. We see however from (365) to (369) that in the combinations of twist-two amplitudes $M_{\lambda'+, \lambda+}$ relevant for an unpolarized or longitudinally polarized target, E always comes with a kinematical suppression factor compared with other GPDs, which should make its separation difficult. To access E , which carries crucial information about orbital angular momentum, transverse target polarization hence seems inevitable. To disentangle the different double flip amplitudes $M_{\lambda'+, \lambda-}$ would require both the Compton and interference terms for longitudinal and transverse targets, given the absence of the highest harmonics in the lepton helicity dependent part of the cross section (see Section 9.1.1).

Using the representation (277) of the twist-two Compton amplitudes in terms of the Compton form factors of Belitsky et al., which are convolutions of the corresponding GPDs with hard-scattering kernels, one can readily see which combinations of GPDs particular observables are sensitive to. For an unpolarized target the Compton cross section involves

$$\begin{aligned} \frac{1}{2} \sum_{\lambda' \lambda} |M_{\lambda'+, \lambda+}|^2 &= (1 - \xi^2) (|\mathcal{H}|^2 + |\tilde{\mathcal{H}}|^2) - \left(\xi^2 + \frac{t}{4m^2} \right) |\mathcal{E}|^2 - \xi^2 \frac{t}{4m^2} |\tilde{\mathcal{E}}|^2 \\ &\quad - 2\xi^2 \operatorname{Re} (\mathcal{H}^* \mathcal{E} + \tilde{\mathcal{H}}^* \tilde{\mathcal{E}}). \end{aligned} \quad (365)$$

The $\cos \phi$ and $\sin \phi$ terms in the interference go with

$$\widehat{M}_{++} = \sqrt{1 - \xi^2} \frac{\sqrt{t_0 - t}}{2m} \left[F_1 \mathcal{H} + \xi (F_1 + F_2) \tilde{\mathcal{H}} - \frac{t}{4m^2} F_2 \mathcal{E} \right]. \quad (366)$$

Note that $\tilde{\mathcal{E}}$ is absent in this term. A numerical study by Korotkov and Nowak [498] found (365) strongly dominated by $(1 - \xi^2) |\operatorname{Im} \mathcal{H}|^2$ in typical HERMES kinematics, and $\operatorname{Im} \widehat{M}_{++}$ strongly dominated by the term with $\operatorname{Im} \mathcal{H}$. Such observations are however dependent on the specific GPD models and kinematics considered and should be taken with due care: Belitsky et al. [244] report for instance that for certain models the \mathcal{E} contribution to \widehat{M}_{++} can be significant in small- x kinematics. While being a useful guide for a rough phenomenological analysis, the neglect of particular GPDs in a particular observable should if at all possible be cross checked with estimates of their size from different observables, or if these are not available by scanning a suitable range of ansätze for the GPDs.

The ϕ independent term in $P(\cos \phi) d\sigma_{\text{INT}}/d\phi$ has been calculated in [244]. To leading order in

$1/Q$ its contribution to $e^{-6} \sum'_{\text{spins}} (\mathcal{T}_{\text{BH}}^* \mathcal{T}_{\text{VCS}} + \mathcal{T}_{\text{VCS}}^* \mathcal{T}_{\text{BH}})$ in (347) can be written as

$$\begin{aligned}
& -e_\ell \frac{1}{Q^2} \frac{8}{\xi} \frac{1}{P} \sqrt{\frac{1+\epsilon}{1-\epsilon}} \text{Re} \left\{ \left[F_1 \mathcal{H} - \xi^2 (F_1 + F_2) (\mathcal{H} + \mathcal{E}) - \frac{t}{4m^2} F_2 \mathcal{E} \right] \right. \\
& \quad \left. - \frac{1+\epsilon}{\epsilon} \frac{t-t_0}{t} (1-\xi) \left[F_1 \mathcal{H} + \xi (F_1 + F_2) \tilde{\mathcal{H}} - \frac{t}{4m^2} F_2 \mathcal{E} \right] \right\}. \tag{367}
\end{aligned}$$

Numerical estimates in [244] show that this term need not be small compared with the $\cos \phi$ term. The second line of (367) involves the same combination of GPDs as the $\cos \phi$ term, whereas the first line, which survives the zero angle limit $t = t_0$, involves a different combination. The difference between the two terms in square brackets is however proportional to $\xi \tilde{\mathcal{H}} + \xi^2 (\mathcal{H} + \mathcal{E})$ and should be rather small unless ξ is large, as was confirmed by numerical estimates in [244]. At sufficiently small ξ the constant and the $\cos \phi$ term in the interference are hence approximately sensitive to the *same* linear combination of Compton form factors or helicity amplitudes.

For longitudinal target polarization the relevant combinations in the Compton cross section and interference term respectively read

$$\begin{aligned}
& \frac{1}{2} \sum_{\lambda'} (|M_{\lambda'+,++}|^2 - |M_{\lambda'+,-+}|^2) \\
& = 2\text{Re} \left[(1 - \xi^2) \mathcal{H}^* \tilde{\mathcal{H}} - \left(\frac{\xi^2}{1+\xi} + \frac{t}{4m^2} \right) \xi \mathcal{E}^* \tilde{\mathcal{E}} - \xi^2 (\tilde{\mathcal{H}}^* \mathcal{E} + \mathcal{H}^* \tilde{\mathcal{E}}) \right] \tag{368}
\end{aligned}$$

and

$$\begin{aligned}
& \frac{1}{2} \sum_{\lambda'} (g_{\lambda'+} M_{\lambda'+,++} - g_{\lambda'-} M_{\lambda'+,-+}) = \sqrt{1 - \xi^2} \frac{\sqrt{t_0 - t}}{2m} \\
& \quad \times \left[F_1 \tilde{\mathcal{H}} + \xi (F_1 + F_2) \mathcal{H} + \frac{\xi^2}{1+\xi} (F_1 + F_2) \mathcal{E} - \left(\frac{\xi^2}{1+\xi} F_1 + \xi \frac{t}{4m^2} F_2 \right) \tilde{\mathcal{E}} \right]. \tag{369}
\end{aligned}$$

Given the kinematical prefactors they should be most sensitive to \mathcal{H} and $\tilde{\mathcal{H}}$, so that together with the unpolarized terms (365), (366) one should be able to separate these two contributions, with the caveats spelled out below (366). Note that the Compton term (368) is only accessible in the double asymmetry for beam and target polarization, in accordance with the rules of Sect. 9.1.2. The imaginary part of (369) appears in the single target spin asymmetry, and its real part in the double spin asymmetry for beam and target.

Observables where \mathcal{E} and $\tilde{\mathcal{E}}$ are not kinematically suppressed compared with \mathcal{H} and $\tilde{\mathcal{H}}$ require *transverse* target polarization, which involves the combinations

$$\begin{aligned}
& \frac{1}{2i} \sum_{\lambda'} (M_{\lambda'+,-+}^* M_{\lambda'+,++} - M_{\lambda'+,++}^* M_{\lambda'+,-+}) \\
& = 2\text{Im} \left[\sqrt{1 - \xi^2} \frac{\sqrt{t_0 - t}}{2m} (\mathcal{E}^* \mathcal{H} - \xi \tilde{\mathcal{E}}^* \tilde{\mathcal{H}}) \right], \tag{370}
\end{aligned}$$

$$\begin{aligned}
& \frac{1}{2} \sum_{\lambda'} (M_{\lambda'+,-+}^* M_{\lambda'+,++} + M_{\lambda'+,++}^* M_{\lambda'+,-+}) \\
& = 2\text{Re} \left[\sqrt{1 - \xi^2} \frac{\sqrt{t_0 - t}}{2m} (\mathcal{E}^* \tilde{\mathcal{H}} - \xi \tilde{\mathcal{E}}^* \mathcal{H} - \frac{\xi^2}{1+\xi} \mathcal{E}^* \tilde{\mathcal{E}}) \right] \tag{371}
\end{aligned}$$

in the Compton cross section, with (370) appearing in the single target spin asymmetry and (371) in the double spin asymmetry for target and beam. In the interference term one has the combinations

$$\begin{aligned}
& \frac{1}{2} \sum_{\lambda'} (g_{\lambda'} - M_{\lambda'+,++} - g_{\lambda'+} M_{\lambda'+,-+}) \\
&= \left[\xi^2 F_1 - \frac{t}{4m^2} (1 - \xi^2) F_2 \right] \mathcal{H} + \left[\xi^2 F_1 + \frac{t}{4m^2} (F_1 + \xi^2 F_2) \right] \mathcal{E} \\
&\quad - \xi^2 (F_1 + F_2) \tilde{\mathcal{H}} - \frac{t}{4m^2} \xi^2 (F_1 + F_2) \tilde{\mathcal{E}}, \tag{372}
\end{aligned}$$

$$\begin{aligned}
& \frac{1}{2} \sum_{\lambda'} (g_{\lambda'} - M_{\lambda'+,++} + g_{\lambda'+} M_{\lambda'+,-+}) \\
&= \left[\xi^2 F_1 - \frac{t}{4m^2} (1 - \xi^2) F_2 \right] \tilde{\mathcal{H}} + \left[\frac{\xi^2}{1 + \xi} F_1 + \frac{t}{4m^2} (F_1 + \xi F_2) \right] \xi \tilde{\mathcal{E}} \\
&\quad - \xi^2 (F_1 + F_2) \mathcal{H} - \left(\frac{\xi^2}{1 + \xi} + \frac{t}{4m^2} \right) \xi (F_1 + F_2) \mathcal{E}, \tag{373}
\end{aligned}$$

which can be separated by the ϕ dependence in the cross section. Their imaginary parts are accessible in the single target spin asymmetry, and their real parts in the double spin asymmetry for target and beam. Only in the combination (372) is \mathcal{E} not kinematically suppressed compared with \mathcal{H} . In [293] it was observed that for $t = t_0$, both (372) and (373) become proportional to $\xi^2 (F_1 + F_2) (\mathcal{H} - \tilde{\mathcal{H}})$ up to terms down by further factors of at least ξ^2 . This extra suppression of \mathcal{E} is however only relevant for very forward angles and no longer effective as soon as $|t - t_0| \sim |t_0|$.

Various asymmetries have been studied using models for GPDs. For the small- x kinematics of the H1 and ZEUS measurements, it was estimated that the beam charge asymmetry may be in the 10% range [293, 244, 110]. The beam spin asymmetry was found sizeable provided that y is not too small. This is because due to the polarization transfer from the lepton to the virtual photon of DVCS, lepton polarization effects at small y come with a suppression factor of $y \sim \sqrt{1 - \epsilon}$ relative to unpolarized contributions, as can be seen in (345) and (347). Estimates of similar size have been obtained in [481, 503] using the simple model of Frankfurt et al. for DVCS at small x (see Section 8.5).

For the fixed-target kinematics of the HERMES or Jefferson Lab experiments the studies [293, 244, 110] found sizeable effects possible for the beam charge asymmetry, as well as for the single spin asymmetries for the lepton and for longitudinal or transverse target polarization. In contrast, the double polarization asymmetry for longitudinal beam and target was estimated to be rather small [293, 110].

For some observables, different models for the GPDs give distinctly different results. Kivel et al. [200] observed that the beam charge asymmetry in HERMES kinematics can change sign when adding the model D -term mentioned in Section 4.3.2 to a double distribution based ansatz. In contrast, the study of Belitsky et al. [244] found that when taking the same D -term the asymmetry becomes close to zero. This was traced back to important differences in the double distribution part of both studies. Note that although the forward quark densities (at not too small x) are rather well constrained by experiment, this is not the case for the nonforward behavior of GPDs, in particular for their t dependence. Given these uncertainties it seems premature to claim evidence e.g. of a sizeable D -term from a single observable.

The importance of different contributions to the cross section changes significantly when going from a proton to a neutron target. The electromagnetic Dirac form factor of the neutron is small at low t , but its Pauli form factor is large. This suppresses the $1/\xi^2$ enhanced term in the Bethe-Heitler cross section (346) so that its contribution is less important compared with the proton case. We see

in (366) that there is also a suppression for the $\cos\phi$ and $\sin\phi$ part of the interference term with an unpolarized target, where the normally dominant contribution from \mathcal{H} is accompanied by the Dirac form factor. Furthermore $\tilde{\mathcal{H}}$ for the neutron may be small due to a cancellation between u and d quark contributions, assuming that their relative sign and size is as for the polarized forward densities [243].

9.1.5 First data

Measurements of DVCS at fixed target energies have been reported by HERMES [260] and CLAS [261]. Both measure the single beam spin asymmetry $A(\phi)$ defined in (363). The results are shown in Fig. 42. With respective lepton beam energies of $E = 27.6$ GeV and $E = 4.25$ GeV the Bethe-Heitler process is prominent in the cross section, except for larger values of x_B at HERMES. The average kinematical values of the HERMES measurement are $Q^2 = 2.6$ GeV², $x_B = 0.11$, $-t = 0.27$ GeV², and $y = 0.46$, whereas the CLAS Collaboration compared their data with theory predictions for fixed $Q^2 = 1.25$ GeV², $x_B = 0.19$, $-t = 0.19$ GeV², and $y = 0.82$. We note that HERMES has detected the final e^+ and γ but not the scattered proton, whereas CLAS measured the e^- and p but not the final-state γ . Important experimental backgrounds are therefore $ep \rightarrow ep\pi^0$ for CLAS and proton dissociation for HERMES.

Both experiments find a sizeable single spin asymmetry $A(\phi)$ compatible with a $\sin\phi$ behavior; a fit by CLAS to $A(\phi) = \alpha \sin\phi + \beta \sin 2\phi$ found β compatible with zero within errors. With the caveats concerning the Bethe-Heitler propagators discussed in Sections 9.1.1 and 9.1.3 this provides evidence that the leading-twist combination $\text{Im} \widehat{M}_{++}$ is sizeable whereas $\text{Im} \widehat{M}_{+0}$ is small. To be sure, by itself this is not a *proof* that one is in the region where the large Q^2 analysis applies. In particular, \widehat{M}_{+0} also has to vanish in the photoproduction limit $Q^2 \rightarrow 0$. More precise data will hopefully allow one to establish the size of the longitudinal photon amplitudes and their behavior with Q^2 .

The sign of the measured $A(\phi)$ translates into $\text{Im} \widehat{M}_{++} > 0$. According to (366) this is expected by a twist-two analysis if one assumes that the observable is dominated by $H^q(\xi, \xi, t)$ and that these GPDs have the same positive sign as their forward limits. The current GPD models discussed in Section 4.3 provide values of $A(\phi)$ with the correct size. This holds for the leading-twist LO analysis of [497], for the leading-twist NLO analysis of [110], and for the LO analyses including twist-three effects in the Wandzura-Wilczek approximation of [244] and of [200] (the latter being shown in the HERMES publication). In all cases the theory predictions are however somewhat above the data. Given the existing uncertainties concerning power corrections and the rather large number of assumptions and parameters in GPD parameterizations it is not simple to identify the ‘‘culprit’’ for this situation. Freund and McDermott [110] argue that the enhancement factor of nonforward to forward distributions (see Section 4.4) is not large according to the data and further conclude that modeling based on double distributions with a profile as in (230) to (233) is problematic.

The DVCS cross section at small x_B has been measured by the H1 and ZEUS Collaborations [259, 299], subtracting the Bethe-Heitler contribution and assuming that after integration over ϕ the interference term can be neglected (see Section 9.1.3). The kinematical region was $Q^2 = 2$ to 20 GeV² and $W = 30$ to 120 GeV for H1, and $Q^2 = 5$ to 100 GeV² and $W = 40$ to 140 GeV for ZEUS. As in meson electroproduction or photoproduction of J/Ψ , a rather steep increase of the cross section with energy was observed. With the GPD models just mentioned, the study [110] found a cross section too large in this kinematics. The analysis in [244] could achieve agreement with the H1 data by taking a large profile parameter b (see Section 4.3.3) and a very steep falloff in t for the sea quarks.³⁰ As in the case of the fixed-target data it may be too early to draw definite conclusion, but it is clear that theoretical predictions are sufficiently different for some of them to be ruled out by data. Both

³⁰Notice that the t -slope parameter B_{sea} used in [244] refers to the amplitude and not to the cross section level, unlike the common parameterization $d\sigma/dt \propto e^{Bt}$.

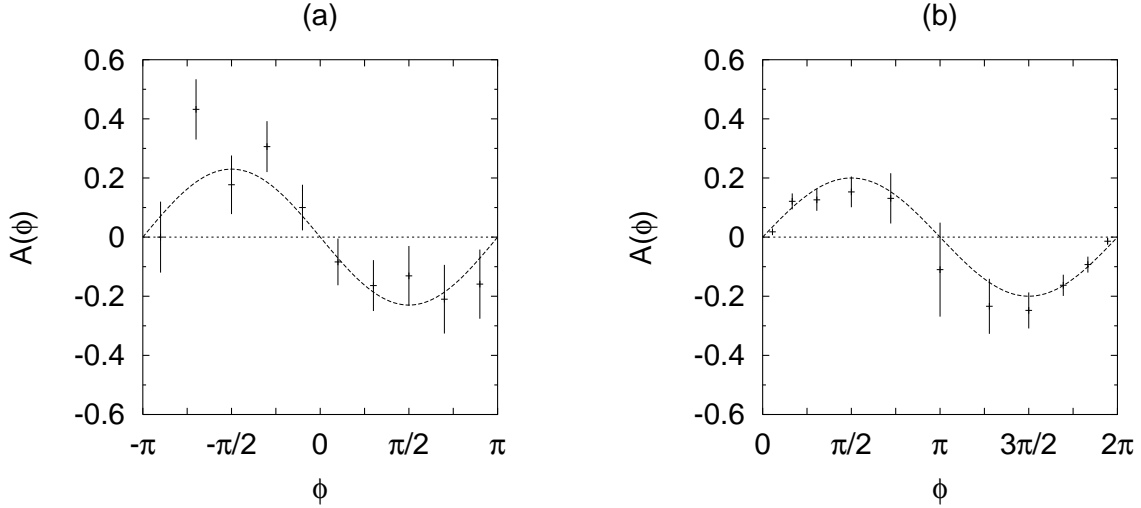


Figure 42: Data for the beam spin asymmetry $A(\phi)$ in DVCS. In both cases the error bars show the statistical errors, which dominate over the systematic ones. (a) The HERMES measurement [260] for $e^+p \rightarrow e^+\gamma X$ with an experimentally reconstructed missing mass of M_X^2 between $-(1.5 \text{ GeV})^2$ and $(1.7 \text{ GeV})^2$. The curve corresponds to $A(\phi) = -0.23 \sin \phi$. (b) The CLAS data for $e^-p \rightarrow e^-\gamma p$ [261] together with the curve $A(\phi) = 0.2 \sin \phi$.

for the fixed-target and the collider experiments, measurement of the t dependence would be of great help to reduce the freedom and uncertainty in modeling the input GPDs.

9.1.6 Targets with spin zero or one

Many theoretical investigations have focused on DVCS on a spinless target, mainly because of its relative simplicity compared with the spin $\frac{1}{2}$ case. The case of a pion target has often been studied as a concrete example, where furthermore rather detailed dynamical predictions are available (see Section 4). One may think of studying DVCS on a virtual pion target in the process $ep \rightarrow e\gamma\pi^+n$ at small invariant momentum transfer from the proton to the neutron.³¹ To obtain the pion GPDs $H_\pi^q(x, \xi, t)$ would then require a careful extrapolation to the pion pole. The analogy with elastic form factors suggests that the situation in this respect should resemble the one for extracting $F_\pi(t)$ at small t from $ep \rightarrow e\pi^+n$.

Another context where targets with different spin J appear is scattering on nuclei. Preliminary data for the beam spin asymmetry $A(\phi)$ on neon ($J = 0$) and on the deuteron ($J = 1$) have for instance been reported by HERMES [504]. Model estimates for the cross section and various asymmetries have been given in [262, 264] for a deuteron target and in [263, 264] for neon. The cross section dependence on the azimuthal angle ϕ and on the lepton beam polarization follows the principles spelled out in Sections 9.1.1 and 9.1.2 for an unpolarized target of *any* spin. Analogous observables hence project out the real or imaginary parts of Compton amplitudes in an analogous way. In contrast, the structure of observables with target polarization is different. A general analysis in the framework of Belitsky et al. [244] has been presented in [264] for a spin-one target. The case of a spin zero target was studied along the same lines to twist-three accuracy in [130].

Note that for DVCS on a spinless target there are only three independent helicity amplitudes,

³¹I thank M. Amarian for discussions on this issue.

M_{++} , M_{+0} , M_{+-} , where the first index refers to the outgoing and the second to the incoming photon. This makes the analysis rather simple. The beam spin independent part of the interference term depends on $\text{Re } M_{++}$, $\text{Re } M_{+0}$, $\text{Re } M_{+-}$ and offers four observable quantities, given as Fourier coefficients of $P(\cos \phi) d\sigma_{\text{INT}}/d\phi$, whereas the beam spin dependent part depends on $\text{Im } M_{++}$, $\text{Im } M_{+0}$ and contains two independent Fourier coefficients. One can hence extract all independent dynamical quantities from the ϕ distribution of the interference, using either its $1/Q$ expanded or its exact expression in terms of the Compton amplitudes. A spin zero target hence presents a clean environment for testing the large Q^2 expansion underlying a GPD based analysis.

9.2 Timelike Compton scattering

The phenomenology of TCS is very similar to the one of DVCS and has been presented in [243], closely following the DVCS treatment we have just discussed. The Compton subprocess in

$$\gamma(q) + p(p) \rightarrow \ell^-(k) + \ell^+(k') + p(p') \quad (374)$$

interferes with a Bethe-Heitler process as shown in Fig. 43. As we have seen in Section 5.2 it is natural to compare TCS and DVCS at the same ξ and t and at corresponding values of Q'^2 and Q^2 . According to the kinematical relation (261) the analog of $x_B \approx 2\xi/(1+\xi) \approx Q'^2/(Q'^2 + W^2)$ in DVCS is thus $2\xi/(1+\xi) \approx Q'^2/W^2$ in the timelike process. The full kinematics of lepton pair production is suitably described by two further variables θ and ϕ , the polar angles of ℓ^- in the c.m. of the lepton pair, with the z -axis pointing opposite to the scattered proton. The azimuth ϕ plays the same role as its analog in DVCS and is the key to obtain information on Compton scattering from its interference with the Bethe-Heitler process. The analogous roles played in the cross section formulae by θ in TCS and the inelasticity y in DVCS are elucidated by the correspondence

$$\frac{1 + \cos \theta}{2} \approx \frac{k \cdot p'}{(k + k') \cdot p'} \leftrightarrow \frac{k \cdot p}{(k - k') \cdot p} = \frac{1}{y}, \quad (375)$$

where in the first relation we have neglected the masses of the lepton and the target. This relation reveals a crucial difference in the phenomenology of the two processes: whereas at small y a factor $1/y^2 \sim 1/(1-\epsilon)$ enhances the DVCS cross section over Bethe-Heitler (see Section 9.1) the corresponding factor in TCS is bounded between -1 and 1 . Given the relative factors $1/t$ and $1/Q'^2$ from the photon propagators, the Bethe-Heitler process hence tends to dominate over TCS in deeply virtual kinematics, so that information about the Compton amplitudes must be gained through the interference term.

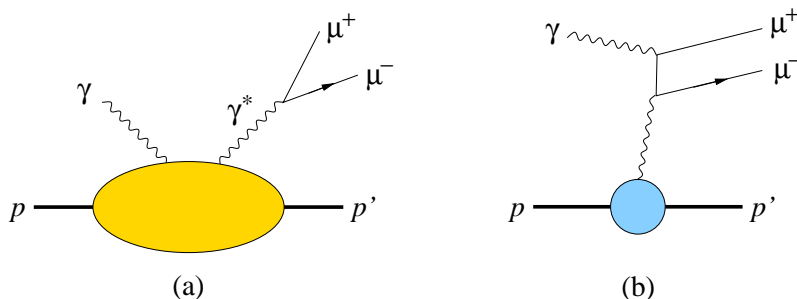


Figure 43: (a) Compton scattering and (b) Bethe-Heitler contribution to $\gamma p \rightarrow \mu^+ \mu^- p$. A second Bethe-Heitler diagram is obtained by reversing the charge flow of the muon line.

To filter out the interference term one can use that the $\ell^+\ell^-$ pair is produced in a C odd state by Compton scattering and in a C even state by the Bethe-Heitler process. Any observable that changes sign under the exchange of ℓ^- and ℓ^+ momenta hence projects out the interference. This is the analog of the beam charge asymmetry in DVCS, and it is readily available from the angular distribution of the leptons instead of requiring beams of opposite charge. The structure of the interference term is analogous to (347) in DVCS: the linear combinations $\text{Re } \widehat{M}_{--}$, $\text{Re } \widehat{M}_{0-}$, $\text{Re } \widehat{M}_{+-}$ of Compton amplitudes appear multiplied with $\cos \phi$, $\cos 2\phi$, $\cos 3\phi$ and with a known lepton propagator factor $1/P(\cos \phi)$. A suitable observable to extract the leading-twist amplitudes $\text{Re } \widehat{M}_{--}$ is for instance the cross section weighted by $\cos \phi$ or by $\cos \phi P(\cos \phi)$. Note that this requires one to reconstruct both the hadronic and leptonic scattering planes in order to measure ϕ . In principle one may also access the amplitudes $\text{Re } M_{\lambda'-\lambda-}$ from ϕ integrated observables. An example is the cross section weighted by $\cos \theta$. This comes however with an additional kinematic suppression factor $1/Q'$ and was estimated to be numerically very small in kinematics of fixed-target experiments [243].

The imaginary parts of the Compton amplitudes can be obtained with a polarized photon beam. With circular photon polarization (obtained for instance by bremsstrahlung from a longitudinally polarized lepton beam) one finds $\text{Im } \widehat{M}_{--}$, $\text{Im } \widehat{M}_{0-}$, $\text{Im } \widehat{M}_{+-}$ multiplied with $\sin \phi$, $\sin 2\phi$, $\sin 3\phi$ times $1/P(\cos \phi)$ in the interference term. Note that unlike in the *lepton* spin asymmetry of DVCS, the contribution with $\sin 3\phi$ is not absent here and provides access to the double helicity flip amplitudes of the photon.

No experimental results on TCS have been reported so far. A numerical estimate of the $\cos \phi$ asymmetry in [243] found rather small effects for fixed-target kinematics and Q^2 around 5 GeV^2 , but the estimate strongly depended on the model for GPDs in the ERBL region and should be taken with care. This is typical of observables involving the real parts of Compton amplitudes, which crucially depend on GPDs in the region where least is known about them.

The yet unexplored phenomenology of DDVCS, to be measured in $ep \rightarrow ep \ell^+\ell^-$, will combine the elements of DVCS and of TCS, with Bethe-Heitler processes of both types in Figs. 40 and 43 contributing to the cross section. In the limit where one of the two photon virtualities becomes small one expects to find the features of either DVCS or TCS in the pattern of observable quantities.

9.3 Two-photon annihilation

The analysis strategy we have presented for Compton scattering carries over to the crossed-channel process of exclusive $\gamma^*\gamma$ annihilation and has been developed in detail in [85] for the case of $e\gamma \rightarrow e\pi\pi$. The analog of the Bethe-Heitler process is now bremsstrahlung of a timelike γ^* which decays into the final state hadrons, as shown in Fig. 44. It can be calculated given the timelike pion form factor $F_\pi(s)$ at low to moderate s , whose square is measured in $e^+e^- \rightarrow \pi^+\pi^-$ and whose phase can be taken from the phase shift analysis of elastic $\pi\pi$ scattering using Watson's theorem (see Section 3.7.2). Modeling the two-pion DA along the lines of Section 4.6.4 one finds that the bremsstrahlung process strongly enhances and dominates the $e\gamma \rightarrow e\pi^+\pi^-$ cross section in a broad region of invariant two-pion masses $m_{\pi\pi}$ around the $\rho(770)$ mass. Angular analysis in the azimuth ϕ between the leptonic and hadronic planes of the process can then be used to filter out the interference with two-photon annihilation, which depends on the helicity amplitudes $M_{\mu'\mu}$ for $\gamma^*\gamma \rightarrow \pi\pi$. This is achieved by using the charge conjugation properties of the hadronic system, which is produced C -even by $\gamma^*\gamma$ annihilation and C -odd by bremsstrahlung. One of the simplest observables for this purpose is the cross section weighted with $\cos \phi$. More refined quantities to separate the three independent quantities $\text{Re}(F_\pi^* M_{++})$, $\text{Re}(F_\pi^* M_{0+})$ and $\text{Re}(F_\pi^* M_{-+})$ appearing in the interference term are discussed in [85], as well as the possibilities to simultaneously perform a partial-wave analysis of the two-pion system.

In the approximation of leading twist and leading $O(\alpha_s)$ the phase of M_{++} is equal to the dy-

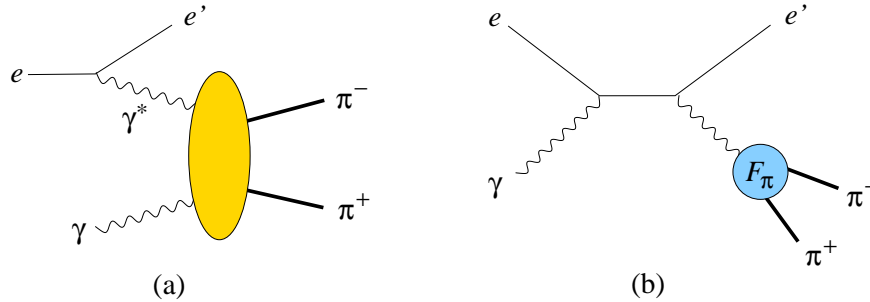


Figure 44: (a) Two-photon annihilation and (b) bremsstrahlung contribution to $e\gamma \rightarrow e\pi^+\pi^-$. A second bremsstrahlung diagram is obtained by interchanging the photon vertices.

namical phase of the isosinglet GDA Φ^{u+d} , so that the interference with bremsstrahlung gives rather clean access to this quantity. Consider $m_{\pi\pi}$ in a region where the two pions are predominantly in the S or P wave and where Watson's theorem can be applied (see Section 3.7.2). Then $\text{Re}(F_\pi^* M_{++})$ is proportional to $\cos(\delta_0 - \delta_1)$, where $\delta_l(m_{\pi\pi})$ is the phase shift of the l th partial wave. Significant structure can thus be expected in the $m_{\pi\pi}$ dependence of interference observables as shown in [85]. Studies at $m_{\pi\pi} \sim 1$ GeV may in particular shed light on the nature of the $f_0(980)$ resonance, in a context where its structure is probed at *short distance*.

$e\gamma$ scattering at large Q^2 can be studied at e^+e^- colliders in events with one lepton scattered at large and the other at small invariant momentum transfer. The estimates in [85] find that the event rate at high-luminosity experiments like BABAR and BELLE should be sufficient to study the interference signal in $e^+e^- \rightarrow e^+e^-\pi^+\pi^-$, as well as the cross section of $e^+e^- \rightarrow e^+e^-\pi^0\pi^0$, where bremsstrahlung does not contribute since the $\pi^0\pi^0$ system is charge conjugation even.

The principles of phenomenological analysis spelled out in [85] generalize to channels with different produced hadrons like $\bar{p}p$ or $\rho\rho$, with the additional complication of having more unknown amplitudes (as in Compton scattering on targets with nonzero spin). Anikin et al. [89] have recently studied $e^+e^- \rightarrow e^+e^-\rho^0\rho^0$ at large Q^2 , where bremsstrahlung is absent for the same reason as in $\pi^0\pi^0$ production. First data on this process has been presented by the L3 Collaboration [505] and is in fair agreement with the Q^2 behavior predicted by the leading-twist mechanism.

9.4 Meson production

In this section we present basics of analyzing meson electroproduction in the framework of GPDs, and point out some salient features of relevant data at fixed-target energies. For a discussion of vector meson production at small x see Section 8.4. A number of numerical estimates of production cross sections in the GPD framework have been made in the literature. Mankiewicz et al. have considered ρ^0 and π^0 production in [123], charged ρ production in [186], and charged pion production and its relation to the pion form factor in [196]. Cross sections for ρ^0 and π^0 in the leading-twist framework were given by Vanderhaeghen et al. [303], whereas the study [304] also estimated the size of power corrections (see Section 6.4). Frankfurt et al. have studied channels where the initial proton is scattered into a Δ or a strange baryon [189], and the production ratio of η and π^0 production was considered by Eides et al. [302]. Several of these predictions are collected in the review by Goeke et al. [37].

With Hand's convention [506] for the virtual photon flux one has the electroproduction cross

section for a meson M on an unpolarized target given by

$$\frac{d\sigma(ep \rightarrow epM)}{dt dQ^2 dx_B} = \frac{\alpha_{\text{em}}}{2\pi} \frac{y^2}{1-\epsilon} \frac{1-x_B}{x_B} \frac{1}{Q^2} \left[\frac{d\sigma_T}{dt} + \epsilon \frac{d\sigma_L}{dt} \right] \quad (376)$$

with γ^*p cross sections

$$\frac{d\sigma_i}{dt} = \frac{1}{16\pi} \frac{x_B^2}{1-x_B} \frac{1}{Q^4} \frac{1}{\sqrt{1+4x_B^2 m^2/Q^2}} \sum'_{\text{spins}} \left| \mathcal{A}(\gamma_i^* p \rightarrow Mp) \right|^2, \quad i = T, L \quad (377)$$

for transverse and longitudinal photon polarization. y and ϵ are defined in (343). We have not explicitly labeled the dependence of the scattering amplitude \mathcal{A} on the hadron polarizations, which are summed or averaged over in \sum'_{spins} .

The leading-twist expression for $d\sigma_L/dt$ is readily obtained from the amplitudes given in Section 5.3. The relevant combinations of GPDs are obtained as

$$\frac{1}{2} \sum_{\lambda'\lambda} |\mathcal{F}_{\lambda'\lambda}|^2 = (1-\xi^2) |\mathcal{H}|^2 - \left(\xi^2 + \frac{t}{4m^2} \right) |\mathcal{E}|^2 - 2\xi^2 \text{Re}(\mathcal{E}^* \mathcal{H}) \quad (378)$$

for mesons with natural parity, and

$$\frac{1}{2} \sum_{\lambda'\lambda} |\tilde{\mathcal{F}}_{\lambda'\lambda}|^2 = (1-\xi^2) |\tilde{\mathcal{H}}|^2 - \xi^2 \frac{t}{4m^2} |\tilde{\mathcal{E}}|^2 - 2\xi^2 \text{Re}(\tilde{\mathcal{E}}^* \tilde{\mathcal{H}}). \quad (379)$$

for mesons with unnatural parity. Here \mathcal{F} and $\tilde{\mathcal{F}}$ are appropriate convolutions of the proton matrix elements F and \tilde{F} , summed over quark flavors and gluons as specified by the scattering amplitudes (281) to (283). \mathcal{H} , \mathcal{E} , $\tilde{\mathcal{H}}$, $\tilde{\mathcal{E}}$ are defined in analogy from the corresponding quark or gluon GPDs. Note that the flavor structure and the hard-scattering kernels in the convolution differ from those in Compton scattering, where we have used the same notation. Since they only reflect the decomposition of $F_{\lambda'\lambda}$ and $\tilde{F}_{\lambda'\lambda}$ in terms of proton spinors, the structures (378) and (379) readily generalize to higher order corrections in α_s .

In addition to the cross section for a longitudinal photon and unpolarized target there is one more observable which involves only leading-twist amplitudes and can be expressed using the factorization theorem, namely the single spin asymmetry for a transversely polarized target (again with a longitudinal photon). This was first discussed for pseudoscalar production by Frankfurt et al. [187], and the analog for vector meson production was given in [37]. The cross section difference for target polarization along the positive and negative y axis (with the coordinate system defined as for Compton scattering in Fig. 41) involves the GPD combinations

$$\frac{1}{2i} \sum_{\lambda'} (\mathcal{F}_{\lambda'-}^* \mathcal{F}_{\lambda'+} - \mathcal{F}_{\lambda'+}^* \mathcal{F}_{\lambda'-}) = \sqrt{1-\xi^2} \frac{\sqrt{t_0-t}}{m} \text{Im}(\mathcal{E}^* \mathcal{H}) \quad (380)$$

for mesons with natural parity, and

$$\frac{1}{2i} \sum_{\lambda'} (\tilde{\mathcal{F}}_{\lambda'-}^* \tilde{\mathcal{F}}_{\lambda'+} - \tilde{\mathcal{F}}_{\lambda'+}^* \tilde{\mathcal{F}}_{\lambda'-}) = -\sqrt{1-\xi^2} \frac{\sqrt{t_0-t}}{m} \xi \text{Im}(\tilde{\mathcal{E}}^* \tilde{\mathcal{H}}) \quad (381)$$

for mesons with unnatural parity. The corresponding normalized polarization asymmetry goes with the ratio of (380) and (378) or of (381) and (379), and thus depends on \mathcal{E}/\mathcal{H} or on $\tilde{\mathcal{E}}/\tilde{\mathcal{H}}$. Restricting ourselves to $O(\alpha_s)$ accuracy we find from the discussion of Section 5.3 that for suitable mesons like π or ρ the amplitude depends on the meson structure only through a global factor, which cancels

in these normalized asymmetries. As emphasized in [187] the difference of polarized cross sections for pseudoscalar production gives access to the product of the GPDs \tilde{H} and \tilde{E} , whereas in large kinematical domains either \tilde{H} or \tilde{E} is estimated to dominate the unpolarized cross section. In analogy, the transverse asymmetry in vector meson production is sensitive to E even in kinematics where H dominates the cross section (379). Numerical estimates [187, 37] found that both for pseudoscalar and for vector meson production the transverse asymmetry may be sizeable.

9.4.1 Leading twist and beyond

The above predictions refer to the γ^*p cross section with longitudinal polarization of the photon and of the meson if applicable. In the case where the final meson has spin zero or where its polarization is unobserved, one needs to extract the longitudinal cross section from $\sigma_T + \epsilon\sigma_L$ by a Rosenbluth separation: measuring at different ϵ but equal values of Q^2 , x_B , t (on which $\sigma_{T,L}$ depend) requires different ep collision energies. There are however indirect ways of constraining the size of power suppressed amplitudes. For a target with no polarization or longitudinal polarization in the γ^*p c.m. a ϕ dependence of $d\sigma(ep \rightarrow epM)/(d\phi dt dQ^2 dx_B)$ is due to the interference of different γ^* polarizations. $\cos\phi$ or $\sin\phi$ terms go with the product of γ_L^* and γ_T^* amplitudes and are predicted to be power suppressed as $1/Q$ relative to σ_L . A $\cos 2\phi$ or $\sin 2\phi$ dependence comes from the interference of amplitudes with positive and negative photon helicity, resulting in the same $1/Q^2$ suppression as for σ_T . HERMES has observed a nonzero $\sin\phi$ dependence of the single spin asymmetry for $ep \rightarrow e\pi^+n$ on a longitudinally polarized target [507]. Since the longitudinal polarization is with respect to the beam direction it induces a small transverse polarization in the hadronic process $\gamma^*p \rightarrow Mp$ (see Section 9.1.2), but this effect alone cannot account for the asymmetry observed. A quantitative analysis will require data with transverse target polarization so that both effects can be separated, but the above observation already implies that the γ_T^* amplitude cannot be negligible in the kinematics of the measurement, with average values of $Q^2 = 2.2 \text{ GeV}^2$, $x_B = 0.15$, $-t = 0.46 \text{ GeV}^2$.

For the production of ρ mesons, the decay angular distribution of $\rho \rightarrow \pi^+\pi^-$ contains information on the ρ helicity and in combination with the ϕ dependence can be used for a detailed polarization analysis, worked out in the classical work of Schilling and Wolf [491]. Data for ρ production in the large- Q^2 region has in particular been taken by HERMES [508] for $W = 3.8 \text{ GeV}$ to 6.5 GeV and $Q^2 \leq 4 \text{ GeV}^2$ and by E665 at Fermilab [509] for W from about 10 GeV to 25 GeV and $Q^2 \leq 20 \text{ GeV}^2$. In both experiments angular analysis found approximate helicity conservation between the photon and meson in the γ^*p c.m. This can then be used to translate a measurement of the cross sections for transverse and longitudinal ρ mesons (separated via the decay angular distribution) into a measurement of σ_T and σ_L for transverse and longitudinal photons, without Rosenbluth separation. The ratio $R = \sigma_L/\sigma_T$ reaches a value of 1 at Q^2 around 2 to 3 GeV^2 , providing a clear indication of nonnegligible power suppressed amplitudes. HERMES has also observed a nonzero double spin asymmetry for longitudinal beam and target polarization [510, 511]. The effect cannot be explained alone by the induced transverse target polarization with respect to the γ^*p axis, and is evidence for an asymmetry between the γ_T^* cross sections with the target spin in the same or in the opposite direction as the spin of the photon. As to the longitudinal cross section itself, the HERMES data [380] for $\gamma_L^*p \rightarrow \rho_L p$ with $W = 4 \text{ GeV}$ to 6 GeV and $Q^2 \leq 5 \text{ GeV}^2$ and the data from E665 [509] are reasonably well reproduced by the calculation of [304], which contains a substantial amount of power suppression from parton k_T in this kinematics.

9.4.2 Meson pair production

As we have discussed in Section 5.4.2, measurement of $ep \rightarrow ep(\pi^+\pi^-)$ with the pion pair off the ρ mass peak offers a possibility to access the two-pion system both in the C -even and in the C -odd state.

At large enough Q^2 the process contains information about the two-pion distribution amplitude. The angular distribution of the pion pair in its rest frame carries again detailed information about the angular momentum state of the two-pion system, as it does on the ρ peak. The general framework of angular analysis including $J = 0, 1, 2$ partial waves has been given by Sekulin [512], and results specific to leading twist dynamics were presented by Lehmann-Dronke et al. [272]. Access to the C -even component, i.e., to S and D waves can in particular be obtained by interference with the C -odd component in the tail of the ρ peak. Any angular observable reversing sign under exchange of the pion momenta projects out the interference of the production amplitudes for C -even and C -odd two-pion states, as we discussed for $e\gamma \rightarrow e\pi^+\pi^-$ in Section 9.3. This interference is very sensitive to the dynamical phases of the GDAs, with phase differences $\delta_J(m_{\pi\pi}) - \delta_{J'}(m_{\pi\pi})$ resulting in a characteristic structure in the $m_{\pi\pi}$ distribution.

A simple observable projecting out the interference is the $\cos\theta$ moment of the cross section, where θ is the polar angle of the π^+ in the two-pion c.m. Preliminary data for a nonzero signal has been reported by HERMES [513]. Leading-twist factorization only applies to amplitudes with $J^3 = 0$. As pointed out in [272] these can be selected by taking the moment³²

$$\langle P_1(\cos\theta) + \frac{7}{3}P_3(\cos\theta) \rangle = \frac{2}{\sqrt{3}} \operatorname{Re} \left[\rho_{00}^{10} + \sqrt{5} \rho_{00}^{12} \right] \quad (382)$$

with $P_1(x) = x$ and $P_3(x) = \frac{1}{2}(5x^3 - 3x)$. Partial waves with $J > 2$ have been neglected in (382). The moment $\langle f(\cos\theta) \rangle$ is defined through

$$\int_{-1}^1 d(\cos\theta) f(\cos\theta) \frac{d\sigma}{d(\cos\theta)} = \langle f(\cos\theta) \rangle \int_{-1}^1 d(\cos\theta) \frac{d\sigma}{d(\cos\theta)}, \quad (383)$$

and the $\pi\pi$ system is described by its spin density matrix $\rho_{\lambda\lambda'}^{JJ'}$, whose diagonal entries $\rho_{\lambda\lambda}^{JJ}$ give the probability of producing the pion pair with quantum numbers J and $J^3 = \lambda$ and whose off-diagonals describe the corresponding interference terms. In contrast, the moment

$$\langle P_1(\cos\theta) - \frac{14}{9}P_3(\cos\theta) \rangle = \frac{2}{\sqrt{3}} \operatorname{Re} \left[\rho_{00}^{10} + 2\sqrt{\frac{5}{3}} \rho_{11}^{12} \right] \quad (384)$$

is sensitive to the interference of S and P waves with $J^3 = 0$ and to the interference of D and P waves with $J^3 = \pm 1$. Again partial waves with $J > 2$ have been neglected.

9.5 The deconvolution problem

So far we have been concerned with extracting helicity amplitudes from differential cross sections. A different task is to retrieve GPDs or GDAs from the appropriate amplitudes, where they appear convoluted with known hard-scattering kernels as discussed in Section 5.1. For GDAs the situation is analogous to the one for single-meson DAs (see our detailed discussion of the pion case in Section 6.2). One can access integrals of the distribution amplitudes over z , with ζ and s just appearing as additional variables in the GDAs. Notice that at leading $O(\alpha_s)$ the same z integrals appear in two-photon annihilation and in electroproduction of states with even C parity, see Sections 5.3 and 5.4.

Let us turn to the extraction of GPDs. For the leading-twist DVCS amplitudes one has to deconvolute

$$\mathcal{A}(\xi, Q^2, t) = \sum_i \int_{-1}^1 dx T^i(x, \xi, \log(Q^2/\mu_F^2)) F^i(x, \xi, t; \mu_F^2), \quad (385)$$

³²The prefactor $\sqrt{7/3}$ of $P_3(\cos\theta)$ in [272] is mistaken and should be replaced with $7/3$ [42].

where F^i stands for F^q , F^g , \tilde{F}^q , \tilde{F}^g . We have explicitly given the dependence on the factorization scale but suppressed the renormalization scale μ_R . The structure for electroproduction of light mesons is similar, with the kernels T^i replaced by the convolution of hard-scattering kernels and meson distribution amplitudes. Since the variable t appears in the GPDs but not in the hard-scattering kernels, it does not pose particular problems, and one may consider the deconvolution problem at a given value of t . The interplay between the variables x and ξ is however nontrivial.

It is instructive to compare this problem with the extraction of forward parton densities from appropriate inclusive cross sections, where the experimental observables are convolutions of the type

$$\sum_{i=q,g} \int_{-1}^1 dx t^i(x, x_B, \log(Q^2/\mu_F^2)) f^i(x; \mu_F^2), \quad (386)$$

where the f^i denote the forward limits of the F^i . In this case the external scaling variable x_B (or its analog in processes like Drell-Yan or jet production) appears in the hard-scattering kernels but not in the distributions. At leading order in α_s the kernels reduce to delta functions in the momentum fraction and one has a one-to-one correspondence between the measured x_B and the argument of the parton densities. At higher orders in the coupling one has nontrivial convolutions, and the evolution of the parton densities in μ_F is used in an essential way to extract for instance the gluon density from the Q^2 and x_B dependence of the DIS cross sections, where gluons do not appear at Born level.

What makes the convolution in (385) more complicated is the appearance of x and ξ in both the hard-scattering kernels and the distributions. At leading order in α_S the imaginary part of the amplitude involves still a delta function and one has direct access to F^i at the points $x = \pm\xi$ separating DGLAP and ERBL regions. At NLO accuracy the convolution in $\text{Im } \mathcal{A}$ involves only the DGLAP regions, whereas the ones in $\text{Re } \mathcal{A}$ involve the full interval $x \in [-1, 1]$ already starting at Born level. It is not known whether as a mathematical problem the system (385) can be solved for the GPDs, given the nontrivial properties of GPDs as functions of x and ξ and given their known evolution behavior in μ_F^2 . That this might be the case is suggested by a study of Freund [514]. The particular method considered there is based on the expansion of GPDs in polynomials discussed at the end of Section 3.8.3, and can hardly be used in practice unless one finds a set of polynomials where such an expansion can be truncated after a sufficiently small number of terms.

The only other known way to constrain GPDs is to choose a particular parameterization for them, calculate process amplitudes (or directly the relevant observables) and to fit the free parameters to data. This is just the analog of what is done in conventional extractions of forward parton distributions. To make it reliable in our context requires sufficient understanding of the functional dependence of GPDs on x , ξ , and t . To make use of the information from the Q^2 dependence of the observables and the evolution of the GPDs requires of course to be in a region where the Q^2 variation of amplitudes is adequately described by the leading-twist approximation, as in the case of forward distributions.

A possibility to gain more direct information on the shape of GPDs in their two momentum variables is provided by DDVCS, where one has two measured scaling variables

$$\mathcal{A}(\xi, \rho, Q^2, t) = \sum_i \int_{-1}^1 dx T^i(x, \xi, \rho, \log(Q^2/\mu_F^2)) F^i(x, \xi, t; \mu_F^2) \quad (387)$$

and hence an inversion problem more akin to the forward case. At Born level the imaginary part of the amplitude gives GPDs at $x = \pm\rho$ and hence in the ERBL region as discussed in Section 5.2. We note that at NLO accuracy $\text{Im } \mathcal{A}$ involves now both ERBL and DGLAP regions, unlike in the case of DVCS. Especially since the ERBL region is the region where GPDs are most different from their forward counterparts, DDVCS has a unique potential. Data and phenomenological analysis will have to show to what extent this potential can be realized.

10 Processes at large s , t and u

This section deals with exclusive processes with a large momentum transfer to a hadron, such as elastic form factors and Compton scattering at large t , and with their counterparts in the crossed channel, such as timelike form factors and two-photon annihilation into hadrons at large s . These processes receive contributions from handbag-type diagrams, which can be expressed in terms of GPDs at large t or of GDAs at large s . Following the historical development, we will first concentrate on large- t scattering processes and discuss large- s annihilation processes at the end of this section.

10.1 Hard scattering and soft overlap contributions

Consider the spacelike Dirac form factor $F_1(t)$ of the nucleon at large t , or Compton scattering $\gamma p \rightarrow \gamma p$ at large $s \sim -t \sim -u$. In a frame where both initial and final particles are fast, the nucleon is deviated by a large angle, and so is each of its partons. An exception are partons with soft momenta, which “fit” into both the initial and final wave function without undergoing a large momentum transfer. As shown by Brodsky and Lepage [38, 50], the dominant reaction mechanism in the large- t limit (at fixed ratios t/s , u/s of the large invariants) involves for each nucleon the Fock state with minimal number of partons, which undergo a hard scattering process described by a connected graph, as shown in Fig. 45 for Compton scattering. The amplitude is given as a convolution of the leading-twist distribution amplitude for each nucleon with a hard scattering kernel evaluated in the collinear approximation. This is the exact analog of the hard-scattering mechanism described in Section 5 when applied to meson form factors. It leads in particular to “dimensional counting rules” [515, 516], which predict the power-law dependence in the hard scale up to logarithmic corrections.

Compared with the meson case, scattering on baryons involves more internal lines in the hard scattering, where hence the external hard scale becomes more “diluted”. In such processes one may thus expect power suppressed effects to be more prominent at moderate values of the hard scale. Evaluation of the proton form factor $F_1(t)$, where data exist up to just over $-t = 30 \text{ GeV}^2$, with the leading-twist formula leads to values well below the data unless one takes distribution amplitudes strongly concentrated in the endpoint regions. Configurations with soft partons in a hadron wave function, for which the approximations of the hard scattering approach break down, then provide a substantial part of the leading-twist result, although they are power suppressed in the asymptotic analysis. This has been pointed out long ago by Isgur and Llewellyn Smith and by Radyushkin [517, 518, 519]. Such regions of phase space are additionally suppressed when taking into account the Sudakov form factors in the “modified hard scattering” approach of Sterman and collaborators [365, 366]. Yet stronger suppression results when one includes the k_T dependence of the hadronic wave functions in the hard scattering subprocess. This led to results well below the data for all distribution amplitudes considered in a study by Bolz et al. [520]. More recently, Kundu et al. [521] claimed agreement between the data for $F_1(t)$ at $-t \gtrsim 10 \text{ GeV}^2$ and a calculation using the modified hard scattering approach. Bolz et al. [522] have however remarked that the main numerical contributions to this result are still from regions, where it is not justified to neglect the k_T dependence of the hadronic wave functions when evaluating the hard scattering.

The analysis of wide-angle Compton scattering in the collinear hard scattering framework leads to results below the available data, even when endpoint concentrated DAs are used [523]. In the same analysis the ratio of the Compton cross section and the square of F_1 at the same t came out too small. From the analogy with the pion form factor (Section 5.3.1) one may expect enhancement of the leading-order result from radiative corrections to the hard scattering kernel, but their calculation for baryon scattering processes has not been attempted so far.

A contribution to elastic form factors that involves only small virtualities is the Feynman mech-

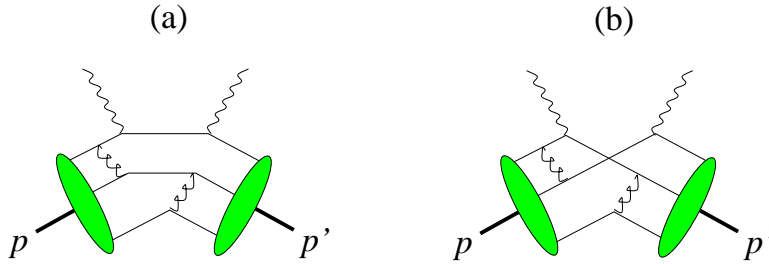


Figure 45: Hard-scattering diagrams for wide-angle Compton scattering. Removing one photon one obtains diagrams for the elastic form factor.

anism, where almost all momentum transfer to the nucleon is absorbed by a single quark (Fig. 46a). This quark carries nearly the full momentum of the nucleon before and after the scattering, whereas all other partons in the hadron have soft momenta and hence need not be “turned around”. This corresponds to quite rare configurations in the nucleon wave function, but the configurations required for the hard scattering mechanism are rare as well, namely three quarks in a small transverse area of size $1/Q^2$ as encoded in the distribution amplitude at factorization scale Q . To decide which of these rare configurations dominates is difficult to judge from intuition. Evaluating the soft overlap contribution to $F_1(t)$ using light-cone wave functions with a Gaussian falloff (216) in \mathbf{k}_i and an x_i dependence rather close to the asymptotic form, a rather good description of the large- t data can be achieved [221], whereas strongly endpoint concentrated wave functions strongly overshoot the data. Modeling the wave functions for the next higher Fock states with an additional gluon or $q\bar{q}$ pair, the study [31] found that their importance in the overlap decreases with increasing t . This is in line with naive expectation: larger t requires a smaller momentum fraction of the spectator system, which should be more difficult for states with more partons. One expects that the soft overlap contribution of Fig. 46 receives radiative corrections from the quark-photon vertex, which can be resummed into a Sudakov form factor and will lead to a suppression for spacelike momentum transfer t [16]. How to evaluate these effects for the processes of interest here is however not known.

In agreement with the leading-twist analysis one finds that the soft overlap mechanism evaluated with the above wave function models falls off faster with t than the hard-scattering mechanism. In particular, the soft overlap contribution to the scaled Dirac form factor $t^2 F_1(t)$ decreases with t . This happens however only at t of several 10 GeV^2 . As explained in Section 4.1.6 and emphasized in [30, 524], one finds that the relevant scale of the t -dependence for the soft overlap mechanism is *several* GeV^2 , although the basic nonperturbative parameters in the wave functions are around 1 GeV^2 . This

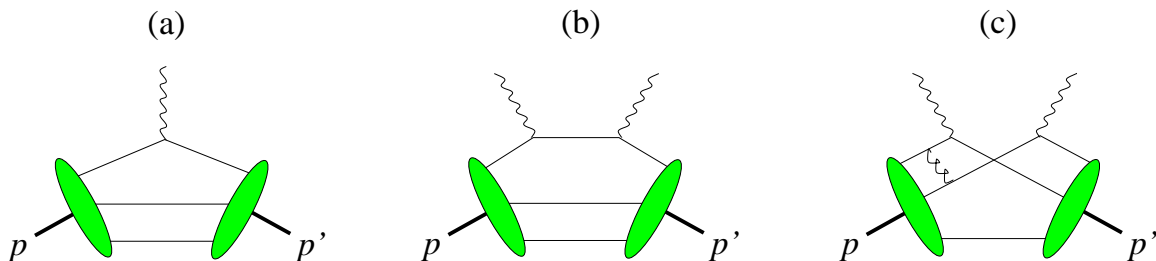


Figure 46: Soft overlap mechanism for (a) the elastic proton form factor and (b) wide-angle Compton scattering. (c) A soft overlap contribution with “cat’s ears” topology.

warns us that asymptotic power counting cannot simply be used for soft overlap contributions to processes involving baryons unless the hard scale is *very* large. One can explicitly show how the form (219) of the soft overlap contributions to form factors can mimic the scaling behavior of dimensional counting rules over a rather wide but finite range of t in the multi-GeV region [524]. For various form factors differing by their flavor or spin structure this happens in approximately the same region of t and may be seen as a rather universal property of the hadron in question. Apparent dimensional counting behavior can thus be found in several processes where the physics of the soft overlap mechanism can be parameterized by such form factors. This shows that, although the mimicking of dimensional counting behavior by the soft overlap may be seen as a numerical “accident”, it can occur on a systematic basis in several places.

The situation for wide-angle Compton scattering is similar to the elastic form factors but more complex. There is a soft overlap contribution to this process, shown in Fig. 46b, which involves the same low-virtuality parton configurations in the nucleon as the form factors, and Compton scattering $\gamma q \rightarrow \gamma q$ on one quark. The Compton subprocess is hard and suggests the factorized description of this mechanism we will discuss in the following. As discussed in [30, 31] there are other overlap contributions where the photons couple to two different quarks, as shown in Fig. 46c, whereas the remaining spectator partons have soft momenta. For large s , t , u kinematics does not allow such a process to be entirely soft, and if the wave functions in the figure are understood as soft wave functions, at least one hard gluon exchange is required. This type of contribution is intermediate between the soft overlap in Fig. 46b and the hard-scattering mechanism of Fig. 45 with respect to the number of hard internal propagators and the restrictions on the nucleon wave functions, and one may expect that its size is intermediate between the two extreme mechanisms. There are further power-suppressed mechanisms (see [30]), for instance those with hadron-like configurations of the photons, which one might model in terms of vector dominance and wide-angle meson-nucleon scattering. To date there is no formalism allowing a systematic treatment of all relevant contributions to the amplitude in a situation where the leading-twist mechanism is not dominant, and phenomenological analysis is required to identify situations where one particular mechanism turns out to dominate.

Generalized parton distributions provide a unified description of the soft physics involved in soft overlap contributions. The Feynman mechanism for the elastic form factor just corresponds to the overlap of soft wave functions in the relevant GPDs we discussed in Section 4.1.6. As we describe in the next section, one may also evaluate the soft overlap contributions of Fig. 46b in terms of GPDs. This leads to a description of the Compton amplitude involving a calculable short-distance process and quantities encoding the relevant soft physics, which one may extract from measurement and confront with efforts to calculate or model them theoretically.

10.2 The soft overlap for Compton scattering and meson production

10.2.1 Calculating the handbag diagrams

The soft overlap diagrams in Fig. 46b can be rearranged in the form of the familiar handbag diagrams of Fig. 1b (with external photons on shell). The details of the wave function overlap (including summation over the number of soft spectators) are lumped together in the matrix element of the bilocal operator $\bar{q}_\alpha(-\frac{1}{2}z)q_\beta(\frac{1}{2}z)$ between the external hadrons. To be more precise, only the *soft* part of this matrix element is implied here. Contributions involving large virtualities are not part of what is to be calculated. They are implied to be subtracted, unless they are sufficiently small to be simply neglected. Part of such hard contributions within the handbag are in fact included in leading-twist hard scattering diagrams as in Fig. 45a. This situation precludes one from using certain familiar arguments based on dimensional analysis, since the matrix element $\langle p' | \bar{q}_\alpha(-\frac{1}{2}z)q_\beta(\frac{1}{2}z) | p \rangle_{\text{soft}}$ depends on a large invariant t but by definition contains no internal virtualities of that size.

The calculation of the soft handbag has been carried out in [30] and in [31] using different techniques, whose results agree if suitable approximations are made within each scheme. The calculation of [31] is in momentum space and organizes the diagrams into Compton scattering on an on-shell quark and Fourier transformed matrix elements of $\bar{q}(-\frac{1}{2}z)\gamma^+q(\frac{1}{2}z)$ and $\bar{q}(-\frac{1}{2}z)\gamma^+\gamma_5 q(\frac{1}{2}z)$ at $z^2 = 0$. They are given as $1/x$ moments of GPDs,

$$\begin{aligned} R_V(t) &= \sum_q e_q^2 \int_{-1}^1 \frac{dx}{x} H^q(x, 0, t), & R_T(t) &= \sum_q e_q^2 \int_{-1}^1 \frac{dx}{x} E^q(x, 0, t), \\ R_A(t) &= \sum_q e_q^2 \int_{-1}^1 \frac{dx}{|x|} \tilde{H}^q(x, 0, t), \end{aligned} \quad (388)$$

and referred to as ‘‘Compton form factors’’. The calculation explicitly chooses a frame where $\xi = 0$, and where all external particles have energies and momenta of order $\sqrt{-t}$. (The wave function representation of the matrix elements is simplest in such a frame because it avoids the parton number changing overlap in the ERBL region.) At $\xi = 0$ no Compton form factor related to \tilde{E}^q appears, since these distributions are multiplied with Δ^+ in their definition (14). An attempt was made to quantify the approximations of the calculation parametrically, assuming that the soft wave functions ensure $\mathbf{k}_i^2/x_i \lesssim \Lambda^2$ for all partons at the wave function vertices in Fig. 46b. This ensures that all virtualities at these vertices are bounded by a soft physics scale $\Lambda^2 \sim 1 \text{ GeV}^2$. The final result for the Compton amplitude was then found to be accurate up to corrections of $O(\Lambda^2/t)$.

The calculation of Radyushkin [30] starts with the handbag diagrams in position space and expands the operator $\bar{q}_\alpha(-\frac{1}{2}z)q_\beta(\frac{1}{2}z)$ around light-like distances $z^2 = 0$. Representing the resulting matrix elements by double distributions according to (123) and Fourier transforming to momentum space, one obtains quark propagators with denominators

$$\begin{aligned} \hat{s} &= \beta(s - m^2) - \frac{1}{4}[(1 - \beta)^2 - \alpha^2]t + \beta^2 m^2, \\ \hat{u} &= \beta(u - m^2) - \frac{1}{4}[(1 - \beta)^2 - \alpha^2]t + \beta^2 m^2 \end{aligned} \quad (389)$$

for $\beta > 0$, respectively corresponding to the s and u channel handbag graphs. The calculation proceeds by approximating $\hat{s} \approx \beta(s - m^2)$ and $\hat{u} \approx \beta(u - m^2)$, which in [30] is justified on numerical rather than parametrical grounds. After further approximations the integration over the double distribution parameters leads to

$$\sum_q e_q^2 \int d\beta d\alpha \frac{1}{\beta} f^q(\beta, \alpha, t) \quad (390)$$

and its analog for the other double distributions, and hence to the same $1/x$ moments of GPDs as above. The form factors corresponding to E^q and \tilde{E}^q were explicitly neglected in [30], and as a further simplification R_A was approximated by R_V .

The result of both calculations, whose phenomenology we shall discuss in the next subsection, quite clearly involves approximations which one would like to improve on, especially when faced with data at values of s , t and u that are not significantly above 1 GeV^2 . How this can be done consistently is not clear at the present stage. Electromagnetic gauge invariance for Compton scattering on a quark is ensured if the quarks are approximated to be on shell. To be consistent with kinematical constraints, this approximation requires one to set the quark momentum equal to the momentum of its parent hadron and to neglect the target mass. Since the quark handbag diagrams in Fig. 1 are not gauge invariant by themselves, improvement over these approximations will require careful study, as the case of $1/Q$ corrections to DVCS has shown (see Section 6.1). Whether one obtains a gauge invariant Compton amplitude when keeping the full propagators (389) in the approach of Radyushkin is for

instance not known. The same caveat concerns the inclusion of the t -dependent terms in (389) up to linear accuracy in t/s , considered by Bakulev et al. [231].

Identifying the momenta of the struck parton and its parent hadron implies in particular setting the quark light-cone momentum fraction x to 1 in the hard scattering. One of the theoretical uncertainties of this approximation concerns the factors $1/x$ and $1/|x|$ in the GPD moments (388), since the way they appear in the calculation of [31] does not unambiguously assign them to either the hard scattering or the soft matrix element. Within the present accuracy of the approach, one might also choose to replace them respectively with $\text{sgn}(x)$ and 1. For an individual quark flavor, the Compton form factor R_A^q is then replaced by the axial form factor g_A^q . In the case of R_V^q and R_T^q one does not obtain form factors of local currents because the region $x < 0$ is explicitly weighted with a factor of -1 . This region corresponds to scattering on an antiquark in the proton, which is much less likely than a quark to carry most of the hadron momentum. Neglecting these configurations one may count the integral over this region with the “wrong sign”, and then finds the Dirac and Pauli form factors F_1^q and F_2^q of the local vector current. We remark however that with the model wave functions used in [31] the omission of the $1/x$ factors in the Compton form factors is of some numerical importance, since the x values dominating the integral for experimentally relevant t are not very close to 1 (see Section 4.1.6). This calls for an improvement of the theoretical description beyond the $x = 1$ approximation in the hard scattering.

Different possibilities of approximately taking into account the nucleon mass when relating the subprocess kinematics to the external Mandelstam variables have been explored in [525]. Their comparison may be taken as an estimate of theoretical uncertainties in kinematics where the target mass is not negligible. They were found to significantly depend on the observable and on the scattering angle, and to decrease substantially when going from the energies of present experiments at Jefferson Lab [526] to those of the proposed 12 GeV upgrade [527].

10.2.2 Phenomenology of Compton scattering

With the approximations we have discussed, the helicity amplitudes $e^2 M_{\lambda'\mu',\lambda\mu}$ for Compton scattering at large $s \sim -t \sim -u$ are given by [31, 528]

$$M_{\lambda'+,\lambda+} = \left(\delta_{\lambda'\lambda} R_V(t) - 2\lambda \delta_{\lambda'-\lambda} \frac{\sqrt{-t}}{2m} R_T(t) \right) \frac{s-u}{\sqrt{-su}} + 2\lambda \delta_{\lambda'\lambda} R_A(t) \frac{s+u}{\sqrt{-su}}, \quad (391)$$

$M_{\lambda'+,\lambda-} = 0$, and the parity relations (272). The light-cone helicities λ, λ' of the initial and final state proton are normalized to $\frac{1}{2}$ and refer to a frame with momentum components $(p-p')^+ = 0$, $(p-p')^1 > 0$, $(p-p')^2 = 0$. Their explicit transformation to usual helicities in the γp c.m. is given in [528]. The amplitudes for virtual Compton scattering $\gamma^* p \rightarrow \gamma p$ with Q^2 at most of the same order as the other large invariants can readily be calculated in the same formalism and are given in [31], where various observables have been estimated. Amplitudes which flip the photon helicity by one or two units are respectively found to be proportional to Q and Q^2 .

The result (391) corresponds to the hard parton subprocess at Born level. Radiative corrections of $O(\alpha_s)$ have been calculated by Huang et al. [528] for the case of real photons. It was found that the collinear and soft divergences obtained with on-shell external partons are multiplied with the leading-order scattering amplitudes and hence can be absorbed into the Compton form factors. It is suggestive to assume that this can be implemented by an appropriate renormalization prescription, although this has not been studied in detail. The $O(\alpha_s)$ corrections also induce nonzero amplitudes that flip the photon helicity by two units. They further involve handbag diagrams where the scattering is on a fast gluon instead of a quark. In line with expectations, the corresponding moments of gluon

GPDs estimated in [528] are smaller compared with their quark analogs, although not negligible. The $O(\alpha_s)$ kernels for virtual Compton scattering have recently been evaluated by Huang and Morii [529].

From (391) one obtains for the unpolarized cross section

$$\frac{d\sigma}{dt} = \frac{\pi\alpha_{\text{em}}^2}{(s-m^2)^2} \left[\frac{(s-u)^2}{|su|} \left(R_V^2(t) - \frac{t}{4m^2} R_T^2(t) \right) + \frac{(s+u)^2}{|su|} R_A^2(t) \right] \quad (392)$$

where here and in the following we keep the target mass in the phase space and flux factor while neglecting it in the squared process amplitudes. The dependence on the scattering angle in the collision c.m. is readily obtained from the relations $t \approx -\frac{1}{2}s(1 - \cos\theta)$, $u \approx -\frac{1}{2}s(1 + \cos\theta)$, which are valid up to $O(m^2/s)$ corrections. The $O(\alpha_s)$ corrections to the cross section have been estimated to increase the cross section by about 10% for backward angles and by about 30% in the forward direction [528]. In that study the range of θ was restricted to $|\cos\theta| < 0.6$ in order to ensure that $-t$ or $-u$ do not become significantly smaller than s , and this restriction will be implied in the following.

Whereas the form factors R_V and R_A may be obtained from the overlap of soft model wave functions [30, 31], modeling of R_T along the same lines would require wave functions with nonzero orbital angular momentum between the partons and has not been attempted. Instead one may assume that R_T/R_V behaves approximately like the ratio F_2/F_1 of Pauli and Dirac form factors, given the similarity of these quantities. Measurements from Jefferson Lab using the recoil polarization of the scattered proton find a behavior $F_2(t)/F_1(t) \approx 0.37 \times 2m/\sqrt{-t}$ for t between 1 and 5.6 GeV² [530], whereas older measurements using Rosenbluth separation found a steeper falloff $F_2(t)/F_1(t) \propto 4m^2/(-t)$. Which result is correct awaits clarification, for recent discussions see [531, 532]. If $R_T(t)/R_V(t) \sim 2m/\sqrt{-t}$ then R_T contributes to the cross section at the same level as R_V and R_A , and proton helicity conserving and helicity changing amplitudes in (391) are of comparable size.

The wave function model in [30, 31] gave form factors $R_V(t)$ and $R_A(t)$ which for $-t$ between about 5 and 15 GeV² behave approximately like t^{-2} and thus mimic dimensional counting behavior in this range. The cross section (392) of the soft handbag then mimics the dimensional counting behavior $d\sigma/(dt) \sim s^{-6}$ at fixed t/s . It is only at larger values of t that the soft part of the form factors implied in the handbag formulas is power suppressed compared to t^{-2} , with a corresponding power suppression of the soft overlap contribution to the Compton cross section as required by the asymptotic analysis.

Using these model form factors, the handbag result (391) gives a fair description of the available data for $d\sigma/(dt)$ from experiments with photon beam energies E_γ from 3 GeV to 6 GeV in the target rest frame [31, 528]. As discussed in Section 10.1, the hard scattering mechanism has difficulties to reproduce the cross section. A satisfactory description can however be obtained in the diquark model [494]. This treats the proton as an effective quark-diquark system, thus implying nonperturbative correlations among the quarks, and evaluates hard exclusive processes as hard scattering on the quark-diquark system, with phenomenological diquark form factors describing again effects beyond perturbation theory.

To establish which dynamics is actually at work in the process it is important to find features of the different mechanisms that are independent of the nonperturbative physics input, i.e., of the Compton form factors in our case. As we have seen, the s behavior of the cross section at fixed t/s cannot be used to distinguish experimentally between different reaction mechanisms in Compton scattering, given that values of t much above 15 GeV² will hardly be realizable in experiment. Among the generic features of the soft handbag mechanism is that photon helicity flip for $\gamma p \rightarrow \gamma p$ only occurs at $O(\alpha_s)$, which directly reflects a feature of real Compton scattering on massless fermions. This can be tested with suitable polarization observables. An example is the asymmetry Σ of cross sections for linear photon polarization either normal to or in the scattering plane, for which the soft handbag generically predicts $\Sigma = O(\alpha_s)$. Under weak assumptions on the gluon Compton form factors one

further obtains that $\Sigma < 0$, and numerical estimates suggest that this quantity may indeed be a good discriminator between different mechanism [528].

As another generic feature, the soft overlap mechanism predicts small phases of the amplitudes for real and virtual Compton scattering: since the Compton form factors are real valued, imaginary parts of the amplitude are only generated by the partonic subprocess at $O(\alpha_s)$. In the hard-scattering mechanism and its diquark variant, imaginary parts arise at leading order in the strong coupling and phases are generically large. As emphasized by Kroll et al. [494], the imaginary part of the virtual Compton amplitude can be accessed in the lepton polarization asymmetry of $ep \rightarrow ep\gamma$ using the interference between Compton and Bethe-Heitler amplitudes, i.e., the same principle we discussed for DVCS in Section 9.1.

It follows from (391) that the soft handbag mechanism makes specific predictions about the s -dependence of amplitudes at fixed t : each helicity amplitude can be written as a finite sum of known functions of s , whose coefficients are determined by the Compton form factors. Including $O(\alpha_s)$ corrections, the s -dependent functions are modified, and additional terms due to gluon form factors appear. This structure can be tested, as observed by Nathan [533]. Dividing for convenience the Compton cross section (392) by the Klein-Nishina cross section $d\sigma_{\text{KN}}/dt$ on a pointlike target, one obtains

$$\frac{d\sigma/dt}{d\sigma_{\text{KN}}/dt} = f_V \left(R_V^2(t) - \frac{t}{4m^2} R_T^2(t) \right) + (1 - f_V) R_A^2(t) \quad (393)$$

with

$$f_V = \frac{(s - u)^2}{2(s^2 + u^2)}, \quad (394)$$

where we neglect the proton mass throughout. Note that $d\sigma_{\text{KN}}/dt$ is obtained from (392) by setting $R_A = R_V$ and $R_T = 0$, which fixes the coefficient of R_A^2 in (393). The $O(\alpha_s)$ corrections to the quark handbag diagrams are readily taken into account using the results of [528]: if one divides $d\sigma/dt$ by $d\sigma/dt|_{R_A=R_V, R_T=0}$, the structure of (393) is preserved with a modified function f_V . The remaining $O(\alpha_s)$ corrections due to the gluon form factors were estimated to be at most 10% in [528].

As observed in [533], confronting (393) with data at equal t and different s would not only provide a distinctive test of the mechanism but may in principle be used to separate R_A from the other form factors. The lever arm for this is however rather small since f_V is rather close to 1 in most kinematics, so that sensitivity to R_A will be smaller than to the combination of R_V and R_T in (393). An alternative way to separate the different form factors is given by spin asymmetries, which were studied in detail in [524, 528]. An example are the correlation parameters between the helicity of the incoming photon and the helicity of the incoming (A_{LL}) or outgoing (K_{LL}) proton, which in the handbag are equal and given by

$$A_{LL} \frac{d\sigma}{dt} = K_{LL} \frac{d\sigma}{dt} = \frac{2\pi\alpha_{\text{em}}^2}{(s - m^2)^2} \frac{s^2 - u^2}{|su|} R_A(t) \left(R_V(t) - \frac{t}{s + \sqrt{-su}} R_T(t) \right) \quad (395)$$

to lowest order in α_s . Dividing by the Klein-Nishina value $A_{LL}^{\text{KN}} = K_{LL}^{\text{KN}} = (s^2 - u^2)/(s^2 + u^2)$ for a target without structure and mass one obtains

$$\frac{A_{LL}}{A_{LL}^{\text{KN}}} = \frac{K_{LL}}{K_{LL}^{\text{KN}}} \simeq \frac{R_A}{R_V} \left[1 - \frac{t^2}{2(s^2 + u^2)} \left(1 - \frac{R_A^2}{R_V^2} \right) \right]^{-1}, \quad (396)$$

where we have neglected terms involving R_T . The kinematical prefactor in brackets is small in typical kinematics, so that this ratio is approximately a measure of R_A/R_V .

An observable sensitive to the tensor form factor R_T is for instance the correlation K_{LS} between the helicity of the initial photon and the transverse (“sideways”) polarization of the recoil proton in the scattering plane. With the sign convention of [528] this parameter is

$$K_{LS} \frac{d\sigma}{dt} = \frac{2\pi\alpha_{\text{em}}^2}{(s-m^2)^2} \frac{s^2-u^2}{|su|} \frac{\sqrt{-t}}{2m} \left(\frac{4m^2}{s+\sqrt{-su}} R_V(t) - R_T(t) \right) R_A(t) \quad (397)$$

to leading $O(\alpha_s)$. A useful variable is the ratio K_{LS}/K_{LL} , where the form factor R_A drops out [528] and where the target mass corrections were estimated to be small [525].

10.2.3 Meson production

The soft overlap mechanism gives contributions to a number of exclusive wide-angle processes. Huang et al. [534] have investigated exclusive photo- and electroproduction of mesons at large scattering angle, generalizing the approach to Compton scattering described in the previous two subsections. The photon-meson transition was described within the collinear hard scattering mechanism, so that the resulting diagrams had the form of Fig. 2. The scattering amplitudes for the production of longitudinally polarized mesons can then be expressed in terms of *(i)* form factors which apart from the flavor structure are the same as for wide-angle Compton scattering and of *(ii)* the leading-twist meson distribution amplitudes $\Phi^q(z)$ convoluted with hard scattering kernels depending on z and on the external invariants s , t and Q^2 . As already remarked in Section 10.1, dimensional counting behavior for these processes is again mimicked by the mechanism in the t range where the corresponding form factors approximately fall off as t^{-2} .

Compared with available data for large angle photoproduction of π^0 , ρ^0 and ω at $s \sim 10 \text{ GeV}^2$, Huang et al. find that the soft overlap cross sections are too small by orders of magnitude. The authors suggest that these data may be dominated by the hadronic component of the photon, arguing that the s dependence of available cross section data is more compatible with that of meson-hadron scattering than with the dimensional counting behavior of $\gamma p \rightarrow Mp$ in the hard-scattering approach or its soft overlap analog. This hadronic component may be modeled in terms of vector meson dominance as was for instance done in [535]. Its relevance should decrease when the incident photon is virtual, but data in the relevant kinematics are not yet available. Kroll and Passek-Kumerički [94] have pointed out that large-angle electroproduction of η' has some sensitivity to the two-gluon component of the η' , unlike its counterpart in the small- t region. For large-angle real Compton scattering, Huang et al. found that the hadronic component of the photon is not dominant for s around 10 GeV^2 , using available data and vector meson dominance to estimate the corresponding contribution to $\gamma p \rightarrow \gamma p$.

10.3 Two-photon annihilation

Let us now discuss processes related to Compton scattering by crossing symmetry. Exclusive two-photon annihilation offers the possibility to investigate a variety of final states. Data at high energies is available from VENUS [536], CLEO [537, 538, 539], LEP [540, 541, 542, 543], and results with yet higher statistics can be expected from Belle at KEK [543]. The time reversed process of exclusive $p\bar{p}$ annihilation into photon pairs would likely be accessible at the planned HESR facility at GSI [544].

10.3.1 Baryon pair production

The dynamics of $\gamma\gamma \rightarrow p\bar{p}$ at large $s \sim -t \sim -u$ shares important features with wide-angle Compton scattering on the proton. The problems of the hard-scattering approach at s of order 10 GeV^2 are the same as those discussed in Section 10.1, with the leading-twist calculation of [545] being far below

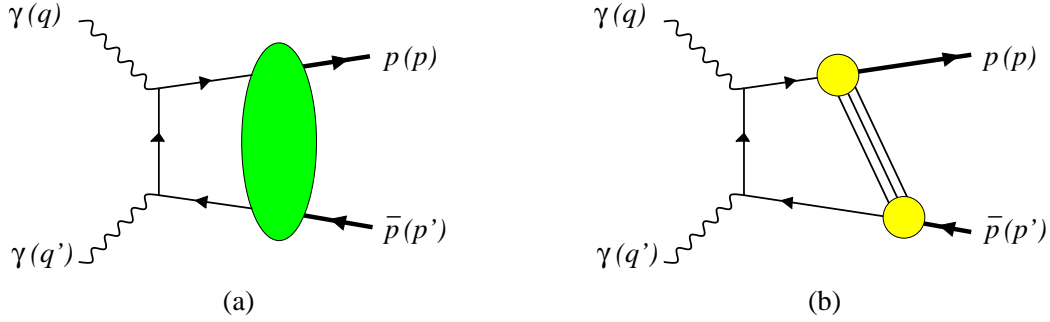


Figure 47: (a) Handbag factorization of $\gamma\gamma \rightarrow p\bar{p}$ at large s , t , u . A second graph is obtained by interchanging the photon vertices. (b) The physical mechanism of handbag factorization. Any number of soft partons connect the two parton-hadron vertices.

the available cross section data for baryon pair production. The diquark model gives a rather good description of the data [546], as it does for wide-angle Compton scattering.

The analog of the soft overlap mechanism for this process is shown in Fig. 47: a hard photon-photon collision produces a quark-antiquark pair, which then hadronizes into $p\bar{p}$ in a soft process. For the hadronization to involve no large virtualities, the additional partons created must have soft momenta, so that the initial quark and antiquark respectively carry almost the full momentum of one of the final-state baryons. This process cannot be represented in terms of a light-cone wave function overlap since one of the soft vertices in Fig. 47b has both incoming and outgoing partons. It can however be treated within a covariant framework starting with Bethe-Salpeter wave functions, as remarked in Section 4.6. In any case, the soft dynamics can be parameterized in terms of crossed versions of the Compton form factors introduced above. Our discussion of Compton scattering at the end of Section 10.1 has its equivalent in the annihilation channel: whether the soft handbag provides the dominant mechanism in given kinematics must be investigated phenomenologically. Since the detailed dynamics is different in the time- and spacelike domains, the ranges in s and $-t$ where the soft handbag is relevant need not be the same.

In [33] the soft handbag diagrams for $\gamma\gamma \rightarrow p\bar{p}$ have been calculated within the same momentum-space formalism as wide-angle Compton scattering [31]. This was done in a reference frame where the baryons are produced back to back and have zero three-momentum along the z axis. The skewness parameter of GDAs is then $\zeta = \frac{1}{2}$, and the baryon and antibaryon appear in a symmetrical fashion. The approximation of setting $x = 1$ in wide-angle Compton scattering now corresponds to approximating the quark plus-momentum fraction z with $\frac{1}{2}$. In order to obtain a representation of the amplitude in terms of GDAs it turned out necessary to neglect configurations where the *antiquark* hadronizes into the proton, in a similar way as discussed at the end of Section 10.2.1. The scattering amplitude is then parameterized in terms of three annihilation form factors,

$$\begin{aligned}
 R_V(s) &= \sum_q e_q^2 \int_0^1 dz \Phi_V^q(z, \frac{1}{2}, s), \\
 R_A(s) &= \sum_q e_q^2 \int_0^1 dz \Phi_A^q(z, \frac{1}{2}, s), & R_P(s) &= \sum_q e_q^2 \int_0^1 dz \Phi_P^q(z, \frac{1}{2}, s), \quad (398)
 \end{aligned}$$

defined from the proton GDAs $\Phi^q(z, \zeta, s)$ we introduced in (80). Up to the different weighting of quark flavors these form factors respectively correspond to the magnetic form factor $G_M(s) = F_1(s) + F_2(s)$ and the axial and pseudoscalar form factors $g_A(s)$, $g_P(s)$ in the timelike region. Because of time

reversal invariance, the helicity amplitudes of $\gamma\gamma \rightarrow p\bar{p}$ and $p\bar{p} \rightarrow \gamma\gamma$ are of course equal.

Freund et al. [34] have considered the same process using the position space method of Radyushkin [30]. In this approach, the amplitudes are expressed in terms of integrals over double distributions of the type

$$\sum_q e_q^2 \int d\beta d\alpha \frac{1}{\beta} f^q(\beta, \alpha, s). \quad (399)$$

From the reduction formula (149) one sees that this cannot be written as a moment of a GDA because of the factor $1/\beta$. The approximations made in [33] correspond to replacing this factor with 1, after which the results of both approaches agree.

For the unpolarized cross section one obtains [33]

$$\frac{d\sigma}{dt}(\gamma\gamma \rightarrow p\bar{p}) = \frac{\pi\alpha_{\text{em}}^2}{s^2} \left[\frac{s^2}{tu} (|R_A(s) + R_P(s)|^2 + \frac{s}{4m^2}|R_P(s)|^2) + \frac{(t-u)^2}{tu}|R_V(s)|^2 \right], \quad (400)$$

where in the calculation of the amplitude we have neglected hadron masses as we did for Compton scattering. For $p\bar{p} \rightarrow \gamma\gamma$ one obtains the same cross section times a factor $(1 - 4m^2/s)^{-1}$ due to the different phase space and flux.

Many phenomenological aspects in the annihilation channel are quite similar to the case of Compton scattering. As one difference we point out that in the annihilation channel it is a combination of the form factors R_A , R_P associated with the axial current, rather than the one associated with the vector current, which tends to dominate the cross section. This is due to the relative kinematical factor $(t-u)^2/s^2 \approx \cos^2\theta$, which is small except in the forward and backward regions, where the approach is not valid. In [33] the size of $|R_A(s)|$ was estimated using $\gamma\gamma \rightarrow p\bar{p}$ data between $s = 6.5 \text{ GeV}^2$ and 11 GeV^2 , finding $s^2|R_A(s)| \approx 5 \div 8 \text{ GeV}^4$ in this region. This is somewhat larger than the estimate $s^2|R_V(s)| \approx 2.5 \div 5 \text{ GeV}^4$ obtained from the data on the magnetic form factor $G_M(s)$, but there is no known constraint that would require $|R_A(s)| \leq |R_V(s)|$. Note that, as in the spacelike region, the s -dependence of these form factors is compatible with dimensional scaling for these values of s . The $\cos\theta$ distribution obtained with these form factor estimates is well approximated by $d\sigma/dt \propto 1/\sin^2\theta$ and was found in reasonable agreement with available data.

A particularity of the soft handbag mechanism is that the final hadron pair originates from an intermediate $q\bar{q}$ state and can therefore only carry isospin $I = 0$ or $I = 1$, but not $I = 2$. Together with flavor SU(3) symmetry this allows one to express the annihilation form factors for all ground state octet baryons in terms of the individual flavor contributions R_i^u , R_i^d , R_i^s ($i = V, A, P$) in the proton [33]. One may expect that for large values of s the strange quark contributions R_i^s are negligible compared with R_i^u and R_i^d , since the quark is required to carry almost all the proton momentum. To the extent that the form factor combination $R_A + R_P$ dominates the cross section (400) one then obtains a simple approximate relation between the cross sections for all octet channels in terms of the ratio of the relevant form factors for $u\bar{u}$ and $d\bar{d}$ fragmenting into $p\bar{p}$. This relation was found to be in reasonable agreement with data for $\Sigma^0\bar{\Sigma}^0$ and $\Lambda\bar{\Lambda}$ pair production in two-photon annihilation, and predicts in particular that the cross section for the mixed $\Lambda\bar{\Sigma}^0 + \Sigma^0\bar{\Lambda}$ channel should be much lower than for $p\bar{p}$ pairs.

10.3.2 Meson pair production

Two-photon annihilation into pairs of pseudoscalar mesons is in some respects simpler than annihilation into baryons. The hard-scattering mechanism involves a partonic subprocess with fewer internal off-shell lines, and one might expect it to be relevant at lower values of s than for baryons. Comparing with the data for $\gamma\gamma \rightarrow \pi^+\pi^-$ at s of order 10 GeV^2 , one finds however [32] that the leading-twist

cross section is well below the observed one, except if one takes a strongly endpoint concentrated pion DA, which is in conflict with the measurements of $\gamma^*\gamma \rightarrow \pi^0$ (see Section 6.2). The situation does not improve when the effect of parton k_T is included in the hard scattering [547].

The soft handbag contribution to meson pair production was studied in [32] using the same methods as for baryon pair production [33]. Evaluating the hard scattering subprocess with the parton momenta approximated by the momenta of the final-state mesons, one obtains however a zero result, due to a conspiracy of invariance under rotation and charge conjugation (which is not effective in the case of baryons because of their spin degree of freedom). The calculation in [32] hence included the first subleading term of the Taylor expansion in the quark plus-momentum fraction z around $\frac{1}{2}$. The scattering amplitude is then expressed in terms of the $(2z-1)$ moment of the two-pion distribution amplitude,

$$R_{\pi\pi}(s) = \frac{1}{2} \sum_q e_q^2 \int_0^1 dz (2z-1) \Phi_{\pi\pi}^q(z, \frac{1}{2}, s). \quad (401)$$

According to Section 3.7.2 this form factor belongs to the quark part of the energy-momentum tensor, except for the weighting by the quark charges. The unpolarized annihilation cross section is found to be

$$\frac{d\sigma}{dt}(\gamma\gamma \rightarrow \pi^+\pi^-) = \frac{\pi\alpha_{\text{em}}^2}{2s^2} \left(\frac{s^2}{tu}\right)^2 |R_{\pi\pi}(s)|^2. \quad (402)$$

Notice that by expanding the hard scattering subprocess to first order in $(2z-1)$ one obtains a cross section going like $s^4/(4tu)^2 \approx 1/\sin^4\theta$, instead of $s^2/(4tu) \approx 1/\sin^2\theta$ in the baryon case. This gives a rather good description of the angular dependence seen in preliminary data on $\gamma\gamma \rightarrow \pi^+\pi^-$ and $\gamma\gamma \rightarrow K^+K^-$ [32]. Fitting to the normalization of preliminary cross section data, the same study obtained an annihilation form factor $|R_{\pi\pi}(s)|$ compatible with dimensional scaling behavior s^{-1} for s between about 6 GeV² and 30 GeV², with a size comparable to the timelike pion form factor (where data is available for $s \lesssim 9$ GeV²).

As in the baryon channels, the absence of isospin $I = 2$ states in the handbag mechanism allows one to relate the cross section for different final states. Using in addition SU(3) flavor symmetry (which is approximately seen in the comparison of $\pi^+\pi^-$ and K^+K^- production data) and neglecting the strange quark contribution to $R_{\pi\pi}(s)$, one predicts a cross section ratio $\sigma(K^0\bar{K}^0) : \sigma(K^+K^-) \simeq 4 : 25$ for kaons. In the two-pion channel only $I = 0$ is allowed in the handbag mechanism, so that one obtains

$$\frac{d\sigma}{dt}(\gamma\gamma \rightarrow \pi^0\pi^0) = \frac{d\sigma}{dt}(\gamma\gamma \rightarrow \pi^+\pi^-). \quad (403)$$

This is in stark contrast to the hard-scattering mechanism, where due to destructive interference between $I = 0$ and $I = 2$ amplitudes the cross section for neutral pions is about an order of magnitude smaller when a pion DA close to the asymptotic form is used [548]. The relation (403) is very robust as it follows only from isospin invariance and from the assumption that the relevant diagrams have handbag topology, i.e., both photons coupling to the same quark line. Its test at large s may thus be one of the cleanest discriminators between the two reaction mechanisms. On the basis of parton-hadron duality Close and Zhang [549] have suggested that this relation may be valid at smaller s values, where the detailed mechanism we have discussed may not yet be applicable. We finally note that $\rho^0\rho^0$ and $\rho^+\rho^-$ production are connected as in (403) by the handbag mechanism.

11 Conclusions

To conclude, let us return to the introduction and take a second look at the different motivations for studying generalized parton distributions and generalized distribution amplitudes.

The link which GPDs provide between the scale evolution of forward parton densities and of distribution amplitudes gives insight into the inner working of evolution itself. It points to a similarity between GPDs in the ERBL region and meson distribution amplitudes which persists beyond the formal level: in both cases one probes quark-antiquark or gluon pairs of small transverse size in a hadron, and dynamical considerations have shown intimate relations between the two types of quantities. A further extension is given by GDAs, which may be seen as probing small-size parton configurations in the hadron continuum, or as describing hadronization in a very specific setting. Both the interplay between GPDs in the DGLAP and the ERBL regions imposed by Lorentz invariance and the crossing symmetry between GPDs and GDAs relate “spacelike” and “timelike” dynamics at the interface between partons and hadrons. To understand these relations at a dynamical level remains a challenge.

Distributions like E^q and E^g are only nonzero because partons carry orbital angular momentum, as can be seen in the helicity balance, in the wave function representation, and in Ji’s sum rule. The state of the art does not yet allow us to quantify how precisely one may evaluate this sum rule from experimental data. Ji’s sum rule provides a very concise way of quantifying the role of orbital angular momentum, but one should not forget that comparing for instance the ξ and t dependence of $E^q(\xi, \xi, t)$ and $H^q(\xi, \xi, t)$ (which is more directly accessible in measurements) would already give information about this poorly known degree of freedom. The wave function and impact parameter representations provide heuristic tools to interpret this information.

Whereas the evaluation of Ji’s sum rule puts a focus on the region of small t (to be eventually continued to $t = 0$), the t dependence by itself opens up a new dimension. Going beyond the “one dimensional projection” inherent in conventional parton densities, it provides access to the transverse structure of hadrons. The impact parameter representation formulates this in a manner well adapted to the parton picture and to relativistic field theory. Elastic form factors like the electromagnetic ones specify the size of hadrons in a “global” way, independent of whether the hadron is probed at a resolution of 0.5 fm or 0.05 fm. Higher moments of GPDs, or the combined dependence of GPDs on longitudinal and transverse variables, will give specific information about spatial structure at parton level, distinguishing slow from fast partons and quarks from gluons, which play very different roles in the dynamics.

The impact parameter picture of GPDs is most simple for $\xi = 0$, where it extends the density interpretation which makes the parton model so intuitive. The relevant processes are however measured at finite ξ . We do not see this as a terrible shortcoming. On one hand the transverse “shift” induced by nonzero ξ is not large in an important part of experimental phase space. Having ξ not exactly zero is on the other hand what gives access to the rather unique points $x = \pm\xi$ and to the region $-\xi < x < \xi$. To adequately describe them is a test for major approaches to understanding hadron structure: examples we have discussed are chiral dynamics and the large- N_c limit, the concept of constituent quarks, and efforts starting from light-cone quantization and wave functions. The points $x = \pm\xi$ are rather directly accessible in DVCS and light meson production, and if DDVCS can be experimentally realized the region $-\xi < x < \xi$ will be as well.

Even in small- x physics, where one initially expected the difference between forward and nonforward distributions to be least important, theoretical studies and comparison with data have revealed important effects of nonzero skewness ξ . Whether for experimentally relevant kinematics these effects can be ascribed to perturbative evolution from a low starting scale (which would allow one to constrain the ordinary gluon distribution in exclusive processes) remains a matter of appreciation. Given our arguments in Section 4.4 we feel that results like the Shuvaev formula (249) should rather be tested than used. Better understanding GPDs in this region is ultimately related with understanding the dynamics of small- x partons beyond the leading $\log \frac{1}{x}$ approximation.

Other fields of study are still rather unexplored, like transition GPDs and GPDs of nuclei. To the

extent that these can be studied in experiment, theoretical investigation will hopefully reveal their physics potential in more detail.

The dynamics of exclusive processes at large s and large t remains a poorly understood area of QCD. The concept of GPDs and GDAs allows one to describe soft Feynman-type contributions in a two-step strategy, separating the dynamical mechanism from quantitative aspects of the hadronic structure. Applying this strategy to processes like wide-angle Compton scattering or two-photon annihilation into meson pairs has identified a number of key observables which should help to pin down the underlying dynamics.

Where do we stand? The wealth of physics information in the functions we have discussed comes with a considerable degree of complexity, which must be managed in practice. The theory for calculating two-photon processes like DVCS from given GPDs is well advanced, at the level of NLO for leading twist and for part of the leading power-suppressed terms. Likewise, theoretical tools are in place to attempt an extraction of information at amplitude level from experimental observables. To take the final step and reconstruct GPDs from amplitudes will require some prior understanding of the interplay between x and ξ in these functions, and the most promising strategy at present is to combine theory studies of dynamics and phenomenological analysis of data in a learning process.

A quantitative description of hard meson production in the framework of GPDs remains a challenge to theory. In a sense these processes have “inherited” the dynamical complexity of meson form factors at large momentum transfer concerning the importance of radiative and power corrections. It should however not be overlooked that meson production provides a wealth of observables from which different aspects of dynamics can be studied phenomenologically. A minimum requirement is to substantiate which observables are least prone to theory uncertainties. Then one may gain quantitative information, both about GPDs and nucleon structure, and about the small-scale structure of mesons and continuum states from their distribution amplitudes. The latter can be studied independently in exclusive reactions at high-luminosity e^+e^- colliders, which would be most valuable.

Experiment has seen impressive progress in the study of hard exclusive processes in the last years, with important measurements at facilities that have not been specifically designed to this end. Further progress in the immediate future can be expected in a wide range of kinematics, from collider energies at H1 and ZEUS to fixed-target energies of HERMES (who already have preliminary results on the beam charge asymmetry in DVCS [550]) and of the Jefferson Lab experiments [551, 552]. Measurements in a region between these extremes will hopefully come from COMPASS at CERN [499]. On an intermediate time scale there is the proposed energy upgrade to 12 GeV at JLAB [527] and the project of an Electron-Ion-Collider EIC [553]. At a certain level of detail and precision, studying the physics described in the review will likely require a dedicated experimental facility.

Acknowledgments

I have very much benefited from discussions with many experimental and theoretical colleagues over the years. Space does not permit to list them all. Thanks go in particular to E. R. Berger, S. J. Brodsky, F. Cano, J. C. Collins, Th. Feldmann, T. Gousset, H. W. Huang, D. S. Hwang, R. Jakob, P. Kroll, B. Pire, J. P. Ralston, O. Teryaev, and C. Vogt, with whom I had the pleasure to collaborate on subjects reviewed here. Special thanks go to D. Müller and M. V. Polyakov for patiently answering innumerable questions concerning their work. I am indebted to M. Amarian, J. C. Collins, Th. Feldmann, G. Iacobucci, R. Jakob, X. Janssen, A. D. Martin, B. Pire, and M. V. Polyakov for valuable remarks on parts of the manuscript.

I thank the Institute for Nuclear Theory at the University of Washington for its hospitality and the Department of Energy for partial support during the completion of this work.

Note added

Concerning the behavior of GPDs at $x = \xi$ (Sections 3.13 and 7.1), Braun et al. [554] have observed that for the perturbatively calculated gluon GPD of a free quark target not only $H^g(x, \xi, t)$ but also its first derivative in x is continuous at this point.

Chen and Savage [555] have investigated the GPDs for the transition from a nucleon to a nucleon and a soft pion (Section 4.1.1). They argue that chiral symmetry is insufficient to reduce these quantities to the elastic nucleon GPDs and claim that the results by Guichon et al. [190] are incorrect.

Hoodbhoy et al. [556] have recalculated the GPDs of the pion in the large t limit (Section 4.1.7) and revealed an error in the result by Vogt [233].

A Acronyms

In the following we list the acronyms used in the text and refer to sections where the corresponding notions are defined or discussed in detail.

DA	Distribution amplitude (Section 3.7)
DIS	Deeply inelastic scattering
DGLAP	Dokshitzer, Gribov, Lipatov, Altarelli, Parisi (Sections 3.2, 3.8)
DVCS	Deeply virtual Compton scattering (Sections 5.1, 5.2, 9.1)
DDVCS	Double deeply virtual Compton scattering (Sections 5.1, 5.2)
ERBL	Efremov, Radyushkin, Brodsky, Lepage (Sections 3.2, 3.7, 3.8)
GDA	Generalized distribution amplitude (Section 3.7)
GPD	Generalized parton distribution
LO	Leading order
NLO	Next-to-leading order
OPE	Operator product expansion (Section 6.1.1)
QCD	Quantum Chromodynamics
TCS	Timelike Compton scattering (Sections 5.1, 5.2, 9.2)

B Light-cone helicity spinors

Here we give the explicit spinors we have used in calculations for fermions with definite light-cone helicity [54]. In the usual Dirac representation they read

$$\begin{aligned}
 u(p, +) &= N \begin{pmatrix} p^0 + p^3 + m \\ p^1 + ip^2 \\ p^0 + p^3 - m \\ p^1 + ip^2 \end{pmatrix}, & u(p, -) &= N \begin{pmatrix} -p^1 + ip^2 \\ p^0 + p^3 + m \\ p^1 - ip^2 \\ -p^0 - p^3 + m \end{pmatrix}, \\
 v(p, +) &= -N \begin{pmatrix} -p^1 + ip^2 \\ p^0 + p^3 - m \\ p^1 - ip^2 \\ -p^0 - p^3 - m \end{pmatrix}, & v(p, -) &= -N \begin{pmatrix} p^0 + p^3 - m \\ p^1 + ip^2 \\ p^0 + p^3 + m \\ p^1 + ip^2 \end{pmatrix},
 \end{aligned} \tag{404}$$

where $N^{-1} = \sqrt{2(p^0 + p^3)}$. For quark spinors this corresponds to the phase conventions of Brodsky and Lepage [51], whereas for antiquark spinors we differ from [51] by the overall sign. The spinors in (404) satisfy the charge conjugation relations $v(p, \nu) = S(C) \bar{u}^T(p, \nu)$ with $S(C) = i\gamma^2\gamma^0$. For

massless spinors one simply has $v(p, \nu) = -u(p, -\nu)$. The covariant spin vectors belonging to our spinors are given by

$$s = \frac{2\nu}{m} \left(p - \frac{m^2}{pn_-} n_- \right) \quad (405)$$

for helicity $\nu = \pm \frac{1}{2}$. This vector is normalized as $s^2 = -1$. In the frame where the particle is at rest, $s = (0, \mathbf{s})$ points into the spin direction. It appears in the projector relations

$$\begin{aligned} u(p, \nu) \bar{u}(p, \nu) &= (\not{p} + m) \frac{1 + \gamma_5 \not{s}}{2}, \\ v(p, \nu) \bar{v}(p, \nu) &= (\not{p} - m) \frac{1 + \gamma_5 \not{s}}{2}. \end{aligned} \quad (406)$$

For states with ordinary helicity we use the convention

$$\begin{aligned} u(p, +) &= \begin{pmatrix} \sqrt{p^0 + m} \chi_+(p) \\ \sqrt{p^0 - m} \chi_+(p) \end{pmatrix}, & u(p, -) &= \begin{pmatrix} \sqrt{p^0 + m} \chi_-(p) \\ -\sqrt{p^0 - m} \chi_-(p) \end{pmatrix}, \\ v(p, +) &= - \begin{pmatrix} \sqrt{p^0 - m} \chi_-(p) \\ -\sqrt{p^0 + m} \chi_-(p) \end{pmatrix}, & v(p, -) &= - \begin{pmatrix} \sqrt{p^0 - m} \chi_+(p) \\ \sqrt{p^0 + m} \chi_+(p) \end{pmatrix} \end{aligned} \quad (407)$$

with two-spinors

$$\begin{aligned} \chi_+(p) &= \frac{1}{\sqrt{2|\vec{p}|(|\vec{p}| + p^3)}} \begin{pmatrix} |\vec{p}| + p^3 \\ p^1 + ip^2 \end{pmatrix} = \begin{pmatrix} \cos \frac{1}{2}\vartheta \\ e^{i\varphi} \sin \frac{1}{2}\vartheta \end{pmatrix}, \\ \chi_-(p) &= \frac{1}{\sqrt{2|\vec{p}|(|\vec{p}| + p^3)}} \begin{pmatrix} -p^1 + ip^2 \\ |\vec{p}| + p^3 \end{pmatrix} = \begin{pmatrix} -e^{-i\varphi} \sin \frac{1}{2}\vartheta \\ \cos \frac{1}{2}\vartheta \end{pmatrix}, \end{aligned} \quad (408)$$

where $\vec{p} = (p^1, p^2, p^3)$ is the three-momentum vector and ϑ, φ are its polar angles. The transformation from the light-cone spinors $u_{\text{LC}}, v_{\text{LC}}$ in (404) to the spinors $u_{\text{H}}, v_{\text{H}}$ in (407) reads

$$\begin{pmatrix} u_{\text{H}}(+), \\ u_{\text{H}}(-) \end{pmatrix} = U \begin{pmatrix} u_{\text{LC}}(+), \\ u_{\text{LC}}(-) \end{pmatrix}, \quad \begin{pmatrix} v_{\text{H}}(+), \\ v_{\text{H}}(-) \end{pmatrix} = U^* \begin{pmatrix} v_{\text{LC}}(+), \\ v_{\text{LC}}(-) \end{pmatrix} \quad (409)$$

with a unitary matrix

$$\begin{aligned} U &= \frac{\sqrt{p^0 + |\vec{p}|}}{\sqrt{2|\vec{p}|(|\vec{p}| + p^3)}(p^0 + p^3)} \begin{pmatrix} |\vec{p}| + p^3, & (p^1 + ip^2) \frac{m}{p^0 + |\vec{p}|} \\ -(p^1 - ip^2) \frac{m}{p^0 + |\vec{p}|}, & |\vec{p}| + p^3 \end{pmatrix} \\ &= \frac{\sqrt{p^0 + |\vec{p}|}}{\sqrt{p^0 + p^3}} \begin{pmatrix} \cos \frac{1}{2}\vartheta, & e^{i\varphi} \sin \frac{1}{2}\vartheta \frac{m}{p^0 + |\vec{p}|} \\ -e^{-i\varphi} \sin \frac{1}{2}\vartheta \frac{m}{p^0 + |\vec{p}|}, & \cos \frac{1}{2}\vartheta \end{pmatrix}. \end{aligned} \quad (410)$$

We see that the ratio $|U_{+-}/U_{++}| = |U_{-+}/U_{--}|$ between off-diagonal and diagonal elements in this matrix is not greater than $(\tan \frac{1}{2}\vartheta) m/(2|\vec{p}|)$. This means that for a particle moving fast at an angle $\vartheta \neq \pi$ the difference between usual and light-cone helicity is small.

References

- [1] G. Altarelli and G. Preparata, Phys. Lett. **B39**, 371 (1972).
- [2] R. Gatto and G. Preparata, Nucl. Phys. **B47**, 313 (1972).
- [3] A. De Rújula and E. De Rafael, Annals Phys. **78**, 132 (1973).
- [4] E. Wieczorek, V. A. Matveev, and D. Robaschik, Theor. Math. Phys. **19**, 315 (1974).
- [5] K. Watanabe, Prog. Theor. Phys. **66**, 1003 (1981).
- [6] K. Watanabe, Prog. Theor. Phys. **67**, 1834 (1982).
- [7] B. Geyer, D. Robaschik, M. Bordag, and J. Hořejši, Z. Phys. **C26**, 591 (1985).
- [8] T. Braunschweig, B. Geyer, J. Hořejši, and D. Robaschik, Z. Phys. **C33**, 275 (1986).
- [9] F. M. Dittes, D. Müller, D. Robaschik, B. Geyer, and J. Hořejši, Phys. Lett. **B209**, 325 (1988).
- [10] D. Müller, D. Robaschik, B. Geyer, F. M. Dittes, and J. Hořejši, Fortschr. Phys. **42**, 101 (1994), hep-ph/9812448.
- [11] V. N. Gribov and L. N. Lipatov, Sov. J. Nucl. Phys. **15**, 438 (1972).
- [12] L. N. Lipatov, Sov. J. Nucl. Phys. **20**, 94 (1975).
- [13] G. Altarelli and G. Parisi, Nucl. Phys. **B126**, 298 (1977).
- [14] Y. L. Dokshitzer, Sov. Phys. JETP **46**, 641 (1977).
- [15] A. V. Efremov and A. V. Radyushkin, Phys. Lett. **B94**, 245 (1980).
- [16] G. P. Lepage and S. J. Brodsky, Phys. Lett. **B87**, 359 (1979).
- [17] J. Bartels and M. Loewe, Zeit. Phys. **C12**, 263 (1982).
- [18] M. G. Ryskin, Z. Phys. **C57**, 89 (1993).
- [19] S. J. Brodsky, L. Frankfurt, J. F. Gunion, A. H. Mueller, and M. Strikman, Phys. Rev. **D50**, 3134 (1994), hep-ph/9402283.
- [20] X.-D. Ji, Phys. Rev. Lett. **78**, 610 (1997), hep-ph/9603249.
- [21] A. V. Radyushkin, Phys. Lett. **B380**, 417 (1996), hep-ph/9604317.
- [22] X.-D. Ji, Phys. Rev. **D55**, 7114 (1997), hep-ph/9609381.
- [23] A. V. Radyushkin, Phys. Lett. **B385**, 333 (1996), hep-ph/9605431.
- [24] J. C. Collins, L. Frankfurt, and M. Strikman, Phys. Rev. **D56**, 2982 (1997), hep-ph/9611433.
- [25] P. Jain and J. P. Ralston, hep-ph/9305250.
- [26] M. Burkardt, Phys. Rev. **D62**, 071503 (2000), hep-ph/0005108, Erratum-ibid. D **66**, 119903 (2002).

- [27] A. G. Grozin, *Sov. J. Nucl. Phys.* **38**, 289 (1983).
- [28] V. A. Baier and A. G. Grozin, *Sov. J. Part. Nucl.* **16**, 1 (1985).
- [29] M. Diehl, T. Gousset, B. Pire, and O. Teryaev, *Phys. Rev. Lett.* **81**, 1782 (1998), hep-ph/9805380.
- [30] A. V. Radyushkin, *Phys. Rev.* **D58**, 114008 (1998), hep-ph/9803316.
- [31] M. Diehl, T. Feldmann, R. Jakob, and P. Kroll, *Eur. Phys. J.* **C8**, 409 (1999), hep-ph/9811253.
- [32] M. Diehl, P. Kroll, and C. Vogt, *Phys. Lett.* **B532**, 99 (2002), hep-ph/0112274.
- [33] M. Diehl, P. Kroll, and C. Vogt, *Eur. Phys. J.* **C26**, 567 (2003), hep-ph/0206288.
- [34] A. Freund, A. V. Radyushkin, A. Schäfer, and C. Weiss, *Phys. Rev. Lett.* **90**, 092001 (2003), hep-ph/0208061.
- [35] X.-D. Ji, *J. Phys.* **G24**, 1181 (1998), hep-ph/9807358.
- [36] A. V. Radyushkin, hep-ph/0101225.
- [37] K. Goeke, M. V. Polyakov, and M. Vanderhaeghen, *Prog. Part. Nucl. Phys.* **47**, 401 (2001), hep-ph/0106012.
- [38] G. P. Lepage and S. J. Brodsky, *Phys. Rev.* **D22**, 2157 (1980).
- [39] A. V. Radyushkin, *Phys. Rev.* **D56**, 5524 (1997), hep-ph/9704207.
- [40] K. J. Golec-Biernat and A. D. Martin, *Phys. Rev.* **D59**, 014029 (1999), hep-ph/9807497.
- [41] M. Diehl, T. Feldmann, R. Jakob, and P. Kroll, *Nucl. Phys.* **B596**, 33 (2001), hep-ph/0009255, Erratum-ibid. B **605**, 647 (2001).
- [42] M. V. Polyakov, private communication (2003).
- [43] P. V. Pobylitsa, *Phys. Rev.* **D67**, 034009 (2003), hep-ph/0210150.
- [44] B. C. Tiburzi and G. A. Miller, *Phys. Rev.* **D67**, 013010 (2003), hep-ph/0209178.
- [45] P. V. Landshoff, J. C. Polkinghorne, and R. D. Short, *Nucl. Phys.* **B28**, 225 (1971).
- [46] L. Frankfurt, A. Freund, V. Guzey, and M. Strikman, *Phys. Lett.* **B418**, 345 (1998), hep-ph/9703449.
- [47] M. Diehl and T. Gousset, *Phys. Lett.* **B428**, 359 (1998), hep-ph/9801233.
- [48] R. L. Jaffe, *Nucl. Phys.* **B229**, 205 (1983).
- [49] J. B. Kogut and D. E. Soper, *Phys. Rev.* **D1**, 2901 (1970).
- [50] S. J. Brodsky and G. P. Lepage, in: A. H. Mueller (Ed.), *Perturbative Quantum Chromodynamics* (World Scientific, Singapore, 1989) p. 93.
- [51] S. J. Brodsky, H.-C. Pauli, and S. S. Pinsky, *Phys. Rept.* **301**, 299 (1998), hep-ph/9705477.
- [52] R. L. Jaffe, hep-ph/9602236.

- [53] K. Yamawaki, hep-th/9802037.
- [54] D. E. Soper, Phys. Rev. **D5**, 1956 (1972).
- [55] M. Diehl, Eur. Phys. J. **C19**, 485 (2001), hep-ph/0101335.
- [56] A. V. Belitsky and D. Müller, Phys. Lett. **B486**, 369 (2000), hep-ph/0005028.
- [57] P. Hoodbhoy and X.-D. Ji, Phys. Rev. **D58**, 054006 (1998), hep-ph/9801369.
- [58] J. P. Ralston and D. E. Soper, Nucl. Phys. **B152**, 109 (1979).
- [59] R. L. Jaffe, hep-ph/9710465.
- [60] V. Barone, A. Drago, and P. G. Ratcliffe, Phys. Rept. **359**, 1 (2002), hep-ph/0104283.
- [61] R. L. Jaffe and A. Manohar, Phys. Lett. **B223**, 218 (1989).
- [62] X. Artru and M. Mekhfi, Z. Phys. **C45**, 669 (1990).
- [63] X.-D. Ji and R. F. Lebed, Phys. Rev. **D63**, 076005 (2001), hep-ph/0012160.
- [64] R. Windmolders, Nucl. Phys. Proc. Suppl. **79**, 51 (1999), hep-ph/9905505.
- [65] B. W. Filippone and X.-D. Ji, Adv. Nucl. Phys. **26**, 1 (2001), hep-ph/0101224.
- [66] L. M. Sehgal, Phys. Rev. **D10**, 1663 (1974), Erratum-ibid. D **11**, 2016 (1975).
- [67] P. G. Ratcliffe, Phys. Lett. **B192**, 180 (1987).
- [68] X.-D. Ji, Phys. Rev. **D58**, 056003 (1998), hep-ph/9710290.
- [69] S. J. Brodsky, D. S. Hwang, B.-Q. Ma, and I. Schmidt, Nucl. Phys. **B593**, 311 (2001), hep-th/0003082.
- [70] O. V. Teryaev, hep-ph/9904376.
- [71] QCDSF Collaboration, M. Göckeler *et al.*, hep-ph/0304249.
- [72] LHPC and SESAM Collaborations, P. Hägler *et al.*, hep-lat/0304018.
- [73] P. Hoodbhoy, X.-D. Ji, and W. Lu, Phys. Rev. **D59**, 074010 (1999), hep-ph/9808305.
- [74] R. L. Jaffe and A. Manohar, Nucl. Phys. **B337**, 509 (1990).
- [75] P. Hoodbhoy, X.-D. Ji, and W. Lu, Phys. Rev. **D59**, 014013 (1999), hep-ph/9804337.
- [76] R. L. Jaffe, Phil. Trans. Roy. Soc. Lond. **A359**, 391 (2001), hep-ph/0008038.
- [77] I. Balitsky and X.-D. Ji, Phys. Rev. Lett. **79**, 1225 (1997), hep-ph/9702277.
- [78] V. Barone, T. Calarco, and A. Drago, Phys. Lett. **B431**, 405 (1998), hep-ph/9801281.
- [79] N. Mathur, S. J. Dong, K. F. Liu, L. Mankiewicz, and N. C. Mukhopadhyay, Phys. Rev. **D62**, 114504 (2000), hep-ph/9912289.
- [80] V. Gadiyak, X.-D. Ji, and C.-W. Jung, Phys. Rev. **D65**, 094510 (2002), hep-lat/0112040.

- [81] S. D. Bass, Phys. Rev. **D65**, 074025 (2002), hep-ph/0102036.
- [82] M. V. Polyakov and A. G. Shuvaev, hep-ph/0207153.
- [83] M. V. Polyakov, Phys. Lett. **B555**, 57 (2003), hep-ph/0210165.
- [84] R. G. Sachs, Phys. Rev. **126**, 2256 (1962).
- [85] M. Diehl, T. Gousset, and B. Pire, Phys. Rev. **D62**, 073014 (2000), hep-ph/0003233.
- [86] N. Kivel, L. Mankiewicz, and M. V. Polyakov, Phys. Lett. **B467**, 263 (1999), hep-ph/9908334.
- [87] M. V. Polyakov, Nucl. Phys. **B555**, 231 (1999), hep-ph/9809483.
- [88] B. Pire and O. V. Teryaev, Phys. Lett. **B496**, 76 (2000), hep-ph/0007014.
- [89] I. V. Anikin, B. Pire, and O. V. Teryaev, hep-ph/0307059.
- [90] M. V. Polyakov and C. Weiss, Phys. Rev. **D60**, 114017 (1999), hep-ph/9902451.
- [91] K. M. Watson, Phys. Rev. **95**, 228 (1954).
- [92] M. K. Chase, Nucl. Phys. **B174**, 109 (1980).
- [93] A. G. Baier, V. A. Grozin, Sov. J. Nucl. Phys. **35**, 596 (1982).
- [94] P. Kroll and K. Passek-Kumerički, Phys. Rev. **D67**, 054017 (2003), hep-ph/0210045.
- [95] L. V. Gribov, E. M. Levin, and M. G. Ryskin, Phys. Rept. **100**, 1 (1983).
- [96] A. D. Martin and M. G. Ryskin, Phys. Rev. **D57**, 6692 (1998), hep-ph/9711371.
- [97] I. I. Balitsky and A. V. Radyushkin, Phys. Lett. **B413**, 114 (1997), hep-ph/9706410.
- [98] A. V. Radyushkin, Phys. Rev. **D59**, 014030 (1999), hep-ph/9805342.
- [99] J. Blümlein, B. Geyer, and D. Robaschik, Phys. Lett. **B406**, 161 (1997), hep-ph/9705264.
- [100] J. Blümlein, B. Geyer, and D. Robaschik, Nucl. Phys. **B560**, 283 (1999), hep-ph/9903520.
- [101] A. V. Belitsky and D. Müller, Nucl. Phys. **B527**, 207 (1998), hep-ph/9802411.
- [102] A. V. Belitsky and D. Müller, Nucl. Phys. **B537**, 397 (1999), hep-ph/9804379.
- [103] A. V. Belitsky, D. Müller, and A. Freund, Phys. Lett. **B461**, 270 (1999), hep-ph/9904477.
- [104] A. V. Belitsky and D. Müller, Phys. Lett. **B464**, 249 (1999), hep-ph/9906409.
- [105] A. V. Belitsky, A. Freund, and D. Müller, Nucl. Phys. **B574**, 347 (2000), hep-ph/9912379.
- [106] A. V. Belitsky, A. Freund, and D. Müller, Phys. Lett. **B493**, 341 (2000), hep-ph/0008005.
- [107] A. P. Bukhvostov, G. V. Frolov, L. N. Lipatov, and E. A. Kuraev, Nucl. Phys. **B258**, 601 (1985).
- [108] I. I. Balitsky and V. M. Braun, Nucl. Phys. **B311**, 541 (1989).

- [109] A. V. Belitsky, D. Müller, L. Niedermeier, and A. Schäfer, Nucl. Phys. **B546**, 279 (1999), hep-ph/9810275.
- [110] A. Freund and M. McDermott, Eur. Phys. J. **C23**, 651 (2002), hep-ph/0111472.
- [111] A. Freund and V. Guzey, Phys. Lett. **B462**, 178 (1999), hep-ph/9806267.
- [112] K. Golec-Biernat, J. Kwieciński, and A. D. Martin, Phys. Rev. **D58**, 094001 (1998), hep-ph/9803464.
- [113] K. J. Golec-Biernat, A. D. Martin, and M. G. Ryskin, Phys. Lett. **B456**, 232 (1999), hep-ph/9903327.
- [114] A. V. Belitsky, B. Geyer, D. Müller, and A. Schäfer, Phys. Lett. **B421**, 312 (1998), hep-ph/9710427.
- [115] I. V. Musatov and A. V. Radyushkin, Phys. Rev. **D61**, 074027 (2000), hep-ph/9905376.
- [116] A. V. Belitsky, D. Müller, L. Niedermeier, and A. Schäfer, Phys. Lett. **B437**, 160 (1998), hep-ph/9806232.
- [117] A. Freund and M. F. McDermott, Phys. Rev. **D65**, 056012 (2002), hep-ph/0106115.
- [118] A. V. Efremov and A. V. Radyushkin, Theor. Math. Phys. **42**, 97 (1980).
- [119] Y. M. Makeenko, Sov. J. Nucl. Phys. **33**, 440 (1981).
- [120] T. Ohrndorf, Nucl. Phys. **B198**, 26 (1982).
- [121] A. Shuvaev, Phys. Rev. **D60**, 116005 (1999), hep-ph/9902318.
- [122] N. Kivel and L. Mankiewicz, Nucl. Phys. **B557**, 271 (1999), hep-ph/9903531.
- [123] L. Mankiewicz, G. Piller, and T. Weigl, Eur. Phys. J. **C5**, 119 (1998), hep-ph/9711227.
- [124] A. V. Belitsky, D. Müller, L. Niedermeier, and A. Schäfer, Phys. Lett. **B474**, 163 (2000), hep-ph/9908337.
- [125] J. D. Noritzsch, Phys. Rev. **D62**, 054015 (2000), hep-ph/0004012.
- [126] A. G. Shuvaev, K. J. Golec-Biernat, A. D. Martin, and M. G. Ryskin, Phys. Rev. **D60**, 014015 (1999), hep-ph/9902410.
- [127] A. V. Radyushkin, Phys. Lett. **B449**, 81 (1999), hep-ph/9810466.
- [128] A. V. Radyushkin, Phys. Lett. **B131**, 179 (1983).
- [129] O. V. Teryaev, Phys. Lett. **B510**, 125 (2001), hep-ph/0102303.
- [130] A. V. Belitsky, D. Müller, A. Kirchner, and A. Schäfer, Phys. Rev. **D64**, 116002 (2001), hep-ph/0011314.
- [131] N. Kivel and M. V. Polyakov, hep-ph/0203264.
- [132] J. C. Collins and D. E. Soper, Nucl. Phys. **B193**, 381 (1981), Erratum-ibid. B **213**, 545 (1983).
- [133] M. Burkardt, Int. J. Mod. Phys. **A18**, 173 (2003), hep-ph/0207047.

- [134] M. Diehl, Eur. Phys. J. **C25**, 223 (2002), hep-ph/0205208, Erratum-ibid. to appear.
- [135] J. P. Ralston and B. Pire, Phys. Rev. **D66**, 111501 (2002), hep-ph/0110075.
- [136] D. E. Soper, Phys. Rev. **D15**, 1141 (1977).
- [137] M. Burkardt, hep-ph/0008051.
- [138] J. B. Kogut and L. Susskind, Phys. Rev. **D9**, 3391 (1974).
- [139] P. V. Pobylitsa, Phys. Rev. **D66**, 094002 (2002), hep-ph/0204337.
- [140] A. V. Belitsky and D. Müller, Nucl. Phys. **A711**, 118 (2002), hep-ph/0206306.
- [141] A. V. Belitsky, hep-ph/0307256.
- [142] X.-D. Ji, hep-ph/0304037.
- [143] P. J. Mulders and R. D. Tangerman, Nucl. Phys. **B461**, 197 (1996), hep-ph/9510301.
- [144] P. J. Mulders, hep-ph/9912493.
- [145] M. Burkardt, Phys. Rev. **D66**, 114005 (2002), hep-ph/0209179.
- [146] M. Burkardt, hep-ph/0302144.
- [147] B. Pire and L. Szymanowski, Phys. Lett. **B556**, 129 (2003), hep-ph/0212296.
- [148] S. J. Brodsky, M. Diehl, and D. S. Hwang, Nucl. Phys. **B596**, 99 (2001), hep-ph/0009254.
- [149] M. Burkardt, X.-D. Ji, and F. Yuan, Phys. Lett. **B545**, 345 (2002), hep-ph/0205272.
- [150] X.-D. Ji, J.-P. Ma, and F. Yuan, Nucl. Phys. **B652**, 383 (2003), hep-ph/0210430.
- [151] P. Ball and V. M. Braun, hep-ph/9808229.
- [152] P. Ball, JHEP **01**, 010 (1999), hep-ph/9812375.
- [153] V. Braun, R. J. Fries, N. Mahnke, and E. Stein, Nucl. Phys. **B589**, 381 (2000), hep-ph/0007279.
- [154] B. C. Tiburzi and G. A. Miller, Phys. Rev. **D67**, 054015 (2003), hep-ph/0210305.
- [155] L. Mankiewicz and A. Schäfer, Phys. Lett. **B265**, 167 (1991).
- [156] L. Mankiewicz and Z. Ryzak, Phys. Rev. **D43**, 733 (1991).
- [157] A. Mukherjee and M. Vanderhaeghen, Phys. Rev. **D67**, 085020 (2003), hep-ph/0211386.
- [158] S. D. Drell and T.-M. Yan, Phys. Rev. Lett. **24**, 181 (1970).
- [159] S. J. Brodsky and S. D. Drell, Phys. Rev. **D22**, 2236 (1980).
- [160] J. P. Ralston, P. Jain, and R. V. Buniy, AIP Conf. Proc. **549**, 302 (2000), hep-ph/0206074.
- [161] X.-D. Ji, J.-P. Ma, and F. Yuan, hep-ph/0301141.
- [162] X.-D. Ji, J.-P. Ma, and F. Yuan, hep-ph/0304107.

- [163] M. Sawicki, Phys. Rev. **D46**, 474 (1992).
- [164] S. J. Brodsky and D. S. Hwang, Nucl. Phys. **B543**, 239 (1999), hep-ph/9806358.
- [165] A. Mukherjee and M. Vanderhaeghen, Phys. Lett. **B542**, 245 (2002), hep-ph/0206159.
- [166] S. J. Brodsky, P. Hoyer, N. Marchal, S. Peigné, and F. Sannino, Phys. Rev. **D65**, 114025 (2002), hep-ph/0104291.
- [167] J. C. Collins, Phys. Lett. **B536**, 43 (2002), hep-ph/0204004.
- [168] J. C. Collins, Acta Phys. Polon. **B34**, 3103 (2003), hep-ph/0304122.
- [169] X.-D. Ji and F. Yuan, Phys. Lett. **B543**, 66 (2002), hep-ph/0206057.
- [170] A. V. Belitsky, X.-D. Ji, and F. Yuan, Nucl. Phys. **B656**, 165 (2003), hep-ph/0208038.
- [171] S. J. Brodsky, D. S. Hwang, and I. Schmidt, Phys. Lett. **B530**, 99 (2002), hep-ph/0201296.
- [172] S. J. Brodsky, D. S. Hwang, and I. Schmidt, Nucl. Phys. **B642**, 344 (2002), hep-ph/0206259.
- [173] B. Pire, J. Soffer, and O. Teryaev, Eur. Phys. J. **C8**, 103 (1999), hep-ph/9804284.
- [174] M. Burkardt, hep-ph/0105324.
- [175] P. V. Pobylitsa, Phys. Rev. **D65**, 077504 (2002), hep-ph/0112322.
- [176] P. V. Pobylitsa, Phys. Rev. **D65**, 114015 (2002), hep-ph/0201030.
- [177] P. V. Pobylitsa, Phys. Rev. **D67**, 094012 (2003), hep-ph/0210238.
- [178] P. V. Pobylitsa, hep-ph/0211160.
- [179] J. Soffer, Phys. Rev. Lett. **74**, 1292 (1995), hep-ph/9409254.
- [180] G. Altarelli, S. Forte, and G. Ridolfi, Nucl. Phys. **B534**, 277 (1998), hep-ph/9806345.
- [181] J. C. Collins and A. Freund, Phys. Rev. **D59**, 074009 (1999), hep-ph/9801262.
- [182] L. Theussl, S. Noguera, and V. Vento, nucl-th/0211036.
- [183] M. Burkardt, Phys. Rev. **D62**, 094003 (2000), hep-ph/0005209.
- [184] G. 't Hooft, Nucl. Phys. **B75**, 461 (1974).
- [185] F. Antonuccio, S. J. Brodsky, and S. Dalley, Phys. Lett. **B412**, 104 (1997), hep-ph/9705413.
- [186] L. Mankiewicz, G. Piller, and T. Weigl, Phys. Rev. **D59**, 017501 (1999), hep-ph/9712508.
- [187] L. L. Frankfurt, P. V. Pobylitsa, M. V. Polyakov, and M. Strikman, Phys. Rev. **D60**, 014010 (1999), hep-ph/9901429.
- [188] L. L. Frankfurt, M. V. Polyakov, and M. Strikman, hep-ph/9808449.
- [189] L. L. Frankfurt, M. V. Polyakov, M. Strikman, and M. Vanderhaeghen, Phys. Rev. Lett. **84**, 2589 (2000), hep-ph/9911381.
- [190] P. A. M. Guichon, L. Mossé, and M. Vanderhaeghen, hep-ph/0305231.

- [191] J. Blümlein, J. Eilers, B. Geyer, and D. Robaschik, Phys. Rev. **D65**, 054029 (2002), hep-ph/0108095.
- [192] T. Feldmann and P. Kroll, Eur. Phys. J. **C12**, 99 (2000), hep-ph/9905343.
- [193] E. R. Berger, F. Cano, M. Diehl, and B. Pire, Phys. Rev. Lett. **87**, 142302 (2001), hep-ph/0106192.
- [194] P. Hoodbhoy, R. L. Jaffe, and A. Manohar, Nucl. Phys. **B312**, 571 (1989).
- [195] F. E. Close and S. Kumano, Phys. Rev. **D42**, 2377 (1990).
- [196] L. Mankiewicz, G. Piller, and A. Radyushkin, Eur. Phys. J. **C10**, 307 (1999), hep-ph/9812467.
- [197] M. Penttinen, M. V. Polyakov, and K. Goeke, Phys. Rev. **D62**, 014024 (2000), hep-ph/9909489.
- [198] S. Weinberg, *The quantum theory of fields. Vol. II: Modern applications* (Cambridge University Press, 1996).
- [199] A. V. Belitsky and X.-D. Ji, Phys. Lett. **B538**, 289 (2002), hep-ph/0203276.
- [200] N. Kivel, M. V. Polyakov, and M. Vanderhaeghen, Phys. Rev. **D63**, 114014 (2001), hep-ph/0012136.
- [201] G. 't Hooft, Nucl. Phys. **B72**, 461 (1974).
- [202] E. Witten, Nucl. Phys. **B160**, 57 (1979).
- [203] V. Y. Petrov *et al.*, Phys. Rev. **D57**, 4325 (1998), hep-ph/9710270.
- [204] D. Diakonov, V. Y. Petrov, P. V. Pobylitsa, M. V. Polyakov, and C. Weiss, Phys. Rev. **D56**, 4069 (1997), hep-ph/9703420.
- [205] D. Diakonov and V. Y. Petrov, hep-ph/0009006.
- [206] C. V. Christov *et al.*, Prog. Part. Nucl. Phys. **37**, 91 (1996), hep-ph/9604441.
- [207] P. Schweitzer, S. Boffi, and M. Radici, Phys. Rev. **D66**, 114004 (2002), hep-ph/0207230.
- [208] P. Schweitzer, M. Colli, and S. Boffi, Phys. Rev. **D67**, 114022 (2003), hep-ph/0303166.
- [209] E. R. Berger, M. Diehl, and B. Pire, Phys. Lett. **B523**, 265 (2001), hep-ph/0110080.
- [210] M. Praszalowicz and A. Rostworowski, Acta Phys. Polon. **B34**, 2699 (2003), hep-ph/0302269.
- [211] A. Chodos, R. L. Jaffe, K. Johnson, C. B. Thorn, and V. F. Weisskopf, Phys. Rev. **D9**, 3471 (1974).
- [212] X.-D. Ji, W. Melnitchouk, and X. Song, Phys. Rev. **D56**, 5511 (1997), hep-ph/9702379.
- [213] I. V. Anikin, D. Binosi, R. Medrano, S. Noguera, and V. Vento, Eur. Phys. J. **A14**, 95 (2002), hep-ph/0109139.
- [214] S. Scopetta and V. Vento, Eur. Phys. J. **A16**, 527 (2003), hep-ph/0201265.
- [215] S. Boffi, B. Pasquini, and M. Traini, Nucl. Phys. **B649**, 243 (2003), hep-ph/0207340.

- [216] G. A. Miller and M. R. Frank, Phys. Rev. **C65**, 065205 (2002), nucl-th/0201021.
- [217] H.-M. Choi, C.-R. Ji, and L. S. Kisslinger, Phys. Rev. **D66**, 053011 (2002), hep-ph/0204321.
- [218] H.-M. Choi, C.-R. Ji, and L. S. Kisslinger, Phys. Rev. **D64**, 093006 (2001), hep-ph/0104117.
- [219] B. C. Tiburzi and G. A. Miller, Phys. Rev. **D65**, 074009 (2002), hep-ph/0109174.
- [220] B. C. Tiburzi and G. A. Miller, Phys. Rev. **D67**, 054014 (2003), hep-ph/0210304.
- [221] J. Bolz and P. Kroll, Z. Phys. **A356**, 327 (1996), hep-ph/9603289.
- [222] S. J. Brodsky, T. Huang, and G. P. Lepage, in: *Particles and Fields 2*, Proc. of the Banff Summer Institute, Banff, Alberta, 1981, Eds. A. Z. Capri and A. N. Kamal (Plenum, New York, 1981) p. 143.
- [223] A. Szczepaniak, A. Radyushkin, and C.-R. Ji, Phys. Rev. **D57**, 2813 (1998), hep-ph/9708237.
- [224] A. R. Zhitnitsky, Phys. Lett. **B357**, 211 (1995), hep-ph/9410228.
- [225] I. E. Halperin and A. Zhitnitsky, Phys. Rev. **D56**, 184 (1997), hep-ph/9612425.
- [226] N. G. Stefanis, W. Schroers, and H.-C. Kim, Eur. Phys. J. **C18**, 137 (2000), hep-ph/0005218.
- [227] C. Vogt, Phys. Rev. **D63**, 034013 (2001), hep-ph/0007277.
- [228] A. V. Afanasev, hep-ph/9808291.
- [229] P. Stoler, Phys. Rev. **D65**, 053013 (2002), hep-ph/0108257.
- [230] P. Stoler, hep-ph/0307162.
- [231] A. P. Bakulev, R. Ruskov, K. Goeke, and N. G. Stefanis, Phys. Rev. **D62**, 054018 (2000), hep-ph/0004111.
- [232] B. C. Tiburzi and G. A. Miller, Phys. Rev. **C64**, 065204 (2001), hep-ph/0104198.
- [233] C. Vogt, Phys. Rev. **D64**, 057501 (2001), hep-ph/0101059.
- [234] V. N. Gribov, hep-ph/0006158.
- [235] S. Dalley, hep-ph/0306121.
- [236] E. Ruiz Arriola and W. Broniowski, hep-ph/0307198.
- [237] J. W. Negele, Nucl. Phys. **A699**, 18 (2002), hep-lat/0107010.
- [238] M. Göckeler *et al.*, hep-lat/0209160.
- [239] M. Göckeler *et al.*, hep-ph/0108105.
- [240] M. Göckeler *et al.*, hep-lat/0303019.
- [241] A. D. Martin and T. D. Spearman, *Elementary Particle Theory* (North-Holland, Amsterdam, 1970).
- [242] P. D. B. Collins, *An Introduction to Regge Theory and High-Energy Physics* (Cambridge University Press, Cambridge, 1977).

- [243] E. R. Berger, M. Diehl, and B. Pire, *Eur. Phys. J.* **C23**, 675 (2002), hep-ph/0110062.
- [244] A. V. Belitsky, D. Müller, and A. Kirchner, *Nucl. Phys.* **B629**, 323 (2002), hep-ph/0112108.
- [245] A. D. Martin, R. G. Roberts, W. J. Stirling, and R. S. Thorne, *Phys. Lett.* **B531**, 216 (2002), hep-ph/0201127.
- [246] Asymmetry Analysis Collaboration, Y. Goto *et al.*, *Phys. Rev.* **D62**, 034017 (2000), hep-ph/0001046.
- [247] E. Leader, A. V. Sidorov, and D. B. Stamenov, *Eur. Phys. J.* **C23**, 479 (2002), hep-ph/0111267.
- [248] M. Glück, E. Reya, and A. Vogt, *Eur. Phys. J.* **C5**, 461 (1998), hep-ph/9806404.
- [249] M. Glück, E. Reya, M. Stratmann, and W. Vogelsang, *Phys. Rev.* **D63**, 094005 (2001), hep-ph/0011215.
- [250] B. Lehmann-Dronke, M. Maul, S. Schaefer, E. Stein, and A. Schäfer, *Phys. Lett.* **B457**, 207 (1999), hep-ph/9901283.
- [251] A. Freund, M. McDermott, and M. Strikman, *Phys. Rev.* **D67**, 036001 (2003), hep-ph/0208160.
- [252] C. Weiss, private communication (2001).
- [253] P. A. M. Guichon and M. Vanderhaeghen, *Prog. Part. Nucl. Phys.* **41**, 125 (1998), hep-ph/9806305.
- [254] P. Mergell, U. G. Meissner, and D. Drechsel, *Nucl. Phys.* **A596**, 367 (1996), hep-ph/9506375.
- [255] E. J. Brash, A. Kozlov, S. Li, and G. M. Huber, *Phys. Rev.* **C65**, 051001 (2002), hep-ex/0111038.
- [256] V. Bernard, L. Elouadrhiri, and U. G. Meissner, *J. Phys.* **G28**, R1 (2002), hep-ph/0107088.
- [257] A. Mukherjee, I. V. Musatov, H. C. Pauli, and A. V. Radyushkin, *Phys. Rev.* **D67**, 073014 (2003), hep-ph/0205315.
- [258] B. C. Tiburzi and G. A. Miller, *Phys. Rev.* **D67**, 113004 (2003), hep-ph/0212238.
- [259] H1 Collaboration, C. Adloff *et al.*, *Phys. Lett.* **B517**, 47 (2001), hep-ex/0107005.
- [260] HERMES Collaboration, A. Airapetian *et al.*, *Phys. Rev. Lett.* **87**, 182001 (2001), hep-ex/0106068.
- [261] CLAS Collaboration, S. Stepanyan *et al.*, *Phys. Rev. Lett.* **87**, 182002 (2001), hep-ex/0107043.
- [262] F. Cano and B. Pire, hep-ph/0307231.
- [263] V. Guzey and M. Strikman, hep-ph/0301216.
- [264] A. Kirchner and D. Müller, hep-ph/0302007.
- [265] A. Freund and M. Strikman, hep-ph/0307211.
- [266] J. Osborne and X.-N. Wang, *Nucl. Phys.* **A710**, 281 (2002), hep-ph/0204046.
- [267] M. V. Polyakov and C. Weiss, *Phys. Rev.* **D59**, 091502 (1999), hep-ph/9806390.

- [268] M. Diehl, T. Feldmann, P. Kroll, and C. Vogt, Phys. Rev. **D61**, 074029 (2000), hep-ph/9912364.
- [269] B. Lehmann-Dronke, P. V. Pobylitsa, M. V. Polyakov, A. Schäfer, and K. Goeke, Phys. Lett. **B475**, 147 (2000), hep-ph/9910310.
- [270] V. Y. Petrov, M. V. Polyakov, R. Ruskov, C. Weiss, and K. Goeke, Phys. Rev. **D59**, 114018 (1999), hep-ph/9807229.
- [271] N. Kivel and L. Mankiewicz, Eur. Phys. J. **C18**, 107 (2000), hep-ph/0008168.
- [272] B. Lehmann-Dronke, A. Schäfer, M. V. Polyakov, and K. Goeke, Phys. Rev. **D63**, 114001 (2001), hep-ph/0012108.
- [273] P. Hägler, B. Pire, L. Szymanowski, and O. V. Teryaev, Eur. Phys. J. **C26**, 261 (2002), hep-ph/0207224.
- [274] B. Andersson, G. Gustafson, G. Ingelman, and T. Sjöstrand, Phys. Rept. **97**, 31 (1983).
- [275] M. Maul, Phys. Rev. **D63**, 036003 (2001), hep-ph/0003254.
- [276] J. C. Collins, hep-ph/9907513.
- [277] J. C. Collins, D. E. Soper, and G. Sterman, in: A. H. Mueller (Ed.), *Perturbative Quantum Chromodynamics* (World Scientific, Singapore, 1989) p. 1.
- [278] X.-D. Ji and J. Osborne, Phys. Rev. **D58**, 094018 (1998), hep-ph/9801260.
- [279] C. W. Bauer, S. Fleming, D. Pirjol, I. Z. Rothstein, and I. W. Stewart, Phys. Rev. **D66**, 014017 (2002), hep-ph/0202088.
- [280] S. E. Derkachov and R. Kirschner, Phys. Rev. **D64**, 074013 (2001), hep-ph/0101174.
- [281] J. C. Collins, private communication (2001).
- [282] M. Guidal and M. Vanderhaeghen, Phys. Rev. Lett. **90**, 012001 (2003), hep-ph/0208275.
- [283] A. Freund, Phys. Rev. **D61**, 074010 (2000), hep-ph/9903489.
- [284] S. Coleman and R. E. Norton, Nuovo Cim. **38**, 438 (1965).
- [285] A. Hebecker and P. V. Landshoff, Phys. Lett. **B419**, 393 (1998), hep-ph/9710296.
- [286] A. Freund and M. F. McDermott, Phys. Rev. **D65**, 074008 (2002), hep-ph/0106319.
- [287] J. C. Collins and M. Diehl, Phys. Rev. **D61**, 114015 (2000), hep-ph/9907498.
- [288] J. Blümlein and D. Robaschik, Nucl. Phys. **B581**, 449 (2000), hep-ph/0002071.
- [289] P. Hoodbhoy, Phys. Rev. **D65**, 077501 (2002), hep-ph/0108214.
- [290] M. Diehl, T. Gousset, and B. Pire, Phys. Rev. **D59**, 034023 (1999), hep-ph/9808479.
- [291] S. J. Brodsky and G. P. Lepage, Phys. Rev. **D24**, 2848 (1981).
- [292] M. V. Polyakov, private communication (2001).

- [293] A. V. Belitsky, D. Müller, L. Niedermeier, and A. Schäfer, Nucl. Phys. **B593**, 289 (2001), hep-ph/0004059.
- [294] A. V. Belitsky and D. Müller, Phys. Lett. **B417**, 129 (1998), hep-ph/9709379.
- [295] L. Mankiewicz, G. Piller, E. Stein, M. Vanttinen, and T. Weigl, Phys. Lett. **B425**, 186 (1998), hep-ph/9712251.
- [296] X.-D. Ji and J. Osborne, Phys. Rev. **D57**, 1337 (1998), hep-ph/9707254.
- [297] D. Müller, private communication (2000).
- [298] A. Freund and M. F. McDermott, Phys. Rev. **D65**, 091901 (2002), hep-ph/0106124.
- [299] ZEUS Collaboration, S. Chekanov *et al.*, hep-ex/0305028.
- [300] ZEUS Collaboration, J. Breitweg *et al.*, Eur. Phys. J. **C12**, 35 (2000), hep-ex/9908012.
- [301] H1 Collaboration, C. Adloff *et al.*, Phys. Lett. **B528**, 199 (2002), hep-ex/0108039.
- [302] M. I. Eides, L. L. Frankfurt, and M. I. Strikman, Phys. Rev. **D59**, 114025 (1999), hep-ph/9809277.
- [303] M. Vanderhaeghen, P. A. M. Guichon, and M. Guidal, Phys. Rev. Lett. **80**, 5064 (1998).
- [304] M. Vanderhaeghen, P. A. M. Guichon, and M. Guidal, Phys. Rev. **D60**, 094017 (1999), hep-ph/9905372.
- [305] L. Frankfurt, W. Koepf, and M. Strikman, Phys. Rev. **D54**, 3194 (1996), hep-ph/9509311.
- [306] T. Feldmann, Int. J. Mod. Phys. **A15**, 159 (2000), hep-ph/9907491.
- [307] T. Feldmann and P. Kroll, Phys. Scripta **T99**, 13 (2002), hep-ph/0201044.
- [308] C. E. Carlson and J. Milana, Phys. Rev. Lett. **65**, 1717 (1990).
- [309] D. Bollini *et al.*, Nuovo Cim. Lett. **14**, 418 (1975).
- [310] A. V. Belitsky and D. Müller, Phys. Lett. **B513**, 349 (2001), hep-ph/0105046.
- [311] S. J. Brodsky, G. P. Lepage, and P. B. Mackenzie, Phys. Rev. **D28**, 228 (1983).
- [312] A. P. Bakulev, A. V. Radyushkin, and N. G. Stefanis, Phys. Rev. **D62**, 113001 (2000), hep-ph/0005085.
- [313] B. Melić, B. Nizić, and K. Passek, Phys. Rev. **D60**, 074004 (1999), hep-ph/9802204.
- [314] J. P. Ma and J.-S. Xu, Phys. Lett. **B510**, 161 (2001), hep-ph/0103225.
- [315] J. P. Ma and J.-S. Xu, hep-ph/0109055.
- [316] M. Maul, Eur. Phys. J. **C21**, 115 (2001), hep-ph/0104078.
- [317] C.-H. Chen and H.-n. Li, Phys. Lett. **B561**, 258 (2003), hep-ph/0209043.
- [318] V. M. Braun and N. Kivel, Phys. Lett. **B501**, 48 (2001), hep-ph/0012220.

- [319] CLEO Collaboration, J. Gronberg *et al.*, Phys. Rev. **D57**, 33 (1998), hep-ex/9707031.
- [320] L3 Collaboration, M. Acciarri *et al.*, Phys. Lett. **B418**, 399 (1998).
- [321] M. Diehl, P. Kroll, and C. Vogt, Eur. Phys. J. **C22**, 439 (2001), hep-ph/0108220.
- [322] B. Clerbaux and M. V. Polyakov, Nucl. Phys. **A679**, 185 (2000), hep-ph/0001332.
- [323] M. Diehl, T. Gousset, and B. Pire, hep-ph/9909445.
- [324] R. K. Ellis, W. Furmanski, and R. Petronzio, Nucl. Phys. **B212**, 29 (1983).
- [325] P. Ball, V. M. Braun, and N. Kivel, Nucl. Phys. **B649**, 263 (2003), hep-ph/0207307.
- [326] J. Chay and C. Kim, Phys. Rev. **D65**, 114016 (2002), hep-ph/0201197.
- [327] M. Beneke, A. P. Chapovsky, M. Diehl, and T. Feldmann, Nucl. Phys. **B643**, 431 (2002), hep-ph/0206152.
- [328] M. Beneke and T. Feldmann, Phys. Lett. **B553**, 267 (2003), hep-ph/0211358.
- [329] D. Pirjol and I. W. Stewart, Phys. Rev. **D67**, 094005 (2003), hep-ph/0211251.
- [330] C. W. Bauer, D. Pirjol, and I. W. Stewart, Phys. Rev. **D67**, 071502 (2003), hep-ph/0211069.
- [331] I. Z. Rothstein, hep-ph/0301240.
- [332] J.-W. Qiu and G. Sterman, Nucl. Phys. **B353**, 105 (1991).
- [333] J.-W. Qiu and G. Sterman, Nucl. Phys. **B353**, 137 (1991).
- [334] N. Kivel and L. Mankiewicz, hep-ph/0305207.
- [335] Z. Chen, Nucl. Phys. **B525**, 369 (1998), hep-ph/9705279.
- [336] B. E. White, J. Phys. **G28**, 203 (2002), hep-ph/0102121.
- [337] S. A. Anikin and O. I. Zavvalov, Annals Phys. **116**, 135 (1978).
- [338] B. Geyer, M. Lazar, and D. Robaschik, Nucl. Phys. **B559**, 339 (1999), hep-th/9901090.
- [339] B. Geyer and M. Lazar, Nucl. Phys. **B581**, 341 (2000), hep-th/0003080.
- [340] B. Geyer, M. Lazar, and D. Robaschik, Nucl. Phys. **B618**, 99 (2001), hep-ph/0108061.
- [341] A. V. Radyushkin and C. Weiss, Phys. Rev. **D63**, 114012 (2001), hep-ph/0010296.
- [342] A. V. Belitsky and D. Müller, Nucl. Phys. **B589**, 611 (2000), hep-ph/0007031.
- [343] D. V. Kiptily and M. V. Polyakov, hep-ph/0212372.
- [344] N. Kivel, M. V. Polyakov, A. Schäfer, and O. V. Teryaev, Phys. Lett. **B497**, 73 (2001), hep-ph/0007315.
- [345] A. V. Radyushkin and C. Weiss, Phys. Lett. **B493**, 332 (2000), hep-ph/0008214.
- [346] A. V. Radyushkin and C. Weiss, Phys. Rev. **D64**, 097504 (2001), hep-ph/0106059.

- [347] S. Wandzura and F. Wilczek, Phys. Lett. **B72**, 195 (1977).
- [348] E155 Collaboration, P. L. Anthony *et al.*, Phys. Lett. **B553**, 18 (2003), hep-ex/0204028.
- [349] N. Kivel and M. V. Polyakov, Nucl. Phys. **B600**, 334 (2001), hep-ph/0010150.
- [350] I. V. Anikin and O. V. Teryaev, Phys. Lett. **B509**, 95 (2001), hep-ph/0102209.
- [351] P. Ball and M. Lazar, Phys. Lett. **B515**, 131 (2001), hep-ph/0103080.
- [352] M. Penttinen, M. V. Polyakov, A. G. Shuvaev, and M. Strikman, Phys. Lett. **B491**, 96 (2000), hep-ph/0006321.
- [353] H. Burkhardt and W. N. Cottingham, Annals Phys. **56**, 453 (1970).
- [354] A. V. Efremov, O. V. Teryaev, and E. Leader, Phys. Rev. **D55**, 4307 (1997), hep-ph/9607217.
- [355] I. V. Anikin, B. Pire, and O. V. Teryaev, Phys. Rev. **D62**, 071501 (2000), hep-ph/0003203.
- [356] A. Khodjamirian, Eur. Phys. J. **C6**, 477 (1999), hep-ph/9712451.
- [357] A. Khodjamirian, Nucl. Phys. **B605**, 558 (2001), hep-ph/0012271.
- [358] P. Gosdzinsky and N. Kivel, Nucl. Phys. **B521**, 274 (1998), hep-ph/9707367.
- [359] M. Beneke, Phys. Rept. **317**, 1 (1999), hep-ph/9807443.
- [360] A. Schmedding and O. I. Yakovlev, Phys. Rev. **D62**, 116002 (2000), hep-ph/9905392.
- [361] A. P. Bakulev, S. V. Mikhailov, and N. G. Stefanis, Phys. Rev. **D67**, 074012 (2003), hep-ph/0212250.
- [362] A. V. Radyushkin and R. Ruskov, Phys. Lett. **B374**, 173 (1996), hep-ph/9511270.
- [363] A. V. Radyushkin and R. Ruskov, Nucl. Phys. **B481**, 625 (1996), hep-ph/9603408.
- [364] I. V. Musatov and A. V. Radyushkin, Phys. Rev. **D56**, 2713 (1997), hep-ph/9702443.
- [365] J. Botts and G. Sterman, Nucl. Phys. **B325**, 62 (1989).
- [366] H.-n. Li and G. Sterman, Nucl. Phys. **B381**, 129 (1992).
- [367] R. Jakob and P. Kroll, Phys. Lett. **B315**, 463 (1993), hep-ph/9306259.
- [368] R. Jakob, P. Kroll, and M. Raulfs, J. Phys. **G22**, 45 (1996), hep-ph/9410304.
- [369] S. Descotes-Genon and C. T. Sachrajda, Nucl. Phys. **B625**, 239 (2002), hep-ph/0109260.
- [370] B. Melić, D. Müller, and K. Passek-Kumerički, Phys. Rev. **D68**, 014013 (2003), hep-ph/0212346.
- [371] B. Melić, B. Nizic, and K. Passek, Phys. Rev. **D65**, 053020 (2002), hep-ph/0107295.
- [372] S. J. Brodsky, C.-R. Ji, A. Pang, and D. G. Robertson, Phys. Rev. **D57**, 245 (1998), hep-ph/9705221.
- [373] P. Kroll and M. Raulfs, Phys. Lett. **B387**, 848 (1996), hep-ph/9605264.

- [374] A. V. Belitsky and D. Müller, Phys. Lett. **B507**, 173 (2001), hep-ph/0102224.
- [375] J. Eilers and B. Geyer, Phys. Lett. **B546**, 78 (2002), hep-ph/0207104.
- [376] A. V. Belitsky and A. Schäfer, Nucl. Phys. **B527**, 235 (1998), hep-ph/9801252.
- [377] M. Vanttinen, L. Mankiewicz, and E. Stein, hep-ph/9810527.
- [378] A. Donnachie, J. Gravelis, and G. Shaw, Eur. Phys. J. **C18**, 539 (2001), hep-ph/0009235.
- [379] F. Cano and J. M. Laget, Phys. Lett. **B551**, 317 (2003), hep-ph/0209362v2, Erratum-ibid. to appear.
- [380] HERMES Collaboration, A. Airapetian *et al.*, Eur. Phys. J. **C17**, 389 (2000), hep-ex/0004023.
- [381] N. Kivel and L. Mankiewicz, Eur. Phys. J. **C21**, 621 (2001), hep-ph/0106329.
- [382] H.-n. Li, Phys. Rev. **D48**, 4243 (1993).
- [383] The Jefferson Lab F_π Collaboration, J. Volmer *et al.*, Phys. Rev. Lett. **86**, 1713 (2001), nucl-ex/0010009.
- [384] V. M. Braun, A. Khodjamirian, and M. Maul, Phys. Rev. **D61**, 073004 (2000), hep-ph/9907495.
- [385] B. Postler, hep-ph/0110271.
- [386] T. Gousset and B. Pire, Phys. Rev. **D51**, 15 (1995), hep-ph/9403293.
- [387] NA3 Collaboration, J. Badier *et al.*, Phys. Lett. **B142**, 446 (1984).
- [388] K. Freudenreich, Int. J. Mod. Phys. **A5**, 3643 (1990).
- [389] BES Collaboration, J. Z. Bai *et al.*, Phys. Rev. Lett. **88**, 101802 (2002), hep-ex/0102003.
- [390] M. L. Swartz, Phys. Rev. **D53**, 5268 (1996), hep-ph/9509248.
- [391] S. Jeschonnek and J. W. Van Orden, hep-ph/0209157.
- [392] F. E. Close and Q. Zhao, Phys. Rev. **D66** (2002), hep-ph/0202181.
- [393] L. Mankiewicz and G. Piller, Phys. Rev. **D61**, 074013 (2000), hep-ph/9905287.
- [394] I. V. Anikin and O. V. Teryaev, Phys. Lett. **B554**, 51 (2003), hep-ph/0211028.
- [395] N. Kivel, Phys. Rev. **D65**, 054010 (2002), hep-ph/0107275.
- [396] D. Y. Ivanov and R. Kirschner, Phys. Rev. **D58**, 114026 (1998), hep-ph/9807324.
- [397] D. Y. Ivanov, B. Pire, L. Szymanowski, and O. V. Teryaev, Phys. Lett. **B550**, 65 (2002), hep-ph/0209300.
- [398] G. T. Bodwin, E. Braaten, and G. P. Lepage, Phys. Rev. **D51**, 1125 (1995), hep-ph/9407339, Erratum-ibid. **D 55**, 5853 (1997).
- [399] P. Hoodbhoy, Phys. Rev. **D56**, 388 (1997), hep-ph/9611207.
- [400] M. G. Ryskin, Phys. Lett. **B403**, 335 (1997).

- [401] M. Vänttinen and L. Mankiewicz, Phys. Lett. **B434**, 141 (1998), hep-ph/9805338.
- [402] M. Vänttinen and L. Mankiewicz, Phys. Lett. **B440**, 157 (1998), hep-ph/9807287.
- [403] B. Lehmann-Dronke and A. Schäfer, Phys. Lett. **B521**, 55 (2001), hep-ph/0107312.
- [404] J. C. Collins, J. Phys. **G28**, 1069 (2002), hep-ph/0107252.
- [405] J. C. Collins, Phys. Rev. **D57**, 3051 (1998), hep-ph/9709499, Erratum-ibid. D **61**, 019902 (2000).
- [406] L. Alvero, J. C. Collins, J. Terron, and J. J. Whitmore, Phys. Rev. **D59**, 074022 (1999), hep-ph/9805268.
- [407] H. Jung, R. Peschanski, and C. Royon, Acta Phys. Polon. **B33**, 3645 (2002), hep-ph/0209143.
- [408] V. A. Khoze, A. D. Martin, and M. G. Ryskin, Phys. Lett. **B401**, 330 (1997), hep-ph/9701419.
- [409] V. A. Khoze, A. D. Martin, and M. G. Ryskin, Eur. Phys. J. **C14**, 525 (2000), hep-ph/0002072.
- [410] A. De Roeck, V. A. Khoze, A. D. Martin, R. Orava, and M. G. Ryskin, Eur. Phys. J. **C25**, 391 (2002), hep-ph/0207042.
- [411] V. A. Khoze, A. D. Martin, and M. G. Ryskin, Eur. Phys. J. **C26**, 229 (2002), hep-ph/0207313.
- [412] A. De Roeck and C. Royon, Acta Phys. Polon. **B33**, 3491 (2002), hep-ph/0209171.
- [413] J. B. Bronzan, G. L. Kane, and U. P. Sukhatme, Phys. Lett. **B49**, 272 (1974).
- [414] J. R. Forshaw and D. A. Ross, *Quantum Chromodynamics and the Pomeron* (Cambridge University Press, 1997).
- [415] A. Donnachie, H. G. Dosch, P. V. Landshoff, and O. Nachtmann, *Pomeron physics and QCD* (Cambridge University Press, Cambridge, 2002).
- [416] A. Donnachie and P. V. Landshoff, Nucl. Phys. **B267**, 690 (1986).
- [417] A. Donnachie and P. V. Landshoff, Phys. Lett. **B296**, 227 (1992), hep-ph/9209205.
- [418] J. R. Cudell, A. Donnachie, and P. V. Landshoff, Phys. Lett. **B448**, 281 (1999), hep-ph/9901222.
- [419] S. Catani, M. Ciafaloni, and F. Hautmann, Phys. Lett. **B242**, 97 (1990).
- [420] J. C. Collins and R. K. Ellis, Nucl. Phys. **B360**, 3 (1991).
- [421] Small x Collaboration, B. Andersson *et al.*, Eur. Phys. J. **C25**, 77 (2002), hep-ph/0204115.
- [422] A. D. Martin and M. G. Ryskin, Phys. Rev. **D64**, 094017 (2001), hep-ph/0107149.
- [423] L. N. Lipatov, Sov. J. Nucl. Phys. **23**, 338 (1976).
- [424] E. A. Kuraev, L. N. Lipatov, and V. S. Fadin, Sov. Phys. JETP **45**, 199 (1977).
- [425] I. I. Balitsky and L. N. Lipatov, Sov. J. Nucl. Phys. **28**, 822 (1978).
- [426] N. N. Nikolaev and B. G. Zakharov, Z. Phys. **C49**, 607 (1991).

- [427] A. H. Mueller, Nucl. Phys. **B415**, 373 (1994).
- [428] A. H. Mueller and B. Patel, Nucl. Phys. **B425**, 471 (1994), hep-ph/9403256.
- [429] H. Navelet and S. Wallon, Nucl. Phys. **B522**, 237 (1998), hep-ph/9705296.
- [430] J. Bartels, B. I. Ermolaev, and M. G. Ryskin, Z. Phys. **C72**, 627 (1996), hep-ph/9603204.
- [431] B. Ermolaev, R. Kirschner, and L. Szymanowski, Eur. Phys. J. **C7**, 65 (1999), hep-ph/9806439.
- [432] A. Bialas, H. Navelet, and R. Peschanski, Nucl. Phys. **B593**, 438 (2001), hep-ph/0009248.
- [433] J. Bartels, S. Gieseke, and A. Kyrieleis, Phys. Rev. **D65**, 014006 (2002), hep-ph/0107152.
- [434] A. H. Mueller, hep-ph/0111244.
- [435] K. Golec-Biernat and M. Wüsthoff, Phys. Rev. **D59**, 014017 (1999), hep-ph/9807513.
- [436] J. Czyżewski, J. Kwieciński, L. Motyka, and M. Sadzikowski, Phys. Lett. **B398**, 400 (1997), hep-ph/9611225.
- [437] J. Bartels, M. A. Braun, D. Colferai, and G. P. Vacca, Eur. Phys. J. **C20**, 323 (2001), hep-ph/0102221.
- [438] R. Engel, D. Y. Ivanov, R. Kirschner, and L. Szymanowski, Eur. Phys. J. **C4**, 93 (1998), hep-ph/9707362.
- [439] P. Hägler, B. Pire, L. Szymanowski, and O. V. Teryaev, Phys. Lett. **B535**, 117 (2002), hep-ph/0202231, Erratum-ibid. B **540**, 324 (2002).
- [440] A. D. Martin, M. G. Ryskin, and T. Teubner, Phys. Rev. **D55**, 4329 (1997), hep-ph/9609448.
- [441] H. Abramowicz, L. Frankfurt, and M. Strikman, Surveys High Energ. Phys. **11**, 51 (1997), hep-ph/9503437.
- [442] J. Bartels, K. Golec-Biernat, and K. Peters, Acta Phys. Polon. **B34**, 3051 (2003), hep-ph/0301192.
- [443] J. Bartels and H. Kowalski, Eur. Phys. J. **C19**, 693 (2001), hep-ph/0010345.
- [444] J. A. Crittenden, hep-ex/9704009.
- [445] A. Kreisel, hep-ex/0208013.
- [446] H1 Collaboration, S. Aid *et al.*, Nucl. Phys. **B468**, 3 (1996), hep-ex/9602007.
- [447] H1 Collaboration, C. Adloff *et al.*, Z. Phys. **C75**, 607 (1997), hep-ex/9705014.
- [448] H1 Collaboration, C. Adloff *et al.*, Eur. Phys. J. **C13**, 371 (2000), hep-ex/9902019.
- [449] H1 Collaboration, C. Adloff *et al.*, Phys. Lett. **B483**, 360 (2000), hep-ex/0005010.
- [450] H1 Collaboration, C. Adloff *et al.*, Phys. Lett. **B539**, 25 (2002), hep-ex/0203022.
- [451] ZEUS Collaboration, M. Derrick *et al.*, Phys. Lett. **B356**, 601 (1995), hep-ex/9507001.
- [452] ZEUS Collaboration, M. Derrick *et al.*, Phys. Lett. **B380**, 220 (1996), hep-ex/9604008.

- [453] ZEUS Collaboration, J. Breitweg *et al.*, Eur. Phys. J. **C6**, 603 (1999), hep-ex/9808020.
- [454] ZEUS Collaboration, J. Breitweg *et al.*, Eur. Phys. J. **C12**, 393 (2000), hep-ex/9908026.
- [455] ZEUS Collaboration, J. Breitweg *et al.*, Phys. Lett. **B487**, 273 (2000), hep-ex/0006013.
- [456] H1 Collaboration, S. Aid *et al.*, Nucl. Phys. **B472**, 3 (1996), hep-ex/9603005.
- [457] H1 Collaboration, C. Adloff *et al.*, Phys. Lett. **B421**, 385 (1998), hep-ex/9711012.
- [458] H1 Collaboration, C. Adloff *et al.*, Eur. Phys. J. **C10**, 373 (1999), hep-ex/9903008.
- [459] H1 Collaboration, C. Adloff *et al.*, Phys. Lett. **B483**, 23 (2000), hep-ex/0003020.
- [460] H1 Collaboration, C. Adloff *et al.*, Phys. Lett. **B541**, 251 (2002), hep-ex/0205107.
- [461] ZEUS Collaboration, J. Breitweg *et al.*, Z. Phys. **C75**, 215 (1997), hep-ex/9704013.
- [462] ZEUS Collaboration, J. Breitweg *et al.*, Phys. Lett. **B437**, 432 (1998), hep-ex/9807020.
- [463] ZEUS Collaboration, S. Chekanov *et al.*, Eur. Phys. J. **C24**, 345 (2002), hep-ex/0201043.
- [464] A. Donnachie and P. V. Landshoff, Phys. Lett. **B185**, 403 (1987).
- [465] L. Frankfurt, W. Koepf, and M. Strikman, Phys. Rev. **D57**, 512 (1998), hep-ph/9702216.
- [466] L. L. Frankfurt, M. F. McDermott, and M. Strikman, JHEP **02**, 002 (1999), hep-ph/9812316.
- [467] L. Frankfurt, M. McDermott, and M. Strikman, JHEP **03**, 045 (2001), hep-ph/0009086.
- [468] M. G. Ryskin, R. G. Roberts, A. D. Martin, and E. M. Levin, Z. Phys. **C76**, 231 (1997), hep-ph/9511228.
- [469] A. D. Martin, M. G. Ryskin, and T. Teubner, Phys. Lett. **B454**, 339 (1999), hep-ph/9901420.
- [470] A. D. Martin, M. G. Ryskin, and T. Teubner, Phys. Rev. **D62**, 014022 (2000), hep-ph/9912551.
- [471] E. M. Levin, A. D. Martin, M. G. Ryskin, and T. Teubner, Z. Phys. **C74**, 671 (1997), hep-ph/9606443.
- [472] J. P. Ma and J.-S. Xu, hep-ph/0111391.
- [473] H. G. Dosch, T. Gousset, G. Kulzinger, and H. J. Pirner, Phys. Rev. **D55**, 2602 (1997), hep-ph/9608203.
- [474] J. Hüfner, Y. P. Ivanov, B. Z. Kopeliovich, and A. V. Tarasov, Phys. Rev. **D62**, 094022 (2000), hep-ph/0007111.
- [475] A. C. Caldwell and M. S. Soares, Nucl. Phys. **A696**, 125 (2001), hep-ph/0101085.
- [476] H. G. Dosch and E. Ferreira, Eur. Phys. J. **C29**, 45 (2003), hep-ph/0212257.
- [477] S. Munier, A. M. Staśto, and A. H. Mueller, Nucl. Phys. **B603**, 427 (2001), hep-ph/0102291.
- [478] E. Gotsman, E. Ferreira, E. Levin, U. Maor, and E. Naftali, Phys. Lett. **B503**, 277 (2001), hep-ph/0101142.

- [479] J. Nemchik, N. N. Nikolaev, and B. G. Zakharov, Phys. Lett. **B341**, 228 (1994), hep-ph/9405355.
- [480] E. V. Kuraev, N. N. Nikolaev, and B. G. Zakharov, JETP Lett. **68**, 696 (1998), hep-ph/9809539.
- [481] L. L. Frankfurt, A. Freund, and M. Strikman, Phys. Rev. **D58**, 114001 (1998), hep-ph/9710356.
- [482] A. Freund, private communication (2003).
- [483] A. Donnachie and H. G. Dosch, Phys. Lett. **B502**, 74 (2001), hep-ph/0010227.
- [484] M. McDermott, R. Sandapen, and G. Shaw, Eur. Phys. J. **C22**, 655 (2002), hep-ph/0107224.
- [485] L. Favart and M. V. T. Machado, hep-ph/0302079.
- [486] L. L. Frankfurt, A. Freund, and M. Strikman, Phys. Lett. **B460**, 417 (1999), hep-ph/9806535.
- [487] J. Bartels, K. Golec-Biernat, and K. Peters, Eur. Phys. J. **C17**, 121 (2000), hep-ph/0003042.
- [488] M. Wüsthoff and A. D. Martin, J. Phys. **G25**, R309 (1999), hep-ph/9909362.
- [489] A. Hebecker and T. Teubner, Phys. Lett. **B498**, 16 (2001), hep-ph/0010273.
- [490] M. Diehl, T. Gousset, B. Pire, and J. P. Ralston, Phys. Lett. **B411**, 193 (1997), hep-ph/9706344.
- [491] K. Schilling and G. Wolf, Nucl. Phys. **B61**, 381 (1973).
- [492] A. V. Belitsky and D. Müller, Phys. Rev. Lett. **90**, 022001 (2003), hep-ph/0210313.
- [493] S. J. Brodsky, F. E. Close, and J. F. Gunion, Phys. Rev. **D6**, 177 (1972).
- [494] P. Kroll, M. Schürmann, and P. A. M. Guichon, Nucl. Phys. **A598**, 435 (1996), hep-ph/9507298.
- [495] A. V. Belitsky, A. Kirchner, D. Müller, and A. Schäfer, Phys. Lett. **B510**, 117 (2001), hep-ph/0103343.
- [496] P. Y. Bertin, Y. Roblin, and C. E. Hyde-Wright, Fizika **B8**, 207 (1999), hep-ph/9910381.
- [497] V. A. Korotkov and W. D. Nowak, Eur. Phys. J. **C23**, 455 (2002), hep-ph/0108077.
- [498] V. A. Korotkov and W. D. Nowak, Nucl. Phys. **A711**, 175 (2002), hep-ph/0207103.
- [499] N. d'Hose *et al.*, hep-ex/0212047.
- [500] A. Freund, hep-ph/0306012.
- [501] J. H. Ely, Dissertation, University of Colorado (2002).
- [502] S. Stepanyan, private communication (2003).
- [503] A. Freund and M. Strikman, Phys. Rev. **D60**, 071501 (1999), hep-ph/9906205.
- [504] HERMES Collaboration, F. Ellinghaus, R. Shanidze, and J. Volmer, hep-ex/0212019.
- [505] L3 Collaboration, P. Achard *et al.*, hep-ex/0305082.
- [506] L. N. Hand, Phys. Rev. **129**, 1834 (1963).

- [507] HERMES Collaboration, A. Airapetian *et al.*, Phys. Lett. **B535**, 85 (2002), hep-ex/0112022.
- [508] HERMES Collaboration, K. Ackerstaff *et al.*, Eur. Phys. J. **C18**, 303 (2000), hep-ex/0002016.
- [509] E665 Collaboration, M. R. Adams *et al.*, Z. Phys. **C74**, 237 (1997).
- [510] HERMES Collaboration, A. Airapetian *et al.*, Phys. Lett. **B513**, 301 (2001), hep-ex/0102037.
- [511] HERMES, A. Airapetian *et al.*, Eur. Phys. J. **C29**, 171 (2003), hep-ex/0302012.
- [512] R. L. Sekulin, Nucl. Phys. **B56**, 227 (1973).
- [513] HERMES Collaboration, P. di Nezza and R. Fabbri, hep-ex/0211008.
- [514] A. Freund, Phys. Lett. **B472**, 412 (2000), hep-ph/9903488.
- [515] S. J. Brodsky and G. R. Farrar, Phys. Rev. Lett. **31**, 1153 (1973).
- [516] V. A. Matveev, R. M. Muradian, and A. N. Tavkhelidze, Nuovo Cim. Lett. **7**, 719 (1973).
- [517] N. Isgur and C. H. Llewellyn Smith, Phys. Lett. **B217**, 535 (1989).
- [518] N. Isgur and C. H. Llewellyn Smith, Nucl. Phys. **B317**, 526 (1989).
- [519] A. V. Radyushkin, Nucl. Phys. **A532**, 141 (1991).
- [520] J. Bolz, R. Jakob, P. Kroll, M. Bergmann, and N. G. Stefanis, Z. Phys. **C66**, 267 (1995), hep-ph/9405340.
- [521] B. Kundu, H.-n. Li, J. Samuelsson, and P. Jain, Eur. Phys. J. **C8**, 637 (1999), hep-ph/9806419.
- [522] J. Bolz, R. Jakob, P. Kroll, and N. G. Stefanis, hep-ph/9807328.
- [523] T. C. Brooks and L. J. Dixon, Phys. Rev. **D62**, 114021 (2000), hep-ph/0004143.
- [524] M. Diehl, T. Feldmann, R. Jakob, and P. Kroll, Phys. Lett. **B460**, 204 (1999), hep-ph/9903268.
- [525] M. Diehl, T. Feldmann, H. W. Huang, and P. Kroll, Phys. Rev. **D67**, 037502 (2003), hep-ph/0212138.
- [526] Jefferson Lab Hall A Collaboration, J. P. Chen *et al.*, *Exclusive Compton Scattering on the Proton*, Jefferson Lab Report PCCF-RI-99-17 (2000).
- [527] L. Cardman *et al.*, *The Science Driving the 12 GeV Upgrade of CEBAF*, Jefferson Lab Report (2001).
- [528] H. W. Huang, P. Kroll, and T. Morii, Eur. Phys. J. **C23**, 301 (2002), hep-ph/0110208, Erratum-*ibid.* to appear.
- [529] H. W. Huang and T. Morii, Phys. Rev. **D68**, 014016 (2003), hep-ph/0305132.
- [530] Jefferson Lab Hall A Collaboration, O. Gayou *et al.*, Phys. Rev. Lett. **88**, 092301 (2002), nucl-ex/0111010.
- [531] J. Arrington, hep-ph/0209243.
- [532] P. A. M. Guichon and M. Vanderhaeghen, hep-ph/0306007.

- [533] A. M. Nathan, hep-ph/9908522.
- [534] H. W. Huang and P. Kroll, Eur. Phys. J. **C17**, 423 (2000), hep-ph/0005318.
- [535] F. Cano and J. M. Laget, Phys. Rev. **D65**, 074022 (2002), hep-ph/0111146.
- [536] VENUS Collaboration, H. Hamasaki *et al.*, Phys. Lett. **B407**, 185 (1997).
- [537] CLEO Collaboration, J. Dominick *et al.*, Phys. Rev. **D50**, 3027 (1994), hep-ph/9403379.
- [538] CLEO Collaboration, M. Artuso *et al.*, Phys. Rev. **D50**, 5484 (1994).
- [539] CLEO Collaboration, S. Anderson *et al.*, Phys. Rev. **D56**, 2485 (1997), hep-ex/9701013.
- [540] L3 Collaboration, P. Achard *et al.*, Phys. Lett. **B536**, 24 (2002), hep-ex/0204025.
- [541] OPAL Collaboration, G. Abbiendi *et al.*, Eur. Phys. J. **C28**, 45 (2003), hep-ex/0209052.
- [542] L3 Collaboration, P. Achard *et al.*, hep-ex/0306017.
- [543] F. Anulli, S. Braccini, and G. Pancheri, Proceedings of PHOTON 2003, Frascati, Italy, 7–11 April 2003, to appear in Nucl. Phys. Proc. Suppl.
- [544] H. H. Gutbrod *et al.*, *An International Accelerator Facility for Beams of Ions and Antiprotons*, Conceptual Design Report, GSI Darmstadt (2001).
- [545] G. R. Farrar, E. Maina, and F. Neri, Nucl. Phys. **B259**, 702 (1985).
- [546] C. F. Berger and W. Schweiger, Eur. Phys. J. **C28**, 249 (2003), hep-ph/0212066.
- [547] C. Vogt, hep-ph/0010040.
- [548] S. J. Brodsky and G. P. Lepage, Phys. Rev. **D24**, 1808 (1981).
- [549] F. E. Close and Q. Zhao, Phys. Lett. **B553**, 211 (2003), hep-ph/0210277.
- [550] HERMES Collaboration, F. Ellinghaus, Nucl. Phys. **A711**, 171 (2002), hep-ex/0207029.
- [551] Jefferson Lab Hall A Collaboration, J. P. Chen *et al.*, *Deeply Virtual Compton Scattering at 6 GeV*, Jefferson Lab Experiment E 00-110 (2000).
- [552] F. Sabatié, hep-ex/0207016.
- [553] R. Holt *et al.*, *The Electron Ion Collider: A high luminosity probe of the partonic substructure of nucleons and nuclei*, Brookhaven Report BNL-68933 (2002).
- [554] V. M. Braun, D. Y. Ivanov, A. Schäfer, and L. Szymanowski, Nucl. Phys. B **638**, 111 (2002), hep-ph/0204191.
- [555] J. W. Chen and M. J. Savage, nucl-th/0308033.
- [556] P. Hoodbhoy, X.-D. Ji, and F. Yuan, hep-ph/0309085.